Mathematical and numerical modelling of cell migration

Christèle Etchegaray

Université Paris-Saclay

École doctorale de mathématiques Hadamard (EDMH, ED 574)

Établissement d'inscription : Université Paris-Sud

Établissements d'accueil : Université Paris-Sud
Université Paris Descartes

Laboratoires d'accueil : Laboratoire de mathématiques d'Orsay, UMR 8628 CNRS
Laboratoire MAP5, UMR CNRS 8145

THÈSE DE DOCTORAT ÈS MATHÉMATIQUES

Spécialité : Mathématiques appliquées

Christèle ETCHEGARAY

Modélisation mathématique et numérique de la migration cellulaire

Date de soutenance : 29 Novembre 2016

Après avis des rapporteurs : M. Clair POIGNARD (Université de Bordeaux)
M. Viet Chi TRAN (Université de Lille)

Jury de soutenance :

M. Alexis GAUTREAU	(École Polytechnique) Codirecteur de thèse
Mme Danielle HILHORST	(Université Paris-Sud) Présidente du jury
M. Bertrand MAURY	(Université Paris-Sud) Codirecteur de thèse
M. Nicolas MEUNIER	(Université Paris Descartes) Codirecteur de thèse
M. Clair POIGNARD	(Université de Bordeaux) Rapporteur
M. Viet Chi TRAN	(Université de Lille) Rapporteur
Mme Amandine VEBER	(École Polytechnique) Invitée

NNT : 2016SACLS428

Table des matières

Page

Remerciements 1

Introduction - Synthèse en français 4

I Particle approach 39

1 A stochastic model for cell adhesion to the vascular wall 41
- 1.1 Introduction . . . 41
- 1.2 Construction of the discrete stochastic model . . . 43
- 1.3 Mathematical properties and numerical simulations . . . 45
- 1.4 Continuous bonds approximations . . . 50
- 1.5 Stopping time . . . 62
- 1.6 Conclusions and perspectives . . . 73
- 1.7 Appendix . . . 73

2 A stochastic model for 2D cell crawling 77
- 2.1 Introduction . . . 77
- 2.2 Construction of the model . . . 78
- 2.3 Mathematical properties . . . 91
- 2.4 Annex . . . 96

3 Scaling limits 99
- 3.1 Scaling the force and dynamics . . . 99
- 3.2 Deterministic limits . . . 104
- 3.3 Accelerated demography . . . 112
- 3.4 Annex . . . 133

4 The continuous limiting models 137
- 4.1 Time-space continuous dynamics . . . 137
- 4.2 Angular discretization . . . 143
- 4.3 One dimensional migration . . . 147
- 4.4 Conclusions and perspectives . . . 155

II Fluid approach **157**

5 Construction of the fluid model **159**
5.1 Introduction . . . 159
5.2 The cytoskeleton as an active polar gel . . . 161
5.3 Existing works . . . 164
5.4 The free boundary model . . . 171
5.5 The problem in a rigid domain . . . 178

6 Analysis of a 1D non-local and non-linear Fokker-Planck equation **189**
6.1 The boundary non-linear Fokker-Planck equation . . . 190
6.2 Global existence and asymptotic analysis for sub-critical mass $M < 1$ . . . 193
6.3 Critical case $M = 1$ . . . 198
6.4 The Super-critical case $M > 1$ . . . 200
6.5 Dynamical exchange of markers at the boundary: prevention of blow-up and asymptotic behaviour . . . 204
6.6 Perspectives . . . 207

7 The discoidal 2D model **209**
7.1 Introduction . . . 209
7.2 Models under study . . . 211
7.3 Cell intrinsic activity: first results . . . 212
7.4 Stochastic effects . . . 217
7.5 Stimulation by a chemical signal . . . 223
7.6 Mechanical interaction . . . 230
7.7 Conclusions . . . 233
7.8 Discretization . . . 234

III Appendices **I**

A An integro-differential equation for 1D cell migration **III**

B Algorithm for numerical trajectories analysis **XIII**

C Un modèle de régulation moléculaire oscillatoire **XVII**
C.1 Modélisation locale . . . XIX
C.2 Modèle 2 : diffusion sur la membrane . . . XXIV

Abstract/Résumé **XXVIII**
*

Remerciements

Tout d'abord, je tiens à exprimer ma profonde gratitude envers mes directeurs de thèse Alexis Gautreau, Bertrand Maury et Nicolas Meunier, autant pour leurs appuis scientifiques que leurs qualités humaines. Merci infiniment Nicolas d'avoir été aussi présent et de m'avoir soutenue depuis ce projet de modélisation en M2 jusqu'à cette thèse. Je te suis très reconnaissante de m'avoir proposé un sujet de recherche aussi beau, passionnant et riche que celui de la migration cellulaire, qui n'a d'ailleurs pas fini de nous occuper! Merci de m'avoir fait confiance. J'ai beaucoup apprécié nos discussions ainsi que ton enthousiasme communicatif! Merci beaucoup Bertrand pour ta confiance et ton intérêt pour ce sujet. Merci également pour ton soutien, tes conseils, ainsi que pour la liberté que tu m'as donnée. Nos discussions sur la modélisation ont enrichi ma réflexion. Merci beaucoup Alexis d'avoir accepté d'encadrer cette thèse de mathématiques sans hésiter, et de t'être montré curieux de notre approche. Merci pour ta disponibilité et les échanges que nous avons eus.

Je remercie très sincèrement Clair Poignard et Viet Chi Tran pour l'intérêt qu'ils ont porté à mes travaux, et pour avoir accepté de rapporter ma thèse. Merci pour votre efficacité et vos remarques pertinentes. Merci également à Danielle Hilhorst et Amandine Veber d'avoir accepté de faire partie de mon jury de soutenance.

Un grand merci à Raphaël Voituriez qui a joué un rôle important dans le développement de ces travaux. Merci également à Daniel Riveline et David Caballero pour leur ouverture et leur enthousiasme. I would like to sincerely thank Alex Mogilner and Dietmar Oelz for their kindness and helpful discussions at the CIMS. Merci également au LMO ainsi qu'à Nicolas et Bertrand pour cette opportunité. Je remercie également vivement Antoine Mellet pour notre collaboration. Enfin, merci également à Vincent Calvez et Matthieu Piel pour l'intérêt qu'ils portent à nos travaux, ainsi que pour leurs remarques.

J'ai eu la chance de bénéficier de très bons environnements de travail dans deux laboratoires. Au LMO, un grand merci aux membres de l'équipe ANEDP que j'ai eu plaisir à côtoyer, ainsi qu'à David Harari, Frédéric Paulin, Frédéric Lagoutière et Stéphane Nonnenmacher pour l'école doctorale. Merci également à Sylvain Faure pour son aide. J'ai été accueillie au MAP5 depuis mon stage de M2, jusqu'à cette année d'ATER. Merci aux directrices Christine Graffigne, Annie Raoult et Fabienne Comte, ainsi qu'aux membres permanents du laboratoire, pour cette ambiance chaleureuse. Merci en particulier à l'équipe de Modélisation numérique, ainsi qu'à Florent Benaych-Georges, Rachid Lounès, Éric Luçon, et Camille Male. Je suis fière d'avoir produit la vidéo du laboratoire avec Charlotte. Un grand merci à Nicolas Muller, mon brillant grand frère de thèse, pour son aide et son soutien.

Je suis très reconnaissante à l'équipe enseignante du département Mesures Physiques de l'IUT d'Orsay pour le cadre convivial dans lequel j'ai fait mes débuts d'enseignante : merci à Maximilien Lagron, Sabine Marduel, Florence Alberge et Thierry Guilbaud.

Enfin, mon quotidien a été grandement facilité par le dynamisme et l'efficacité des équipes

administratives et informatiques. Je leur en suis très reconnaissante. En particulier, merci à Valérie Lavigne, Catherine Poupon, Florence Rey, Estelle Savinien et Florence Furbatto à Orsay. Merci également à Marie-Hélène Gbaguidi, Isabelle Valéro, Christophe Castellani, Clémence Misseboukpo, ainsi qu'à Thierry Rardersdorff, Arnaud Meunier, et Azedine Mani au MAP5.

Je tiens également à remercier mes professeurs qui ont joué un rôle important dans mon orientation. A Bordeaux, merci à Christophe Bavard et à Qing Liu de m'avoir donné l'opportunité de premières expériences de recherche et excursions (au soleil) chez les groupes Fuchsiens et les courbes algébriques. Je suis profondément reconnaissante aux responsables du M2 MathSV d'Orsay, Christophe Giraud et Pascal Massart, pour m'avoir permis de découvrir les maths appliquées aux sciences du vivant. Merci en particulier à Christophe pour ses encouragements. Je remercie également Sylvie Méléard et Laurent Desvillettes. Enfin, merci à la FMJH qui a facilité ma venue à Orsay.

Merci à tous les doctorants, anciens doctorants, stagiaires avec qui j'ai partagé ces années ! Merci aux doctorants des bureaux 256-258 à Orsay : Pierre, Tony, Jean, Yeyuan, Alpar, Antonin, Paul, Samer, Perla, Andrea S.; Nina (& Jérémie), Anthony, Clémentine, et Fatima. J'ai beaucoup apprécié les pauses goûters/batailles de pistolets à ventouse/luttes de pouvoir pour être chef de bureau. Au MAP5, merci d'abord à Arthur, papa Ours et roi du karaoké. Merci à la team GTTJD, Jean, Gwen et Charlotte pour ces années d'innovation. Un Big Up à José Bigre, son jury et son orchestre pour ce concert triomphal ! Merci à l'ensemble des doctorants pour leur bonne humeur et les soirées mémorables : Claire, Anne-Claire, Charlotte L., Alkéos, Maud ; Rémy, Fanny, Anne-So, Sonia, Alasdair, Nora, Vincent (le géographe) ; Fabien, mon petit bro de thèse qui ira loin! Mes co-bureaux Léon, Rébecca (merci à vous deux pour l'accueil), Fu-Chen, Pierre-Alexandre, Aniket, Ronan, Léo. Merci en particulier à Julie avec qui je partage le bureau depuis longtemps maintenant. Grazie à Andrea pour m'avoir supporté pendant la rédaction. Merci pour les petit-déjs, les harmonies vocales et aussi pour avoir fermé le bureau :). Bienvenue aux nouveaux doctorants enthousiastes!

Merci aux autres doctorants avec qui j'ai partagé des moments : merci à Emeric, Ludovick, Fabien P., Thibault (merci pour les slides!). Merci aux plus gros brigands de Londres, Pierre et Caz : big Up, force, peace. Merci à Mélina, Céline (& Igor) Maxime, et Chloé M. Merci aussi aux anciens du M2 MathSV. En particulier, merci à Arus, Aurora et Chloé A. (& Adrien) : bientôt le diamant !! Charlotte, merci pour tout ce que tu m'as apporté depuis le projet!
La période de la thèse a également été riche en danse. Merci aux danseurs pour leur talent, leur simplicité, la force qu'ils donnent et surtout les valeurs qu'ils transmettent partout où ils passent. Merci à Stéf pour son amitié depuis le théâtre de la Plaine jusqu'à aujourd'hui. Notre évolution commune fait plaisir à voir. Merci à Cathy et Claire pour leurs énergies, depuis les freestyles du cours de Jay jusqu'à ceux de Guillaume et Sonia. Merci à Jennifer pour les discussions sur l'Inde, et à Abdel pour les joutes verbales. Merci à Laure d'être merveilleuse. J'en profite également pour remercier Lady Sev pour son courage et sa détermination qui la font déplacer des montagnes (basques). Un grand merci à Claudine pour sa gentillesse et sa folie. Une pensées aux filles de Btz depuis le Zion festival jusqu'à la BDS.

Je tiens également à remercier Sandy, Mario, et BenJ pour leurs amitiés. Une pensée pour Xavier et tout ce qu'il a accompli. Comment ne pas citer Elodie HD : merci pour toutes ces années et ta présence durant la période de rédaction. J'admire le chemin que tu as parcouru.

Je remercie profondément ma grande famille, depuis le lotissement Etchegaray à Lar-

ressore jusqu'à Souraïde, de Louhossoa à Romans-sur-Isère et Valence, en passant par Biarritz/St-Palais et Cambo. Une pensée pour Amatxi, Mamie et Jérôme. Evidemment, cette thèse n'existerait pas sans mascottes, Ophélie, Paula et surtout Luna. Merci à Serge d'être là, paré de sa plus belle moustache (la prochaine fête sera pour toi !), ainsi qu'à Yvonne pour son enthousiasme. J'ai la chance d'avoir le meilleur beauf du monde, Mick-Mick, qui sait parfaitement toaster en jamaïcain (je suis jalouse).

Loïc, mon frère de coeur-coeur-coeur, je ne peux pas surpasser la force de tes remerciements, mais je peux citer Youssoupha, qui a très justement dit : "à quoi ça sert de faire des maths si on ne peut pas compter les uns sur les autres?". Merci pour ce voyage jusqu'à Montigny-le-Bretonneux, et pour les innombrables bêtises qu'on a pu dire depuis.

Un merci tout particulier à ma grande sœur Elodie pour notre relation unique et tout ce qu'on partage depuis toujours. Merci de me faire rire de tout, et même de moi-même en situation de rédaction. 2Be2 for ever.

Enfin, je termine ces remerciements par mes parents. Merci pour tout ce que vous avez fait pour nous. Vous avez toujours été présents, et d'un soutien inconditionnel. Par vos exemples, vous nous avez appris à persévérer, à rester curieuses et ouvertes d'esprit et à profiter des bons moments. J'espère que vous apprécierez autant la "mécanique" de migration que les hiéroglyphes. Je suis admirative de ce que vous nous avez transmis, et je suis fière de vous dédier cette thèse.

Introduction générale

Dans cette thèse, nous abordons des problèmes de modélisation de la migration cellulaire. Ce phénomène universel, impliqué dans de nombreux processus biologiques, est également extrêmement complexe et a été ainsi étudié depuis plusieurs dizaines d'années par les biologistes, puis plus récemment du point de vue de la physique et des mathématiques.

La cellule est généralement définie comme la plus petite structure fonctionnelle du vivant. Elle est en effet capable de se spécialiser pour assurer différents rôles dans un organisme (contraction pour les cellules musculaires, formation de tissus pour les cellules épithéliales, etc.), et peut notamment se déplacer dans ce but. Cette notion d'activité provient de son organisation interne complexe comportant des éléments moléculaires, mais aussi des biopolymères et des organites fonctionnels (noyau, centrosome, mitochondries, etc.) qui entrent tous régulièrement en interaction chimique ou mécanique, et ce dans des échelles de temps très différentes.

Cette activité intrinsèque résulte en un comportement macroscopique observable par les expérimentateurs, et dont l'origine est souvent peu ou mal comprise.

L'apport de la modélisation est donc non négligeable afin de tester diverses intuitions ou hypothèses, ou parfois même d'en proposer de nouvelles. Modéliser un tel phénomène est également un défi en soi. Dans un tel cadre, il s'agit d'appréhender cette complexité et de réussir à en extraire une problématique pour laquelle formuler une question pertinente en délimitant soigneusement ses limites. La construction d'un modèle doit alors se faire dans cette perspective, en vue de fournir des éléments de réponse.

Dans cette thèse, nous abordons plus particulièrement la notion de motilité et de persistance dans le déplacement. La motilité désigne la capacité des cellules à se déplacer. Les cellules migrent de façon plus ou moins directionnelle selon leur type et l'environnement. Certaines adoptent un mouvement très peu persistant et changent constamment de direction, tandis que d'autres ont un déplacement franc dans une direction fixe. Ces caractères prennent leurs origines dans l'activité intracellulaire en lien avec l'environnement. Nous nous attachons donc à construire des modèles de migration cellulaire tenant compte du caractère multi-échelle de ce phénomène, et permettant d'aborder la question de la variabilité des phénotypes migratoires observés.

La migration cellulaire

Généralités

Le déplacement de cellules est un mécanisme fondamental du vivant, impliqué dans de nombreux processus physiologiques comme pathologiques chez un organisme. Nous présentons maintenant des exemples de tels phénomènes, afin d'en mesurer l'importance.

Enjeux

L'embryogenèse [Aman and Piotrowski, 2010] Il s'agit du développement d'un organisme vivant pluricellulaire à partir d'une cellule-oeuf [Keller, 2002]. Le développement des axes de polarité (antéro-postérieur, dorso-ventral, droite-gauche) en constitue une étape fondamentale, gérée par les gènes dits *homéotiques*. Cependant, la réponse cellulaire à l'expression de ces gènes se produit par la migration.

La bonne marche de ce processus dépend de la capacité des cellules à répondre collectivement aux signaux de polarisation pour migrer entre leurs congénères. Pour s'intercaler, elles forment des extensions de leurs membranes dans le sens de polarisation, appelées *protrusions*, qui vont adhérer aux cellules adjacentes (voir figure 1). Par ces adhésions, les cellules peuvent alors exercer une force de traction sur leurs voisines, et effectuer la migration adéquate de manière collective.

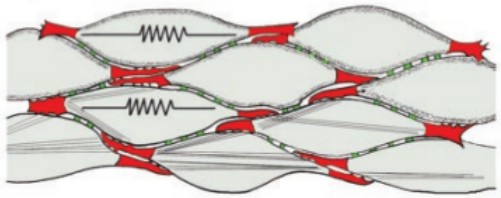

Figure 1 – Intercalation des cellules grâce à une activité protrusive polarisée. Les protrusions envoyées latéralement (en rouge) exercent des forces de traction sur la surface des cellules adjacentes, qui s'allongent sous la tension, ce qui induit leur intercalation. En vert, les adhésions cellulaires préservant l'intégrité du tissu malgré les tensions. Source : Keller [2002].

Lésion vasculaire et inflammation Lorsqu'une lésion apparaît dans des vaisseaux sanguins, la cicatrisation débute par la formation d'un caillot. Outre la protection des zones découvertes par la lésion, il contient tous les facteurs de croissance et cytokines nécessaires au recrutement chimiotactique des cellules immunitaires mais aussi dermiques et épidermiques. Il sert aussi de matrice extra-cellulaire provisoire, ce qui permet la migration de ces cellules.

Remarque 1. *Les facteurs de croissance et les cytokines sont des molécules de signalisation cellulaire. Les premières envoient des signaux pour promouvoir la prolifération des cellules. Les secondes sont des molécules permettant notamment de recruter des cellules ayant les récepteurs membranaires correspondants.*

La phase inflammatoire démarre ensuite, avec la migration de **neutrophiles** de la moelle osseuse vers la zone lésée. Ce sont des cellules immunitaires qui ont une action anti-infectieuse locale, et favorisent l'arrivée des **monocytes** dans la même zone. Les neutrophiles font partie des cellules les plus motiles de l'organisme [Jones et al., 2014; Kolaczkowska and Kubes, 2013]. Les monocytes sont des globules blancs qui peuvent infiltrer les tissus, et se différencier en macrophages. Là, ils sont chargés d'éliminer les éléments pathogènes ainsi que les débris cellulaires par phagocytose.

L'arrivée des monocytes se fait via les vaisseaux sanguins. Ces cellules adhèrent à la paroi des vaisseaux pour être externalisées dans le derme et migrer vers la lésion. C'est la migration transendothéliale [Yadav et al., 2003]. Elles ont également un rôle dans le remodelage de la matrice extra-cellulaire, et favorisent la prolifération des fibroblastes, qui interviendront dans la phase suivante de cicatrisation.

Un exemple pathologique : le cancer Nous avons vu comment la migration cellulaire est déterminante dans des phénomènes physiologiques courants. Elle peut également jouer un rôle important dans le développement de pathologies telles que le cancer, et ce à plusieurs niveaux [Bravo-Cordero et al., 2013; Yamaguchi et al., 2005]. Lorsque la tumeur primaire se développe, ses besoins en nutriments augmentent. Par conséquent, les cellules tumorales envoient des signaux dans le milieu pour activer le processus d'angiogenèse, et vasculariser la tumeur. Ainsi nourrie, elle pourra se développer d'autant plus rapidement. Ce phénomène se produit grâce à la capacité des cellules endothéliales à percevoir et à répondre aux signaux qui les font migrer pour former les nouveaux vaisseaux sanguins.

L'impact le plus fort de la migration sur le développement tumoral réside cependant dans l'apparition de métastases, qui passe par le phénomène de transition épithélio-mésenchymateuse, ou EMT. Elle se produit lorsque des cellules de nature épithéliale (non motiles et incorporée dans un tissu) développent un phénotype migratoire bien plus développé. Elles sont ainsi capables de se déplacer vers les vaisseaux sanguins les plus proches, notamment en dégradant la matrice extracellulaire afin de pouvoir y progresser. Si elles y parviennent, elles pourront rejoindre le sang et se disséminer dans l'organisme. L'apparition de métastases étant le principal facteur de morbidité d'un cancer, différentes stratégies thérapeutiques visent à limiter la motilité des cellules cancéreuses. Cependant, le caractère hautement adaptatif des cellules contre leur efficacité [Friedl and Wolf, 2003].

Une meilleure compréhension de la motilité cellulaire et de sa plasticité est donc un outil nécessaire pour développer des stratégies thérapeutiques plus précises et adaptées à la nature des tumeurs.

Développons maintenant une description précise des éléments cellulaires principaux de la migration.

Anatomie cellulaire

Le cytosquelette Le principal acteur de l'intégrité physique et mécanique de la cellule est le cytosquelette. C'est un ensemble de biopolymères très dynamiques qui s'assemblent en structures branchées ou en faisceaux. Il est responsable des caractères physiques (forme, rhéologie, génération de forces) et dynamiques (division cellulaire, transport interne, motilité) de la cellule, si bien qu'on le considère comme à la fois son muscle et son squelette. Étant rattaché à la fois à la membrane plasmique et à certains organites, le cytosquelette se pose en cadre dynamique de l'activité intracellulaire [Fletcher and Mullins, 2010; Howard et al., 2001; Lee and Dominguez, 2010; R. Ananthakrishna, 2007; Risler, 2009]. Le cytosquelette se compose de trois sortes de polymères.

Les microtubules Ce sont sont les composants du cytosquelette les plus rigides et les plus gros, avec un diamètre de 25 nm. Chaque microtubule est un tube creux formé de 13 filaments, eux-mêmes formés à partir d'une protéine, la tubuline. Une de ses extrémités est toujours attachée au **centrosome** ou Centre d'Organisation des MicroTubules. Les microtubules sont responsables du transport intracellulaire, un rôle primordial notamment lors de la division cellulaire : les chromosomes migrent vers les pôles de la cellule via ces filaments. Ils sont également impliqués dans le signalement chimique et la polarisation: l'orientation des microtubules et leur répartition inhomogène induisent des réactions de natures différentes, renforçant ainsi l'asymétrie fonctionnelle de la cellule [Etienne-Manneville, 2013; Ganguly et al., 2012]. Enfin, il faut noter que les microtubules sont des filaments dynamiques, capables de croître par polymérisation et de se raccourcir. Nous détaillerons ce processus par la suite.

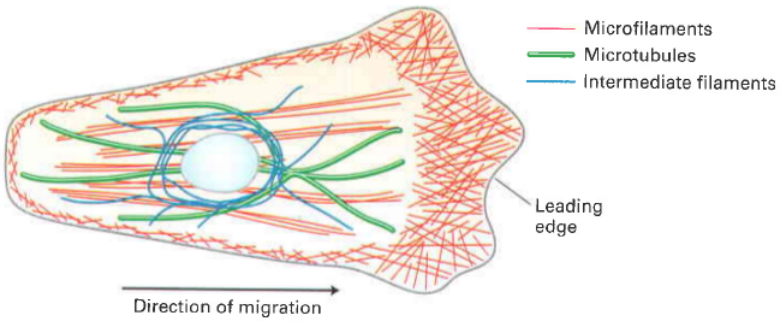

Figure 2 – Une cellule polarisée, des microfilaments d'actine en rouge, des microtubules en vert, et des filaments intermédiaires en bleu foncé. En bleu ciel, le noyau. On remarque le front avant très riche en actine comparé à l'arrière. Dans le corps de la cellule, les fibres de stress sont représentées par des droites rouges. Source : H. Lodish [2008].

Les filaments intermédiaires Ce sont les filaments les plus flexibles des trois, et ils ont un diamètre de l'ordre de 10 nm. Ils ne sont pas polarisés, et se dépolymérisent très peu comparé aux autres filaments. Ce sont donc les éléments les plus statiques du cytosquelette, qui supportent la structure de la cellule.

Les microfilaments d'actine L'ensemble des filaments d'actine est appelé le cytosquelette d'actine. Il est responsable de la forme, de la stabilité et de la motilité de la cellule.

L'actine existe sous deux formes. La plus simple est la forme monomérique ou *globulaire*, appelée **actine G**. Ces monomères peuvent se polymériser pour former de l'actine *filamenteuse*, ou **actine F**, qui est un polymère semi-flexible d'environ 8 nm de diamètre. Le déclenchement de la polymérisation, ou de la dépolymérisation, est lié à la concentration en monomères d'actine dans le milieu. Au delà d'un seuil de concentration critique, le bout du filament d'actine va grandir par polymérisation. A l'inverse, si une extrémité du filament est placée dans un milieu dont la concentration en monomères est en dessous du seuil critique, il dépolymérise.

Il est important de noter que les filaments d'actine sont polarisés : les deux extrémités n'ont pas le même seuil de concentration critique, et ne se polymérisent donc pas au même rythme. L'extrémité *positive*, ou **barbue**, a un seuil critique 6 fois plus petit que l' extrémité *négative* (ou **pointue**) [R. Ananthakrishna, 2007]. La polymérisation est également plus rapide sur le bout barbu.

Il existe un régime intéressant pour ce phénomène. C'est celui où la concentration du milieu en actine G se situe entre les deux seuils. Ainsi, du côté barbu, le filament polymérise, tandis qu'il dépolymérise du côté pointu. Le filament garde ainsi une longueur globalement constante, tout en avançant. C'est le régime dit du "tapis de course", ou encore "**treadmilling**".

Les réactions ayant lieu à l'échelle du cytosquelette sont régies par l'hydrolyse de l'ATP qui génère de l'énergie. Ce procédé permanent est à l'origine du caractère intrinsèquement dynamique du cytosquelette. Comme nous le verrons à nouveau plus tard, c'est une structure qui n'atteint jamais l'état d'équilibre thermodynamique. Cela permet en outre de s'adapter facilement aux signaux et stimuli, tout en gardant une organisation fonctionnelle.

Les filaments d'actine peuvent s'assembler en différentes structures sous l'action de protéines capables d'associer des filaments. Nous nous attachons maintenant à décrire ces

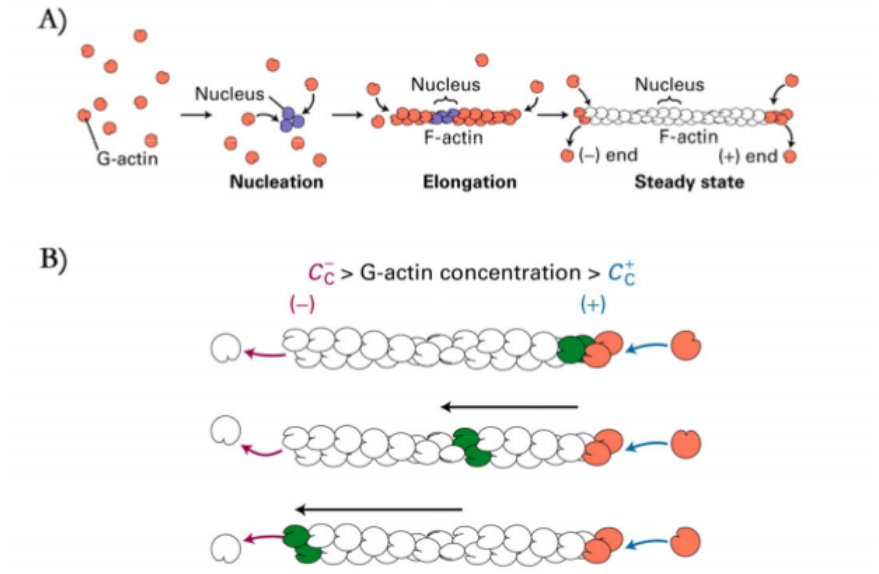

Figure 3 – A) Schéma du mécanisme de polymérisation de l'actine. B) Représentation du phénomène de tapis roulant ou "treadmilling". Le complexe moléculaire actine G-ATP (en rose) est hydrolysé en actine G-ADP (vert) pour se lier au filament, et finira par être relâché dans le milieu par dépolymérisation. Source : H. Lodish [2008].

structures [Lee and Dominguez, 2010].

Les filaments d'actine peuvent être associés en réseau par des molécules telles que Arp2/3, dont la géométrie impose un angle préférentiel entre filaments de 70°. Connecté à la membrane plasmique, ce réseau forme ce qu'on appelle le cortex cellulaire. Disposé en couche large et fine (1 µm) chez une cellule adhérente à une surface, il s'agit du **lamellipode**, une structure impliquée dans la migration.

D'autres molécules comme la fimbrine sont également responsables du regroupement parallèle de filaments en faisceaux longs et fins. Ces faisceaux peuvent ainsi croître dans la même direction : ce sont les **filopodes**, également impliqués dans la migration. En général, les filopodes démarrent en bout de lamellipode (voir figure 8).

Enfin, lorsque des molécules comme la myosine II ou l'α-actinine associent des filaments de manière anti-parallèle, il se forme une fibre d'acto-myosine. Ces molécules sont des sortes de moteurs capables de faire glisser les filaments les uns par rapport aux autres, et la différence de polarité des filaments donne lieu à une dynamique contractile. Lorsque les fibres se regroupent, le faisceau résultant est appelé **fibre de stress**. Les fibres de stress sont présentes sur la partie ventrale de la cellule, et sont liées par les extrémités à des zones adhérentes au substrat (voir la figure 8). Ainsi, si les fibres de stress se contractent, c'est tout la cellule qui va pouvoir se contracter, ce qui est déterminant pour la migration. Ce dispositif permet au cytosquelette d'exercer des forces sur le substrat.

La polymérisation de l'actine contre la membrane dans les structures protrusives (lamellipodes et filopodes) s'accompagne d'un mouvement d'éloignement des filaments de la membrane appelé **flot rétrograde**. Cela est illustré dans la figure 3, où un monomère d'actine (en vert) est transporté vers l'arrière du filament au fur et à mesure que celui-ci polymérise. Ce phénomène peut également être accentué sous l'effet des fibres de stress dans le corps cellulaire. Chez tous types de cellule, le flot rétrograde existe, que ce soit à l'échelle de la cellule ou bien seulement dans les parties protrusives. Nous verrons par la suite qu'il fait partie des processus fondamentaux de la migration.

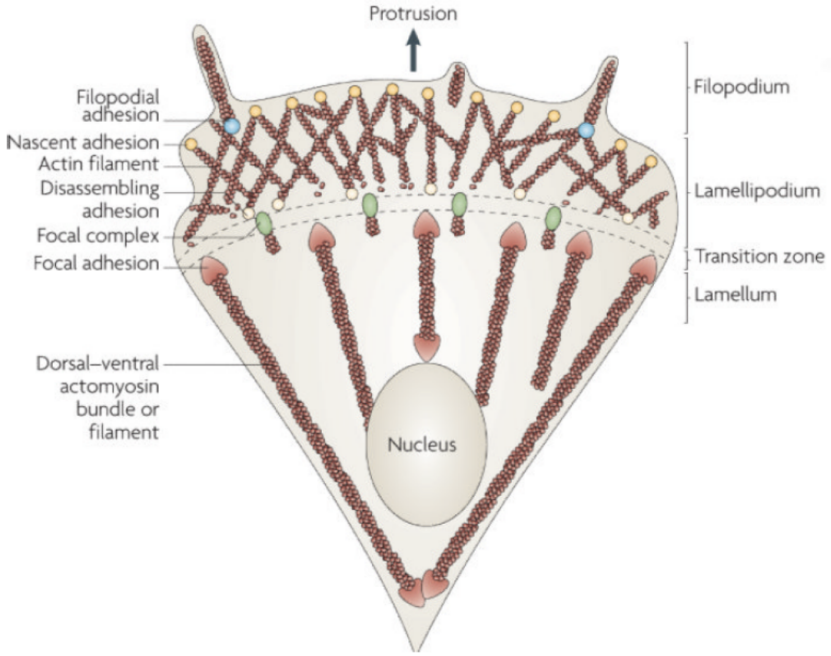

Figure 4 – Schema des structures d'actine chez une cellule rampante. Réimprimé avec la permission de Macmillan Publishers Ltd: Nature Reviews Molecular Cell Biology [Parsons et al., 2010], copyright 2010.

Remarque 2. *Il existe d'autres types de protrusions, comme les podosomes, qui se développent chez les cellules migrant dans la matrice extra-cellulaire en trois dimensions, et les arcs. Les podosomes se créent sur la face ventrale de la cellule, et ont la capacité de dégrader la matrice afin de permettre à la cellule de s'y introduire. Les arcs sont des faisceaux longs et épais de filaments d'actine qui servent de support structural transverse à la cellule. Ils ne sont pas toujours liés à des adhésions.*

Étudions maintenant quelques-unes des molécules régulant la motilité :

Les molécules régulatrices de la migration directionnelle

Les principales molécules impliquées dans la régulation de la motilité sont celles de la famille Rho des GTPases (Guanosine TriPhosphate), et plus précisément les molécules Rho, Rac, et Cdc42 [Hall, 1998]. Nous donnons simplement ici leur rôle dans le mécanisme de migration directionnelle des fibroblastes, avant d'aborder la variété des modes de migration existants.

- La protéine **Cdc42** est la première à être exprimée durant la migration, en réaction aux signaux de polarisation. Elle est responsable du positionnement du noyau et de la polarisation des microtubules, et va surtout activer la machinerie de polymérisation de l'actine à l'avant de la cellule. Enfin, elle induit la formation de filopodes exploratoires, puis l'activation de la molécule Rac.

- **Rac** régule la formation de lamellipodes, et de complexes focaux à la frontière lamellipode/lamellum. Son activité est antagoniste à celle de la molécule Rho (lorsque Rac est activée à l'avant de la cellule, Rho n'y est pas activée, mais joue un rôle dans le reste de la cellule).

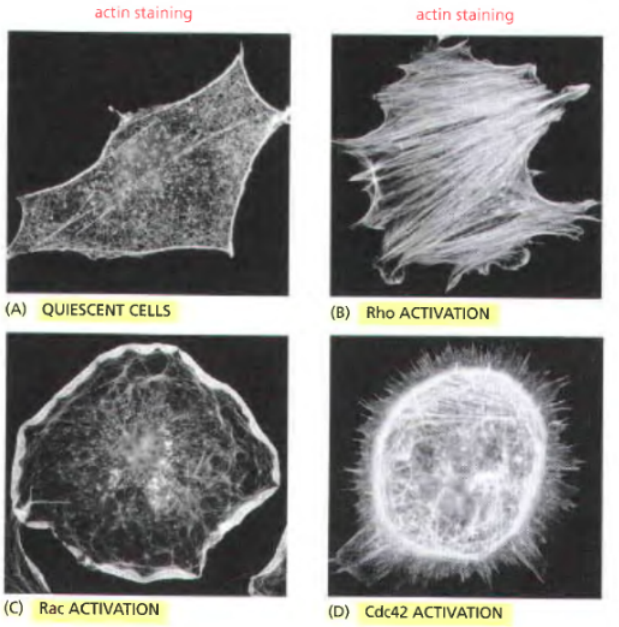

Figure 5 – Les effets des molécules Rho, Rac et Cdc42 sur le cytosquelette d'actine d'un fibroblaste. L'actine est marquée par fluorescence. A) Le fibroblaste dans son état initial. B) Après injection de molécules Rho actives, les fibres de stress sont très nombreuses. C) Après injection de molécules Rac actives, tout le pourtour de la cellule forme un grand lamellipode. D) Après injection de la forme active de Cdc42, on observe la formation de filopodes sur toute la périphérie de la cellule. Source : Hall [1998].

- La molécule **Rho** induit la formation des fibres de stress et des adhésions focales. (Elle est donc la principale responsable des liens entre le substrat et le cytosquelette.) Lors d'une migration directionnelle, cette molécule s'exprime à l'arrière de la cellule (puisque Rac s'exprime à l'avant), et elle est donc responsable de l'absence de protrusions à l'arrière, et de l'avancée de la cellule vers la zone protrusive par contraction des fibres de stress.

Phénotypes de migration

Nous avons vu à quel point les éléments constituant la machinerie cellulaire de migration peuvent être nombreux et de différentes natures. Il est maintenant établi que le cytosquelette possède une souplesse qui rend la cellule capable de s'adapter à différentes contraintes [Liu et al., 2015]. Nous présentons maintenant les deux grands modes de migration qui se distinguent (voir la figure 6).

La **migration amiboïde** est typique des cellules les plus rapides (dictyostelium, leucocytes, cellules dendritiques). Elle est basée sur une forte contractilité et une très faible interaction avec le substrat. Sous l'effet de la contraction, qui génère une forte pression hydrostatique, la membrane cellulaire se détache du cortex et il se créé des excroissances remplies de cytosol (fluide contenu dans la cellule) appelées les blebs. La faible adhésion au substrat implique que les cellules migrant de manière amiboïde ont en général besoin d'être confinées pour se déplacer.

La **migration mésenchymateuse** est à l'opposé basée sur une forte adhésion au substrat, ce qui induit une vitesse de migration plus faible. Les cellules caractéristiques adoptant une migration mésenchymateuse sont les fibroblastes. Lorsque des cellules migrant de manière mésenchymateuse sont placées librement sur un substrat plan et adhérent, elles

migrent par reptation. Nous nous sommes concentrés dans cette thèse sur la migration de la reptation cellulaire, c'est pourquoi nous détaillons son mécanisme à présent.

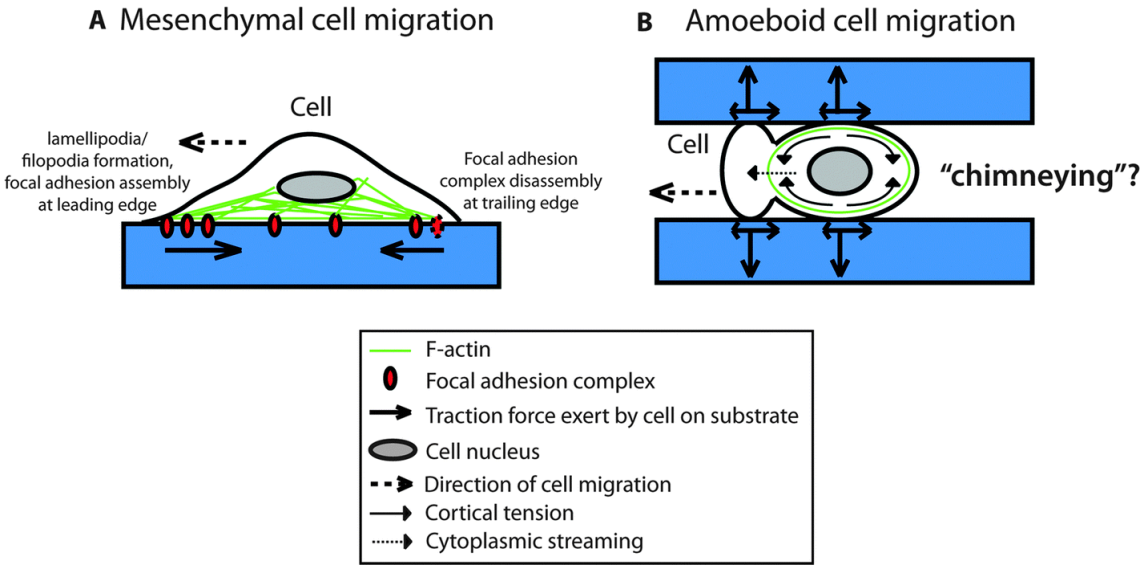

Figure 6 – Schéma des deux principaux modes de migration. Source : Yip et al. [2015].

La reptation Près de la membrane, les filaments d'actine organisés en réseau ou en faisceaux polymérisent et finissent pas déformer la membrane. Des excroissances se forment, appelés *protrusions*. La cellule adhère initialement sur le substrat au moyen de complexes moléculaires d'adhésion. Lors de la croissance de protrusions, de nouvelles adhésions se forment de façon à les lier mécaniquement au substrat. Puis, les fibres de stress présentes dans la cellule, et couplées aux adhésions, se contractent pour générer des forces transmises au substrat. Cela se traduit par l'éventuel détachement des adhésions à l'arrière, et par le déplacement de la cellule. Ce phénomène est représenté dans la figure 7.

L'adhésion au substrat L'adhésion entre une cellule et son substrat (la Matrice Extra-Cellulaire ou MEC) est un régulateur important de la migration cellulaire. Les adhésions sont des complexes locaux qui se forment à partir de protéines transmembranaires comme l'intégrine, auxquelles se lient le cytosquelette d'actine d'une part, et des molécules d'adhésion du substrat d'autre part (fibronectine). Ces structures dynamiques sont plus ou moins stables selon leur maturité. Les *adhésions naissantes* sont des complexes petits et très instables, qui évoluent très rapidement, soit en disparaissant, soit en se développant en adhésions plus importantes, appelées *complexes focaux*. Ceux-ci sont liés à la myosine II à l'intérieur de la cellule. Ces deux premiers complexes d'adhésion, très dynamiques, sont caractéristiques des cellules très motiles, comme les leucocytes ou les cellules tumorales. Ce n'est pas le cas des fibroblastes, qui présentent en général des adhésions plus larges et plus stables. Les *adhésions focales* sont très stables, et sont capables de se lier aux fibres de stress. C'est ce qui permet à la cellule d'exercer des forces sur le substrat en se contractant.

Avec la contraction D'autres facteurs se joignent à la contraction de l'actomyosine afin de rétracter l'arrière de la cellule en y désagrégeant les adhésions. Les microtubules sont en général liés à des adhésions à l'arrière de la cellule. Lorsqu'ils se polarisent vers l'avant, cela donne un signal de relâchement à ces adhésions, qui deviennent plus faciles

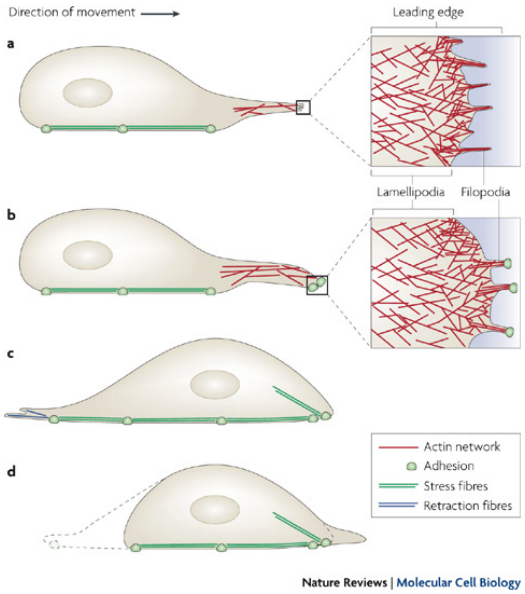

Figure 7 – Schéma représentant une cellule rampante. Les filaments d'actine sont organisés en réseau et faisceaux, et polymérisent contre la membrane cellulaire pour former des protrusions (a). Des complexes d'adhésion se forment entre les filaments d'actine et le substrat (b). La cellule s'avance tandis que l'arrière se rétracte (c et d). Réimprimé avec la permission de Macmillan Publishers Ltd: Nature Reviews Molecular Cell Biology [Mattila and Lappalainen, 2008], copyright 2008.

à désassembler. De plus, l'avancée de la cellule vers l'avant induit parfois l'internalisation des molécules d'adhésion à l'arrière. Elles peuvent également être directement dégradées.

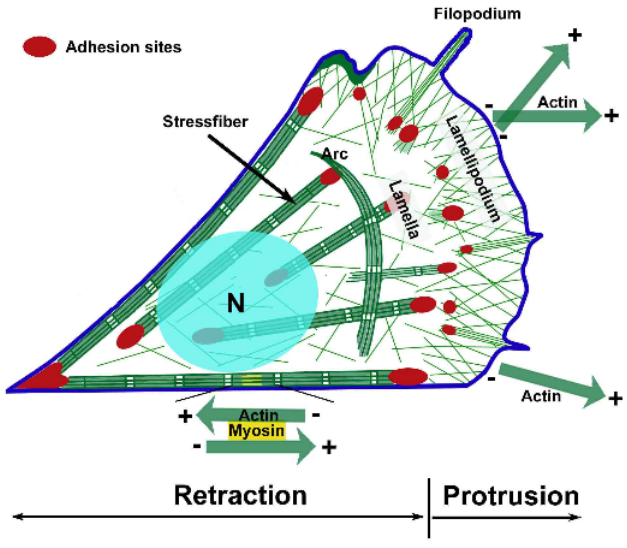

Figure 8 – Schéma récapitulatif des acteurs de la reptation cellulaire. A l'avant de la cellule se trouve le lamellipode constitué de filaments d'actine assemblés en maillage. Des filopodes peuvent se former par assemblage en faisceaux parallèles. Entre le noyau et le lamellipode se trouve le lamellum. Dans le corps de la cellule, des fibres de stress sont liées à des adhésions focales (en rouge), et permettent à l'arrière de la cellule de se rétracter lors du mouvement. Source : Risler [2009].

Nous abordons maintenant la question de la persistance des déplacements cellulaires.

Migration et persistance

Les cellules ont la particularité de répondre aux informations fournies par l'environnement. En particulier, des stimulations chimiques et/ou mécaniques ont la capacité d'agir sur le mouvement de manière attractive ou répulsive.

Stimuli

Différents signaux dans l'environnement sont capables de diriger la migration des cellules. Le phénomène le plus connu est le **chimiotactisme**, opérant à la fois pour les cellules eucaryotes et pour les bactéries [Wang, 2009]. Ce phénomène se produit lorsque des molécules du milieu sont perçues par des récepteurs membranaires. En réaction, ceux-ci sont activés, ce qui déclenche une cascade de signalisation moléculaire et l'amplification interne du signal perçu. Ainsi, le gradient senti à la membrane aura un effet plus prononcé sur le fonctionnement interne.

D'autres facteurs sont capables de diriger la migration, notamment de façon mécanique [Caballero et al., 2015]. Par exemple, dans le cas de la reptation, des substrats présentant un gradient de concentration en molécules d'adhésion a un effet sur le déplacement des cellules : celles-ci migrent vers les zone les plus adhérentes. C'est l'**haptotaxie** [Carter, 1967]. De manière analogue, des gradients de rigidité du substrat induisent une migration directionnelle, ce qui est appelé la **durotaxie** [Filippo Stefanoni, 2011].

Il existe également des cadres expérimentaux dénués de gradient à proprement parler, mais présentant des asymétries géométriques qui induisent également le mouvement. Par exemple, dans Caballero et al. [2014], des cellules sont déposées sur un substrat qui n'est adhésif que sur des zones triangulaires non connectées. Il est apparu que l'activité filopodiale couplée à l'asymétrie géométrique suffisait à diriger la migration dans le sens des extrémités pointues.

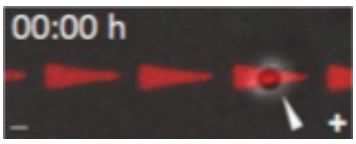

Figure 9 – Dispositif expérimental dans Caballero et al. [2014].

Il existe d'autres procédés par lesquels des asymétries de natures chimique ou mécanique peuvent diriger la migration. Mais la persistance du mouvement dans un cadre dénué de telles stimulations dépend d'abord de la capacité à maintenir un état polarisé.

Polarisation

Nous avons vu comment les éléments intracellulaires forment une structure complexe et organisée régissant l'activité de la cellule. En particulier, celle-ci est capable d'adopter un état morphologique et fonctionnel asymétrique qui perdure dans le temps. C'est la **polarisation**. Elle s'exprime et s'exerce à tous les niveaux dans l'organisation intracellulaire (activité protrusive, position de certains organites, concentration en certaines molécules, etc.). En effet, la répartition spatiale de certaines molécules sont caractéristiques d'un état polarisé, et par leur action régulatrice contribuent à maintenir cet état asymétrique. Par exemple, les molécules régulant la persistance du cytosquelette font partie de ces éléments

[Krause and Gautreau, 2014]. A l'échelle mésoscopique, les microtubules et le centrosome induisent également des réactions différentiées selon leur polarité. De plus, le cytosquelette d'actine présente aussi une activité asymétrique, avec des structures protrusives à l'avant responsables de la migration, et des structures contractiles à l'arrière.

Dans des travaux récents [Maiuri et al., 2015], la corrélation positive existant entre la vitesse de déplacement et la persistance des trajectoires a été mise en évidence. Une corrélation plus précise encore existe entre la vitesse du flot rétrograde d'actine et la persistance des trajectoires : les cellules possédant les flots rétrogrades les plus rapides sont aussi les plus persistantes. Des expériences suggèrent qu'un flot rétrograde fort contribue à l'établissement et au maintien d'une configuration unipolaire avec des protrusions peu nombreuses et orientées de la même façon. Ils proposent également un mécanisme caractéristique d'un état polarisé qui place le flot rétrograde au centre de la machinerie de migration : ce flot est capable de transporter des molécules, de façon à ce que des flots importants engendrent une asymétrie spatiale dans la répartition des molécules. Ces travaux seront détaillés dans le chapitre 5.

Nous nous intéressons maintenant à la modélisation de la migration, en donnant des exemples de modèles existants, avant de présenter l'approche que nous développons dans la thèse.

Modéliser la migration

Modèles existants

Devant l'immense complexité de la migration, l'apport de la modélisation est non négligeable. Intégrer les résultats de différentes expériences dans un cadre unifié, tester des hypothèses d'interaction non linéaire et de redondance, mais également étudier les relations inter-échelles dans la migration sont des approches que peuvent adopter les modélisateurs.

Nous présentons maintenant quelques modèles liés à la migration.

Modèles de phénomènes intracellulaires

Il est considéré que le premier modèle de migration est dû à Abercrombie [1980], pour sa description des étapes de la reptation (polarisation, protrusion, adhésion, contraction). Depuis, de nombreux modèles se sont intéressés à l'une de ces étapes, et ont contribué à une meilleure compréhension des mécanismes sous-jacents. Par exemple, des modèles de polymérisation de l'actine contre la membrane cellulaire ont permis d'étudier les forces relatives à ce phénomène en relation avec la résistance de la membrane [Mogilner and Oster, 1996; Peskin et al., 1993]. Des modèles actuels permettent également d'appréhender la complexité de l'organisation du cytosquelette, comme dans Oelz et al. [2008]. La question du phénomène d'embrayage d'adhésion a été étudiée dans Li et al. [2010]; Sabass and Schwarz [2010]. Lorsque les filaments d'actine polymérisent, la résistance membranaire engendre un mouvement rétrograde, qui peut être ralenti par interaction avec les adhésion. Si les frictions sont grandes, alors ce flot est bas et la protrusion se forme au delà de la membrane. A l'inverse, pour de faibles frictions, il y a peu d'interaction et les filaments "patinent" [Gardel et al., 2008]. Les modèles cités ci-dessus représentent les molécules d'adhésion comme des ressorts élastiques s'accrochant régulièrement au réseau d'actine. Ils ont montré que pour des vitesses faibles, l'adhésion est "pleine" et se déforme peu, tandis que pour des grandes vitesses, les adhésions s'attachent, s'étirent et relâchent les filaments rapidement, de telle sorte que les filaments glissent et poursuivent leur mouvement.

Modèles intégratifs

Intéressons nous maintenant aux modèles ayant servi à intégrer différents phénomènes locaux dans un modèle de migration global. Ces modèles sont la plupart du temps computationnels, et permettent parfois de comparer des quantités numériques avec leurs analogues expérimentales (vitesse du flot rétrograde, densité d'actine, densité d'adhésion, etc.) [Barnhart et al., 2015; Holmes and Edelstein-Keshet, 2012; Prass et al., 2006]. Ils sont particulièrement utiles pour étudier la question de la forme des cellules motiles grâce à des problèmes à frontière libre. De ce point de vue-là, les modèles les plus aboutis concernent le cas du kératinocyte, qui est une cellule très stable du point de vue de la forme, de la vitesse et de la persistance. De plus, ses parties protrusives et contractiles sont également clairement localisées.

La question de la polarisation a suscité le développement de modèles computationnels permettant d'étudier le rôle de la contraction, de l'adhésion et de la polymérisation de l'actine chez les kératinocytes ou les cellules épithéliales. Ces modèles ont fourni des prédictions pertinentes et ont pu être confrontés à des données expérimentales [Barnhart et al., 2015; Lomakin et al., 2015; Recho et al., 2015]. D'autres modèles mécano-chimiques ont été construits pour mener des expériences in silico [Dawes and Edelstein-Keshet, 2007; Marée et al., 2006], mais ne constituent pas un cadre minimal assez simple pour expliquer la persistance des déplacements cellulaires du point de vue théorique.

Chimiotactisme et signaux

De nombreux modèles s'intéressent au phénomène de chimiotactisme pour les cellules eucaryotes comme pour les bactéries [Calvez, 2007; Chalub et al., 2006; Emako et al., 2016; Winkler, 2010]. Les modèles sont en général de type Keller-Segel, et abordent la question de l'existence des solutions ou de leur explosion en temps fini.

Approche développée dans la thèse

Motivations

Dans cette thèse, nous cherchons à développer des modèles de migration intégrant les différentes échelles du processus migratoire. Nous cherchons à étudier la question de la persistance dans le déplacement, et à expliquer les différents types de trajectoires observées expérimentalement. Ainsi, le modèle doit tenir compte des caractères suivants :

→ l'aspect actif. Les cellules sont capables de se déplacer sans stimulus extérieur grâce à leur activité intrinsèque.

→ l'intégration d'interactions multi-échelles produisant un circuit de régulation de la migration. En particulier, le développement de la polarisation cellulaire se produit à tous les niveaux, et doit donc être décrite par le modèle.

→ la stochasticité, jouant un rôle important à l'intérieur de la cellule, en particulier dans les interactions multi-échelles.

De plus, nous cherchons à construire des modèles assez souples pour s'adapter à différentes situations de migration (environnement, drogues, etc.), et pour décrire des phénomènes assez génériques afin de gérer la redondance des processus cellulaires.

Il s'agit donc de former un cadre mathématique rigoureux pour une dynamique générale afin de retrouver qualitativement des observations expérimentales. La présence de différents niveaux d'interaction permet d'aborder la question des perturbations de la dynamique

(perturbations internes, signaux chimiques, mécaniques, interaction cellulaire) et de leur effet macroscopique.

Choix de modélisation

Nous cherchons donc à construire des modèles répondant au caractère actif, multi-échelle et stochastique de la migration cellulaire, tout en restant dans une démarche de description assez générique pour s'adapter à différentes situations.

Afin de combiner des approches à la fois multi-échelle et générique, il est naturel de développer un modèle minimal, s'appuyant sur des principes fondamentaux (lois physiques, interaction simple).

Détaillons maintenant les caractéristiques des modèles développés dans la thèse.

Modèles développés

Modèle particulaire Un premier modèle de trajectoires se base sur la nature active de la dynamique. Il s'agit d'un modèle de particule active de type mouvement Brownien persistant, où les paramètres sont liés à l'activité de protrusion, et comportent un feedback lié au déplacement. Le modèle porte donc sur l'interaction stochastique entre les échelles mésoscopique et macroscopique. La simplicité de la description de la cellule permet d'envisager la description de la réponse à un signal extérieur, chimique ou mécanique, si tant est que ce signal agit sur l'activité protrusive.

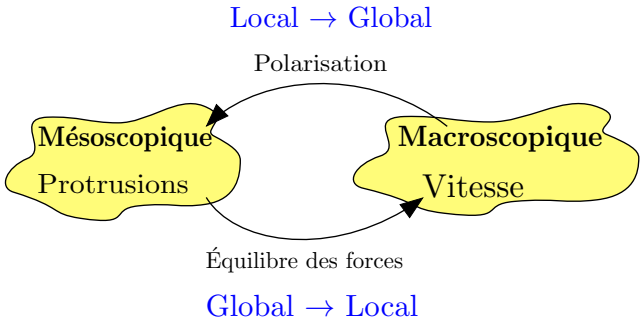

Figure 10 – Les échelles de description du modèle particulaire.

Modèle fluide discoïdal Dans une deuxième approche, nous cherchons à décrire plus précisément la dynamique intracellulaire responsable de la migration. Pour cela, nous considérons un domaine cellulaire non déformable qui est un disque.

L'activité mésoscopique correspond ici à la dynamique du cytosquelette, tandis que l'échelle microscopique correspond aux activités moléculaires, avec une espèce moléculaire régulant l'activité du cytosquelette. Le système actif (le cytosquelette) est décrit par un fluide qui est porté par un contenant passif macroscopique (le domaine cellulaire). Les interaction modélisées sont les suivantes:

→ la molécule régule la dynamique du cytosquelette,

→ le cytosquelette influe sur le déplacement global par sa friction avec le substrat (équilibre des forces),

→ le déplacement joue à son tour sur la dynamique du fluide par friction passive (équilibre des forces),

→ le fluide transporte le marqueur.

La base du modèle est maintenant son caractère multi-échelle, avec des règles de rétroaction clairement définies, et basées sur des principes simples (approximation fluide, équilibre des forces, transport). Le caractère actif, lui, vient d'une perturbation stochastique ajoutée au système.

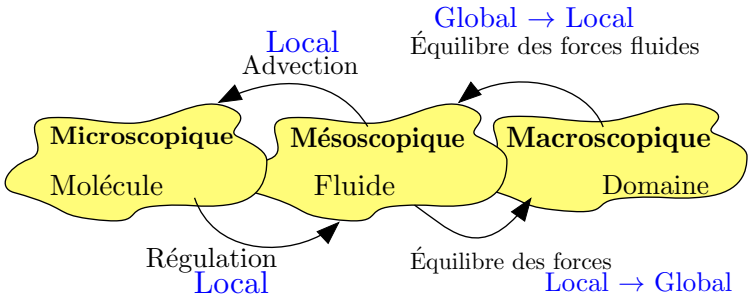

Modèle fluide déformable Une dernière approche de modélisation consiste à considérer le domaine cellulaire non pas comme une forme rigide mais comme un domaine déformable, sans description d'une partie passive. Le déplacement cellulaire étant maintenant local, les interactions précédemment décrites ne peuvent plus nécessairement être considérées.

Les nouvelles lois d'interaction sont les suivantes:

→ la molécule et le fluide engendrent un déplacement du bord du domaine.

→ En réaction, des effets de géométrie et de tension de surface en lien avec la courbure du domaine rétroagissent naturellement sur la dynamique du fluide et sur celle du marqueur.

Le couplage multi-échelle est donc ici bien plus complexe que dans les cas précédents. Le travail relatif à ce domaine est en cours, et nous ne détaillerons pas son cas dans cette thèse.

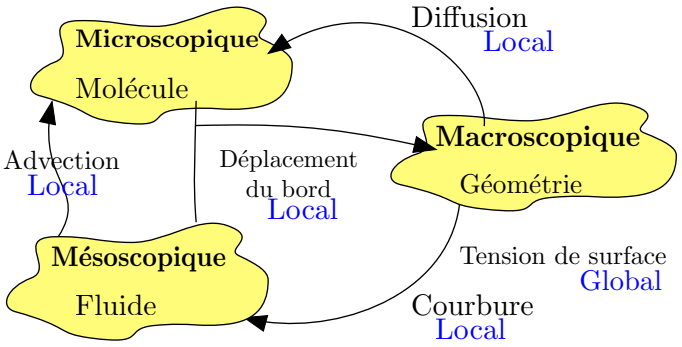

Dans la partie suivante, nous détaillons les travaux qui ont été réalisés sur des modèles de type particulaires.

Modèles particulaires

Dynamique d'adhésion d'un leucocyte à la paroi des artères

Ce travail a été effectué en collaboration avec Nicolas Meunier. Il porte sur la modélisation stochastique de la dynamique d'adhésion d'un leucocyte transporté par le sang lorsqu'il entre en contact avec la paroi artérielle.

Contexte biologique

Afin d'assurer leurs fonctions immunitaires, les leucocytes ou globules blancs sont amenés à se déplacer dans l'organisme notamment en étant transportés par le flux sanguin [Granger and Senchenkova, 2010]. La façon dont ils finissent par s'arrêter sur la paroi endothéliale avant de traverser la paroi se déroule en plusieurs étapes. La cellule est d'abord en contact éphémère avec la paroi, de façon à former des liaisons d'adhésion faibles. Au-delà d'un certain seuil, les forces d'adhésion sont telles que la cellule ralentit et est "capturée" : elle n'est plus sous l'influence principale du flux sanguin. Puis, une dynamique intermédiaire se met en place, durant laquelle le leucocyte forme des liaisons en avant, tandis que celles à l'arrière se dissolvent par l'action des forces de courant. C'est la phase de "roulement". L'interaction plus stable avec la paroi entraîne le recrutement de liaisons plus fortes composées d'intégrines. Elles sont responsables de l'adhésion totale qui stoppe la cellule et lui permet de s'extraire de l'artère (voir figure 11).

Le modèle

Des modèles de dynamique des liaisons en interaction avec la dynamique du leucocyte ont déjà été étudiés [Grec et al., 2012; Milišić and Oelz, 2011], et portent sur une description déterministe tenant compte de la nature mécanique des liaisons (élasticité) ou de leurs âges (effet mémoire).

Dans notre travail, nous proposons une approche minimale où, de même, la géométrie n'est pas décrite. De plus, les liaisons sont simplement décrites par leur nombre et leur dynamique au cours du temps.

Plus précisément, nous considérons un milieu homogène correspondant à la paroi interne d'un vaisseau sanguin. Le principe d'équilibre des forces s'exerçant sur un système microscopique nous donne une expression pour la vitesse de la cellule :

$$V_t = u - \gamma N_t \,,$$

où V_t est la vitesse de la particule au temps t, N_t le nombre de liaisons, et u la vitesse du sang supposée constante. Le paramètre γ correspond à un coefficient d'adhésion entre chaque lien et la paroi.

La dynamique de formation de liaison est décrite de la façon suivante : la rencontre entre un récepteur d'adhésion à la surface de la cellule et une protéine d'adhésion sur la paroi est décrite comme un événement de *création* (ou immigration). La croissance d'une zone d'adhésion après contact avec la paroi se traduit par un processus d'auto-renforcement

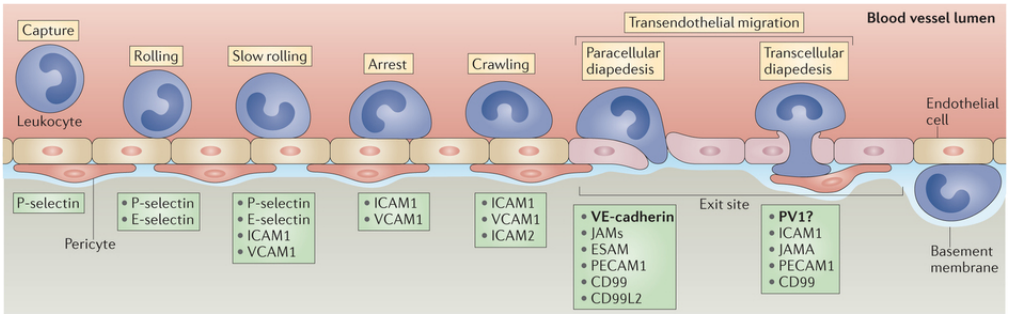

Figure 11 – Schéma de la cascade d'exravasation d'un leucocyte hors d'une artère. Réimprimé avec la permission de Macmillan Publishers Ltd: Nature Reviews Immunology [Vestweber, 2015], copyright (2007)

porté par la notion de *reproduction*. Enfin, le détachement des liaisons correspond à une *disparition* ou mort. Une telle dynamique stochastique est modélisée par un processus stochastique de type naissances, morts et immigration.

La dynamique du leucocyte joue ici directement un rôle dans la formation et le maintien de liaisons avec la paroi. Un couplage est donc proposé entre la vitesse cellulaire et le taux de disparition des liaisons : plus la cellule se déplace vite, plus les liaisons existantes se détachent rapidement. Ce choix provient de l'observation de l'effet mécanique du déplacement sur le détachement des liaisons. A l'opposé, le renforcement plus faible des adhésions pour un déplacement rapide est un phénomène passif.

Le processus ainsi défini est un processus markovien de sauts à valeurs dans $\mathbb{N}$, qui vérifie la propriété de martingale suivante :

$$M_t = N_t - N_0 - \int_0^t (\lambda(N_s) - \mu(N_s))\,\mathrm{d}s \tag{1}$$

est une martingale càdlàg de carré intégrable, issue de 0, et donc la variation quadratique s'exprime par

$$\langle M \rangle_t = \int_0^t (\lambda(N_s) + \mu(N_s))\ \mathrm{d}s\,. \tag{2}$$

Dans ces expressions, $\lambda(N_s) = c + rN_s$ et $\mu(N_s) = de^{\alpha(V_s)}N_s$, avec c le taux de création, r le taux de reproduction, et $de^{\alpha(V_s)}$ l'expression du taux de disparition en fonction de la vitesse, pour $\alpha > 0$.

Résultats obtenus

Des simulations numériques du modèle montrent que des cas d'arrêt de la cellule peuvent se produire, de même que des cas où la cellule se libère de l'interaction avec la paroi et rejoint le flux sanguin. Ces situations dépendent du contexte extérieur (u) ainsi que de la dynamique interne d'adhésion.

Limite continue A l'échelle du déplacement de la cellule, le temps de vie d'une liaison est infinitésimal, et l'ensemble des liaisons est organisé en adhésions de tailles variables, composées d'un grand nombre d'éléments. Ainsi, une description continue des liaisons est mieux adaptée aux échelles du déplacement. C'est pourquoi nous renormalisons le processus de population ainsi que sa dynamique, de façon à obtenir un modèle limite continu de densité d'adhésion, mieux adapté aux échelles. En posant pour $K \geq 1$,

$$X_t^K = \frac{1}{K} N_t^K \in \frac{1}{K}\mathbb{N}\,, \tag{3}$$

où N_t^K est le processus de population correspondant aux taux renormalisés, nous supposons que le nombre de liens croît vers l'infini tandis que les forces correspondantes tendent vers 0.

En accélérant seulement le taux de création dans la dynamique, proportionnellement à K, nous obtenons à la limite un modèle déterministe:

$$n(t) = n_0 + \int_0^t \Big(c(n(s)) + (r(n(s)) - d(n(s)))\, n(s)\Big)\,\mathrm{d}s\,.$$

L'interprétation donnée à cette limite consiste à faire croitre les évènements de rencontres entre des protéines cellulaires et celles de la paroi, tout en conservant la même dynamique

de renforcement des adhésions existantes. Cette limite semble plus réaliste pour décrire des situations extrêmes ou les fluctuations stochastiques sont négligeables, comme le cas où u est grand.

En adoptant une renormalisation de toute la dynamique relativement à K, nous pouvons obtenir à la limite une équation différentielle stochastique. Plus précisément, pour $c^K = Kc$, $r^K = r + Ka$ et $d^K(\nu) = d(\nu) + Ka$, avec $a > 0$, nous obtenons à la limite l'équation différentielle stochastique suivante :

$$\mathrm{d}N_t = b(N_t)\,\mathrm{d}t + \sigma(N_t)\,\mathrm{d}B_t\,, \tag{4}$$

avec B_t un mouvement Brownien, $b(N_t) = c + (r - de^{\alpha(V_s)})N_t$ et $\sigma(N_t) = \sqrt{2aN_t}$.

Modèle CIR Pour des coefficients constants, nous nous ramenons au processus de Cox–Ingersoll–Ross, introduit en 1985 pour décrire l'évolution de taux d'intérêt en finance [Göing-Jaeschke and Yor, 1999a; Shreve, 2004].

Des résultats concernant le temps d'atteinte d'un état existent déjà pour ce processus. En effet, le modèle CIR peut s'exprimer par un carré de processus d'Ornstein-Uhlenbeck radial via un changement de variables. Celui-ci est lui-même lié à un carré de processus de Bessel par un théorème de type Girsanov. La transformée de Laplace du temps d'atteinte d'un état s'obtient en exploitant des propriétés de réversibilité en temps pour le processus de Bessel, et ce résultat se propage aux autres processus par ces relations [Göing-Jaeschke and Yor, 1999b].

Nous nous intéressons à la possibilité d'arrêt de la cellule sur la paroi du vaisseau. En particulier, nous cherchons à déterminer si ce modèle simple est suffisamment riche pour décrire à la fois la situation d'arrêt et la situation où la cellule poursuit son déplacement dans le sang. Au niveau du modèle, nous nous intéressons au temps d'atteinte d'une taille de population donnée, correspondant à l'atteinte d'une vitesse nulle. Ici, nous arrivons à simuler la densité de probabilité du temps d'atteinte d'un état donné à partir de sa transformée de Laplace, en utilisant une décomposition spectrale démontrée dans Linetsky [2004]. Cependant, le lien avec la dynamique cellulaire n'existe plus, et ce résultat ne peut s'interpréter dans notre situation.

Approche Fokker-Planck Nous étudions enfin le modèle stochastique continu complet au moyen de la dérivation de l'équation de Fokker-Panck à partir de l'équation différentielle stochastique. La dynamique étant homogène en temps, il est possible d'exploiter le lien avec l'équation de Fokker-Planck rétrograde afin de dériver une expression du temps moyen d'atteinte d'une densité d'adhésion donnée.

Les simulations de ce résultat montrent une bifurcation basée sur les valeurs de la vitesse du flux sanguin : pour un flux assez faible, la cellule s'arrête en temps moyen fini, tandis que pour des valeurs trop importantes, la cellule ne s'arrête pas.

Ce modèle permet donc de relier la dynamique sanguine et la dynamique d'adhésion au "destin" de la cellule, dans le sang ou hors des artères.

Modèle de reptation 2D

Motivations

Dans le chapitre 2, nous nous intéressons à la construction d'un modèle de migration unicellulaire sur une surface, où la cellule est ponctuelle, et sa dynamique est décrite en fonction de son activité observable. Ce travail a été réalisé en collaboration avec Nicolas Meunier et Raphaël Voituriez.

Les modèles de trajectoires individuelles de particules les plus simples sont les marches aléatoires ainsi que leur analogue continu en espace. D'abord utilisés pour décrire le mouvement de particules inertes dans un champ de vitesse extérieur, ils ont bien vite été étendus au cas de particules auto-propulsées *actives* (voir Codling et al. [2008]; Romanczuk et al. [2012]). En particulier, le mouvement persistant peut être associé à une marche aléatoire persistante, et la migration directionnelle (par exemple par chimiotactisme) par une marche aléatoire orientée. Dans le cas continu, pour les équations de Langevin, la dynamique hors équilibre est modélisée par un terme de friction négatif pour des vitesses faibles. Ces modèles fournissent des informations telles que les distributions stationnaires des vitesses, le coefficient de diffusion effectif, ou des estimations sur le premier temps de passage [Campos et al., 2010; Lindnera and Nicola, 2008]. La confrontation du modèle à des trajectoires expérimentales permet ainsi de quantifier l'efficacité de la migration.

Globalement, ces modèles fournissent donc un cadre pour mieux comprendre la migration individuelle et même collective [Bechinger et al., 2016; Speck, 2015]. L'interaction avec l'environnement peut également être inclus, tel que le confinement, et les signaux chimiques. Des résultats explicites sont aisément dérivés grâce au caractère minimal de ces modèles. Pourtant, la description phénoménologique de l'activité interne empêche l'obtention d'informations au delà de leur caractère descriptif, puisqu'ils n'expliquent pas les processus internes liés à la dynamique observable.

A l'inverse, les modèles basés sur des processus intracellulaires n'ont pas la simplicité nécessaire pour dériver les quantités caractéristiques de la persistance des trajectoires.

Dans ce travail, nous tentons d'adopter une approche intermédiaire, en formulant un modèle particulaire stochastique, dont la dynamique est décrite à l'échelle mésoscopique. Pour cela, nous nous basons sur un travail de Caballero et al. [2014] qui montre que les fluctuations stochastiques observées dans la dynamique de protrusions filopodiales jouent un rôle non négligeable dans la migration directionnelle. Nous nous attachons donc à décrire l'évolution stochastique de cette dynamique en lien avec la migration cellulaire.

Le modèle

Comme pour le travail précédent, nous nous basons sur l'équilibre des forces dans un contexte microscopique : la cellule est soumise à des forces passives de friction, ainsi qu'à des forces actives liées à l'adhésion des filopodes sur le substrat.

$$\gamma \vec{V_t} = \sum_{i=1}^{N_t} \vec{F_i}(t)\,,$$

où $(\vec{F_i})_i$ correspond aux forces liées à l'adhésion des filopodes sur le substrat, et γ est la force de friction s'exerçant sur la cellule en mouvement.

Sous des hypothèses simplificatrices, les forces filopodiales sont considérées unitaires, et donc caractérisées uniquement par leur orientation θ_i. Nous obtenons alors

$$\gamma \vec{V_t} = \sum_{i=1}^{N_t} \begin{pmatrix} \cos(\theta_i) \\ \sin(\theta_i) \end{pmatrix}\,.$$

Cette hypothèse revient à considérer les forces de protrusion par unités. L'apparition de nouvelles protrusions sur une même orientation correspond alors à l'intensification de la force associée.

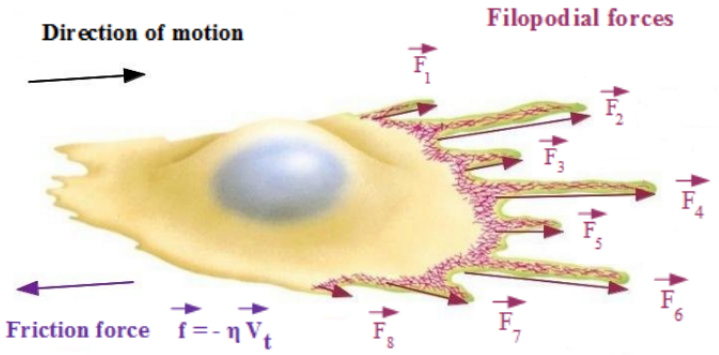

Figure 12 – Schema d'une cellule avec les forces considérées (modifiée depuis [Lodish and Zipursky, 2001]).

Formalisme mathématique

Afin de décrire l'évolution de la population de filopodes simplement, nous utilisons le formalisme des processus de populations structurées par un trait [Bansaye and Méléard, 2015; Champagnat et al., 2008; Fournier and Méléard, 2004], où le trait correspond à l'orientation de chaque filopode. Les filopodes sont donc décrits par une mesure ponctuelle finie, où chaque masse de Dirac porte l'information sur l'orientation d'un filopode. Nous avons

$$\nu_t = \sum_{i=1}^{N_t} \delta_{\theta_i} ,$$

ce qui nous permet d'écrire

$$\gamma \vec{V_t} = \begin{pmatrix} < \nu_t, \cos > \\ < \nu_t, \sin > \end{pmatrix} .$$

L'évolution de la mesure ponctuelle se fait selon une dynamique de naissances et morts avec immigration. En effet, nous considérons que des filopodes peuvent se former de manière isotrope, de la même manière qu'un phénomène d'immigration. Puis, l'activité protrusive étant auto-entretenue, chaque filopode existant est capable d'engendrer la formation d'un nouveau filopode (ce qui est similaire à de la reproduction). L'orientation du nouvel individu est alors d'orientation identique ou proche à celle du filopode originel). Ce phénomène est dû à la régulation microscopique des protrusions.

La prise en compte de la polarisation cellulaire se fait à partir de la considération suivante : dans Maiuri et al. [2015], il est établi que le flot rétrograde d'actine renforce la polarisation notamment en favorisant une activité protrusive orientée. De plus, la vitesse du flot rétrograde peut être considérée comme proportionnelle à la vitesse cellulaire, avec un coefficient de couplage α. Ainsi, nous choisissons un taux de reproduction dépendant de façon non linéaire de V_t, de façon à ce que pour des valeurs de vitesses importantes, les filopodes dans le sens du déplacement soient les plus promptes à induire de nouvelles protrusions. L'orientation des filopodes engendrés par la reproduction est déterminée de façon stochastique, et centrée sur l'orientation initiale. Cependant, nous ne tenons pas compte d'une quelconque influence du déplacement dans ce phénomène, qui est considéré comme local.

Finalement, nous obtenons un modèle discontinu de trajectoires de type marche aléatoire persistante basée sur la dynamique mésoscopique. Des simulations numériques de trajec-

toires nous permettent d'observer que les persistances des déplacements sont largement dépendantes de la valeur du paramètre de couplage α.

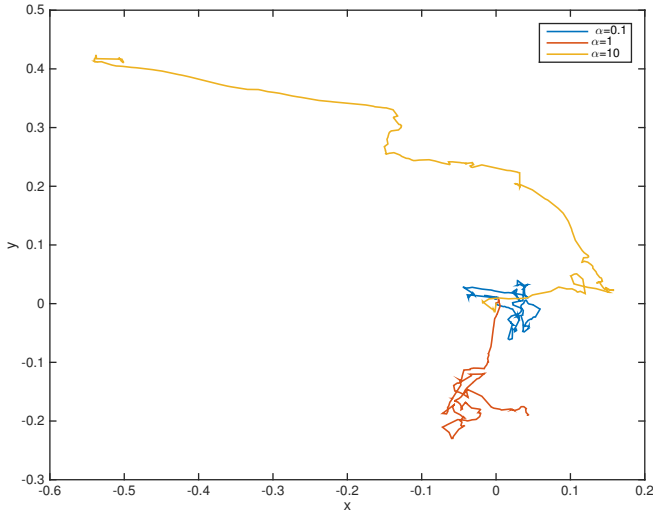

Figure 13 – Trajectoires numériques obtenues pour un coefficient de couplage α variable.

Changement d'échelle et limite continue

Comme pour le travail sur la dynamique d'adhésion du leucocyte, bien que nous ayons défini la dynamique cellulaire sur la base de l'activité protrusive, celle-ci se produit à des échelles de temps et d'espace inférieures à celles de la migration cellulaire. En particulier, si les filopodes sont des protrusions discrètes et dénombrables, ce n'est pas le cas du lamellipode, qui intervient également dans la migration.

Nous procédons donc à une renormalisation de la population, ainsi que de sa dynamique, afin d'obtenir une description continue.

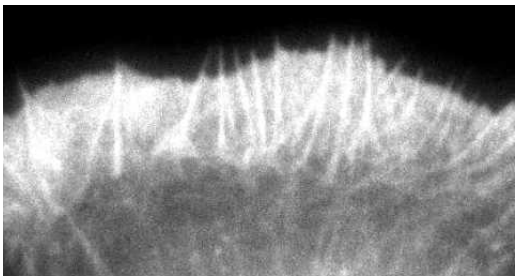

Figure 14 – Une cellule XTC marquée pour les filaments d'actine. On observe les filopodes ainsi que le lamellipode. Réimprimé depuis Ryan et al. [2012], avec la permission d'Elsevier.

Posons

$$X_t^K = \frac{1}{K}\nu_t^K\,, \tag{5}$$

avec K le paramètre d'échelle, et $(\nu_t^K)_t$ le processus correspondant aux taux renormalisés.

Nous étudions différentes renormalisations de la dynamique, menant à des limites continues déterministes ou stochastiques. Du point de vue mathématique, nous abordons donc des preuves de convergence de processus stochastiques dans l'espace des mesures finies sur un espace borné. La démarche est adaptée de celle développée sans immigration dans Bansaye and Méléard [2015]; Champagnat et al. [2008]; Fournier and Méléard [2004]. La

justification de la limite repose sur une formulation du problème en problème de martingale, puis en utilisant des arguments de type compacité-unicité.

Parmi les limites obtenues, nous obtenons le problème de martingale suivant : pour tout $f \in \mathcal{C}^2([0, 2\pi))$ périodique,

$$\begin{aligned} \widetilde{M^f}_t =& < X_t, f > - < X_0, f > - \frac{c}{2\pi} \int_0^t \int_\chi f(\theta) \, \mathrm{d}\theta \, \mathrm{d}s \\ & - \int_0^t \int_\chi (r(\theta, X_s) - d(\theta, X_s)) f(\theta) X_s(\, \mathrm{d}\theta) \, \mathrm{d}s - \frac{1}{2} \mu \sigma^2 a \int_0^t \int_\chi f''(\theta) X_s(\, \mathrm{d}\theta) \, \mathrm{d}s \end{aligned} \tag{6}$$

est une martingale continue, de carré intégrable et de variation quadratique

$$\left\langle \widetilde{M^f} \right\rangle_t = 2a \int_0^t \int_\chi f(\theta)^2 X_s(\, \mathrm{d}\theta) \, \mathrm{d}s \, . \tag{7}$$

Appliquant cela aux expressions de la vitesse de la cellule, nous obtenons

$$V_t = V_0 + \begin{pmatrix} M_1 \\ M_2 \end{pmatrix} + \int_0^t \left\langle X_s, r(., V_s) \begin{pmatrix} \cos \\ \sin \end{pmatrix} \right\rangle - \left(d + \frac{1}{2} \mu a \sigma^2 \right) V_s \, \mathrm{d}s \, ,$$

où $(X_t)_t$ est le processus de protrusion continu.

Le caractère non linéaire et infini-dimensionnel de ce problème nous empêche d'aller plus loin dans ce cas.

Le cas 1D

Dans la situation unidimensionnelle, la population de protrusions se partage en deux sous-populations à droite et à gauche. Plus précisément, nous écrivons

$$\gamma V_t = N_t^+ - N_t^- \, ,$$

avec $(N_t^+)_t$ le processus de population à droite, et $(N_t^-)_t$ le processus à gauche. La prise en compte de la polarisation dans le terme de reproduction est maintenant porté par la fonction antisymétrique

$$r_{1,2}(Y_t) = \frac{\beta}{2} \left(1 \pm \tanh \left(\alpha V_t \right) \right) \, .$$

Dans ce cas, il nous est possible d'écrire l'équation de Fokker-Planck vérifiée par (N_t^+, N_t^-). L'état stationnaire correspondant à un flux de probabilité nul partout s'exprime en fonction d'un potentiel, sous lequel la particule évolue. Il est également possible de dériver un potentiel similaire sur le processus (N_t, V_t), où N_t est la densité totale de protrusions. Des simulations numériques de ce potentiel montrent une transition de phase sur la vitesse liée au paramètre de couplage α (les zones sombres correspondant aux puits de potentiel).

Finalement, nous avons construit un modèle de trajectoires cellulaires en 2D et 1D capable de décrire la polarisation à partir d'une description mésoscopique. Des simulations numériques et l'expression d'un potentiel dans le cas 1D nous permettent de mettre en évidence une transition de phase en fonction du paramètre de couplage α de la polarisation avec le mouvement.

Ce modèle porte une richesse supplémentaire par rapport à des modèles de type particules actives, puisque la dynamique est décrite à l'échelle mésoscopique. Néanmoins, elle ne permet pas la dérivation de quantités macroscopiques sur la persistance des trajectoires. Cependant, ce modèle fournit des perspectives nouvelles dans l'analyse de trajectoires expérimentales, ainsi que dans l'étude de la migration sous l'action d'un signal extérieur.

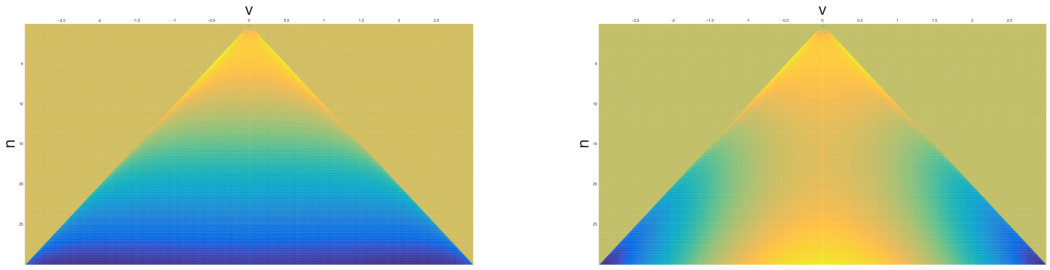

(a) $\alpha = 0.01$ (b) $\alpha = 0.1$

Figure 15 – Potentiel sur (N, V).

Modèle fluide

Dans la seconde partie de la thèse, nous nous intéressons à la construction et à l'étude de modèles capables d'intégrer une dynamique microscopique. Ce travail a été effectué en collaboration avec Nicolas Meunier et Raphaël Voituriez.

Nous développons une approche minimale pour tenir compte de trois échelles en interaction : moléculaire, mésoscopique, et macroscopique. Nous nous appuyons pour cela sur des principes physiques généraux.

D'une part, nous considérons la cellule comme rigide et discoïdale, de façon à négliger les effets hautement non linéaires liés à la forme dans la dynamique. De plus, nous tenons compte des composantes "passives" de la cellule pour la migration (noyau, organites, etc.).

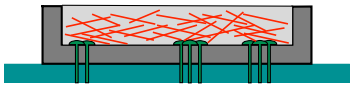

Figure 16 – Représentation schématique de la cellule. La partie en gris foncé correspond à la partie passive, tandis que les traits rouge correspondent aux filaments d'actine du cytosquelette. Les molécules d'adhésions sont représentées en vert.

D'autre part, nous nous plaçons sur des échelles de temps et d'espace assez grandes pour adopter une description du cytosquelette continue, au moyen de la théorie des gels actifs [Jülicher et al., 2007].

Enfin, l'interaction avec l'échelle moléculaire est définie suivant des observations et analyses effectuées dans Maiuri et al. [2015] : nous supposons qu'une molécule inhibitrice de la polymérisation possède une grande affinité avec les filaments d'actine, et peut ainsi être transportée par le flot rétrograde. Par conséquent, les régimes où le flot rétrograde est fort peut engendrer et maintenir une asymétrie dans la concentration en marqueurs. Ces molécules étant régulatrices de la dynamique du cytosquelette, cette interaction forme une boucle de régulation.

Formulation du modèle

La formulation du modèle repose sur la description physique du fluide, ainsi que sur le principe d'équilibre des forces vérifié sur le système entier. Notons $\Omega(\,\cdot\,)$ le domaine cellulaire en déplacement dans $\mathbb{R}^2$.

Problème fluide

Notons $\tilde{U}$ la vitesse du fluide dans le référentiel de la cellule, $\tilde{P}$ sa pression, et V la vitesse globale de la cellule. De plus, notons ρ la densité du fluide. D'une part, l'équilibre des forces exercées sur le fluide s'écrit

$$-\text{div } \left(\eta \left(\nabla(\tilde{U}(t,\mathbf{X}) + V(t)) + {}^t\nabla(\tilde{U}(t,\mathbf{X}) + V(t))\right) - \tilde{P}(t,\mathbf{X})\ \text{Id}\right) = -\xi(\tilde{U}(t,\mathbf{X}) + V(t))\,, \tag{8}$$

avec η la viscosité du fluide et ξ le coefficient de friction. Sous l'hypothèse de grande friction, nous négligeons la viscosité et obtenons une loi de Darcy sur la pression :

$$\nabla\tilde{P}(t,\mathbf{X}) = -\xi(\tilde{U}(t,\mathbf{X}) + V(t)) \qquad \text{dans } \Omega(t)\,.$$

D'autre part, nous supposons de manière caricaturale que la polymérisation de l'actine se produit au bord du domaine de manière discontinue: pour $\varepsilon > 0$, notons ρ_ε la densité de l'actine. Ainsi,

$$\begin{aligned} \frac{\partial}{\partial t}\rho_\varepsilon(t,\mathbf{X}) + \text{div } (\rho_\varepsilon(t,\mathbf{x})(\tilde{U}(t,\mathbf{X}) + V(t))) = -K_d\rho_\varepsilon(t,\mathbf{X}) \quad &\text{dans } \Omega(t)\,. \\ \rho_\varepsilon(t,\mathbf{X}) = \rho_0 + \varepsilon k_p \quad &\text{sur } \partial\Omega(t)\,, \end{aligned} \tag{9}$$

où ρ_0 est une constante, et ε représente la discontinuité au bord. La constante k_d représente la dépolymérisation se produisant dans tout le domaine.

En définissant une loi de pression de la forme

$$\tilde{P}_\varepsilon = \frac{1}{\varepsilon}(\rho_\varepsilon - \rho_0)\,,$$

il est possible de dériver formellement le problème limite pour une densité d'actine constante. Nous avons

$$\begin{cases} -\Delta\tilde{P}(t,\mathbf{X}) = -\xi K_d & \text{dans } \Omega(t)\,, \\ \tilde{P}(t,\mathbf{X}) = k_p & \text{sur } \partial\Omega(t)\,, \end{cases}$$

Équilibre des forces global

Le système que nous étudions vérifie la propriété d'équilibre des forces instantané, dû au caractère non-inertiel d'un système microscopique. Ainsi, en considérant à la fois le système fluide et la charge passive, nous obtenons

$$\xi_1 V(t) + \xi \int_{\Omega(t)} \tilde{U}(t,\mathbf{X}) + V(t)\,\mathrm{d}\mathbf{X} = 0\,,$$

avec ξ_1 le coefficient de friction global lié à la charge passive.

Nous obtenons alors les équation finales pour la vitesse du fluide et celle du domaine :

$$\tilde{U}(t,\mathbf{X}) = -\frac{1}{\xi}\nabla\tilde{P}(t,\mathbf{X}) - \frac{1}{\xi_1}\int_{\Omega(t)} \nabla\tilde{P}(t,\mathbf{X})\,\mathrm{d}\mathbf{X}\,,$$

avec

$$V(t) = \frac{1}{\xi_1}\int_{\Omega(t)} \nabla\tilde{P}(t,\mathbf{X})\,\mathrm{d}\mathbf{X}\,.$$

Le problème que nous étudions a donc la particularité d'évoluer sous l'influence d'une quantité globale, correspondant à la vitesse du domaine.

Formulation dans un domaine fixe

Nous réécrivons maintenant le problème dans un domaine Ω_0 fixe. Notons (P, U) les analogues à $(\tilde{P}, \tilde{U})$ définis sur Ω_0. De plus, nous définissons

$$\begin{array}{rccl} L(.,t): & \Omega_0 & \longrightarrow & \Omega(t) \\ & \mathbf{x} & \mapsto & \mathbf{X} = \mathbf{x} + \int_0^t V(s)\,\mathrm{d}s = L(t,\mathbf{x}), \end{array}$$

d'où $P(t,\mathbf{x}) = \tilde{P}(t, L(t,\mathbf{x})) = \tilde{P}(t,\mathbf{X})$ (par exemple pour P). Pour $\mathbf{x} \in \Omega_0$ et tout $t > 0$, le problème s'écrit maintenant

$$\begin{cases} -\Delta P(t,\mathbf{x}) = -\xi K_d & \text{dans } \Omega_0\,, \\ P(t,\mathbf{x}) = k_p & \text{sur } \partial\Omega_0\,, \end{cases} \tag{10}$$

avec

$$V(t) = \frac{1}{\xi_1} \int_{\Omega_0} \nabla P(t,\mathbf{x})\,\mathrm{d}\mathbf{x}\,, \tag{11}$$

et pour $\mathbf{x} \in \Omega_0$,

$$U(t,\mathbf{x}) = -\frac{1}{\xi}\nabla P(t,\mathbf{x}) - \frac{1}{\xi_1} \int_{\Omega_0} \nabla P(t,\mathbf{x})\,\mathrm{d}\mathbf{x}\,. \tag{12}$$

Le régulateur moléculaire

Nous considérons maintenant un régulateur moléculaire du cytosquelette, qui a la propriété d'inhiber la polymérisation. Notons $C : \mathbb{R}_+ \times \Omega_0 \to \mathbb{R}_+$ sa concentration. Alors son évolution dans le référentiel de la cellule suit une dynamique d'advection-diffusion, où le champ d'advection correspond au champ de vitesse du fluide dans le référentiel de la cellule. Nous avons

$$\partial_t C(t,\mathbf{x}) + \mathrm{div}\ (C(t,\mathbf{x})U(t,\mathbf{x}) - D\nabla C(t,\mathbf{x})) = 0 \quad \text{pour } \mathbf{x} \in \Omega_0,\, t > 0\,,$$

avec la condition de flux nul

$$(D\nabla C(t,\mathbf{x}) - C(t,\mathbf{x})U(t,\mathbf{x})) \cdot \mathbf{n} = 0 \quad \text{pour } \mathbf{x} \in \partial\Omega_0,\, t > 0\,,$$

avec $\mathbf{n}$ la normale unitaire sortante au bord du domaine. La formulation du problème garantit la conservation de la masse.

Cette molécule est supposée inhiber la polymérisation de l'actine au bord du domaine. C'est pourquoi nous définissons une loi d'interaction sur la condition de Dirichlet sur la pression du fluide. Plus précisément, le problème fluide s'écrit

$$\begin{cases} U(t,\mathbf{x}) = -\frac{1}{\xi}\nabla P(t,\mathbf{x}) - \frac{1}{\xi_1}\int_{\Omega_0} \nabla P(t,\mathbf{x})\,\mathrm{d}\mathbf{x} & \text{pour } \mathbf{x} \in \Omega_0,\, t > 0\,, \\ -\Delta P(t,\mathbf{x}) = -\xi K_d & \text{pour } \mathbf{x} \in \Omega_0,\, t > 0\,, \\ P(t,\mathbf{x}) = [\alpha - \beta C(t,\mathbf{x})]_+ & \text{pour } \mathbf{x} \in \partial\Omega_0,\, t > 0\,, \end{cases}$$

avec $[\,\cdot\,]_+$ la fonction partie positive, et α, β des constantes positives.

L'activation à la membrane Le modèle introduit précédemment peut se montrer trop singulier. Une façon de régulariser légèrement la dynamique consiste à considérer l'activation du régulateur lorsqu'il se trouve à la membrane. Ainsi, seules les molécules activées peuvent exercer une action sur la polymérisation.

Plus précisément, notons μ la concentration en marqueur activé. Nous avons pour des taux d'attachement/détachement K_{on}, , K_{off},

$$\frac{\partial}{\partial t}\mu(t,\mathbf{x}) = K_{\text{on}}C(t,\mathbf{x}) - K_{\text{off}}\mu(t,\mathbf{x}) \quad \text{dans } \Omega_0\,,$$

et la condition de bord sur la concentration cytoplasmique C devient

$$(C(t,\mathbf{x})U(t,\mathbf{x}) - D\nabla C(t,\mathbf{x}))\cdot\mathbf{n} = -K_{\text{on}}C(t,\mathbf{x}) + K_{\text{off}}\mu(t,\mathbf{x}) \quad \text{sur } \partial\Omega_0\,.$$

La masse totale est également conservée :

$$\int_{\Omega_0} C(t,\mathbf{x})\,\mathrm{d}\mathbf{x} + \int_{\partial\Omega_0} \mu(t,\mathbf{x})\,\mathrm{d}\mathbf{x} = M \quad \text{pour } t>0\,. \tag{13}$$

Enfin, la dynamique du fluide correspond au problème

$$\begin{cases} U(t,\mathbf{x}) = -\frac{1}{\xi}\nabla P(t,\mathbf{x}) - \frac{1}{\xi_1}\int_{\Omega_0}\nabla P(t,\mathbf{x})\,\mathrm{d}\mathbf{x} & \text{pour } \mathbf{x}\in\Omega_0,\ t>0\,,\\ -\Delta P(t,\mathbf{x}) = -\xi K_d & \text{pour } \mathbf{x}\in\Omega_0,\ t>0\,,\\ P(t,\mathbf{x}) = [\alpha-\beta\mu(t,\mathbf{x})]_+ & \text{pour } \mathbf{x}\in\partial\Omega_0,\ t>0\,, \end{cases}$$

Dans la thèse, nous avons d'abord étudié ce modèle dans le cadre 1D, et avons obtenu des résultats théoriques.

Le cas 1D : étude théorique

Supposons maintenant que $\Omega=(-1,1)$ fixé, et posons toutes les constantes égales à 1. Le problème précédent, sans activation à la membrane, et pour une pression au bord linéaire, se reformule comme ceci : pour $t>0$,

$$\begin{cases} \partial_t c(t,x) = \partial_x\Big(\partial_x c(t,x) + (x + c(t,-1) - c(t,1))\,c(t,x)\Big) & \text{sur } (-1,1)\,,\\ \partial_x c(t,-1) + (c(t,-1) - c(t,1) - 1)\,c(t,-1) = 0\,,\\ \partial_x c(t,1) + (c(t,-1) - c(t,1) + 1)\,c(t,1) = 0\,, \end{cases} \tag{14}$$

avec une vitesse cellulaire

$$v(t) = \frac{\delta\xi}{\xi_1}(c(t,-1) - c(t,1))\,.$$

Il s'agit donc d'une équation de Fokker-Planck non linéaire et non-locale en raison de l'expression de la vitesse, qui fait par ailleurs intervenir des quantités au bord du domaine. Ce modèle présente une structure similaire au modèle de polarisation étudié dans Calvez et al. [2012, 2010]; Hawkins et al. [2009]; Lepoutre et al. [2014]; Muller et al. [2016].

Dans notre cas, différents éléments entrent en compétition. La diffusion tend à homogénéiser la concentration en molécules, tandis que le biais vers 0 présent dans le terme d'advection est en compétition avec le biais lié aux concentrations en marqueur sur les deux bords.

Les résultats obtenus sur ce système sont de nature dichotomique. En dessous d'une masse critique, nous démontrons l'existence globale d'une solution ainsi que la convergence de la solution vers son unique état stationnaire, qui est symmétrique et donc non motile.

Théorème 1. *Supposons que la condition initiale c_0 soit telle que $c_0 \in L^1(-1,1)$ et $\int_{-1}^{1} c_0(x)\log c_0(x)\,\mathrm{dx} < +\infty$. De plus, supposons que $M \leq 1$. Alors, il existe une solution faible globale au problème (14) qui vérifie les estimations suivantes : pour tout $T > 0$,*

$$\begin{aligned}\sup_{t\in(0,T)} \int_{-1}^{1} c(t,x)\log c(t,x)\,\mathrm{dx} &< +\infty\,,\\ \int_0^T \int_{-1}^{1} c(t,x)\left(\partial_x \log c(t,x)\right)^2\,\mathrm{dx}\,\mathrm{dt} &< +\infty\,.\end{aligned}$$

De plus, la solution converge fortement sur L^1 vers l'unique état stationnaire $G_M(x)$ du système, et le taux de convergence est exponentiel:

$$\|c(t,x) - G_M(x)\|_{L^1} \leq \sqrt{2M\mathbf{L}(0)}\exp(-t)\,.$$

Ce résultat de convergence est démontré par l'existence d'une fonctionnelle de Lyapunov. De plus, le taux de convergence est obtenu grâce à l'utilisation de l'inégalité log-Sobolev. De plus, dans le cas critique $M = 1$, un résultat similaire est démontré grâce à la convergence vers 0 de l'entropie relative.

Dans le cas sur-critique, la situation est plus compliquée. Nous explicitons une condition suffisante pour que la solution devienne non bornée en temps fini.

Théorème 2. *Supposons que $M > 1$, et que le premier moment initial de la solution décalé de 1 est petit : $\int_{-1}^{1}(x+1)c_0(\mathbf{x})\,\mathrm{d}x < (M-1)/2$ pour une condition initiale notée c_0. De plus, supposons que $c_0(-1) - c_0(1) > 1$. Alors, la solution au problème (14) issue de c_0 devient non bornée en temps fini.*

Afin de démontrer ce théorème, nous formulons dans un premier temps un résultat similaire pour le problème annexe.

$$\begin{aligned}\partial_t c(t,x) = \partial_x\Big(\partial_x c(t,x) + \left(-1 + c(t,-1) - c(t,1)\right)c(t,x)\Big) \quad &\text{dans } \Omega_0\,,\\ \partial_x c(t,-1) + \left(c(t,-1) - c(t,1) - 1\right)c(t,-1) = 0\,,&\\ \partial_x c(t,1) + \left(c(t,-1) - c(t,1) - 1\right)c(t,1) = 0\,.&\end{aligned} \tag{15}$$

Il s'agit donc d'un problème similaire où le champ d'advection est uniforme. Nous démontrons le résultat suivant :

Proposition 1. *Supposons que $M > 1$, et que le premier moment décalé de 1 est initialement petit : $\int_{-1}^{1} c_0(\mathbf{x})\,\mathrm{d}x < (M-1)/2$. De plus, supposons que la condition initiale c_0 est décroissante et telle que $c_0(-1) - c_0(1) > 1$. Alors, la solution au problème(15) issue de c_0 devient non bornée en temps fini.*

Ce résultat est démontré en mettant en évidence une quantité positive dont la dérivée en temps est strictement négative. En notant $\tilde{\mathbf{J}}(0) = \int_{-1}^{1} c(0,\mathbf{x})\,\mathrm{d}x$, nous définissons

$$\mathbf{K}(t) = \tilde{\mathbf{J}}(0) + \frac{(1-M)M^2}{2}\left(1 - \frac{2\tilde{\mathbf{J}}(0)}{M-1}\right)\int_0^t \tilde{\mathbf{J}}(s)^{-1}\,\mathrm{d}s\,.$$

Nous pouvons alors montrer que

$$\frac{\mathrm{d}}{\mathrm{dt}}\mathbf{K}(t)^2 \leq (1-M)M^2\left(1 - \frac{2\tilde{\mathbf{J}}(0)}{M-1}\right) < 0\,.$$

Puis, pour conclure, nous établissons un résultat de concentration-comparaison similaire à celui établi par Lepoutre et al. [2014], s'appliquant au problème intégré en espace, et permettant de comparer les quantités intégrées entre les deux problèmes.

Le cas 2D : étude numérique

Dans une dernière partie, nous effectuons des simulations numériques du problème bidimensionnel, afin de mettre en évidence sa capacité à produire des trajectoires cellulaires de persistance variée, ainsi que ses possibilités notamment dans la modélisation de l'interaction avec l'environnement extérieur.

Les simulations sont effectuées suivant une discrétisation par la méthode des volumes finis sur Matlab, et par éléments finis sur FreeFem++.

Comportement général

Dans un premier temps, nous effectuons des simulations numériques de la dynamique pure, principalement dans le cas de l'activation du marqueur au bord. Puisque la non-linéarité dans le terme d'advection a deux origines distinctes, nous étudions d'abord le cas où la vitesse cellulaire est nulle, et la comparons au cas classique. Nous observons que le biais global introduit par la vitesse est un élément fondamental pour la mise en place d'un profil polarisé maintenu dans le temps.

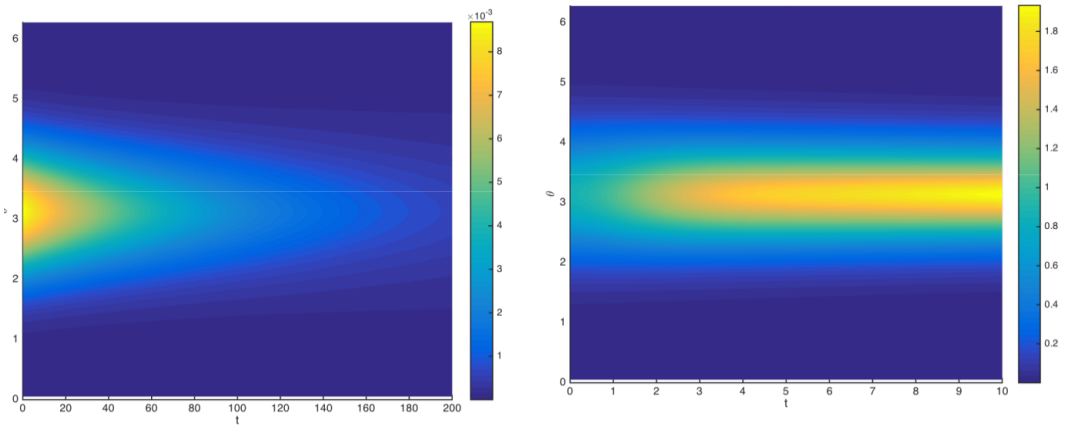

Figure 17 – Kymographes représentant la concentration en marqueurs activés dans un cas de dépolarisation et de polarisation. Le temps est représenté en abscisses, et les angles en ordonnées.

Fluctuations stochastiques et signal extérieur

Puis, nous introduisons des fluctuations stochastiques dans la dynamique d'advection au moyen d'un processus de Q-Wiener, qui a la particularité d'être un bruit blanc en temps et corrélé en espace.

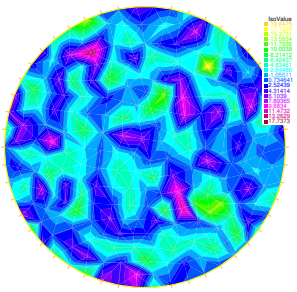

Figure 18 – Réalisation d'un processus de Q-Wiener pour une corrélation de $\zeta = 0.1$.

Cette perturbation se justifie par la régulation microscopique de l'activité du cytosquelette. En effet, les boucles moléculaires de signalisation comportant des réactions complexes d'activation et d'inhibition, cela pourrait générer des oscillations visibles dans la dynamique du cytosquelette. Les équations fluides correspondantes étant basées sur des lois de conservation, il est plus naturel dans notre cas d'introduire une perturbation stochastique dans l'activité découlant de l'écoulement, à savoir le terme d'advection de la molécule étudiée.

Nous mettons alors en évidence la capacité du bruit à perturber le système de façon à amorcer le processus de polarisation, et à mettre la cellule en mouvement. De plus, nous obtenons des simulations numériques de trajectoires qui sont de natures plus ou moins persistantes selon la valeur du paramètre de couplage entre le marqueur et le fluide.

Suite à ces résultats encourageants, nous avons abordé la question du signal chimique extérieur induisant localement une plus forte polymérisation de l'actine. L'effet du signal est donc considéré comme antagoniste à celui du marqueur moléculaire. Nous avons effectué des simulations numériques associant l'effet du signal et les perturbations stochastiques du processus de Q-Wiener. Dans le cas d'un signal localisé dans l'espace de concentration S, nous définissons une réponse cellulaire directement dans le terme d'advection, qui dépend de ∇S. Nous obtenons les résultats suivants pour une cellule initialement polarisée : lorsque la dynamique de polarisation l'emporte sur la perception du signal extérieur, la cellule ne perçoit pas le signal et poursuit sa route. Dans le cas contraire, la cellule est capable de sentir le signal et de rejoindre la source.

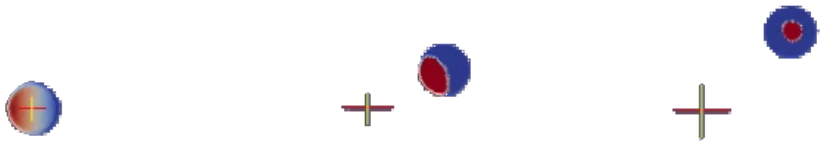

Figure 19 – Simulations numériques de l'effet d'un signal attracteur dominant la polarisation.

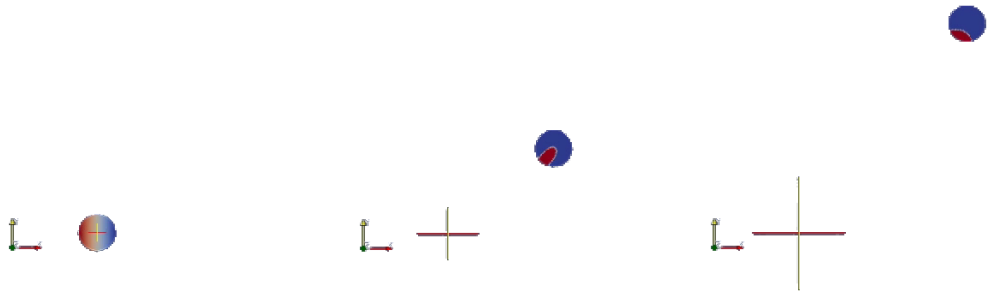

Figure 20 – Simulations numériques de l'effet d'un signal attracteur dominé la polarisation.

Contact mécanique

Enfin, nous abordons le cas du contact mécanique avec un obstacle, ainsi que la question de sa gestion numérique. Puisque le modèle est multi-échelle, il est possible de stopper

la cellule lors d'un contact sans pour autant empêcher la dynamique intracellulaire de s'adapter afin d'adopter un mouvement différent.

Des premières simulations sont réalisées dans le cas d'une cellule fortement polarisée se déplaçant vers un mur de manière orthogonale. Le contact a pour effet de stopper la cellule. Puis l'activité interne bruitée s'adapte et la cellule se remet par la suite en mouvement.

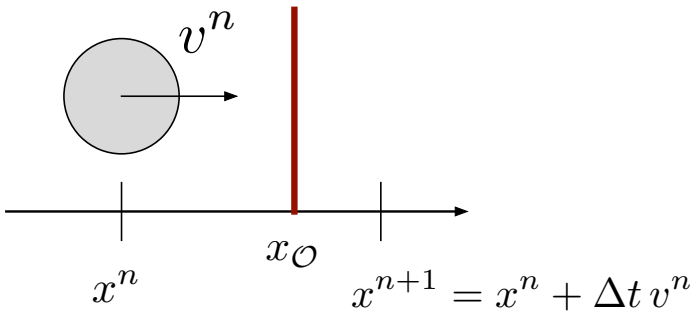

Figure 21 – Contact numérique.

Ces résultats constituent une première étape vers le développement d'une méthode efficace de gestion des contacts mécaniques, ce qui pourra ouvrir la voie vers la modélisation d'interaction entre cellules.

Bibliography

Abercrombie, M. (1980). The croonian lecture, 1978: the crawling movement of metazoan cells. Proceedings of the Royal Society of London B: Biological Sciences, 207(1167):129–147. 15

Aman, A. and Piotrowski, T. (2010). Cell migration during morphogenesis. Developmental biology, 341(1):20–33. 6

Bansaye, V. and Méléard, S. (2015). Some stochastic models for structured populations : scaling limits and long time behavior. 23, 24

Barnhart, E., Lee, K.-C., Allen, G. M., Theriot, J. A., and Mogilner, A. (2015). Balance between cell-substrate adhesion and myosin contraction determines the frequency of motility initiation in fish keratocytes. Proc Natl Acad Sci U S A, 112(16):5045–50. 16

Bechinger, C., Leonardo, R. D., Löwen, H., Reichhardt, C., Volpe, G., and Volpe, G. (2016). Active Brownian Particles in Complex and Crowded Environments. 22

Bravo-Cordero, J. J., Hodgson, L., and Condeelis, J. (2013). Directed cell invasion and migration during metastasis. Current Opinion in Cell Biology, pages 277–283. 7

Caballero, D., Comelles, J., Piel, M., Voituriez, R., and Riveline, D. (2015). Ratchetaxis: Long-range directed cell migration by local cues. Trends Cell Biol, 25(12):815–27. 14

Caballero, D., Voituriez, R., and Riveline, D. (2014). Protrusion fluctuations direct cell motion. Biophys J, 107(1):34–42. 14, 22

Calvez, V. (2007). Modèles et analyses mathématiques pour les mouvements collectifs de cellules. PhD thesis, Université Pierre et Marie Curie-Paris VI. 16

Calvez, V., Hawkins, R. J., Meunier, N., and Voituriez, R. (2012). Analysis of a Nonlocal Model for Spontaneous Cell Polarization. SIAM Journal on Applied Mathematics, 72(2):594–622. 29

Calvez, V., Meunier, N., and Voituriez, R. (2010). A one-dimensional Keller–Segel equation with a drift issued from the boundary. Comptes Rendus Mathematique, 348(11):629–634. 29

Campos, D., Méndez, V., and Llopis, I. (2010). Persistent random motion: uncovering cell migration dynamics. J Theor Biol, 267(4):526–34. 22

Carter, S. B. (1967). Haptotaxis and the mechanism of cell motility. Nature, pages 256–260. 14

Chalub, F., Dolak-Struss, Y., Markowich, P., Oelz, D., Schmeiser, C., and Soreff, A. (2006). Model hierarchies for cell aggregation by chemotaxis. Mathematical Models and Methods in Applied Sciences, 16(supp01):1173–1197. 16

Champagnat, N., Ferrière, R., and Méléard, S. (2008). From individual stochastic processes to macroscopic models in adaptive evolution. 24:2–44. 23, 24

Codling, E. A., Plank, M. J., and Benhamou, S. (2008). Random walk models in biology. Journal of the Royal Society Interface, 5(25):813–834. 22

Dawes, A. T. and Edelstein-Keshet, L. (2007). Phosphoinositides and rho proteins spatially regulate actin polymerization to initiate and maintain directed movement in a one-dimensional model of a motile cell. Biophysical journal, 92(3):744–768. 16

Emako, C., Gayrard, C., Buguin, A., de Almeida, L. N., and Vauchelet, N. (2016). Traveling pulses for a two-species chemotaxis model. PLoS Comput Biol, 12(4):e1004843. 16

Etienne-Manneville, S. (2013). Microtubules in cell migration. Annual review of cell and developmental biology, 29:471–499. 7

Filippo Stefanoni, e. a. (2011). A numerical model for durotaxis. Journal of Theoretical Biology. 14

Fletcher, D. A. and Mullins, R. D. (2010). Cell mechanics and the cytoskeleton. Nature, 463(7280):485–492. 7

Fournier, N. and Méléard, S. (2004). A microscopic probabilistic description of a locally regulated population and macroscopic approximations. 14(4):1880–1919. 23, 24

Friedl, P. and Wolf, K. (2003). Tumour-cell invasion and migration: diversity and escape mechanisms. Nature Reviews Cancer, 3(5):362–374. 7

Ganguly, A., Yang, H., Sharma, R., Patel, K. D., and Cabral, F. (2012). The role of microtubules and their dynamics in cell migration. Journal of Biological Chemistry, 287(52):43359–43369. 7

Gardel, M. L., Sabass, B., Ji, L., Danuser, G., Schwarz, U. S., and Waterman, C. M. (2008). Traction stress in focal adhesions correlates biphasically with actin retrograde flow speed. The Journal of cell biology, 183(6):999–1005. 15

Göing-Jaeschke, A. and Yor, M. (1999a). A survey and some generalizations of bessel processes. Bernoulli, 9:313–349. 21

Göing-Jaeschke, A. and Yor, M. (1999b). A survey and some generalizations of bessel processes. Bernoulli, 9:313–349. 21

Granger, D. N. and Senchenkova, E. (2010). Inflammation and the microcirculation. In Colloquium Series on Integrated Systems Physiology: From Molecule to Function, volume 2, pages 1–87. Morgan & Claypool Life Sciences. 19

Grec, B., Maury, B., Meunier, N., and Navoret, L. (2012). The role of ligands binding in shear induced leukocyte rolling. 19

H. Lodish, e. a. (2008). Molecular Cell Biology. W. H. Freeman. 8, 9

Hall, A. (1998). Rho GTPases and the actin cytoskeleton. Science, 279(5350):509–514. 10, 11

Hawkins, R. J., Bénichou, O., Piel, M., and Voituriez, R. (2009). Rebuilding cytoskeleton roads: active-transport-induced polarization of cells. Phys Rev E Stat Nonlin Soft Matter Phys, 80(4 Pt 1):040903. 29

Holmes, W. R. and Edelstein-Keshet, L. (2012). A comparison of computational models for eukaryotic cell shape and motility. PLoS Comput Biol, 8(12):e1002793. 16

Howard, J. et al. (2001). Mechanics of motor proteins and the cytoskeleton. 7

Jones, C. N., Moore, M., Dimisko, L., Alexander, A., Ibrahim, A., Hassell, B. A., Warren, H. S., Tompkins, R. G., Fagan, S. P., and Irimia, D. (2014). Spontaneous neutrophil migration patterns during sepsis after major burns. PloS one, 9(12):e114509. 6

Jülicher, F., Kruse, K., Prost, J., and Joanny, J.-F. (2007). Active behavior of the cytoskeleton. Physics Reports, 449(1):3–28. 26

Keller, R. (2002). Shaping the vertebrate body plan by polarized embryonic cell movements. Science. 6

Kolaczkowska, E. and Kubes, P. (2013). Neutrophil recruitment and function in health and inflammation. Nature Reviews Immunology, 13(3):159–175. 6

Krause, M. and Gautreau, A. (2014). Steering cell migration: lamellipodium dynamics and the regulation of directional persistence. Nat Rev Mol Cell Biol, 15(9):577–90. 15

Lee, S. H. and Dominguez, R. (2010). Regulation of actin cytoskeleton dynamics in cells. Molecules and cells, 29(4):311–325. 7, 9

Lepoutre, T., Meunier, N., and Muller, N. (2014). Cell polarisation model : the 1D case. Journal des Mathematiques Pures et Appliquees, 101(2):152–171. 29, 30

Li, Y., Bhimalapuram, P., and Dinner, A. R. (2010). Model for how retrograde actin flow regulates adhesion traction stresses. Journal of Physics: Condensed Matter, 22(19):194113. 15

Lindnera, B. and Nicola, E. (2008). (diffusion in different models of active brownian particles). Eur. Phys. J. Special Topics, 157:43–52. 22

Linetsky, V. (2004). Computing hitting time densities for cir and ou diffusions: Applications to mean-reverting models. Journal of Computational Finance, 7:1–22. 21

Liu, Y.-J., Le Berre, M., Lautenschlaeger, F., Maiuri, P., Callan-Jones, A., Heuzé, M., Takaki, T., Voituriez, R., and Piel, M. (2015). Confinement and low adhesion induce fast amoeboid migration of slow mesenchymal cells. Cell, 160(4):659–672. 11

Lodish, H. and Zipursky, S. L. (2001). Molecular cell biology. Biochemistry and Molecular Biology Education, 29:126–133. 23

Lomakin, A. J., Lee, K.-C., Han, S. J., Bui, D. A., Davidson, M., Mogilner, A., and Danuser, G. (2015). Competition for actin between two distinct f-actin networks defines a bistable switch for cell polarization. Nat Cell Biol, 17(11):1435–45. 16

Maiuri, P., Rupprecht, J.-F., Wieser, S., Ruprecht, V., Bénichou, O., Carpi, N., Coppey, M., De Beco, S., Gov, N., Heisenberg, C.-P., Lage Crespo, C., Lautenschlaeger, F., Le Berre, M., Lennon-Dumenil, A.-M., Raab, M., Thiam, H.-R., Piel, M., Sixt, M., and Voituriez, R. (2015). Actin flows mediate a universal coupling between cell speed and cell persistence. Cell, 161(2):374–86. 15, 23, 26

Marée, A. F. M., Jilkine, A., Dawes, A., Grieneisen, V. A., and Edelstein-Keshet, L. (2006). Polarization and movement of keratocytes: a multiscale modelling approach. Bull Math Biol, 68(5):1169–211. 16

Mattila, P. K. and Lappalainen, P. (2008). Filopodia: molecular architecture and cellular functions. Nat Rev Mol Cell Biol, 9(6):446–54. 13

Milišić, V. and Oelz, D. (2011). On the asymptotic regime of a model for friction mediated by transient elastic linkages. Journal de mathématiques pures et appliquées, 96(5):484–501. 19

Mogilner, A. and Oster, G. (1996). The physics of lamellipodial protrusion. European biophysics journal, 25(1):47–53. 15

Muller, N., Piel, M., Calvez, V., Voituriez, R., Gonçalves-Sá, J., Guo, C.-L., Jiang, X., Murray, A., and Meunier, N. (2016). A predictive model for yeast cell polarization in pheromone gradients. PLoS Comput Biol, 12(4):e1004795. 29

Oelz, D., Schmeiser, C., and Small, J. V. (2008). Modeling of the actin-cytoskeleton in symmetric lamellipodial fragments. Cell adhesion & migration, 2(2):117–126. 15

Parsons, J. T., Horwitz, A. R., and Schwartz, M. A. (2010). Cell adhesion: integrating cytoskeletal dynamics and cellular tension. Nat Rev Mol Cell Biol, 11(9):633–43. 10

Peskin, C. S., Odell, G. M., and Oster, G. F. (1993). Cellular motions and thermal fluctuations: the brownian ratchet. Biophysical journal, 65(1):316. 15

Prass, M., Jacobson, K., Mogilner, A., and Radmacher, M. (2006). Direct measurement of the lamellipodial protrusive force in a migrating cell. J Cell Biol, 174(6):767–72. 16

R. Ananthakrishna, a. A. E. (2007). The forces behind cell movement. Int. J. Biol. Sci. 7, 8

Recho, P., Putelat, T., and Truskinovsky, L. (2015). Mechanics of motility initiation and motility arrest in crawling cells. Journal of the Mechanics and Physics of Solids, 84:469–505. 16

Risler, T. (2009). Cytoskeleton and cell motility. In Encyclopedia of Complexity and Systems Science, pages 1738–1774. Springer. 7, 13

Romanczuk, P., Bär, M., Ebeling, W., Lindner, B., and Schimansky-Geier, L. (2012). Active Brownian Particles. From Individual to Collective Stochastic Dynamics. Eur.Phys.J. 22

Ryan, G. L., Petroccia, H. M., Watanabe, N., and Vavylonis, D. (2012). Excitable actin dynamics in lamellipodial protrusion and retraction. Biophysical Journal, 102(7):1493–1502. 24

Sabass, B. and Schwarz, U. S. (2010). Modeling cytoskeletal flow over adhesion sites: competition between stochastic bond dynamics and intracellular relaxation. Journal of Physics: Condensed Matter, 22(19):194112. 15

Shreve, S. E. (2004). Stochastic calculus for finance II: Continuous-time models, volume 11. Springer Science & Business Media. 21

Speck, T. (2015). Collective behavior of Active Brownian particles: From microscopic clustering to macroscopic phase separation. 22

Vestweber, D. (2015). How leukocytes cross the vascular endothelium. Nature Reviews Immunology. 19

Wang, F. (2009). The signaling mechanisms underlying cell polarity and chemotaxis. Cold Spring Harbor perspectives in biology, 1(4):a002980. 14

Winkler, M. (2010). Aggregation Vs. global diffusive behavior in the higher-dimensional Keller–Segel model. Journal of Differential Equations, 248(12):2889–2905. 16

Yadav, R., Larbi, K. Y., Young, R. E., and Nourshargh, S. (2003). Migration of leukocytes through the vessel wall and beyond. Thrombosis and haemostasis, 90(4):598–606. 6

Yamaguchi, H., Wyckoff, J., and Condeelis, J. (2005). Cell migration in tumors. Current opinion in cell biology, 17(5):559–564. 7

Yip, A. K., Chiam, K.-H., and Matsudaira, P. (2015). Traction stress analysis and modeling reveal that amoeboid migration in confined spaces is accompanied by expansive forces and requires the structural integrity of the membrane–cortex interactions. Integrative Biology, 7(10):1196–1211. 12

Part I

Particle approach

Chapter 1

A stochastic model for cell adhesion to the vascular wall

Contents

1.1 Introduction 41
1.2 Construction of the discrete stochastic model 43
1.2.1 Velocity model 43
1.2.2 Discrete stochastic model for the adhesive force 44
1.3 Mathematical properties and numerical simulations 45
1.3.1 A population approach 45
1.3.2 Trajectorial representation 46
1.3.3 Martingale property 48
1.3.4 Moment equation 49
1.3.5 Numerical Simulations 50
1.4 Continuous bonds approximations 50
1.4.1 Renormalization 51
1.4.2 Deterministic limits 52
1.4.3 Accelerated demography 57
1.5 Stopping time 62
1.5.1 General remarks 62
1.5.2 Constant rates: the CIR process 63
1.5.3 General rates 69
1.6 Conclusions and perspectives 73
1.7 Appendix 73
1.7.1 Stochastic processes 73
1.7.2 Discretization of EDS 74

1.1 Introduction

Leukocytes adhesion on the vascular wall is a major process involved during inflammation or metastasis invasion [Granger and Senchenkova, 2010]. The adhesive interaction between leukocytes and endothelial cells occurs in the presence of the hemodynamic forces exerted on the adhering leukocytes by the blood flow. The first step of interaction happens when

enough bonds between the cell and the wall are stabilized so that the cell is slowed down, this is the so called **capture phase**. Then, leukocytes roll along the stimulated endothelial cells. This step is mediated by adhesion molecules of the selectin family. During **rolling**, the leukocytes may also be stimulated, and consequently another family of cell adhesion molecules, the integrins, is activated on the leukocyte surface. The integrins mediate the **firm adhesion** which slows the cell enough so that the leukocyte penetrates the vascular wall allowing for the further development of the phenomenon at play (growth of a lesion, invasion of tissues by metastatic cells e.g, see for example [Ley et al., 2007]).

Leukocyte rolling has been observed in vivo and in vitro in flow chambers, in which isolated leukocytes are rolling on either monolayers of cultured endothelial cells or surfaces coated with selectin or other molecules. It has been observed that the velocities of rolling cells are orders of magnitudes lower than the velocities of non-adherent cells freely moving close to the substratum surface. This indicates adhesive interaction between the rolling cells and the substratum [Springer et al., 1990].

The motion of leukocyte rolling has been observed to be stochastic both in vivo, [Schmid-Schöounbein et al., 1987], and in vitro, [Goetz et al., 1994]. Variation of the rolling velocities of individual cells in time has also been observed for experiments in which the leukocytes roll on a flat surface bearing a uniform layer of ligands, [Springer et al., 1990]. This suggests that the fluctuation in leukocyte dynamics in the vicinity of the wall is a reflection of the stochastic nature of the adhesive interaction.

The aim of the present paper is to build and study a continuous model to describe the motion of a cell that develops adhesive interaction with the vascular wall. To do so, we start with a minimal discrete stochastic model to describe the individual bond dynamics and then we derive the continuous model by performing a scaling limit. More precisely, in the discrete model that describes the individual bond dynamics, we assume the cell to be a point particle submitted to blood flow with 1D constant velocity. Units of resistive force appear/disappear stochastically and discontinuously in time, following a stochastic jump process. The stochastic character of the dynamics is due to the large number of molecules interacting to form bonds. We neglect the growth of an adhesion so that the binding dynamics is discontinuous in time. Since the number of bonds involved in cellular adhesion is very high, in a second step we let the number of bonds go to infinity while the contribution of each bond goes to zero. In the spirit of Bansaye and Méléard [2015]; Champagnat and Méléard [2007]; Tran [2006] by the renormalization of the population of bonds and its dynamics, we rigorously derive a continuous limiting model for the cellular adhesion dynamics. Depending on the renormalization assumptions, we obtain either a deterministic or a stochastic equation, that we both study. The deterministic model successfully predicts the threshold wall shear stress above which rolling does not occur and, for some parameter

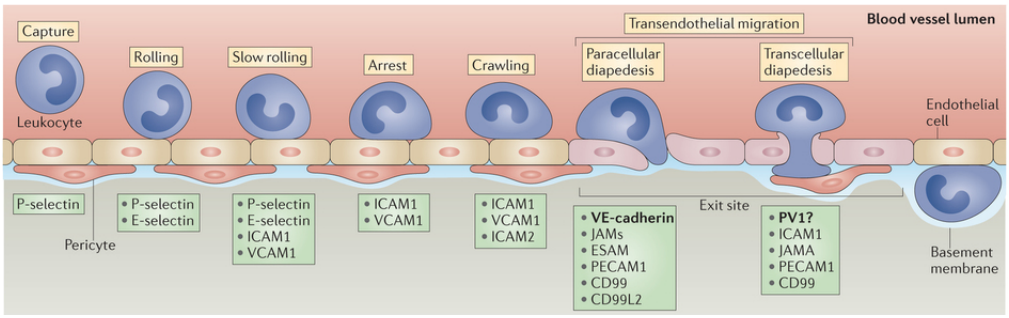

Figure 1.1 – Scheme of the multistep cascade of leukocyte extravasation. Reprinted by permission from Macmillan Publishers Ltd: Nature Reviews Immunology [Vestweber, 2015], copyright (2007)

values, it predicts the cell stationary adhesion. We also study the continuous stochastic model and derive information on the time needed for the cell to stop. To do so we use two approaches: a comparison principle together with an explicit Laplace transform for the Cox-Ingersoll-Ross (CIR) process, and the direct derivation of the mean stopping time using a Fokker-Planck equation. We believe that this work is a first step in the construction of a permeability law for leukocytes, characterizing the different regimes that can arise: cells either slip or grip to the wall. This work was made in collaboration with Nicolas Meunier, and is submitted for publication.

The plan of this article is the following. In Section 2, we detail the construction of the discrete stochastic model for the individual bond dynamics. We provide a mathematical analysis of the discrete model in Section 3. In Section 4, using a renormalization technique we build continuous versions of the model and we exhibit different behaviours according to the chosen renormalization: deterministic or stochastic. In section 4 we also give the behaviour of the solution to the deterministic model. Finally, in Section 5, we use the continuous stochastic model to compute the probability distribution of the time needed for the cell to stop.

1.2 Construction of the discrete stochastic model

Let us consider a cell (a leukocyte e.g.) carried by the blood flow. We suppose that the size of the gap between the cell and the blood vessel wall is small enough so that bonds between the cell and the vascular wall may continuously form in the contact area. Since the cell is in the vicinity of the wall, we assume that the blood shear flow is 1D, parallel to the vascular wall and with a constant velocity, denoted by $u \in \mathbb{R}_+$.

In previous studies, see Chang and Hammer [1999]; Jadhav et al. [2005] e.g., it was shown that approximating the contact area by a simple geometrical figure (a circle or a rectangle) and neglecting the increase of the contact area with the flow shear rate due to cell deformability do not change qualitatively the analysis. Moreover, as suggested in Bhatia et al. [2003], the cell adhesion is primarily determined by physicochemical properties of adhesion proteins and, thus, to a first approximation, we assume the cell to be a point particle whose position at time $t \geq 0$ is denoted by $x(t)$.

1.2.1 Velocity model

To describe the cell motion in our model, we use a non-inertial approximation. Indeed, in the limit of low Reynolds number, viscous forces dominate over inertial forces and the momentum equation reduces to the force balance principle:

$$V_t = u - F_t, \tag{1.1}$$

where $V_t \in \mathbb{R}$ is the cell velocity, u is the blood shear flow and the cell is subjected to a macroscopic resistive force, denoted by $F_t \in \mathbb{R}_+$, induced by the bonds that contribute to decelerating the cell, see Figure 1. The previous equation is valid only for $F_t \leq u$, as for a maximal force the cell stops, and the model is no longer valid.

Depending on the ratio between the adhesion force exerted by the stabilized bonds and the load and torque created by the blood flow, which is characterized by the shear rate, two situations might occur:

- either the adhesion force is strong enough to first capture and then slow down the leukocyte (in that case it allows the cell to roll on the wall),

- or the tension exerted by the blood flow on the bonds is too high and the bonds rupture immediately without capturing the cell.

Modeling leukocyte dynamics near a vessel wall now amounts to modeling the time evolution of the adhesive force.

1.2.2 Discrete stochastic model for the adhesive force

The resistive force arises from the strength of the cell adhesion to the vessel wall. Cellular adhesion is a macroscopic readout of the forces exerted by the wall on the cell through each bond. Moreover, the formation of each bond is based on a highly complex and dynamic set of microscopic (physical and chemical) reactions [Bhatia et al., 2003].

Let us now present the very simple mesoscopic discrete model we will use to describe the individual bond dynamics. We denote by N_t the number of stabilized bonds at time t. We assume that each stabilized bond mediates a unit force in the opposite direction of the moving fluid and we denote by $\gamma > 0$ a global friction coefficient. Thus, the total force exerted by all the stabilized bonds is

$$F_t = \gamma N_t \,.$$

The quantity N_t is a random variable that we assume follow a classical birth and death dynamics with creation rate c, dissociation rate d and reproduction rate r as follows.

- As the leukocyte is assumed to be close enough to the arterial wall to interact, bonds might appear spontaneously at rate c. Since the rate for a single bond formation between two proteins is mostly determined by the time the two proteins spend near one another, the rate c should depend on the cell velocity when the relative velocity between the cell surface and the wall is non zero. A natural choice for c is to consider that there exists a threshold velocity value above which no bond is created. The simplest way is to use a step function of the blood-flow velocity u: $c(u) = c$ if $u \leq u_*$ and $c(u) = 0$ otherwise. In the following, we will always work with a constant u, but both configurations will be considered.

- A more realistic choice for c would be to consider a decreasing function of the instantaneous cell velocity V_t. A prototypical behaviour would be given by $c(v) = (u_* - v)_+$ where $(\,\cdot\,)_+$ denotes the positive part. Recalling that V_t is related to N_t this would amount to choose a rate c depending on N_t the number of stabilized bonds: $c(n) = (u_* - u + \gamma n)_+$. Such a choice would mean to include individual reproduction of the bonds in the birth and death process. Let us now see whether reproduction is well suited to our case. Cellular adhesions are modulated by cytoskeletal forces or external stresses and adapt to the mechanical properties of the extracellular matrix. It is now well accepted that this mechanosensitivity can be driven in part by the elastic, cell-contractility-induced deformations of protein molecules that form the adhesion, [Nicolas et al., 2004]. As a consequence, the formation of bonds promotes the reinforcement of the connexion to the wall. Another way to see the reinforcement is that it results from the cooperation between the clustered adhesion proteins located on the cell or on the wall. If there is only one bond consisting of a single pair of interacting proteins, these proteins quickly become separated after the bond between them breaks. Thus, chances that they will form the bond again are negligible. Now consider a second case, that of an adhesion formed by a large number of bonds (hence involving clustering proteins), the situation is different. When one of the bonds inside the adhesion site breaks, the unbound proteins do not move apart

(as long as this is not the last bond). Therefore, the unbound proteins can rapidly restore the ruptured bond, because they do not need to diffuse over a long distance in a search of a binding partner. Hence, the natural assumption for the model is to impose a reproduction dynamics for each bond and we denote by r the individual reproduction rate.

- Each bond dissociates at rate d. The simplest assumption would be to consider that the average lifetime is independent of the cell velocity but this is not realistic. Indeed, the average lifetime of an adhesion site changes with the applied tension. Moreover, for a given number of bonds, the faster the cell goes, the more force is exerted on each bond and likely existing bonds are to disassemble. This way, a realistic choice is to take d as an increasing function of V_t. We choose this relation to be exponential: $d(V_t) = de^{\alpha V_t} = de^{\alpha(u-\gamma N_t)}$, where d is the unstressed bonds dissociation rate. As the cell velocity is bounded by u, so is the dissociation rate.

Finally to describe the bonds dynamics we will use a birth and death process with the following choice for the rates:

$$c(N_t) = c\mathbb{1}_{u\leq u_*} \text{ with } c>0\,, \quad r(N_t) = r > 0\,, \quad \text{and} \quad d(N_t) = de^{\alpha(u-\gamma N_t)}\,. \tag{1.2}$$

The key point here is that the bond dynamics depends on the instantaneous cell velocity. More elaborate dependence could be analyzed (see e.g Milišić and Oelz [2011]; Milisic and Oelz [2015]), in particular involving age dependences to model the bond elasticity (see Grec et al. [2012]), but we choose to keep a minimal set of parameters, as for simplicity as for the sake of clarity.

1.3 Mathematical properties and numerical simulations

In this section we consider general rates and we derive mathematical properties of the discrete stochastic process. We first study the well-posedness character and the infinitesimal generator. Then, we introduce a trajectorial representation for this process. This allows to deduce some moment and martingale properties. Finally we present numerical simulations of the discrete model.

1.3.1 A population approach

Let $(\Omega, \mathcal{F}, \mathbb{P})$ be a probability space. Denote $\mathbb{D}(\mathbb{R}_+, \mathbb{R}_+)$ the Skorohod space of càdàg functions from $\mathbb{R}_+$ to $\mathbb{R}_+$. We consider the following hypothesis:

Hypothesis 1. *There exist positive constants $\overline{C}$, $\overline{R}$, $\overline{D}$ such that*

$$\forall n \in \mathbb{N}_+, \quad 0 \leq c(n) \leq \overline{C}, \quad 0 \leq r(n) \leq \overline{R} \quad \textit{and} \quad 0 \leq d(n) \leq \overline{D}.$$

We are interested in the following dynamics:

$$n \mapsto \begin{cases} n+1 & \text{at rate } \lambda(n) = c(n) + r(n)n\,, \\ n-1 & \text{at rate } \mu(n) = d(n)n\,, \end{cases}$$

together with hypothesis 1, and λ and μ are defined on $\mathbb{N}$. As a consequence, we can write

$$0 \leq \lambda(n) \leq \overline{C} + \overline{R}n\,, \quad \text{and} \quad 0 \leq \mu(n) \leq \overline{D}n\,.$$

Proposition 2 (Well-posedness, infinitesimal generator)**.** *The Markovian jump process* $(N_t)_{t\geq 0}$ *defined by the transitions above is well defined on* $\mathbb{R}_+$*, and its infinitesimal generator* $(Q_{i,j})_{(i,j)\in\mathbb{N}^2}$ *writes*

$$Q_{i,i+1} = \lambda(i)\,, \quad Q_{i,i-1} = \mu(i)\,, \quad Q_{i,i} = -(\lambda(i)+\mu(i))\,, \quad Q_{i,j} = 0 \text{ otherwise.} \tag{1.3}$$

Proof. This is a classical result that can be found e.g in Bansaye and Méléard [2015]. □

1.3.2 Trajectorial representation

We introduce here a stochastic differential equation for $(N_t)_t$ driven by a Poisson Point Measure. We will show existence and uniqueness of the solution, and prove that it follows the dynamics described before.

Let N_0 be an integer-valued random variable, and $M(\mathrm{d}s, \mathrm{d}w)$ an independent Poisson Point Measure on $\mathbb{R}_+^2$, of intensity measure $\mathrm{d}s\,\mathrm{d}w$. Finally, $(\mathcal{F}_t)_{t\geq 0}$ denotes the canonical filtration generated by these objects. Let us construct the $(\mathcal{F}_t)_{t\geq 0}$-adapted càdàg process $(N_t)_{t\geq 0}$ as the solution of the following SDE: $\forall t \geq 0$,

$$N_t = N_0 + \int_0^t \int_{\mathbb{R}_+} \left(\mathbb{1}_{0\leq w\leq \lambda(N_{s^-})} - \mathbb{1}_{\lambda(N_{s^-})<w\leq \lambda(N_{s^-})+\mu(N_{s^-})} \right) M(\mathrm{d}s, \mathrm{d}w)\,. \tag{1.4}$$

This representation is classical (see e.g Champagnat and Méléard [2007]; Fournier and Méléard [2004]). The Poisson jumps related to the measure are accepted or rejected thanks to the indicator functions. The variable w is then used as an acceptance parameter in order to get the desired rates for each event.

Proposition 3 (Existence, uniqueness, moments propagation)**.** *Assume hypothesis 1, and that there exists* $p \geq 1$ *such that* $\mathbb{E}\left[N_0^p\right] < +\infty$*. Then,*

1. $\forall\, T > 0$,
$$\mathbb{E}\left[\sup_{t\in[0,T]} N_t^p\right] < +\infty\,,$$
2. *the process* $(N_t)_t$ *exists and is unique in law.*

Proof. Although the proof is similar to proposition 2.7 in Bansaye and Méléard [2015] we recall it here for clarity. In the following C will denote a positive constant which value can change from line to line. The proof is broken into three steps.

1. We know that $\mathbb{P}-a.s$, for a test function Φ positive and measurable,
$$\begin{aligned}\Phi(N_t) = \Phi(N_0) + \int_0^t \int_{\mathbb{R}_+} \Big[&(\Phi(N_{s^-}+1) - \Phi(N_{s^-})\mathbb{1}_{w\leq\lambda(N_{s^-})} \\ &+(\Phi(N_{s^-}-1) - \Phi(N_{s^-})\mathbb{1}_{\lambda(N_{s^-})\leq w\leq\lambda(N_{s^-})+\mu(N_{s^-})}\Big] M(\mathrm{d}s, \mathrm{d}w)\,,\end{aligned}$$
so that
$$\Phi(N_t) = \Phi(N_0) + \sum_{s\leq t} \Phi(N_{s^-} + (N_s - N_{s^-})) - \Phi(N_{s^-})\,. \tag{1.5}$$
Then, for $\Phi(N_t) = N_t^p$, using equation (1.4), and neglecting the negative death term, we get

$$N_t^p \leq N_0^p + \int_0^t \int_{\mathbb{R}_+} \left((N_{s^-}+1)^p - N_{s^-}^p\right) \mathbb{1}_{0\leq u\leq \lambda(N_{s^-})} M(\mathrm{d}s,\, \mathrm{d}w)\,.$$

For $n \geq 0$, consider the stopping time $\tau_n = \inf_{t\geq 0}\{N_t \geq n\}$. Then, taking expectations,

$$\begin{aligned}\mathbb{E}\left[\sup_{t\in[0,T\wedge\tau_n]} N_t^p\right] &\leq \mathbb{E}[N_0^p] + \mathbb{E}\left[\int_0^{T\wedge\tau_n} \lambda(N_{t^-})\left((N_{t^-}+1)^p - N_{t^-}^p\right)\,\mathrm{d}t\right],\\ &\leq \mathbb{E}[N_0^p] + \mathbb{E}\left[\int_0^{T\wedge\tau_n} C(1+N_{t^-})\left[(N_{t^-}+1)^p - N_{t^-}^p\right]\,\mathrm{d}t\right].\end{aligned}$$

We use now the following lemma, which can be proved by a direct computation:

Lemma 1. *Let $x \in \mathbb{R}_+$, and p a positive integer. Then, there exists a positive constant $C(p)$ such that*

$$(1+x)^p - x^p \leq C(p)(1+x^{p-1})\,.$$

$$\begin{aligned}\mathbb{E}\left[\sup_{t\in[0,T\wedge\tau_N]} N_t^p\right] &\leq \mathbb{E}[N_0^p] + C(p)\mathbb{E}\left[\int_0^{T\wedge\tau_N} (1+N_{t^-})\left(1+N_{t^-}^{p-1}\right)\,\mathrm{d}t\right]\\ &\leq \mathbb{E}[N_0^p] + C(p)\left(T + \int_0^T \mathbb{E}\left[\sup_{u\in[0,t\wedge\tau_N]} N_{u^-}^p\right]\,\mathrm{d}t\right).\end{aligned}$$

We use now the Gronwall inequality together with the assumption on the initial term to get a partial result.

Let us now prove that $\lim_{n\to+\infty}\tau_n = +\infty\ \mathbb{P}-a.s$: if not, there exists $T^* < +\infty$ such that $\mathbb{P}\left(\sup_n \tau_n < T^*\right) > 0$. Then, by the Markov inequality, for all $n \in \mathbb{N}$, the following inequalities hold true:

$$\begin{aligned}\mathbb{E}\left[\sup_{t\in[0,T^*\wedge\tau_n]} N_t^p\right] &\geq \mathbb{P}\left(\sup_{t\in[0,T^*\wedge\tau_n]} N_t^p \geq n^p\right) n^p\\ &\geq \mathbb{P}\left(\tau_n < T^*\right) n^p\\ &\geq \underbrace{\mathbb{P}\left(\sup_n \tau_n < T^*\right)}_{>0} n^p\,,\end{aligned}$$

which contradicts the previous inequality since $\mathbb{E}\left[\sup_{t\in[0,T\wedge\tau_N]} N_t^p\right]$ was bounded independantly of n.

Finally, by the Fatou inequality:

$$\mathbb{E}\left[\sup_{t\in[0,T]} N_t^p\right] = \mathbb{E}\left[\liminf_{n\to+\infty}\sup_{t\in[0,T\wedge\tau_n]} N_t^p\right] \leq \liminf_{n\to+\infty}\mathbb{E}\left[\sup_{t\in[0,T\wedge\tau_n]} N_t^p\right] \leq C(p,T) < +\infty\,.$$

2. Let $T_0 = 0$ be the first time of event, and $t \in \mathbb{R}_+$. Then, the global jump rate of N_t is smaller than $\overline{C} + (\overline{R} + \overline{D})N_t \leq C(1 + N_t)$. One can $\mathbb{P} - a.s$ define the sequence $(T_k)_{k\in\mathbb{N}^*}$ of jumping times, as well as $T_\infty := \lim_{k\to+\infty} T_k$. By definition, the process $(N_t)_t$ can be inductively constructed on $[0, T_\infty[$. Showing existence of a solution $(N_t)_{t\in\mathbb{R}_+} \in \mathbb{D}(\mathbb{R}_+, \mathbb{R}_+)$ amounts to showing that $\mathbb{P} - a.s$, $T_\infty = +\infty$. From the first step, the population size stays controlled in finite time. As a consequence, the appearance of events can be compared to a Poisson variable, leading to the result.

3. Uniqueness is clear by construction. It is possible to derive a rigorous proof by induction, using the trajectorial representation of the process. We do not detail this here.

□

Now, the process $(N_t)_t$ is classically a Markov process in the Skorohod space $\mathbb{D}(\mathbb{R}_+, \mathbb{R}_+)$ of càdlàg $\mathbb{R}_+$-valued processes, and its infinitesimal generator is defined for all $\Phi : \mathbb{R}_+ \to \mathbb{R}$ measurable bounded by

$$L\Phi(n) = \lambda(n)\left[\Phi(n+1) - \Phi(n)\right] + \mu(n)\left[\Phi(n-1) - \Phi(n)\right] . \tag{1.6}$$

In particular, it corresponds to the dynamics described by (1.3).

1.3.3 Martingale property

Markov processes are usually associated with a semimartingale structure. We prove now that for some $\Phi : \mathbb{R}_+ \to \mathbb{R}$ measurable, there exists a martingale $(M_t)_t$ and a finite variation process $(A_t)_t$ such that for all $t \geq 0$, $\Phi(N_t) = \Phi(N_0) + A_t + M_t$.

Theorem 1. *Assume that there exists $p \geq 2$ such that $\mathbb{E}[(N_0)^p] < +\infty$. Then,*

1. *for all $\Phi : \mathbb{R}_+ \to \mathbb{R}$ measurable, for which there exists C such that for all $N \in \mathbb{R}_+$, $|\Phi(N)| + |L\Phi(N)| \leq C(1 + N^p)$,*

$$\Phi(N_t) - \Phi(N_0) - \int_0^t L\Phi(N_s)\,\mathrm{d}s \tag{1.7}$$

is a càdlàg $(\mathcal{F}_t)_{t\geq 0}$-martingale starting from 0.

2. *This applies in particular to functions $\Phi : N \mapsto N^q$, for $0 \leq q \leq p$.*

As a consequence, the $\mathbb{R}$-valued process $(M_t)_{t\geq 0}$ defined by

$$M_t = N_t - N_0 - \int_0^t (\lambda(N_s) - \mu(N_s))\,\mathrm{d}s \tag{1.8}$$

is a càdlàg square-integrable martingale starting from 0 and of quadratic variation

$$\langle M\rangle_t = \int_0^t (\lambda(N_s) + \mu(N_s))\ \mathrm{d}s\,. \tag{1.9}$$

Proof of Theorem 1. 1. This is a direct consequence of Dynkin's theorem combined with the integrability of each term.

2. Take $N \in \mathbb{R}_+$ and $\Phi(N) = N^q$ for $0 \leq q \leq p$. Then,

$$|\Phi(N)| + |L\Phi(N)| \leq N^q + (\overline{C} + \overline{R}N)\left|(N+1)^q - N^q\right| + \overline{D}N\left|(N-1)^q - N^q\right| .$$

Now notice that as $|(N+1)^q - N^q| \leq C(1+N^{q-1})$ and $|(N-1)^q - N^q| \leq C(1+N^{q-1})$,

$$|\Phi(N)| + |L\Phi(N)| \leq C(1+N^q) .$$

3. Let us now prove the semimartingale formulation. We first notice that expression (1.8) comes from (1.7) for $\Phi_1(N) := N$. Now, let us compute the quadratic variation of this martingale.

   → As a first step, compute the Doob decomposition of $\Phi(N_t) := N_t^2$ using (1.7). Notice that

$$(N+1)^2 - N^2 = 2N+1, \quad (N-1)^2 - N^2 = -2N+1 .$$

   Hence we can write

$$L\Phi(N) \quad = \quad [\lambda(N) + \mu(N)] + 2N\left[\lambda(N) - \mu(N)\right] .$$

   By point 2, we have

$$N_t^2 - N_0^2 - \int_0^t \lambda(N_s) + \mu(N_s) + 2N_s\left[\lambda(N_s) - \mu(N_s)\right] \mathrm{d}s$$

   is a càdlàg martingale starting from 0.

   → Now, applying Itô 's formula to equation (1.8) leads to another decomposition that involves the quadratic variation of $(M)_t$:

$$N_t^2 - N_0^2 - \int_0^t 2N_s\left[\lambda(N_s) - \mu(N_s)\right] \mathrm{d}s - < M >_t$$

   is a martingale. From uniqueness of such a decomposition, we find that

$$< M >_t = \int_0^t \lambda(N_s) + \mu(N_s)\, \mathrm{d}s ,$$

   that is exactly equation (1.9).

□

1.3.4 Moment equation

Let us now investigate the mean path of this process. Using the martingale formulation, we can write

$$\mathbb{E}\left[N_t\right] = \mathbb{E}\left[N_0\right] + \int_0^t \mathbb{E}\left[c(N_s) + (r(N_s) - d(N_s))N_s\right] \mathrm{d}s .$$

It is clear that with the choice of $d(N_t) = de^{\alpha(u-\gamma N_t)}$ (with $N_t \leq u/\gamma$ to ensure the model validity), the resulting nonlinearity would prevent the closure of the previous equation.

In the particular case where $c(N_s) = c$, $r(N_s) = r$ and $d(N_s) = d$, we get $\mathbb{E}[N_t] = \mathbb{E}[N_0] + ct + (r-d)\int_0^t \mathbb{E}[N_s]\,\mathrm{d}s$, leading to

$$\mathbb{E}[N_t] = \begin{cases} \mathbb{E}[N_0] + ct & \text{if } r = d, \\ \mathbb{E}[N_0]e^{(r-d)t} + \frac{c}{r-d}\left(e^{(r-d)t} - 1\right) & \text{otherwise.} \end{cases}$$

At steady state, one finds the steady states

$$\mathbb{E}[N]_\infty := \begin{cases} \frac{c}{d-r} & \text{for } r < d, \\ +\infty & \text{otherwise, and the value } n^* \text{ for which the velocity reaches zero is attained.} \end{cases}$$

For the velocity,

$$\mathbb{E}[V]_\infty := \begin{cases} u - \gamma\frac{c}{d-r} & \text{for } r < d, \\ -\infty & \text{otherwise, that is to say the velocity reaches 0.} \end{cases}$$

These results show that it is already possible to get a mean dichotomy behaviour based on the bonds dynamics in the discrete case. In order to get deeper analytical results, we will derive a continuous limiting stochastic process associated to this dynamics.

1.3.5 Numerical Simulations

Algorithm

The bonds population model being a markovian jump process, it is piecewise constant, and the evolution of the process depends only on the present state. Its simulation is therefore straightforward. Consider the population size at time T_k (N_{T_k}). Then,

- the global jump rate is $\varsigma_k = \lambda(N_{T_k}) + \mu(N_{T_k})$. This means that the time before the next event is a random variable following an exponential law of parameter ς_k. A realization of this law gives T_{k+1}.
- Next, we have to determine the type of event occurring: a new bond is created with probability $\frac{\lambda(N_{T_k})}{\varsigma_k}$, while a bond disassemble with probability $\frac{\mu(N_{T_k})}{\varsigma_k}$. Hence, we can compute $N_{T_{k+1}}$.

It is now sufficient to reiterate this procedure to get the time evolution of the process.

Numerical results

Some numerical simulations of the process are displayed in figure 1.2. It is observed that the velocity either shrinks to zero or remains close to u.

1.4 Continuous bonds approximations

In this part we separate the scale of the bond dynamics from the one of the cell motion, since the number of bonds is very large, and the binding dynamics very fast compared to the cell displacement. For that purpose, we let the number of bonds grow to infinity while the individual contribution to the adhesion force shrinks to zero, so that the global adhesive force keeps its range. We also renormalize the dynamics of the bond turnover and this leads to different limiting continuous models.

1.4.1 Renormalization

Let $K \geq 1$ be a parameter scaling the number of the discrete adhesions we consider. We assume that $\frac{1}{K}$ scales the force generated by each one. This amounts to looking at the adhesion sites at a smaller and smaller scale. Moreover, we assume that the dynamics gets faster and faster. Hence, we consider now K-dependent rates c^K, r^K, and d^K as functions of the corresponding process N_t^K defined by equation (1.4). We define the renormalized process $(X_t^K)_t \in \mathbb{D}(\mathbb{R}_+, \mathbb{R}_+)$ by

$$X_t^K = \frac{1}{K} N_t^K \in \frac{1}{K}\mathbb{N}. \tag{1.10}$$

In this subsection, we work with K fixed, and assume that the rates satisfy the following boundedness and continuity hypothesis:

Hypothesis 2. *For all $N \in \mathbb{R}_+$, the following inequalities hold true*

$$0 \leq c^K(N) \leq K\overline{C}, \quad 0 \leq r^K(N) \leq \overline{R} + Ka \quad \text{and} \quad 0 \leq d^K(N) \leq \overline{D} + Ka,$$

where $\overline{C}$, $\overline{R}$, $\overline{D}$ and a are positive constants. In addition the rates $N \mapsto c^K(N)$ (resp. $r^K(N)$, resp. $d^K(N)$) are continuous. The global demographic parameters write

$$\lambda^K(N) = c^K(N) + r^K(N)N\,, \quad \mu^K(N) = d^K(N)N\,.$$

Markov property By construction, $(X_t^K)_{t\geq 0}$ is also a Markov process, and for $\Phi : \mathbb{R}_+ \to \mathbb{R}$ measurable bounded, its infinitesimal generator writes

$$L^K\Phi(X) = \lambda^K(KX)\left[\Phi(X + \frac{1}{K}) - \Phi(X)\right] + \mu^K(KX)\left[\Phi(X - \frac{1}{K}) - \Phi(X)\right]. \tag{1.11}$$

As before, for fixed K, we can prove that $(X_t^K)_{t\geq 0}$ satisfies the following proposition.

Proposition 4 (Moment, martingale property)**.** *Assume that there exists $p \geq 2$ such that $\mathbb{E}\left[(X_0^K)^p\right] < +\infty$. Then, under hypothesis 2, one has*

1. *$\forall\, T > 0$,*
$$\mathbb{E}\left[\sup_{t\in[0,T]} (X_t^K)^p\right] < +\infty, \tag{1.12}$$
2. *for all measurable function $\Phi : \mathbb{R}_+ \to \mathbb{R}$ for which there exists C such that $\forall X \in \mathbb{R}_+$, $|\Phi(X)| + |L^K\Phi(X)| \leq C(1 + X^p)$,*
$$\Phi(X_t^K) - \Phi(X_0^K) - \int_0^t L^K\Phi(X_s^K)\,\mathrm{d}s \tag{1.13}$$
is a càdlàg $(\mathcal{F}_t)_{t\geq 0}$-martingale starting from 0.
3. *This applies in particular to functions $\Phi : X \mapsto X^q$, for $0 \leq q \leq p$.*
4. *The process*
$$M_t^K = X_t^K - X_0^K - \int_0^t \frac{1}{K} c^K(KX_s^K) + \left(r^K(KX_s^K) - d^K(KX_s^K)\right) X_s^K\,\mathrm{d}s \tag{1.14}$$
is a càdlàg square-integrable martingale starting from 0 and of quadratic variation
$$\left\langle M^K \right\rangle_t = \frac{1}{K}\int_0^t \left\{\frac{1}{K}c^K(KX_s^K) + (r^K(KX_s^K) + d^K(KX_s^K))X_s^K\right\}\mathrm{d}s\,. \tag{1.15}$$

The semimartingale formulation (1.14) allows us to study the convergence of $(X_t^K)_t$ for $K \to +\infty$ in $\mathbb{D}(\mathbb{R}_+, \mathbb{R}_+)$ for different renormalizations of the adhesive dynamics.

1.4.2 Deterministic limits

In this section, we study two sets of parameters leading to deterministic limits. The first one consists in only accelerating the creation rate. In the second one, the whole dynamics is unchanged. For both cases, we consider an additional assumption on the Lipschitz-continuity of the rates.

Hypothesis 3. *The rates are Lipschitz-continuous and satisfy:*

$$0 \leq c^K(KX_t^K) \leq K\overline{C}, \quad r^K(KX_t^K) \leq \overline{R} \quad \text{and} \quad d^K(KX_t^K) \leq \overline{D}.$$

In this context, we can prove the following K-uniform moment property:

Proposition 5. *Assume hypothesis 3 and that there exists $p \geq 1$ such that $\sup_{K>0} \mathbb{E}\left[(X_0^K)^p\right] < +\infty$, then*

$$\forall\, T > 0,\ \sup_{K>0} \mathbb{E}\left[\sup_{t\in[0,T]} (X_t^K)^p\right] < +\infty\,. \tag{1.16}$$

Proof. The proof is similar to the one for proposition (3). Indeed, in equation (1.14), the coefficient $\frac{1}{K}$ in the creation term compensates for the bound on c^K, and the new bound on r^K is K-independent. As a consequence, taking the supremum of the estimate over $\{K > 0\}$ leads to the result. □

Accelerated creation

Let us consider the following set of parameters:

$$c^K(KX_t^K) = Kc(X_t^K), \quad r^K(KX_t^K) = r(X_t^K) \quad \text{and} \quad d^K(KX_t^K) = d(X_t^K),$$

where hypothesis 3 is fulfilled. In other words, while we consider an increasing number of smaller adhesions, only their creation is intensified, while their positive effect on the adhesion and their lifetime stay the same.

From the modeling viewpoint such an assumption amounts to consider an increasing number of smaller adhesions, each of them involving a few number of proteins on each side (wall and cell). Note that this corresponds to an intermediate scale (the cell scale) since the clustering process in the adhesion sites is not described. This latter process will be described below, see paragraph 1.4.3, when the individual dynamics of the bonds will also be accelerated.

We will prove the following convergence theorem:

Theorem 2. *Assume hypothesis 3. If $X_0^K \underset{K\to+\infty}{\longrightarrow} n_0 \in \mathbb{R}_+$ in probability, and if*

$$\sup_{K>0} \mathbb{E}\left[(X_0^K)^2\right] < +\infty\,, \tag{1.17}$$

then, for $T > 0$, $(X^K)_{K>0}$ converges in law in $\mathbb{D}([0,T],\mathbb{R}_+)$ to the unique continuous function $n \in \mathcal{C}([0,T],\mathbb{R}_+)$ solution to

$$n(t) = n_0 + \int_0^t c(n(s)) + (r(n(s)) - d(n(s)))n(s)\,\mathrm{d}s\,. \tag{1.18}$$

Remark 1. *By the Gronwall lemma, one has*

$$\sup_{t\in[0,T]} n(t) \quad \leq \quad (n_0 + \overline{c}T)e^{\overline{r}T} < +\infty\,,$$

showing that the global density stays finite in finite time.

Proof of theorem 2. The proof is similar to the one in Ethier and Kurtz [2009]; Joffe and Metivier [1986]. It is based on a compactness-uniqueness argument. First, the tightness of the sequence of laws $(Q^K)_K$ of $(X^K)_K$ is proved. Then, we establish that for any accumulation point Q, a process X of law Q is almost surely continuous, and solution to equation (1.18). Finally, the convergence is proved by showing uniqueness in $\mathcal{C}([0,T],\mathbb{R}_+)$ of the solution to (1.18). Throughout this proof, C will denote a constant that may change during computations, and $C(T)$ a constant depending on T.

Tightness of $(Q^K)_K$: We use the Aldous and Rebolledo criterion [Aldous, 1989] as detailled in Joffe and Metivier [1986]. Let us denote $(A^K_t)_{t\geq 0}$ the finite variation process related to the semimartingale $(X^K_t)_{t\geq 0}$:

$$A^K_t \;=\; X^K_0 + \frac{1}{K}\int_0^t c^K(KX^K_s)\,\mathrm{d}s + \int_0^t \left(r^K(KX^K_s) - d^K(KX^K_s)\right) X^K_s\,\mathrm{d}s\,.$$

We need to prove that for all $T>0$ the following inequalities hold true:

1. $$\sup_{K>0}\mathbb{E}\left[\sup_{t\in[0,T]}\left|X^K_t\right|\right] < +\infty.$$

2. $\forall\varepsilon>0,\ \forall\eta>0,\ \exists\delta>0,\ K_0\in\mathbb{N}^*$ such that for all sequence $(\sigma_K,\tau_K)_K$ of stopping times with $\sigma_K\leq\tau_K\leq T$,

   (a) $$\sup_{K\geq K_0}\mathbb{P}\left(\left|< M^K >_{\tau_K} - < M^K >_{\sigma_K}\right|\geq\eta,\ \tau_K\leq\sigma_K+\delta\right)\leq\varepsilon,$$

   (b) $$\sup_{K\geq K_0}\mathbb{P}\left(\left|A^K_{\tau_K} - A^K_{\sigma_K}\right|\geq\eta,\ \tau_K\leq\sigma_K+\delta\right)\leq\varepsilon\,.$$

1. The first point is straightforward from proposition 5 together with the assumption (1.17) made on the initial condition.

2. Take $T>0$, $\varepsilon>0$, $\eta>0$ and a sequence of pairs of stopping times $(\sigma_K,\tau_K)_K$ such that $\sigma_K\leq\tau_K\leq T$ and $\tau_K\leq\sigma_K+\delta$.

   (a) From equation (1.15) together with the moment proposition 5, we obtain

   $$\mathbb{E}\left[\left|< M^K >_{\tau_K} - < M^K >_{\sigma_K}\right|\right] \;\leq\; \frac{C}{K}\left(\delta + \mathbb{E}\left[\left|\int_{\sigma_K}^{\tau_K} X^K_s\,\mathrm{d}s\right|\right]\right) \leq \frac{C(T)}{K}\delta\,.$$

   Hence, using the Markov inequality, for all $\varepsilon>0$, for all $\eta>0$, there exists δ and K_0 such that 2.a) is satisfied.

   (b) Similarly, by proposition 5,

   $$\mathbb{E}\left[\left|A^K_{\tau_K} - A^K_{\sigma_K}\right|\right] \;\leq\; C\delta\left(1+\mathbb{E}[\sup_{[0,T]}X^K_t]\right)\leq C(T)\delta\,.$$

   As before, we conclude by the Markov inequality.

This proves that the sequence $(Q^K)_K$ is uniformly tight in $\mathcal{L}(\mathbb{D}([0,T],\mathbb{R}_+))$.

Identification of the limit : From the Prokhorov theorem we deduce the relative compactness of the family of laws $(Q^K)_K$ on $\mathbb{D}([0,T],\mathbb{R}_+)$. Consider a convergent subsequence, and denote by Q its limit. Next, consider a corresponding sequence of processes $(X^K)_K$ in $\mathbb{D}([0,T],\mathbb{R}_+)$ converging in distribution to $n \in \mathbb{D}([0,T],\mathbb{R}_+)$ of law Q. First, for all $K>0$, by construction, we know that the jumps of $(X_t^K)_t$ are of the form $1/K$. As a consequence, almost surely, one has

$$\sup_{t\in[0,T]} \left|X_t^K - X_{t^-}^K\right| \leq \frac{1}{K},$$

and as $X \mapsto \sup_{t\in[0,T]} |X_t - X_{t^-}|$ is continuous from $\mathbb{D}([0,T],\mathbb{R}_+)$ to $\mathbb{R}_+$, any process of law Q is almost surely strongly continuous.

Now, let us establish that the process n is solution to equation (1.18). Using the moment proposition 5, we deduce that $\mathbb{E}\left[\sup_{[0,T]} n_t\right] < +\infty$, which almost surely leads to

$$\sup_{[0,T]} n_t \ < +\infty\,. \tag{1.19}$$

For $T>0$, take $t \leq T$ and $n \in \mathcal{C}([0,T],\mathbb{R}_+)$. Denote

$$\Psi_t(n) \ := \ n_t - n_0 - \int_0^t \{c(n_s) + (r(n_s) - d(n_s))n_s\}\, \mathrm{d}s\,.$$

We have to prove that for all $t \leq T$, $\mathbb{E}_Q\left[|\Psi_t(n)|\right] = 0$. For that purpose, we see that

1. Since $\mathbb{E}\left[\left|\Psi_t(X^K)\right|\right] = \mathbb{E}\left[\left|M_t^K\right|\right]$, we have

$$\mathbb{E}\left[\left|\Psi_t(X^K)\right|\right]^2 \ \leq \ \mathbb{E}\left[\left|M_t^K\right|^2\right] = \mathbb{E}\left[\left\langle M^K\right\rangle_t\right] \leq C\frac{T}{K}\left(1 + \mathbb{E}\left[\sup_{[0,T]} X_t^K\right]\right),$$

   and recalling the moment property given in proposition 5, it follows that for all $t\in[0,T]$, $\lim_{K\to+\infty}\mathbb{E}\left[\left|\Psi_t(X^K)\right|\right] = 0$.

2. (a) Recalling that n is almost surely continuous and that the parameter rates are continuous, it follows that Ψ_t is continuous in n, and that $\lim_K \Psi_t(X^K) = \Psi_t(n)$ in distribution.

   (b) Moreover, the inequality

$$|\Psi_t(n)| \leq C(T)(1 + \sup_{[0,T]} n_s)$$

   together with proposition 5 yield that $\left(\Psi_t(X^K)\right)_K$ is uniformly integrable. Hence,

$$\lim_{K\to+\infty}\mathbb{E}\left[\left|\Psi_t(X^K)\right|\right] = \mathbb{E}\left[\left|\lim_{K\to+\infty}\Psi_t(X^K)\right|\right] = \mathbb{E}\left[|\Psi_t(n)|\right] = 0.$$

Finally, uniqueness follows from the Lipschitz-continuous hypothesis 3 again. □

Non accelerated dynamics

As mentioned before, we can also choose not to accelerate any part of the dynamics. From the modeling viewpoint such an assumption is relevant when the cell velocity is high. In such a case newly formed bonds are instantaneously broken. Note that this situation was already described in the previous section when $u > u_*$. More precisely, consider the following rates:

$$\boldsymbol{c^K(N_t^K) = c(X_t^K)} \quad \boldsymbol{r^K(N_t^K) = r(X_t^K)} \quad \boldsymbol{d^K(N_t^K) = d(X_t^K)}$$

We can prove the following result:

Theorem 3. *Under hypothesis 3, if* $X_0^K \underset{K\to+\infty}{\longrightarrow} n_0$ *in probability on* $\mathbb{R}_+$ *for some deterministic* n_0*, and*

$$\sup_{K>0} \mathbb{E}\left[(X_0^K)^2\right] < +\infty, \tag{1.20}$$

then $(X^K)_{K>0}$ *converges in law in* $\mathbb{D}([0,T],\mathbb{R}_+)$ *to the unique* $n \in \mathcal{C}([0,T],\mathbb{R}_+)$ *such that*

$$n(t) = n_0 + \int_0^t (r(n(s)) - d(n(s)))n(s)\,\mathrm{d}s, \tag{1.21}$$

The proof is exactly the same as in theorem (1.4.2).

Analysis of the continuous deterministic equation obtained when creation is accelerated

Let us recall that when creation is accelerated the limiting equation is:

$$n(t) = n_0 + \int_0^t \Big(c(n(s)) + (r(n(s)) - d(n(s)))\,n(s)\Big)\,\mathrm{d}s\,, \tag{1.22}$$

where

$$c(n) = c\mathbb{1}_{u<u_*} \text{ with } c>0\,, \quad r(n) = r > 0 \quad \text{and} \quad d(n) = de^{\alpha(u-\gamma n)}\,. \tag{1.23}$$

The equation satisfied by the cell velocity is

$$v(t) = (u - \gamma n(t))_+\,. \tag{1.24}$$

Let us define the function F by: $F(n) = c\mathbb{1}_{u\le u_*} + \left(r - de^{\alpha(u-\gamma n)}\right) n$.

Proposition 6. *Let* $n_0 \in [0, n^*]$*, where* n^* *corresponds to number of bonds for which the cell velocity vanishes. Assume that the rates are given by (1.23), then the stationary state* n_∞ *of (1.22) satisfies*

1. *If* $u > u_*$*, then*
   (a) *If* $u > \frac{1}{\alpha}\ln(\frac{r}{d})$*, then there are two stationary states* $n_\infty^1 = 0$ *and* $n_\infty^2 = \frac{u}{\gamma} - \frac{1}{\alpha\gamma}\ln(\frac{r}{d}) > 0$*. The smallest is stable and the largest is unstable.*
   (b) *Otherwise, then* $n_\infty = 0$*.*
2. *If* $u \le u_*$*, then*
   (a) *If* $u \le \frac{1}{\alpha}\ln\left(\frac{r}{d}\right)$*, then* $n_\infty = +\infty$*.*

(b) *If* $u > \frac{1}{\alpha}\ln\left(\frac{r}{d}\right)$, *then there exists a unique* $0 < \bar{n} < \frac{2}{\alpha\gamma}$ *such that* $F'(\bar{n}) = 0$ *and*
   i. *If* $F(\bar{n}) > 0$, *then* $n_\infty = +\infty$.
   ii. *If* $F(\bar{n}) = 0$, *then* $\bar{n}$ *is the unique stationary solution.*
   iii. *If* $F(\bar{n}) < 0$, *then there exists two stationary solutions* n_∞^1 *and* n_∞^2, *such that* $0 < n_\infty^1 < \bar{n} < n_\infty^2 < +\infty$, *the smallest being stable and the largest unstable.*

Proof. The case $u > u_*$ follows from a direct computation. Consider the case where $u \leq u_*$, then one has

$$n'(t) = c + \left(r - de^{\alpha(u-\gamma n(t))}\right) n(t) = F(n(t))\,. \tag{1.25}$$

A quick computation shows that

$$\begin{aligned} F'(n) &= r + d\,(\alpha\gamma n - 1)\, e^{\alpha(u-\gamma n)}\,, \\ F''(n) &= \alpha\gamma d\,(2 - \alpha\gamma n)\, e^{\alpha(u-\gamma n)}\,. \end{aligned}$$

We can study the sign of $F'(n)$ and get the following variation table:

n	0		$\frac{2}{\alpha\gamma}$		$+\infty$
$F''(n)$		$+$	0	$-$	
$F'(n)$	$r - de^{\alpha u}$	↗	$F'(\frac{2}{\alpha\gamma}) > 0$	↘	r

As a consequence,

- If $u \leq \frac{1}{\alpha}\ln\left(\frac{r}{d}\right)$, then $\forall n \in \mathbb{R}_+$, $F(n) \geq c > 0$, hence $n_\infty = +\infty$.
- If $u > \frac{1}{\alpha}\ln\left(\frac{r}{d}\right)$, then there exists a unique $\bar{n} > 0$ such that $F'(\bar{n}) = 0$. Since $\bar{n} < \frac{2}{\alpha\gamma}$, we obtain the following variation table from which the result follows:

n	0		$\bar{n} < \frac{2}{\alpha\gamma}$		$+\infty$
$F'(n)$		$-$	0	$+$	
$F(n)$	$c > 0$	↘	$F(\bar{n})$	↗	$+\infty$

Notice that since $u > \frac{1}{\alpha}\ln\left(\frac{r}{d}\right) \Leftrightarrow de^{\alpha u} > r$, both behaviours arise according to the comparison between the reproduction and death rates. □

Let us comment on these results. First of all, not surprisingly, our model successfully predicts the threshold wall shear stress above which nor capture nor rolling does occur. This is due to the regulation by shear of the number of bonds: the number of bonds falls below one. Moreover, the model predicts existence of cell adhesion bistability, which results from the competition between the two processes taking place in the cell-wall contact area: bond formation and rupture. Finally, the model predicts stationary adhesion which is observed during the leukocytes extravasation.

Remark 2. *Note that if* $u_* \geq u > \frac{1}{\alpha}\ln\left(\frac{r}{d}\right)$ *the three cases described in the proposition above may occur. Indeed, consider the particular case where* $d > r$ *and* $u = \frac{1-\frac{r}{d}}{\alpha}$, *then* $\bar{n} = \frac{u}{\gamma}$ *and* $F(\bar{n}) = c - \frac{(d-r)^2}{\alpha d\gamma}$ *whose sign depends on the value of* c.

1.4.3 Accelerated demography

In this section, we accelerate also the individual dynamics, so that the smaller the scale of adhesion we consider, the faster the dynamics is. From the modeling viewpoint such an assumption amounts to consider an increasing number of smaller adhesions, each of them involving a large number of proteins on each side (wall and cell), so that the attachment/detachment dynamics is faster. Note that this corresponds to the description of the clustering process in the adhesion sites.

For that purpose, let us introduce the parameter $0 < \eta \leq 1$ related to the speed of acceleration compared to the scale reduction. Now, for $K > 0$, and $a > 0$, consider

$$c^K(KX_t^K) = Kc(X_t^K), \quad r^K(KX_t^K) = r(X_t^K) + K^\eta a, \quad d^K(KX_t^K) = d(X_t^K) + K^\eta a.$$

The same acceleration for reproduction and death events permits to keep the same bounded individual growth rate $r^K - d^K = r - d$. This way, even if conceptually, each adhesion unity reproduces and dies infinitely faster, its contribution the the global adhesion growth remains the same. The martingale property (1.14) now writes

$$M_t^K = X_t^K - X_0^K - \int_0^t c(X_s^K)\,\mathrm{d}s - \int_0^t \left(r(X_s^K) - d(X_s^K)\right) X_s^K\,\mathrm{d}s \tag{1.26}$$

is a càdlàg square-integrable martingale starting from 0 and of quadratic variation

$$\left\langle M^K \right\rangle_t = \frac{1}{\mathbf{K}} \int_0^t \left\{c(X_s^K) + (r(X_s^K) + d(X_s^K) + 2K^\eta a)X_s^K\right\}\,\mathrm{d}s. \tag{1.27}$$

For either $0 < \eta < 1$ or $\eta = 1$, deterministic or stochastic limiting equations will be obtained at the limit. In all cases, we will need moment properties established below. First, we prove a moment estimate uniform in time and K. The method developped in proposition 5 can't be used anymore, as the bound on r is now K-dependent.

Proposition 7. *Consider the process $(X_t^K)_{t\geq 0}$ defined in equation (1.10). Under hypothesis 2, for $\eta = 1$, and if $\sup_{K>0} \mathbb{E}[(X_0^K)^2] < +\infty$, then for $T < +\infty$,*

$$\sup_K \sup_{t\in[0,T]} \mathbb{E}[(X_t^K)^2] < +\infty. \tag{1.28}$$

Proof. Let us use equation (1.13) for $\Phi(X) = X^2$. We obtain

$$\begin{aligned} L^K\Phi(X_s^K) &= K\left\{c(X_s^K) + (r(X_s^K) + Ka)X_s^K\right\} \overbrace{\left[\left(X_s^K + \frac{1}{K}\right)^2 - (X_s^K)^2\right]}^{=:B_+} \\ &+ K(d(X_s^K) + Ka)X_s^K \underbrace{\left[\left((X_s^K - \frac{1}{K}\right)^2 - (X_s^K)^2\right]}_{=:B_-}. \end{aligned}$$

Then,

$$L^K\Phi(X_s^K) = K(c(X_s^K) + X_s^K r(X_s^K))B_+ + KX_s^K d(X_s^K)B_- + K^2 a X_s^K (B_+ + B_-).$$

Now, as $B_- \leq 0$, we can neglect the second death terms and study an inequality. Moreover, we compute

$$B_+ = \frac{2}{K}X_s^K + \frac{1}{K^2}, \quad B_- = -\frac{2}{K}X_s^K + \frac{1}{K^2}, \quad B_+ + B_- = \frac{2}{K^2},$$

leading to

$$L^K\Phi(X_s^K) \leq \left(\overline{C} + \overline{R}X_s^K\right)\left(2X_s^K + \frac{1}{K}\right) + 2aX_s^K \leq C\left(1 + X_s^K + (X_s^K)^2\right).$$

Hence, we can deduce from (1.13) that

$$\begin{aligned}\mathbb{E}[(X_t^K)^2] &= \mathbb{E}[(X_0^K)^2] + \int_0^t \mathbb{E}[L^K\Phi(X_s^K)]\,\mathrm{d}s \\ &\leq \mathbb{E}[(X_0^K)^2] + C\left(t + \int_0^t \mathbb{E}[X_s^K] + \mathbb{E}[(X_s^K)^2]\,\mathrm{d}s\right).\end{aligned}$$

Finally, since $\mathbb{E}[X_s^K] \leq C(1 + \mathbb{E}[(X_t^K)^2])$, by the Gronwall lemma, there exists a constant $C(t)$ such that $\mathbb{E}[(X_t^K)^2] \leq C(t)$, hence

$$\sup_{K>0}\sup_{[0,T]} \mathbb{E}[(X_t^K)^2] < +\infty.$$

□

We show now a K-uniform control on $\mathbb{E}\left[\sup_{t\in[0,T]} X_t^K\right]$.

Proposition 8. *Consider the process $(X_t^K)_{t\geq 0}$ defined in equation (1.10) for all $K > 0$. Assume that $\sup_{K>0}\mathbb{E}[(X_0^K)^2] < +\infty$. Then, for $T < +\infty$,*

$$\sup_K \mathbb{E}\left[\sup_{t\in[0,T]} X_t^K\right] < +\infty. \tag{1.29}$$

Proof. Recall (1.14) that rewrites

$$X_t^K = M_t^K + X_0^K + \int_0^t c(X_s^K) + \left(r(X_s^K) - d(X_s^K)\right)X_s^K\,\mathrm{d}s.$$

As a consequence,

$$\sup_{t\in[0,T]} X_t^K \leq \sup_{t\in[0,T]} |M_t^K| + X_0^K + \overline{C}T + \overline{R}\int_0^t X_s^K\,\mathrm{d}s.$$

Now, by the Burkholder-Davis-Gundy inequality,

$$\mathbb{E}\left[\sup_{t\in[0,T]} |M_t^K|\right]^2 \leq \mathbb{E}\left[\sup_{t\in[0,T]} |M_t^K|^2\right] \leq 4\mathbb{E}\left[|M_T^K|^2\right] = 4\mathbb{E}\left[\left\langle M^K\right\rangle_T\right],$$

and as $\mathbb{E}[X_0^K] < +\infty$,

$$\mathbb{E}\left[\sup_{t\in[0,T]} X_t^K\right] \leq 2\mathbb{E}\left[\left\langle M^K\right\rangle_T\right]^{1/2} + C(T) + \overline{R}\mathbb{E}\left[\int_0^t X_s^K\,\mathrm{d}s\right].$$

We use (1.15) to get

$$\mathbb{E}[\left\langle M^K\right\rangle_T] \leq \overline{C}T + (\overline{R} + \overline{D} + 2a)\int_0^t \mathbb{E}[X_s^K]\,\mathrm{d}s \leq C(T)$$

thanks to (7). We conclude by using the Gronwall lemma. □

The deterministic case: $0 < \eta < 1$ We consider here the case where the individual dynamics is less accelerated as the scale gets smaller and smaller. As a consequence, the stochastic fluctuations in the adhesion dynamics are not important enough to impact the migration dynamics, and get a deterministic limit. We assume the following:

Hypothesis 4 (Deterministic limit)**.** *For $\overline{C}$, $\overline{R}$, $\overline{D}$ positive constants, consider the positive rates*

$$c^K(KX_t^K) = Kc(X_t^K) \leq K\overline{C}, \quad r^K(KX_t^K) = r(X_t^K) + K^\eta a, \quad d^K(KX_t^K) = d(X_t^K) + K^\eta a,$$

with $r(.) \leq \overline{R}$ and $d(.) \leq \overline{D}$. Moreover, c, r and d are Lipschitz-continuous functions.

Theorem 4. *Under hypothesis 4, if for $K \to +\infty$ the initial measure X_0^K converges in probability on $\mathbb{R}_+$ to a constant n_0, and if*

$$\sup_{K>0} \mathbb{E}\left[(X_0^K)^2\right] < +\infty, \tag{1.30}$$

then $(X^K)_{K>0}$ converges in law in $\mathbb{D}([0,T],\mathbb{R}_+)$ to the unique deterministic function $n \in \mathcal{C}([0,T],\mathbb{R}_+)$ such that

$$n_t = n_0 + \int_0^t \{c(n_s) - (r(n_s) - d(n_s))\, n_s\}\, \mathrm{d}s\,. \tag{1.31}$$

Proof. The proof is similar to the one of theorem 2. Indeed, the only difference is the K^η terms in the reproduction and death terms, but as $\eta < 1$, this doesn't prevent the quadratic variation from going to 0 as K tends to infinity. □

The stochastic case: $\eta = 1$ Now, we study the case where the binding dynamics is accelerated enough so that stochastic fluctuations remain at the limit. We consider now the following hypothesis:

Hypothesis 5 (Stochastic limit)**.** *For $\overline{C}$, $\overline{R}$, $\overline{D}$ positive constants,*

$$c^K(KX_t^K) = Kc(X_t^K) \leq K\overline{C}, \qquad r^K(KX_t^K) = r(X_t^K) + Ka \leq \overline{R} + Ka,$$

$$d^K(kx_t^K) = d(X_t^K) + Ka \leq \overline{D} + Ka$$

Moreover, c, r and d are Lipschitz-continuous.

Theorem 5. *Under hypothesis 5, if for $K \to +\infty$ the initial value X_0^K converges in law to a $\mathbb{R}_+$-valued random variable N_0, with*

$$\sup_{K>0} \mathbb{E}\left[(X_0^K)^2\right] < +\infty, \tag{1.32}$$

then $(X^K)_{K>0}$ converges in law in $\mathbb{D}([0,T],\mathbb{R}_+)$ to the continuous process $N = (N_t)_{t\in[0,T]} \in \mathcal{C}([0,T],\mathbb{R}_+)$ solution of

$$\mathrm{d}N_t = b(N_t)\,\mathrm{d}t + \sigma(N_t)\,\mathrm{d}B_t \tag{1.33}$$

with B_t a Brownian Motion, $b(N_t) = c(N_t) + (r(N_t) - d(N_t))N_t$ and $\sigma(N_t) = \sqrt{2aN_t}$.

Proof. The proof is here again based on a compactness-uniqueness argument: we prove that the sequence of laws $(Q^K)_K$ of the processes $(X^K)_K$ is tight. Then, we identify its limiting values as solutions of (1.33), for which uniqueness is stated.

Uniform tightness of $(Q^K)_K$. As in the proof of theorem 2, denote $(A_t^K)_{t\geq 0}$ the finite variation process related to the semimartingale $(X_t^K)_{t\geq 0}$:

$$A_t^K = X_0^K + \frac{1}{K}\int_0^t c^K(KX_s^K)\,\mathrm{d}s + \int_0^t \left(r^K(KX_s^K) - d^K(KX_s^K)\right) X_s^K\,\mathrm{d}s\,.$$

We need to prove that for all $T>0$ the following inequalities hold true:

1. $$\sup_{K>0}\mathbb{E}\left[\sup_{t\in[0,T]}\left|X_t^K\right|\right] < +\infty.$$
2. $\forall\varepsilon>0,\ \forall\eta>0,\ \exists\delta>0,\ K_0\in\mathbb{N}^*$ such that for all sequence $(\sigma_K,\tau_K)_K$ of stopping times with $\sigma_K\leq\tau_K\leq T$,
   (a) $$\sup_{K\geq K_0}\mathbb{P}\left(\left|< M^K >_{\tau_K} - < M^K >_{\sigma_K}\right|\geq\eta,\ \tau_K\leq\sigma_K+\delta\right)\leq\varepsilon,$$
   (b) $$\sup_{K\geq K_0}\mathbb{P}\left(\left|A^K_{\tau_K} - A^K_{\sigma_K}\right|\geq\eta,\ \tau_K\leq\sigma_K+\delta\right)\leq\varepsilon\,.$$

1. The first point is straightforward from proposition 8 together with the assumption (1.32) made on the initial condition.
2. Take $T>0$, $\varepsilon>0$, $\eta>0$ and a sequence of pairs of stopping times $(\sigma_K,\tau_K)_K$ such that $\sigma_K\leq\tau_K\leq T$ and $\tau_K\leq\sigma_K+\delta$.
   (a) From equation (1.15) together with the moment proposition 8, we obtain
   $$\begin{aligned}\mathbb{E}\left[\left|< M^K >_{\tau_K} - < M^K >_{\sigma_K}\right|\right] &\leq \frac{C}{K}\left(\delta + \mathbb{E}\left[\left|\int_{\sigma_K}^{\tau_K} X_s^K\,\mathrm{d}s\right|\right]\right) + 2a\mathbb{E}\left[\left|\int_{\sigma_K}^{\tau_K} X_s^K\,\mathrm{d}s\right|\right]\\ &\leq C(T)\delta\,.\end{aligned}$$
   Hence, using the Markov inequality, for all $\varepsilon>0$, for all $\eta>0$, there exists δ and K_0 such that 2.a) is satisfied.
   (b) Similarly, by proposition 8,
   $$\mathbb{E}\left[\left|A^K_{\tau_K} - A^K_{\sigma_K}\right|\right] \leq C\delta\left(1+\mathbb{E}[\sup_{[0,T]} X_t^K]\right)\leq C(T)\delta\,.$$
   As before, we conclude by the Markov inequality.

This proves that the sequence $(Q^K)_K$ is uniformly tight in $\mathcal{L}(\mathbb{D}([0,T],\mathbb{R}_+))$.

Identification of the limit Using the Prokhorov theorem, we can consider a convergent subsequence $(Q^K)_K$, and denote Q its limit. Let $(X^K)_K$ be a corresponding sequence of processes in $\mathbb{D}([0,T],\mathbb{R}_+)$ converging in law to $N\in\mathbb{D}([0,T],\mathbb{R}_+)$. As in the proof of 2, we can show that N is almost surely strongly continuous.

Now, we show that if for $Y=(Y_t)_{t\geq 0}\in\mathbb{D}(\mathbb{R}_+,\mathbb{R}_+)$, we write

$$\widetilde{M}_t(Y) = Y_t - Y_0 - \int_0^t \left\{c(Y_s) + \left(r(Y_s) - d(Y_s)\right)Y_s\right\}\,\mathrm{d}s\,, \tag{1.34}$$

then $\widetilde{M}_t(N)$ is a twice-integrable continuous martingale with quadratic variation

$$\left\langle \widetilde{M} \right\rangle_t = 2a \int_0^t Y_s \, \mathrm{d}s. \tag{1.35}$$

First, we show that $\widetilde{M}(N)$ is a martingale. Take $0 \leq s_1 < ... < s_n < s < t$, and $\Phi_1, ..., \Phi_n$ continuous bounded functions from $\mathbb{R}$ to $\mathbb{R}$. Define $\Psi : \mathbb{D}([0,T], \mathbb{R}) \to \mathbb{R}$ by

$$\Psi(Y) = \Phi_1(Y_{s_1})...\Phi_n(Y_{s_n})[Y_t - Y_s - \int_s^t \{c(Y_s) + (r(Y_s) - d(Y_s))\, Y_s\} \, \mathrm{d}u].$$

We need to show that

$$\mathbb{E}[\Psi(N)] = 0\,.$$

This can be made similarly as in the determinist case, and we refer to the proof of theorem 2 for the details.

The new argument in this proof consists in showing that the bracket of $\widetilde{M}$ is given by (1.35).

1. First, consider the K-dependent semimartingale obtained from equation (1.13) with $\Phi(X^K) = (X^K)^2$, that is related to the generator:

$$\begin{aligned} L^K \Phi(X_s^K) = 2X_s^K \left(c(X_s^K) + (r(X_s^K) - d(X_s^K))X_s^K\right) \\ + \frac{1}{K}\left(c(X_s^K) + (r(X_s^K) + d(X_s^K) + 2Ka)X_s^K\right)\,. \end{aligned}$$

   As in the previous point we can show that we have at the limit the following martingale:

$$\widetilde{N}_t = (N_t)^2 - (N_0)^2 - \int_0^t \{2N_s\left(c(N_s) + (r(N_s) - d(N_s))N_s\right) + 2aN_s\} \, \mathrm{d}s\,.$$

2. Moreover, applying the Itô formula to equation (1.34) shows that

$$N_t^2 - N_0^2 - <\widetilde{M}>_t - \int_0^t 2N_s\left(c(N_s) + (r(N_s) - d(N_s))N_s\right) \, \mathrm{d}s$$

   is a martingale. We conclude by the uniqueness of the semimartingale decomposition of N_t^2.

It remains to show the equivalence between the martingale problem (1.34)-(1.35) and the SDE (1.33). This is a consequence of the classical martingale identification

$$M_t = \int_0^t \sqrt{2aN(s)}\, \mathrm{d}B_s\,,$$

(see for example Karatzas and Shreve [1998]).

Finally, the pathwise uniqueness of the solution to this SDE is classical in 1D since the drift is Lipschitz-continuous and the diffusion coefficient is 1/2-Hölder (see e.g Ikeda and Watanabe [1989]).

□

Remark 3. *The solution is strong and has the strong Markov property.*

Numerical simulations We performed numerical simulations of the SDE (1.33) with rates as in 1.23, using a symmetrized Euler scheme (taking the absolute value of the Euler scheme) in order to preserve the positivity of the process (see e.g Berkaoui, Abdel et al. [2008]). More precisely, the scheme is the following: write $(N_k)_k$ for the discretization of $(N_t)_t$, with N_k corresponding to the time $t_k = k\Delta t$. Then,

$$N_0 = n_0 \tag{1.36}$$

$$N_{k+1} = \mid N_k + b(N_k)\Delta t + \sqrt{2a\Delta t N_k} Z \mid \quad \text{for } k \geq 0\,, \tag{1.37}$$

with $Z \sim \mathcal{N}(0,1)$. It is proved in Berkaoui, Abdel et al. [2008] that strong L^1 convergence holds for this scheme if

$$\frac{\sigma^2}{8}\left(\frac{2b(0)}{\sigma^2} - 1\right)^2 > 3P \vee 4\sigma^2\,,$$

for $P \geq |r-d|$ and $\Delta t \leq \frac{1}{2P}$. This condition allows to deal with the non lipschitz diffusion coefficient, and rewrites in our case

$$\frac{a}{4}\left(\frac{c}{a} - 1\right)^2 > 3P \vee 8a\,.$$

As an example, $\frac{a}{4}\left(\frac{c}{a} - 1\right)^2 > 8a$ is equivalent to $\left(\frac{c}{a} - 1\right)^2 > 32$, that is verified for $c > 7a$. The numerical simulations are displayed in figure 1.3.

1.5 Stopping time

The rolling motion of individual cells has been observed to fluctuate randomly both in vivo and in vitro, hence it is natural to study in more details the stochastic limit continuous model previously obtained (after a renormalizaton procedure). In particular we are interested in the probability for a rolling cell to stop, that is to say for the velocity to reach 0. More precisely, in this section we will compute the probability distribution of the time T_{n^*} needed for the process to reach $n^* := u/\gamma$ starting from n_0 (say 0). Hence, we focus here on the process $(N_t)_{t \leq T_{n^*}}$, for which almost surely, $N_t \leq n^*$. We start by general remarks on the stochastic differential equation (1.33).

1.5.1 General remarks

Positivity Even if we obtained a positive solution in the construction of the last section, we can also show positivity in general if $b(n) \geq 0$ for all $n \geq 0$, and for a positive initial state (see the 1D comparison principle in Karatzas and Shreve [1998] e.g.).

Change of variable The Itô formula allows us to write SDE (1.33) on N-dependent quantities.

- For $Y_t = \sqrt{N_t}$, we can show that for $Y_t \in (0, +\infty)$,

$$\mathrm{d}Y_t = \frac{b(Y_t^2) - a/2}{2Y_t}\,\mathrm{d}t + \sqrt{\frac{a}{2}}\,\mathrm{d}B_t\,.$$

  The diffusion coefficient is now non-degenerate, but the 0-state is excluded.

- For $V_t = u - \gamma N_t \in [0, u]$ if $N_t \in [0, n^*]$, we obtain

$$\mathrm{d}V_t = (u(d(N_t) - r(N_t)) - \gamma c(N_t) + (r(N_t) - d(N_t))V_t)\,\mathrm{d}t + \sqrt{2a\gamma(u - V_t)}\,\mathrm{d}B_t\,. \quad (1.38)$$

  Using this equation is tempting, as we are interested in the time needed for this quantity to reach 0. However, the diffusion coefficient is now less simple than the one for $(N_t)_t$, as we will see in the sequel.

1.5.2 Constant rates: the CIR process

For constant rates, the model given by (1.33) reduces to a CIR process, see Göing-Jaeschke and Yor [1999]; Ikeda and Watanabe [1989]; Shreve [2004]:

$$\mathrm{d}N_t = (c + (r - d)N_t)\,\mathrm{d}t + \sqrt{2aN_t}\,\mathrm{d}B_t\,, \quad (1.39)$$

with $c > 0$, $a > 0$ and $r - d \in \mathbb{R}$. It is known for demographical processes that the diffusion limit of discrete branching processes with immigration results in such processes [Athreya and Ney, 1972]. Simulations of this process are displayed in figure 1.4. In this case, the adhesion dynamics is not directly related to the cell velocity, nor on the proximity with the vessel wall. Different behaviours may occur only based on the range of the dynamics: if too low compared to the blood blow, the cell does not stop, and does for a large enough adhesive dynamics.

Some generalities

In this paragraph, we give some classical results about the CIR process. For more details we refer to Göing-Jaeschke and Yor [1999]; Shreve [2004].

Reaching zero: As mentioned in Göing-Jaeschke and Yor [1999], for $c > 0$ and a positive initial state, $\{N = 0\}$ is naturally a reflective barrier for the process (1.39). We can also provide information about the probability to hit 0, depending on the quantity $\delta := \frac{2c}{a}$, or equivalently on the comparison between a and c: denote $\mathbb{P}^0$ the probability to hit 0 in finite time, then one has

$c < a$		$c \geq a$
$r - d \leq 0$	$r - d > 0$	
$\mathbb{P}^0 = 1$	$\mathbb{P}^0 \in (0, 1)$	$\mathbb{P}^0 = 0$

These results can be intuitively understood following the correspondance between CIR processes and Orstein-Uhlenbeck processes for $r - d < 0$. Indeed, consider D such processes $(X^1, \cdots, X^D)$ such that $\forall i = 1, \cdots, D$,

$$\mathrm{d}X_t^i = -\frac{1}{2}\beta X_t^i\,\mathrm{d}t + \frac{1}{2}\sigma\,\mathrm{d}B_t^i\,,$$

with $(B^i)_i \in \{1, \cdots, D\}$ independent Brownian motions and $\beta > 0$. Each process follows a stochastic dynamics that is drifted to zero. Now, similarly as for Brownian motion, for $D = 1$, the process almost surely hits zero infinitely many times, while for $D \geq 2$, it has a null probability of reaching zero even once.

Using the Itô formula, it is possible to write the SDE that verifies the squared euclidean norm of $(X^1, \cdots, X^D)$, that is to say $R = (X^1)^2 + \cdots + (X^D)^2$: we have

$$\mathrm{d}R_t = \left(\frac{\sigma^2 D}{4} - \beta R_t\right)\mathrm{d}t + \sigma\sqrt{R(t)}\,\mathrm{d}B_t\,,$$

with B a Brownian motion. Then, denoting $D = 4c/\sigma^2 > 0$, where $\sigma^2 = 2a$, it is possible to derive equation (1.39) with $r - d = -\beta \leq 0$. Therefore, if D is an integer, the CIR process admits a representation as the squared norm of D Ornstein-Uhlenbeck processes. More generally, the CIR process relates rigorously to the Squared Radial Ornstein-Uhlenbeck process, as it will be precised below.

Remark 4. *It is also possible to relate a CIR process to a Squared Bessel process by a space-time transformation. This process is itself in correspondance with a Squared Radial Ornstein-Uhlenbeck process. Take S a squared Bessel process of dimension $\delta \geq 0$ (denoted BESQ$^\delta$). For a fixed initial condition, it is the unique strong solution of the SDE*

$$\mathrm{d}S_t = \delta\,\mathrm{d}t + 2\sqrt{S_t}\,\mathrm{d}B_t\,. \tag{1.40}$$

Now, for $\delta = \frac{4c}{2a} = \frac{2c}{a}$, the correspondance between N and S writes

$$N_t = e^{(r-d)t} S_{\frac{a}{2(r-d)}(1-e^{-(r-d)t})}\,.$$

For $\delta \in \mathbb{N}$, a squared Bessel process also admits a representation as the square norm of a δ-dimensional Brownian motion. Therefore, the previous result can be deduced by the same reasoning [Göing-Jaeschke and Yor, 1999].

Distribution: It is known that for $\delta = \frac{2c}{a} \in \mathbb{N}$ and $r - d < 0$, we have $N_t|n_0 = \frac{(1-e^{(r-d)t})2a}{2(d-r)} Y_t$, with Y_t following a non-central chi-square distribution with δ degrees of freedom, and a non-centrality parameter $\xi_t = n_0 \frac{2(d-r)}{(1-e^{(r-d)t})a} e^{(r-d)t}$. This also results from the representation as the squared euclidean norm of a δ-dimensional Ornstein-Uhlenbeck process. The integral form of the SDE (1.39) allows to compute the mean solution directly, and the variance of the solution (using additionally the Ito formula). We compute

$$\begin{aligned}
\mathbb{E}[N_t|n_0] &= n_0 e^{(r-d)t} + \frac{c}{d-r}\left(1 - e^{(r-d)t}\right)\,,\\
Var(N_t|n_0) &= n_0 \frac{2a}{d-r}\left(e^{(r-d)t} - e^{2(r-d)t}\right) + \frac{ac}{(d-r)^2}\left(1 - e^{(r-d)t}\right)^2\,.
\end{aligned}$$

The corresponding probability density p_{n_0} writes for $n \geq 0$, $n_0 > 0$ and $\kappa_t = \frac{d-r}{(1-e^{(r-d)t})a}$:

$$p_{n_0}(n; k, \xi_t) = \kappa_t \left(\frac{n}{n_0 e^{(r-d)t}}\right)^{\frac{c}{a}-1} e^{-\kappa_t\left[n_0 e^{(r-d)t}+n\right]} I_{\frac{c}{a}-1}\left(2\kappa_t\sqrt{n_0 n e^{(r-d)t}}\right)\,,$$

where I_α is the modified Bessel function of the first kind whose definition we recall now:

$$I_\alpha(x) := \Sigma_{m=0}^{\infty} \frac{1}{m!\Gamma(m+\alpha+1)}\left(\frac{x}{2}\right)^{2m+\alpha}\,,$$

where Γ is the Gamma function $\Gamma(t) = \int_0^\infty x^{t-1}e^{-x}\,\mathrm{d}x$.

A stationary distribution exists if and only if $r - d < 0$. In that case, the previous approach gives a possible stationary probability density. Then, writing the Fokker-Planck equation associated to equation (1.39), we can check that the stationary density writes

$$p_\infty(n) = \left(\frac{d-r}{a}\right)^{\frac{c}{a}} \frac{1}{\Gamma\left(\frac{c}{a}\right)} n^{\frac{c}{a}-1} e^{\frac{r-d}{a}n}\,.$$

It can be noticed that

$$p_\infty(n) = \mathcal{N} e^{-\phi(n)}$$

for $\phi(n) = \left(1 - \frac{c}{a}\right)\ln(n) + \frac{d-r}{a}n$ the corresponding potential, and $\mathcal{N}$ a normalization constant. Simulations are displayed in figure 1.5.

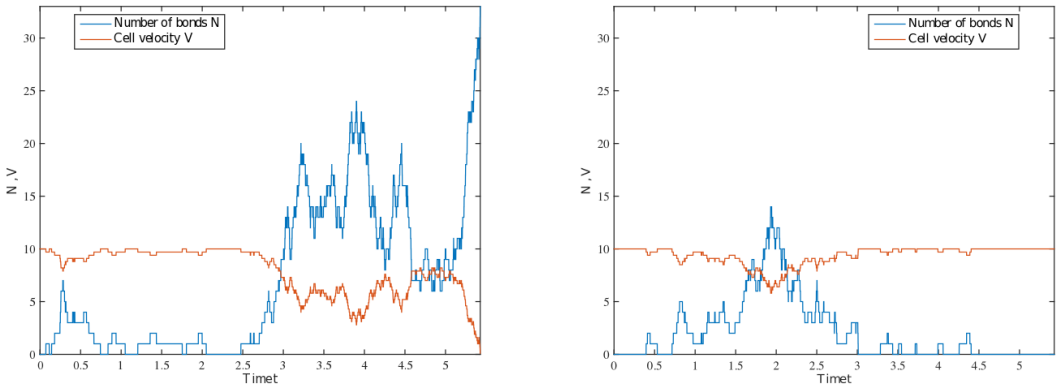

Figure 1.2 – Numerical simulations of the discrete process. Parameters: $u = 10$, $\gamma = 0.3$, $c = 4$, $r = 5$, $d = 3$, $\alpha = 0.1$.

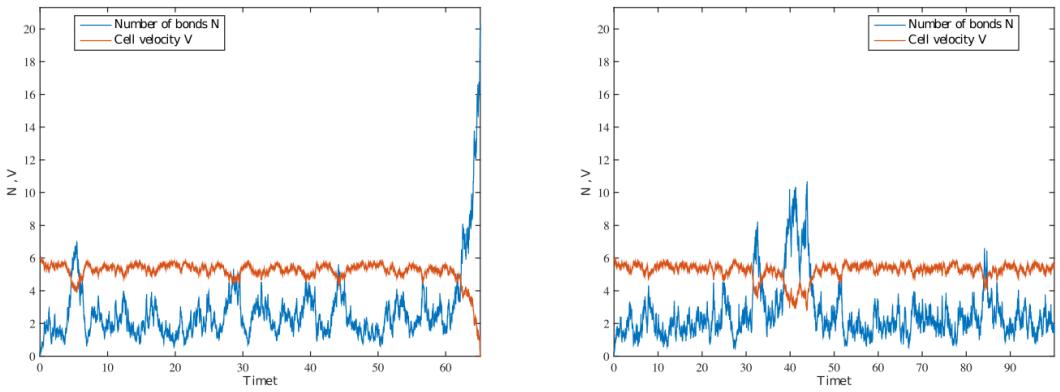

Figure 1.3 – Numerical simulations of the solution of the SDE (1.33). Parameters: $u = 6$, $\gamma = 0.3$, $c = 4$ (left) and $c = 5$ (right), $r = 5$, $d = 4$, $\alpha = 0.1$, $a = 0.55$.

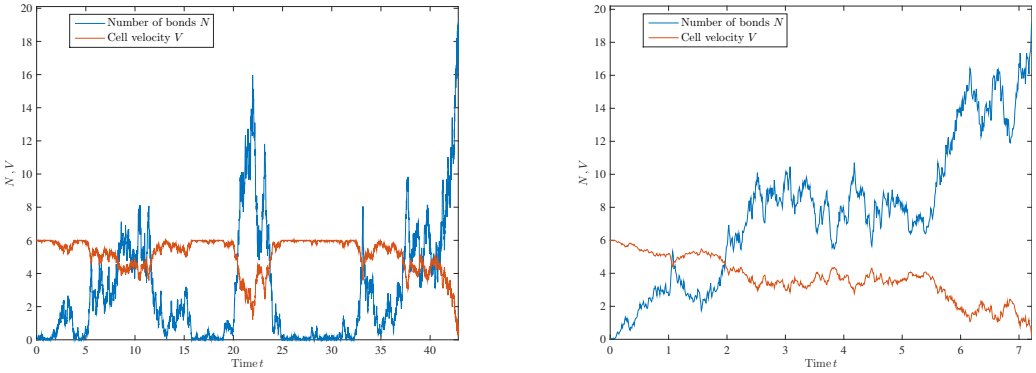

(a) Subcritical case: $(c, a, r, d) = (0.5, 1.5, 4.45, 4.5)$.

(b) Supercritical case: $(c, a, r, d) = (2, 1, 4, 4)$.

Figure 1.4 – Numerical simulations of the CIR process (1.39)

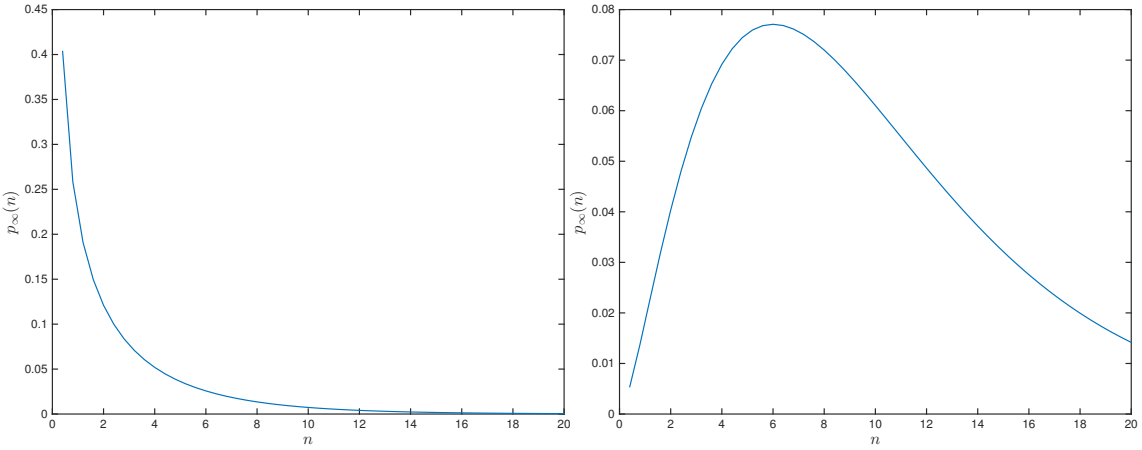

(a) Subcritical case: $c = 1$, $a = 2$.

(b) Supercritical case: $c = 5$, $a = 2$.

Figure 1.5 – Numerical simulations of the stationary probability density of the CIR process for $u = 6$, $\eta = 0.3$, $\alpha = 0.1$, $r = 4$, and $d = 4.5$.

Time to reach n^*: For the CIR process, it is possible to explicit the Laplace transform of the first hitting time of any value, starting at a given point [Göing-Jaeschke and Yor, 1999; Leblanc and Scaillet, 1998]. It is not possible to proceed to its inversion analytically. Numerical inversions procedures exist, and some of them are compared in Leblanc and Scaillet [1998]. They do not always provide satisfactory results: the integral of the output may not be equal to one, and negative values may appear. The procedure proposed by Abate and Whitt [1992] seems satisfactory in this viewpoint. However in Linetsky [2004a], a spectral expansion of the probability density is used, and we will follow this method.

We start by giving an outline of the ideas leading to the expressions of the Laplace transform of first hitting times of CIR processes. For more details we refer to Göing-Jaeschke and Yor [1999].

We exploit the rigorous link that exists between the CIR process and the Squared δ-dimensional Radial Ornstein-Uhlenbeck process of parameter $-\kappa$, denoted SROU in the sequel, corresponding to the SDE

$$\mathrm{d}Z_t = (\delta - 2\kappa Z_t)\,\mathrm{d}t + 2\sqrt{Z_t}\,\mathrm{d}B_t\,. \tag{1.41}$$

Recalling equation (1.39), we obtain the SROU using the change of variable $Z_t = \frac{2}{a}N_t$. Then, we have $\delta = \frac{2c}{a}$ and $-2\kappa = r - d$.

Now, the squared root of a δ-SROU process is called a δ-dimensional Radial Ornstein-Uhlenbeck process (or δ-ROU, denoted by $(R_t)_t$). A Girsanov theorem relates its law and the law of a Bessel process [Göing-Jaeschke and Yor, 1999]. Briefly, the Laplace transform of first hitting times for Bessel process are obtained by exploiting time-reversal arguments. These expressions transfer to ROU processes, allowing to get explicit Laplace transforms in the case of CIR processes. Detailed proofs are displayed in Göing-Jaeschke and Yor [1999]. Take $x, y \geq 0$, and denote ${}^{P}T_{x\to y}$ the random variable corresponding to the time needed for a process P to reach y starting from x. Then,

$${}^{N}T_{x\to y} \overset{\text{law}}{=} {}^{Z}T_{\frac{2x}{a}\to\frac{2y}{a}} \overset{\text{law}}{=} {}^{R}T_{\sqrt{\frac{2x}{a}}\to\sqrt{\frac{2y}{a}}}\,.$$

Let us introduce now the Whittaker's functions

$$M_{k,\mu}(z) := z^{\mu+1/2}e^{-z/2}\Phi(\mu - k + 1/2, 2\mu + 1; z),$$

and the Kummer confluent hypergeometric function defined for $b \notin \mathbb{Z}^-$,

$$\Phi(a,b;z) := \sum_{j=0}^{\infty} \frac{(a)_j}{(b)_j} \frac{z^j}{j!},$$

with $(r)_0 = 1$, $(r)_j = \frac{\Gamma(r+j)}{\Gamma(r)} = r(r+1)...(r+j-1)$ for $j \geq 1$. Moreover, $I_\nu(\,\cdot\,)$ is the first modified Bessel function of order ν. Then, the following expressions are verified [Göing-Jaeschke and Yor, 1999].

Theorem 6 (0 to x, Göing-Jaeschke and Yor [1999]). *Denote $T_x = \inf\{t | R_t = x, R_0 = 0\}$ for $(R_t)_t$ a δ-ROU process with parameter $-\kappa$ (we drop the R superscript for simplicity). Then, its Laplace Transform writes*

$$\begin{aligned}
\mathbb{E}_0\left[e^{-\alpha T_x}\right] &= \frac{2^{\alpha/\kappa-\nu-1} x^\nu \Gamma(\alpha/(2\kappa)) \kappa^{\alpha/(2\kappa)}}{\Gamma(\nu+1)\int_0^{+\infty} I_\nu(\gamma x) e^{-\gamma^2/(4\kappa)} \gamma^{\alpha/\kappa-\nu-1}\,\mathrm{d}\gamma} \\
&= \frac{(\sqrt{\kappa}x)^{\nu+1} e^{-\kappa x^2/2}}{M_{(-\alpha/\kappa+\nu+1)/2,\nu/2}(\kappa x^2)} \\
&= \frac{1}{\Phi(\alpha/(2\kappa),\nu+1;\kappa x^2)}\,.
\end{aligned}$$

Then, since for $0 < y < x$, we have $T_x = T_y + T_{y\to x}$ in law, and as by the strong Markov property, T_y and $T_{y\to x}$ are independent, we get the following corollary.

Corollary 1 ($0 < y < x$ to x [Göing-Jaeschke and Yor, 1999]).

$$\begin{aligned}
\mathbb{E}_y\left[e^{-\alpha T_x}\right] &= \left(\frac{x}{y}\right)^{\nu+1} e^{\kappa(y^2-x^2)/2} \frac{M_{(-\alpha/\lambda+\nu+1)/2,\nu/2}(\kappa y^2)}{M_{(-\alpha/\lambda+\nu+1)/2,\nu/2}(\kappa x^2)} \\
&= \frac{\Phi(\alpha/(2\kappa),\nu+1;\kappa y^2)}{\Phi(\alpha/(2\kappa),\nu+1;\kappa x^2)}\,.
\end{aligned}$$

Remark 5. *Analogous results exist for the case $0 < x < y$, but are not useful for our purpose.*

We follow now the work of Linetsky [2004a,b] to compute numerically the first hitting time density using an eigenfunction decomposition, following an approach used for diffusions [Davydov and Linetsky, 2003; Itô and McKean, 1965; McKean, 1956]. For the CIR process, it is established in Linetsky [2004b,c] that the same type of decomposition holds. More precisely, the infinitesimal generator $\mathcal{G}$ associated to the CIR diffusion (1.39) writes for $y > 0$

$$(\mathcal{G}u)(y) = \frac{1}{2}\sigma^2 y u''(y) + (c + (r-d)y)u'(y)\,,$$

with $\sigma^2 = 2a$. For $c/a < 1$, the origin is attainable and instantaneously reflecting. In this case, the state space is $I = [0, +\infty)$, and we have the boundary condition at zero

$$\lim_{y\downarrow 0} \frac{u'(y)}{s(y)} = 0\,, \tag{1.42}$$

where $s(y) = y^{-c/a}\exp(-(r-d)y/a)$. For $c/a \geq 1$, the origin in unattainable, $I = (0, +\infty)$, and the previous boundary condition is directly satisfied. The infinitesimal generator is

thus defined on $D(\mathcal{G}) := \{u \in \mathcal{C}_b(\mathbb{R}) : \mathcal{G}(u) \in \mathcal{C}_b(\mathbb{R})$ and the condition (1.42) holds.$\}$. The infinitesimal generator can be rewritten for $x \in [0, +\infty)$,

$$(\mathcal{G}u)(y) = m(y)\left(\frac{u'(y)}{s(y)}\right)',$$

where $m(y) = \frac{1}{ays(y)}$. Notice that s and m are continuous and strictly positive on $(0, +\infty)$.

Since the CIR process admits a stationary distribution (for $r - d < 0$), it is positively recurrent: $\mathbb{P}_y(T_{y\to x} < +\infty) = 1$ and $\mathbb{E}_y[T_{y\to x}] < +\infty$. We apply now a result proved in Linetsky [2004b] and applied in Linetsky [2004a] to the CIR process.

Proposition 9. *[Linetsky, 2004b] For $y < x \in I$ and $t > 0$, we have*

$$\mathbb{P}_y(t < T_{y\to x}) = \sum_{n=1}^{+\infty} o_n e^{-\lambda_n t}, \tag{1.43}$$

with $0 < \lambda_1 < \lambda_2 < \ldots$, $\lambda_n \to_{n\to+\infty} +\infty$. The families $\{\lambda_n\}_n$ and $\{o_n\}_n$ are defined as follows.

Let us introduce the Sturm-Liouville problem associated to $\mathcal{G}$:

$$-\mathcal{G}u = \lambda u, \tag{1.44}$$

for $\lambda \in \mathbb{C}$. Denote $\psi(y, \lambda)$ the unique (up to a multiplicative constant) non-trivial solution of (1.44), square-integrable with $m(y)$ near $\{y = 0\}$, satisfying the boundary condition (1.42), and such that $(y, \lambda) \mapsto \psi(y, \lambda)$, $\psi_y(y, \lambda)$ are continuous in $(0, x] \times \mathbb{C}$, and continuous on $\mathbb{C}$ as functions of λ for $y < x$ fixed.

Then, equipping equation (1.44) of the Dirichlet boundary condition $u(y) = 0$, the family $\{\lambda_n\}_{n\in\mathbb{N}^*}$ is defined as the set of simple positive zeros of the solution:

$$\psi(y, \lambda_n) = 0. \tag{1.45}$$

Now, $\{o_n\}_{n\in\mathbb{N}^*}$ is defined by

$$o_n = \frac{-\psi(x, \lambda_n)}{\lambda_n \psi_\lambda(y, \lambda_n)}. \tag{1.46}$$

We state now the result of Linetsky [2004a] that gives explicit expressions for $\{\lambda_n\}_{n\in\mathbb{N}^*}$ and $\{o_n\}_{n\in\mathbb{N}^*}$, as well as a series expansion for the first hitting time density $f_{T_{y\to x}}$. Its uniform convergence is a consequence of estimates given on λ_n and o_n.

Proposition 10. *[Linetsky, 2004a] For $0 < x < y \in I$, and $t > 0$ we have*

$$f_{T_{y\to x}}(t) = \sum_{n=1}^{+\infty} o_n \lambda_n e^{-\lambda_n t}, \tag{1.47}$$

with uniform convergence on $[t_0, +\infty)$, $t_0 > 0$, and $0 < \lambda_1 < \ldots$, with $\lambda_n \underset{n\to+\infty}{\to} +\infty$. More precisely, recall that $\Phi(w_1; w_2; w_3)$ denotes the Kummer confluent hypergeometric function. Then, for

$$\overline{y} := -\frac{r-d}{a}y, \quad \overline{x} := -\frac{r-d}{a}x, \quad s_n := \frac{\lambda_n}{r-d},$$

with $\{s_n\}$ such that $0 > a_1 > \ldots$, and $s_n \underset{n\to+\infty}{\to} -\infty$, $\{s_n\}_n$ are the negative roots of $\varphi(\,\cdot\,; c/a; \overline{x}) = 0$. The family $\{o_n\}_n$ is then defined by

$$o_n = -\frac{\Phi(s_n; c/a; \overline{y})}{s_n \partial_s(\Phi(s_n; c/a; \overline{x}))}. \tag{1.48}$$

Moreover, the following large-n asymptotics hold:

$$\lambda_n \underset{n\to+\infty}{\sim} \frac{(d-r)\pi^2}{4\overline{x}}\left(n+\frac{c}{2a}-\frac{3}{4}\right)^2-\frac{(r-d)c}{2a}\,, \tag{1.49}$$

as well as

$$o_n \underset{n\to+\infty}{\sim} \frac{(-1)^{n+1}2\pi(n+c/(2a)-3/4)}{\pi^2(n+c/(2a)-3/4)^2-\frac{2c}{a}\overline{x}}\times e^{\frac{1}{2}(\overline{y}-\overline{x})}\left(\frac{\overline{y}}{\overline{x}}\right)^{\frac{1}{4}-\frac{c}{2a}}\cos\left(\pi\left(n+\frac{c}{2a}-\frac{3}{4}\right)\sqrt{\frac{\overline{y}}{\overline{x}}}-\frac{\pi c}{2a}+\frac{\pi}{4}\right)\,. \tag{1.50}$$

Therefore, the proposed numerical method requires to compute the set of negative roots of φ to get approximations of the families $\{\lambda_n\}_n$ and $\{o_n\}_n$. The choice of the level of truncation for the approximation of (1.47) can be made using the following estimate resulting from the expressions above:

$$\left|o_n\lambda_N e^{-\lambda_N t_0}\right| \underset{N\to+\infty}{\sim} ANe^{-BN^2t_0}\,,$$

for

$$A=\frac{2a\pi}{4x}e^{\frac{\overline{y}-\overline{x}}{2}}\left(\frac{x}{y}\right)^{\frac{1}{4}-\frac{c}{2a}}\,,\quad B=\frac{a\pi^2}{4x}\,.$$

Linetsky also remarks that using the large-n estimates (1.49)-(1.50) instead of computating zeros of the Kummer function provides quite satisfactory results, in particular for c/a small. For a better accuracy, one can also use the exact expression for the first term, then the estimates. The following numerical simulation was performed using only the asymptotic expansion of λ_n and o_n even for n small, since it is observed that this approximation does not change qualitatively the profile (see figure 1.6). Obviously, in this case, the obtained function is not a probability density. An inconsistency tends to appear near $\{t=0\}$ due to the approximation, but the overall shape was conserved.

1.5.3 General rates

Let us now focus on the general case of equation (1.33), assuming hypothesis 5. The first result to state consists in using the 1D comparison result that was already mentioned.

Comparison principle

We assume $0\le n_0<n^*$, hence before the hitting time of n^* we can assume $d(N_t)\le \underline{D}=d$ (as $u-\gamma n^*=0$).

Using the bounds on the parameters, it is possible to use a 1D comparison principle (see e.g Revuz and Yor [2005]) to deduce bounds on the hitting time of n^* for our process. We have

$$c+(r-\underbrace{de^{\alpha u}}_{\overline{D}})N_t\le b(N_t)\le c+(r-\underbrace{d}_{\underline{D}})N_t\,,$$

for $N_t\in[0,n^*]$. Denote $\overline{N}$ (resp. $\underline{N}$) the solution related to the death rate $\overline{D}$ (resp. $\underline{D}$). Almost surely, for $t\in[0,T_{n^*}]$,

$$\underline{n}_t\le n_t\le \overline{n}_t\,,$$

and for the same initial condition $0\le n_0<n^*$, almost surely,

$${}^{\overline{N}}T_{n^*}\le {}^{N}T_{n^*}\le {}^{\underline{N}}T_{n^*}\,.$$

However, these bounds are not precise enough for our study, and we develop in the following a Fokker-Planck approach.

The Fokker-planck approach

We associate to the SDE (1.33) the Fokker-Planck equation on $p(n,t) := p(n,t|n_0,t_0)$ the probability density of $(N_t)_t$ conditionnally to its initial condition:

$$\frac{\partial p(n,t)}{\partial t} = \frac{\partial}{\partial n} \underbrace{\left(-b(n)p(n,t) + \frac{1}{2}\frac{\partial}{\partial n}(\sigma^2(n)p(n,t))\right)}_{\mathbf{J}(n,t)}, \tag{1.51}$$

where we recall that $b(n) = c + (r(n) - d(n))n$, while $\sigma(n) = \sqrt{2an}$ and $\mathbf{J}(n,t)$ is the associated probability current. The natural boundary conditions are the following:

$$\begin{aligned} \mathbf{J}(0,t) &= 0\,, \\ \lim_{n\to+\infty} p(n,t) &= 0\,, \\ p(n,0) &= \delta_{n=n_0}\,. \end{aligned}$$

We are interested in the time necessary for the process to reach the value $n^* > 0$ if it starts at $n_0 \in (0,n^*)$, and with 0 a reflecting barrier. This question can be adressed by considering the Fokker-Planck equation on $(0,n^*)$ with 0 reflecting and n^* an absorbing barrier. More precisely, write $G(n_0,t)$ the probability that a particle starting at n_0 is still in $(0,n^*)$ at time t. Then,

$$G(n_0,t) = \int_0^{n^*} p(n,t|n_0,0)\,\mathrm{d}n = \mathbb{P}(T \geq t)\,,$$

where T is the exit time from $(0,n^*)$.

Since the dynamics is homogeneous in time, we deduce that $p(n,t|n_0,0) = p(n,0|n_0,-t)$ and $n_0 \mapsto p(n,t|n_0,0)$ satisfy the backward Fokker-Planck equation:

$$\frac{\partial p(n,t|n_0,0)}{\partial t} = b(n_0)\frac{\partial}{\partial n_0}p(n,t|n_0,0) + \frac{1}{2}\sigma^2(n_0)\frac{\partial}{\partial {n_0}^2}p(n,t|n_0,0)\,, \tag{1.52}$$

and that $(n_0,t) \mapsto G(n_0,t)$ satisfies

$$\frac{\partial G(n_0,t)}{\partial t} = b(n_0)\frac{\partial}{\partial n_0}G(n_0,t) + \frac{1}{2}\sigma^2(n_0)\frac{\partial}{\partial {n_0}^2}G(n_0,t)\,. \tag{1.53}$$

The initial and boundary conditions are the following:

$$\begin{aligned} G(n_0,0) &= \int_0^{n^*} \delta(n-n_0)\,\mathrm{d}n = \mathbb{1}_{[0,n^*]}(n_0)\,, \\ \frac{\partial}{\partial n_0}G(0,t) &= 0\,, \\ G(n^*,t) &= 0\,. \end{aligned}$$

Take $f : \mathbb{R} \mapsto \mathbb{R}_+$ non-decreasing and $\mathcal{C}^1$. Then, classically, $\mathbb{E}[f(T)] = \int_0^{+\infty} f'(t)\mathbb{P}(T > t)\,\mathrm{d}t = \int_0^{+\infty} f'(t)G(n_0,t)\,\mathrm{d}t$. Hence, we get for $k > 1$,

$$\begin{aligned} \tau(n_0) &:= \mathbb{E}[T] = \int_0^{+\infty} G(n_0,t)\,\mathrm{d}t\,, \\ \tau_k(n_0) &:= \mathbb{E}[T^k] = k\int_0^{+\infty} t^{k-1}G(n_0,t)\,\mathrm{d}t\,. \end{aligned}$$

Finally, by integration of equation (1.53) in time, we get ODEs on the family $(\tau_k)_{k\geq 1}$:

$$\begin{cases} b(n_0)\tau'(n_0) + \frac{1}{2}\sigma^2(n_0)\tau''(n_0) = -1\,, \\ \tau'(0) = 0\,, \\ \tau(n^*) = 0\,, \end{cases} \tag{1.54}$$

and for $k > 1$,

$$\begin{cases} b(n_0)\tau_k'(n_0) + \frac{1}{2}\sigma^2(n_0)\tau_k''(n_0) = -k\tau_{k-1}(n_0)\,, \\ \partial_{n_0}\tau_k(0) = 0\,, \\ \tau_k(n^*) = 0\,. \end{cases} \tag{1.55}$$

By direct integration, we can directly solve equation (1.54), which allows then to solve successively the sequence of problems (1.55). Write

$$\Psi(n_0) = e^{\int_0^{n_0} \frac{2b(n')}{\sigma^2(n')}\,\mathrm{d}n'}\,. \tag{1.56}$$

Then, we have

$$\tau(n_0) = 2\int_{n_0}^{n^*} \frac{1}{\Psi(y)} \int_0^y \frac{\Psi(z)}{\sigma^2(z)}\,\mathrm{d}z\,\mathrm{d}y\,. \tag{1.57}$$

In practice, denoting $\epsilon > 0$ for the below bound instead of zero, we find

$$\Psi(n_0) = \left(\frac{n_0}{\epsilon}\right)^{\frac{c}{a}} \exp\left(\frac{r}{a}n_0 - \frac{d}{\alpha\gamma a}e^{\alpha u}(1 - e^{-\alpha\gamma n_0})\right)\,.$$

Explicit computations lead to

$$\tau(n_0) = \frac{1}{a}\int_{n_0}^{n^*}\int_0^y \left(\frac{z}{y}\right)^{\frac{c}{a}} z^{-1} e^{\frac{r}{a}(z-y)} \exp\left(\frac{d}{a\alpha\gamma}e^{\alpha u}\left(e^{-\alpha\gamma z} - e^{-\alpha\gamma y}\right)\right)\,\mathrm{d}z\,\mathrm{d}y\,. \tag{1.58}$$

We perform numerical simulations of $\tau(0)$ for varying flow velocity u (see figure 1.7).

The simulations show that below a treshold flow velocity, the particle reaches a zero velocity very fast, while it gets extremely slow above the treshold. This dichotomy on u can be numerically modulated by γ corresponding to the adhesion force, and a corresponding to the noise. Increasing adhesion forces allows to stop cells in settings of higher flow, so as increasing the stochastic fluctuations due to the bonds dynamics.

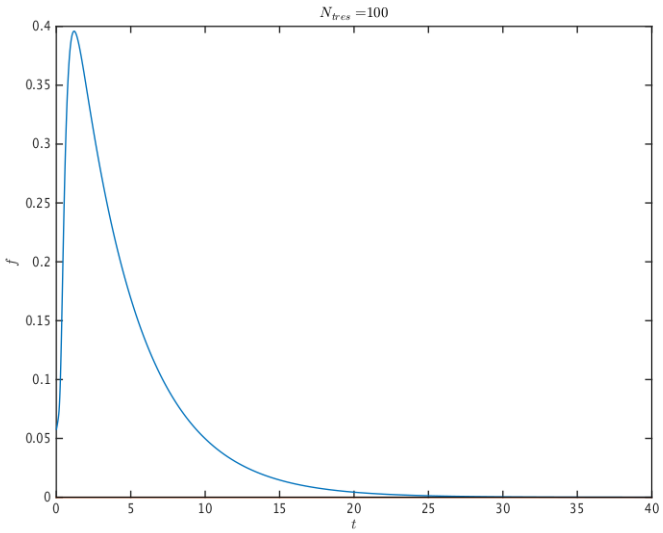

Figure 1.6 – Numerical simulation of an asymptotic spectral decomposition of the probability density of the first hitting time of 1 of a CIR process starting at 0.01. Parameters: $\Delta t = 0.01$, $c = 0.45$, $a = 0.5$, $r = 0.2$ and $d = 1$. The sum is truncated at $N_{tres} = 100$.

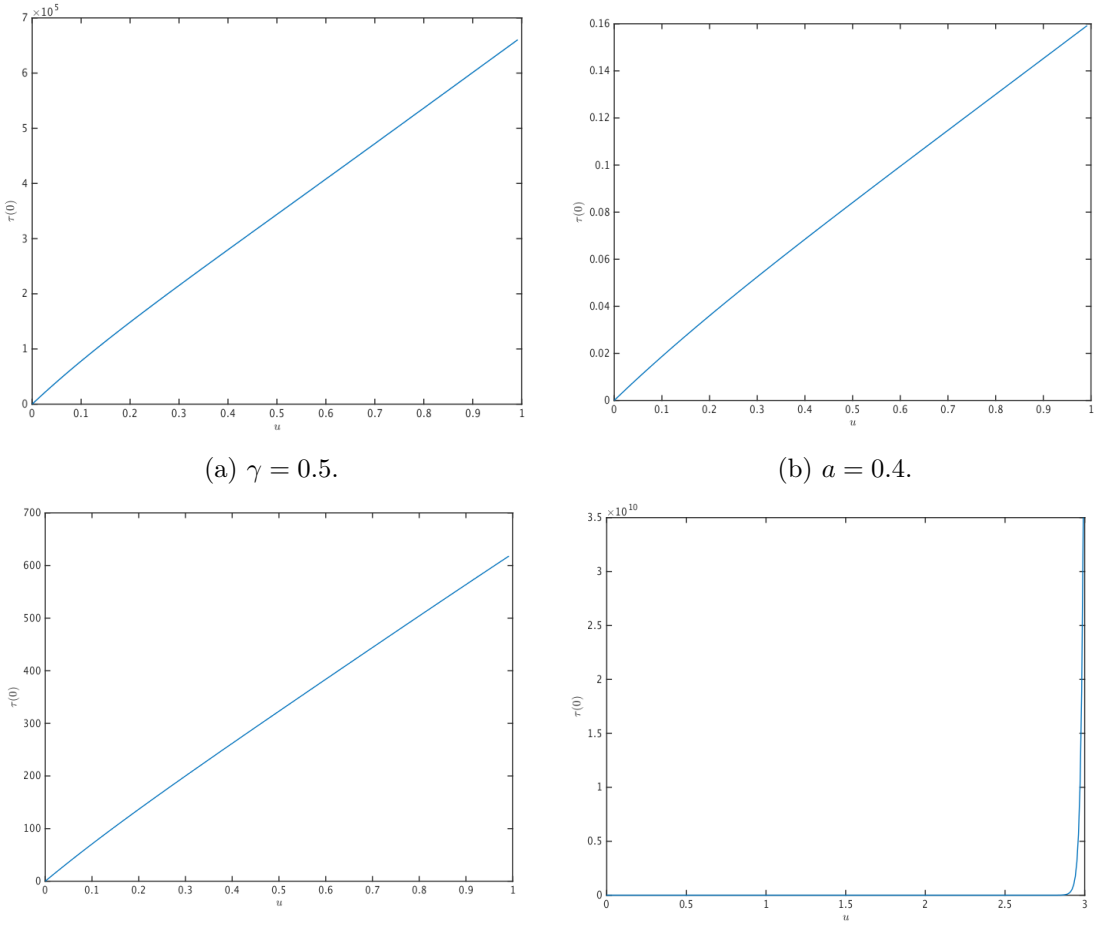

(a) $\gamma = 0.5$.

(b) $a = 0.4$.

Figure 1.7 – Mean first hitting time of a zero velocity for u variable. Parameters: $\gamma = 0.5$, $\alpha = 0.8$, $c = 1$, $r = 0.6$, $d = 0.7$, $a = 0.1$. The figures below depict the same simulation on different scales.

1.6 Conclusions and perspectives

In this part, we have presented a discrete model for ligands binding on artery walls. The model is based on a stochastic description of the formation of weak bonds between the cell and the adhesive molecules on the wall, and of the stronger ones arising by self-reinforcement. This phenomenon is modelled by a stochastic population model. The bonds dynamics are affected by the cell displacement by an interaction on their breaking rate: faster cells have shorter-lived bonds with the wall.

We are interested in the stopping time of the cell, that amounts to the first hitting time of a treshold value for the bond population. For this purpose, we derive a continuous model by scaling, so that the adhesion dynamics follows a diffusive stochastic differential equation. For constant parameters, no interaction or feedback is described, and the model resumes to a CIR process, for which properties of first hitting times are known. We provide its Laplace transform, and use a spectral method to make simulations of the corresponding probability density. Finally, for the model with interaction, we use a Fokker-Planck approach to have an integral formulation of the mean time to stop. Numerical simulations of this quantity as a function of the flow velocity show interesting results. First, a dichotomy appears in relation with the flow velocity: for low flows, the particle is stopped very fast, while above some treshold, the mean time to stop grows very steeply. Next, we checked that the simulations were the most sensitive on the adhesion coefficient γ, and on the stochastic parameter a. Indeed, larger adhesion forces favors the stopping of the cell. A larger noise also induces stops more easily, which is in agreement with the observations stated at the beginning. Finally, comparison with experimental measures is promising to enlighten conditions of stopping for the cell.

1.7 Appendix

1.7.1 Stochastic processes

We recall here some definitions from Revuz and Yor [2005].

Definition 1. *Let σ and b be predictable functions with values in $d \times r$ matrices and d-vectors. A solution to the stochastic differential equation $e(\sigma, b)$ is a pair (X, B) of adapted processes defined on a filtered probability space $(\Omega, \mathcal{F}_t, \mathbb{P})$ such that*

- *B is a standard $(\mathcal{F}_t)-$Brownian motion in $\mathbb{R}^r$,*
- *$X_t = X_0 + \int_0^t \sigma(X_s)\,\mathrm{d}B_s + \int_0^t b(X_s)\,\mathrm{d}s$, and we denote $e_x(\sigma, b)$ if we impose as initial condition $X_0 = x$ a.s.*

Definition 2. *Uniqueness of solutions*

- *There is pathwise uniqueness for $e(\sigma, b)$ if whenever (X, B) and (X', B') are two solutions defined on the same filtered space with $B = B'$ and $X_0 = X'_0$ a.s, then X and X' are indistinguishable.*
- *There is uniqueness in law for $e(\sigma, b)$ if whenever (X, B) and (X', B') are two solutions (with possibly different Brownian motion, and defined on different probability spaces) such that $X_0 \overset{=}{\mathcal{L}} x'_0$, then the laws of X and X' are equal. In other words, X and X' are two versions of the same process.*
- *The latter definition is equivalent to: $\forall x \in \mathbb{R}^d$, whenever (X, B) and (X, B') are solutions such that $X_0 = x$ and $X'_0 = x$ a.s, then the laws of X and X' are equal.*

Definition 3. *Strong solution A solution (X, B) of $e(\sigma, b)$ on $(\Omega, \mathcal{F}, \mathcal{F}_t, \mathbb{P})$ is said to be a strong solution if X is adapted to the filtration $(\mathcal{F}_t^B)$ of B completed with respect to $\mathbb{P}$.*

The link between pathwise uniqueness, uniqueness in law, and the strongness of solutions is explicited in the following theorem.

Theorem 7. *If pathwise uniqueness holds for $e(\sigma, b)$, then*

1. *uniqueness in law holds for $e(\sigma, b)$,*
2. *every solution to $e_x(\sigma, b)$ is strong.*

1.7.2 Discretization of EDS

We recall here definitions from Shao [2012].

Definition 4 (Strong convergence)**.** *Consider a sequence of discrete time approximation $\{\overline{X}_0, ... \overline{X}_{nh}, ...\}$ of a continuous time process X, for $h = T/n$, T fixed. We say $\overline{X}$ converges strongly to X if it converges in L^1, that is to say*

$$\lim_{n \to +\infty} \mathbb{E}[|\overline{X}(nh) - X(T)|] = 0\,.$$

Definition 5 (Weak convergence)**.** *Consider a sequence of discrete time approximation $\{\overline{X}_0, ... \overline{X}_{nh}, ...\}$ of a continuous time process X, for $h = T/n$, T fixed. We say $\overline{X}$ converges weakly to X with order 1 if for f with its $4_t h$ first derivatives polynomially bounded,*

$$\lim_{n \to +\infty} \mathbb{E}[f(\overline{X}(nh))] = \mathbb{E}[f(\overline{X}(T))]\,.$$

Bibliography

Abate, J. and Whitt, W. (1992). The fourier-series method for inverting transforms of probability distributions. Queueing systems, 10(1-2):5–87. 66

Aldous, D. (1989). Stopping times and tightness. ii. The Annals of Probability, 17(2):pp. 586–595. 53

Athreya, K. B. and Ney, P. E. (1972). Branching processes, volume 196 of die grundlehren der mathematischen wissenschaften. 63

Bansaye, V. and Méléard, S. (2015). Some stochastic models for structured populations : scaling limits and long time behavior. 42, 46

Berkaoui, Abdel, Bossy, Mireille, and Diop, Awa (2008). Euler scheme for SDEs with non-Lipschitz diffusion coefficient: strong convergence. ESAIM: PS, 12:1–11. 62

Bhatia, S. K., King, M. R., and Hammer, D. A. (2003). The state diagram for cell adhesion mediated by two receptors. Biophysical journal, 84(4):2671–2690. 43, 44

Champagnat, N. and Méléard, S. (2007). Invasion and adaptive evolution for individual-based spatially structured populations. Journal of Mathematical Biology, 55(2):147–188. 42, 46

Chang, K.-C. and Hammer, D. A. (1999). The forward rate of binding of surface-tethered reactants: effect of relative motion between two surfaces. Biophysical Journal, 76(3):1280–1292. 43

Davydov, D. and Linetsky, V. (2003). Pricing options on scalar diffusions: an eigenfunction expansion approach. Operations research, 51(2):185–209. 67

Ethier, S. N. and Kurtz, T. G. (2009). Markov processes: characterization and convergence, volume 282. John Wiley & Sons. 53

Fournier, N. and Méléard, S. (2004). A microscopic probabilistic description of a locally regulated population and macroscopic approximations. 14(4):1880–1919. 46

Goetz, D. J., El-Sabban, M. E., Pauli, B. U., and Hammer, D. A. (1994). Dynamics of neutrophil rolling over stimulated endothelium in vitro. Biophysical journal, 66(6):2202. 42

Göing-Jaeschke, A. and Yor, M. (1999). A survey and some generalizations of Bessel processes. Bernoulli, 9:313–349. 63, 64, 66, 67

Granger, D. N. and Senchenkova, E. (2010). Inflammation and the microcirculation. In Colloquium Series on Integrated Systems Physiology: From Molecule to Function, volume 2, pages 1–87. Morgan & Claypool Life Sciences. 41

Grec, B., Maury, B., Meunier, N., and Navoret, L. (2012). The role of ligands binding in shear induced leukocyte rolling. 45

Ikeda, N. and Watanabe, S. (1989). Stochastic differential equations and diffusion processes. Kodansha scientific books. North-Holland. 61, 63

Itô, K. and McKean, H. P. (1965). Diffusion processes and their sample paths. Grundlehren der Mathematischen Wissenschaften, 125. 67

Jadhav, S., Eggleton, C. D., and Konstantopoulos, K. (2005). A 3-D computational model predicts that cell deformation affects selectin-mediated leukocyte rolling. Biophysical journal, 88(1):96–104. 43

Joffe, A. and Metivier, M. (1986). Weak convergence of sequences of semimartingales with applications to multitype branching processes. Advances in Applied Probability, 18(1):20. 53

Karatzas, I. and Shreve, S. E. (1998). Brownian Motion and Stochastic Calculus, volume 113 of Graduate Texts in Mathematics. Springer New York, New York, NY. 61, 62

Leblanc, B. and Scaillet, O. (1998). Path dependent options on yields in the affine term structure model. Finance and Stochastics, 2(4):349–367. 66

Ley, K., Laudanna, C., Cybulsky, M. I., and Nourshargh, S. (2007). Getting to the site of inflammation: the leukocyte adhesion cascade updated. Nature Reviews Immunology, 7(9):678–689. 42

Linetsky, V. (2004a). Computing hitting time densities for CIR and OU diffusions: Applications to mean-reverting models. Journal of Computational Finance, 7:1–22. 66, 67, 68

Linetsky, V. (2004b). Lookback options and diffusion hitting times: A spectral expansion approach. Finance and Stochastics, 8(3):373–398. 67, 68

Linetsky, V. (2004c). The spectral decomposition of the option value. International Journal of Theoretical and Applied Finance, 7(03):337–384. 67

McKean, H. P. (1956). Elementary solutions for certain parabolic partial differential equations. 67

Milišić, V. and Oelz, D. (2011). On the asymptotic regime of a model for friction mediated by transient elastic linkages. Journal de mathématiques pures et appliquées, 96(5):484–501. 45

Milisic, V. and Oelz, D. (2015). On a structured model for load-dependent reaction kinetics of transient elastic linkages mediating nonlinear friction. SIAM Journal on Mathematical Analysis, 47(3):2104–2121. 45

Nicolas, A., Geiger, B., and Safran, S. A. (2004). Cell mechanosensitivity controls the anisotropy of focal adhesions. Proceedings of the National Academy of Sciences of the United States of America, 101(34):12520–12525. 44

Revuz, D. and Yor, M. (2005). Continuous martingales and Brownian motion. Number 293 in Grundlehren der mathematischen Wissenschaften. Springer, Berlin, corr. 3. print. of the 3. ed edition. 69, 73

Schmid-Schöounbein, G. W., Skalak, R., Simon, S. I., and Engler, R. L. (1987). The interaction between leukocytes and endothelium in vivoa. Annals of the New York Academy of Sciences, 516(1):348–361. 42

Shao, A. (2012). A fast and exact simulation for CIR process. University of Florida. 74

Shreve, S. E. (2004). Stochastic calculus for finance II: Continuous-time models, volume 11. Springer Science & Business Media. 63

Springer, T. A. et al. (1990). Adhesion receptors of the immune system. Nature, 346(6283):425–434. 42

Tran, V. C. (2006). Modèles particulaires stochastiques pour des problèmes d'évolution adaptative et pour l'approximation de solutions statistiques. phdthesis, Université Paris X. 42

Vestweber, D. (2015). How leukocytes cross the vascular endothelium. Nature Reviews Immunology. 42

Chapter 2

A stochastic model for 2D cell crawling

Contents

2.1 Introduction 77
2.2 Construction of the model 78
2.2.1 Modelling assumptions 78
2.2.2 Mathematical formulation 83
2.2.3 Numerical simulations 88
2.3 Mathematical properties 91
2.3.1 Moment property 91
2.3.2 Martingale property 92
2.3.3 Moment equation 95
2.4 Annex 96
2.4.1 Gronwall lemma 96
2.4.2 Itô formula 96

2.1 Introduction

In this model, we study cell migration under a large scale assumption so that the cell's geometry is neglected, and we end up with a particle model. In classical particle models like Active Brownian models, key-features of the motion are quantified, such as the mean persistence time, or the stationary distribution of the particle's velocity [Romanczuk et al., 2012]. However, the dynamics is macroscopic and processes such as polarisation are taken into account by an arbitrary positive feedback at the scale of the trajectory.

In our case, we try to develop the same framework for a macroscopic dynamics (the cell velocity) that is defined by a mesoscopic activity (the protrusion dynamics) arising from the intracellular scale. Protrusions are visible at the cellular scale, so that it is a measurable feature in our setting.

The model relies on the force balance principle that holds in a microscopic setting. We obtain the cell velocity as a function of the (discrete) protrusive forces exerted by filopodia on the substrate.

Normalizing the protrusive forces, they get characterized by their orientation. Therefore, the time evolution of these forces correspond to the time evolution of a population structured by a quantitative trait.

As a consequence, we use the corresponding mathematical framework of structured population processes developed by Champagnat et al. [2006, 2008]; Fournier and Méléard [2004]. The protrusive forces are described by a finite point measure that evolves in time by a markovian jump process, so that forces appear and disappear with a stochastic dynamics. This demographic description uses the notions of protrusion rates, so that the model is related to measurable cellular features. The cell polarisation ability is visible in the feedback that the cell motion exerts on the protrusion rates: faster cells form preferentially protrusions in the direction of motion.

In the following, we will introduce rigorously the mathematical model and derive some of its fundamental properties. Moreover, numerical simulations will show that different types of trajectories may be obtained: Brownian-like, persistent, or intermittent when the cell switches between both previous regimes. We find back the trajectories usually described in the literature for cell migration with a dynamics based on cellular processes. This work was made in collaboration with Nicolas Meunier and Raphaël Voituriez (LJP,LPTMC, Univ. Paris 6).

2.2 Construction of the model

2.2.1 Modelling assumptions

We define now the velocity model that is based on force equilibrium.

Velocity model

At each time, the cell velocity writes $\vec{V}_t$, and its polar coordinates (v_t, θ_t). At the scale of a cell (μm), Newton's second law of motion reduces to instantaneous force equilibrium: at all time $t \geq 0$,

$$\sum \vec{F}_{ext}(t) = \vec{0}\,.$$

The cell being an active system, macroscopic forces that apply can be either passive or active. In this case appear

→ a passive force: the **friction force** exerted by the substrate on the cell due to motion, that writes $\vec{f} = -\gamma \vec{V}_t$, with γ the global friction coefficient (of range $10^5 - 10^9 \mathrm{Pa}\cdot\mathrm{s}$ for keratocytes with an averaged radius $R_0 = 1-10\,\mu\mathrm{m}$, see Dembo and Wang [1999]; Oliver et al. [1999]; Theriot and Mitchison [1992]).

→ active forces related to the protrusion process. Indeed, a complex internal activity gives rise to forces in the body of the cell. Filopodial protrusions can be considered as good readouts [Caballero et al., 2014]. As a consequence, in the following, only **filopodial forces** will be considered.

Combining these informations, we get:

$$\gamma \vec{V}_t = \sum_{i=1}^{N_t} \vec{F}_i(t), \tag{2.1}$$

with N_t the number of filopodia adhering on the substrate at time t, and $(\vec{F}_i(t))_i$ the filopodial forces. The cell motion is then entirely described by the protrusions.

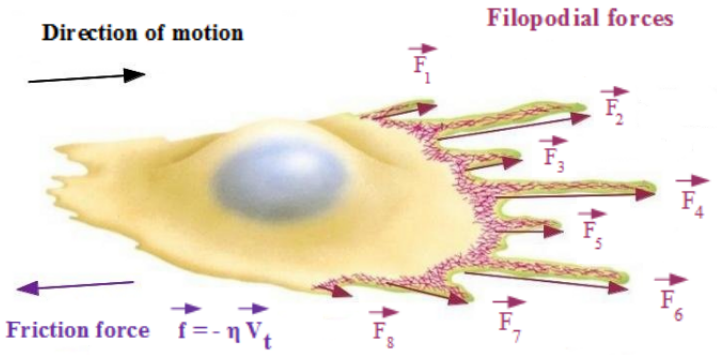

Figure 2.1 – Scheme of a cell with the corresponding forces. Lodish [2002]

Remark 6. *The chosen space scale does not provide any information about intracellular processes (actin polymerization, adhesion, evolution, etc.), nor about the time evolution of a filopodial force. It is therefore natural to assume that each filopodial force is constant and (dis)appears instantaneously: the cell velocity evolves by jumps.*

Hypothesis 6. *Each filopodial force vector is unitary and constant in time.*

Now, denoting $\theta_i = arg(\vec{F_i})$, one can write

$$\vec{F_i}(t) = \begin{pmatrix} \cos(\theta_i) \\ \sin(\theta_i) \end{pmatrix}.$$

Modeling cell motion then accounts to modeling the time evolution of the filopodial population in terms of individual orientation. In what follows we'll indifferently use the term "individual", "filopodium" or "filopodial force".

Mathematical description of filopodia

Each filopodium is characterized by a quantitative parameter, its orientation $\theta \in [0, 2\pi)$. Then we are studying the evolution of a population structured by a phenotypic trait. In that case, at time t, N_t individuals carry traits $(\theta_1, ..., \theta_{N_t})$. However, this vector has a non-constant size. A more natural formalism consists in using finite point measures as in structured population models [Fournier and Méléard, 2004].

Let us denote $\mathcal{M}_F(\overline{\chi})$ the set of positive finite measures on $\overline{\chi} = [0, 2\pi]$, equipped with the weak topology. Notice that as $\overline{\chi}$ is compact, weak and vague topologies on $\mathcal{M}_F(\overline{\chi})$ coincide. Write $\mathcal{M}$ for the subset of $\mathcal{M}_F(\overline{\chi})$ composed of all finite point measures. Then, a filopodium of orientation θ is described by a Dirac measure δ_θ on χ, and the whole population by

$$\nu_t = \sum_{i=1}^{N_t} \delta_{\theta_i} \in \mathcal{M}.$$

For any measurable function f on $\overline{\chi}$ and any $\mu \in \mathcal{M}_F(\overline{\chi})$, we have $< \mu, f >= \int_\chi f(\theta)\mu(\,\mathrm{d}\theta)$. In particular, $< \nu_t, f >= \sum_{i=1}^{N_t} f(\theta_i)$, and the population size corresponds to $N_t =< \nu_t, 1 >$. A simple way to express the velocity equation (2.1) together with hypothesis (6) is to write

$$\gamma \vec{V}_t = \begin{pmatrix} < \nu_t, \cos > \\ < \nu_t, \sin > \end{pmatrix}.$$

Now, the cell motion is entirely described by the time evolution of the population measure ν_t. We already noticed that the scaling choice brings discontinuities in the problem. It also has to be pointed out that by the same argument, the description of the population dynamics is necessarily stochastic.

Finally, we ought to construct a stochastic measure-valued (markovian) jump process $(\nu_t)_t$, as in adaptive stuctured population models.

The dynamics

- The basic dynamics arising is the **isotropic appearance** of filopodia. It is responsible for the spontaneous activity that is observed experimentally. We write **c** for the creation rate.

  A negative feedback driven by the cell velocity could be included. Indeed, as observed in Maiuri et al. [2015], a large cell speed is coupled to a large persistance, due to mechanisms that favor protrusions in the direction of motion. A first step in that process is to inhibit the formation of randomly-oriented filopodia for a growing velocity.

- Each filopodium ends up disappearing: the disappearance or **death** rate is denoted $\mathbf{d}(\theta_\mathbf{i}, \nu_\mathbf{t})$. The choice of an eventual feedback is tricky, as no simple global rule seems to emerge. For simplicity, we take $d(\theta, \nu) = d$ constant.

- Polarisation is characterized by a morphological and functional asymmetry visible both on cell shape and at the microscopic scale. Our model does not allow for these direct descriptions of polarisation (see Wolgemuth et al. [2011] for an example). A macroscopic approach would consist in a particle which velocity is explicitly self-reinforced, as in active Brownian particle models (see Romanczuk et al. [2012]). Here, we use the mesoscopic scale of the model to account for polarisation by its feedback on the protrusive activity. Two phenomena have to be distinguished:

  → The formation of a protrusion is induced by several microscopic regulators (see introduction) and generates a local positive feedback on the protrusive machinery. Following that, we assume that each filopodium is able to **reproduce**. Denote $\mathbf{r}(\theta_\mathbf{i}, \nu_\mathbf{t})$ the individual reproduction rate of a filopodium of orientation θ_i.

  → Polarisation is also reinforced by actin flows, (see Maiuri et al. [2015]). In particular, faster actin flows favor the formation of protrusions in a single stable configuration. Denoting $\vec{u}$ for the space-averaged actin flow velocity over the cell. As actin flows are inwardly directed, $-\vec{u}$ characterizes the reinforced direction for protrusions. Moreover, we know that $\vec{V} = -1/\alpha\, \vec{u}$, where $1/\alpha$ depends on the cell type and the experimental setting. Therefore, we consider a positive coupling between the reproduction rate and $-\vec{u} = \alpha \vec{V}$, imposing a global feedback.

Remark 7 (A local feedback)**.** *Following arguments for a reproduction process as a local feedback, notice that it is possible to define a more powerful one. One can consider a reproduction rate related to the neighbourhood of the individual: the more neighbours there are, the more it is likely to reproduce. This recalls competition kernels in classical population*

models taking into account competition for resources (e.g the Verhulst model). Here, the interaction would be positive, since we assume that the protrusive reinforcement by chemical signalling dominates the local limitations of resources (actin monomers). For example, one can write

$$r(\theta, W * \nu(\theta)) = b\left(\theta, \sum_{i=1}^{N(t)} W(\theta - \theta_i)\right), \tag{2.2}$$

with W an interaction kernel.

This local dependance seems richer, as with the only feedback from the cell velocity, only one axis of polarisation is favored. In the case of the rate (2.2), multipolar configurations could appear. However, the dependance on cell velocity is needed to account for a global polarisation, so that we keep only this global feedback in this work.

Remark 8 (An external feedback)**.** *The environment can also affect the protrusive activity. One can think of reproduction rates depending on external signal, other cells, the nature of the substrate, etc.*

- Reproduction of spatially localized filopodia questions the localization of the new protrusions. An individual can reproduce to form a filopodium with the same orientation, or it can have a slightly different location. This phenomenon accounts for the stochastic fluctuations arising in the cell signalling pathways involved in protrusions. In our model, we describe this using the notion of **heredity** and subsequent **mutation event** for the orientation of the "offspring".

  For simplicity, we assume that at each reproduction event, the mutation probability μ is constant. In the case of a mutant new protrusion, its orientation is determined following a probability distribution $\mathbf{g}(\mathbf{z}; \theta_\mathbf{i})$ assumed centered in the parent's orientation θ_i, with a constant variance.

- Finally, one has to describe the **limitation of resources** for the formation of protrusions. In macroscopic populations usually described by demographic models, resources are necessary for survival, justifying an impact on the death rate. In our case, resources are actin monomers, the main components of filopodia. Their limitation in the medium thus results in a decrease in protrusion formation. This translates to a multiplicative non-increasing term involved in the creation and reproduction rates such as $(1 - {}^{N_t}/\lambda)_+$, with λ accounting for the carrying capacity related to the medium.

The possible events are summed up in the following graph:

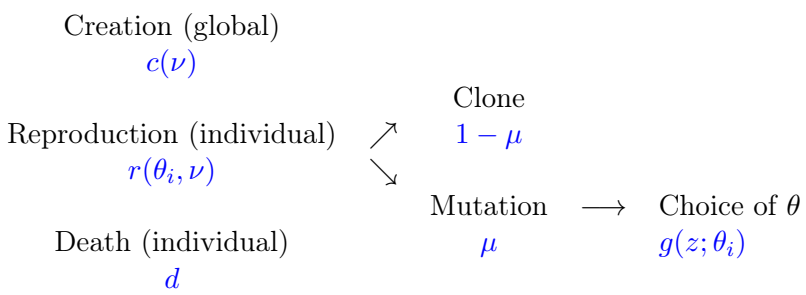

Let us comment on the mathematical features of the model. In the case of no interaction between individuals, or global feedback, the process $(N_t)_t$ simply follows an immigration, birth and death dynamics, and mathematical information can be derived. In particular,

the branching property still holds. This is no longer the case when adding interactions. For example, if the interaction relies on V_t, then one has to know about the structured quantities $(N^{\theta_1}, N^{\theta_2}, ...)$ at all time, for which knowing only N_t is not sufficient.

A practical example For application of our model to the cell migration problem, we choose the following rates:

Creation: For simplicity, we choose a constant isotropic creation rate c.

Reproduction rate: as protrusions are located on $[0, 2\pi)$, it is natural to consider reproduction rates as circular functions. We chose a reproduction function that is positively correlated to $\alpha\vec{V_t}$ to account for polarisation. The idea is to have a function centered in θ_t the direction of motion, that gets sharper with increasing v_t.

We introduce now circular probability distributions that can be used, up to a multiplicative constant, since we don't need particularly a probability density. Recall that characteristic functions ϕ of such distributions are defined only for integer values:

$$\phi_p = \mathbb{E}\left[e^{ip\theta}\right] = \rho_p e^{i\mu_p} = \alpha_p + i\beta_p\,,$$

with $\rho_p \in [0, 1]$. We have $\phi_\theta(0) = 1$, and ρ_1 quantifies the mean concentration of the distribution, while μ_1 is its mean direction. For more details, we refer to Jammalamadaka and SenGupta [2001].

The cardioid distribution has a density

$$f(\theta_i; \theta_t, \rho) = \frac{1}{2\pi}(1 + 2\rho\cos(\theta_i - \theta_t)),$$

with $-1/2 < \rho < 1/2$, and θ_t the mean orientation. We can show that the first circular moment is $\phi_1 = |\rho|e^{i\mu}$, and $\phi_p = 0\ \forall p \geq 1$.

The circular normal distribution has a density

$$f(\theta_i; \theta_t, \kappa) = \frac{1}{2\pi I_0(\kappa)}\exp(\kappa\cos(\theta_i - \theta_t)),$$

with $\kappa \geq 0$ a shape parameter, and I_0 the 0-order modified Bessel function of the first kind. We can show that the p^{eth} trigonometric moment for this density is

$$\phi_P = \int e^{ip\theta} f(\theta; \mu, \kappa)\,\mathrm{d}\theta = \frac{I_p(\kappa)}{I_0(\kappa)}e^{i\mu}\,,$$

for $p \in \mathbb{Z}$.

Mutation event: as explained before, we assume the simplest hypothesis on the mutation parameters: μ is the mutation probability, and $g(z; \theta_i)$ is a circular normal distribution on $[0, 2\pi)$ centered in θ_i and with a constant shape parameter (resp. variance) κ (resp. σ^2).

Death rate: we consider simply a constant individual death rate d.

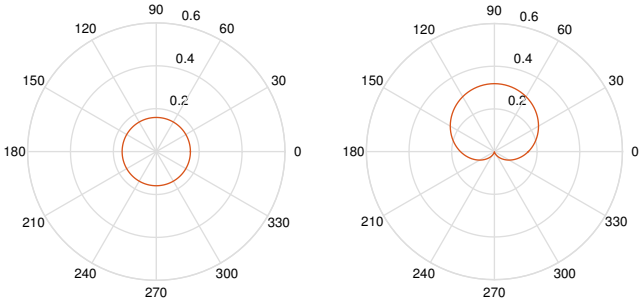

Figure 2.2 – Cardioid distribution for $\theta_t = \pi/2$, $\rho = 0$ (left) and $\rho = 1/2$ (right).

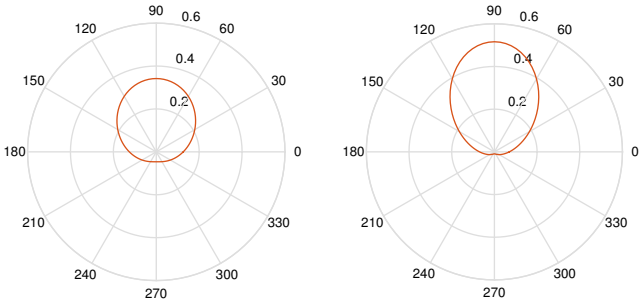

Figure 2.3 – Circular distribution for $\theta_t = \pi/2$, $\kappa = 1$ (left) and $\kappa = 2$ (right).

2.2.2 Mathematical formulation

From now on, we will use the notation C for any constant, that will change from line to line.

We introduce here a stochastic differential equation for $(\nu_t)_t$ driven by Point Poisson Measures. We will show existence and uniqueness of a solution, and prove that it follows the dynamics previously described.

In order to pick a specific individual in the population, we have to be able to order them or their trait. Indeed, from the n-uplet $(\theta_1, ..., \theta_N)$, one can recover $\nu = \sum_{i=1}^N \delta_{\theta_i}$, but from ν it is only possible to know $\{\theta_1, ..., \theta_N\}$.

Definition 6. *Let us define the function*

$$\begin{aligned} H = (H^1, ..., H^k, ...) : \qquad \mathcal{M} \qquad &\longrightarrow \quad (\chi)^{\mathbb{N}^*} \\ \nu = \sum_{i=1}^n \delta_{\theta_i} \quad &\longmapsto \quad (\theta_{\sigma(1)}, ..., \theta_{\sigma(n)}, ...), \end{aligned}$$

with $\theta_{\sigma(1)} \preceq \theta_{\sigma(2)} \preceq ... \preceq \theta_{\sigma(n)}$, for an arbitrary order $\preceq$. Now, an individual can be picked by its label i, and the corresponding trait writes $H^i(\nu) = \theta_{\sigma(i)}$.

Let $(\Omega, \mathcal{F}, \mathbb{P})$ be a probability space, and $n(\,\mathrm{d}i)$ the counting measure on $\mathbb{N}^*$. We introduce the following objects:

- $\nu_0 \in \mathcal{M}$ the finite point measure describing the initial population, eventually equal to the null measure. It can be chosen stochastic as soon as $\mathbb{E}[< \nu_0, 1 >] < +\infty$.
- $M_0(\,\mathrm{d}s, \,\mathrm{d}\theta, \,\mathrm{d}u)$ a Poisson Point Measure on $[0, +\infty) \times \chi \times \mathbb{R}_+$, of intensity measure $\mathrm{d}s \,\mathrm{d}\theta \,\mathrm{d}u$,
- $M_1(\,\mathrm{d}s, \,\mathrm{d}i, \,\mathrm{d}u)$ and $M_3(\,\mathrm{d}s, \,\mathrm{d}i, \,\mathrm{d}u)$ Poisson Point Measures on $[0, +\infty) \times \mathbb{N}^* \times \mathbb{R}_+$, both of intensity measure $\mathrm{d}s\, n(\,\mathrm{d}i) \,\mathrm{d}u$,

- $M_2(\mathrm{d}s, \mathrm{d}i, \mathrm{d}\theta, \mathrm{d}u)$ a Poisson Point Measure on $[0, +\infty) \times \mathbb{N}^* \times \chi \times \mathbb{R}_+$, of intensity measure $\mathrm{d}s n(\mathrm{d}i)\, \mathrm{d}\theta\, \mathrm{d}u$.

The Poisson Measures are independent. Finally, $(\mathcal{F}_t)_{t\geq 0}$ denotes the canonical filtration generated by these objects. Let us construct the $(\mathcal{F}_t)_{t\geq 0}$-adapted process $(\nu_t)_{t\geq 0}$ as the solution of the following SDE: $\forall t \geq 0$,

$$
\begin{aligned}
\nu_t \;=\; & \nu_0 \\
& + \int_0^t \int_{\chi\times\mathbb{R}_+} \delta_\theta \qquad\qquad \mathbb{1}_{u\leq \frac{c(\nu_s)}{2\pi}} \qquad\qquad M_0(\mathrm{d}s, \mathrm{d}\theta, \mathrm{d}u) \\
& + \int_0^t \int_{\mathbb{N}^*\times\mathbb{R}_+} \delta_{H^i(\nu_s)} \mathbb{1}_{i\leq N_s} \mathbb{1}_{u\leq (1-\mu) r(H^i(\nu_s),\nu_s)} \qquad M_1(\mathrm{d}s, \mathrm{d}i, \mathrm{d}u) \\
& + \int_0^t \int_{\mathbb{N}^*\times\chi\times\mathbb{R}_+} \delta_\theta \mathbb{1}_{i\leq N_s} \mathbb{1}_{u\leq \mu r(H^i(\nu_s),\nu_s) g(\theta; H^i(\nu_s)))} \qquad M_2(\mathrm{d}s, \mathrm{d}i, \mathrm{d}\theta, \mathrm{d}u) \\
& - \int_0^t \int_{\mathbb{N}^*\times\mathbb{R}_+} \delta_{H^i(\nu_s)} \mathbb{1}_{i\leq N_s} \mathbb{1}_{u\leq d(H^i(\nu_s),\nu_s)} \qquad M_3(\mathrm{d}s, \mathrm{d}i, \mathrm{d}u).
\end{aligned}
\tag{2.3}
$$

In this equation, each term describes a different event. The Poisson Point Measures generate atoms homogeneously in time. However, the dynamics we want to describe follows state-dependent rates. Hence, we use indicator functions to keep only some of the events in order to get the wanted rates. Then, the Dirac measures correspond to the individuals added to or removed from the population.

In this chapter, we will need boundedness hypothesis on the rates of events.

Hypothesis 7 (Boundedness of rates)**.** *Let $\bar{c}$, $\bar{r}$, $\bar{d}$ be positive constants. Then, $\forall \nu \in \mathcal{M}$, $\forall (\theta, \nu) \in \chi \times \mathcal{M}$, $0 \leq \frac{c(\nu)}{2\pi} \leq \bar{c}$, $0 \leq r(\theta, \nu) \leq \bar{r}$, $0 \leq d(\theta, \nu) \leq \bar{d}$.*

Existence and uniqueness

Let us now show existence and uniqueness of a solution for equation (2.3).

Proposition 11. *Recall that $N_t =< \nu_t, 1 >$. Assume hypothesis 7, and that $\mathbb{E}[N_0] < +\infty$.*

1. *There exists a solution $\nu \in \mathbb{D}(\mathbb{R}_+, \mathcal{M}(\chi))$ of equation (2.3) such that*

$$
\forall T > 0,\ \mathbb{E}\left[\sup_{t\in[0,T]} N_t\right] < \mathbb{E}\left[N_0\right] e^{\bar{r}T} + \frac{\bar{c}}{\bar{r}}(e^{\bar{r}T} - 1) < +\infty\,. \tag{2.4}
$$

2. *There is strong (pathwise) uniqueness of the solution.*

Proof of 11. The proof is similar to prop.2.2.5 and 2.2.6 in Fournier and Méléard [2004].

1. Let $T_0 = 0$, and $t \in \mathbb{R}_+$. Then, the global jump rate of ν_t is smaller than $\bar{c} + (\bar{r} + \bar{d}) N_t$. Hence one can $\mathbb{P} - a.s$ define the sequence $(T_k)_{k\in\mathbb{N}^*}$ of jumping times, as well as $T_\infty := \lim_{k\to+\infty} T_k$.

   Now, by construction, it is $\mathbb{P} - a.s$ possible to build "step-by-step" a solution of equation (2.3) on $[0, T_\infty[$. Showing existence of a solution $(\nu_t)_{t\in\mathbb{R}_+} \in \mathbb{D}(\mathbb{R}_+, \mathcal{M}(\chi))$ amounts to showing that $\mathbb{P} - a.s$, $T_\infty = +\infty$. That is equivalent to saying that there cannot be an infinite number of jumps in a finite time interval.

- **First, we show the control property (2.4).** For $n > 0$ define the sequence of stopping times $(\tau_n)_n$ by

$$\tau_n = \inf_{t\geq 0}\{N_t \geq n\}.$$

→ **Let us show that $(\boldsymbol{\tau_n})_{\boldsymbol{n\geq 0}}$ is a sequence of stopping times for $(\boldsymbol{\mathcal{F}_t})_{\boldsymbol{t}}$.** Denote $\sigma_t = \sigma(\nu_s,\ 0 \leq s \leq t)$ the σ-algebra generated by $\{\nu_s,\ 0 \leq s \leq t\}$. Then $\forall t \geq 0$, $\sigma_t \subseteq \mathcal{F}_t$. For $(n, m) \in (\mathbb{N}^*)^2$, notice that

$$\begin{aligned}\{\tau_n \leq m\} &= \{\inf\{t \geq 0,\ \langle \nu_t, 1\rangle \geq n\} \leq m\}\\ &\in \sigma_m \subseteq \mathcal{F}_m,\end{aligned}$$

and $(\tau_n)_{n\geq 0}$ is indeed a sequence of stopping times.

→ **Now, we prove that for all $\boldsymbol{T < +\infty}$, the quantity $\mathbb{E}\left[\sup_{\boldsymbol{t\in[0,T\wedge\tau_n]}} \boldsymbol{N_t}\right]$ is bounded $\forall \boldsymbol{n \geq 0}$.**
For $t \in \mathbb{R}_+$, using equation (2.3) and dropping the non-positive term, one has

$$\begin{aligned}N_{t\wedge\tau_n} &= <\nu_{t\wedge\tau_n}, 1> \leq N_0 + \int_0^{t\wedge\tau_n}\int_{\chi\times\mathbb{R}_+} \mathbb{1}_{u\leq c(\nu_s)} M_0(\mathrm{d}s, \mathrm{d}\theta, \mathrm{d}u)\\ &+ \int_0^{t\wedge\tau_n}\int_{\mathbb{N}^*\times\mathbb{R}_+} \mathbb{1}_{i\leq N_s}\mathbb{1}_{u\leq(1-\mu)r(H^i(\nu_s),\nu_s)} M_1(\mathrm{d}s, \mathrm{d}i, \mathrm{d}u)\\ &+ \int_0^{t\wedge\tau_n}\int_{\mathbb{N}^*\times\chi\times\mathbb{R}_+} \mathbb{1}_{i\leq N_s}\mathbb{1}_{u\leq\mu r(H^i(\nu_s),\nu_s)g(\theta;H^i(\nu_s))} M_2(\mathrm{d}s, \mathrm{d}i, \mathrm{d}\theta, \mathrm{d}u).\end{aligned}$$

As each integrand is positive, bounded, and integrable with respect to the intensity measure, taking the expectation and using the Fubini theorem, we can write

$$\begin{aligned}\mathbb{E}\left[\sup_{t\in[0,T\wedge\tau_N]} N_t\right] &\leq \mathbb{E}[N_0] + \mathbb{E}\left[\int_0^{T\wedge\tau_N}\left(c(\nu_t) + \sum_{i=1}^{N_t} r(\theta_i, \nu_t)\right)\mathrm{d}t\right]\\ &\leq \mathbb{E}[N_0] + \bar{c}T + \bar{r}\int_0^T \mathbb{E}\left[\sup_{s\in[0,t\wedge\tau_N]} N_s\right]\mathrm{d}t\end{aligned} \tag{2.5}$$

leading to the T-dependent bound using the Gronwall inequality.

→ **Let us prove that $\mathbb{P} - \boldsymbol{a.s}$, $\lim_{\boldsymbol{n\to+\infty}} \boldsymbol{\tau_n} = \boldsymbol{+\infty}$.** If this wasn't the case, there would exist $M < +\infty$ and a set $A_M \subset \Omega$ such that $\mathbb{P}(A_M) > 0$, and $\forall\omega \in A_M$, $\lim_{n\to+\infty}\tau_n(\omega) < M$. By the Markov inequality, $\forall T > M$,

$$\mathbb{E}\left[\sup_{t\in[0,T\wedge\tau_n]} N_t\right] \geq n\,\underbrace{\mathbb{P}\left(\sup_{t\in[0,T\wedge\tau_n]} N_t \geq n\right)}_{\geq\mathbb{P}(A_M)>0},$$

which is in contradiction with equation (2.5).

→ **Property (2.4) is proved by the Fatou lemma:**

$$\mathbb{E}\left[\sup_{t\in[0,T]} N_t\right] = \mathbb{E}\left[\liminf_{n\to+\infty} \sup_{t\in[0,T\wedge\tau_n]} N_t\right]$$
$$\leq \liminf_{n\to+\infty} \mathbb{E}\left[\sup_{t\in[0,T\wedge\tau_n]} N_t\right] \leq \mathbb{E}[N_0]e^{\overline{r}T} + \frac{\overline{c}}{\overline{r}}\left(e^{\overline{r}T}-1\right) < +\infty.$$

- **Now, let us show that $\mathbb{P}-a.s$, $T_\infty = +\infty$.** If this is not the case, then there exists $\overline{M} < +\infty$ and a set $A_{\overline{M}} \subset \Omega$ such that $\mathbb{P}(A_{\overline{M}}) > 0$ and $\forall w \in A_{\overline{M}}$, $T_\infty(\omega) < \overline{M}$. Moreover, if the assertion

$$\forall \omega \in A_{\overline{M}},\ \lim_{k\to+\infty} N_{T_k}(\omega) = +\infty, \tag{2.6}$$

is true, then we would have

$$\forall N > 0,\ \forall \omega \in A_{\overline{M}},\ \tau_N(\omega) \leq \overline{M},$$

which contradicts $\lim_{n\to+\infty}\tau_n = +\infty$. As a consequence, if we prove (2.6), the proposition is proved. If (2.6) is not true, there would exist $N' > 0$ and a set $B \subset A_{\overline{M}}$ such that $\mathbb{P}(B) > 0$ and

$$\forall \omega \in B,\ \forall k \in \mathbb{N},\ N_{T_k}(\omega) < N'.$$

Then, $\forall \omega \in B$, $(T_k(\omega))_k$ can be seen as the subsequence of a sequence of jumping times $(T_k^1(\omega))_k$ of a Point Poisson Process of intensity $\overline{c} + (\overline{r}+\overline{d})N'$. The only accumulation point of $(T_k^1(\omega))_k$ being $\mathbb{P}-a.s\ +\infty$, it contradicts the definition of B, and proves (2.6).

2. The sequence of jumping times $(T_k)_{k\in\mathbb{N}}$ being already defined, we only have to show that $(T_k, \nu_{T_k})_{k\in\mathbb{N}}$ are uniquely determined by $D = (\nu_0, M_0, M_1, M_2, M_3)$ defined above. But this is clear by construction of the process.

□

Markov property

Now, we can show that the solution $(\nu_t)_t$ of equation (2.3) is a Markov process in the Skorohod space $\mathbb{D}(\mathbb{R}_+, \mathcal{M}_F(\chi))$ of càdlàg finite measure-valued processes on χ. For that purpose, we introduce $\forall \nu \in \mathcal{M}$, $\Phi : \mathcal{M} \to \mathbb{R}$ measurable and bounded, the operator L defined by

$$\begin{aligned} L\Phi(\nu) &= \int_\chi \frac{c(\nu)}{2\pi}\left[\Phi(\nu+\delta_\theta)-\Phi(\nu)\right]\mathrm{d}\theta \\ &+ \int_\chi (1-\mu)r(\theta,\nu)\left[\Phi(\nu+\delta_\theta)-\Phi(\nu)\right]\nu(\mathrm{d}\theta) \\ &+ \int_\chi \mu r(\theta,\nu)\int_\chi \left[\Phi(\nu+\delta_z)-\Phi(\nu)\right]g(z;\theta)\,\mathrm{d}z\,\nu(\mathrm{d}\theta) \\ &+ \int_\chi d(\theta,\nu)\left[\Phi(\nu-\delta_\theta)-\Phi(\nu)\right]\nu(\mathrm{d}\theta). \end{aligned} \tag{2.7}$$

Proposition 12. *Assume that the boundedness hypothesis 7 is fulfilled. Take $(\nu_t)_{t\geq 0}$ the solution of equation (2.3) with $\mathbb{E}[< \nu_0, 1 >] < +\infty$. Then, $(\nu_t)_{t\geq 0}$ is a Markovian process of infinitesimal generator L.*

In particular, this proposition ensures that the law of $(\nu_t)_{t\geq 0}$ is independent of the order $\preceq$ involved in (6).

Proof of proposition 12. The process $(\nu_t)_{t\geq 0} \in \mathbb{D}(\mathbb{R}_+, \mathcal{M}(\overline{\chi}))$ is markovian by construction. Now, let $N_0 < N < +\infty$, and consider again the stopping time τ_N. Let $\Phi : \mathcal{M} \to \mathbb{R}$ be measurable and bounded. As $\mathbb{P} - a.s$ we can write

$$\Phi(\nu_t) = \Phi(\nu_0) + \sum_{s\leq t} \Phi(\nu_{s^-} + (\nu_s - \nu_{s^-})) - \Phi(\nu_{s^-}), \tag{2.8}$$

we have

$$\begin{aligned}
\Phi(\nu_{t\wedge\tau_N}) = \Phi(\nu_0) &+ \int_0^{t\wedge\tau_N} \int_{\chi\times\mathbb{R}_+} [\Phi(\nu_{s^-} + \delta_\theta) - \Phi(\nu_{s^-})]\, \mathbb{1}_{u\leq \frac{c(\nu)}{2\pi}} M_0(\mathrm{d}s, \mathrm{d}\theta, \mathrm{d}u) \\
+ &\int_0^{t\wedge\tau_N} \int_{\mathbb{N}^*\times\mathbb{R}_+} \left[\Phi(\nu_{s^-} + \delta_{H^i(\nu_{s^-})}) - \Phi(\nu_{s^-})\right] \mathbb{1}_{i\leq N_{s^-}} \mathbb{1}_{u\leq (1-\mu)r(H^i(\nu_{s^-}),\nu_{s^-})} M_1(\mathrm{d}s, \mathrm{d}i, \mathrm{d}u) \\
+ &\int_0^{t\wedge\tau_N} \int_{\mathbb{N}^*\times\chi\times\mathbb{R}_+} [\Phi(\nu_{s^-} + \delta_z) - \Phi(\nu_{s^-})]\, \mathbb{1}_{i\leq N_{s^-}} \mathbb{1}_{u\leq \mu r(H^i(\nu_{s^-}),\nu_{s^-}) g(z;H^i(\nu_s))} M_2(\mathrm{d}s, \mathrm{d}i, \mathrm{d}z, \mathrm{d}u) \\
+ &\int_0^{t\wedge\tau_N} \int_{\mathbb{N}^*\times\mathbb{R}_+} \left[\Phi(\nu_{s^-} - \delta_{H^i(\nu_{s^-})}) - \Phi(\nu_{s^-})\right] \mathbb{1}_{i\leq N_{s^-}} \mathbb{1}_{u\leq d(H^i(\nu_s),\nu_s)} M_3(\mathrm{d}s, \mathrm{d}i, \mathrm{d}u).
\end{aligned}$$

Again, as all integrands are bounded, we can take expectations to get

$$\begin{aligned}
\mathbb{E}\left[\Phi(\nu_{t\wedge\tau_N})\right] &= \mathbb{E}\left[\Phi(\nu_0)\right] + \mathbb{E}\left[\int_0^{t\wedge\tau_N} \int_\chi [\Phi(\nu_{s^-} + \delta_\theta) - \Phi(\nu_{s^-})] \frac{c(\nu)}{2\pi} \mathrm{d}\theta\, \mathrm{d}s\right] \\
&+ \mathbb{E}\left[\int_0^{t\wedge\tau_N} \sum_{i=1}^{N_{s^-}} \left[\Phi(\nu_{s^-} + \delta_{H^i(\nu_{s^-})}) - \Phi(\nu_{s^-})\right] (1-\mu) r(H^i(\nu_{s^-}), \nu_{s^-})\, \mathrm{d}s\right] \\
&+ \mathbb{E}\left[\int_0^{t\wedge\tau_N} \sum_{i=1}^{N_{s^-}} \mu r(H^i(\nu_{s^-}), \nu_{s^-}) \int_\chi [\Phi(\nu_{s^-} + \delta_z) - \Phi(\nu_{s^-})]\, g(z; H^i(\nu_s))\, \mathrm{d}z\, \mathrm{d}s\right] \\
&+ \mathbb{E}\left[\int_0^{t\wedge\tau_N} \sum_{i=1}^{N_{s^-}} \left[\Phi(\nu_{s^-} - \delta_{H^i(\nu_{s^-})}) - \Phi(\nu_{s^-})\right] d(H^i(\nu_s), \nu_s)\, \mathrm{d}s\right], \\
&=: \mathbb{E}\left[\Phi(\nu_0)\right] + \mathbb{E}\left[\psi(t\wedge\tau_N, \nu)\right].
\end{aligned}$$

On the one hand, $\forall t \in [0, T]$,

$$\begin{aligned}
\| \psi(t\wedge\tau_N, \nu) \|_\infty &\leq 2T \| \Phi \|_\infty \overline{c} + 2T \| \Phi \|_\infty (1-\mu)\overline{r}N + 2T \| \Phi \|_\infty \mu\overline{r}N + 2T \| \Phi \|_\infty \overline{d}N \\
&\leq CT \| \Phi \|_\infty (\overline{c} + (\overline{r} + \overline{d})N) < +\infty.
\end{aligned}$$

On the other hand, $t \mapsto \psi(t\wedge\tau_N, \nu)$ is derivable in $t = 0$ $\mathbb{P} - a.s$ (as $\nu \in \mathbb{D}(\mathbb{R}_+, \mathcal{M}(\chi))$), and for a given ν_0, we have

$$\begin{aligned}\frac{\partial\psi}{\partial t}(0,\nu_0) &= \int_\chi \left[\Phi(\nu_0+\delta_\theta)-\Phi(\nu_0)\right]\frac{c(\nu_0)}{2\pi}\,\mathrm{d}\theta \\ &+ \sum_{i=1}^{N_0}\left[\Phi(\nu_0+\delta_{H^i(\nu_0)})-\Phi(\nu_0)\right](1-\mu)r(H^i(\nu_0),\nu_0) \\ &+ \sum_{i=1}^{N_0}\mu r(H^i(\nu_0),\nu_0)\int_\chi \left[\Phi(\nu_0+\delta_z)-\Phi(\nu_0)\right]g(z;H^i(\nu_0))\,\mathrm{d}z \\ &+ \sum_{i=1}^{N_0}\left[\Phi(\nu_0-\delta_{H^i(\nu_0)})-\Phi(\nu_0)\right]d(H^i(\nu_0),\nu_0)\,.\end{aligned}$$

Moreover, $\| \frac{\partial\psi}{\partial t}(0,\nu_0) \| \leq C \| \Phi \|_\infty (\overline{c}+N_0(\overline{r}+\overline{d}))$. Now,

$$\begin{aligned}L\phi(\nu_0) &:= \left.\frac{\partial\mathbb{E}\left[\phi(\nu_t)\right]}{\partial t}\right|_{t=0} \\ &= \int_\chi \left[\Phi(\nu_0+\delta_\theta)-\Phi(\nu_0)\right]\frac{c(\nu_0)}{2\pi}\,\mathrm{d}\theta + \sum_{i=1}^{N_0}\left[\Phi(\nu_0+\delta_{H^i(\nu_0)})-\Phi(\nu_0)\right](1-\mu)r(H^i(\nu_0),\nu_0) \\ &+ \sum_{i=1}^{N_0}\mu r(H^i(\nu_0),\nu_0)\int_\chi \left[\Phi(\nu_0+\delta_z)-\Phi(\nu_0)\right]g(z;H^i(\nu_0))\,\mathrm{d}z \\ &+ \sum_{i=1}^{N_0}\left[\Phi(\nu_0-\delta_{H^i(\nu_0)})-\Phi(\nu_0)\right]d(H^i(\nu_0),\nu_0),\end{aligned}$$

or equivalently

$$\begin{aligned}L\phi(\nu_0) &= \int_\chi \left[\Phi(\nu_0+\delta_\theta)-\Phi(\nu_0)\right]\frac{c(\nu_0)}{2\pi}\,\mathrm{d}\theta + \sum_{i=1}^{N_0}\left[\Phi(\nu_0+\delta_{H^i(\nu_0)})-\Phi(\nu_0)\right]r(H^i(\nu_0),\nu_0) \\ &+ \sum_{i=1}^{N_0}\left[\Phi(\nu_0-\delta_{H^i(\nu_0)})-\Phi(\nu_0)\right]d(H^i(\nu_0),\nu_0) \\ &+ \mu\sum_{i=1}^{N_0} r(H^i(\nu_0),\nu_0)\left(\int_\chi \Phi(\nu_0+\delta_z)g(z;H^i(\nu_0))\,\mathrm{d}z - \Phi(\nu_0+\delta_{H^i(\nu_0)})\right).\end{aligned}$$

□

2.2.3 Numerical simulations

The construction of the process $(\nu_t)_t$ furnishes directly an algorithm for simulations. We proceed as follows: start with the population measure ν_k at time t_k, for a particle located at X_k.

Time of next event let $\tau = c(\nu_k)+ < \nu_k, r+d >$ denote the global jump rate of the process. Then, the time of the next event writes $t_{k+1} := t_k + \Delta t$, where

$$\Delta t \sim Exp(\tau)\,.$$

Nature of the event what happens at time t_{k+1} is determined as follows:

- creation of a protrusion occurs with probability $\frac{c(\nu_k)}{\tau}$. Its orientation is chosen uniformly on $[0, 2\pi)$.
- reproduction of the protrusion number i occurs with probability $\frac{r(H^i(\nu_k),\nu_k)}{\tau}$. Then,
  - $\rightarrow$ with probability $(1-\mu)$, the new protrusion has orientation $H^i(\nu_k)$,
  - $\rightarrow$ with probability μ, its orientation is chosen with the realization of a random variable having a probability density $g(\,\cdot\,; H^i(\nu_k), \nu_k)$.
- protrusion number i disappears with probability $\frac{d(H^i(\nu_k),\nu_k)}{\tau}$.

The measure ν_{k+1} is then obtained from ν_k and the information of the event occuring at time t_{k+1}.

Updates the particle's new position is

$$X_{k+1} = X_k + \Delta t\, V_k\,,$$

while $V_{k+1} = \frac{1}{\gamma}\begin{pmatrix} < \nu_{k+1}, \cos > \\ < \nu_{k+1}, \sin > \end{pmatrix}$.

One only has to start again to get a trajectory over time.

Results

Let us now present the numerical trajectories we obtained, that are displayed in figures 2.4 and 2.5. Recall that polarisation is quantified by $-\alpha v$, so that the larger α is, the more concentrated in the direction of motion the protrusions are formed. We observe indeed different types of trajectories for varying α, from Brownian-like to persistent. In figure 2.4, the mutation probability is $\mu = 0.2$, whereas it is $\mu = 0.8$ in figure 2.5. We observe that the territory exploration is significantly lower for a higher mutation probability. This shows that the mutation events can not be neglected.

We derive now some classical properties on the model.

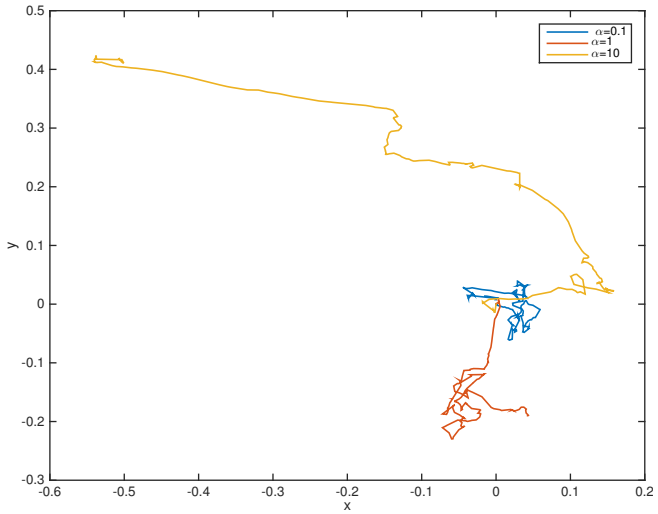

Figure 2.4 – Numerical trajectories obtained for a varying polarisation parameter α. Parameters: $T = 100$, $\Delta t = 10^{-4}$, $c = d = 1$, $r = 0.95$, $\gamma = 90$, $\mu = 0.2$. Mutation concentration parameter $k = 10$.

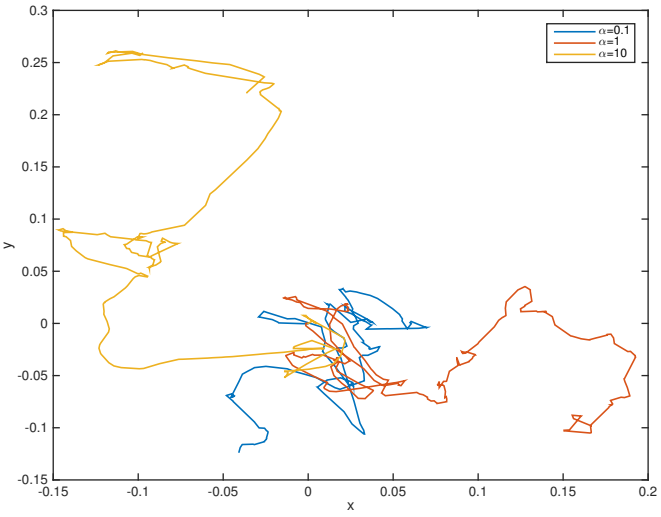

Figure 2.5 – Numerical trajectories obtained for a varying polarisation parameter α. Parameters: $T = 100$, $\Delta t = 10^{-4}$, $c = d = 1$, $r = 0.95$, $\gamma = 90$, $\mu = 0.8$.

2.3 Mathematical properties

2.3.1 Moment property

The first feature of our model concerns the control of moments for the population size.

Proposition 13. *Under the boundedness hypothesis 7, if the exists $p \geq 1$ such that $\mathbb{E}\left[< \nu_0, 1 >^p\right] < +\infty$, then $\forall\, T > 0$,*

$$\mathbb{E}\left[\sup_{t\in[0,T]} < \nu_t, 1 >^p\right] < +\infty.$$

Proof of 13. Using equation (2.8) with $\Phi(\nu_t) =< \nu_t, 1 >^p$ and the expression of ν_t in equation (2.3),

$$\begin{aligned}
< \nu_t, 1 >^p \leq N_0^p &+ \int_0^t \int_{\chi\times\mathbb{R}_+} \left(< \nu_{s^-} + \delta_\theta, 1 >^p - < \nu_{s^-}, 1 >^p\right) \mathbb{1}_{u\leq \frac{c(\nu_s)}{2\pi}} M_0(\mathrm{d}s, \mathrm{d}\theta, \mathrm{d}u) \\
+ \int_0^t \int_{\mathbb{N}^*\times\mathbb{R}_+} &\left(< \nu_{s^-} + \delta_{H^i(\nu_s)}, 1 >^p - < \nu_{s^-}, 1 >^p\right) \mathbb{1}_{i\leq <\nu_{s^-},1>} \mathbb{1}_{u\leq(1-\mu)r(H^i(\nu_s),\nu_s)} M_1(\mathrm{d}s, \mathrm{d}i, \mathrm{d}u) \\
+ \int_0^t \int_{\mathbb{N}^*\times\chi\times\mathbb{R}_+} &\left(< \nu_{s^-} + \delta_z, 1 >^p - < \nu_{s^-}, 1 >^p\right) \mathbb{1}_{i\leq <\nu_{s^-},1>} \mathbb{1}_{u\leq\mu r(H^i(\nu_s),\nu_s) g(z;H^i(\nu_s))} M_2(\mathrm{d}s, \mathrm{d}i, \mathrm{d}z, \mathrm{d}u)\,.
\end{aligned}$$

As before all integrands are bounded, allowing us to take expectations. Using again the stopping time $\tau_n = \inf_{t\geq 0}\{< \nu_t, 1 >\geq n\}$ for $n \geq 0$, we get

$$\mathbb{E}\left[\sup_{s\in[0,t\wedge\tau_n]} < \nu_s, 1 >^p\right] \leq \mathbb{E}\left[N_0^p + C\int_0^{t\wedge\tau_n} (1+ < \nu_{s^-}, 1 >)\left((< \nu_{s^-}, 1 > +1)^p - < \nu_{s^-} 1 >^p\right) \mathrm{d}s\right].$$

We use now the following lemma:

Lemma 2. *Let $x \in \mathbb{R}_+$, and p a positive integer. Then, there exists a positive constant C_p such that*

$$(1+x)^p - x^p \leq C_p(1 + x^{p-1})\,.$$

Proof. Notice that

$$\begin{aligned}
(1+x)^p &= \sum_{k=0}^{p} \binom{p}{k} x^k 1^{p-k} = x^p + \sum_{k=0}^{p-1} \binom{p}{k} x^k\,, \\
&= x^p + (1 + px^{p-1}) + \sum_{k=1}^{p-2} \binom{p}{k} x^k\,.
\end{aligned}$$

Now $\forall 1 \leq k \leq p-2$, we have either $x \leq 1$, and $x^k \leq 1$, either $x \geq 1$ and then $x^k \leq x^{p-1}$. Then,

$$\begin{aligned}
(1+x)^p &\leq x^p + (1 + px^{p-1}) + \sum_{k=1}^{p-2} \binom{p}{k} (1 + x^{p-1}) \\
&\leq x^p + (1 + x^{p-1}) \underbrace{\left[p + \sum_{k=1}^{p-2} \binom{p}{k}\right]}_{=2^{p-1}-1}.
\end{aligned}$$

□

Then for some constant C_p,

$$\begin{aligned}\mathbb{E}\left[\sup_{s\in[0,t\wedge\tau_N]} <\nu_s,1>^p\right] &\leq \mathbb{E}[N_0^p] + C(p)\mathbb{E}\left[\int_0^{t\wedge\tau_N} (1+<\nu_{s^-},1>)\left(1+<\nu_{s^-},1>^{p-1}\right)\,\mathrm{d}s\right]\\ &\leq \mathbb{E}[N_0^p] + C(p)\int_0^t 1+\mathbb{E}[\sup_{u\in[0,s\wedge\tau_N]} <\nu_{u^-},1>^{p-1}]\,\mathrm{d}s\,,\\ &\quad + C(p)\int_0^t \mathbb{E}[\sup_{u\in[0,s\wedge\tau_N]} <\nu_{u^-},1>] + \mathbb{E}[\sup_{u\in[0,s\wedge\tau_N]} <\nu_{u^-},1>^p]\,\mathrm{d}s\,.\end{aligned}$$

Now, it is clear that for $k\in\{1,p-1\}$, $\mathbb{E}\left[\sup_{u\in[0,s\wedge\tau_N]} <\nu_{u^-},1>^k\right] \leq 1+\mathbb{E}\left[\sup_{u\in[0,s\wedge\tau_N]} <\nu_{u^-},1>^p\right]$, and

$$\mathbb{E}\left[\sup_{s\in[0,t\wedge\tau_N]} <\nu_s,1>^p\right] \leq \mathbb{E}[N_0^p] + C(p,t)\left(1+\int_0^t \mathbb{E}\left[\sup_{u\in[0,s\wedge\tau_N]} <\nu_{u^-},1>^p\right]\,\mathrm{d}s\right),$$

and by the Gronwall inequality,

$$\mathbb{E}\left[\sup_{t\in[0,T\wedge\tau_N]} <\nu_t,1>^p\right] \leq C(p,T)\,,$$

by the assumption on the initial measure.

- As before, we have $\lim_{n\to+\infty} \tau_n = +\infty$ $\mathbb{P}-a.s$.
- **Finally, by the Fatou inequality,** :

$$\begin{aligned}\mathbb{E}\left[\sup_{t\in[0,T]} <\nu_t,1>^p\right] &= \mathbb{E}\left[\liminf_{n\to+\infty}\sup_{t\in[0,T\wedge\tau_n]} <\nu_t,1>^p\right]\\ &\leq \liminf_{n\to+\infty}\mathbb{E}\left[<\nu_t,1>^p\right] \leq C(p,T) < +\infty.\end{aligned}$$

□

2.3.2 Martingale property

Markov processes are usually associated with a semimartingale structure. We are able to prove that for any real-valued process $(\Phi(\nu_t))_t$, with $\Phi:\mathcal{M}\to\mathbb{R}$ measurable, there exists a martingale $(M_t)_t$ and a finite variation process $(A_t)_t$ such that $\forall t\geq 0$, $\Phi(\nu_t) = \Phi(\nu_0)+A_t+M_t$.

Theorem 8. *Assume there exists $p\geq 2$ such that $\mathbb{E}[\langle\nu_0,1\rangle^p] < +\infty$. Then, under the boundedness hypothesis 7,*

1. *$\forall$ measurable $\Phi:\mathcal{M}\to\mathbb{R}$ for which there exists C such that $\forall\nu\in\mathcal{M}$, $|\Phi(\nu)| + |L\Phi(\nu)| \leq C(1+<\nu,1>^p)$,*

$$\Phi(\nu_t) - \Phi(\nu_0) - \int_0^t L\Phi(\nu_s)\,\mathrm{d}s \tag{2.9}$$

is a càdlàg $(\mathcal{F}_t)_{t\geq 0}$-martingale starting from 0.

2. *This applies in particular to functions* $\Phi : \nu \mapsto < \nu, f >^q$, *for* $0 \leq q \leq p$, *and* f *measurable bounded on* χ.

3. *For such* f *and* $q = 1$, *the process*

$$\begin{aligned} M_t^f =& < \nu_t, f > - < \nu_0, f > - \int_0^t \int_\chi \frac{c(\nu_s)}{2\pi} f(\theta) \, \mathrm{d}\theta \, \mathrm{d}s \\ & - \int_0^t \int_\chi \left(r(\theta, \nu_s) - d(\theta, \nu_s) \right) f(\theta) \nu(\, \mathrm{d}\theta) \, \mathrm{d}s \\ & - \int_0^t \int_\chi \mu r(\theta, \nu_s) \left(\int_\chi f(z) g(z; \theta) \, \mathrm{d}z - f(\theta) \right) \nu_s(\, \mathrm{d}\theta) \, \mathrm{d}s \end{aligned} \tag{2.10}$$

is a càdlàg square-integrable martingale starting from 0 *and of quadratic variation*

$$\begin{aligned} \left\langle M^f \right\rangle_t = & \int_0^t \int_\chi \frac{c(\nu_s)}{2\pi} f(\theta)^2 \, \mathrm{d}\theta + \int_\chi (r(\theta, \nu_s) + d(\theta, \nu_s)) f(\theta)^2 \nu_s(\, \mathrm{d}\theta) \\ & + \int_\chi \mu r(\theta, \nu_s) \left[\int_\chi f(z)^2 g(z; \theta) \, \mathrm{d}z - f(\theta)^2 \right] \nu_s(\, \mathrm{d}\theta) \, \mathrm{d}s \, . \end{aligned} \tag{2.11}$$

Proof of 8. 1. Point 1 is a direct consequence of the definition of infinitesimal generator, as proposition 13 ensures integrability of the expression.

2. Take $\nu \in \mathcal{M}$, f measurable bounded on χ, and $\Phi(\nu) =< \nu, f >^q$ for $0 \leq q \leq p$. Then,

$$\begin{aligned} |\Phi(\nu)| + |L\Phi(\nu)| \leq & \| f \|_\infty^q < \nu, 1 >^q + \overline{c} \int_\chi |(< \nu, f > + f(\theta))^q - < \nu, f >^q| \, \mathrm{d}\theta \\ & + (1 - \mu) \overline{r} \int_\chi |(< \nu, f > + f(\theta))^q - < \nu, f >^q| \, \nu(\, \mathrm{d}\theta) \\ & + \mu \overline{r} \iint_{\chi \times \chi} |(< \nu, f > + f(z))^q - < \nu, f >^q| \, g(z; \theta) \, \mathrm{d}z \nu(\, \mathrm{d}\theta) \\ & + \overline{d} \int_\chi |(< \nu, f > - f(\theta))^q - < \nu, f >^q| \, \nu(\, \mathrm{d}\theta) \, . \end{aligned}$$

Now notice that

$$\begin{aligned} (< \nu, f > + f(\theta))^q &= \sum_{i=0}^q \binom{q}{k} < \nu, f >^k f(\theta)^{q-k} \\ &=< \nu, f >^q + \sum_{i=0}^{q-1} \binom{q}{k} < \nu, f >^k f(\theta)^{q-k} \, , \end{aligned}$$

hence

$$\begin{aligned} |(< \nu, f > + f(\theta))^q - < \nu, f >^q| &\leq \sum_{i=0}^{q-1} \binom{q}{k} |< \nu, f >|^k |f(\theta)|^{q-k} \\ &\leq \sum_{i=0}^{q-1} \binom{q}{k} \left(1 + | < \nu, f > |^{q-1} \right) (1 + \| f \|_\infty^q) \\ &\leq C(1 + < \nu, 1 >^{q-1}) \end{aligned}$$

for a constant C, and similarly

$$|(<\nu, f> - f(\theta))^q - <\nu, f>^q| \quad \leq \quad C(1+ <\nu, 1>^{q-1}).$$

This leads to

$$\begin{aligned}
|\Phi(\nu)| + |L\Phi(\nu)| \leq & \| f \|_\infty^q <\nu, 1>^q + C(1+ <\nu, 1>^{q-1}) \\
& + C \int_\chi 1+ <\nu, 1>^{q-1} \nu(\,\mathrm{d}\theta) \\
& \leq C(1+ <\nu, 1> + <\nu, 1>^{q-1} + <\nu, 1>^q) \\
& \leq C(1+ <\nu, 1>^q)\,,
\end{aligned}$$

because $<\nu, 1>$ and $<\nu, 1>^{q-1}$ are always smaller than $1+ <\nu, 1>^q$.

3. **Semimartingale formulation:** the expression (2.10) comes from equation (2.9) for $\Phi_1(\nu) := <\nu, f>$. In this case, one can write

$$\begin{aligned}
L\Phi_1(\nu) \quad = \quad & \int_\chi \frac{c(\nu)}{2\pi} f(\theta)\,\mathrm{d}\theta + \int_\chi (1-\mu) r(\theta,\nu) f(\theta) \nu(\,\mathrm{d}\theta) \\
& + \int_\chi \mu r(\theta,\nu) \int_\chi f(z) g(z;\theta)\,\mathrm{d}z\, \nu(\,\mathrm{d}\theta) - \int_\chi d(\theta,\nu) f(\theta) \nu(\,\mathrm{d}\theta) \\
= \quad & \int_\chi \frac{c(\nu)}{2\pi} f(\theta)\,\mathrm{d}\theta + \int_\chi (r(\theta,\nu) - d(\theta,\nu)) f(\theta) \nu(\,\mathrm{d}\theta) \\
& + \int_\chi \mu r(\theta,\nu) \underbrace{\left[\int_\chi f(z) g(z;\theta)\,\mathrm{d}z - f(\theta) \right]}_{(1)} \nu(\,\mathrm{d}\theta),
\end{aligned}$$

and directly obtain formulation (2.10).

Remark 9. *For g a distribution of mean θ, the term (1) corresponds to $\mathbb{E}[f(Z)] - f(\mathbb{E}[Z])$, Z being the random variable of the offspring's orientation.*

Quadratic variation:

→ As a first step, compute the Doob decomposition of $\Phi(\nu_t) := <\nu_t, 1>^2$ using (2.9). Notice that

$$\begin{aligned}
(<\nu, f> + f(\theta))^2 - <\nu, f>^2 \quad &= \quad 2 <\nu, f> f(\theta) + f(\theta)^2, \\
(<\nu, f> - f(\theta))^2 - <\nu, f>^2 \quad &= \quad -2 <\nu, f> f(\theta) + f(\theta)^2.
\end{aligned}$$

Hence we can write

$$\begin{aligned}
L\Phi(\nu) \quad = \quad & \int_\chi \frac{c(\nu)}{2\pi} f(\theta)^2\,\mathrm{d}\theta + \int_\chi (r(\theta,\nu) + d(\theta,\nu)) f(\theta)^2 \nu(\,\mathrm{d}\theta) \\
& + \int_\chi \mu r(\theta,\nu) \left[\int_\chi f(z)^2 g(z;\theta)\,\mathrm{d}z - f(\theta)^2 \right] \nu(\,\mathrm{d}\theta) \\
& + 2 <\nu, f> \left(\int_\chi \frac{c(\nu)}{2\pi} f(\theta)\,\mathrm{d}\theta + \int_\chi (r(\theta,\nu) - d(\theta,\nu)) f(\theta) \nu(\,\mathrm{d}\theta) \right) \\
& + 2 <\nu, f> \int_\chi \mu r(\theta,\nu) \left[\int_\chi f(z) g(z;\theta)\,\mathrm{d}z - f(\theta) \right] \nu(\,\mathrm{d}\theta) \\
= \quad & L\Phi_2(\nu) + 2 <\nu, f> L\Phi_1(\nu)\,,
\end{aligned}$$

with $\Phi_2(\nu) :=< \nu, f^2 >$. By (2), we know that

$$< \nu_t, f >^2 - < \nu_0, f >^2 - \int_0^t L\Phi_2(\nu_s) + 2 < \nu_s, f > L\Phi_1(\nu_s)\,\mathrm{d}s$$

is a càdlàg martingale starting from 0.

→ As a second step, applying Itô's formula to equation (2.10) leads to another decomposition that involves the quadratic variation of $(M^f)_t$:

$$< \nu_t, f >^2 - < \nu_0, f >^2 - \int_0^t 2 < \nu_s, f > L\Phi_1(\nu_s)\,\mathrm{d}s - < M^f >_t$$

is a martingale. From the uniqueness of such decomposition, we find

$$< M^f >_t = \int_0^t L\Phi_2(\nu_s)\,\mathrm{d}s,$$

that is exactly formula (2.11).

□

2.3.3 Moment equation

Let us now investigate the mean path of this process. For $\nu \in \mathcal{M}(\chi)$ a random measure, define its mean measure $\mathbb{E}[\nu]$ by

$$\int_\chi f(\theta)\mathbb{E}[\nu](\,\mathrm{d}\theta) = \mathbb{E}\left[\int_\chi f(\theta)\nu(\,\mathrm{d}\theta)\right].$$

Then, taking expectations in (2.10), we have for f measurable and bounded on χ,

$$\begin{aligned} < \mathbb{E}[\nu_t], f > =< \mathbb{E}[\nu_0], f > &+ \int_0^t \mathbb{E}\left[\int_\chi \frac{c(\nu_s)}{2\pi} f(\theta)\,\mathrm{d}\theta\right]\,\mathrm{d}s \\ &+ \int_0^t \mathbb{E}\left[\int_\chi \left((1-\mu)r(\theta,\nu_s) - d(\theta,\nu_s)\right) f(\theta)\nu_s(\,\mathrm{d}\theta)\right]\,\mathrm{d}s \\ &+ \int_0^t \mathbb{E}\left[\int_\chi \mu r(\theta,\nu_s)\int_\chi f(z)g(z;\theta)\,\mathrm{d}z\,\nu_s(\,\mathrm{d}\theta)\right]\,\mathrm{d}s\,, \end{aligned} \tag{2.12}$$

and the non linearities prevent us from going further on the computation. In the particular case where c, r and d are independent of the population measure, we get

$$\begin{aligned} < \mathbb{E}[\nu_t], f > =< \mathbb{E}[\nu_0], f > + \int_0^t \frac{c}{2\pi}\int_\chi f(\theta)\,\mathrm{d}\theta\,\mathrm{d}s + ((1-\mu)r - d)\int_0^t < \mathbb{E}[\nu_s], f >\,\mathrm{d}s \\ + \int_0^t \mu r\left\langle \mathbb{E}[\nu_s], \int_\chi f(z)g(z;\theta)\,\mathrm{d}z\right\rangle\,\mathrm{d}s, \end{aligned}$$

and we can see that the dependance of g on θ prevent us from closing the system. However, we can have informations on the mean population size: take $f \equiv 1$:

$$< \mathbb{E}[\nu_t], 1 > \;=\; < \mathbb{E}[\nu_0], 1 > + ct + (r-d)\int_0^t < \mathbb{E}[\nu_s], 1 >\,\mathrm{d}s,$$

leading to

$$\mathbb{E}[N_t] = \mathbb{E}[N_0]e^{(r-d)t} + \frac{c}{r-d}\left(e^{(r-d)t} - 1\right)$$

for $r \neq d$.

Finally, it is possible to prove an absolute continuity result for (2.12).

Proposition 14. *Under hypothesis 7, if $\mathbb{E}[< \nu_0, 1 >] < +\infty$, and $\mathbb{E}[\nu_0]$ is absolutely continuous with respect to the Lebesgue measure $\mathrm{d}\theta$, then for all $t \geq 0$, $\mathbb{E}[\nu_t]$ is also absolutely continuous with respect to $\mathrm{d}\theta$.*

Proof. Take $f = \mathbf{1}_A(\theta)$ with A a Borel subset of χ of null Lebesgue measure. Then, for $n \in \mathbb{N}$, we have

$$\begin{aligned}
\mathbb{E}[< \nu_{t\wedge\tau_n}, \mathbf{1}_A >] &= \mathbb{E}[< \nu_0, \mathbf{1}_A >] + \int_0^t \overbrace{\int_\chi \frac{c}{2\pi}\mathbf{1}_A(\theta)\,\mathrm{d}\theta}^{=0}\,\mathrm{d}s \\
&\quad + \mathbb{E}\left[\int_0^{t\wedge\tau_n}\int_\chi \left(r(\theta,\nu_s) - d(\theta,\nu_s)\right)\mathbf{1}_A(\theta)\nu_s(\,\mathrm{d}\theta)\,\mathrm{d}s\right] \\
&\quad + \mathbb{E}\left[\int_0^{t\wedge\tau_n}\int_\chi \mu r(\theta,\nu_s)\left(\underbrace{\int_\chi \mathbf{1}_A(z)g(z;\theta)\,\mathrm{d}z}_{=0} - \mathbf{1}_A(\theta)\right)\nu_s(\,\mathrm{d}\theta)\,\mathrm{d}s\right], \\
&\leq ((1-\mu)\overline{r} + \overline{d})\mathbb{E}\left[\int_0^{t\wedge\tau_n}\int_\chi \mathbf{1}_A(\theta)\nu_s(\,\mathrm{d}\theta)\,\mathrm{d}s\right],
\end{aligned}$$

thanks to our assumptions. The Gronwall lemma gives us $\mathbb{E}[< \nu_{t\wedge\tau_n}, \mathbf{1}_A >] = 0$, and the moment property 13 allows us to take the limit $\tau_n \to +\infty$ almost surely with n, and to conclude the proof. □

2.4 Annex

2.4.1 Gronwall lemma

Lemma 3 (Gronwall [Rudin, 1987])**.** *Soient $T \in \mathbb{R}_+$, $a, b \in L^\infty(0,T)$, et $\lambda \geq 0$ une constante. Si pour presque tout $t \in [0,T]$, on a*

$$a(t) \leq b(t) + \lambda\int_0^t a(s)\,\mathrm{d}s,$$

alors pour presque tout $t \in [0,T]$, on a

$$a(t) \leq b(t) + \lambda\int_0^t e^{\lambda(t-s)}b(s)\,\mathrm{d}s.$$

2.4.2 Itô formula

Theorem 9 (Itô formula [Ikeda and Watanabe, 1989])**.** *Let X be a semimartingale and F a real $\mathcal{C}^2$ function. Then $F(X)$ is also a semimartingale and*

$$F(X_t) = F(X_0) + \int_0^t F'(X_{s^-})dX_s + \frac{1}{2}\int_0^t F''(X_{s^-})d < X, X >_s$$

Bibliography

Caballero, D., Voituriez, R., and Riveline, D. (2014). Protrusion fluctuations direct cell motion. Biophys J, 107(1):34–42. 78

Champagnat, N., Ferrière, R., and Méléard, S. (2006). Unifying evolutionary dynamics: from individual stochastic processes to macroscopic models. Theor Popul Biol, 69(3):297–321. 78

Champagnat, N., Ferrière, R., and Méléard, S. (2008). From Individual Stochastic Processes to Macroscopic Models in Adaptive Evolution. Stochastic Models, 24(sup1):2–44. 78

Dembo, M. and Wang, Y.-L. (1999). Stresses at the cell-to-substrate interface during locomotion of fibroblasts. Biophysical journal, 76(4):2307–2316. 78

Fournier, N. and Méléard, S. (2004). A microscopic probabilistic description of a locally regulated population and macroscopic approximations. The Annals of Applied Probability, 14(4):1880–1919. 78, 79, 84

Ikeda, N. and Watanabe, S. (1989). Stochastic differential equations and diffusion processes. Kodansha scientific books. North-Holland. 96

Jammalamadaka, S. and SenGupta, A. (2001). Topics in Circular statistics, volume 5 of Series on multivariate analysis. World scientific edition. 82

Lodish, et al Harvey, D. B. (2002). Molecular Cell Biology, 4th Edition. W H Freeman & Co, fourth edition edition edition. 79

Maiuri, P., Rupprecht, J.-F., Wieser, S., Ruprecht, V., Bénichou, O., Carpi, N., Coppey, M., De Beco, S., Gov, N., Heisenberg, C.-P., Lage Crespo, C., Lautenschlaeger, F., Le Berre, M., Lennon-Dumenil, A.-M., Raab, M., Thiam, H.-R., Piel, M., Sixt, M., and Voituriez, R. (2015). Actin flows mediate a universal coupling between cell speed and cell persistence. Cell, 161(2):374–86. 80

Oliver, T., Dembo, M., and Jacobson, K. (1999). Separation of propulsive and adhesive traction stresses in locomoting keratocytes. The Journal of cell biology, 145(3):589–604. 78

Romanczuk, P., Bär, M., Ebeling, W., Lindner, B., and Schimansky-Geier, L. (2012). Active brownian particles. from individual to collective stochastic dynamics. Eur.Phys.J. 77, 80

Rudin, W. (1987). Real and complex analysis. Mathematics series. McGraw-Hill. 96

Theriot, J. A. and Mitchison, T. J. (1992). Comparison of actin and cell surface dynamics in motile fibroblasts. The Journal of cell biology, 119(2):367–377. 78

Tran, V. C. (2006). Modèles particulaires stochastiques pour des problèmes d'évolution adaptative et pour l'approximation de solutions statistiques. phdthesis, Université de Nanterre - Paris X.

Wolgemuth, C. W., Stajic, J., and Mogilner, A. (2011). Redundant mechanisms for stable cell locomotion revealed by minimal models. Biophys J, 101(3):545–53. 80

Chapter 3

Scaling limits

Contents

3.1 Scaling the force and dynamics 99
3.1.1 Motivations 99
3.1.2 The renormalized sequence of processes 100
3.2 Deterministic limits 104
3.2.1 Accelerated creation - deterministic limit 105
3.2.2 Non accelerated dynamics 111
3.3 Accelerated demography 112
3.3.1 Preliminary results 112
3.3.2 Rare mutations case 114
3.3.3 Small mutation step approximation 122
3.4 Annex 133
3.4.1 A Cameron Martin Girsanov formula 133

3.1 Scaling the force and dynamics

3.1.1 Motivations

The trajectory model that we built in the previous chapter was scaled to describe the filopodial protrusive dynamics, that is discontinuous in both time and space. If this scaling facilitates the formulation of the model, it does not fully characterize the continuous protrusive dynamics. However, as pointed out in Caballero et al. [2014], filopodial dynamics can be taken as a readout of the whole motile machinery, generally acting at smaller scales in time and space/force. Its most prominent component is the lamellipodium, which dynamics can be considered as continuous compared to the filopodial dynamics. Hence, renormalizing the model in time and space/force, one can hope to get a continuous limiting equation for cell motion.

In the following, we will work in the space $(\mathcal{M}_F(\overline{\chi}), w)$ equipped with the weak topology [Billingsley, 1999; Li, 2010]:

Definition 7. *For $\nu \in \mathcal{M}_F(\overline{\chi})$, a family $(\nu_k)_k \subset \mathcal{M}_F(\overline{\chi})$ is said to converge weakly to ν if for every $f \in \mathcal{C}_b(\overline{\chi})$, $\lim_{k\to+\infty} < \nu_k, f >=< \nu, f >$.*

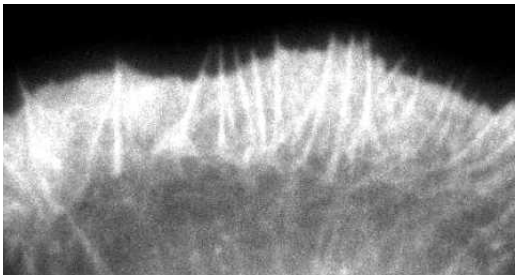

Figure 3.1 – Picture of an XTC cell marked for actin filaments. One can observe the filopodia and the continuous lamellipodium. Reprinted from Ryan et al. [2012], with permission from Elsevier.

3.1.2 The renormalized sequence of processes

Let K be a parameter scaling the number of isolated/discrete protrusions we consider. We assume that the cell can generate a constant maximal force range, so that when K grows, the corresponding individual force ranges in $\frac{1}{K}$. Overall, this amounts to looking at protrusions at a smaller and smaller scale (from a filopodium to actin filaments, see figure 2.1). As a consequence, the demographic dynamics can also get faster and faster, so that we consider now parameters and rates c_K, r_K, d_K, μ_K and g_K that can depend on K.

In this section, we work with K fixed, and assume that they satisfy the following boundedness and continuity hypothesis:

Hypothesis 8 (Boundedness, continuity)**.** *Let $\overline{c}$, $\overline{r}$, and $\overline{d}$, be positive constants. Then, for all $\nu \in \mathcal{M}_F$, $\theta \in \overline{\chi}$,*

$$0 \leq c_K(\nu) \leq K\overline{c}, \quad 0 \leq r_K(\theta, \nu) \leq \overline{r} + Ka, \quad 0 \leq d_K(\theta, \nu) \leq \overline{d} + Ka,$$

and the rates are continuous.

Denote $(\nu_t^K)_t$ the corresponding process, defined as in equation (2.3), and having the infinitesimal generator $\overline{L}^K$ defined by (2.7) with the corresponding parameters.

Finally, let us define the $\mathcal{M}_F(\overline{\chi})$-valued process $(X_t^K)_t$ by

$$X_t^K = \frac{1}{K}\nu_t^K. \tag{3.1}$$

The notational function H defined in the last chapter in 6 classically generalizes to measures of the form $\frac{1}{K}\nu$ with $K > 0$ and $\nu \in \mathcal{M}$.

Let $(\Omega, \mathcal{F}, \mathbb{P})$ be a probability space, and define $\forall K > 0$ $X_0^K \in \mathcal{M}_F(\overline{\chi})$ the finite non-negative measure describing the initial population, such that $\sup_{K>0} \mathbb{E}[< X_0^K, 1 >] < +\infty$. The Poisson Point Measures M_0, M_1, M_2, M_3 are the same as before, and independent with $(X_0^K)_{K>0}$. Finally, $(\mathcal{F}_t)_{t\geq 0}$ denotes the canonical filtration generated by these objects.

As before, the $(\mathcal{F}_t)_{t\geq 0}$-adapted process $(X_t^K)_{t\geq 0}$ can be defined as the solution of an SDE. Denote $N_t^K := K < X_t^K, 1 >$. Then, $\forall K > 0$, $\forall t \geq 0$,

$$
\begin{aligned}
X_t^K &= X_0^K \\
&+ \int_0^t \int_{\chi\times\mathbb{R}_+} \tfrac{1}{K}\delta_\theta \mathbb{1}_{u\leq \frac{c_K(X_s^K)}{2\pi}} M_0(\mathrm{d}s, \mathrm{d}\theta, \mathrm{d}u) \\
&+ \int_0^t \int_{\mathbb{N}^*\times\mathbb{R}_+} \tfrac{1}{K}\delta_{H^i(X_s^K)} \mathbb{1}_{i\leq N_s^K} \mathbb{1}_{u\leq(1-\mu_K)r_K(H^i(X_s^K))} M_1(\mathrm{d}s, \mathrm{d}i, \mathrm{d}u) \\
&+ \int_0^t \int_{\mathbb{N}^*\times\chi\times\mathbb{R}_+} \tfrac{1}{K}\delta_\theta \mathbb{1}_{i\leq N_s^K} \mathbb{1}_{u\leq\mu_K r_K(H^i(X_s^K))g_K(\theta;H^i(X_s^K)))} M_2(\mathrm{d}s, \mathrm{d}i, \mathrm{d}\theta, \mathrm{d}u) \\
&- \int_0^t \int_{\mathbb{N}^*\times\mathbb{R}_+} \tfrac{1}{K}\delta_{H^i(X_s^K)} \mathbb{1}_{i\leq N_s^K} \mathbb{1}_{u\leq d_K(H^i(X_s^K))} M_3(\mathrm{d}s, \mathrm{d}i, \mathrm{d}u).
\end{aligned}
\tag{3.2}
$$

Existence and uniqueness

Analogously, we can prove existence and uniqueness of a solution $(X_t^K)_{t\geq 0}$ of equation (3.2).

Proposition 15. *Assuming that* $\mathbb{E}[< X_0^K, 1 >] < +\infty$, *and under hypothesis 8,*

1. *there exists a solution* $(X_t^K)_{t\in\mathbb{R}_+} \in \mathbb{D}(\mathbb{R}_+, \mathcal{M}_F(\overline{\chi}))$ *of (3.2) such that* $\forall T > 0$,

$$
\mathbb{E}\left[\sup_{t\in[0,T]} < X_t^K, 1 >\right] \leq \mathbb{E}[< X_0^K, 1 >]e^{(\overline{r}+Ka)T} + \frac{\overline{c}}{\overline{r}+Ka}\left(e^{(\overline{r}+Ka)T} - 1\right) < +\infty, \tag{3.3}
$$

2. *there is strong pathwise uniqueness of the solution.*

Proof. The proof is similar to the one of proposition 11.

- The uniqueness directly follows from the construction of the process, as detailed in (11).

□

Markov property

By construction, $(X_t^K)_{t\geq 0}$ is also a Markov process. Let us express its infinitesimal generator L^K . Recall that $\overline{L}^K$, the generator of $(\nu_t^K)_t$ is defined by (2.7) for the K-dependant parameters. Take $\phi : \mathcal{M}_F(\overline{\chi}) \to \mathbb{R}$ measurable and $\nu \in \mathcal{M}_F(\overline{\chi})$. Then,

$$
L^K\phi(\nu) = \frac{\partial}{\partial t}\mathbb{E}_\nu\left(\phi(X_t^K)\right)_{t=0} = \frac{\partial}{\partial t}\mathbb{E}_{K\nu}\left(\phi\left(\frac{\nu_t^K}{K}\right)\right)_{t=0} = \overline{L}^K\phi^K(K\nu)
$$

for $\phi^K(\nu) := \phi\left(\frac{\nu}{K}\right)$. As a consequence we can use (2.7) to express $L^K\phi(\nu)$:

$$
\begin{aligned}
L^K\Phi(\nu) &= \int_\chi \frac{c_K(\nu)}{2\pi}\left[\Phi\left(\nu+\frac{1}{\mathbf{K}}\delta_\theta\right)-\Phi(\nu)\right]\mathrm{d}\theta \\
&+ \mathbf{K}\int_\chi (1-\mu_K) r_K(\theta,\nu)\left[\Phi\left(\nu+\frac{1}{\mathbf{K}}\delta_\theta\right)-\Phi(\nu)\right]\nu(\mathrm{d}\theta) \\
&+ \mathbf{K}\int_\chi \mu_K r_K(\theta,\nu)\int_\chi\left[\Phi\left(\nu+\frac{1}{\mathbf{K}}\delta_z\right)-\Phi(\nu)\right] g_K(z;\theta)\,\mathrm{d}z\,\nu(\mathrm{d}\theta) \\
&+ \mathbf{K}\int_\chi d_K(\theta,\nu)\left[\Phi\left(\nu-\frac{1}{\mathbf{K}}\delta_\theta\right)-\Phi(\nu)\right]\nu(\mathrm{d}\theta).
\end{aligned}
\tag{3.4}
$$

Moment and martingale properties

For K fixed, one can prove moment and martingale properties for $(X_t^K)_t$:

Proposition 16. *Assume the boundedness of rates as in hypothesis (8). Then,*

1. *if $\exists\, p \geq 1$ such that $\mathbb{E}\left[< X_0^K, 1 >^p\right] < +\infty$, then*

$$\forall\, T>0,\ \mathbb{E}\left[\sup_{t\in[0,T]} < X_t^K, 1 >^p\right] < +\infty.$$

2. *assume there exists $p \geq 2$ such that $\mathbb{E}[\langle X_0^K, 1\rangle^p] < +\infty$. Then,*

   (a) *$\forall$ measurable $\Phi : \mathcal{M}_F \to \mathbb{R}$ for which there exists C such that $\forall X \in \mathcal{M}_F$, $|\Phi(X)| + |L^K\Phi(X)| \leq C(1+ < X, 1 >^p)$,*

$$\Phi(X_t^K) - \Phi(X_0^K) - \int_0^t L^K\Phi(X_s^K)\,\mathrm{d}s \tag{3.5}$$

   is a càdlàg $(\mathcal{F}_t)_{t\geq 0}$-martingale starting from 0.

   (b) *This applies in particular to functions $\Phi : X \mapsto < X, f >^q$, for $0 \leq q \leq p$, and f measurable bounded on $\overline{\chi}$.*

   (c) *For such f, the process*

$$
\begin{aligned}
M_t^{K,f} =& < X_t^K, f > - < X_0^K, f > - \frac{1}{\boldsymbol{K}}\int_0^t \frac{c_K(X_s^K)}{2\pi}\int_\chi f(\theta)\,\mathrm{d}\theta\,\mathrm{d}s \\
&- \int_0^t\int_\chi \left(r_K(\theta, X_s^K) - d_K(\theta, X_s^K)\right) f(\theta) X^K(\mathrm{d}\theta)\,\mathrm{d}s \\
&- \int_0^t\int_\chi \mu_K r_K(\theta, X_s^K)\left(\int_\chi f(z) g_K(z;\theta)\,\mathrm{d}z - f(\theta)\right) X_s^K(\mathrm{d}\theta)\,\mathrm{d}s
\end{aligned}
\tag{3.6}
$$

is a càdlàg square-integrable martingale starting from 0 and of quadratic variation

$$
\begin{aligned}
\left\langle M^{K,f}\right\rangle_t = \int_0^t \frac{1}{\mathbf{K^2}}\int_\chi \frac{c_K(X_s^K)}{2\pi} f(\theta)^2\,\mathrm{d}\theta + \frac{1}{\mathbf{K}}\int_\chi (r_K(\theta, X_s^K) + d_K(\theta, X_s^K)) f(\theta)^2 X_s^K(\mathrm{d}\theta) \\
+ \frac{1}{\mathbf{K}}\int_\chi \mu_K r_K(\theta, X_s^K)\left[\int_\chi f(z)^2 g_K(z;\theta)\,\mathrm{d}z - f(\theta)^2\right] X_s^K(\mathrm{d}\theta)\,\mathrm{d}s.
\end{aligned}
\tag{3.7}
$$

Proof. 1. The proof is similar to the one of proposition 15. Using (2.8) for $\Phi(\nu_t) =< \nu_t, 1 >^p$, the expression of X_t^K in (3.2), and neglecting the non-positive death term, we have

$$\Phi(X_t^K) \leq \Phi(X_0^K) + \int_0^t \int_{\chi\times\mathbb{R}_+} \left(< X_{s^-}^K + \frac{1}{K}\delta_\theta, 1 >^p - < X_{s^-}^K, 1 >^p \right) \mathbb{1}_{u\leq \frac{c_K(X_s^K)}{2\pi}} M_0(\mathrm{d}s, \mathrm{d}\theta, \mathrm{d}u)$$
$$+ \int_0^t \int_{\mathbb{N}^*\times\mathbb{R}_+} \left(< X_t^K s^- + \frac{1}{K}\delta_{H^i(X_s^K)}, 1 >^p - < X_{s^-}^K, 1 >^p \right) \mathbb{1}_{i\leq N_{s^-}^K} \mathbb{1}_{u\leq m_1} M_1(\mathrm{d}s, \mathrm{d}i, \mathrm{d}u)$$
$$+ \int_0^t \int_{\mathbb{N}^*\times\chi\times\mathbb{R}_+} \left(< X_{s^-}^K + \frac{1}{K}\delta_\theta, 1 >^p - < X_{s^-}^K, 1 >^p \right) \mathbb{1}_{i\leq N_{s^-}^K} \mathbb{1}_{u\leq m_2} M_2(\mathrm{d}s, \mathrm{d}i, \mathrm{d}\theta, \mathrm{d}u),$$

with $m_1 = (1-\mu_K) r_K(H^i(X_s^K), X_s^K)$ and $m_2 = \mu_K r_K(H^i(X_s^K), X_s^K) g_K(\theta; H^i(X_s^K))$. Integrands involved in the previous expression are bounded, and we can take expectations. Using again the stopping time $\tau_n^K = \inf_{t\geq 0}\{< X_t^K, 1 >\geq n\}$ for $n \geq 0$, we get

$$\mathbb{E}\left[\sup_{s\in[0,t\wedge\tau_n^K]} < X_s^K, 1 >^p \right] \leq \mathbb{E}[< X_0^K, 1 >^p] + \mathbb{E}\left[\int_0^{t\wedge\tau_n^K} K\left(\bar{c} + < X_{s^-}^K, 1 > (\bar{r} + Ka)\right) \left(\left(< X_{s^-}^K, 1 > + \frac{1}{K} \right)^p - < X_{s^-}^K, 1 >^p \right) \mathrm{d}s \right].$$

We use now an analogous to lemma (2):

Lemma 4. *Let $x \in \mathbb{R}_+$, and $p > 0$ an integer. Then, there exists a positive constant C_p such that*

$$\left(\frac{1}{K} + x \right)^p - x^p \leq \frac{C_p}{K}(1 + x^{p-1}).$$

Proof. Notice that

$$\left(\frac{1}{K} + x \right)^p = \sum_{k=0}^{p} \binom{p}{k} \frac{x^k}{K^{p-k}} = x^p + \left(\frac{1}{K^p} + p\frac{x^{p-1}}{K} \right) + \sum_{k=1}^{p-2} \binom{p}{k} \frac{x^k}{K^{p-k}}.$$

Now $\forall 1 \leq k \leq p-2$, we have either $x \leq 1$, and $x^k \leq 1$, either $x \geq 1$ and then $x^k \leq x^{p-1}$. Moreover, $\forall k \in \{1, ..., p-2\}$, $\frac{1}{K^{p-k}} \leq \frac{1}{K}$. Then,

$$\left(\frac{1}{K} + x \right)^p \leq x^p + \left(\frac{1}{K^p} + p\frac{x^{p-1}}{K} \right) + \sum_{k=1}^{p-2} \binom{p}{k} \frac{(1 + x^{p-1})}{K}$$
$$\leq x^p + \frac{1}{K}(1 + x^{p-1}) \underbrace{\left[p + \sum_{k=1}^{p-2} \binom{p}{k} \right]}_{=2^{p-1}-1=:C_p}.$$

□

Then, for some constant C_p,

$$\left(< X^K_{s^-}, 1 > + \frac{1}{K}\right)^p - < X^K_{s^-}, 1 >^p \leq \frac{C_p}{K}\left(1 + < X^K_{s^-}, 1 >^{p-1}\right),$$

and

$$\mathbb{E}\left[\sup_{s\in[0,t\wedge\tau^K_n]} \Phi(X^K_s)\right] \leq \sup_{K>0} \mathbb{E}[< X^K_0, 1 >^p] + C(p,K,t)\left(1 + \int_0^t \mathbb{E}\left[\sup_{u\in[0,s\wedge\tau_N]} < X^K_{u^-}, 1 >^p\right] \mathrm{d}s\right),$$

since for $k \in \{1, p-1\}$, $\mathbb{E}\left[\sup_{u\in[0,s\wedge\tau^K_N]} < X^K_{u^-}, 1 >^k\right] \leq 1 + \mathbb{E}\left[\sup_{u\in[0,s\wedge\tau^K_N]} < X^K_{u^-}, 1 >^p\right]$.
By the Gronwall inequality,

$$\mathbb{E}\left[\sup_{t\in[0,T\wedge\tau^K_N]} < X^K_t, 1 >^p\right] \leq C(p,T,K).$$

- **Now let us show that $\lim_{n\to+\infty} \tau^K_n = +\infty$ $\mathbb{P} - a.s$:**

if not, there exists $T_0 < +\infty$ such that $\mathbb{P}\left(\sup_n \tau^K_n < T_0\right) > 0$. By the Markov inequality, one can write $\forall n \in \mathbb{N}$,

$$\begin{aligned}\mathbb{E}\left[\sup_{t\in[0,T_0\wedge\tau^K_n]} < X^K_t, 1 >^p\right] &\geq \mathbb{P}\left(\sup_{t\in[0,T_0\wedge\tau^K_n]} < X^K_t, 1 >^p \geq n^p\right) n^p \\ &\geq \mathbb{P}\left(\sup_n \tau^K_n < T_0\right) n^p\end{aligned}$$

which contradicts the previous inequality.

- **Finally, by the Fatou inequality,** :

$$\begin{aligned}\mathbb{E}\left[\sup_{t\in[0,T]} < X^K_t, 1 >^p\right] &= \mathbb{E}\left[\liminf_{n\to+\infty} \sup_{t\in[0,T\wedge\tau^K_n]} < X^K_t, 1 >^p\right] \\ &\leq \liminf_{n\to+\infty} \mathbb{E}\left[\sup_{t\in[0,T\wedge\tau^K_n]} < X^K_t, 1 >^p\right] \leq C_{p,T} < +\infty.\end{aligned}$$

2. The rest of the proposition can be proven exactly as in proposition (8).

□

The semimartingale formulation (3.6) allows us to study the convergence of $(X^K_t)_t$ for $K \to +\infty$ in $\mathbb{D}([0,T], \mathcal{M}_F(\overline{\chi}))$ for different renormalizations.

3.2 Deterministic limits

In this section, we are going to study two sets of parameters leading to deterministic limits. The first one consists in accelerating only the creation rate in order to keep this information at the limit. This can be interpreted as follows: as the scale diminishes, the model switches from the description of a filopodium growth to the one of actin filaments growth, whose dynamics is faster: more filaments grow instantaneously over the cell membrane than

filopodia. At the contrary, the demographic rates do not grow as the protrusions get smaller and more numerous. In particular, this means that the polarisation effect stays the same.

In the second case, one keeps all parameters unchanged. This has no meaning from the modelling point of vue, and we will only briefly present this result. For both cases, we consider an additional assumption on the Lipschitz-continuity in ν of the rates.

Hypothesis 9. *Take rates c_K, r_K and d_K such that they are bounded by constants:*

$$c_K(X_t^K) \leq K\overline{c} \quad r_K(\theta, X_t^K) \leq \overline{r} \quad d_K(\theta, X_t^K) \leq \overline{d}$$

Moreover, these rates are expressed from c, r d, and we assume that

- *The applications c, r, d are continuous.*
- *$\forall \theta \in \overline{\chi}$, $\nu \mapsto c(\nu)$, $\nu \mapsto r(\theta, \nu)$ and $\nu \mapsto d(\theta, \nu)$ are Lipschitz-continuous with respective parameters L_c, L_r, L_d for the variation norm defined for $(\mu_1, \mu_2) \in \mathcal{M}_F(\overline{\chi})^2$ by*

$$\| \mu_1 - \mu_2 \| = \sup_{\substack{f \in L^\infty(\overline{\chi}) \\ \|f\|_\infty \leq 1}} |< \mu_1 - \mu_2, f >| .$$

.

In this context, we can prove the following moment property:

Proposition 17. *Assume assumption 9, if $\exists\, p \geq 1$ such that $\sup_{K>0} \mathbb{E}\left[< X_0^K, 1 >^p\right] < +\infty$, then*

$$\forall\, T > 0,\ \sup_{K>0} \mathbb{E}\left[\sup_{t \in [0,T]} < X_t^K, 1 >^p\right] < +\infty.$$

Proof. The proof is similar to the one in proposition 16, with the only exception that the bound on r_K is sharper and independent on K. Hence, it suffices to transpose the proof for $a = 0$, and to take the supremum on $\{K > 0\}$. □

3.2.1 Accelerated creation - deterministic limit

Let us consider the following set of parameters:

$$\boldsymbol{c_K(X_t^K) = Kc(X_t^K) \quad r_K(\theta, X_t^K) = r(\theta, X_t^K) \quad d_K(\theta, X_t^K) = d(\theta, X_t^K)}$$

$$\boldsymbol{g_K(z;\theta) = g \qquad \mu_K = \mu}$$

where hypothesis 7 and 9 are fulfilled. In other words, while we consider an increasing number of smaller protrusions, only their isotropic creation is intensified, while their individual effect on the dynamics (reproduction or death) stays unchanged.

Convergence result

We can prove the following theorem:

Theorem 10. *Assume boundedness and regularity hypothesis 7 and 9. If* $X_0^K \underset{K\to+\infty}{\longrightarrow} \xi_0$ *in law on* $(\mathcal{M}_F(\overline{\chi}), w)$ *with* ξ_0 *deterministic, and if*

$$\sup_{K>0} \mathbb{E}\left[< X_0^K, 1 >^2\right] < +\infty, \tag{3.8}$$

then for $T > 0$, $(X^K)_{K>0}$ *converges in law in* $\mathbb{D}([0,T], \mathcal{M}_F(\overline{\chi})))$ *to the unique* $\xi \in \mathcal{C}([0,T], \mathcal{M}_F(\overline{\chi}))$ *such that* $\forall f : \overline{\chi} \to \mathbb{R}$ *measurable and bounded,*

$$\begin{aligned} < \xi_t, f > &= < \xi_0, f > + \int_0^t \frac{c(\xi_s)}{2\pi} \int_\chi f(\theta)\,\mathrm{d}\theta\,\mathrm{d}s + \int_0^t \int_\chi (r(\theta,\xi_s) - d(\theta,\xi_s)) f(\theta) \xi_s(\,\mathrm{d}\theta)\,\mathrm{d}s \\ &\quad + \int_0^t \int_\chi \mu r(\theta,\xi_s) \left[\int_\chi f(z) g(z;\theta)\,\mathrm{d}z - f(\theta)\right] \xi_s(\,\mathrm{d}\theta)\,\mathrm{d}s. \end{aligned} \tag{3.9}$$

Remark 10. *For* $f \equiv 1$, *one finds*

$$\begin{aligned} < \xi_t, 1 > &= < \xi_0, 1 > + \int_0^t c(\xi_s)\,\mathrm{d}s + \int_0^t \int_\chi (r(\theta,\xi_s) - d(\theta,\xi_s)) \xi_s(\,\mathrm{d}\theta)\,\mathrm{d}s \\ &\leq < \xi_0, 1 > + \overline{c}t + \overline{r} \int_0^t < \xi_s, 1 >\,\mathrm{d}s, \end{aligned}$$

and taking the supremum over $[0,T]$ $\forall T > 0$ *before using Gronwall inequality, one gets*

$$\sup_{t\in[0,T]} < \xi_t, 1 > \leq (< \xi_0, 1 > + \overline{c}T) e^{\overline{r}T} < +\infty, \tag{3.10}$$

showing that the global mass stays finite in finite time.

Remark 11. *As mentionned before, the creation dynamics is accelerated so that this information stays at the limit, as visible in the renormalized martingale formulation (3.6). A convergence result for a* K*-independant dynamics will be obtained in the next section, where the creation term is missing.*

Proof of proposition 10

The proof is similar to the one in Champagnat et al. [2006], and is based on a compactness-uniqueness argument: first, we show the tightness of the sequence of laws $(Q^K)_K$ of $(X^K)_K$. Then, we prove that for any accumulation point Q, a process X of law Q is almost surely continuous, and solution of (3.9). Finally, we prove uniqueness in law of the limit by showing that uniqueness property for (3.9) in $\mathcal{C}(\mathbb{R}_+, \mathcal{M}_F(\overline{\chi}))$. In the following, C will denote a constant that can change during computations, and $C(T)$ a constant depending on T.

Tightness of $(Q^K)_K$ As $\overline{\chi}$ is compact, topologies on $\mathcal{M}_F(\overline{\chi})$ coincide.

- By a criterion established by Roelly-Coppoletta [1986], it is enough to show that $\forall f \in \mathcal{C}(\overline{\chi})$, the sequence of laws of the processes $(< X^K, f >)_K$ is tight in $\mathcal{L}(\mathbb{D}(\mathbb{R}_+, \mathbb{R}))$.
- Then, we use the Aldous and Rebolledo criteria [Aldous, 1989] as detailed in Joffe and Metivier [1986]. Let us denote $(V_t^{K,f})_{t\geq 0}$ the finite variation process related to the semimartingale $(< X_t^K, f >)_{t\geq 0}$, that is to say $(< X_t^K, f > - M_t^{K,f})_{t\geq 0}$:

$$
\begin{aligned}
V_t^{K,f} &= < X_0^K, f > + \frac{1}{K} \int_0^t \frac{c_K(X_s^K)}{2\pi} \int_\chi f(\theta)\, \mathrm{d}\theta\, \mathrm{d}s \\
&+ \int_0^t \int_\chi \left(r_K(\theta, X_s^K) - d_K(\theta, X_s^K) \right) f(\theta) X^K(\,\mathrm{d}\theta)\, \mathrm{d}s \\
&+ \int_0^t \int_\chi \mu_K r_K(\theta, X_s^K) \left(\int_\chi f(z) g_K(z;\theta)\, \mathrm{d}z - f(\theta) \right) X_s^K(\,\mathrm{d}\theta)\, \mathrm{d}s.
\end{aligned}
$$

We need to show the following:

$\forall f \in \mathcal{C}(\overline{\chi}),\ \forall T > 0,$

1. $$\sup_{K>0} \mathbb{E}\left[\sup_{t\in[0,T]} \left| < X_t^K, f > \right| \right] < +\infty.$$

2. $\forall \varepsilon > 0,\ \forall \eta > 0,\ \exists \delta > 0,\ K_0 \in \mathbb{N}^*$ such that $\forall (\sigma_K, \tau_K)_K$ sequence of stopping times with $\sigma_K \le \tau_K \le T$,

   (a) $$\sup_{K \ge K_0} \mathbb{P}\left(\left| < M^{K,f} >_{\tau_K} - < M^{K,f} >_{\sigma_K} \right| \ge \eta,\ \tau_K \le \sigma_K + \delta \right) \le \varepsilon,$$

   (b) $$\sup_{K \ge K_0} \mathbb{P}\left(\left| V_{\tau_K}^{K,f} - V_{\sigma_K}^{K,f} \right| \ge \eta,\ \tau_K \le \sigma_K + \delta \right) \le \varepsilon,$$

1. As $\overline{\chi}$ is compact and f continuous, we know that f is bounded. Point (1) is then a consequence of the moment property 17 together with the hypothesis 3.8.

2. Take $T > 0,\ \varepsilon > 0,\ \eta > 0$ and a sequence of pairs of stopping times $(\sigma_K, \tau_K)_K$ such that $\sigma_K \le \tau_K \le T$ and $\tau_K \le \sigma_K + \delta$.

   (a) We have

   $$
   \begin{aligned}
   &\mathbb{E}\left[\left| < M^{K,f} >_{\tau_K} - < M^{K,f} >_{\sigma_K} \right| \right] \le \overline{c} \frac{\| f \|_\infty^2}{K} \delta + C \frac{\| f \|_\infty^2}{K} \mathbb{E}\left[\left| \int_{\sigma_K}^{\tau_K} < X_s^K, 1 >\, \mathrm{d}s \right| \right] \\
   &\le \frac{\| f \|_\infty^2}{K} (\overline{c} + C\mathbb{E}[\sup_{[0,T]} < X_t^K, 1 >]) \delta \\
   &\le \frac{C(T)}{K} \delta
   \end{aligned}
   $$

   by the moment property 17. Hence, using the Markov inequality, $\forall \varepsilon > 0$, $\forall \eta > 0$, there exists δ and K_0 such that 2.a) is satisfied.

   (b) Similarly,

   $$
   \begin{aligned}
   \mathbb{E}\left[\left| V_{\tau_K}^{K,f} - V_{\sigma_K}^{K,f} \right| \right] &\le \overline{c} \| f \|_\infty \delta + \left((1+2\mu)\overline{r} + \overline{d} \right) \| f \|_\infty \mathbb{E}\left[\left| \int_{\sigma_K}^{\tau_K} < X_s^K, 1 >\, \mathrm{d}s \right| \right] \\
   &\le \overline{c} \| f \|_\infty \delta + \left((1+2\mu)\overline{r} + \overline{d} \right) \| f \|_\infty \mathbb{E}[\sup_{[0,T]} < X_t^K, 1 >] \delta \\
   &\le C(T)\delta
   \end{aligned}
   $$

by proposition 17. As before, using the Markov inequality, $\forall \varepsilon > 0,\ \forall \eta > 0$, there exists δ such that 2.b) is satisfied.

We have just shown that the sequence $(Q^K)_K$ is uniformly tight in $\mathcal{L}(\mathbb{D}(\mathbb{R}_+, (\mathcal{M}_F(\overline{\chi}), \acute{e})))$.

Identification of the limit Let us consider a convergent subsequence $(Q^K)_K$ and denote Q its limit. By the Prohorov theorem, one can find a corresponding sequence of processes $(X^K)_K$ in $\mathbb{D}(\mathbb{R}_+, \mathcal{M}_F(\overline{\chi}))$ converging to $X \in \mathbb{D}(\mathbb{R}_+, \mathcal{M}_F(\overline{\chi}))$ of law Q.

- By construction, we know that $\forall K > 0$, jumps of $(X_t^K)_t$ are almost surely of the form δ_θ / K. As a consequence, almost surely,

$$\sup_{t \in \mathbb{R}_+} \sup_{f \in L^\infty} \left| < X_t^K, f > - < X_{t^-}^K, f > \right| \leq \frac{\| f \|_\infty}{K}.$$

  Hence, any process of law Q is almost surely strongly continuous: $\forall \varepsilon > 0,\ \forall \eta > 0,\ \exists \delta$ such that $\forall S \subset \mathbb{R}_+$ finite set,

$$\mathbb{P}\left(\forall (t_i, t_k) \in S^2,\ |t_i - t_k| < \delta,\ \left| < X_{t_i}^K, f > - < X_{t_k}^K, f > \right| \leq \varepsilon\right) \geq 1 - \eta.$$

- Now, let us show that the process X is solution of (3.9).

  → Following the moment proposition 17, we have $\mathbb{E}\left[\sup_{[0,T]} < X_t, 1 >^2\right] < +\infty$, leading to, almost surely

$$\sup_{[0,T]} < X_t, 1 > < +\infty. \tag{3.11}$$

  → Using a consequence of the Lusin theorem [Rudin, 1987], showing that X is solution of (3.9) for f measurable bounded amounts to showing the same property for $f \in \mathcal{C}(\overline{\chi})$. For $T > 0$, take $t \leq T$ and $\nu \in \mathcal{C}([0,T], \mathcal{M}_F(\overline{\chi}))$. Denote

$$\begin{aligned}
\Psi_t^f(\nu) \ := \ & < \nu_t, f > - < \nu_0, f > - \int_0^t \frac{c(\nu_s)}{2\pi} \int_\chi f(\theta)\, \mathrm{d}\theta\, \mathrm{d}s \\
& - \int_0^t \int_\chi (r(\theta, \nu_s) - d(\theta, \nu_s)) f(\theta) \nu_s(\,\mathrm{d}\theta)\, \mathrm{d}s \\
& - \int_0^t \int_\chi \mu r(\theta, \nu_s) \left[\int_\chi f(z) g(z; \theta)\, \mathrm{d}z - f(\theta)\right] \nu_s(\,\mathrm{d}\theta)\, \mathrm{d}s.
\end{aligned}$$

  We have to show that $\forall t \leq T,\ \mathbb{E}_Q\left[\left|\Psi_t^f(X)\right|\right] = 0$. For that purpose, we are gonna prove the following:

1. $\lim_{K \to +\infty} \mathbb{E}_{Q^K}\left[\left|\Psi_t^f(X^K)\right|\right] = 0.$
2. $\lim_{K \to +\infty} \mathbb{E}_{Q^K}\left[\left|\Psi_t^f(X^K)\right|\right] = \mathbb{E}_Q\left[\left|\Psi_t^f(X)\right|\right].$

1. As $\mathbb{E}_{Q^K}\left[\left|\Psi_t^f(X^K)\right|\right] = \mathbb{E}_{Q^K}\left[\left|M_t^{f,K}\right|\right]$, we have

$$\begin{aligned}
\mathbb{E}_{Q^K}\left[\left|\Psi_t^f(X^K)\right|\right]^2 \ &\leq \ \mathbb{E}_{Q^K}\left[\left|M_t^{f,K}\right|^2\right] = \mathbb{E}_{Q^K}\left[\left\langle M^{f,K}\right\rangle_t\right] \\
&\leq \ C\frac{t}{K}\left(1 + \mathbb{E}\left[\sup_{[0,T]} < X_t^K, 1 >\right]\right),
\end{aligned}$$

and by the moment property 17, we can conclude that

$$\forall t \in [0,T],\ \lim_{K\to+\infty} \mathbb{E}_{Q^K}\left[\left|\Psi_t^f(X^K)\right|\right] = 0\,.$$

2. (a) We know that X is an almost surely continuous process, $f \in \mathcal{C}(\overline{\chi})$ and all the parameters rates are continuous. Hence Ψ_t^f is continuous in X for all f, and $\lim_K \Psi_t^f(X^K) = \Psi_t^f(X)$ in law.

   (b) Moreover,

$$|\Psi_t(\nu)| \le C(T,f)(1 + \sup_{[0,T]} < \nu_s, 1 >$$

   as f is bounded, showing using (17) that $\left(\Psi_t(X^K)\right)_K$ is uniformly integrable. Hence,

$$\lim_{K\to+\infty} \mathbb{E}_{Q^K}\left[\left|\Psi_t^f(X^K)\right|\right] = \mathbb{E}_Q\left[\left|\lim_{K\to+\infty} \Psi_t^f(X^K)\right|\right] = \mathbb{E}_Q\left[\left|\Psi_t^f(X)\right|\right],$$

   and that finishes the proof.

Uniqueness of a solution for equation (3.9)

- Take $\xi \in \mathcal{C}(\mathbb{R}_+, \mathcal{M}_F(\overline{\chi}))$ solution of (3.9). Then by equation (3.10), $\forall t \ge 0$,

$$< \xi_t, 1 >< +\infty\ \mathbb{P} - a.s.$$

- Consider two solutions of (3.9), denoted $(\xi_t)_{t\ge0}$ and $(\overline{\xi_t})_{t\ge0}$ having the same initial condition $\xi_0 \in \mathcal{M}_F(\overline{\chi})$. By the previous point, $\forall T \ge 0$, we can write

$$\sup_{t\in[0,T]} < \xi_t + \overline{\xi_t}, 1 >= A_T < +\infty. \tag{3.12}$$

  Now, let $f : \overline{\chi} \to \mathbb{R}$ be a measurable bounded function such that $\| f \|_\infty \le 1$. Then, for $t \in [0,T]$, $\mathbb{P} - a.s$, one can write

$$\begin{aligned}
\left|< \xi_t - \overline{\xi_t}, f >\right| &= \left| \int_0^t \frac{1}{2\pi}(c(\xi_s) - c(\overline{\xi_s})) \int_\chi f(\theta)\,\mathrm{d}\theta\,\mathrm{d}s \right. \\
&+ \int_0^t \int_\chi ((1-\mu)r(\theta,\xi_s) - d(\theta,\xi_s))f(\theta)\xi_s(\,\mathrm{d}\theta) - \int_\chi ((1-\mu)r(\theta,\overline{\xi_s}) - d(\theta,\overline{\xi_s}))f(\theta)\overline{\xi_s}(\,\mathrm{d}\theta)\,\mathrm{d}s \\
&+ \left. \int_0^t \mu\left\{ \int_\chi r(\theta,\xi_s) \int_\chi f(z)g(z;\theta)\,\mathrm{d}z\xi_s(\,\mathrm{d}\theta) - \int_\chi r(\theta,\overline{\xi_s}) \int_\chi f(z)g(z;\theta)\,\mathrm{d}z\overline{\xi_s}(\,\mathrm{d}\theta) \right\} \mathrm{d}s \right|.
\end{aligned}$$

  For reproduction and death terms, we introduce an additional integrand and use the inequality $|A - B| = |A - C + C - B| \le |A - C| + |C - B|$:

$$\left|< \xi_t - \overline{\xi_t}, f >\right| \le \int_0^t \frac{1}{2\pi}|c(\xi_s) - c(\overline{\xi_s})| \int_\chi |f(\theta)|\,\mathrm{d}\theta\,\mathrm{d}s \tag{3.13}$$

$$+ \left| \int_0^t \int_\chi ((1-\mu)r(\theta,\xi_s) - d(\theta,\xi_s))f(\theta)\xi_s(\,\mathrm{d}\theta) - \int_\chi ((1-\mu)r(\theta,\overline{\xi_s}) - d(\theta,\overline{\xi_s}))f(\theta)\xi_s(\,\mathrm{d}\theta)\,\mathrm{d}s \right| \tag{3.14}$$

$$+ \left| \int_0^t \int_\chi ((1-\mu)r(\theta,\overline{\xi_s}) - d(\theta,\overline{\xi_s}))f(\theta)\xi_s(\,\mathrm{d}\theta) - \int_\chi ((1-\mu)r(\theta,\overline{\xi_s}) - d(\theta,\overline{\xi_s}))f(\theta)\overline{\xi_s}(\,\mathrm{d}\theta)\,\mathrm{d}s \right| \tag{3.15}$$

$$+ \left| \int_0^t \mu\left\{ \int_\chi r(\theta,\xi_s) \int_\chi f(z)g(z;\theta)\,\mathrm{d}z\xi_s(\,\mathrm{d}\theta) - \int_\chi r(\theta,\overline{\xi_s}) \int_\chi f(z)g(z;\theta)\,\mathrm{d}z\xi_s(\,\mathrm{d}\theta) \right\} \mathrm{d}s \right| \tag{3.16}$$

$$+ \left| \int_0^t \mu\left\{ \int_\chi r(\theta,\overline{\xi_s}) \int_\chi f(z)g(z;\theta)\,\mathrm{d}z\xi_s(\,\mathrm{d}\theta) - \int_\chi r(\theta,\overline{\xi_s}) \int_\chi f(z)g(z;\theta)\,\mathrm{d}z\overline{\xi_s}(\,\mathrm{d}\theta) \right\} \mathrm{d}s \right|. \tag{3.17}$$

The first, second and fourth line can be treated thanks to the Lipschitz rates. We have

$$\begin{aligned}(3.13) &\leq L_c \int_0^t \| \xi_s - \overline{\xi_s} \| \, \mathrm{d}s, \\ (3.14) &\leq (L_r + L_d) A_T \int_0^t \| \xi_s - \overline{\xi_s} \| \, \mathrm{d}s, \\ (3.16) &\leq \mu L_r A_T \int_0^t \| \xi_s - \overline{\xi_s} \| \, \mathrm{d}s.\end{aligned}$$

For (3.15) and (3.17), we use the boundedness of the parameters:

$$\begin{aligned}(3.15) &\leq (\overline{r} + \overline{d}) \int_0^t \| \xi_s - \overline{\xi_s} \| \, \mathrm{d}s \\ (3.17) &\leq \mu \overline{r} \int_0^t \| \xi_s - \overline{\xi_s} \| \, \mathrm{d}s.\end{aligned}$$

Finally, we obtain

$$\left| < \xi_t - \overline{\xi_t}, f > \right| \leq \left(L_c + ((1+\mu)L_r + L_d) A_T + (1+\mu)\overline{r} + \overline{d} \right) \int_0^t \| \xi_s - \overline{\xi_s} \| \, \mathrm{d}s.$$

Taking the supremum over all $f \in L^\infty$ such that $\| f \|_\infty \leq 1$, and using the Gronwall lemma leads to $\forall t \in [0,T]$, $\| \xi_t - \overline{\xi_t} \| = 0$. As the time T can be arbitrarily large, uniqueness holds $\mathbb{P} - a.s$ on $\mathcal{C}([0,T], \mathcal{M}_F(\overline{\chi}))$.

Existence of a density for the limiting function

We prove now a result of regularity of the population measure at all times, provided that the initial measure has no singularity.

Theorem 11. *Still under hypothesis 7 and 9, consider ξ the solution of (3.9). If the initial condition $\xi_0(\mathrm{d}\theta) \in \mathcal{M}_F(\overline{\chi})$ is absolutely continuous with respect to the Lebesgue measure $\mathrm{d}\theta$, then $\forall t \in \mathbb{R}_+$, $\xi_t(\mathrm{d}\theta)$ admits a density n_t with respect to $\mathrm{d}\theta$.*

Then, $n : [0,T] \times \chi \to \mathbb{R}_+$ is solution of the following integro-differential equation:

$$\frac{\partial}{\partial t} n_t(\theta) = \frac{c(n_t)}{2\pi} + \left[(1-\mu) r(\theta, n_t) - d(\theta, n_t) \right] n_t(\theta) + \mu \int_\chi r(z, n_t) g(\theta; z) n_t(z) \, \mathrm{d}z. \quad (3.18)$$

In this equation, the contribution of each term is clear. Notice that the last term, corresponding to reproduction events with mutation, amounts to consider for each orientation z the "probability" that a z-individual that will create a $\theta-$mutant. The function n can be interpreted as a "density" of protrusion for each orientation $\theta \in [0, 2\pi[$.

Proof. Let $t \in \mathbb{R}_+$ and let B be a Lebesgue-negligeable borelian of χ. Considering equation

(3.9) for $f = \mathbf{1}_B$ leads to

$$\begin{aligned} 0 \quad \leq \quad & \int_\chi \mathbf{1}_B(\theta)\xi_t(\,\mathrm{d}\theta) = \underbrace{\int_\chi \mathbf{1}_B(\theta)\xi_0(\,\mathrm{d}\theta)}_{=0}\,\mathrm{d}s + \int_0^t \frac{c(\xi_s)}{2\pi}\underbrace{\int_\chi \mathbf{1}_B(\theta)\,\mathrm{d}\theta}_{=0} \\ & + \int_0^t \int_\chi ((1-\mu)r(\theta,\xi_s) - d(\theta,\xi_s))\mathbf{1}_B(\theta)\xi_s(\,\mathrm{d}\theta)\,\mathrm{d}s \\ & + \int_0^t \int_\chi \mu r(\theta,\xi_s)\underbrace{\int_\chi \mathbf{1}_B(z)g(z;\theta)\,\mathrm{d}z}_{=0}\xi_s(\,\mathrm{d}\theta)\,\mathrm{d}s, \end{aligned}$$

where the null terms come from the hypothesis. Finally,

$$0 \leq \int_\chi \mathbf{1}_B(\theta)\xi_t(\,\mathrm{d}\theta) \quad \leq \quad \overline{r}\int_0^t \int_\chi \mathbf{1}_B(\theta)\xi_s(\,\mathrm{d}\theta)\,\mathrm{d}s,$$

and as $\sup_{t\in[0,T]} < \xi_t, 1 >< +\infty$ by equation (3.10), the Gronwall lemma yields

$$\forall t \geq 0, \quad \int_\chi \mathbf{1}_B(\theta)\xi_t(\,\mathrm{d}\theta) = 0\,.$$

Finally, applying the Radon-Nicodyn theorem leads to the result. The equation (3.18) is directly obtained from (3.9) using the equality $\int_\chi f(\theta)\xi_t(\,\mathrm{d}\theta) = \int_\chi f(\theta)n_t(\theta)\,\mathrm{d}\theta$. □

3.2.2 Non accelerated dynamics

As mentioned before, we can also choose not to accelerate any part of the dynamics. More precisely, consider the following rates:

$$\boldsymbol{c_K(X_t^K) = c(X_t^K) \quad r_K(\theta, X_t^K) = r(\theta, X_t^K) \quad d_K(\theta, X_t^K) = d(\theta, X_t^K)}$$
$$\boldsymbol{g_K(z;\theta) = g \quad \mu_K = \mu}$$

We can prove the following:

Theorem 12. *Under hypothesis 7 and 9, if* $X_0^K \underset{K\to+\infty}{\to} \xi_0$ *in law on* $\mathcal{M}_F(\overline{\chi})$*, with* ξ_0 *deterministic, and*

$$\sup_{K>0} \mathbb{E}\left[< X_0^K, 1 >^2\right] < +\infty, \tag{3.19}$$

then $(X^K)_{K>0}$ *converges in law in* $\mathbb{D}([0,T], \mathcal{M}_F(\overline{\chi}))$ *to the unique* $\xi \in \mathcal{C}([0,T], \mathcal{M}_F(\overline{\chi}))$ *such that* $\forall f : \overline{\chi} \to \mathbb{R}$ *measurable and bounded,*

$$< \xi_t, f > \quad = \quad < \xi_0, f > + \int_0^t \int_\chi (r(\theta,\xi_s) - d(\theta,\xi_s))f(\theta)\xi_s(\,\mathrm{d}\theta)\,\mathrm{d}s \tag{3.20}$$
$$+ \int_0^t \int_\chi \mu r(\theta,\xi_s)\left[\int_\chi f(z)g(z;\theta)\,\mathrm{d}z - f(\theta)\right]\xi_s(\,\mathrm{d}\theta)\,\mathrm{d}s. \tag{3.21}$$

Moreover, if $\xi_0(\mathrm{d}\theta) \in \mathcal{M}_F(\overline{\chi})$ *is absolutely continuous with respect to the Lebesgue measure* $\mathrm{d}\theta$*, then* $\forall t \in \mathbb{R}_+$*,* $\xi_t(\mathrm{d}\theta)$ *admits a density* n_t *with respect to* $\mathrm{d}\theta$*. Then,* $(t,\theta) \mapsto n_t(\theta)$ *verifies*

$$\frac{\partial}{\partial t} n_t(\theta) = \left[(1-\mu) r(\theta, n_t) - d(\theta, n_t)\right] n_t(\theta) + \mu \int_{\chi} r(z, n_t) g(\theta; z) n_t(z)\, \mathrm{d}z. \tag{3.22}$$

The proof is exactly the same as in theorem (3.2.1).

3.3 Accelerated demography

In this section, we choose to accelerate also the reproduction and death dynamics, corresponding to allometric demographies: the individuals are smaller and reproduce and die faster. This can be understood as follows: as the scale gets smaller, we go from the apparition of a filopodium, a bundle of actin filaments, to the growth of individual filaments, that occurs at a faster pace. This justifies why the corresponding dynamics is accelerated. When reproduction happens, the mutation event, that is the choice of a slightly different orientation, accounts for the stochasticity involved in the formation and growth of a lamellipodium. We will consider specific renormalizations for this phenomenon in the following. Now, let us introduce the parameter $0 < \eta \leq 1$ related dynamics acceleration pace compared to the population growth. For $K > 0$ and $a > 0$, consider

$$\boldsymbol{c_K(X_t^K) = Kc(X_t^K)}$$

$$\boldsymbol{r_K(\theta, X_t^K) = r(\theta, X_t^K) + K^\eta a, \quad d_K(\theta, X_t^K) = d(\theta, X_t^K) + K^\eta a.}$$

Let us comment on this choice of parameters. Reproduction and death events are accelerated the same way, with $a > 0$ constant, in order to keep an individual growth rate $r_K - d_K = r - d$ bounded. This also means that the individual growth rate is slower than the individual birth and death dynamics.

In order to have a tractable limit, we'll see the need for additional assumptions on the mutation event: first, we'll study what happens when the mutation probability μ_K becomes smaller and smaller. Then we'll consider a distribution of the mutant trait g_K that concentrates on the parent trait. The modelling implications of these choices will be discussed. Moreover, for either $0 < \eta < 1$ or $\eta = 1$, we'll obtain continuous approximations of different natures: deterministic or stochastic. In all cases, we'll need moment properties established below.

3.3.1 Preliminary results

We prove here time independant, K-independant moment estimates.

Proposition 18. *Consider the processes* $(X_t^K)_{t\geq 0}$*. Under hypothesis 8, and if* $\sup_{K>0} \mathbb{E}[< X_0^K, 1 >^2] < +\infty$*, then for* $T < +\infty$*,*

$$\sup_K \sup_{t\in[0,T]} \mathbb{E}[< X_t^K, 1 >^2] < +\infty. \tag{3.23}$$

Proof. Let us use (3.5) for $\Phi(\nu) =< \nu, 1 >^2$. In that case, the infinitesimal generator (3.4) can be simplified by merging the clonal and mutation reproduction terms, giving

$$\begin{aligned} L^K\Phi(X_s^K) &= K\int_\chi \frac{c(X_s^K)}{2\pi}\left[\left(< X_s^K, 1 > +\frac{1}{K}\right)^2 - < X_s^K, 1 >^2\right] \mathrm{d}\theta \\ &+ K\int_\chi (r(\theta, X_s^K) + K^\eta a)\left[\left(< X_s^K, 1 > +\frac{1}{K}\right)^2 - < X_s^K, 1 >^2\right] X_t^K(\mathrm{d}\theta) \\ &+ K\int_\chi (d(\theta, X_s^K) + K^\eta a)\left[\left(< X_s^K, 1 > -\frac{1}{K}\right)^2 - < X_s^K, 1 >^2\right] X_s^K(\mathrm{d}\theta). \end{aligned}$$

Notice that at this point, we know that no particular condition on μ_K or g_K is needed. Write

$$B_+ = \left[\left(< X_s^K, 1 > +\frac{1}{K}\right)^2 - < X_s^K, 1 >^2\right],$$

$$B_- = \left[\left(< X_s^K, 1 > -\frac{1}{K}\right)^2 - < X_s^K, 1 >^2\right],$$

Then,

$$\begin{aligned} L^K\Phi(X_s^K) &= Kc(X_s^K)B_+ + K < X_s^K, r > B_+ \\ &\quad + K < X_s^K, d > B_- + K^{1+\eta}a < X_s^K, 1 > (B_+ + B_-). \end{aligned}$$

Now, as $B_- \leq 0$, we can neglect the corresponding death term and study an inequality. Moreover, we compute

$$B_+ = \frac{2}{K} < X_s^K, 1 > +\frac{1}{K^2} \quad B_- = -\frac{2}{K} < X_s^K, 1 > +\frac{1}{K^2} \quad B_+ + B_- = \frac{2}{K^2},$$

leading to

$$\begin{aligned} L^K\Phi(X_s^K) &\leq (\overline{c} + \overline{r} < X_s^K, 1 >)\left(2 < X_s^K, 1 > +\frac{1}{K}\right) + 2a < X_s^K, 1 > \\ &\leq \overline{c} + (2\overline{c} + \overline{r} + 2a) < X_s^K, 1 > +2\overline{r} < X_s^K, 1 >^2 . \end{aligned}$$

Hence, we can deduce from (3.5) that

$$\begin{aligned} \mathbb{E}[< X_t^K, 1 >^2] &= \mathbb{E}[< X_0^K, 1 >^2] + \int_0^t \mathbb{E}[L^K\Phi(X_s^K)]\,\mathrm{d}s \\ &\leq \mathbb{E}[< X_0^K, 1 >^2] + C(t)\left(1 + \int_0^t \mathbb{E}[< X_s^K, 1 >] + \mathbb{E}[< X_s^K, 1 >^2]\,\mathrm{d}s\right). \end{aligned}$$

Finally, using the Gronwall lemma, we show that there exists a constant $C(t)$ such that $\mathbb{E}[< X_t^K, 1 >^2] \leq C(t)$, and then

$$\sup_{K>0}\sup_{[0,T]} \mathbb{E}[< X_t^K, 1 >^2] < +\infty.$$

□

We want now a control on $\mathbb{E}\left[\sup_{t\in[0,T]} < X_t^K, 1 >\right]$ that holds independently of K, provided $\mathbb{E}[\langle X_s^K, 1\rangle]$ is bounded independantly of $s \in [0,T]$ and K. This will be of crucial importance for the limit theorems we are going to show.

Proposition 19. *Consider the processes $(X_t^K)_{t\geq 0}$ defined in 3.2 for all $K > 0$. Assume that $\sup_{K>0} \mathbb{E}[< X_0^K, 1 >] < +\infty$. Then, for $T < +\infty$,*

$$\sup_K \mathbb{E}\left[\sup_{t\in[0,T]} < X_t^K, 1 >\right] < +\infty. \tag{3.24}$$

Proof. Apply (3.6) with $f \equiv 1$ to find

$$< X_t^K, 1 > \;=\; M_t^{K,1} + < X_0^K, 1 > + \int_0^t c(X_s^K)\,\mathrm{d}s + \int_0^t \int_\chi \left(r(\theta, X_s^K) - d(\theta, X_s^K)\right) X^K(\,\mathrm{d}\theta)\,\mathrm{d}s.$$

As a consequence,

$$\sup_{t\in[0,T]} < X_t^K, 1 > \;=\; \sup_{t\in[0,T]} |M_t^{K,1}| + < X_0^K, 1 > + \overline{c}T + \overline{r}\int_0^T < X_s^K, 1 > \,\mathrm{d}s.$$

Now $\mathbb{E}[< X_0^K, 1 >] < +\infty$, and by the Doob inequality,

$$\mathbb{E}\left[\sup_{t\in[0,T]} |M_t^{K,1}|\right]^2 \leq \mathbb{E}\left[\sup_{t\in[0,T]} |M_t^{K,1}|^2\right] \leq 4\mathbb{E}\left[|M_T^{K,1}|^2\right] = 4\mathbb{E}\left[< M^{K,1} >_T\right],$$

and

$$\mathbb{E}\left[\sup_{t\in[0,T]} < X_t^K, 1 >\right] \;=\; 2\mathbb{E}\left[< M^{K,1} >_T\right]^{1/2} + C(T) + \overline{r}\mathbb{E}\left[\int_0^T \sup_{s\in[0,t]} < X_s^K, 1 > \,\mathrm{d}s\right].$$

We use (3.7) to get

$$\begin{aligned}\mathbb{E}[\langle M^{K,1}\rangle_T] &\leq \overline{c}T + (\overline{r} + \overline{d} + 2a)\int_0^t \mathbb{E}[< X_s^K, 1 >]\,\mathrm{d}s \\ &\leq C(T)\end{aligned}$$

thanks to proposition 18. Finally, the Gronwall lemma leads to a K-independant bound for $\mathbb{E}[\sup_{t\in[0,T]} < X_t^K, 1 >]$, and taking the supremum over $\{K > 0\}$ finishes the proof. □

3.3.2 Rare mutations case

In this subsection, we renormalize the mutation probability: consider

$$\boldsymbol{g_K = g} \quad \text{and} \quad \boldsymbol{\mu_K = \frac{\mu}{K^\eta}}.$$

This choice means that as the reproduction rate is accelerated by a K^η factor, mutant reproduction events become negligible. Mutation for the orientation of new protrusions is a marker of the stochasticity in the molecular pathway regulating actin polymerization. Therefore, this assumption may be acceptable in the case of protrusions mainly constituted of bundles, but this is not our purpose here. A more satisfying assumption will be made hereafter. For these parameters, the martingale property (3.6) rewrites

$$\begin{aligned} M_t^{K,f} =& < X_t^K, f > - < X_0^K, f > - \int_0^t \frac{c(X_s^K)}{2\pi} \int_\chi f(\theta)\,\mathrm{d}\theta\,\mathrm{d}s \\ & - \int_0^t \int_\chi \left(r(\theta, X_s^K) - d(\theta, X_s^K)\right) f(\theta) X^K(\,\mathrm{d}\theta)\,\mathrm{d}s \\ - \int_0^t \int_\chi & \left(\frac{r(\theta, X_s^K)\mu}{\mathbf{K}^\eta} + \mu a\right) \left(\int_\chi f(z) g(z;\theta)\,\mathrm{d}z - f(\theta)\right) X_s^K(\,\mathrm{d}\theta)\,\mathrm{d}s \end{aligned} \tag{3.25}$$

a càdlàg square-integrable martingale starting from 0 of quadratic variation

$$\begin{aligned} \left\langle M^{K,f} \right\rangle_t = \frac{1}{\mathbf{K}} \int_0^t \Bigg\{ & \int_\chi \frac{c(X_s^K)}{2\pi} f(\theta)^2\,\mathrm{d}\theta + \int_\chi \left[r(\theta, X_s^K) + d(\theta, X_s^K) + 2\mathbf{K}^\eta a\right] f(\theta)^2 X_s^K(\,\mathrm{d}\theta) \\ & + \int_\chi \left(\frac{\mu r(\theta, X_s^K)}{\mathbf{K}^\eta} + \mu a\right) \left[\int_\chi f(z)^2 g(z;\theta)\,\mathrm{d}z - f(\theta)^2\right] X_s^K(\,\mathrm{d}\theta) \Bigg\}\,\mathrm{d}s. \end{aligned} \tag{3.26}$$

Case $0 < \eta < 1$

Here, the demography is not accelerated as much as K grows. More precisely, we assume the following:

Hypothesis 10 (Rare mutations - deterministic limit)**.** *For $\overline{c}$, $\overline{r}$, and $\overline{d}$ positive constants, consider positive rates*

$$c_K(X_t^K) = K c(X_t^K) \leq K\overline{c}$$

$$r_K(\theta, X_t^K) = r(\theta, X_t^K) + K^\eta a \leq \overline{r} + K^\eta a, \quad d_K(\theta, X_t^K) = d(\theta, X_t^K) + K^\eta a \leq \overline{d} + K^\eta a.$$

Moreover, c, r and d are continuous, and Lipschitz-continuous in ν of constants L_c, L_r, L_d.

Theorem 13. *Under hypothesis 10,*

1. *if for $K \to +\infty$ the initial measure X_0^K converges in law on $\mathcal{M}_F(\overline{\chi})$ to a deterministic measure $\xi_0 \in \mathcal{M}_F(\overline{\chi})$, and if*

$$\sup_{K>0} \mathbb{E}\left[< X_0^K, 1 >\right] < +\infty, \tag{3.27}$$

then $(X^K)_{K>0}$ converges in law in $\mathbb{D}([0,T], \mathcal{M}_F(\overline{\chi}))$ to the unique deterministic function $\xi \in \mathcal{C}([0,T], \mathcal{M}_F(\overline{\chi}))$ such that $\forall f : \overline{\chi} \to \mathbb{R}$ measurable and bounded,

$$\begin{aligned} < \xi_t, f > = < \xi_0, f > + \int_0^t \frac{c(\xi_s)}{2\pi} \int_\chi f(\theta)\,\mathrm{d}\theta + \int_0^t \int_\chi (r(\theta, \xi_s) - d(\theta, \xi_s)) f(\theta) \xi_s(\,\mathrm{d}\theta)\,\mathrm{d}s \\ + \int_0^t \int_\chi \mu a \left(\int_\chi f(z) g(z;\theta)\,\mathrm{d}z - f(\theta)\right) \xi_s(\,\mathrm{d}\theta)\,\mathrm{d}s. \end{aligned} \tag{3.28}$$

2. *Moreover, if* $\xi_0(\,\mathrm{d}\theta) \in \mathcal{M}_F(\overline{\chi})$ *is absolutely continuous with respect to the Lebesgue measure* $\mathrm{d}\theta$*, then* $\forall t \in \mathbb{R}_+$*,* $\xi_t(\,\mathrm{d}\theta)$ *admits a density* n_t *with respect to* $\mathrm{d}\theta$*, and* $(t,\theta) \mapsto n_t(\theta)$ *is solution of the following integro-differential equation:*

$$\frac{\partial}{\partial t} n_t(\theta) = \frac{c(n_t)}{2\pi} + \left[r(\theta, n_t) - \mu a - d(\theta, n_t)\right] n_t(\theta) + \mu \int_\chi a g(\theta; z) n_t(z)\,\mathrm{d}z. \tag{3.29}$$

Proof. 1. The proof of the convergence is similar to the one of theorem 10.

Uniform tightness Let us denote $(Q^K)_{K>0}$ the sequence of laws of the processes $(X_t^K)_{t\geq 0}$. We can prove that the sequence is uniformly tight in $\mathcal{L}(\mathbb{D}(\mathbb{R}_+, \mathcal{M}_F(\overline{\chi})))$ as for (10). As before, we use Roelly's criterion, as well as the Aldous-Rebolledo one [Aldous, 1989; Joffe and Metivier, 1986; Roelly-Coppoletta, 1986].

Consider

$$\begin{aligned} V_t^{K,f} &= < X_0^K, f > + \int_0^t \frac{c(X_s^K)}{2\pi} \int_\chi f(\theta)\,\mathrm{d}\theta\,\mathrm{d}s \\ &+ \int_0^t \int_\chi \left(r(\theta, X_s^K) - d(\theta, X_s^K)\right) f(\theta) X^K(\,\mathrm{d}\theta)\,\mathrm{d}s \\ &+ \int_0^t \int_\chi \left(\frac{\mu r(\theta, X_s^K)}{K^\eta} + \mu a\right) \left(\int_\chi f(z) g(z;\theta)\,\mathrm{d}z - f(\theta)\right) X_s^K(\,\mathrm{d}\theta)\,\mathrm{d}s. \end{aligned}$$

(a) As $\overline{\chi}$ is compact and f continuous, we know that f is bounded. Point (a) is then a consequence of the initial assumption (3.27) together with the moment property 19.

(b) Take $T > 0$, $\varepsilon > 0$, $\eta > 0$ and a sequence of pairs of stopping times $(\sigma_K, \tau_K)_K$ such that $\sigma_K \leq \tau_K \leq T$ and $\tau_K \leq \sigma_K + \delta$.

i. We study first $Z := \mathbb{E}\left[\left|< M^{K,f} >_{\tau_K} - < M^{K,f} >_{\sigma_K}\right|\right]$:

$$\begin{aligned} Z &\leq \bar{c}\frac{\| f \|_\infty^2}{K}\delta + ((1+2\mu)\bar{r} + \bar{d})\frac{\| f \|_\infty^2}{K}\mathbb{E}\left[\left|\int_{\sigma_K}^{\tau_K} < X_s^K, 1 > \mathrm{d}s\right|\right] \\ &\quad + \frac{2\| f \|_\infty^2}{K^{1-\eta}}\mu a \mathbb{E}\left[\left|\int_{\sigma_K}^{\tau_K} < X_s^K, 1 > \mathrm{d}s\right|\right] \\ &\leq \| f \|_\infty^2 \left(\bar{c} + \left[(1+2\mu)\bar{r} + \bar{d} + 2\mu a\right] \mathbb{E}[\sup_{[0,T]} < X_t^K, 1 >]\right)\delta \\ &\leq C(T)\delta \end{aligned}$$

by the moment property 19. Hence, there exists δ such that 2.a) is satisfied.

ii. Similarly,

$$\begin{aligned} \mathbb{E}\left[\left|V_{\tau_K}^{K,f} - V_{\sigma_K}^{K,f}\right|\right] &\leq C\delta + C\mathbb{E}\left[\left|\int_{\sigma_K}^{\tau_K} < X_s^K, 1 > \mathrm{d}s\right|\right] \\ &\leq C\delta(1 + \mathbb{E}[\sup_{[0,T]} < X_t^K, 1 >]) \\ &\leq C(T)\delta \end{aligned}$$

by 19. As before, there exists δ such that 2.b) is satisfied.

Identification of the limiting process consider a convergent subsequence still denoted $(Q^K)_K$ for convenience, and denote Q its limit. By the Prohorov theorem, one can find a corresponding sequence of processes $(X^K)_K$ in $\mathbb{D}([0,T],\mathcal{M}_F(\overline{\chi}))$ converging in law to $X \in \mathbb{D}([0,T],\mathcal{M}_F(\overline{\chi}))$. Again, we can prove that X is almost surely strongly continuous.

- Now, let us show that X is solution of (3.28).
  → By the moment property 19, we have $\mathbb{E}\left[\sup_{[0,T]} < X_t, 1 >\right] < +\infty$, leading to, almost surely

$$\sup_{[0,T]} < X_t, 1 >< +\infty. \tag{3.30}$$

  → Using the Lusin theorem [Rudin, 1987], it is enough to show that X is solution of (3.28) for $f \in \mathcal{C}(\overline{\chi})$. For $T > 0$, take $t \leq T$ and $\nu \in \mathcal{C}([0,T],\mathcal{M}_F(\overline{\chi}))$. Denote

$$\begin{aligned}\Psi_t(\nu) :=& < \nu_t, f > - < \nu_0, f > - \int_0^t \frac{c(\nu_s)}{2\pi} \int_\chi f(\theta)\,\mathrm{d}\theta\,\mathrm{d}s \\ &- \int_0^t \int_\chi (r(\theta,\nu_s) - d(\theta,\nu_s)) f(\theta) \nu_s(\,\mathrm{d}\theta)\,\mathrm{d}s \\ &- \int_0^t \int_\chi \mu a \left[\int_\chi f(z) g(z;\theta)\,\mathrm{d}z - f(\theta)\right] \nu_s(\,\mathrm{d}\theta)\,\mathrm{d}s.\end{aligned}$$

  We have to show that $\forall t \leq T$, $\mathbb{E}_Q\left[|\Psi_t(X)|\right] = 0$. Moreover, by the martingale property (3.25), we know that

$$M_t^{K,f} = \Psi_t(X^K) + \Psi_t^{2,K}(X^K),$$

  with

$$\Psi_t^{2,K}(X^K) := -\int_0^t \int_\chi \frac{\mu r(\theta, X_s^K)}{K^\eta} \left[\int_\chi f(z) g(z;\theta)\,\mathrm{d}z - f(\theta)\right] X_s^K(\,\mathrm{d}\theta)\,\mathrm{d}s,$$

  where we omit in our notations the dependence on f. We are going to prove the following:

(a) $\lim_{K\to+\infty} \mathbb{E}\left[\left|\Psi_t(X^K)\right|\right] = \mathbb{E}\left[|\Psi_t(X)|\right]$.

(b) $\lim_{K\to+\infty} \mathbb{E}\left[\left|\Psi_t(X^K) + \Psi_t^{2,K}(X^K)\right|\right] = 0$.

(c) $\lim_{K\to+\infty} \mathbb{E}\left[\left|\Psi_t^{2,K}(X^K)\right|\right] = 0$,

permitting us to conclude with

$$\begin{aligned}\mathbb{E}_Q\left[|\Psi_t(X)|\right] &= \lim_{K\to+\infty} \mathbb{E}\left[\left|\Psi_t(X^K)\right|\right] \\ &\leq \lim_{K\to+\infty} \mathbb{E}\left[\left|\Psi_t(X^K) + \Psi_t^{2,K}(X^K)\right|\right] + \lim_{K\to+\infty} \mathbb{E}\left[\left|\Psi_t^{2,K}(X^K)\right|\right] \\ &\leq 0.\end{aligned}$$

(a) We know that X is almost surely a continuous process, $f \in \mathcal{C}(\overline{\chi})$ and all the parameters rates are continuous. Hence Ψ_t is continuous in X for all f, and $\lim_K \Psi_t(X^K) = \Psi_t(X)$ in law. Moreover, for $\nu \in \mathcal{M}_F(\overline{\chi})$,

$$|\Psi_t(\nu)| \leq C(t,f)(1 + \sup_{[0,T]} < \nu_s, 1 >),$$

showing using the moment property 19 that $\left(\Psi_t(X^K)\right)_K$ is uniformly integrable. Hence,

$$\lim_{K\to+\infty} \mathbb{E}\left[\left|\Psi_t(X^K)\right|\right] = \mathbb{E}\left[\left|\lim_{K\to+\infty} \Psi_t(X^K)\right|\right] = \mathbb{E}\left[\left|\Psi_t(X)\right|\right].$$

(b) As $\mathbb{E}\left[\left|M_t^{f,K}\right|\right] = \mathbb{E}\left[\left|\Psi_t(X^K) + \Psi_t^{2,K}(X^K)\right|\right]$, the result comes from

$$\begin{aligned}\mathbb{E}\left[\left|M_t^{f,K}\right|\right]^2 &\leq \mathbb{E}\left[\left|M_t^{f,K}\right|^2\right] = \mathbb{E}\left[\left\langle M^{f,K}\right\rangle_t\right] \\ &\leq \frac{T}{K}C\left(1 + \mathbb{E}\left[\sup_{[0,T]} < X_t^K, 1 >\right]\right),\end{aligned}$$

together with the moment property 19.

(c) Using classical bounds, we obtain

$$\left|\Psi_t^{2,K}(X^K)\right| \leq \frac{2\mu\overline{r}T \parallel f \parallel_\infty}{K^\eta} \sup_{s\in[0,T]} \left\langle X_s^K, 1\right\rangle,$$

and as $0 < \eta < 1$, the moment property 19 leads to the result.

Uniqueness of a solution for (3.28) the proof is identical to the one for (3.9), as a is bounded, and we do not rewrite it here.

The convergence is now shown.

2. The existence of a density for ξ_t $\forall t > 0$ can be proven exactly as for (11). The corresponding equation is then simply the dual form of (3.28).

□

Case $\eta = 1$

The limit theorem is obtained with the following hypothesis:

Hypothesis 11 (Rare mutations - stochastic limit)**.** *For $\overline{r}$, and $\overline{d}$ positive constants, consider the positive rates*

$$c_K(X_t^K) \equiv Kc$$

$$r_K(\theta, X_t^K) = r(\theta, X_t^K) + K^\eta a \leq \overline{r} + Ka, \quad d_K(\theta, X_t^K) = d(\theta, X_t^K) + K^\eta a \leq \overline{d} + Ka.$$

Moreover, r and d are continuous.

Theorem 14. *Under hypothesis 11, if for $K \to +\infty$ the initial measure X_0^K converges in law to $X_0 \in \mathcal{M}_F(\overline{\chi})$, with*

$$\sup_{K>0} \mathbb{E}\left[< X_0^K, 1 >\right] < +\infty, \tag{3.31}$$

then $(X^K)_{K>0}$ converges in law in $\mathbb{D}\left([0,T], \mathcal{M}_F(\overline{\chi})\right)$ to the unique in law $X \in \mathcal{C}([0,T], \mathcal{M}_F(\overline{\chi}))$ superprocess such that

$$\sup_{t\in[0,T]} \mathbb{E}\left[< X_t, 1 >\right] < +\infty, \tag{3.32}$$

$\forall f \in \mathcal{L}^\infty(\overline{\chi})$,

$$\tilde{M}_t^f = < X_t, f > - < X_0, f > - \frac{ct}{2\pi} \int_\chi f(\theta)\,\mathrm{d}\theta - \int_0^t \int_\chi (r(\theta, X_s) - d(\theta, X_s)) f(\theta) X_s(\,\mathrm{d}\theta)\,\mathrm{d}s \\ - \int_0^t \int_\chi \mu a \left(\int_\chi f(z) g(z;\theta)\,\mathrm{d}z - f(\theta) \right) X_s(\,\mathrm{d}\theta)\,\mathrm{d}s \tag{3.33}$$

is a continuous martingale with quadratic variation

$$\left\langle \tilde{M}^f \right\rangle_t = 2a \int_0^t \int_\chi f(\theta)^2 X_s(\,\mathrm{d}\theta)\,\mathrm{d}s. \tag{3.34}$$

Proof. As usual, the proof is based on a compactness-uniqueness argument: we'll prove that the sequence of laws $(Q^K)_K$ of the processes $(X^K)_K$ is tight. Then, we'll identify its limiting values as solutions of (3.33, 3.34), for which a uniqueness property will be stated.

Uniform tightness of $(Q^K)_K$. We refer to the proof of theorem 13.

Identification of the limit Consider a convergent subsequence $(Q^K)_K$, and denote Q its limit. By the Prohorov theorem, one can find a corresponding sequence of processes $(X^K)_K$ in $\mathbb{D}([0,T], \mathcal{M}_F(\overline{\chi}))$ converging in law to $X \in \mathbb{D}([0,T], \mathcal{M}_F(\overline{\chi}))$.

- By construction, we know that $\forall K > 0$, jumps of $(X_t^K)_t$ are almost surely of the form δ_θ / K. As a consequence, almost surely,

$$\sup_{t\in[0,T]} \sup_{f \in L^\infty(\overline{\chi})} \left| < X_t^K, f > - < X_{t^-}^K, f > \right| \leq \frac{\| f \|_\infty}{K}.$$

  Hence, any process of law Q like X is almost surely strongly continuous.

- Now, X verifies (3.32) because of proposition 18 together with the initial condition(3.31).

- Let us show that $\forall f \in L^\infty(\overline{\chi})$, $\tilde{M}^f$ defined in (3.33) is a martingale. Take $0 \leq s_1 < ... < s_n < s < t$, and $\Phi_1, ..., \Phi_n$ continuous bounded functions from $\mathcal{M}_F(\overline{\chi})$ to $\mathbb{R}$. Define $\Psi : \mathbb{D}([0,T], \mathcal{M}_F(\overline{\chi})) \to \mathbb{R}$ by

$$\Psi(\nu) = \Phi_1(\nu_{s_1}) ... \Phi_n(\nu_{s_n}) \left[< \nu_t, f > - < \nu_s, f > - \int_s^t \left\{ \frac{c}{2\pi} \int_\chi f(\theta)\,\mathrm{d}\theta \right. \right. \\ \left. \left. + \int_\chi (r(\theta, \nu_u) - d(\theta, \nu_u) - \mu a) f(\theta) + \mu a \int_\chi f(z) g(z;\theta)\,\mathrm{d}z\, \nu_u(\,\mathrm{d}\theta) \right\} du \right].$$

  We need to show that

$$\mathbb{E}[\Psi(X)] = 0.$$

  Using the K-dependent martingale expression (3.25), we get :

$$0 = \mathbb{E}\left[\Phi_1(X_{s_1}^K) ... \Phi_n(X_{s_n}^K) \left\{ M_t^{K,f} - M_s^{K,f} \right\} \right] \\ = \mathbb{E}[\Psi(X^K)] \\ \underbrace{- \mathbb{E}\left[\Phi_1(X_{s_1}^K) ... \Phi_n(X_{s_n}^K) \left\{ \int_s^t \int_\chi \frac{\mu r(\theta, X_u^K)}{K} \left(\int_\chi f(z) g(z|\theta)\,\mathrm{d}z - f(\theta) \right) X_u^K(\,\mathrm{d}\theta) du \right\} \right]}_{=: A_K}$$

It is now clear that

$$|A_K| \leq \frac{1}{K}\mathbb{E}\left[|\Phi_1(X^K_{s_1})...\Phi_n(X^K_{s_n})|\left\{2\mu\bar{r} \parallel f \parallel_\infty \int_s^t < X^K_u, 1 > du\right\}\right] \underset{K\to+\infty}{\longrightarrow} 0.$$

Moreover, the moment property 19 ensures that the sequence $(|\Psi(X^K)|)_K$ is uniformly integrable, and

$$0 = \lim_{K\to+\infty} \mathbb{E}[|\Psi(X^K)|] = \mathbb{E}_Q[|\Psi(X)|],$$

and $\tilde{M}^f$ defined in (3.33) is indeed a martingale.

- The last thing to show is that the bracket of $\tilde{M}$ is the one given in (3.34)).
  1. First, we check that

$$\begin{aligned}\tilde{N}^f_t =& < X_t, f >^2 - < X_0, f >^2 - \\ &\int_0^t \left\{2 < X_s, f > \frac{c}{2\pi}\int_\chi f(\theta)\,\mathrm{d}\theta + 2 < X_s, f > \int_\chi (r(\theta, X_s) - d(\theta, X_s))f(\theta)X_s(\,\mathrm{d}\theta)\right.\\ &\left. +2 < X^K_s, f > \int_\chi \mu a\left[\int_\chi f(z)g(z|\theta)\,\mathrm{d}z - f(\theta)\right]X^K_s(\,\mathrm{d}\theta) + 2\int_\chi a f(\theta)^2 X_s(\,\mathrm{d}\theta)\right\}\,\mathrm{d}s\end{aligned}$$

     is a martingale, exactly as in the previous step for $\tilde{M}^f$. This time, we have to use the martingale obtained from (3.5) with $\Phi(\nu) =< \nu, f >^2$, related to the generator:

$$\begin{aligned}L^K\Phi(X^K_s) =& K\int_\chi \frac{c}{2\pi}\left(\frac{2f(\theta)}{K} < X^K_s, f > + \frac{f(\theta)^2}{K^2}\right)\,\mathrm{d}\theta\\ &+ K\int_\chi (r(\theta, X^K_s) + Ka)\left[\frac{2f(\theta)}{K} < X^K_s, f > + \frac{f(\theta)^2}{K^2}\right]X^K_s(\,\mathrm{d}\theta)\\ &+K\int_\chi \frac{\mu}{K}(r(\theta, X^K_s) + Ka)\left[\int_\chi \left(\frac{2f(z)}{K} < X^K_s, f > + \frac{f(z)^2}{K^2}\right)g(z;\theta)\,\mathrm{d}z\right.\\ &\qquad\left. - \left(\frac{2f(\theta)}{K} < X^K_s, f > + \frac{f(\theta)^2}{K^2}\right)\right]X^K_s(\,\mathrm{d}\theta)\\ &+ K\int_\chi (d(\theta, X^K_s) + Ka)\left[-\frac{2f(\theta)}{K} < X^K_s, f > + \frac{f(\theta)^2}{K^2}\right]X^K_s(\,\mathrm{d}\theta)\,.\end{aligned}$$

  2. Now, applying the Itô formula to (3.33) shows that

$$\begin{aligned}&< X_t, f >^2 - < X_0, f >^2 - <\tilde{M}^f>_t\\ &- \int_0^t 2 < X_s, f > \left\{\frac{c}{2\pi}\int_\chi f(\theta)\,\mathrm{d}\theta + \int_\chi (r(\theta, X_s) - d(\theta, X_s))f(\theta)X_s(\,\mathrm{d}\theta)\right.\\ &\qquad\left. + \int_\chi \mu a\left[\int_\chi f(z)g(z|\theta)\,\mathrm{d}z - f(\theta)\right]X^K_s(\,\mathrm{d}\theta)\right\}\,\mathrm{d}s\end{aligned}$$

     is a martingale. We conclude by the uniqueness of the semimartingale decomposition of $< X_t, f >^2$.

Uniqueness of a solution for the martingale problem (3.33)-(3.34): The classical tools to show uniqueness for a martingale problem rely on a Laplace transform approach allowed by the branching property of the problem. This feature does not hold as soon as there is interaction in the population under study. In Champagnat et al. [2008]; Fournier and Méléard [2004]; Tran [2006] , uniqueness for martingale problems with interaction are shown using the Cameron-Martin-Girsanov formula to study an equivalent non interactive martingale problem. As for us, the immigration term brings a new difficulty, but we are able to use a similar path:

1. we prove an equivalence between (3.33)-(3.34) and a martingale problem for a non-interactive immigration process. We'll follow Dawson [1978] to use the Cameron-Martin-Girsanov formula in that case.
2. Then, we show uniqueness for the equivalent problem.

First, we want to use the Cameron-Martin-Girsanov formula (see annex (3.4.1, proposition 22) for the details). Our problem can be written in the (G_2, F_2, Q_2) form, that is to say: $\forall \phi \in \mathcal{C}(\overline{\chi}) \cap D(\overline{\chi})$, $< X_{G_2,F_2}, \phi >$ is an $(\mathcal{F}_t)_t$-continuous martingale, with

$$X_{G_2,F_2}(t) \equiv X(t) - \int_0^t G_2^* X(s) + F_2(s, X(s))\,\mathrm{d}s\,,$$

and a quadratic variation defined by

$$< \phi_1, X_{G_2,F_2}, \phi_2 >_t = \int_0^t \iint_{\chi\times\chi} \phi_1(x)\phi_2(y) Q_2(X(s); dx \times dy)\,\mathrm{d}s\,.$$

The martingale problem we study corresponds to the following:

$\rightarrow$ $G_2 = \mu a g(.;\theta)\,\mathrm{d}z$,
$\rightarrow$ $F_2(\nu) = c\,\mathrm{d}\theta + (r(\theta,\nu) - d(\theta,\nu) - \mu a)\nu$,
$\rightarrow$ $Q_2(\nu;\, \mathrm{d}\theta \times d\lambda) = 2a\delta_{\theta-\lambda}\nu(\,\mathrm{d}\theta)$.

We can check that G_2 is an infinitesimal generator on $\mathcal{C}(\overline{\chi})$ of a Markov process on $\overline{\chi}$, that F_2 is continuous, and Q_2 is a continuous mapping such that for $\phi \in \mathcal{C}(\overline{\chi})$,

$$\iint \phi(\theta)\phi(\lambda) Q_2(\nu;\, \mathrm{d}\theta \times d\lambda) = \int_\chi 2a\phi(\theta)^2 \nu(\,\mathrm{d}\theta) \geq 0,$$

because a is positive, and if $\nu(A) = 0$, obviously

$$\iint_{A\times A} \phi(\theta)\phi(\lambda) Q_2(\nu;\, \mathrm{d}\theta \times d\lambda) \leq 2a \parallel \phi \parallel^2 \nu(A) = 0.$$

Now, define a second martingale problem by $G_1 = G_2 =: G$, $Q_1 = Q_2$, and

$$F_1(\nu) = c\,\mathrm{d}\theta = F_2(\nu) - (r(\theta,\nu) - d(\theta,\nu) - \mu a)\nu.$$

First, we have

$$\begin{aligned}(F_1(\nu) - F_2(\nu))(dx) &= -(r(.,\nu) - d(.,\nu) - \nu a)\nu(dx) \\ &= 2ah(\nu;x)\mu(dx) \text{ for } h(\nu;.) = -\frac{r(.,\nu) - d(.,\nu) - \mu a}{2a},\end{aligned}$$

with h that is indeed a continuous function from $M(\overline{\chi})$ to $\mathcal{C}(\overline{\chi})$. Moreover, it is clear that for every ϖ compact of $M(\overline{\chi})$, $\{P^1_\nu,\ \nu \in \varpi\}$ is uniformly tight in $\Pi(\overline{\chi})$.

Hence by proposition 22 in annex, uniqueness for (3.33)-(3.34) is equivalent to uniqueness for the martingale problem

$$\begin{aligned} \tilde{M}^f_t &=< X_t, f > - < X_0, f > - \int_0^t cf(\theta)\,\mathrm{d}\theta\,\mathrm{d}s - \int_0^t < X_s, Gf > \mathrm{d}s \\ \left\langle \tilde{M}^f \right\rangle_t &= \int_0^t < X_s, 2af^2(\theta)) \,\mathrm{d}s. \end{aligned} \tag{3.35}$$

We conclude with a uniqueness result cited in Fu and Li [2004] and detailed in Konno and Shiga [1988], Li and Shiga [1995].

□

3.3.3 Small mutation step approximation

In this subsection, we choose to fix the mutation probability, while the mutation step probability density is renormalized.

Hypothesis 12.

- $\mu_K = \mu$,
- *every offspring of a θ-oriented individual will have a trait distributed according to a probability density g_K with mean θ, variance $\frac{\sigma^2}{K^\eta}$ and third moment of order $\frac{1}{K^{\eta+\varepsilon}}$.*

This means that the pathway of signalling inducing actin polymerization is local. This is in agreement with the molecular activation of polymerization: if filaments grow under molecular triggers, the immediate neighbors filaments are very likely to grow too, whereas activation further away is much less clear. Following this assumption, the martingale property (3.6)-(3.7) rewrites

$$\begin{aligned} M^{K,f}_t =& < X^K_t, f > - < X^K_0, f > - \int_0^t \frac{c}{2\pi} \int_\chi f(\theta)\,\mathrm{d}\theta\,\mathrm{d}s \\ &- \int_0^t \int_\chi \left(r(\theta, X^K_s) - d(\theta, X^K_s)\right) f(\theta) X^K(\,\mathrm{d}\theta)\,\mathrm{d}s \\ &- \int_0^t \int_\chi \mu(r(\theta, X^K_s) + \mathbf{K}^\eta a) \left(\int_\chi f(z) g_K(z;\theta)\,\mathrm{d}z - f(\theta) \right) X^K_s(\,\mathrm{d}\theta)\,\mathrm{d}s \end{aligned} \tag{3.36}$$

is a càdlàg square-integrable martingale starting from 0 and of quadratic variation

$$\begin{aligned} \left\langle M^{K,f} \right\rangle_t = \frac{1}{\mathbf{K}} \int_0^t \int_\chi \frac{c}{2\pi} f(\theta)^2\,\mathrm{d}\theta + \frac{1}{\mathbf{K}} \int_\chi (r(\theta, X^K_s) + d(\theta, X^K_s) + 2\mathbf{K}^\eta a) f(\theta)^2 X^K_s(\,\mathrm{d}\theta) \\ + \frac{1}{\mathbf{K}} \int_\chi \mu(r(\theta, X^K_s) + \mathbf{K}^\eta a) \left[\int_\chi f(z)^2 g_K(z;\theta)\,\mathrm{d}z - f(\theta)^2 \right] X^K_s(\,\mathrm{d}\theta)\,\mathrm{d}s. \end{aligned} \tag{3.37}$$

Case $0 < \eta < 1$

As before, the demography is not accelerated enough to get a stochastic limit. More precisely, we assume the following:

Hypothesis 13 (Small mutation step - deterministic limit)**.** *For* $\overline{c}$, $\overline{r}$, *and* $\overline{d}$ *positive constants, consider positive rates*

$$c_K(X_t^K) = Kc(X_t^K) \leq K\overline{c}$$

$$r_K(\theta, X_t^K) = r(\theta, X_t^K) + K^\eta a \leq \overline{r} + K^\eta a \quad d_K(\theta, X_t^K) = d(\theta, X_t^K) + K^\eta a \leq \overline{d} + Ka.$$

Moreover, c, r *and* d *are continuous, and Lipschitz-continuity in* ν *of constants* L_c, L_r, L_d.

Theorem 15. *Under hypothesis 13 and 12,*

1. *if for* $K \to +\infty$ *the initial measure* X_0^K *converges in law on* $\mathcal{M}_F(\overline{\chi})$ *to a deterministic measure* $\xi_0 \in \mathcal{M}_F(\overline{\chi})$, *and if*

$$\sup_{K>0} \mathbb{E}\left[< X_0^K, 1 >\right] < +\infty, \tag{3.38}$$

then $(X^K)_{K>0}$ *converges in law in* $\mathbb{D}([0,T], \mathcal{M}_F(\overline{\chi}))$ *to the unique deterministic* $\xi \in \mathcal{C}([0,T], \mathcal{M}_F(\overline{\chi}))$ *such that* $\forall f \in \mathcal{C}^2(\overline{\chi})$ *with periodic boundary conditions,*

$$< \xi_t, f >=< \xi_0, f > + \int_0^t \frac{c(\xi_s)}{2\pi} \int_\chi f(\theta)\,\mathrm{d}\theta + \int_0^t \int_\chi (r(\theta,\xi_s) - d(\theta,\xi_s)) f(\theta) \xi_s(\,\mathrm{d}\theta)\,\mathrm{d}s + \int_0^t \int_\chi \frac{1}{2}\mu\sigma^2 a f''(\theta)\xi_s(\,\mathrm{d}\theta)\,\mathrm{d}s\,. \tag{3.39}$$

2. *Moreover, assume that* $a > 0$. *Then,* $\forall t > 0$, $\xi_t(\,\mathrm{d}\theta)$ *admits a density* n_t *with respect to* $\mathrm{d}\theta$, *defining* $n \in L^\infty([0,T], L^1(\overline{\chi}))$ *that is weak solution of*

$$\begin{aligned} \frac{\partial n_t(\theta)}{\partial t} &= \frac{c(n_t)}{2\pi} + (r(\theta, n_t) - d(\theta, n_t))n_t(\theta) + \frac{1}{2}\mu a\sigma^2 \frac{\partial^2}{\partial\theta^2}(n_t(\theta))\,, \\ n_0(\theta) &= n^0(\theta), \\ n_t(0) &= n_t(2\pi) \quad \forall t \in [0,T]. \end{aligned} \tag{3.40}$$

Proof. 1. Let us first prove the convergence result, that is similar to theorems 10 and 13.

Uniform tightness Let us denote $(Q^K)_{K>0}$ the sequence of laws of the processes $(X_t^K)_{t\geq 0}$. We can prove as before that the sequence is uniformly tight in $\mathcal{L}(\mathbb{D}(\mathbb{R}_+, \mathcal{M}_F(\overline{\chi})))$, using Roelly's criterion and the Aldous-Rebolledo one [Aldous, 1989; Joffe and Metivier, 1986; Roelly-Coppoletta, 1986]. Consider

$$\begin{aligned} V_t^{K,f} \quad = \quad & < X_0^K, f > + \int_0^t \frac{c(X_s^K)}{2\pi} \int_\chi f(\theta)\,\mathrm{d}\theta\,\mathrm{d}s \\ & + \int_0^t \int_\chi \left(r(\theta, X_s^K) - d(\theta, X_s^K)\right) f(\theta) X^K(\,\mathrm{d}\theta)\,\mathrm{d}s \\ & + \int_0^t \int_\chi \left(\mu r(\theta, X_s^K) + \mu K^\eta a\right) \left(\int_\chi f(z) g_K(z;\theta)\,\mathrm{d}z - f(\theta)\right) X_s^K(\,\mathrm{d}\theta)\,\mathrm{d}s. \end{aligned}$$

The novelty here lies in the finite variation part, for which we establish the following lemma:

Lemma 5. *For $f \in \mathcal{C}^2(\overline{\chi})$ and g_K as defined above, we have*

$$\int_\chi f(z) g_K(z;\theta)\,\mathrm{d}z - f(\theta) = \frac{1}{2}\frac{\sigma^2}{K^\eta} f''(\theta) + o\left(\frac{1}{K^\eta}\right). \tag{3.41}$$

Proof of lemma 5. Using the second-order Taylor expansion of f in $\theta \in [0, 2\pi)$, one can write

$$\begin{aligned}
&\int_\chi f(z) g_K(z;\theta)\,\mathrm{d}z \\
&= \int_\chi \left[f(\theta) + (z-\theta) f'(\theta) + \frac{1}{2}(z-\theta)^2 f''(\theta) + O((z-\theta)^3) \right] g_K(z;\theta)\,\mathrm{d}z \\
&= f(\theta) + f'(\theta)\mathbb{E}[Z-\theta] + \frac{1}{2} f''(\theta)(Var(Z-\theta) - \mathbb{E}[Z-\theta]^2) + o\left(\frac{1}{K^\eta}\right) \\
&= f(\theta) + \frac{1}{2} f''(\theta)\frac{\sigma^2}{K^\eta} + o\left(\frac{1}{K^\eta}\right).
\end{aligned}$$

□

Hence,

$$\begin{aligned}
V_t^{K,f} &= < X_0^K, f > + \int_0^t \frac{c(X_s^K)}{2\pi} \int_\chi f(\theta)\,\mathrm{d}\theta\,\mathrm{d}s \\
&\quad + \int_0^t \int_\chi \left(r(\theta, X_s^K) - d(\theta, X_s^K) \right) f(\theta) X^K(\,\mathrm{d}\theta)\,\mathrm{d}s \\
&\quad + \int_0^t \int_\chi \left(\mu r(\theta, X_s^K) + \mu K^\eta a \right) \left(\frac{1}{2}\frac{\sigma^2}{K^\eta} f''(\theta) + o\left(\frac{1}{K^\eta}\right) \right) X_s^K(\,\mathrm{d}\theta)\,\mathrm{d}s,
\end{aligned}$$

and

$$\begin{aligned}
&\mathbb{E}\left[\left| V_{\tau_K}^{K,f} - V_{\sigma_K}^{K,f} \right| \right] \\
&\leq \overline{c} \parallel f \parallel_\infty \delta + \left(\overline{r} + \overline{d}\right) \parallel f \parallel_\infty \mathbb{E}\left[\left| \int_{\sigma_K}^{\tau_K} < X_s^K, 1 > \,\mathrm{d}s \right| \right] \\
&+ \mu(a + \overline{r}) \left[\sigma^2 \parallel f'' \parallel_\infty + K^\eta o\left(\frac{1}{K^\eta}\right) \right] \mathbb{E}\left[\left| \int_{\sigma_K}^{\tau_K} < X_s^K, 1 > \,\mathrm{d}s \right| \right] \delta \\
\leq\ & C\delta + C\delta \left[1 + K^\eta o\left(\frac{1}{K^\eta}\right) \right] \mathbb{E}\left[\sup_{[0,T]} < X_t^K, 1 > \right] \\
\leq\ & C(T)\delta \left(1 + K^\eta o\left(\frac{1}{K^\eta}\right) \right),
\end{aligned}$$

by proposition 19. Moreover, $K^\eta o\left(\frac{1}{K^\eta}\right) \underset{K\to+\infty}{\longrightarrow} 0$, showing that the conditions ensuring tightness are satisfied.

Identification of the limiting process consider a convergent subsequence, denoted $(Q^K)_K$ for notational convenience, with Q its limit. By the Prohorov theorem, one can find a corresponding sequence of processes $(X^K)_K$ in $\mathbb{D}([0,T], \mathcal{M}_F(\overline{\chi}))$ converging in law to $X \in \mathbb{D}([0,T], \mathcal{M}_F(\overline{\chi}))$. Again, we can prove that X is almost surely strongly continuous.

- Now, let us show that X is solution of (3.39).

→ Following the moment proposition 19, we have $\mathbb{E}\left[\sup_{[0,T]} < X_t, 1 >\right] < +\infty$, and almost surely

$$\sup_{[0,T]} < X_t, 1 >< +\infty. \tag{3.42}$$

→ We show now that X is solution of equation (3.39) for $f \in \mathcal{C}^2(\overline{\chi})$. For $T > 0$, take $t \leq T$ and $\nu \in \mathcal{C}([0,T], \mathcal{M}_F(\overline{\chi}))$.
Denote

$$\begin{aligned}\Psi_t^1(\nu) &:= < \nu_t, f > - < \nu_0, f > - \int_0^t \frac{c(\nu_s)}{2\pi} \int_\chi f(\theta)\, \mathrm{d}\theta\, \mathrm{d}s \\ &\quad - \int_0^t \int_\chi (r(\theta, \nu_s) - d(\theta, \nu_s)) f(\theta) \nu_s(\,\mathrm{d}\theta)\, \mathrm{d}s\end{aligned}$$

and

$$\Psi_t^2(\nu) := -\int_0^t \int_\chi \frac{1}{2} \mu\sigma^2 a f''(\theta) \nu_s(\,\mathrm{d}\theta)\, \mathrm{d}s.$$

We have to show that $\forall t \leq T$, $\mathbb{E}_Q\left[\left|\Psi_t^1(X) + \Psi_t^2(X)\right|\right] = 0$. Moreover, by the martingale property (3.36), we know that

$$M_t^{K,f} = \Psi_t^1(X^K) + \Psi_t^{2,K}(X^K),$$

with

$$\begin{aligned}\Psi_t^{2,K}(\nu) &:= -\int_0^t \int_\chi \mu(r(\theta, \nu_s) + K^\eta a) \left[\int_\chi f(z) g_K(z;\theta)\, \mathrm{d}z - f(\theta)\right] \nu_s(\,\mathrm{d}\theta)\, \mathrm{d}s \\ &= -\int_0^t \int_\chi \mu(r(\theta, \nu_s) + K^\eta a) \left[\frac{1}{2}\frac{\sigma^2}{K^\eta} f''(\theta) + o\left(\frac{1}{K^\eta}\right)\right] \nu_s(\,\mathrm{d}\theta)\, \mathrm{d}s\end{aligned}$$

by lemma (5), and omitting in our notations the dependence on f. We are going to prove the following:

(a) $\lim_{K\to+\infty} \mathbb{E}\left[\left|\Psi_t^1(X^K) + \Psi_t^2(X^K)\right|\right] = \mathbb{E}\left[\left|\Psi_t^1(X) + \Psi_t^2(X)\right|\right]$.

(b) $\lim_{K\to+\infty} \mathbb{E}\left[\left|\Psi_t^{2,K}(X^K) - \Psi_t^2(X^K)\right|\right] = 0$.

(c) $\lim_{K\to+\infty} \mathbb{E}\left[\left|\Psi_t^1(X^K) + \Psi_t^{2,K}(X^K)\right|\right] = 0$,

permitting us to conclude with

$$\begin{aligned}\mathbb{E}\left[\left|\Psi_t^1(X) + \Psi_t^2(X)\right|\right] &\overset{(a)}{=} \lim_{K\to+\infty} \mathbb{E}\left[\left|\Psi_t^1(X^K) + \Psi_t^2(X^K)\right|\right] \\ &\leq \lim_{K\to+\infty} \mathbb{E}\left[\left|\Psi_t^1(X^K) + \Psi_t^{2,K}(X^K)\right|\right] \\ &\quad + \lim_{K\to+\infty} \mathbb{E}\left[\left|\Psi_t^{2,K}(X^K) - \Psi_t^2(X^K)\right|\right] \\ &\leq 0.\end{aligned}$$

(a) We know that X is almost surely a continuous process, $f \in \mathcal{C}^2(\overline{\chi})$ and all the rates are continuous. Hence Ψ_t^1 and Ψ_t^2 are continuous in X for all f, and $\lim_K \Psi_t^i(X^K) = \Psi_t^i(X)$ in law, for $i = 1, 2$. Moreover, for $\nu \in \mathcal{M}_F(\overline{\chi})$,

$$\left|\Psi_t^1(\nu) + \Psi_t^2(\nu)\right| \leq C(t, f)(1 + \sup_{[0,T]} < \nu_s, 1 >),$$

showing using proposition 19 that $\left(\Psi_t^1(X^K)+\Psi_t^2(X^K)\right)_K$ is uniformly integrable. Hence,

$$\begin{aligned}\lim_{K\to+\infty}\mathbb{E}\left[\left|\Psi_t^1(X^K)+\Psi_t^2(X^K)\right|\right] &= \mathbb{E}\left[\left|\lim_{K\to+\infty}\left\{\Psi_t^1(X^K)+\Psi_t^2(X^K)\right\}\right|\right]\\ &= \mathbb{E}\left[\left|\Psi_t^1(X)+\Psi_t^2(X)\right|\right].\end{aligned}$$

(b) Using classical bounds, we obtain

$$\begin{aligned}&\left|\Psi_t^{2,K}(X^K)-\Psi_t^2(X^K)\right|\\ &\qquad=\left|\int_0^t\int_\chi \mu\overline{r}\left[\frac{1}{2}\frac{\sigma^2}{K^\eta}f''(\theta)+o\left(\frac{1}{K^\eta}\right)\right]+\mu a K^\eta o\left(\frac{1}{K^\eta}\right)X_s^K(\,\mathrm{d}\theta)\,\mathrm{d}s\right|\\ &\qquad\le C(f)\left(\frac{1}{K^\eta}+o\left(\frac{1}{K^\eta}\right)+K^\eta o\left(\frac{1}{K^\eta}\right)\right)\int_0^t <X_s^K,1>\,\mathrm{d}s;\end{aligned}$$

By the moment property 19, and as $\lim_{K\to+\infty}K^\eta o\left(\frac{1}{K^\eta}\right)=0$, we have the result.

(c) As $\mathbb{E}\left[\left|M_t^{f,K}\right|\right]=\mathbb{E}\left[\left|\Psi_t(X^K)+\Psi_t^{2,K}(X^K)\right|\right]$, the result comes from

$$\begin{aligned}\mathbb{E}\left[\left|M_t^{f,K}\right|\right]^2 &\le \mathbb{E}\left[\left|M_t^{f,K}\right|^2\right]=\mathbb{E}\left[\left\langle M^{f,K}\right\rangle_t\right]\\ &\le C(f)\frac{T}{K^{1-\eta}}\left(1+\mathbb{E}\left[\sup_{[0,T]}<X_t^K,1>\right]\right),\end{aligned}$$

together with proposition 19.

Uniqueness of a solution for equation (3.39) First, let us remark the following: if ξ is solution of (3.39), then

$$<\xi_t,1>\le<\xi_0,1>+t\overline{c}+\overline{r}\int_0^t<\xi_s,1>\,\mathrm{d}s,$$

and the Gronwall lemma shows that its mass is bounded on finite time intervals:

$$A_T:=\sup_{t\in[0,T]}<\xi_t,1>\le(<\xi_0,1>+T\overline{c})e^{CT}.$$

Now, let us prove this lemma:

Lemma 6. *Denote P the semigroup of the diffusion process on χ having periodic boundary conditions and diffusion coefficient $\frac{1}{2}\mu\sigma^2 a$. Let ξ be a solution of (3.39). Then, for any $\phi\in\mathcal{C}(\overline{\chi})$ with periodic boundary values,*

$$\begin{aligned}<\xi_t,\phi>=&<\xi_0,P_t\phi>+\int_0^t c(\xi_s)\int_\chi P_{t-s}\phi(\theta)\,\mathrm{d}\theta\\ &+\int_0^t\int_\chi (r(\theta,\xi_s)-d(\theta,\xi_s))P_{t-s}\phi(\theta)\xi_s(\,\mathrm{d}\theta)\,\mathrm{d}s.\end{aligned}\tag{3.43}$$

Proof. From equation (3.39), one can associate a space-time analogous, for any $\psi\in\mathcal{C}^{1,2}([0,t]\times\overline{\chi})$ such that it satisfies the boundary condition $\psi(t,0)=\psi(t,2\pi)\ \forall t\ge 0$. More precisely, denoting $\psi_t(.)=\psi(t,.)$, we have

$$\begin{aligned}<\xi_t,\psi_t>=<\xi_0,\psi_0>&+\int_0^t\frac{c(\xi_s)}{2\pi}\int_\chi\psi_s(\theta)\,\mathrm{d}\theta+\int_0^t\int_\chi(r(\theta,\xi_s)-d(\theta,\xi_s))\psi_s(\theta)\xi_s(\,\mathrm{d}\theta)\,\mathrm{d}s\\ &+\int_0^t\int_\chi\frac{\partial\psi_s(\theta)}{\partial s}+\frac{1}{2}\mu\sigma^2 a\psi_s''(\theta)\xi_s(\,\mathrm{d}\theta)\,\mathrm{d}s.\end{aligned}$$

Hence, for $t \in [0,T]$, $s \in [0,t]$, and any $\phi \in \mathcal{C}(\overline{\chi})$, define

$$\psi_t(\theta) := P_{t-s}\phi(\theta).$$

Then, by definition of P, ψ is solution of

$$\begin{aligned} \frac{\partial \psi_s(\theta)}{\partial s} &= -\frac{1}{2}\mu\sigma^2 a\psi_s''(\theta) \quad && \text{on } [0,T]\times\chi, \\ \psi(t,0) &= \psi(t,2\pi) && \text{for } t \in [0,T], \\ \psi(t,\theta) &= \phi(\theta) && \text{for } \theta \in \overline{\chi}. \end{aligned}$$

Hence using ψ in the previous space-time equation leads to the result. □

Now, showing the uniqueness of a solution to (3.39) amounts to showing uniqueness for equation (3.43). Then, take $(\xi_t)_{t\geq 0}$ and $(\overline{\xi_t})_{t\geq 0}$ solutions of (3.39) having the same initial condition $\xi_0 \in \mathcal{M}_F(\overline{\chi})$. Let $f \in L^\infty(\overline{\chi})$ such that $\| f \|_\infty \leq 1$. Notice that as P is contractant, $\| P_{t-s}f \|_\infty \leq 1$. Then, for $t \in [0,T]$, $\mathbb{P}-a.s$, one can compute

$$\begin{aligned} |< \xi_t - \overline{\xi_t}, f >| &= \left| \int_0^t (c(\xi_s) - c(\overline{\xi_s})) \int_\chi P_{t-s}f(\theta)\,\mathrm{d}\theta\,\mathrm{d}s \right. \\ &\left. + \int_0^t \int_\chi (r(\theta,\xi_s) - d(\theta,\xi_s))P_{t-s}f(\theta)\xi_s(\,\mathrm{d}\theta) - \int_\chi (r(\theta,\overline{\xi_s}) - d(\theta,\overline{\xi_s}))P_{t-s}f(\theta)\overline{\xi_s}(\,\mathrm{d}\theta)\,\mathrm{d}s \right|. \end{aligned}$$

Now we introduce an additional integrand and consider the resulting inequality:

$$\begin{aligned} |< \xi_t - \overline{\xi_t}, f >| &\leq \int_0^t \frac{1}{2\pi}|c(\xi_s) - c(\overline{\xi_s})| \int_\chi |P_{t-s}f(\theta)|\,\mathrm{d}\theta\,\mathrm{d}s \\ &+ \left| \int_0^t \int_\chi (r(\theta,\xi_s) - d(\theta,\xi_s))P_{t-s}f(\theta)\xi_s(\,\mathrm{d}\theta) - \int_\chi (r(\theta,\overline{\xi_s}) - d(\theta,\overline{\xi_s}))P_{t-s}f(\theta)\xi_s(\,\mathrm{d}\theta)\,\mathrm{d}s \right| \\ &+ \left| \int_0^t \int_\chi (r(\theta,\overline{\xi_s}) - d(\theta,\overline{\xi_s}))P_{t-s}f(\theta)\xi_s(\,\mathrm{d}\theta) - \int_\chi (r(\theta,\overline{\xi_s}) - d(\theta,\overline{\xi_s}))P_{t-s}f(\theta)\overline{\xi_s}(\,\mathrm{d}\theta)\,\mathrm{d}s \right|. \end{aligned}$$

The first, and second lines can be treated thanks to the lipschitz rates, and the boundedness of f. We have

$$\begin{aligned} L_1 &\leq L_c \int_0^t \sup_{\substack{f\in L^\infty(\overline{\chi}) \\ \|f\|_\infty \leq 1}} |< \xi_s - \overline{\xi_s}, f >|\,\mathrm{d}s, \\ L_2 &\leq (L_r + L_d)A_T \int_0^t \sup_{\substack{f\in L^\infty(\overline{\chi}) \\ \|f\|_\infty \leq 1}} |< \xi_s - \overline{\xi_s}, f >|\,\mathrm{d}s. \end{aligned}$$

Concerning the last term, we use the boundedness of rates:

$$L_3 \leq (\overline{r} + \overline{d}) \int_0^t \sup_{\substack{f\in L^\infty(\overline{\chi}) \\ \|f\|_\infty \leq 1}} |< \xi_s - \overline{\xi_s}, f >|\,\mathrm{d}s.$$

Finally, we obtain

$$\left|< \xi_t - \overline{\xi_t}, f >\right| \leq \left(L_c + (L_r + L_d)A_T + \overline{r} + \overline{d}\right) \int_0^t \sup_{\substack{f \in L^\infty(\overline{\chi}) \\ \|f\|_\infty \leq 1}} \left|< \xi_s - \overline{\xi_s}, f >\right| \, \mathrm{d}s.$$

Taking the supremum over all $f \in L^\infty(\overline{\chi})$ such that $\| f \|_\infty \leq 1$, and using the Gronwall lemma leads to $\forall t \in [0,T]$, $\sup_{\substack{f \in L^\infty(\overline{\chi}) \\ \|f\|_\infty \leq 1}} \left|< \xi_s - \overline{\xi_s}, f >\right| = 0$.

The convergence is now shown.

2. As $\mu\sigma^2 a > 0$ for all $\theta \in \chi$, the semigroup $P_t(\theta, dx)$ admits a density $p_t(x,y)$ with respect to the Lebesgue measure $\forall \theta \in \chi$.

   Hence, the evolution equation (3.43) can be rewritten

$$\begin{aligned}\int_\chi \phi(\theta)\xi_t(\theta) = \int_\chi \int_\chi \phi(x) p_t(x,\theta) dx \xi_0(\theta) + \int_0^t \int_\chi \frac{c(\xi_s)}{2\pi} \phi(x) p_{t-s}(x,\theta) \, \mathrm{d}x \, \mathrm{d}\theta \\ + \int_0^t \int_\chi \int_\chi (r(\theta,\xi_s) - d(\theta,\xi_s))\phi(x) p_{t-s}(x,\theta) \, \mathrm{d}x \xi_s(\, \mathrm{d}\theta) \, \mathrm{d}s.\end{aligned}$$

   Moreover, ϕ and the rates are bounded and $\sup_{t\in[0,T]} < \xi_t, 1 >< +\infty$, so that by the Fubini theorem,

$$\begin{aligned}\int_\chi \phi(\theta)\xi_t(\theta) &= \int_\chi \phi(x) \left\{ \int_\chi p_t(x,\theta)\xi_0(\theta) + \int_0^t \frac{c(\xi_s)}{2\pi} \int_\chi p_{t-s}(x,\theta) \, \mathrm{d}\theta \, \mathrm{d}s \right. \\ &\quad \left. + \int_0^t \int_\chi (r(\theta,\xi_s) - d(\theta,\xi_s)) p_{t-s}(x,\theta) \xi_s(\, \mathrm{d}\theta) \, \mathrm{d}s \right\} \mathrm{d}x \\ &=: \int_\chi H_t(x)\phi(x) \, \mathrm{d}x.\end{aligned}$$

   As $H \in L^\infty([0,T], L^1(\overline{\chi}))$, we can deduce that ξ_t has a density with respect to the Lebesgue measure. Then, we get equation (3.40) as the dual form of (3.39), with boundary conditions coming from the fact that g is circular.

□

Case $\eta = 1$

We assume here the following:

Hypothesis 14 (Rare mutations - stochastic limit)**.** *For c, $\overline{r}$, and $\overline{d}$ positive constants, consider positive rates*

$$c_K(X_t^K) \equiv Kc \qquad ,$$

$$r_K(\theta, X_t^K) = r(\theta, X_t^K) + Ka \leq \overline{r} + Ka, \quad d_K(\theta, X_t^K) = d(\theta, X_t^K) + Ka \leq \overline{d} + Ka$$

Moreover, r and d are continuous.

Theorem 16. *Assume hypothesis (14) and (12). If for $K \to +\infty$ the initial measure X_0^K converges in law to $X_0 \in \mathcal{M}_F(\overline{\chi})$, and*

$$\sup_{K>0} \mathbb{E}\left[< X_0^K, 1 >\right] < +\infty, \tag{3.44}$$

then $(X^K)_{K>0}$ converges in law in $\mathbb{D}([0,T], \mathcal{M}_F(\overline{\chi}))$ to the unique in law superprocess $X \in \mathcal{C}([0,T], \mathcal{M}_F(\overline{\chi}))$ such that

$$\sup_{t\in[0,T]} \mathbb{E}\left[< X_t, 1 >\right] < +\infty, \tag{3.45}$$

$\forall f \in \mathcal{C}^2(\overline{\chi})$ periodic,

$$\begin{aligned} \tilde{M^f}_t =& < X_t, f > - < X_0, f > - \frac{c}{2\pi} \int_0^t \int_\chi f(\theta) \,\mathrm{d}\theta \,\mathrm{d}s \\ & - \int_0^t \int_\chi (r(\theta, X_s) - d(\theta, X_s)) f(\theta) X_s(\,\mathrm{d}\theta)\,\mathrm{d}s - \int_0^t \int_\chi \frac{1}{2}\mu\sigma^2 a f''(\theta) X_s(\,\mathrm{d}\theta)\,\mathrm{d}s \end{aligned} \tag{3.46}$$

is a continuous martingale with quadratic variation

$$\left\langle \tilde{M^f} \right\rangle_t = 2a \int_0^t \int_\chi f(\theta)^2 X_s(\,\mathrm{d}\theta)\,\mathrm{d}s. \tag{3.47}$$

Proof. As usual, the proof is based on a compactness-uniqueness argument: we'll prove that the sequence of laws $(Q^K)_K$ of the processes $(X^K)_K$ is tight. Then, we'll identify its limiting values as solutions of (3.46, 3.47), for which a uniqueness result will be stated.

Uniform tightness of $(Q^K)_K$. The proof is similar to the one for theorem 15.

Identification of the limit Consider a convergent subsequence denoted $(Q^K)_K$ for simplicity, and denote Q its limit. By the Prohorov theorem, one can find a corresponding sequence of processes $(X^K)_K$ in $\mathbb{D}([0,T], \mathcal{M}_F(\overline{\chi}))$ converging in law to $X \in \mathbb{D}([0,T], \mathcal{M}_F(\overline{\chi}))$.

- By construction, we know that $\forall K > 0$, jumps of $(X_t^K)_t$ are almost surely of the form δ_θ/K. As a consequence, almost surely,

$$\sup_{t\in\mathbb{R}_+} \sup_{f\in L^\infty} \left| < X_t^K, f > - < X_{t^-}^K, f > \right| \leq \frac{\| f \|_\infty}{K}.$$

  Hence, any process of law Q like X is almost surely strongly continuous.

- Now, X verifies (3.45) because of the initial condition (3.44) and proposition 18.

- Let us show that $\forall f \in \mathcal{C}^2(\overline{\chi})$, $\tilde{M}^f$ defined in (3.46) is a martingale. Take $0 \leq s_1 < ... < s_n < s < t$, and $\Phi_1, ..., \Phi_n$ continuous bounded functions from $\mathcal{M}_F(\overline{\chi})$ to $\mathbb{R}$. Define

$$\begin{aligned} \Psi_t(\nu) \quad := \quad & \Phi_1(\nu_{s_1})...\Phi_n(\nu_{s_n}) \left[< \nu_t, f > - < \nu_0, f > - \frac{c}{2\pi} \int_s^t \int_\chi f(\theta) \,\mathrm{d}\theta \,\mathrm{d}s \right. \\ & \left. - \int_s^t \int_\chi (r(\theta, \nu_s) - d(\theta, \nu_s)) f(\theta) \nu_s(\,\mathrm{d}\theta)\,\mathrm{d}s - \int_0^t \int_\chi \frac{1}{2}\mu\sigma^2 a f''(\theta) \nu_s(\,\mathrm{d}\theta)\,\mathrm{d}s \right]. \end{aligned}$$

We have to show that $\forall t \leq T,\ \mathbb{E}_Q\left[|\Psi_t(X)|\right] = 0$.
By (3.36), we know that

$$0 = \mathbb{E}\left[\Phi_1(X^K_{s_1})...\Phi_n(X^K_{s_n})\left\{M_t^{(K,f)} - M_s^{(K,f)}\right\}\right] = \mathbb{E}\left[\Psi_t(X^K)\right] - A^K,$$

with

$$\begin{aligned}A^K :=& \mathbb{E}\left[\Phi_1(X^K_{s_1})...\Phi_n(X^K_{s_n})\int_s^t\int_\chi\left[\mu(r(\theta,\nu_s)+Ka(\theta))\left(\frac{1}{2}\frac{\sigma^2}{K}f''(\theta)+o\left(\frac{1}{K}\right)\right)\right.\right.\\ &\left.\left.+\frac{1}{2}\mu\sigma^2 a(\theta)f''(\theta)\right]X_s^K(\,\mathrm{d}\theta)\,\mathrm{d}s\right]\\ =&\mu\mathbb{E}\left[\Phi_1(X^K_{s_1})...\Phi_n(X^K_{s_n})\int_s^t\int_\chi\left[r(\theta,\nu_s)\left(\frac{1}{2}\frac{\sigma^2}{K}f''(\theta)+o\left(\frac{1}{K}\right)\right)+aKo\left(\frac{1}{K}\right)\right]X_s^K(\,\mathrm{d}\theta)\,\mathrm{d}s\right],\end{aligned}$$

by (5), and omitting in our notations the dependence on f.

It is now clear that

$$|A^K| \leq C\left(\frac{1}{K}+o\left(\frac{1}{K}\right)+Ko\left(\frac{1}{K}\right)\right)\mathbb{E}\left[|\Phi_1(X^K_{s_1})...\Phi_n(X^K_{s_n})|\int_s^t < X_u^K, 1 > \,\mathrm{d}u\right]$$
$$\underset{K\to+\infty}{\longrightarrow} 0.$$

Indeed, the expectation can be bounded uniformly in K thanks to proposition 19, and $\lim_{K\to+\infty} Ko\left(\frac{1}{K}\right) = 0$.

Moreover, the property 19 ensures that the sequence $(|\Psi(X^K)|)_K$ is uniformly integrable, leading to

$$0 = \lim_{K\to+\infty}\mathbb{E}[|\Psi(X^K)|] = \mathbb{E}_Q[|\Psi(X)|],$$

and $\tilde{M}^f$ defined in (3.46) is indeed a martingale.

- The last thing to show is that the bracket of $\widetilde{M}$ is the one given in (3.47).

  1. First, we compute the martingale obtained from the martingale property (3.5) with $\Phi(\nu) =< \nu, f >^2$, related to the generator (3.4):

$$\begin{aligned}L^K\Phi(\nu) &= K\frac{c}{2\pi}\int_\chi\left[\frac{2}{K}f(\theta) < \nu, f > +\frac{f(\theta)^2}{K^2}\right]\,\mathrm{d}\theta\\ &+ K\int_\chi(1-\mu)(r(\theta,\nu)+Ka)\left[\frac{2}{K}f(\theta) < \nu, f > +\frac{f(\theta)^2}{K^2}\right]\nu(\,\mathrm{d}\theta)\\ &+ K\int_\chi\mu(r(\theta,\nu)+Ka)\int_\chi\left\{\frac{2}{K}f(z) < \nu, f > +\frac{f(z)^2}{K^2}\right\}g_K(z;\theta)\,\mathrm{d}z\,\nu(\,\mathrm{d}\theta)\\ &+ K\int_\chi(d(\theta,\nu)+Ka)\left[-\frac{2}{K}f(\theta) < \nu, f > +\frac{f(\theta)^2}{K^2}\right]\nu(\,\mathrm{d}\theta).\end{aligned}$$

     It can be rewritten

$$
\begin{aligned}
L^K\Phi(\nu) &= \frac{c}{\pi}\int_\chi f(\theta) < \nu, f > + \frac{f(\theta)^2}{K}\,\mathrm{d}\theta + 2\int_\chi (r(\theta,\nu) - d(\theta,\nu))f(\theta) < \nu, f > \nu(\,\mathrm{d}\theta) \\
&+ \int_\chi \left(\frac{r(\theta,\nu) + d(\theta,\nu)}{K} + 2a\right) f(\theta)^2 \nu(\,\mathrm{d}\theta) \\
&+ \int_\chi 2\mu(r(\theta,\nu) + Ka) < \nu, f > \left\{\int_\chi f(z) g_K(z;\theta)\,\mathrm{d}z - f(\theta)\right\} \nu(\,\mathrm{d}\theta) \\
&+ \int_\chi \mu\left(\frac{r(\theta,\nu)}{K} + a\right)\left\{\int_\chi f(z)^2 g_K(z;\theta)\,\mathrm{d}z - f(\theta)^2\right\} \nu(\,\mathrm{d}\theta)
\end{aligned}
$$

Now on the one hand, by lemma (5), $\int_\chi f(z) g_K(z;\theta)\,\mathrm{d}z - f(\theta) = \frac{\sigma^2}{2K} f''(\theta) + o\left(\frac{1}{K}\right)$. On the other hand, following lemma 5, we have that for $f \in \mathcal{C}^2(\overline{\chi})$ and g_K as defined above,

$$
\int_\chi f(z)^2 g_K(z;\theta)\,\mathrm{d}z - f(\theta)^2 = \frac{\sigma^2}{K}\left[f'(\theta)^2 + f(\theta) f''(\theta)\right] + o\left(\frac{1}{K}\right). \tag{3.48}
$$

As a consequence, the infinitesimal generator writes

$$
\begin{aligned}
L^K\Phi(\nu) &= \frac{c}{2\pi}\int_\chi 2f(\theta) < \nu, f > + \frac{f(\theta)^2}{K}\,\mathrm{d}\theta \\
&+ \int_\chi 2(r(\theta,\nu) - d(\theta,\nu)) < \nu, f > f(\theta)\nu(\,\mathrm{d}\theta) \\
&+ \int_\chi \left(\frac{r(\theta,\nu) + d(\theta,\nu)}{K} + 2a\right) f(\theta)^2 \nu(\,\mathrm{d}\theta) \\
&+ \int_\chi 2\mu(r(\theta,\nu) + Ka) < \nu, f > \left\{\frac{\sigma^2}{2K} f''(\theta) + o\left(\frac{1}{K}\right)\right\} \nu(\,\mathrm{d}\theta) \\
&+ \int_\chi \mu\left(\frac{r(\theta,\nu)}{K} + a\right) < \nu, f > \left\{\frac{\sigma^2}{K}\left[f'(\theta)^2 + f(\theta) f''(\theta)\right] + o\left(\frac{1}{K}\right)\right\} \nu(\,\mathrm{d}\theta)
\end{aligned}
$$

Now, from the corresponding martingale, we can show as before for $\tilde{M}^f$ that we have at the limit the following $Q-$martingale :

$$
\begin{aligned}
\tilde{N}_t^f = &< X_t, f >^2 - < X_0, f >^2 - \int_0^t \left\{\frac{c}{\pi} < X_s, f > \int_\chi f(\theta)\,\mathrm{d}\theta \right. \\
&+ 2 < X_s, f > \int_\chi (r(\theta, X_s) - d(\theta, X_s)) f(\theta) X_s(\,\mathrm{d}\theta) \\
&\left. + < X_s^K, f > \int_\chi \mu\sigma^2 a f''(\theta) X_s^K(\,\mathrm{d}\theta) + 2\int_\chi a f(\theta)^2 X_s(\,\mathrm{d}\theta)\right\} \mathrm{d}s.
\end{aligned}
$$

2. Moreover, applying the Itô formula to (3.46) shows that

$$
\begin{aligned}
&< X_t, f >^2 - < X_0, f >^2 - <\tilde{M}^f>_t - \int_0^t 2 < X_s, f > \left\{\frac{c}{2\pi}\int_\chi f(\theta)\,\mathrm{d}\theta \right. \\
&\left. + \int_\chi (r(\theta, X_s) - d(\theta, X_s)) f(\theta) X_s(\,\mathrm{d}\theta) + \int_\chi \frac{1}{2}\mu\sigma^2 a f''(\theta) X_s^K(\,\mathrm{d}\theta)\right\} \mathrm{d}s
\end{aligned}
$$

is a martingale. We conclude by the uniqueness of the semimartingale decomposition of $< X_t, f >^2$.

Uniqueness of a solution for (3.46)-(3.47): As in the proof of uniqueness in theorem 14, we show:

1. an equivalence between (3.46)-(3.47) and a martingale problem for a non-interactive immigration process. We'll use the Cameron-Martin-Girsanov formula as described in Dawson [1978] for that purpose.
2. uniqueness for the equivalent problem.

First, we want to use the Cameron-Martin-Girsanov formula (see annex (3.4.1, proposition 22) for the details). Our problem can be written in the (G_2, F_2, Q_2) form with:

$\rightarrow$ $G_2 = \frac{1}{2}\mu a\sigma^2\Delta$,
$\rightarrow$ $F_2(\nu) = c\,\mathrm{d}\theta + (r(\theta,\nu) - d(\theta,\nu))\nu$,
$\rightarrow$ $Q_2(\nu;\, \mathrm{d}\theta \times d\lambda) = 2a\delta_\theta(d\lambda)\nu(\,\mathrm{d}\theta)$.

We can check that Q_2 is a continuous mapping such that for $\phi \in \mathcal{C}(\overline{\chi})$,

$$\iint \phi(\theta)\phi(\lambda)Q_2(\nu;\, \mathrm{d}\theta \times d\lambda) = \int_\chi 2a\phi(\theta)^2\nu(\,\mathrm{d}\theta) \geq 0,$$

because a is positive, and if $\nu(A) = 0$, obviously

$$\iint_{A\times A} \phi(\theta)\phi(\lambda)Q_2(\nu;\, \mathrm{d}\theta \times d\lambda) \leq 2a \parallel \phi \parallel^2 \nu(A) = 0.$$

Now, define the second martingale problem by $G_1 = G_2$, $Q_1 = Q_2$, and

$$F_1(\nu) = c\,\mathrm{d}\theta = F_2(\nu) - (r(\theta,\nu) - d(\theta,\nu))\nu.$$

First, we have

$$\begin{aligned}(F_1(\nu) - F_2(\nu))(\,\mathrm{d}\theta) &= -(r(.,\nu) - d(.,\nu))\nu(\,\mathrm{d}\theta)\\ &= 2ah(\nu;\theta)\mu(\,\mathrm{d}\theta) \text{ for } h(\nu;.) = -\frac{r(.,\nu) - d(.,\nu)}{2a},\end{aligned}$$

that is indeed a continuous function from $\mathcal{M}_F(\overline{\chi})$ to $\mathcal{C}(\overline{\chi})$. Moreover, it is clear that for every ϖ compact of $\mathcal{M}_F(\overline{\chi})$, $\{P^1_\nu,\ \nu \in \varpi\}$ is uniformly tight in $\Pi(\overline{\chi})$.

Hence by proposition 22, we only need to show uniqueness for the martingale problem

$$\begin{aligned}\tilde{M}^f_t &=< X_t, f > - < X_0, f > -c\int_0^t f(\theta)\,\mathrm{d}\theta - \frac{1}{2}\mu\sigma^2 a\int_0^t < X_s, \triangle f > \,\mathrm{d}s\\ \left\langle \tilde{M}^f \right\rangle_t &= 2a\int_0^t < X_s, f^2 > \,\mathrm{d}s.\end{aligned} \tag{3.49}$$

Finally, as $G = \frac{1}{2}\nu\sigma^2 a\Delta$ is strongly continuous $\mathcal{C}^2(\overline{\chi})$, we can use a uniqueness result stated in Fu and Li [2004] and detailed in Konno and Shiga [1988], Li and Shiga [1995] to conclude.

□

In this chapter, we have used large populations approximations with a rescaled dynamics to switch from a discontinuous representation of discrete filopodia to the continuous representation of protrusions along the cell membrane. We have considered different renormalizations, for which the modelling implications were stated. We can now study these continuous limits and try to reach the aim of our work: deriving an analytical characterization of trajectories, their persistence and their variability.

3.4 Annex

3.4.1 A Cameron Martin Girsanov formula

We state here a few results necessary to show equivalence between two martingale problems. This is useful to prove uniqueness of a solution to a problem, as it allows to study a simpler problem. The detailed proofs can be found in Dawson [1978]

Consider $\mathcal{M}(\overline{\chi})$ the space of positive Borel measures on $\overline{\chi}$, and $\Omega = \mathcal{C}([0,+\infty), \mathcal{M}(\overline{\chi}))$, that is a Polish space when endowed with the topology of uniform convergence on bounded intervals. Denote $\mathcal{F}$ the σ-algebra of Borel subsets of Ω, and $\Pi(\Omega)$ the family of probability measure on Ω.

Define $X(.,.) : [0,\infty) \times \Omega \to M(\overline{\chi})$ by $X(t,w) = w(t)$, and the σ-algebra $\mathcal{F}_t = \sigma(X(s) : s \leq t)$.

Three characterizations of a martingale problem

We are going to give different martingale problems based on either an operator L, or a triplet (G, F, Q) that we are about to define.

→ Let G be an infinitesimal generator on $\mathcal{C}(\overline{\chi})$ of a Feller-Markov process on χ. It corresponds to the "spatial" motion.

→ Let F be defined by :

$$\begin{array}{rcl} F : [0,\infty) \times \mathcal{M}(\overline{\chi}) & \longrightarrow & \mathcal{M}(\overline{\chi}) \\ (s,\mu) & \longmapsto & F_I(s) + F_N(\mu), \end{array}$$

with F_I bounded continuous, and F_N continuous, that corresponds to a nonlinear interaction term.

→ Let $Q : \mathcal{M}(\overline{\chi}) \to \mathcal{M}^c(\overline{\chi} \times \overline{\chi})$ a continuous mapping, with $\mathcal{M}^c(\overline{\chi} \times \overline{\chi})$ the collection of symmetric signed measures on $\overline{\chi} \times \overline{\chi}$ positive definite: we assume that for $\phi \in \mathcal{C}(\overline{\chi})$,

$$\iint \phi(x)\phi(y)Q(\mu; dx \times dy) \geq 0,$$

and

$$\mu(A) = 0 \Rightarrow Q(\mu; A \times A) = 0.$$

As Q will be responsible for the stochastic fluctuations of the process, the latter assumption is used to avoid non negative solutions: if the local population density is zero, then there is no more fluctuations.

→ Let L be an unbounded linear operator defined on $D(L) \subset \mathcal{C}(\overline{\chi})$ by

$$L\psi(\mu) = < \psi'(\mu), G^*\mu + F(\mu) > + \frac{1}{2} < Q(\mu), \psi''(\mu) > .$$

Proposition 20. *There is equivalence between the three formulations of a martingale problem:*

1. *find a mapping $\mu \mapsto P_\mu$ such that $\forall \phi \in \mathcal{C}(\overline{\chi}) \cap D(G)$, $< X_{G,F}, \phi >$ is a P_μ-continuous local martingale, with*

$$X_{G,F}(t) \equiv X(t) - \int_0^t G^* X(s) + F(s, X(s))\, \mathrm{d}s,$$

and a quadratic variation defined by

$$< \phi_1, X_{G,F}, \phi_2 >_t = \int_0^t \iint_{\overline{\chi}\times\overline{\chi}} \phi_1(x)\phi_2(y) Q(X(s); dx \times dy)\, \mathrm{d}s,$$

2. *find a mapping $\mu \mapsto P_\mu$ such that $P_\mu(X(0) = \mu) = 1$, and for $\Psi \in D(L)$,*

$$\Psi(X(t)) - \int_0^t L\Psi(X(s))\, \mathrm{d}s$$

is a P_μ-local martingale,

3. *find a mapping $\mu \mapsto P_\mu$ such that $P_\mu(X(0) = \mu) = 1$, and for $\phi \in \mathcal{C}(\overline{\chi}) \cap D(G)$,*

$$Z(\phi, t) \equiv \exp\left\{ < X_{G,F}(t), \phi > - \frac{1}{2} < \phi, X_{G,F}, \phi >_t \right\}$$

is a P_μ-local martingale, with $X_{G,F}$ defined as in point 1.

We next state a result showing the importance of having a well-posed martingale problem (see Dawson [1978], prop 2.1 for the proof).

Proposition 21. *Assume that the martingale problem on Ω associated with L admits a unique solution $\{P_\mu,\ \mu \in M(\overline{\chi})\}$, and that for every K compact of $M(\overline{\chi})$, $\{P_\mu,\ \mu \in K\}$ is uniformly tight in $\Pi(\overline{\chi})$. Then,*

1. *$\{P_\mu,\ \mu \in M(\overline{\chi})\}$ defines a strong homogeneous Markov process on $M(\overline{\chi})$,*
2. *$D(L)$ is a core for the Markov semigroup on $\mathcal{C}_b(M(\overline{\chi}))$,*
3. *the weak closure $\overline{L}$ of L is the weak infinitesimal generator of the process.*

Equivalence of martingale problems

Let us now state the important result of this section, that corresponds to the Theorem 5.1 in Dawson [1978].

Proposition 22. *Consider two local martingale problems, (G_1, F_1, Q_1) related to the law P^1, and (G_2, F_2, Q_2) related to P^2. Assume that (G_1, F_1, Q_1) has a unique solution, and that*

- *for K a compact in $\mathcal{M}(\overline{\chi})$, $\left\{P^1_\mu : \mu \in K\right\}$ is uniformly tight in $\Pi(\Omega)$, P^1_μ being the law of the process starting at μ.*

Let (G_2, F_2, Q_2) be such that

$$G_2 = G_1,\ Q_2 = Q_1,$$

and there exists $h : M(\overline{\chi}) \to \mathcal{C}(\overline{\chi})$ such that

$$(F_1(\mu) - F_2(\mu))(dx) = \int_\chi h(\mu; y) Q_1(\mu; dx \times dy).$$

Then, the local martingale problem associated with (G_2, F_2, Q_2) has a unique solution.

Bibliography

Aldous, D. (1989). Stopping times and tightness. ii. The Annals of Probability, 17(2):pp. 586–595. 106, 116, 123

Billingsley, P. (1999). Convergence of Probability Measures. John Wiley & Sons, Inc., New York, NY. 99

Caballero, D., Voituriez, R., and Riveline, D. (2014). Protrusion fluctuations direct cell motion. Biophys J, 107(1):34–42. 99

Champagnat, N., Ferrière, R., and Méléard, S. (2006). Unifying evolutionary dynamics: from individual stochastic processes to macroscopic models. Theor Popul Biol, 69(3):297–321. 106

Champagnat, N., Ferrière, R., and Méléard, S. (2008). From Individual Stochastic Processes to Macroscopic Models in Adaptive Evolution. Stochastic Models, 24(sup1):2–44. 121

Dawson, D. A. (1978). Geostochastic Calculus. The Canadian Journal of Statistics / La Revue Canadienne de Statistique, 6(2):pp. 143–168. 121, 132, 133, 134

Fournier, N. and Méléard, S. (2004). A microscopic probabilistic description of a locally regulated population and macroscopic approximations. The Annals of Applied Probability, 14(4):1880–1919. 121

Fu, Z. and Li, Z. (2004). Measure-valued diffusions and stochastic equations with Poisson process. Osaka J. Math., 41(3):727–744. 122, 132

Joffe, A. and Metivier, M. (1986). Weak Convergence of Sequences of Semimartingales with Applications to Multitype Branching Processes. Advances in Applied Probability, 18(1):20. 106, 116, 123

Konno, N. and Shiga, T. (1988). Stochastic partial differential equations for some measure-valued diffusions. Probability Theory and Related Fields, 79(2):201–225. 122, 132

Li, Z. (2010). Measure-valued branching Markov processes. Springer Science & Business Media. 99

Li, Z. and Shiga, T. (1995). Measure-valued branching diffusions: immigrations, excursions and limit theorems. J. Math. Kyoto Univ., 35(2):233–274. 122, 132

Roelly-Coppoletta, S. (1986). A criterion of convergence of measure-valued processes: application to measure branching processes. Stochastics, 17(1-2):43–65. 106, 116, 123

Rudin, W. (1987). Real and complex analysis. Mathematics series. McGraw-Hill. 108, 117

Ryan, G. L., Petroccia, H. M., Watanabe, N., and Vavylonis, D. (2012). Excitable actin dynamics in lamellipodial protrusion and retraction. Biophysical Journal, 102(7):1493–1502. 100

Tran, V. C. (2006). Modèles particulaires stochastiques pour des problèmes d'évolution adaptative et pour l'approximation de solutions statistiques. phdthesis, Université de Nanterre - Paris X. 121

Chapter 4

The continuous limiting models

Contents

4.1 Time-space continuous dynamics 137
4.1.1 Deterministic limits 138
4.1.2 Stochastic continuous models 139
4.2 Angular discretization 143
4.2.1 Fokker-Planck equation 143
4.2.2 Stationary state 146
4.2.3 The case $\ell = 3$ 147
4.3 One dimensional migration 147
4.3.1 Stationary distribution 147
4.3.2 Equation on (N, V) 150
4.4 Conclusions and perspectives 155
4.4.1 Validation of the model 155

In this chapter, we study some of the continuous limits that were obtained in the previous chapter. They correspond to the continuous protrusion dynamics at the cell membrane. First, we investigate the equations of chapter 2. We will see that in opposition with the case of bonds in chapter 1, the dynamics is variable in both time and space, making a closed equation hard to obtain.

Then, we will approximate the protrusion dynamics and consider angular areas, in an attempt to get a closed system of equations. Finally, we will study the one dimensional case, for which further results will be derived on the persistence of trajectories.

4.1 Time-space continuous dynamics

In the following, we use the parameters introduced in part 2.2.1.

Recall that for a friction coefficient $\gamma \geq 0$, one has $\gamma \vec{V}_t = \left\langle X_t, \begin{pmatrix} \cos \\ \sin \end{pmatrix} \right\rangle$. Then, assume that $(c, d, \mu) \in \mathbb{R}_+^3$, $a \in \mathbb{R}^{+*}$, and

- the mutant offspring orientation is distributed according to a circular probability density $g(z; \theta)$ on $[0, 2\pi)$ of mean θ, the parent trait, and with fixed circular variance $\sigma_g^2 = 1/\kappa$ and null third moment, such that:

$$g(\theta; \theta_t, \kappa) = \frac{1}{2\pi I_0(\kappa)} \exp(\kappa \cos(\theta - \theta_t)) .$$

- the individual reproduction rate $r(\theta, \nu)$ corresponds to the circular normal distribution function (up to a multiplicative constant r), centered in $\theta_t = arg(\vec{V}_t)$, and with a shape parameter $\kappa(\| \vec{V}_t \|)$ (typically, $\kappa = k\alpha \| \vec{V}_t \|^2$ or $\kappa = k \tanh(\alpha \| \vec{V}_t \|^2)$).

Let us now consider the continuous models obtained in chapter 2, beginning with the deterministic models for the protrusions density 3.18. We will not fully study these limits, since we are interested in the variability in cell trajectories. However, they can be important to understand the dynamics at play, and will be studied in a future work.

4.1.1 Deterministic limits

Let us briefly recall what were the deterministic equations obtained for various renormalizations, in the case of measures admitting densities.

Accelerated creation limit

When only the creation rate was accelerated, we obtained the following integro-differential equation:

$$\frac{\partial}{\partial t} n_t(\theta) = \frac{c}{2\pi} + [(1-\mu) r(\theta, n_t) - d]\, n_t(\theta) + \mu \int_\chi r(z, n_t) g(\theta; z) n_t(z)\, \mathrm{d}z\,, \tag{3.18}$$

with periodic boundary conditions, following the circular nature of g.

Since g is a circular normal function, and we also choose r to be a circular normal function (with a shape parameter function of the velocity), this integro-differential equation is highly nonlinear. Therefore, obtaining a closed system for

$$\gamma v_x(t) = \int_\chi \cos(\theta) n_t(\theta)\, \mathrm{d}\theta\,, \qquad \gamma v_y(t) = \int_\chi \sin(\theta) n_t(\theta)\, \mathrm{d}\theta\,,$$

is hopeless. We will go further into the details for the stochastic equations these difficulties. However, in the deterministic case, assuming an initially empty protrusion population, we know that the protrusions will stay homogeneously distributed. More precisely, for $n_0(\theta) = 0$ for every $\theta \in [0, 2\pi)$, we know that $v_x(0) = v_y(0) = 0$, so that $r(\theta, n_0) = \frac{r}{2\pi}$, and

$$\frac{\partial}{\partial t} n_0(\theta) = \frac{c}{2\pi} + \left[(1-\mu)\frac{r}{2\pi} - d\right] n_0(\theta) + \mu \frac{r}{2\pi} \int_\chi g(\theta; z) n_0(z)\, \mathrm{d}z = \frac{c}{2\pi}\,,$$

and the protrusion density will stay homogeneous, while the cell will not move.

We performed numerical simulations in the case of a non-homogeneous initial condition, that are displayed in figure 4.1. We can see that when the polarisation coefficient α gets large, the asymmetry is sustained for a while. Larger values of polarisation led to an infinite growth of the protrusion population, since we did not consider limitations in resources in this case.

Rare mutations limit

In the limit of rare mutations, we obtained an integro-differential equation:

$$\frac{\partial}{\partial t} n_t(\theta) = \frac{c}{2\pi} + [r(\theta, n_t) - \mu a - d]\, n_t(\theta) + \mu a \int_\chi g(\theta; z) n_t(z)\, \mathrm{d}z\,, \tag{3.29}$$

with periodic boundary conditions. We already mentioned that the assumption of rare mutations corresponds to an unrealistic situation where the molecular regulation of actin

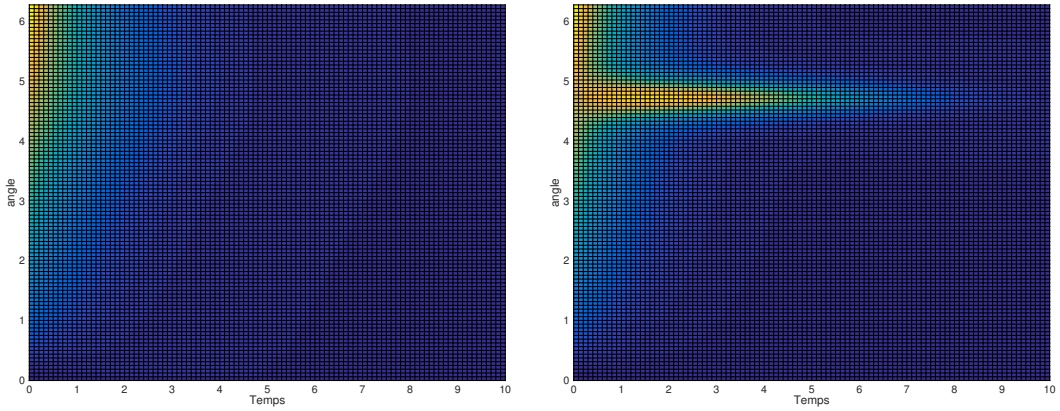

Figure 4.1 – Numerical simulations of the protrusion density as a function of time (so-called kymographs). Parameters: $T = 10$, $\Delta t = 0.1$, $c = d = 1$, $r = 1.1$, $\gamma = 20$, $\mu = 0.2$, $\alpha = 1$ on the left figure, and $\alpha = 10$ on the right.

polymerization can roughly be supposed deterministic as molecules do not diffuse. At this scale, diffusion or molecules and fluctuations in their spatial location are large, and the next model will be preferred.

Diffusive case

When the mutation step is asymptotically zero, this may be interpreted as the regulation of polymerization being local in space. The limiting equation was a reaction-diffusion equation:

$$\begin{aligned} \frac{\partial n_t(\theta)}{\partial t} &= \frac{c}{2\pi} + (r(\theta, n_t) - d)n_t(\theta) + \frac{1}{2}\mu a\sigma^2 \Delta\left(n_t(\theta)\right) , \\ n_t(0) &= n_t(2\pi) \quad \forall t \in [0, T] , \end{aligned} \tag{3.40}$$

with periodic boundary conditions.

These problems can provide useful information on the dynamics, and their comparison is of interest. However, deterministic models can not be used to investigate the variability in cells trajectories. This is why we delay the analysis of these models for a future work, and focus now on the stochastic limits.

4.1.2 Stochastic continuous models

Let us now study the two cases for which we can prove a stochastic limit.

The rare mutation case

In the stochastic limit regime, the rare mutation equation writes $\forall f \in \mathcal{C}^2(\chi)$,

$$\begin{aligned} \tilde{M}{}_t^f = < X_t, f > - < X_0, f > - \frac{ct}{2\pi} \int_\chi f(\theta)\, \mathrm{d}\theta - \int_0^t \int_\chi (r(\theta, X_s) - d(\theta, X_s)) f(\theta) X_s(\, \mathrm{d}\theta)\, \mathrm{d}s \\ + \int_0^t \int_\chi \mu a \left(\int_\chi f(z) g(z; \theta)\, \mathrm{d}z - f(\theta) \right) X_s(\, \mathrm{d}\theta)\, \mathrm{d}s \end{aligned} \tag{3.33}$$

with a quadratic variation

$$\left\langle \widetilde{M}^f \right\rangle_t = 2a \int_0^t \int_\chi f(\theta)^2 X_s(\,\mathrm{d}\theta)\,\mathrm{d}s\,. \tag{3.34}$$

Write

$$Y_t = \left\langle X_t, \begin{pmatrix}\cos\\ \sin\end{pmatrix} \right\rangle \in \mathbb{R}^2,$$

and denote M_1 the martingale associated with the semimartingale $< X_t, \cos >$, and M_2 the one associated with $< X_t, \sin >$. Then, we have the following:

$$\begin{aligned} Y_t &= Y_0 + \begin{pmatrix}M_1\\ M_2\end{pmatrix} + \int_0^t \left\langle X_s, (r(.,Y_s)-d)\begin{pmatrix}\cos\\ \sin\end{pmatrix} + \mu a \begin{pmatrix}\int_\chi \cos(z)g(z,.)\,\mathrm{d}z - \cos(.)\\ \int_\chi \sin(z)g(z,.)\,\mathrm{d}z - \sin(.)\end{pmatrix} \right\rangle \mathrm{d}s\,,\\ &= Y_0 + \begin{pmatrix}M_1\\ M_2\end{pmatrix} + \int_0^t \left\langle X_s, r(.,Y_s)\begin{pmatrix}\cos\\ \sin\end{pmatrix} \right\rangle + \mu a \left\langle X_s, \begin{pmatrix}\int_\chi \cos(z)g(z,.)\,\mathrm{d}z\\ \int_\chi \sin(z)g(z,.)\,\mathrm{d}z\end{pmatrix} \right\rangle - (d+\mu a)Y_s\,\mathrm{d}s\,. \end{aligned}$$

Now, the closure of this equation depends on our choice for r and g.

The cardioid distribution This distribution stays quite large, and thus is not convenient for a distribution of mutant trait. Hence, we expect to use it as a reproduction rate. Take $r(.,Y_t) = \frac{1}{2\pi}(1+2\rho\cos(.-\theta_t))$, with $-1/2 < \rho < 1/2$.

Now,

$$r(\theta,Y_t)\cos(\theta) = \frac{\cos(\theta)}{2\pi} + \frac{\rho}{\pi}\cos(\theta-\theta_t)\cos(\theta).$$

Notice that $\cos(\theta-\theta_t)\cos(\theta) = \cos(\theta_t)\cos(\theta)^2 + \sin(\theta_t)\cos(\theta)\sin(\theta)$, and we have $\cos(\theta)^2 = \frac{1+\cos(2\theta)}{2}$ and $\cos(\theta)\sin(\theta) = \frac{\sin(2\theta)}{2}$. We can deduce that knowing $\left\langle X_s, \begin{pmatrix}r(.,Y_s)\cos\\ r(.,Y_s)\sin\end{pmatrix} \right\rangle$ amounts to knowing $\langle X_s, \cos(p.)\rangle$ and $\langle X_s, \sin(p.)\rangle$ for every $p \geq 1$, and our system can not be closed.

The circular normal distribution Recall that the circular normal density writes

$$h(\theta;\theta_t,\kappa) = \frac{1}{2\pi I_0(\kappa)}\exp(\kappa\cos(\theta-\theta_t)),$$

with $\kappa \geq 0$ describing the concentration around the mean orientation, and I_0 the 0-order modified Bessel function of the first kind.

Then, the term $\int_\chi \cos(z)h(z;\theta_t,\kappa)\,\mathrm{d}z$ (resp. $\int_\chi \sin(z)h(z;\theta_t,\kappa)\,\mathrm{d}z$) is related to the first trigonometric moment of the distribution, and we have

$$\int_\chi \begin{pmatrix}\cos(z)\\ \sin(z)\end{pmatrix} g(z;\theta_t,\kappa)\,\mathrm{d}z = \frac{I_1(\kappa)}{I_0(\kappa)}\begin{pmatrix}\cos(\theta_t)\\ \sin(\theta_t)\end{pmatrix}.$$

Hence the mutation term can be written

$$\mu a \int_0^t \left(\frac{I_p(\kappa)}{I_0(\kappa)} - 1\right)\left\langle X_s, \begin{pmatrix}\cos(.)\\ \sin(.)\end{pmatrix} \right\rangle \mathrm{d}s = \mu a \int_0^t \left(\frac{I_p(\kappa)}{I_0(\kappa)} - 1\right) Y_s\,\mathrm{d}s\,,$$

which is convenient for us.

Now for the reproduction term we need to compute $\langle X_s, r(.,Y_s)\cos\rangle$ and $\langle X_s, r(.,Y_s)\sin\rangle$. However, if $r = h$,

$$r(\theta, Y_s)\cos(\theta) = \frac{\cos(\theta)}{2\pi I_0(\kappa)}\exp(\kappa\cos(\theta - \theta_t)),$$

and as before knowing $\langle X_s, r(.,Y_s)\cos\rangle$ (resp. $\langle X_s, r(.,Y_s)\sin\rangle$) requires to study $\langle X_s, f\rangle$ for infinitely many other functions f.

The diffusive case

In the stochastic limit regime, the small mutation or diffusive equation writes $\forall f \in \mathcal{L}^\infty(\chi)$,

$$\begin{aligned}\widetilde{M^f}_t =& < X_t, f > - < X_0, f > - \frac{c}{2\pi}\int_0^t \int_\chi f(\theta)\,\mathrm{d}\theta\,\mathrm{d}s \\ &- \int_0^t \int_\chi (r(\theta, X_s) - d(\theta, X_s))f(\theta)X_s(\,\mathrm{d}\theta)\,\mathrm{d}s - \int_0^t \int_\chi \frac{1}{2}\mu\sigma^2 a f''(\theta)X_s(\,\mathrm{d}\theta)\,\mathrm{d}s\end{aligned} \tag{3.46}$$

is a continuous martingale with quadratic variation

$$\left\langle \widetilde{M^f} \right\rangle_t = 2a\int_0^t \int_\chi f(\theta)^2 X_s(\,\mathrm{d}\theta)\,\mathrm{d}s. \tag{3.47}$$

Write again M_1 for the martingale associated with the semimartingale $< X_t, \cos >$, and M_2 for the one associated with $< X_t, \sin >$. Then, we have the following:

$$\begin{aligned}Y_t &= Y_0 + \begin{pmatrix} M_1 \\ M_2 \end{pmatrix} + \int_0^t \left\langle X_s, \begin{pmatrix} (r(.,Y_s) - d)\cos \\ (r(.,Y_s) - d)\sin \end{pmatrix} - \frac{1}{2}\mu a\sigma^2 \begin{pmatrix} \cos(.) \\ \sin(.) \end{pmatrix} \right\rangle \mathrm{d}s\,, \\ &= Y_0 + \begin{pmatrix} M_1 \\ M_2 \end{pmatrix} + \int_0^t r(.,Y_s)\left\langle X_s, \begin{pmatrix} \cos \\ \sin \end{pmatrix} \right\rangle - \left(d + \frac{1}{2}\mu a\sigma^2\right) Y_s\,\mathrm{d}s\end{aligned}$$

Juste as before, we can not go any further because of the nonlinearity in the reproduction term.

Another approach consists in considering the superprocess itself rather than its projection on regular functions.

A superprocess density formal approach

For both superprocesses obtained in chapter 3, we can write formally a corresponding integral SDE or SPDE.

Rare mutations Let us consider the martingale problem

$$\begin{aligned}\widetilde{M}^f_t =& < X_t, f > - < X_0, f > - \frac{ct}{2\pi}\int_\chi f(\theta)\,\mathrm{d}\theta - \int_0^t \int_\chi (r(\theta, X_s) - d(\theta, X_s))f(\theta)X_s(\,\mathrm{d}\theta)\,\mathrm{d}s \\ &+ \int_0^t \int_\chi \mu a \left(\int_\chi f(z)g(z;\theta)\,\mathrm{d}z - f(\theta)\right) X_s(\,\mathrm{d}\theta)\,\mathrm{d}s\end{aligned} \tag{3.33}$$

with a quadratic variation

$$\left\langle \widetilde{M}^f \right\rangle_t = 2a\int_0^t \int_\chi f(\theta)^2 X_s(\,\mathrm{d}\theta)\,\mathrm{d}s\,. \tag{3.34}$$

Then, as mentioned in Champagnat et al. [2006], the process X can be formally written as a solution of

$$\partial_t X_t(\theta) = \frac{c}{2\pi} + (r(\theta, X_t) - d - \mu a)X_t(\theta) + \mu a \int_\chi g(\theta;\lambda)X_t(\lambda)d\lambda + \dot{M},$$

with $\dot{M}$ a random fluctuation term, with periodic boundary conditions.

The fluctuation term is a real issue, since in a space-time setting, no representation theorems for martingales such as in the one dimensional case. One could arbitrarily choose a form for these fluctuations, for example using a space correlated noise. A critical choice consists in writing formally $\dot{M} = \sqrt{2aX_t(\theta)}\,\mathrm{d}B_t$, with B_t a real-valued Brownian motion. We get

$$\partial_t X_t(\theta) = \frac{c}{2\pi} + (r(\theta, X_t) - d - \mu a)X_t(\theta) + \mu a \int_\chi g(\theta;\lambda)X_t(\lambda)d\lambda + \sqrt{2aX_t(\theta)}\,\mathrm{d}B_t, \quad (4.1)$$

Remark 12. *This assumption is based on a conjecture on the existence of a density for these superprocesses. It is knows that this is true for the super Brownian Motion or Dawson-Watanabe process, that does not include neither immigration nor interaction.*

Diffusive case In the case of the martingale problem

$$\tilde{M^f}_t = < X_t, f > - < X_0, f > - \frac{c}{2\pi}\int_0^t \int_\chi f(\theta)\,\mathrm{d}\theta\,\mathrm{d}s - \int_0^t \int_\chi (r(\theta, X_s) - d)f(\theta)X_s(\,\mathrm{d}\theta)\,\mathrm{d}s \\ - \frac{1}{2}\mu\sigma^2 a \int_0^t \int_\chi f''(\theta)X_s(\,\mathrm{d}\theta)\,\mathrm{d}s\,, \quad (4.2)$$

continuous martingale with quadratic variation

$$\left\langle \tilde{M^f} \right\rangle_t = 2a\int_0^t \int_\chi f(\theta)^2 X_s(\,\mathrm{d}\theta)\,\mathrm{d}s\,, \quad (4.3)$$

the process X can be formally written as a solution of

$$\partial_t X_t(\theta) = \frac{c}{2\pi} + (r(\theta, X_t) - d)X_t(\theta) - \frac{1}{2}\mu a\sigma^2 \Delta X_t + \sqrt{2aX_t(\theta)}\,\mathrm{d}B_t\,, \quad (4.4)$$

with periodic boundary conditions. This allows to write, for example in the diffusive case:

$$\int_\chi f(\theta)X_t(\theta)\,\mathrm{d}\theta = \int_\chi f(\theta)X_0(\theta)\,\mathrm{d}\theta + \frac{c}{2\pi}t\int_\chi f(\theta)\,\mathrm{d}\theta + \int_0^t\int_\chi (r(\theta, X_s) - d)f(\theta)X_s(\theta)\,\mathrm{d}\theta\,\mathrm{d}s \\ + \frac{1}{2}\mu\sigma^2 a\int_0^t\int_\chi f''(\theta)X_s(\theta)\,\mathrm{d}\theta\,\mathrm{d}s + \int_0^t\int_\chi \sqrt{2aX_s(\theta)}f(\theta)\,\mathrm{d}\theta dB_s,$$

for $f \in \mathcal{C}^2(\chi)$ periodic. In this case, the strong form of this weak equation is 4.4.

It is clear that the issue of non linearity in the reproduction term can not be overcome. In particular, the interaction is non linear and global, so that knowing the cell velocity (by knowing $< X_t, \cos >$ and $< X_t, \sin >$) requires to knowing the whole protrusion density, and we can not reduce the system.

Remark 13. *For the global protrusion density $(N_t)_t$, one can write in the diffusive case*

$$M_t^1 = N_t - N_0 - ct - \int_0^t \int_\chi r(\theta, X_s) X_s(\,\mathrm{d}\theta) - dN_s \,\mathrm{d}s \tag{4.5}$$

a continuous martingale with quadratic variation

$$< M^1 >_t = 2a \int_0^t N_s \,\mathrm{d}s\,, \tag{4.6}$$

We investigate now the case where the orientation space is split into a collection of finite directions. This approach may overcome the nonlinearity barrier to get a closed system.

4.2 Angular discretization

In the case of a finite number of orientations, the framework is simpler: we have $\chi = \{\theta_1, ..., \theta_\ell\}$ with $\ell \in \mathbb{N}^*$. In the following, we'll use the superscript $i \in \{1, ..., \ell\}$ to distinguish the orientations. The problem now reduces to a $\mathbb{R}_+^\ell$-valued continuous markovian process.

The diffusive limit of the continuous case is no longer relevant. However, the objections given for the rare mutation model are no longer valid either. Indeed, since we consider protrusions densities on an angular area, mutation now amounts to induce protrusions to occur in neighboring areas, which can be neglected for a large enough decomposition of the state space. Let us thus write the corresponding equation. We have $Y = (N^i)_{1 \le i \le \ell} \in \mathcal{C}([0,T], \mathbb{R}_+^\ell)$ is solution of the following SDE:

$$dY_t = b(Y_t)dt + \sigma(Y_t)d\mathcal{B}_t \tag{4.7}$$

with $\mathcal{B}_t$ a ℓ-dimensional Brownian Motion, and for $1 \le i \le \ell$, $b_i(Y_t) = c + (r^i(Y_t) - d)Y_t^i$ and $\sigma(Y_t) = \mathrm{diag}(\sqrt{2aY_t})$.

4.2.1 Fokker-Planck equation

Following a classical procedure, one can write a Fokker-Planck equation on the probability distribution of the protrusion population.

Derivation of the equation

In the following, we'll directly use the structure of σ to simplify some expressions, and denote $\sigma_i := \sigma_{ii}$. Take $F \in \mathcal{C}_c^2(\Upsilon, \mathbb{R})$, where Υ will be determined later. Then, by the Itô formula (Ikeda and Watanabe [1989]),

$$F(Y_t) = F(Y_0) + M_t + \int_0^t \sum_{i=1}^\ell \frac{\partial F}{\partial Y^i}(Y_s) b_i(Y_s)\,\mathrm{d}s + \frac{1}{2}\int_0^t \sigma_i^2(Y_s)\frac{\partial^2 F}{\partial {Y^i}^2}(Y_s)\,\mathrm{d}s$$

Write $p(y,t)$ the probability density of Y at (y,t). Taking conditional expectation with respect to the initial condition Y_0 gives:

$$\begin{aligned}\mathbb{E}_{Y_0}[F(Y_t)] = \mathbb{E}_{Y_0}[F(Y_0)] + \int_\Upsilon \int_0^t \sum_{i=1}^\ell \frac{\partial F}{\partial Y^i}(y) b_i(y) p(y,s)\,\mathrm{d}s\,\mathrm{d}y \\ + \frac{1}{2}\int_\Upsilon \int_0^t \sigma_i^2(y)\frac{\partial^2 F}{\partial {Y^i}^2}(y) p(y,s)\,\mathrm{d}s\,\mathrm{d}y.\end{aligned}$$

As all integrands are bounded, we use the Fubini theorem before taking the time derivative of the expression:

$$\int_\Upsilon F(y)\frac{\partial p(y,t)}{\partial t}\,\mathrm{d}y = \sum_{i=1}^{\ell}\left\{\int_\Upsilon \frac{\partial F}{\partial Y^i}(y)b_i(y)p(y,t)\,\mathrm{d}y + \frac{1}{2}\int_\Upsilon \sigma_i^2(y)\frac{\partial^2 F}{\partial {Y^i}^2}(y)p(y,t)\,\mathrm{d}y\right\}$$
$$=: \sum_{i=1}^{\ell}\left\{[U_i] + \frac{1}{2}[V_i]\right\}.$$

In order to deal with boundary conditions, we study two cases for Υ:

- for $F \in \mathcal{C}_c^2({\mathbb{R}_+^*}^\ell)$, we'll obtain the master Fokker-Planck equation on the domain,
- for $F \in \mathcal{C}_c^2({\mathbb{R}_+^*}^{\ell-1} \times \mathbb{R}_+)$, we study the case when $\exists! i,\ y \in \Gamma_i = \{y_i = 0\}$, and get boundary conditions.

The master equation Consider that $F \in \mathcal{C}_c^2({\mathbb{R}_+^*}^\ell)$. We compute $[U_i]$ and $[V_i]$ using integration by parts:

$$[U_i] = \iint_{\mathbb{R}_+^{\ell-1}} [F(y)b_i(y)p(y,t)]_{y^i=0}^{+\infty}\,\mathrm{d}y_{i*} - \iint_{\mathbb{R}_+^\ell} F(y)\frac{\partial}{\partial Y^i}(b_i(y)p(y,t))\,\mathrm{d}y,$$

where $\mathrm{d}y_{i*} = \Pi_{\substack{j=1\\ j\neq i}}^{\ell}\mathrm{d}y^j$. By an abuse of notations, any function of y_{i*} denotes a function of y where $y_i = 0$. By definition of F, and for a vanishing p at infinity, the first term vanishes and

$$[U_i] = -\iint_{\mathbb{R}_+^\ell} F(y)\frac{\partial}{\partial Y^i}(b_i(y)p(y,t))\,\mathrm{d}y.$$

For the second term, we get

$$\begin{aligned}
[V_i] &= \iint_{\mathbb{R}_+^{\ell-1}} \left[\frac{\partial F}{\partial Y^i}(y)\sigma_i^2(y_{i*})p(y_{i*},t)\right]_{y^i=0}^{+\infty}\mathrm{d}y_{i*} - \iint_{\mathbb{R}_+^\ell}\frac{\partial F}{\partial Y^i}(y)\frac{\partial}{\partial Y^i}(\sigma_i^2(y)p(y,t))\,\mathrm{d}y,\\
&= -\iint_{\mathbb{R}_+^{\ell-1}}\left[F(y_{i*})\frac{\partial}{\partial Y^i}(\sigma_i^2(y_{i*})p(y_{i*},t))\right]_{y^i=0}^{+\infty}\mathrm{d}y_{i*} + \iint_{\mathbb{R}_+^\ell} F(y)\frac{\partial^2}{\partial {Y^i}^2}(\sigma_i^2(y)p(y,t))\,\mathrm{d}y,\\
&= \iint_{\mathbb{R}_+^\ell} F(y)\frac{\partial^2}{\partial {Y^i}^2}(\sigma_i^2(y)p(y,t))\,\mathrm{d}y
\end{aligned}$$

as $\frac{\partial F}{\partial Y^i}(y)$ vanishes for y_i at infinity, and $\sigma_i^2(y_{i*}) = 0$. Finally,

$$\iint_{\mathbb{R}_+^\ell} F(y)\frac{\partial p(y,t)}{\partial t}\,\mathrm{d}y = \iint_{\mathbb{R}_+^\ell} F(y)\sum_{i=1}^{\ell}\left\{-\frac{\partial}{\partial Y^i}(b_i(y)p(y,t)) + \frac{1}{2}\frac{\partial^2(\sigma_i^2(y)p(y,t))}{\partial {Y^i}^2}\right\}\mathrm{d}y, \tag{4.8}$$

and we can write

$$\boxed{\frac{\partial \boldsymbol{p(y,t)}}{\partial \boldsymbol{t}} = \sum_{\boldsymbol{i=1}}^{\boldsymbol{\ell}} -\frac{\partial}{\partial \boldsymbol{y^i}}(\boldsymbol{b_i(y)p(y,t)}) + \frac{\boldsymbol{1}}{\boldsymbol{2}}\frac{\boldsymbol{\partial^2(\sigma_i^2(y)p(y,t))}}{\boldsymbol{\partial {y^i}^2}} \text{ on } \boldsymbol{\Omega}.} \tag{4.9}$$

Moreover, this Fokker-Planck equation is usually written

$$\frac{\partial p(y,t)}{\partial t} = \nabla \cdot \mathbf{J}(y,t) = \sum_{i=1}^{\ell} \frac{\partial}{\partial y_i} J_i(y,t),$$

where

$$J_i(y,t) = -b_i(y)p(y,t) + \frac{1}{2}\frac{\partial}{\partial y_i}(\sigma_i^2(y)p(y,t)) \tag{4.10}$$

is the probability current of p in the y_i direction, and we have immediately that $\forall 1 \leq i \leq \ell$ $\lim_{y_i \to +\infty} J(y,t) = 0$.

Boundary conditions Now, assume that $F \in \mathcal{C}_c^2({\mathbb{R}_+^*}^{\ell-1} \times \mathbb{R}_+)$, and that the coordinate allowed to hit 0 is y_i. For $j \neq i$, $[U_j]$ and $[V_j]$ are computed as before. After an integration by parts,

$$[U_i] = \iint_{\mathbb{R}_+^{\ell-1}} \lim_{\epsilon \to 0} \left\{ [F(y)b_i(y)p(y,t)]_{y^i=\epsilon}^{+\infty} - \int_\epsilon^{+\infty} F(y)\frac{\partial}{\partial Y^i}(b_i(y)p(y,t))\,\mathrm{d}y_i \right\} \mathrm{d}y_{i*}.$$

By definition of F, $\lim_{y_i \to +\infty} F(y) = 0$, and we can write

$$[U_i] = \iint_{\mathbb{R}_+^{\ell-1}} \left\{ -F(y_{i*})b_i(y_{i*})p(y_{i*},t) - \lim_{\epsilon \to 0} \int_\epsilon^{+\infty} F(y)\frac{\partial}{\partial Y^i}(b_i(y)p(y,t))\,\mathrm{d}y_i \right\} \mathrm{d}y_{i*}.$$

For the second term, we get

$$\begin{aligned}
[V_i] &= \iint_{\mathbb{R}_+^{\ell-1}} \lim_{\epsilon \to 0} \left\{ \left[\frac{\partial F}{\partial Y^i}(y)\sigma_i^2(y)p(y,t) \right]_{y^i=\epsilon}^{+\infty} - \int_\epsilon^{+\infty} \frac{\partial F}{\partial Y^i}(y)\frac{\partial}{\partial Y^i}(\sigma_i^2(y)p(y,t))\,\mathrm{d}y_i \right\} \mathrm{d}y_{i*}, \\
&= \iint_{\mathbb{R}_+^{\ell-1}} \lim_{\epsilon \to 0} \left\{ -\left[F(y)\frac{\partial}{\partial Y^i}(\sigma_i^2(y)p(y,t)) \right]_{y^i=\epsilon}^{+\infty} + \int_\epsilon^{+\infty} F(y)\frac{\partial^2}{\partial {Y^i}^2}(\sigma_i^2(y)p(y,t))\,\mathrm{d}y_i \right\} \mathrm{d}y_{i*}, \\
&= \iint_{\mathbb{R}_+^{\ell-1}} \left\{ F(y_{i*})\frac{\partial}{\partial Y^i}(\sigma_i^2(y_{i*})p(y_{i*},t)) + \lim_{\epsilon \to 0} \int_\epsilon^{+\infty} F(y)\frac{\partial^2}{\partial {Y^i}^2}(\sigma_i^2(y)p(y,t))\,\mathrm{d}y_i \right\} \mathrm{d}y_{i*},
\end{aligned}$$

as $\frac{\partial F}{\partial Y^i}(y)$ vanishes for y_i at infinity, and $\sigma_i^2(y_{i*}) = 0$. Finally,

$$\iint_{\mathbb{R}_+^\ell} F(y)\frac{\partial p(y,t)}{\partial t}\,\mathrm{d}y = \iint_{\mathbb{R}_+^{\ell-1}} \lim_{\epsilon \to 0} \left\{ \int_0^\epsilon F(y)\frac{\partial p(y,t)}{\partial t}\,\mathrm{d}y_i + \int_\epsilon^{+\infty} F(y)\frac{\partial p(y,t)}{\partial t}\,\mathrm{d}y_i \right\} \mathrm{d}y_{i*}$$

is equal to

$$\begin{aligned}
\sum_{j=1}^{\ell} \iint_{\mathbb{R}_+^{\ell-1}} \lim_{\epsilon \to 0} \int_\epsilon^{+\infty} F(y) \left(-\frac{\partial}{\partial Y^j}(b_j(y)p(y,t)) + \frac{1}{2}\frac{\partial^2}{\partial {Y^j}^2}(\sigma_j^2(y)p(y,t)) \right) \mathrm{d}y_j\,\mathrm{d}y_{j*} \\
+ \iint_{\mathbb{R}_+^{\ell-1}} F(y_{i*}) \left(-b_i(y_{i*})p(y_{i*},t) + \frac{1}{2}\frac{\partial}{\partial Y^i}(\sigma_i^2(y_{i*})p(y_{i*},t)) \right) \mathrm{d}y_{i*},
\end{aligned}$$

as the last term occurs only for $j = 1$.

Using the previous result (4.9), the equality simplifies to

$$\iint_{\mathbb{R}_+^{\ell-1}} \lim_{\epsilon\to 0} \int_0^{\epsilon} F(y)\frac{\partial p(y,t)}{\partial t}\,\mathrm{d}y_i\,\mathrm{d}y_{i*} = \iint_{\mathbb{R}_+^{\ell-1}} F(y_{i*})\left(-b_i(y_{i*})p(y_{i*},t) + \frac{1}{2}\frac{\partial}{\partial Y^i}(\sigma_i^2(y_{i*})p(y_{i*},t))\right)\mathrm{d}y_{i*}.$$

Assuming the boundedness of $\frac{\partial p(y,t)}{\partial t}$, one can deduce that the left-side of the equality vanishes, and we get the no-flux boundary condition

$$\boldsymbol{J_i(y,t)|_{\Gamma_i} = 0.} \tag{4.11}$$

4.2.2 Stationary state

As detailed in Gardiner [2004], we investigate a stationary distribution for p such that the probability courant $\mathbf{J}$ vanishes at each point. More precisely, for all $1 \le i \le \ell$, one has

$$-b_i(y)p(y) + \frac{1}{2}\frac{\partial}{\partial y_i}(\sigma_i^2(y)p(y)) = 0,$$

or equivalently

$$\frac{1}{2}\sigma_i^2(y)\frac{\partial p(y)}{\partial y_i} = p(y)\left[b_i(y) + -\frac{1}{2}\frac{\partial \sigma_i^2(y)}{\partial y_i}\right].$$

As this equality already holds for $y_i = 0$ by the boundary conditions, let us assume that $y_i > 0$. Then, $\sigma_i^2(y) > 0$ as well, and we have

$$\frac{\partial}{\partial y_i}\ln[p(y)] = \sigma_i^2(y)^{-1}\left[2b_i(y) - \frac{\partial \sigma_i^2(y)}{\partial y_i}\right] = \underbrace{2\frac{b_i(y)}{\sigma_i^2(y)} - \frac{\partial}{\partial y_i}\ln[\sigma_i^2(y)]}_{=:Z_i(b,\sigma,y)}.$$

Hence for a stationary solution to exists, $Z_i(b,\sigma,y)$ must be a gradient, which is equivalent to the condition of vanishing curl, that is to say:

$$\forall i \neq j,\ \frac{\partial Z_i}{\partial y_j} = \frac{\partial Z_j}{\partial y_i}.$$

As $\sigma_i^2(y) = 2ay_i$ is independent of $\{y_j,\ j \neq i\}$, this condition recasts to

$$\forall i \neq j,\ y_j\frac{\partial b_i}{\partial y_j} = y_i\frac{\partial b_j}{\partial y_i}. \tag{4.12}$$

In that case, the stationary solution writes

$$\boxed{\boldsymbol{p^\star(y) = \mathcal{N}\exp\left(\int_0^{\boldsymbol{y}} \boldsymbol{Z(b,\sigma,y')}\cdot\,\mathbf{d}\boldsymbol{y'}\right),}} \tag{4.13}$$

or $p^\star(y) = \mathcal{N}\exp(\phi(y))$ with $\phi(y) = -\int_0^y Z(b,\sigma,y')\cdot\mathrm{d}y'$ the corresponding potential, and $\mathcal{N}$ the normalization constant. In the following, we will perform numerical simulations of the potential rather than of the propability distribution. These simulations have to be interpreted as follows: in the phase space, the particle is drifted towards minimizing values of the potential.

4.2.3 The case $\ell = 3$

Since we are interested in the cell velocity in two dimensions, a change of variable can allow deriving equations on $\vec{v}$. Namely, for (N_1, N_2, N_3) the respective protrusion densities on $\Theta_1 = (-\frac{\pi}{3}, \frac{\pi}{3})$ centered in $\theta_1 = 0$, $\Theta_2 = (\frac{\pi}{3}, \pi)$ centered in $\theta_2 = \frac{2\pi}{3}$, and $\Theta_3 = (\pi, \frac{5\pi}{3})$ centered in $\theta_3 = \frac{4\pi}{3}$, one obtains

$$\begin{cases} \gamma V_x = N_1 - \frac{1}{2}N_2 - \frac{1}{2}N_3 \,, \\ \gamma V_y = \frac{\sqrt{3}}{2}(N_2 - N_3) \,, \\ N = N_1 + N_2 + N_3 \,, \end{cases}$$

or equivalently

$$\begin{cases} N_1 = N - \frac{2}{\sqrt{3}}\gamma V_y \,, \\ N_2 = N - \gamma V_x - \frac{1}{\sqrt{3}}\gamma V_y \,, \\ N_3 = N - \gamma V_x - \sqrt{3}\gamma V_y \,. \end{cases}$$

Stationary distribution

In order to investigate a stationary probability distribution for (N_1, N_2, N_3), one has to choose the form of the reproduction rate. A natural adaptation from the continuous case consists in writing for θ_i and the corresponding unit vector e_i in this direction

$$r_i(Y_t) := r \tanh(\alpha V_t \cdot e_i) \,.$$

Then, the potential condition (4.12) rewrites

$$\forall i \neq j, \; N_i N_j \frac{\partial r_i(y)}{\partial N_j} = N_i N_j \frac{\partial r_j(y)}{\partial N_i} \,,$$

and the expressions of (V_x, V_y) immediatly show that the condition is not satisfied, due to the geometric asymmetry of the model, and there is no stationary state for the system.

4.3 One dimensional migration

The minimal situation of one dimensional migration is now investigated. Indeed, the symmetry property of the system allows us to expect getting a stationary distribution for the velocity.

4.3.1 Stationary distribution

We have now

$$\gamma V_t = N_t^+ - N_t^- \,, \tag{4.14}$$

with N_t^+ the protrusion density on the right of the cell, and N_t^- the protrusion density on the left. The dynamics is now defined as follows: for simplicity, we neglect the limitations of resources. Creation and disappearance of protrusions occur at constant rate c and d.

Denote $r_i(Y_t)$ the individual reproduction rate without any logistic constraint. Moreover, denote s_i a positive constant. Then, we take

$$r_{1,2}(Y_t) = \frac{\beta}{2}\left(1 \pm \tanh\left(\alpha V_t\right)\right) \,,$$

where the expression accounts for the antisymmetric effect of retrograde flow.

Remark 14. *Polarisation is also sensitive to the environment, which is sensed by filopodial protrusions. The reproduction rates could then include a dependence on an external signal, other cells, mechanical obstacles, or the nature of the substrate. This will be investigated in a future work.*

In the $1D$ formalism, let us write for $i = 1\,, 2$,

$$\begin{aligned} b_i(y) &= c_i + (r_i(y) - d)y_i, \\ \sigma_i(y)^2 &= 2ay_i. \end{aligned}$$

This choice is made in order to satisfy (4.12) easily. In particular, the interaction being carried by the reproduction term, the condition (4.12) is simplified:

$$y_2 y_1 \frac{\partial r_1(y)}{\partial y_2} = y_1 y_2 \frac{\partial r_2(y)}{\partial y_1},$$

that is ensured for our choice of rate with s_i constants. Finally,

$$Z(b,\sigma,y) = \begin{pmatrix} \frac{c_1-a}{ay_1} + \frac{\beta}{2a}\tanh\left(\frac{\alpha}{\gamma}\left(y_1 - y_2\right)\right) + \frac{\beta}{2a} \\ \frac{c_2-a}{ay_2} + \frac{\beta}{2a}\tanh\left(\frac{\alpha}{\gamma}\left(y_2 - y_1\right)\right) + \frac{\beta-2d}{2a} \end{pmatrix}.$$

Moreover, the boundary conditions at all time t rewrite

$$(a - c_i)p(y_{i*}, t) = 0,$$

and different configurations occur depending on a and $(c_i)_i$.

The compensation case

If $c_1 = c_2 = a$, the probability for the population size is compensated by creation, and Z doesn't have any poles. The sationary distribution is well defined on $\mathbb{R}^2_+$. For $y_2 = n^-$ we compute

$$\begin{aligned} \int_0^{n^+} Z_1(b,\sigma,y)\,\mathrm{d}y_1 &= \int_0^{n^+} \left\{ \frac{\beta}{2a}\tanh\left(\frac{\alpha}{\gamma}\left(y_1 - n^-\right)\right) + \frac{\beta-2d}{2a} \right\} \mathrm{d}y_1 \\ &= \frac{\beta\gamma}{2a\alpha}\left[\ln\circ\cosh(\frac{\alpha}{\gamma}\left(n^+ - n^-\right)) - \ln\circ\cosh(\frac{\alpha}{\gamma}\left(-n^-\right))\right] \\ &+ \frac{\beta-2d}{2a}n^+. \end{aligned}$$

Similarly, for $y_1 = n^+$,

$$\begin{aligned} \int_0^{n^-} Z_2(b,\sigma,y)\,\mathrm{d}y_2 &= \int_0^{n^-} \left\{ \frac{\beta}{2a}\tanh\left(\frac{\alpha}{\gamma}\left(y_2 - n^+\right)\right) + \frac{\beta-2d}{2a} \right\} \mathrm{d}y_2 \\ &= \frac{\beta\gamma}{2a\alpha}\left[\ln\circ\cosh(\frac{\alpha}{\gamma}\left(n^- - n^+\right)) - \ln\circ\cosh(\frac{\alpha}{\gamma}\left(-n^+\right))\right] \\ &+ \frac{\beta-2d}{2a}n^-, \end{aligned}$$

and

$$\begin{aligned} \phi(n^+,n^-) &= -\frac{\beta\gamma}{2a\alpha}\ln\left[\frac{\cosh(\frac{\alpha}{\gamma}\left(n^+ - n^-\right))^2}{\cosh(\frac{\alpha}{\gamma}n^+)\cosh(\frac{\alpha}{\gamma}n^-)}\right] - \frac{\beta-2d}{2a}(n^+ + n^-) \\ &= \frac{\beta\gamma}{2a\alpha}\ln\left[\frac{\cosh(\frac{\alpha}{\gamma}n^+)\cosh(\frac{\alpha}{\gamma}n^-)}{\cosh(\frac{\alpha}{\gamma}\left(n^+ - n^-\right))^2}\right] - \frac{\beta-2d}{2a}(n^+ + n^-)\,. \end{aligned} \tag{4.15}$$

In this expression, we can distinguish two trends:

- the first term describes an eventual asymmetry between the two subpopulations. This is led by the value of α/γ. Numerically, we observe that for $100\alpha/\gamma < 1$, the potential favors a symmetric steady state, while in the other case, the asymmetric cases $(n^+, 0)$ and $(0, n^-)$ are preferred. Further simulations show that the treshold is dependent on the demographic parameters.
- The second term describes the steady total population size. For $\beta > 2d$, the symmetric steady state will be non-zero, as opposed to the case $\beta < 2d$ where the potential favors a null population size.

The figures 4.2 and 4.3 illustrate these trends. The lower corner in figure 4.2 corresponds to the $(0, 0)$ state. We can see that for a low polarisation parameter, the potential shows a minimum at that state. For larger values of α, and a low disappearance rate d, the dynamics tends to a state where one of the two subpopulations is way larger than the other. For an increasing disappearance rate, the possibility that both populations stabilize near zero becomes important enough to compete with the polarised situations.

Not reaching zero

If for $i = 1, 2$, $c_i \neq a$, we know in particular that $p(y_{i*}, t) = 0$ at all time t, and we expect at steady state a potential that prevents the hitting of a boundary.

Take $\epsilon_{1,2} > 0$. As before, for $y_2 = n^- > 0$ and $n^+ \in]0, +\infty)$, we compute

$$\begin{aligned}\int_{\epsilon_1}^{n^+} Z_1(b,\sigma,y)\,\mathrm{d}y_1 &= \int_{\epsilon_1}^{n^+} \left\{ \frac{c_1 - a}{a y_1} + \frac{\beta}{2a} \tanh\left(\frac{\alpha}{\gamma}\left(y_1 - n^-\right)\right) + \frac{\beta - 2d}{2a} \right\} \mathrm{d}y_1 \\ &= \frac{c_1 - a}{a}\left[\ln(n^+) - \ln(\epsilon_1)\right] + \frac{\beta\gamma}{2a\alpha}\left[\ln\circ\cosh(\frac{\alpha}{\gamma}\left(n^+ - n^-\right)) - \ln\circ\cosh(\frac{\alpha}{\gamma}\left(\epsilon_1 - n^-\right))\right] \\ &+ \frac{\beta - 2d}{2a}[n^+ - \epsilon_1].\end{aligned}$$

Similarly, for $y_1 = n^+$,

$$\begin{aligned}\int_{\epsilon_2}^{n^-} Z_2(b,\sigma,y)\,\mathrm{d}y_2 &= \int_{\epsilon_2}^{n^-} \left\{ \frac{c_2 - a}{a y_2} + \frac{\beta}{2a} \tanh\left(\frac{\alpha}{\gamma}\left(y_2 - n^+\right)\right) + \frac{\beta - 2d}{2a} \right\} \mathrm{d}y_2 \\ &= \frac{c_2 - a}{a}\left[\ln(n^-) - \ln(\epsilon_2)\right] + \frac{\beta\gamma}{2a\alpha}\left[\ln\circ\cosh(\frac{\alpha}{\gamma}\left(n^- - n^+\right)) - \ln\circ\cosh(\frac{\alpha}{\gamma}\left(\epsilon_2 - n^+\right))\right] \\ &+ \frac{\beta - 2d}{2a}[n^- - \epsilon_2],\end{aligned}$$

and

$$\begin{aligned}\phi(n^+, n^-) &= -\frac{\beta\gamma}{2a\alpha}\left[2\ln\circ\cosh(\frac{\alpha}{\gamma}\left(n^+ - n^-\right)) - \ln\circ\cosh(\frac{\alpha}{\gamma}(\epsilon_1 - n^-)) - \ln\circ\cosh(\frac{\alpha}{\gamma}(\epsilon_2 - n^+))\right] \\ &\quad - \frac{\beta - 2d}{2a}(n^+ + n^- - \epsilon_1 - \epsilon_2) - \frac{c_1 - a}{a}\left[\ln(n^+) - \ln(\epsilon_1)\right] \\ &\quad - \frac{c_2 - a}{a}\left[\ln(n^-) - \ln(\epsilon_2)\right], \\ &= \frac{\beta\gamma}{2a\alpha}\ln\left[\frac{\cosh(\frac{\alpha}{\gamma}(n^+ - \epsilon_2))\cosh(\frac{\alpha}{\gamma}(n^- - \epsilon_1))}{\cosh(\frac{\alpha}{\gamma}\left(n^+ - n^-\right))^2}\right] - \frac{\beta - 2d}{2a}(n^+ + n^- - \epsilon_1 - \epsilon_2) \\ &\quad - \ln\left[(n^+)^{\frac{c_1 - a}{a}}(n^-)^{\frac{c_2 - a}{a}}\right] + \ln\left[(\epsilon_1)^{\frac{c_1 - a}{a}}(\epsilon_2)^{\frac{c_2 - a}{a}}\right].\end{aligned} \tag{4.16}$$

The corresponding simulations for equal creation rates are qualitatively similar to the ones in the compensation case, as we arbitrarily stay away from zero. They are displayed in figures 4.4 and 4.5.

4.3.2 Equation on (N, V)

We want to express the probability distribution on the couple

$$w = (n, v) = (n^+ + n^-, \frac{1}{\gamma}(n^+ - n^-))$$

rather than on $y = (n^+, n^-)$. First, notice that

$$n_\pm \in [0, +\infty) \Leftrightarrow \left\{ \begin{array}{l} n \in [0, +\infty) \\ v \in [-\frac{1}{\gamma}n, \frac{1}{\gamma}n] \end{array} \right. .$$

Moreover, as

$$\begin{pmatrix} n^+ \\ n^- \end{pmatrix} = \frac{1}{2}\begin{pmatrix} 1 & \gamma \\ 1 & -\gamma \end{pmatrix}\begin{pmatrix} n \\ v \end{pmatrix},$$

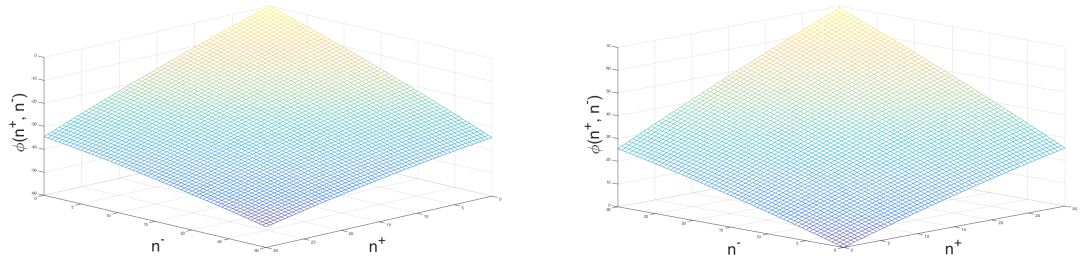

(a) $d = 9$ (b) $d = 11$

Figure 4.2 – Stationary distributions for $(\beta, a) = (20, 1)$ and $\boldsymbol{(\alpha, \gamma) = (1, 1000)}$.

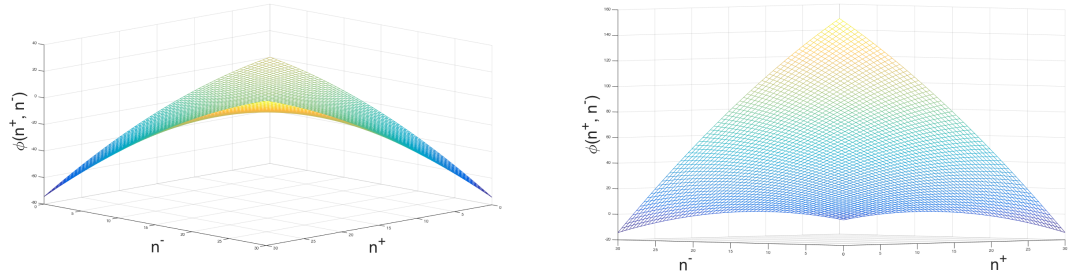

(a) $d = 9$ (b) $d = 11$

Figure 4.3 – Stationary distributions for $(\beta, a) = (20, 1)$ and $\boldsymbol{(\alpha, \gamma) = (10, 1000)}$.

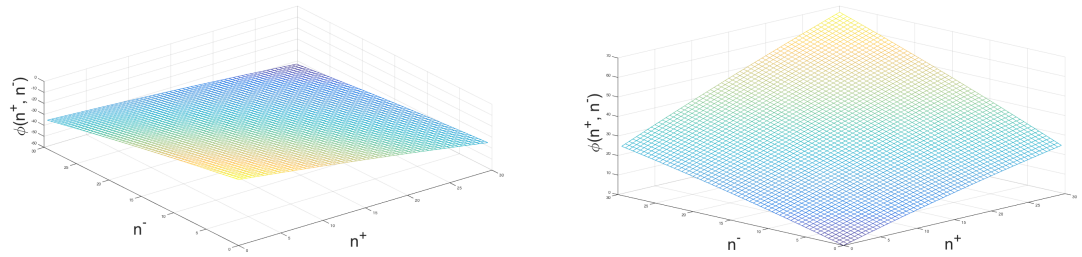

(a) $d = 9$ (b) $d = 11$

Figure 4.4 – Stationary distributions for $(\beta, a) = (20, 1)$ and $\boldsymbol{(\alpha, \gamma) = (1, 1000)}$.

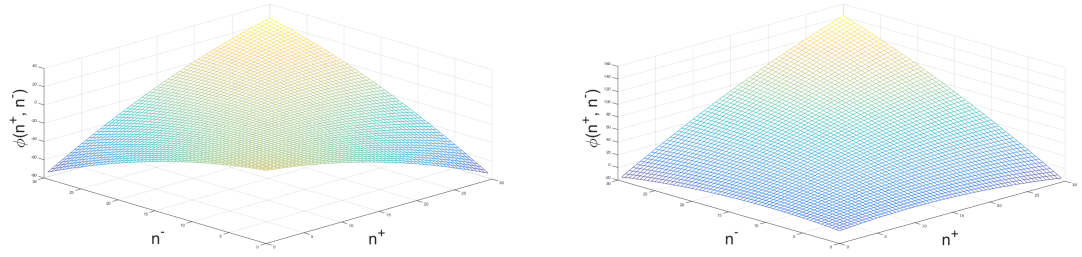

(a) $d = 9$ (b) $d = 11$

Figure 4.5 – Stationary distributions for $(\beta, a) = (20, 1)$ and $\boldsymbol{(\alpha, \gamma) = (10, 1000)}$.

the Jacobian writes $\frac{\partial(n^+,n^-)}{\partial(n,v)} = \frac{\gamma}{2}$, and we have

$$p^\star(w) = \frac{\gamma}{2} p^\star(y). \tag{4.17}$$

Now, we have to compute the change of variables in $\int_0^y Z(b,\sigma,y')\cdot \mathrm{d}y'$:

$$\int_0^{n^+} Z_1(y)\,\mathrm{d}y_1 + \int_0^{n^-} Z_2(y)\,\mathrm{d}y_2 = \underbrace{\int_0^n \frac{Z_1(w)+Z_2(w)}{2} dn}_{=:A} + \gamma \underbrace{\int_{-\frac{1}{\gamma}n}^v \frac{Z_1(w)-Z_2(w)}{2} dv}_{=:B},$$

with

$$A = \int_0^n \frac{c_1-a}{a(n+\gamma v)} + \frac{c_2-a}{a(n-\gamma v)} + \frac{\beta+s_1+s_2-2d}{2a} dn,$$
$$B = \int_{-\frac{1}{\gamma}n}^v \frac{c_1-a}{a(n+\gamma v)} - \frac{c_2-a}{a(n-\gamma v)} + \frac{\beta}{2a}\tanh(\alpha v).$$

It is clear that these expressions are not well defined for all values of (n,v). In the following, we'll introduce infinitesimal parameters as soon as needed to prevent any problem, and denote A_ϵ, B_ϵ the corresponding integrals.

Computation of A. For $n \in [\epsilon_1, +\infty[$, with $\epsilon_1 > 0$, we have

$$\begin{aligned} A_{\epsilon_1} &= \int_{\epsilon_1}^n \frac{c_1-a}{a(n+\gamma v)} + \frac{c_2-a}{a(n-\gamma v)} + \frac{\beta-2d}{2a} dn \\ &= \frac{c_1-a}{a}\left[\ln(n+\gamma v) - \ln(|\epsilon_1+\gamma v|)\right] + \frac{c_2-a}{a}\left[\ln(n-\gamma v) - \ln(|\epsilon_1-\gamma v|)\right] \\ &+ \frac{\beta-2d}{2a}(n-\epsilon_1)\,. \end{aligned}$$

Computation of B. Let us consider $v \in \left[-\frac{1}{\gamma}n+\epsilon_3, \frac{1}{\gamma}n-\epsilon_4\right]$ for $\epsilon_3, \epsilon_4 > 0$. Then it is clear that $n \pm \gamma v > 0$. Hence,

$$\begin{aligned} B_{\epsilon_3} &= \frac{c_1-a}{a\gamma}\left(\ln(n+\gamma v) - \ln(\gamma\epsilon_3)\right) + \frac{c_2-a}{a\gamma}\left(\ln(n-\gamma v) - \ln(2n+\gamma\epsilon_3)\right) \\ &+ \frac{\beta}{2a\alpha}\left(\ln\circ\cosh(\alpha v) - \ln\circ\cosh\left(-\frac{\alpha}{\gamma}n + \alpha\epsilon_3\right)\right)\,. \end{aligned}$$

In this expression, using ϵ_3 is important for the first term, as it ensures that for v close the the bottom boundary the expression doesn't go to infinity.

Now, consider the second term of coefficient $\frac{c_2-a}{a\gamma}$. As $\lim_{v\to\frac{1}{\gamma}n} \ln(n-\gamma v) = -\infty$,

- → for $c_2 > a$, it leads to a term going to $+\infty$ in the potential ϕ, and $\lim_{v\to\frac{1}{\gamma}n} p(w) = 0$. This means that if creation is strong enough on the "minus" side, all the population can't be concentrated on the "plus" side, and the velocity is almost surely strictly bounded by $\frac{1}{\gamma}n$.
- → for $c_2 < a$, the opposite happens. Intuitively, the population created on the "minus" side instantaneously disappears, and the stationnary velocity is almost surely concentrated at the state $\frac{1}{\gamma}n$. Rigorously, it leads to $\lim_{v\to\frac{1}{\gamma}n} p(w) = +\infty$ and the distribution is degenerate.

Following these arguments, we arbitrarily avoid the degenerate polarization at the minus side with the parameter ϵ_4.

Expression of the potential Finally, the potential $\phi(w) = -A - \gamma B$ writes

$$\begin{aligned}\Phi(w) = &-\frac{c_1 - a}{a}\left(2\ln(n+\gamma v) - \ln(|\gamma\epsilon_3|) - \ln(|\epsilon_1 + \gamma v|)\right)\\ &-\frac{c_2 - a}{a}\left(2\ln(n-\gamma v) - \ln(|2n - \gamma\epsilon_3|) - \ln(|\epsilon_1 - \gamma v|)\right)\\ &-\frac{\beta - 2d}{2a}(n - \epsilon_1)\\ &-\frac{\beta\gamma}{2a\alpha}\left(\ln\circ\cosh(\alpha v) - \ln\circ\cosh\left(-\frac{\alpha}{\gamma}n + \alpha\epsilon_3\right)\right).\end{aligned}$$

Simulations led to figures 4.6 and 4.7. In figure 4.6, we can see that for lower values of α, the potential is symmetric, whereas for larger values, the potential has a double well shape symmetric with respect to $\{v = 0\}$, corresponding to non zero velocities in one or another direction. Figure 4.7 shows that increasing the disappearance rate prevents the particle from maintaining a directional motion.

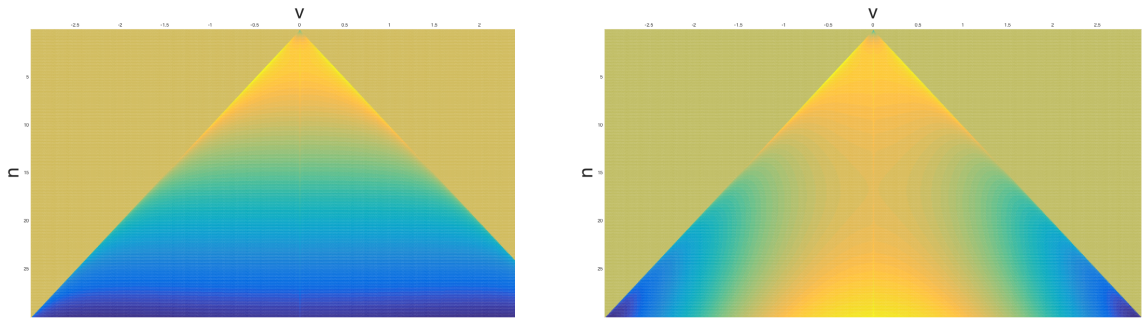

(a) $\alpha = 0.01$ (b) $\alpha = 0.1$

Figure 4.6 – Potential for $(\beta, a, c_i, d, \gamma) = (20, 1, 2, 8, 10)$.

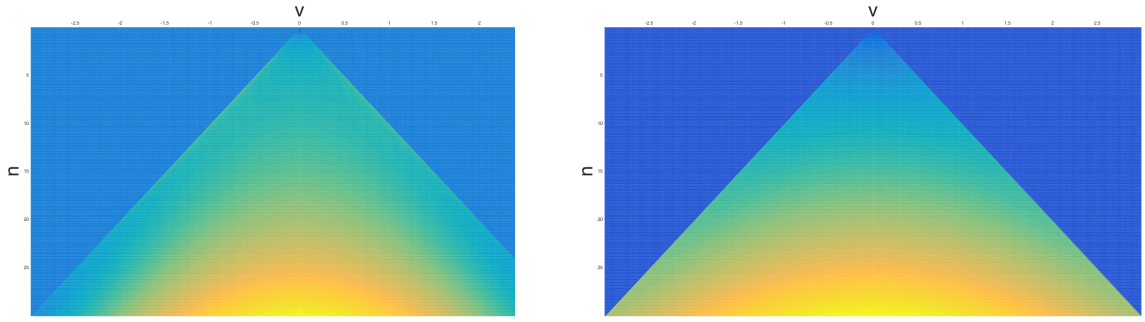

(a) $d = 9$ (b) $d = 11$

Figure 4.7 – Potential for $(\beta, a, c_i, \gamma) = (20, 1, 2, 10)$ and $\boldsymbol{\alpha = 0.1}$.

4.4 Conclusions and perspectives

In chapters 2, 3 and in this chapter, we have rigorously built a stochastic particle model for two dimensional cell migration based on the protrusive activity. It is based on a individual-based population model to describe a discrete population of filopodia. We have assumed that it evolved in interaction, in order for the cell velocity to exert a feedback on the protrusive dynamics. This feedback involved a parameter α quantifying the coupling between cell velocity and polarisation.

From the mathematical viewpoint, the resulting model is expressed as a markovian measure-valued jump process. The nonlinearity brought by the global feedback of the displacement led to difficulties to derive specific information on the cell velocity. However, numerical simulations of trajectories showed different behaviours, from Brownian-like trajectories to directed paths. This dichotomy was also observed on the distribution of velocities obtained by sampling numerical trajectories.

Then, in order to get an analytical characterization of this variety, we performed a scaling limit to obtain a time continuous model for continuous protrusions. The scaling was a natural hypothesis, since the description of protrusions require not only filopodia but also continuous protrusions such as lamellipodia.

We then tried to derive analytical information on the probability density for the cell velocity. The non linear interaction term made the attempts unsuccessful in the two dimensional setting.

Finally, we investigated the particular cases where the state space $[0, 2\pi)$ was discretized in angular areas. In the one dimensional case, the stationnary distribution of the couple (N, V) can be obtained, with N the global protrusion density. Numerical simulations allowed to observe symmetric and asymmetric potentials according to the value of α.

Overall, the modelling approach we developped in this part allowed to describe cell crawling based on an intracellular activity and a feedback of the velocity on this dynamics. The model is able to provide variable cell trajectories of different natures in terms of persistence. An analytical study provide the stationnary velocity distribution of the cell in one dimension, based on its protrusive dynamics and on the value of the polarisation parameter α.

Since the model is minimal, it is tempting to investigate interaction with external cues or other cells. Indeed, chemical signals and mechanical obstacles are generally sensed by filopodial protrusions during the cell motion. The intracellular response thus occurs in reaction, and affect the protrusive dynamics. This feedback could be included in the model by a biais in protrusion rates depending on the concentration in a chemical signal, or on the distance to an obstacle.

4.4.1 Validation of the model

We have built a minimal trajectory model spanning two different scales, and able to provide different types of trajectories with a minimal set of parameters. Moreover, only the polarisation parameter can not be determined by experimental measures, so that confrontation with experimental trajectories could lead to a classification of cells depending on the value of α. Validation of the model on experimental data is a joint work in progress with Nicolas Meunier, Raphaël Voituriez, David Caballero and Daniel Riveline. The algorithm to analyze the trajectories is presented in annex B.

Bibliography

Champagnat, N., Ferrière, R., and Méléard, S. (2006). Unifying evolutionary dynamics: from individual stochastic processes to macroscopic models. Theor Popul Biol, 69(3):297–321. 142

Gardiner, C. (2004). Handbook of Stochastic Methods: for Physics, Chemistry and the Natural Sciences (Springer Series in Synergetics). Springer, 3rd edition. 146

Ikeda, N. and Watanabe, S. (1989). Stochastic differential equations and diffusion processes. Kodansha scientific books. North-Holland. 143

Part II

Fluid approach

Chapter 5

Construction of the fluid model

Contents

5.1 Introduction 159
5.2 The cytoskeleton as an active polar gel 161
5.3 Existing works 164
5.3.1 A minimal model for cell lamellar fragments 164
5.3.2 On the impact of the polarisation field 165
5.3.3 Spontaneous motility of actin lamellar fragments 167
5.3.4 A universal law for cell migration 168
5.4 The free boundary model 171
5.4.1 The fluid problem 171
5.4.2 The molecular marker's dynamics 174
5.4.3 Non-dimensionalization 177
5.5 The problem in a rigid domain 178
5.5.1 The fluid problem 178
5.5.2 The marker's dynamics: two choices 181
5.5.3 Non-dimensionalization 182
5.5.4 The one-dimensional case 183

5.1 Introduction

In this chapter, we present our modeling approach to construct a minimal multi-scale model of migration. It is based on the actin cytoskeleton and molecular agents. The resulting model is expected to provide typical migration patterns, and highlight common processes to a wide range of cell types. Moreover, a generic model is a useful tool to investigate the effect of various constraints and stimulations on the cell motion (stochastic fluctuations, external signals, mechanical obstacles). In particular, stochasticity in the system is needed to provide realistic cell trajectories, that allow confrontation with experimental data. Finally, notice that this generic model can be enriched and precised to fit a particular cell type. This work is a joint work with Nicolas Meunier and Raphaël Voituriez.

The cytoskeleton, an active polar medium The actin cytoskeleton is a highly complex and dynamical medium, composed of actin filaments organized in bundles and networks by their transient interaction with cross-linking molecules. Actin filaments are **polar**: they continuously polymerize at their "plus" end near the cell membrane, and depolymerize at their "minus" end. An inward flow can arise from this process, and transient attachment to the substrate generates friction forces. Filaments also interact with myosin motors assembled in minifilaments, that generate contractile or dilative stresses in the network (see figure 5.3). These stresses can be transmitted to the substrate by molecular adhesion complexes. Finally, the cell being a microscopic system, low Reynolds number physics apply, and the force balance principle is verified: the cell is at mechanical equilibrium. As a consequence, these local forces are balanced by the global friction force associated with the cell motion.

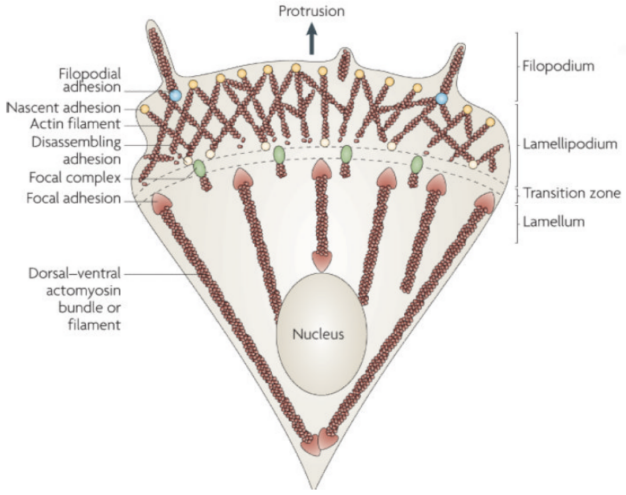

Figure 5.1 – Scheme of actin structures inside a crawling cell. At the protrusive edge, actin filaments are assembled in bundles or cross-linked in networks, and polymerize against the cell membrane. In the cell body, actin filaments assemble with myosin to form contractile bundles. These structures are in mechanical interaction with the substrate thanks to adhesion structures all over the cell. Reprinted by permission from Macmillan Publishers Ltd: Nature Reviews Molecular Cell Biology [Parsons et al., 2010], copyright 2010.

This activity continuously occurs thanks to a permanent energy consumption via ATP hydrolysis. The resulting system is highly complex and intrinsically out-of-equilibrium: one speaks of an **active** system.

Therefore, the will for a minimal model justifies a macroscopic description of the actin cytoskeleton, that needs to be able to capture its distinctive features. We choose to use an active polar gel description. It consists in considering the system on large length and long time scales compared to the cross-linking dynamics, so that the cytoskeleton is described as a continuum depending on macroscopic variables. This theory, already applied to the study of liquid crystals [De Gennes and Prost, 1993], is based on conservation laws and symmetry properties. It does not rely on any detailed microscopic description, and ought to be **generic**. The small set of phenomenological physical parameters involved allows for a simple framework and eventually a phase space description. However, if they are accessible using experimental data, their dependance on biological conditions can be hard to understand. In the case of cell migration, even if the cross-linking dynamics is neglected, this theory has helped to explain the retrograde flow of actin, to build a qualitative description of an advancing lamellipodium, and to estimate active stresses on the keratocyte

cell [Joanny and Prost, 2009].

In the following, we will briefly present the basis of the active polar gel theory. In our minimal approach however, simplifying assumptions will be made.

The cytoskeleton dynamics is regulated at a smaller scale by molecular reactions, that control filaments branching, polymerization and depolymerization. It also exerts a feedback on the dynamics of some molecules that can bind to actin filaments. We discuss now our choice for the interaction between the cytoskeleton and the molecular scale.

Interaction with molecular dynamics The model being generic, it makes it possible to choose several interaction laws depending on the cell type, and on the molecules described in the system.

It is known that a large number of molecular complexes interact and form signalling pathways that regulate cellular functions related to motility. Their architecture is redundant and variable among cell types. As a minimal approach, we choose to consider a single generic molecule as a marker of cell polarisation: its aggregation in a part of the membrane characterizes the rear of the cell. This marker could be an antagonist to polymerization-inducing molecules (Rac1, Cdc42), such as RhoA, Arpin, or even myosin II (see Dang et al. [2013]; Krause and Gautreau [2014]).

It has been observed that some molecules can bind to actin filaments. Furthermore, polymerization on the cell edge combined with depolymerization, and eventually with myosin-mediated contraction, induce an **inward actin flow**. Hence, the advection of rear markers by actin flows away from the membrane can durably modify their spatial repartition. For markers of polarisation, interaction with actin flows is therefore a part of the polarisation-enhancing machinery. We choose to describe this process in our model, as a minimal interaction between actin and the molecular scale.

This mechanism was proposed in Maiuri et al. [2015] as an explanation for a generic feature of cell migration: the Universal Coupling between cell Speed and Persistence (UCSP). Based on an extensive set of experimental measures for different cell types, migration modes, and experimental settings, it was observed that faster cells have more directional trajectories. This work will be detailed further on. Furthermore, the model will make it possible to testing this explanation.

The plan of this chapter is as follows: in section 5.2, we introduce the active gel approach used to describe the cytoskeleton. In section 5.3, we develop three studies related to a minimal description of the cytoskeleton, as well as the work of Maiuri et al. [2015] on the UCSP. Then, in section 5.4, we construct a free boundary problem that accounts for the fluid description and the interaction with the marker. Finally, in section 5.5, we pursue a similar construction for a domain of fixed circular shape. Formulation in a one-dimensional setting is also given.

5.2 The cytoskeleton as an active polar gel

We introduce here the main principles of a hydrodynamic description of the actin cytoskeleton as an active polar gel, before introducing some works made using this approach. Our modelling approach will be detailled in a next section.

As a passive material, the cross-linked network of actin filaments has been described as a **viscoelastic gel** [De Gennes, 1979; Head et al., 2003; Wilhelm and Frey, 2003]. At short time scales, it behaves as an elastic solid characterized by a finite elastic shear modulus $E = 10^3$ Pa [MacKintosh et al., 1995; Wottawah et al., 2005]. At long time scales, it behaves like a fluid of viscosity η.

We use the simplest viscoelastic model, that is the Maxwell model. It corresponds to an elastic spring of elastic modulus E, connected in series with a purely viscous dashpot of viscosity η (see figure 5.2). The total strain then writes $\varepsilon = \varepsilon_e + \varepsilon_v$, with ε_e its elastic part and ε_v its viscous part. Its total stress σ is defined by $\sigma = E\varepsilon_e = \eta\varepsilon_v'(t)$. It can be shown that the corresponding characteristic equation writes

$$\tau_{\text{visc}} \frac{\mathrm{d}\sigma}{\mathrm{d}t} + \sigma = \eta \frac{\mathrm{d}\varepsilon}{\mathrm{d}t},$$

with $\tau_{\text{visc}} = \frac{\eta}{E}$ the viscoelastic response time of the gel. For time scales larger than $\tau_{\text{visc}} = \frac{\eta}{E}$, the cytoskeleton behaves as a fluid. It is generally closely related to the lifetime of cross-links in the network, and has been estimated in the range of 10 s [Wottawah et al., 2005]. As a consequence, under our hypothesis of large time scales, the short term elastic response of the gel is negligible, and we describe the actin cytoskeleton as a fluid of viscosity η. We deduce that $\eta \sim 10^4$ Pa · s.

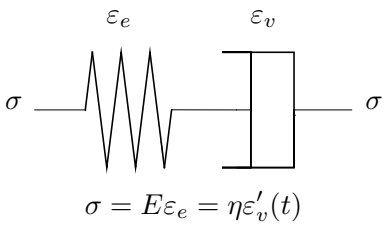

Figure 5.2 – The Maxwell viscoelastic model.

Now, its intrinsic polarity and out-of-equilibrium state requires a complement in the description. The active gel theory is an answer to that need, as the fluid's constitutive equations contain the polar and active characteristics. We refer to Joanny and Prost [2009]; Jülicher et al. [2007]; Kruse et al. [2005]; Prost et al. [2015] for a complete description of these issues.

Active polar gel theory

The cell interior can be roughly decomposed as the cytoskeleton and its solvent, the cytosol. This fluid surrounds actin filaments, and contains the diffusing actin monomers. Some fluid descriptions of the cell use a two-components theory to take into account both media and their interaction, polymer-solvent friction forces. This is the case for example for a cell using amoeboid migration in confinement [Callan-Jones and Voituriez, 2013]. In our case, actin-based motility is based on large friction forces arising between the actin filaments and the substrate. In that condition, the respective importance of both forces can be estimated: as explained in Kruse et al. [2006]; Prost et al. [2015], the friction generated by the cytosol flow through the actin network is negligible for a length scale smaller than 100 µm. Cells having generally smaller sizes, a **one component theory** is acceptable in this work.

Building a **linear hydrodynamic theory** consists in identifying conserved quantities and the relevant fluxes in the system. Each flux can be expressed as a function of a conjugate force. Expanding these expressions and keeping only the lower linear terms leads to a dynamical description of the gel. Let us give now some examples of constitutive equations for different fluids.

→ For a **simple isotropic fluid** of viscosity η, such as water, its stress tensor σ is considered as a flux. The corresponding force is its velocity gradient ∇u. Hence, we have $\sigma = \eta(\nabla u + {}^t\nabla u)$, with η the viscosity.

→ Consider now a **polar liquid**, that is to say a liquid composed of polar molecules. The orientation is described by a polarisation vector field denoted $\mathbf{p}$, giving the local mean orientation of molecules. Its rate of change $\partial\mathbf{p}/\partial t$ is identified as a flux. In reaction to any perturbation, a torque acts to drive the field back to equilibrium, and corresponds to an orientational field $h = K\Delta\mathbf{p}$. The gel description is then enriched with the flux/force couple $(\partial\mathbf{p}/\partial t,\, h)$.

Remark 15. *It is known that at the front of a cell crawling on a substrate, the actin filaments grow against the membrane with a mean orientation of $\pm 35°$ from the normal direction to the edge [Svitkina and Borisy, 1999]. Hence the corresponding polarisation vector is oriented in the normal direction from the cell edge.*

→ The **cytoskeleton** is a polar gel that has an intrinsic activity, as treadmilling and the molecular motors activity consumes energy by ATP hydrolysis. The corresponding flux is the ATP consumption rate, and its conjugate force is the so-called active stress $-\zeta\delta\mu\mathbf{M}$ with $\mathbf{M}$ a non-diagonal tensor, non-zero only in the radial direction. The parameter ζ is called the activity coefficient. This stress corresponds to the differences between the chemical potential of ATP and the ones of its hydrolysis products (ADP and inorganic phosphate). Experimentally, it is observed that the active stress is contractile in the direction of polarisation, and dilative in the perpendicular direction. Therefore, the interaction between the dynamics of $\mathbf{p}$ and the one of the active stress is intricate. Experimental measures yield $-\zeta\delta\mu = 10^3$ Pa for the keratocyte's lamellipodium [Jülicher et al., 2007].

The linear hydrodynamic theory for active polar gels is based on the description of three fluxes: the stress tensor σ, the polarisation field's evolution rate $\partial\mathbf{p}/\partial t$, and the ATP consumption rate. Nevertheless, the theory comprises some limitations. For example, the *stochastic fluctuations* associated with intracellular active processes (treadmilling, myosin-motors activity) are not included, as more generally non-mechanical processes (signalling pathways). Also, a *linear theory* implicitly assumes that the system is close to thermodynamical equilibrium, which is not realistic for an active matter. These non-linear features can therefore be added arbitrarily when needed.

Even if the description of the cytoskeleton as an active gel constitutes the basis of our model, the complete theory is far too complex for our minimal approach. In the construction of the model, we will make simplifying assumptions in particular on the intrinsic activity and the polarity of the cytoskeleton. Such assumptions were already made in several works on migration, that we briefly consider now.

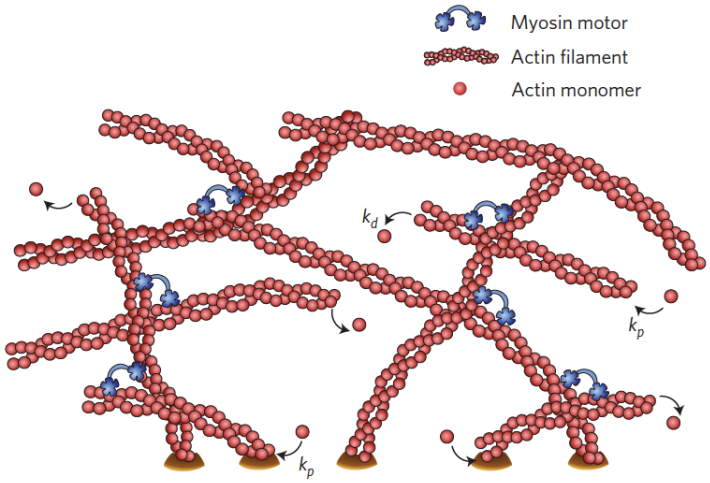

Figure 5.3 – Illustration of the structure of an actin filaments cross-linked network with polymerization at rate k_p, depolymerization at rate k_d, and myosin motors. Reprinted by permission from Macmillan Publishers Ltd: Nature Physics [Prost et al., 2015], copyright 2015.

5.3 Existing works

We introduce now three works on cell motility that used polar active gel theory, in a minimal approach. We briefly account here the main results of these three works, and recall the modelling assumptions that were made.

We will also present the paper of Maiuri et al. [2015] on the Universal Coupling between cell Speed and Persistance (UCSP).

5.3.1 A minimal model for cell lamellar fragments, Callan-Jones et al. [2008]

In this work, Callan-Jones et al. are interested in identifying minimal mechanisms responsible for **shape polarisation** that occurs before motion. This phenomenon, observed for cells, was also witnessed for cell fragments containing only the actin cytoskeleton and myosin motors. Hence, they proposed a simplified model for such a cell fragment based on the active polar gel theory.

As a cell fragment is very thin and shows little thickness variation, they assume a **constant thickness** and neglect all processes eventually occurring in this direction. The cytosol, actin cytoskeleton, monomers and molecular motors are described as a **one component gel**. This assumption was justified in section 5.2 by the fact that the friction generated by the cytosol flow through the actin network is negligible at this scale. Moreover, the short term elastic response is neglected, and the fluid is considered as **non inertial, newtonian and incompressible**, with a **constant and homogeneous density**. The authors neglect the dynamics of the polarisation field, as it seems not relevant for their purpose of linear stability analysis. Therefore, **p** is **uniform, normalized, and radially oriented at the boundary**.

Finally, actin polymerization is mediated by activators such as WASP proteins, preferentially located along the cell membrane [Ridley, 2011]. Therefore, polymerization is supposed to occur at the cell edge, and in the normal direction, following the polarisation field. Depolymerization occurs in the cell bulk, and is assumed uniform in space, and of rate k_d.

Constitutive equations

Denote $\Omega \subset \mathbb{R}^2$ the two-dimensional description of the cellular domain, that is a function of time. We denote $\Omega(0)$ the initial domain, a disc of radius $R > 0$. The actin cytoskeleton is modeled by a single-component 2D fluid bounded by a membrane. For ρ the actin density (assumed constant) and u the flow velocity, the continuity equation writes

$$\nabla \cdot (\rho u) = -\rho k_d \quad \text{in } \Omega(t)\,.$$

Moreover, the velocity of the domain's boundary $V_{\partial\Omega}$ has a prescribed normal component:

$$V_{\partial\Omega} \cdot \mathbf{n} = u \cdot \mathbf{n} + v_p\,,$$

with v_p the polymerization speed.

The momentum equation describes an isotropic viscous fluid of viscosity η, having an additional active term in the radial direction to account for the actin of myosin on filaments along the polarisation field:

$$\sigma = \eta(\nabla u + {}^t\nabla u) - P\mathrm{Id} - \zeta\delta\mu\mathbf{M}\,,$$

with P the fluid pressure. Force balance at low Reynolds number applied on the fluid yields

$$-\nabla \cdot \sigma = -\xi u\,,$$

with ξ a friction coefficient characterizing the interaction between the actin filaments and the substrate. After non-dimensionalization, the respective scale of viscosity and friction is quantifies by the parameter $\lambda^2 = \eta/\xi R^2$. A large value for λ^2 means a predominent viscosity over friction, while low values of λ^2 are characteristic of friction-dominated systems. Experimental values give $\eta = 10^4\mathrm{Pa}\cdot\mathrm{s}$ [Wottawah et al., 2005], $\xi = 10^5 - 10^7\mathrm{Pa}\cdot\mathrm{s}/\mu\mathrm{m}^2$ for keratocytes [Dembo and Wang, 1999; Oliver et al., 1999; Theriot and Mitchison, 1992], and $R = 1 - 10\mu\mathrm{m}$. Overall, $\lambda^2 \sim 10^{-1} - 10^{-5}$, justifying the large friction limit leading to a Darcy flow hypothesis:

$$u \sim -\lambda^2 \nabla P\,.$$

Using linear stability analysis of an initially circular shape, the authors were able to show that polymerization and a large friction were sufficient to make the circular cell fragment linearly unstable. In particular, the instability does not depend on cell signalling or on the molecular motors.

5.3.2 On the impact of the polarisation field Ben Amar et al. [2011]

This paper is based on the previous work of Callan-Jones et al. [2008], and explores the impact of the orientational order of actin filaments in the dynamics, that brings an intrinsic symmetry breaking in the system. Indeed, it is observed experimentally that shape bifurcation is coupled to a reorganisation of the cytoskeleton. Hence, they study the case of a boundary layer accounting for a disoriented cortex, and either an isotropic or fully oriented core. These assumptions bring non linear terms in the active gel formulation.

Modelling hypothesis

The actin cytoskeleton is assumed to be a incompressible newtonian fluid in three dimensions. Assuming that the layer thickness is constant, and that any effect in this direction is negligible, the model is reduced to a two-dimensional description.

Constitutive equations

The continuity equation writes

$$\partial_t \rho + \nabla \cdot (\rho u) = -\rho k_d + \rho \mathcal{F} V_p \mathbf{n} \delta((r - r_{int}) \cdot \mathbf{n}) \,, \quad \text{in } \Omega(t) \,,$$

with u the velocity of actin in the moving frame, V_p the polymerization velocity, r_{int} the position of a point at the interface. The dimensionless shape function $\mathcal{F}$ accounts for the fact that the actin density at the border may vary from point to point. It can be expressed as a function of the local curvature. Assume that the fluid density is now constant. Then, mass conservation and integration of the continuity equation locally around the border and in the bulk give

$$\begin{aligned} k_d |\Omega| &= V_p \int_{\partial\Omega} \mathcal{F} \, \mathrm{d}s \,, \\ V_{\partial\Omega} \cdot \mathbf{n} &= u \cdot \mathbf{n} + \mathcal{F} V_p \quad \text{on } \partial\Omega(t) \,, \\ \nabla \cdot u &= -k_d \quad \text{in } \Omega(t) \,, \end{aligned}$$

where $V_{\partial\Omega}$ is the local boundary velocity, and we write $u_n = u \cdot \mathbf{n}$. The detailed calculations will be found in subsection 5.4.1. The kinematic boundary condition states that the normal displacement of the boundary (hence the cell motion) at velocity $V_{\partial\Omega} \cdot \mathbf{n}$ does not follow the actin flows normal displacements (at velocity $u \cdot \mathbf{n}$): actin polymerization induces an additional movement with velocity $\mathcal{F} V_p$.

Force balance equation For an isotropic homogeneous fluid, the momentum equation writes

$$-\nabla P - \xi u + \eta \Delta u = 0 \,.$$

Adding an *isotropic* diagonal active stress $-\zeta \delta \mu \mathrm{Id}$ inside the cell does not change this equation since its divergence is zero. However, the boundary conditions are affected:

$$V_{\partial\Omega} \cdot \mathbf{n} = u \cdot \mathbf{n} + \mathcal{F} V_p \quad \text{on } \partial\Omega(t) \,, \tag{5.1}$$

$$\sigma_{nn} = -P + 2\eta \frac{\partial u_n}{\partial n} = \zeta \delta \mu \,, \tag{5.2}$$

$$\sigma_{ns} = \eta \left(\frac{\partial u_n}{\partial s} + \frac{\partial u_s}{\partial n} - |\kappa| u_s \right) = \zeta \delta \mu \,, \tag{5.3}$$

with κ the local curvature of the boundary.

Laplacian law with $\eta = 0$ Surface tension appears from a Laplace law for the pressure. In this case, the equation on σ_{nn} admits an additional term $\gamma\kappa$, where γ is the surface tension and κ the boundary curvature. Such a choice will be justified in the construction of our free boundary model. Moreover, as explained before, in the large friction regime we can assume $\eta = 0$ and the flow velocity follows a Darcy law. Then, the equation on σ_{ns} can be ignored. In this case we can write $u = -1/\xi \nabla P$ such that the continuity equation $\nabla \cdot u = -k_d$ rewrites as a Poisson equation

$$\Delta P = \xi k_d \,.$$

This problem is close to the sliding drop problem in a partial wetting setting studied in Ben Amar et al. [2003]. It was proved in Ben Amar et al. [2011] that the model is sufficient to explain a sustained motile state.

5.3.3 Spontaneous motility of actin lamellar fragments Blanch-Mercader and Casademunt [2013]

In this work, Blanch-Mercader and Casademunt performed a nonlinear analysis of the minimal model proposed by Callan-Jones et al. [2008], for which linear instability of the circular shape was proved. They promote this morphological instability together with large friction forces, polymerization dynamics and shape as a minimal mechanism for motility. Neither molecular motors, global polarisation of the filaments nor any implicit symmetry breaking factors are necessary to provide spontaneous motion, even if they may improve motility in real cells.

They also provide a simple relation between shape and the cell's center of mass velocity, from which emerge a bifurcation phenomenon from static configurations to motile traveling solutions.

Let us know recall the modelling choices made.

Modelling hypothesis

As in Callan-Jones et al. [2008], the actin lamellar fragment is assumed of constant thickness, and is modeled by a single-component 2D fluid bounded by a membrane. The short-term elastic effect is neglected, as well as the polarisation field dynamics and the molecular intrinsic activity.

Polymerization occurs at the membrane with uniform velocity v_p, in the normal direction to the edge, whereas depolymerization occurs uniformly in the domain with constant rate k_d. In the large friction regime, one has $u = -1/\xi \nabla P$, and

$$\nabla \cdot u = -k_d \quad \text{in} \quad \Omega(t)\,, \tag{5.4}$$

$$V_n = u \cdot \mathbf{n} + v_p \quad \text{on} \quad \partial\Omega(t)\,, \tag{5.5}$$

$$P = -\gamma\kappa \quad \text{on} \quad \partial\Omega(t)\,, \tag{5.6}$$

assuming a Laplace law for the pressure at the boundary. We have assumed that the external medium is a fluid with a zero pressure. We denoted γ the surface tension of the interface, and κ its curvature.

Equation on centers of mass

Now let us briefly present the simple equation obtained in the paper relating the area of $\Omega(t)$, $A(t)$, its center of mass, $R_A(t)$, and the contour center of mass $R_L(t)$, for a boundary of length $L(t)$.

By definition,

$$\frac{\mathrm{d}}{\mathrm{d}t}(A(t)R_A(t)) = \frac{\mathrm{d}}{\mathrm{d}t}\int_{\Omega(t)} z \,\mathrm{d}a = \int_{\partial\Omega(t)} z V_n \,\mathrm{d}l\,,$$

for $z = x + iy$. Using equation (5.5) and the mass balance equation $A'(t) = v_p L - k_d A$, one has

$$R_A'(t) = \frac{v_p L}{A}(R_L - R_A)\,. \tag{5.7}$$

It is now clear how the geometric asymmetry is related to the center of mass velocity. A stationary motile shape corresponds to a configuration where $R_L \neq R_A$, for which we have $R_A'(t) = V_{\text{cell}} = k_d(R_L - R_A)$.

This work provides a minimal system for sustained motile shapes, based on the relative asymmetry between the center of mass of the domain and the center of mass of its boundary, accounting respectively for depolymerization and polymerization geometric centers.

Spontaneous motion occurs as a result of the instability of the initial shape. However, as precised in the paper, the motile shapes and velocities obtained furnish qualitative proofs of principle rather than realistic cell shapes. Enhancement in that direction would arise from extension of the model.

Up to now, we have developped some physical approaches aiming at capturing the active character of the cytoskeleton, and the resulting instabilities. Let us now focus on the interaction between the cytoskeleton and the molecular scale. It was studied in Maiuri et al. [2015] in a physical model, and was proven enough to explain the positive correlation that exists between cell speed and its persistance, cited before as the UCSP. In the following, we detail the interdisciplinary work that gave rise to the UCSP.

5.3.4 A universal law for cell migration Maiuri et al. [2015]

We introduce now the work of Maiuri et al. [2015], that put to light a generic positive coupling between cell speed and persistence.

Discovering the UCSP

The First World Cell Race took place in 2011, when 54 different adherent cell types performed a one dimensional migration assay on adhesive tracks [Maiuri et al., 2012]. Experimental measures showed a positive correlation between the global averaged values of persistence time τ of the trajectories and the mean linear instantaneous cell speed v. Such a result on such an extensive cell zoology suggested a strong common process between these cell types.

The authors then performed further experiments to investigate this correlation at the single cell level. For that purpose, cells having mesenchymal (hTERT-immortalized retinal pigment epithelial cells, RPE1) and amoeboid (bone marrow dendritic cells, BMDC) migration modes were used on various experimental settings: for one dimensional migration, adhesive tracks and microchannels, and for two dimensional migration, adhesive non confined and confined configurations. A population-specific exponential correlation was observed for low velocities: $\tau = Ae^{\lambda v}$, for $(A,\, \lambda) \in \mathbb{R}^2$.

Further experiments on complex geometries confirmed this observation: BMDCs migrating in a 3D collagen gel, and macrophages *in vivo* in Medaka fish. Overall, by the diversity of cell types and migration settings employed, this coupling was qualified as *universal*.

Coupling actin flow velocity and persistence time

In order to explain the UCSP, the authors pointed out that a conserved aspect of migration ought to be responsible for the coupling. Actin retrograde flow can be witnessed in all cell types, either in the whole cell (amoeboid migration) or only in its protrusive parts (mesenchymal migration). Experimental proof of its implication in the UCSP required the use of mature BMDCs. Indeed, it is known for these cells that modulating the substrate's adhesiveness also modifies the actin retrograde flow velocity, without affecting cell speed [Renkawitz et al., 2009]. A cell type-dependent linear relation exists between the cell velocity v and the actin retrograde flow velocity u, for low velocities:

$$v = \alpha u\,,$$

where α is a dimensionless parameter that quantifies friction, and is specific of the experimental conditions. Therefore, modifying α leads to an adaptation on the retrograde flow so that v stays constant.

Moreover, the cell velocity can be modulated by a pharmacological control on the acto-myosin contractility, and by a control of the temperature. Overall, the influence of both velocities can be investigated independently.

Measures were taken for 9 experimental conditions. They highlighted an exponential correlation between the mean persistence time and the mean retrograde velocity among each setting: $\tau = A' e^{\lambda' u}$, whereas no correlation was witnessed between τ and v. This experiment suggested that the UCSP can be explained by a more specific **coupling between cell persistence and actin flows velocity**.

Moreover, it was measured that faster actin flows were combined with less protrusions, but larger and more stable in time, with a lifetime τ_p characterizing the polarisation time. Measures of τ_p showed an exponential correlation with u. Therefore, **actin flows favor a stable polar configuration** of the cell, leading to more persistent trajectories.

Effect of actin flows on polarity cues

A proposed explanation is that actin flows reinforce cell polarity by advection of polarity cues. These cues may depend on the cell type, and impact the myosin or microtubules activity for example.

In a simple 1D model, the authors consider the advection-diffusion of a marker on the cell domain $\Omega =]0, L[$, for $L > 0$, that is in translation with velocity v. For $t > 0$ and $\mathbf{x} \in \Omega$, write $c(t, \mathbf{x})$ for the marker's concentration, and assume it is a rear marker. Then, for a constant velocity u, at steady state, the concentration profile is exponential

$$\overline{c}(\mathbf{x}) = C e^{-\frac{u\mathbf{x}}{D}} ,$$

with D the diffusion coefficient. Hence, according to this model, the retrograde flow velocity is responsible for the steepness of the concentration profile.

Experiments on mBMDCs were performed to measure the concentration profile for various markers and retrograde velocities. They showed that only molecules with high actin affinity saw their concentration profile get steeper. Therefore, experimental results agree with the hypothesis of advection of polarity markers by actin flows.

A general physical model

In order to push further the theoretical analysis, the advection-diffusion problem for the marker is generalized to two dimensions, and coupled to a stochastic polar equation for the actin velocity $\mathbf{U}$, vector of modulus u and polar angle ϕ. Note that $\mathbf{U}$ accounts for a space-averaged actin flow, and that its stochastic dynamics is prescribed phenomenologically.

For a given concentration profile, the mean actin flow modulus is phenomenologically written as

$$u^* = \beta(c^*(t, 0) - c^*(t, L)) ,$$

where the one dimensional notation accounts for the polarity axis of the cell. The coefficient β accounts for the tightness of the correlation between the actin flow and the asymmetry in the polarity cue. It can also be interpreted as the maximal possible velocity for the flow. The notation c^* is for the concentration of activated markers that exert a feedback on the flow. Its expression is a Hill response function of index n, and with a saturation treshold for activation C_s:

$$c^*(t, \mathbf{x}) = \frac{c^n(t, \mathbf{x})}{C_s^n + c^n(t, \mathbf{x})} .$$

The parameter C_s can be interpreted as a maximal concentration of activated molecules.

Resolution The typical diffusion time of the markers over the cell length is in the order of seconds, while the typical time scale for actin flows is in the order of minutes. Therefore, the advection-diffusion problem is taken at steady state. The problem on u is then linearized and gives rise to a SDE on u, or on v assuming $v = -u$.

Classical steps allow to obtain a Fokker-Planck equation on the cell velocity distribution. Now, the steady state is characterized by an explicit effective potential $W(v)$, from which one obtains analytically the polarisation time $\tau_p(v)$ as the mean first-passage time to the $\{v = 0\}$ state. The persistence time of trajectories $\tau(v)$ is obtained numerically using the autocorrelation function.

These results can be fitted by exponential function: τ, $\tau_p \simeq Ae^{\lambda v}$, for $0.7 \lesssim n \lesssim 1.5$. Finally, this relation was used to successfully fit all the data, reproducing the UCSP law and therefore validating the model.

Generic phase diagram of cell migration patterns

The analysis of the linearized problem on (U, ϕ) leads to a phase diagram of migration patterns depending on two parameters: β, the maximal actin flow, and C_s the maximal concentration in activated markers. For each couple (β, C_s), there exists critical values ($\overline{\beta}(C_s)$, $\overline{C_s}(\beta)$) splitting the phase space of migratory behaviours into three parts:

- for $\beta < \overline{\beta}(C_s)$, trajectories are **Brownian**, with a zero mean cell velocity. Actin flows are too slow to sustain an asymmetry in the repartition of the marker.
- for $\beta > \overline{\beta}(C_s)$ and $C_s > \overline{C_s}(\beta)$, the trajectories correspond to a **persistent** random walk, with a non-zero mean velocity, fast actin flows and large concentrations in activated markers.
- for $\beta > \overline{\beta}(C_s)$ and $C_s < \overline{C_s}(\beta)$, actin flows are fast and the concentration in activated markers is low. As a result, fluctuations are large, preventing any asymmetry from being stable in time. The resulting trajectories are **intermittent**, alternating between brownian and persistent phases.

Finally, the phase diagram was confronted to experimental data, and β and C_s alone were enough to get a velocity distribution $\mathcal{P}(v)$ fitting experimental data. This simple framework based on microscopic parameters is an opening towards control of the efficiency of trajectories.

Remark 16. *Saturation effects arise either for large velocities or for large polarisation time τ_p. Explanations can be proposed in both cases. For large velocities, non linear phenomena can happen, such as clutch processes. If the characteristic polarisation time is large enough, that is larger than the characteristic angular diffusion time, the latter is limiting for cell persistence.*

This work provides a powerful idea of a universal mechanism for cell migration, and allows further analysis of cell trajectories from microscopic features. However, the actin flows were described as averaged in space, and following a phenomenological, although realistic description. With that in mind, we developped a fully two-dimensional free boundary problem based on the association of the fluid description of the cytoskeleton and the same interaction with the microscopic scale: actin flows are able to transport molecular markers of polarisation away from the polymerizing edges, following the cell geometry. Moreover, the concentration of markers on the cell membrane acts on the fluid flow from the boundary, closing the feedback system. Therefore, we proposed an enriched minimal model containing geometric and molecular feedbacks.

5.4 The free boundary model

5.4.1 The fluid problem

We start from the same modelling assumptions as in Blanch-Mercader and Casademunt [2013]. We consider the cell as a 2D domain, where the motility material (actin cytoskeleton, monomers, cytosol) is modeled by a one-component viscous fluid bounded by a membrane (see 5.2 about the single-component assumption). More precisely, no thickness effect nor myosin-related activity are taken into account. The polarisation field $\mathbf{p}$ is taken constant, of unit norm, and normally oriented at the boundary: we neglect its dynamics in the following. Finally, the short-time elastic response of the actin gel is also neglected, as we consider time scales larger than the characteristic viscoelastic relaxation time τ_{visc}.

Continuity equation

Write $\rho : [0, +\infty) \times \mathbb{R}^2 \to \mathbb{R}_+$ the density of actin filaments, $\Omega(t) = \{\rho(t, \cdot) > 0\} \subset \mathbb{R}^2$ for the cellular domain at time $t \geq 0$, and $U : [0, +\infty) \times \Omega \to \mathbb{R}^2$ the local actin velocity. We assume that $\Omega(0)$ is a disc of radius $R > 0$. By its definition, $\Omega(\cdot)$ is a domain with moving boundary. We denote $V_{\partial\Omega} : \partial\Omega \to \mathbb{R}^2$ the boundary velocity, and $V_n = V_{\partial\Omega} \cdot \mathbf{n}$ the normal velocity of the boundary. Let us construct formally the model in $\Omega(t)$, regardless of the boundary regularity.

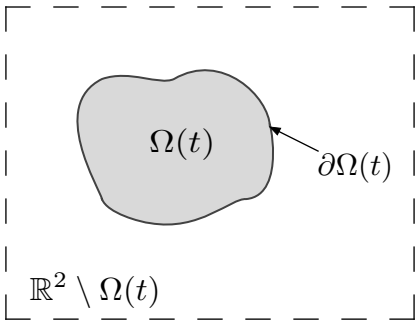

Figure 5.4 – The cell domain.

As the actin polymerization activators WASP are preferentially located on the cell membrane, we assume that polymerization occurs on $\partial\Omega$ (see Ridley [2011]), at rate v_p. Moreover, polymerization occurs following the polarisation field $\mathbf{p}$, hence normally to the cell edge. Uniform depolymerization inside the domain occurs with rate K_d. Then, writing $\mathrm{d}H^1_{\partial\Omega(t)}(\mathbf{X})$ for the one-dimensional Hausdorff measure, continuity equation writes

$$\frac{\partial}{\partial t}\rho + \nabla \cdot (\rho U) = -\rho K_d + \rho v_p \, \mathrm{d}H^1_{\partial\Omega(t)}(\mathbf{X}) \,. \tag{5.8}$$

Remark 17. *Compared to Ben Amar et al. [2011], we also neglect the shape factor $\mathcal{F}$ for polymerization, and write directly v_p for the polymerization rate.*

Remark 18. *A more realistic assumption would be to consider that the polymerization process occurs on a band of constant width $\lambda > 0$ at the boundary.*

Write φ a test function with compact support in $\mathbb{R}_+ \times \mathbb{R}^2$. Then, the corresponding weak formulation writes

$$-\int_0^\infty \int_{\mathbb{R}^2} \rho \left[\frac{\partial \varphi}{\partial t} + U \cdot \nabla \varphi - k_d \varphi \right] \mathrm{d}\mathbf{X} \, \mathrm{d}t = \int_0^\infty \int_{\partial\Omega(t)} \rho v_p \varphi \, \mathrm{d}H^1(\mathbf{X}) \, \mathrm{d}t \,. \tag{5.9}$$

Since $\rho = 0$ outside $\Omega(t)$, we also have

$$-\int_0^\infty \int_{\Omega(t)} \rho \left[\frac{\partial \varphi}{\partial t} + U \cdot \nabla \varphi - k_d \varphi \right] \, \mathrm{d}\mathbf{X} \, \mathrm{d}t = \int_0^\infty \int_{\partial\Omega(t)} \rho v_p \varphi \, \mathrm{d}H^1(\mathbf{X}) \, \mathrm{d}t \,.$$

We use a formal integration by parts to get

$$\begin{aligned} -\int_0^\infty \int_{\Omega(t)} \rho \frac{\partial \varphi}{\partial t} \, \mathrm{d}\mathbf{X} \, \mathrm{d}t - \int_0^\infty \int_{\partial\Omega(t)} \varphi \rho U \cdot \mathbf{n} \, \mathrm{d}H^1(\mathbf{X}) \, \mathrm{d}t \\ \underbrace{+ \int_0^\infty \int_{\Omega(t)} \varphi \nabla \cdot (\rho U) + K_d \rho \varphi \, \mathrm{d}\mathbf{X} \, \mathrm{d}t}_{= -\int_0^\infty \int_{\Omega(t)} \varphi \frac{\partial \rho}{\partial t} \, \mathrm{d}\mathbf{X} \, \mathrm{d}t} = \int_0^\infty \int_{\partial\Omega(t)} \rho v_p \varphi \, \mathrm{d}H^1(\mathbf{X}) \, \mathrm{d}t \,. \end{aligned}$$

Now, we use the formula $\frac{\mathrm{d}}{\mathrm{d}t} \int_{\Omega(t)} \phi \, \mathrm{d}\mathbf{X} = \int_{\Omega(t)} \frac{\partial \phi}{\partial t} \, \mathrm{d}\mathbf{X} + \int_{\partial\Omega(t)} V_n \phi \, \mathrm{d}H^1(\mathbf{X})$, where V_n is the normal component of the boundary velocity:

$$V_n = V_{\partial\Omega(t)} \cdot \mathbf{n} \,. \tag{5.10}$$

For a test-function that does not vanish on $\partial\Omega(t)$, we get a characterization of V_n that defines the free boundary motion:

$$\int_0^\infty \int_{\partial\Omega(t)} \phi(\rho V_n(\mathbf{X}) - \rho U \cdot \mathbf{n}) \, \mathrm{d}H^1(\mathbf{X}) \, \mathrm{d}t = \int_0^\infty \int_{\partial\Omega(t)} \rho v_p \varphi \, \mathrm{d}H^1(\mathbf{X}) \, \mathrm{d}t \,.$$

Moreover, using a test function with compact support in $\Omega(t)$ for the main equation, we find that equation (5.8) is equivalent to the following free boundary problem:

$$\begin{aligned} \frac{\partial}{\partial t}\rho + \operatorname{div}(\rho U) &= -\rho K_d \qquad \text{in } \Omega(t) \,, & (5.11) \\ \rho V_n - \rho U \cdot \mathbf{n} &= \rho v_p \qquad \text{on } \partial\Omega(t) \,, & (5.12) \end{aligned}$$

where $\mathbf{n}$ is the outward unit normal vector to $\Omega(t)$, and the free boundary's motion is prescribed by equation (5.12).

Finally, we also assume that the actin density is constant in time and space, so that

$$\begin{aligned} \operatorname{div}(U) &= -K_d \qquad \text{in } \Omega(t) \,, & (5.13) \\ V_n &= U \cdot \mathbf{n} + v_p \qquad \text{on } \partial\Omega(t) \,. & (5.14) \end{aligned}$$

Notice that the actin polymerization dynamics corresponds to non trivial characteristics for the model. Indeed, polymerization corresponds to a direct prescription of the domain's boundary velocity, whereas depolymerization is responsible for a non-zero divergence of the fluid velocity field.

Momentum equation

In the limit of low Reynolds number, viscous forces dominate over inertial forces and the momentum equation reduces to the force balance principle:

$$-\operatorname{div} \sigma = f \qquad \text{in } \Omega(t) \,, \tag{5.15}$$

where f is a body force, and the stress tensor, σ, is given by

$$\sigma = \eta \left(\nabla U + {}^t\nabla U \right) - P \, \mathrm{Id} \,, \tag{5.16}$$

with η the viscosity, P the fluid pressure. Since the layer is placed on a substrate, a mechanical interaction arises from the transient formation of adhesion complexes between the actin filaments and the substrate. Despite the active nature of the adhesion dynamics, this phenomenon can be approximated by a passive friction force (see remark 20 below):

$$f = -\xi U\,, \tag{5.17}$$

where ξ is the effective friction coefficient It yields

$$-\eta\Delta U + \nabla P = -\xi U\,. \tag{5.18}$$

Remark 19. *As U is a vector field, we have*

$${}^t\nabla U = \begin{pmatrix} \frac{\partial U_1}{\partial x_1} & \frac{\partial U_2}{\partial x_1} \\ \frac{\partial U_1}{\partial x_2} & \frac{\partial U_2}{\partial x_2} \end{pmatrix}, \quad \text{and} \quad \nabla\cdot({}^t\nabla U) = \begin{pmatrix} \frac{\partial^2 U_1}{\partial x_1^2} + \frac{\partial^2 U_2}{\partial x_1 \partial x_2} \\ \frac{\partial^2 U_1}{\partial x_1 \partial x_2} + \frac{\partial^2 U_2}{\partial x_2^2} \end{pmatrix}.$$

Now, assuming $\nabla\cdot U = A$, with $A \in \mathbb{R}$, we can deduce that $\nabla\cdot({}^t\nabla U) = \begin{pmatrix} 0 \\ 0 \end{pmatrix}$.

Remark 20. *Write a for the size of an adhesion molecule (for example an integrin), and τ its mean lifetime. Then if the cell velocity relative to the substrate v verifies $v << a/\tau$, then the adhesion force is similar to a friction force [Kruse et al., 2006].*

Let us briefly consider non-dimensionalization of equation (5.18). For $\overline{V} = v_p$ the polymerization velocity, $\overline{L} = R$, $\overline{F} = \xi v_p$ and $\overline{P} = \frac{\overline{F}\overline{L}^2}{\overline{L}} = \xi v_p R$, we get

$$\nabla P - \lambda^2 \Delta U = -U$$

with $\lambda^2 = \eta/\xi R^2$ defined in 5.3.1 (see Callan-Jones et al. [2008]), and for which experimental values yield $\lambda^2 \sim 10^{-1} - 10^{-5}$. As a consequence, we effectively neglect the viscosity related to polymer-polymer and polymer-cytosol interaction.

For $\eta \to 0$, force balance simplifies to a Darcy law

$$U = -\frac{1}{\xi}\nabla P \qquad \text{in } \Omega(t)\,. \tag{5.19}$$

Boundary condition In order to impose a boundary condition on σ, it is useful to discuss the role of cell membrane in motility.

The cell membrane is a lipid bilayer that acts for the cell physical integrity, and in numerous functional processes. Transmembrane proteins are involved in interaction with the external medium, as well as in intracellular biochemical signalling cascades. Molecules can be activated for some function by binding the membrane, that changes their spatial configuration. The actin cytoskeleton also transiently binds, and this close association is responsible for bilateral influence on their respective dynamics.

Cell membrane is particularly active for the regulation of migration and polarisation processes thanks to its tension. Membrane tension is defined as a resistance to an increase in membrane area. It is based on the quantity of lipids available, and can be regulated due to lipids resources and exo-endocytosis.

The strong interaction with the cytoskeleton leads to mechanical and biochemical feedbacks. For example, it is known that surface tension can block protrusion in a srong adhesion setting, and favor retrograde flows for low adhesion forces. Polarisation is also

reinforced by its effect on protrusions: protruding filopodia-like structures can be forced to coalesce in a single protrusion, preventing the development of multiple lamellipodia. More generally, the relation between membrane tension and motility fits in the framework of the UCSP (see 5.3.4). On the other way, cell spreading by means of adhesion and actin assembly increases membrane tension. More details can be found for example in the review [Sens and Plastino, 2015]. Based on these facts, accounting for membrane tension in our model is natural.

In our model, the cell domain $\Omega(t)$ is implicitly defined as a function of the actin density $\rho(t, \cdot)$. Since the fluid is supposed homogeneous inside $\Omega(t)$, $\rho(t, \cdot)$ is a discontinuous function on $\mathbb{R}^2$. The interface between the cell and the external medium being defined by this discontinuity, membrane thickness is therefore neglected.

Now, imposing a boundary condition on σ ought to characterize the mechanical equilibrium of the membrane. The natural choice is to impose a Laplace law, that is to say a pressure jump in the normal direction between the cell and the external medium, that depends on the membrane's tension and curvature [Sens and Plastino, 2015; Vigneaux, 2007]. For simplicity, we assume that the external pressure is zero. Hence,

$$P = -\gamma\kappa \quad \text{on } \partial\Omega(t)\,, \tag{5.20}$$

with γ the surface tension and κ the local curvature of the boundary.

The final problem

Overall, the global problem is the following:

$$\begin{aligned}
-\Delta P &= -\xi K_d \qquad \text{in } \Omega(t)\,, && (5.21)\\
P &= -\gamma\kappa \qquad \text{on } \partial\Omega(t)\,, && (5.22)\\
V_n &= U\cdot\mathbf{n} + v_p \quad \text{on } \partial\Omega(t)\,, && (5.23)\\
U &= -\frac{1}{\xi}\nabla P \qquad \text{in } \Omega(t)\,. && (5.24)\\
& && (5.25)
\end{aligned}$$

On the definition of velocity In a minimal modeling framework, simplifications may lead to non physical quantities or may inforce phenomenological choices. It is of interest in our case to precise the velocities we consider.

As a cell crawls on a solid substrate, the arising friction may come from two factors: first, from the adhesion dynamics between actin filaments and adhesion molecules attached on the substrate ; then, from the cell membrane rubbing when the cell translocates.

Our modeling approach consists in describing the cell as a fluid on a solid substrate, enclosed by a line membrane. Therefore, the base membrane is not taken into account, nor is the related friction force. As a consequence, we can only take into account the friction related to the actin filaments in this model.

The cell velocity corresponds here to the local displacement of the domain boundary. A global cell velocity may be expressed as the center of mass velocity as in Blanch-Mercader and Casademunt [2013], but has no direct effect on the fluid dynamics.

5.4.2 The molecular marker's dynamics

The main novelty of our work consists in considering the dynamics of a molecule inside the cell, that interacts with the actin cytoskeleton. This choice follows two goals: first, the

spatial repartition of the molecule is correlated to the polarisation process. It therefore serves as a **quantifier for polarisation**. Moreover, we consider a molecule that is part of a **regulatory pathway for the cytoskeleton activity**. As a consequence, the resulting system forms a closed multi-scale self-regulated functional structure. Let us detail now the assumptions we made.

It has been observed in experiments described in Maiuri et al. [2015] that molecules with high-affinity to actin filaments show a steeper concentration profile for higher retrograde flow velocities. Moreover, the same work highlights the positive correlation between retrograde flow velocities and a stable polarised state for the cell. As a consequence, it is natural to consider a molecule whose spatial concentration profile characterizes the polarisation level of the cell: it plays the role of **biological marker** of polarisation. We will assume that it can diffuse in the cell domain, and be transported by the actin filaments, modelled by the previously described fluid.

We have now to precise the role of this molecule in the cell machinery. As proposed in Maiuri et al. [2015], it could be involved in a regulatory pathway for the cytoskeleton dynamics, for example for contractility functions (myosin motors, RhoA), or in the activity of microtubules (see e.g Akhshi et al. [2014]; Machacek et al. [2009]; Sackmann [2015]; Wittmann and Waterman-Storer [2001]). The choice of a molecule and its role being cell type specific, we will work with a generic molecular cue and arbitrarily choose its effect in the regulation of migration.

The accumulation of markers on some part of the membrane ought to reinforce rear-specific functions involved in migration, such as contractility. However, our minimal fluid model for the cytoskeleton only describes actin polymerization, which is characteristic of the cell front. The intracellular activity results partly from signalling pathways, that mediate a global regulation of polarised functions [Ridley et al., 2003]. For example, the Rho family of small GTPases is involved in the regulation of adhesion, protrusion and contraction dynamics. In particular, three molecules arise as key players for the cytoskeleton dynamics: RhoA that promotes the growth of adhesions and contractility, Rac1 that acts on the formation of lamellipodia, and Cdc42 that upregulates polarity and filopodia formation. In a polarized cell, RhoA is generally located at the rear, while Rac1 and Cdc42 are found at the cell front, where they promote polymerization. In particular, RhoA and Rac1 are regulated in antagonist ways [Lawson and Burridge, 2014]. A precise description of their crosstalk is unreachable and would be cell type-specific. Nevertheless, it is reasonable for our work to consider that there exists a molecule that locally inhibits polymerization [Dang et al., 2013]. This way, a simple interaction rule with the actin cytoskeleton closes the feedback loop between elements of the migration machinery: asymmetry in the molecular concentration results in an asymmetric protrusive dynamics, thus reinforcing polarisation.

Write $C : \mathbb{R}_+ \times \Omega(\,\cdot\,) \to \mathbb{R}_+$ for the concentration in marker inside Ω. It is assumed to diffuse and to be transported by the actin filaments at velocity U. The corresponding problem writes

$$\partial_t C(t,\mathbf{X}) + \operatorname{div}\,\left(C(t,\mathbf{X})U(t,\mathbf{X}) - D\nabla C(t,\mathbf{X})\right) = 0 \quad \text{for } \mathbf{X} \in \Omega(t),\, t > 0\,,$$

with the boundary condition

$$\left(C(t,\mathbf{X})U(t,\mathbf{X}) - D\nabla C(t,\mathbf{X})\right)\cdot \mathbf{n} = C(t,\mathbf{X})(U(t,\mathbf{X})\cdot\mathbf{n} + v_p(t,\mathbf{X})) \quad \text{for } \mathbf{X} \in \partial\Omega(t),\, t > 0\,,$$

where $\mathbf{n}$ is the outward unit normal to the boundary and D the cytoplasmic diffusion coefficient. Note that as $v_p \geq 0$ on $\Omega(t)$, we have $V_n \geq U\cdot\mathbf{n}$. This means that polymerization acts for the domain's growth, thus provides extra-space for the marker. The boundary

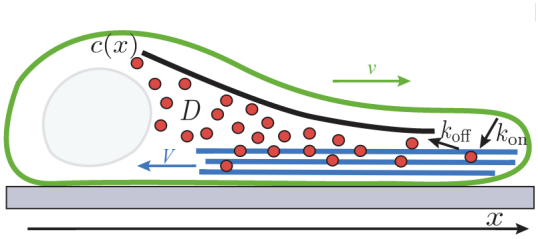

Figure 5.5 – Interaction between actin flows and a molecular polarity marker. The actin network in blue experiences a backward motion with velocity V, whereas the cell moves in the positive direction with velocity v. The molecular marker transiently bind to the actin filaments, leading to a gradient of concentration along the polarity axis. Reprinted from Maiuri et al. [2015], Copyright 2015, with permission from Elsevier.

condition ensures that the diffusion adapts to the changing domain, and that the marker's mass is preserved:

$$\begin{aligned}
&\frac{\mathrm{d}}{\mathrm{d}t}\int_{\Omega(t)} C\,\mathrm{d}\mathbf{X} = \int_{\Omega(t)} \frac{\partial}{\partial t} C\,\mathrm{d}\mathbf{X} + \int_{\partial\Omega(t)} C V_n\,\mathrm{d}H^1(\mathbf{X}) \\
&= \int_{\Omega(t)} -\mathrm{div}\ (CU - D\nabla C)\ \mathrm{d}\mathbf{X} + \int_{\partial\Omega(t)} C(U\cdot\mathbf{n} + v_p)\,\mathrm{d}H^1(\mathbf{X}) \\
&= \int_{\partial\Omega(t)} -(CU - D\nabla C)\cdot\mathbf{n} + C(U\cdot\mathbf{n} + v_p)\,\mathrm{d}H^1(\mathbf{X}) \\
&= 0\,.
\end{aligned}$$

Feedback on the fluid The main novelty of our work is to consider that the polymerization rate v_p is a function of C. In the spirit of Maiuri et al. [2015], we will assume that polymerization occurs more likely at the boundary points where the marker concentration is the lower (the marker inhibits polymerization). Moreover, we choose the simplest expression for this feedback, that is to say a decreasing linear feedback with a treshold: We write $v_p(t,\mathbf{X}) = [\alpha - \beta C(t,\mathbf{X})]_+$ for $\mathbf{X}\in\partial\Omega(t)$, $\alpha,\beta\geq 0$. This choice is acceptable in a first approach for the sake of simplicity. It means that in the absence of marker, polymerization occurs at a constant rate. If the marker's concentration levels rise, then polymerization is slowed down. The coefficient β quantifies the tightness of the feedback of the molecule on the fluid. For low values, the marker can only slow polymerization whereas for higher values this can be stopped.

Recalling what was explained previously, the fluid problem writes

$$\begin{aligned}
-\Delta P(t,\mathbf{X}) &= -\xi K_d \qquad \text{in } \Omega(t)\,,\\
P(t,\mathbf{X}) &= -\gamma\kappa(t,\mathbf{X}) \qquad \text{on } \partial\Omega(t)\,,\\
V_n(t,\mathbf{X}) &= U(t,\mathbf{X})\cdot\mathbf{n} + [\alpha - \beta C(t,\mathbf{X})]_+ \qquad \text{on } \partial\Omega(t)\,,\\
U(t,\mathbf{X}) &= -\frac{1}{\xi}\nabla P(t,\mathbf{X}) \qquad \text{in } \Omega(t)\,,
\end{aligned}$$

and for $t>0$, the advection-diffusion problem on C rewrites

$$\begin{aligned}
\partial_t C(t,\mathbf{X}) + \mathrm{div}\ (U(t,\mathbf{X})C(t,\mathbf{X}) - D\nabla C(t,\mathbf{X})) &= 0 \quad \text{in } \Omega(t),\ t>0\,,\\
-D\nabla C(t,\mathbf{X})\cdot\mathbf{n} &= C(t,\mathbf{X})\,[\alpha - \beta C(t,\mathbf{X})]_+ \quad \text{on } \partial\Omega(t),\ t>0\,.
\end{aligned}$$

The boundary condition for the flux is therefore nonlinear.

Remark 21. *The expression of the feedback of C on the polymerization is arbitrarily oversimplified, since it assumes that polymerization always takes place where the concentration in marker is low. Regulation of polymerization by a front-specific molecule could be considered in further studies, in relation with observations of the RhoA/Rac1 signalling crosstalk. A first approach of modelling such a self-regulated system is presented in annex. Enrichment of the model with a second molecular agent is relevant also for interaction with the environment. Indeed, external chemical signals can be sensed by protrusions [Heckman and Plummer, 2013; Lidke et al., 2005]. It is reasonable to think that the first cellular response to such a signal would occur at the front, and impacts the dynamics of front-specific molecules.*

5.4.3 Non-dimensionalization

Let us introduce the following typical quantities for non-dimensionalization:

$$\begin{array}{lll} \overline{L} = R, & \overline{V} = \alpha, & \overline{F} = \xi\overline{V} = \xi\alpha, \\ \overline{P} = \frac{\overline{F}\,\overline{L}^2}{\overline{L}} = \xi\alpha R, & \overline{T} = \frac{\overline{L}}{\overline{V}} = \frac{R}{\alpha}, & \overline{C} = N_c\overline{L}^{-2}, \end{array}$$

with N_c the total number of molecules, and α the maximal polymerization velocity.

Remark 22. *It has to be noticed that the force we consider is actually a force per unit area. This explains the expression used for the typical pressure $\overline{P}$, corresponding to a force divided by a length (in 2D).*

Now, write (p, u, c, v) the non-dimensionalized analogous to (P, U, C, V). Moreover, write $\beta' = \frac{\beta N_c}{\alpha R^2}$ and $D' = \frac{D}{\alpha R}$.

The nondimensionalized problem writes:

$$\begin{cases} -\Delta p(t,\mathbf{X}) = -\frac{R}{\alpha}K_d =: -k_d & \text{in } \Omega(t)\,, \\ p(t,\mathbf{X}) = -\frac{\gamma}{\xi\alpha R}\kappa(t,\mathbf{X}) & \text{on } \partial\Omega(t)\,, \\ v_n(t,\mathbf{X}) = u(t,\mathbf{X})\cdot\mathbf{n} + [1-\beta' c(t,\mathbf{X})]_+ & \text{on } \partial\Omega(t)\,, \\ u(t,\mathbf{X}) = -\nabla p(t,\mathbf{X}) & \text{in } \Omega(t)\,, \end{cases} \tag{5.26}$$

and for $t > 0$, the convection-diffusion problem writes

$$\begin{aligned} \partial_t c(t,\mathbf{X}) + \operatorname{div}\,\big(c(t,\mathbf{X})u(t,\mathbf{X}) - D'\nabla c(t,\mathbf{X})\big) &= 0 \quad \text{in } \Omega(t)\,, \\ \big(c(t,\mathbf{X})u(t,\mathbf{X}) - D'\nabla c(t,\mathbf{X})\big)\cdot\mathbf{n} &= c(t,\mathbf{X})(u(t,\mathbf{X})\cdot\mathbf{n} + \big[1-\beta' c(t,\mathbf{X})\big]_+) \quad \text{in } \partial\Omega(t)\,. \end{aligned}$$

Remark 23 (Steady disc)**.** *Let us consider briefly a simple example of the dynamics involved in the model. For $\Omega(0)$ a disc of radius R, consider uniform polymerization on the boundary at rate v_p, and uniform depolymerization inside the domain at rate k_d. Then, the system is axisymmetric, and the velocity of the fluid can be expressed as a radial function, and the domain expands or shrinks but keeps its circular shape and does not move. Equation $\nabla\cdot u = -k_d$ can be solved, and for $u(r=0) = 0$, one obtains*

$$u(r) = -\frac{k_d}{2}r.$$

We can now use the equation on the velocity of the boundary to get the radius for which the domain has a steady shape, i.e $V_n = 0$:

$$V_n = u.n + v_p = 0 \Leftrightarrow R = \frac{2v_p}{k_d}\,.$$

In this configuration, actin filaments continue to polymerize at the domain boundary, but it is exactly compensated by depolymerization inside the domain. Thus, even for a steady non motile cell, the mesoscopic dynamics is never at equilibrium.

5.5 The problem in a rigid domain

The free boundary problem presented above ought to be a minimal model for cell locomotion that includes shape, the cytoskeleton, forces, and molecular interactions. However, as we will see, the resulting system is too complex to provide analytical results.

We are now interested in studying a simpler model, built on the same basis, that allows for a deeper investigation on the persistence of a motile behaviour, in terms of mathematical results and numerical simulations. This is why we want now to focus on the feedback system between the fluid and the molecular dynamics, neglecting the shape and its feedbacks. Therefore, we present now a similar model in a rigid domain in translation.

5.5.1 The fluid problem

Let us consider the cell domain as a two-dimensional disc of radius R, that contains the motility material, described as an active one-component fluid. The non-deformable setting allows to make the distinction between the actin cytoskeleton and the whole cell, composed in particular by passive components (nucleus, centrosome, etc.) that play a part in the domain motion via friction forces (see also Callan-Jones and Voituriez [2013]). In the following, we will therefore consider first force balance equation on the fluid, then on the whole cell.

Figure 5.6 – Figures depicting the notion of passive parts of the cell, seen respetively from above and from the side (for a non-zero thickness). The light grey parts with the red segments account for the actin cytoskeleton. The dark grey zones correspond to the passive components of the cell, that are not localized but taken as a global characteristic.

Let us briefly account for the assumptions made on the fluid. As in the free boundary case, we neglect any thickness effect, myosin-related activity, short-term elastic effect. The polarisation field is assumed constant, unitary, and radially oriented.

Denote Ω the moving domain that defines the cell. Notice that as its shape is fixed, the cell velocity $V : \mathbb{R}_+ \to \mathbb{R}^2$ can only be defined globally. Indeed, one has now to think of the model as a fluid contained in a box that moves according to the intrinsic activity of the fluid in interaction with the substrate, together with the passive loads also rubbing on the substrate. Therefore, polymerization cannot be described as a boundary velocity term any more.

Force balance on the fluid

Let us introduce the quantities of interest. For $t > 0$ and $\mathbf{X} \in \Omega(t)$, define the fluid pressure $\tilde{P}(t, \mathbf{X})$, and the local actin filaments velocity field $\tilde{U}(t, \mathbf{X})$.

In the limit of low Reynolds number, the force balance principle in the frame of reference of the lab writes:

$$-\operatorname{div}\sigma = f(t,\mathbf{X}) \qquad \text{in } \Omega(t)\,, \tag{5.27}$$

where σ, the stress tensor, is given by

$$\begin{aligned}\sigma &= \eta\left(\nabla(\tilde{U}(t,\mathbf{X})+V(t)) + {}^t\nabla(\tilde{U}(t,\mathbf{X})+V(t))\right) - \tilde{P}(t,\mathbf{X})\ \mathrm{Id}\,,\\ &= \eta\left(\nabla\tilde{U}(t,\mathbf{X}) + {}^t\nabla\tilde{U}(t,\mathbf{X})\right) - \tilde{P}(t,\mathbf{X})\ \mathrm{Id}\,,\end{aligned} \tag{5.28}$$

with η the viscosity. We consider a friction force

$$f(t,\mathbf{X}) = -\xi(\tilde{U}(t,\mathbf{X})+V(t))\,, \tag{5.29}$$

where ξ is an effective friction coefficient.

Remark 24. *Following the observations in 5.4.1, notice that a global cell velocity being defined, one can take into account friction arising from both the actin filaments and the cell displacement with velocity V, which is not the case in the free boundary problem.*

Following Callan-Jones et al. [2008], we neglect the viscosity arising from the polymer-polymer and polymer-solvent friction forces and consider the limit $\eta \to 0$. This reduces to

$$\nabla\tilde{P}(t,\mathbf{X}) = -\xi(\tilde{U}(t,\mathbf{X})+V(t)) \qquad \text{in } \Omega(t)\,. \tag{5.30}$$

Continuity equation for the fluid

We introduce the fluid density $\rho(t,\mathbf{X})$, defined for $t>0$ and $\mathbf{X}\in\Omega(t)$. The continuity equation inside the domain writes

$$\frac{\partial}{\partial t}\rho(t,\mathbf{X}) + \operatorname{div}\left(\rho(t,\mathbf{X})(\tilde{U}(t,\mathbf{X})+V(t))\right) = -K_d\rho(t,\mathbf{X})\,. \tag{5.31}$$

To account for polymerization that takes place at the edge of the cell and which consists in a local increase in actin concentration, we impose on the cell membrane a jump on the actin concentration, that depends on a small parameter ε. Denote $\rho_\varepsilon(t,\mathbf{X})$ the corresponding density. We write

$$\rho_\varepsilon(t,\mathbf{X}) = \rho_0 + \varepsilon k_p \qquad \text{on } \partial\Omega(t)\,, \tag{5.32}$$

where ρ_0 is a constant, and k_p accounts for polymerization. One can also assume that the polymerization rate is a continuous non-zero polar function in an annulus initially defined as $\overline{\Omega}(0)\setminus B(0,R-\lambda)$, of width $\lambda>0$, see e.g Kruse et al. [2006].

As it is classical, see Callan-Jones and Voituriez [2013], in addition, we assume that $\tilde{P}_\varepsilon$ is a function of ρ_ε:

$$\tilde{P}_\varepsilon = \frac{1}{\varepsilon}(\rho_\varepsilon - \rho_0)\,.$$

This means that the pressure tends to smooth the polymer concentration. Overall, we get the following problem:

$$\begin{aligned}\partial_t\rho_\varepsilon + \operatorname{div}\left(-\frac{1}{\xi}\rho_\varepsilon\nabla\left(\frac{\rho_\varepsilon}{\varepsilon}\right)\right) &= -K_d\rho_\varepsilon \qquad && \text{in } \Omega(t)\,,\\ \rho_\varepsilon &= \rho_0+\varepsilon k_p \qquad && \text{on } \partial\Omega(t)\,.\end{aligned}$$

Formally, in the limit $\varepsilon \to 0$, $\rho = \lim_{\varepsilon\to 0} \rho_\varepsilon \equiv \rho_0$ and $\tilde{P} = \lim_{\varepsilon\to 0} \tilde{P}_\varepsilon$ is solution of the following Poisson problem:

$$\begin{cases} -\Delta \tilde{P}(t,\mathbf{X}) = -\xi K_d & \text{in } \Omega(t)\,, \\ \tilde{P}(t,\mathbf{X}) = k_p & \text{on } \partial\Omega(t)\,. \end{cases} \tag{5.33}$$

The boundary condition accounts for polymerization at the edge of the cell, while K_d describes depolymerization in the cell body. Notice that in the free boundary case, polymerization was described by a velocity term.

This amounts to saying that the pressure $\tilde{P}$ ensures at all time that the polymer density stays constant. The rigorous justification of this limit is not our purpose here, and will be the object of a future work.

Global force balance

As explained before (see figure 5.6), the cell is composed by a fluid part, and a passive part that rubs on the substrate when the cell moves forward at velocity $V(t)$. Therefore, force balance for the global cell description leads to

$$\xi_1 V(t) + \xi \int_{\Omega(t)} \tilde{U}(t,\mathbf{X}) + V(t)\,\mathrm{d}\mathbf{X} = 0\,, \tag{5.34}$$

where ξ_1 is a global friction coefficient for all the passive loads inside the cell domain. This rewrites

$$V(t) = -\frac{\xi}{\xi_1 + |\Omega|\xi} \int_{\Omega(t)} \tilde{U}(t,\mathbf{X})\,\mathrm{d}\mathbf{X}\,. \tag{5.35}$$

Finally, we can combine equations (5.30) and (5.35) to get expressions for $\tilde{U}$ and V:

$$V(t) = \frac{1}{\xi_1} \int_{\Omega(t)} \nabla \tilde{P}(t,\mathbf{X})\,\mathrm{d}\mathbf{X}\,, \tag{5.36}$$

and

$$\begin{aligned} \tilde{U}(t,\mathbf{X}) &= -\frac{1}{\xi}\nabla \tilde{P}(t,\mathbf{X}) - V(t)\,, \\ &= -\frac{1}{\xi}\nabla \tilde{P}(t,\mathbf{X}) - \frac{1}{\xi_1}\int_{\Omega(t)} \nabla \tilde{P}(t,\mathbf{X})\,\mathrm{d}\mathbf{X}\,. \end{aligned} \tag{5.37}$$

Formulation in a non moving domain

We now rewrite the fluid problem on a fixed domain $\Omega_0 := \Omega(0)$. As $(\tilde{P}, \tilde{U})$ are defined on $\Omega(t)$, we denote (P, U) their analogous on Ω_0. Moreover we define the following map:

$$\begin{array}{rccc} L(.,t): & \Omega_0 & \longrightarrow & \Omega(t) \\ & \mathbf{x} & \mapsto & \mathbf{X} = \mathbf{x} + \int_0^t V(s)\,\mathrm{d}s = L(t,\mathbf{x}), \end{array}$$

which gives $P(t,\mathbf{x}) = \tilde{P}(t, L(t,\mathbf{x})) = \tilde{P}(t,\mathbf{X})$ (for example for P).

Let us now rewrite the fluid problem on Ω_0. To do so we observe that the Jacobian matrix related to L is the identity matrix, since V is space-independent. This leads to $\Delta_{\mathbf{X}} \tilde{P}(t,\mathbf{X}) = \Delta_{\mathbf{x}} P(t,\mathbf{x})$, $\tilde{U}(t,\mathbf{X}) = U(t,\mathbf{x})$, and for all $\mathbf{x} \in \Omega_0$ and for all $t > 0$, the fluid problem writes

$$\begin{cases} -\Delta P(t,\mathbf{x}) = -\xi K_d & \text{in } \Omega_0\,, \\ P(t,\mathbf{x}) = k_p & \text{on } \partial\Omega_0\,, \end{cases} \tag{5.38}$$

together with

$$V(t) = \frac{1}{\xi_1}\int_{\Omega_0} \nabla P(t,\mathbf{x})\,\mathrm{d}\mathbf{x}\,, \tag{5.39}$$

and

$$U(t,\mathbf{x}) = -\frac{1}{\xi}\nabla P(t,\mathbf{x}) - \frac{1}{\xi_1}\int_{\Omega_0} \nabla P(t,\mathbf{x})\,\mathrm{d}\mathbf{x}\,. \tag{5.40}$$

5.5.2 The marker's dynamics: two choices

Denote $C(t,\mathbf{x})$ the concentration of molecular marker inside Ω_0. The advection-diffusion dynamics is similar to the one in the free boundary case. In particular, it does not depend on the global cell velocity. Moreover, the boundary conditions are different: we prescribe a zero-flux in order to conserve mass.

The feedback of the marker on the polymerization is now described in the boundary pressure term, and we keep the same expression. We present now two configurations. In the first one, we simply consider the advection-diffusion dynamics of the marker, such that its concentration on the boundary exerts a feedback on the fluid. This case will be refered to as the *no exchange case*.

As in the work of Muller [2013] on yeast cell polarisation, the latter model can be too simple and yield singularities. Moreover, we saw in Maiuri et al. [2015] that the activation of the marker is an important feature of the system. Therefore, we describe this activation dynamics, that corresponds to attachment and detachment to the membrane. The feedback on the fluid comes from the attached molecules. This case will be refered to as the "*dynamical exchange case*". We did not consider activation of the marker in the case of a free boundary domain, since the boundary deformation and elongation have to be taken into account in the dynamics of activated molecules. The formulation and study of such a model will be the object of a future work.

No exchange case

In the frame of reference of the moving cell, we write

$$\partial_t C(t,\mathbf{x}) + \mathrm{div}\ \left(C(t,\mathbf{x})U(t,\mathbf{x}) - D\nabla C(t,\mathbf{x})\right) = 0 \quad \text{for } \mathbf{x}\in\Omega_0,\ t>0\,,$$

with the zero-flux boundary condition

$$\left(D\nabla C(t,\mathbf{x}) - C(t,\mathbf{x})U(t,\mathbf{x})\right)\cdot\mathbf{n} = 0 \quad \text{for } \mathbf{x}\in\partial\Omega_0,\ t>0\,,$$

where $\mathbf{n}$ is the outward unit normal to the boundary. We can easily check that the total mass is preserved: $\frac{\mathrm{d}}{\mathrm{d}t}\int_{\Omega_0} C(t,\mathbf{x})\,\mathrm{d}\mathbf{x} = 0$. The fluid problem writes now

$$\begin{cases} U(t,\mathbf{x}) = -\frac{1}{\xi}\nabla P(t,\mathbf{x}) - \frac{1}{\xi_1}\int_{\Omega_0}\nabla P(t,\mathbf{x})\,\mathrm{d}\mathbf{x} & \text{for } \mathbf{x}\in\Omega_0,\ t>0\,, \\ -\Delta P(t,\mathbf{x}) = -\xi K_d & \text{for } \mathbf{x}\in\Omega_0,\ t>0\,, \\ P(t,\mathbf{x}) = [\alpha - \beta C(t,\mathbf{x})]_+ & \text{for } \mathbf{x}\in\partial\Omega_0,\ t>0\,, \end{cases}$$

where $[\,\cdot\,]_+$ denotes the positive part function.

Dynamical exchange case

Write $\mu : \mathbb{R}_+ \times \partial\Omega_0 \to \mathbb{R}_+$ for the concentration in activated markers on the boundary. The exchange dynamics write for $t > 0$ and $\mathbf{x} \in \partial\Omega_0$,

$$\frac{\partial}{\partial t}\mu(t,\mathbf{x}) = K_{\text{on}}C(t,\mathbf{x}) - K_{\text{off}}\mu(t,\mathbf{x})\,,$$

with K_{on} , K_{off} the attachment and detachment rates. For the cytoplasmic markers, the exchange brings a new term on the boundary condition: for $\mathbf{x} \in \partial\Omega_0$ and $t > 0$,

$$(CU - D\nabla C)\cdot\mathbf{n} = -K_{\text{on}}C + K_{\text{off}}\mu\,.$$

There is conservation of the total mass:

$$\int_{\Omega_0} C(t,\mathbf{x})\,\mathrm{d}\mathbf{x} + \int_{\partial\Omega_0} \mu(t,\mathbf{x})\,\mathrm{d}\mathbf{x} = M \quad \text{for } t > 0\,. \tag{5.41}$$

The fluid problem then writes

$$\begin{cases} U(t,\mathbf{x}) = -\frac{1}{\xi}\nabla P(t,\mathbf{x}) - \frac{1}{\xi_1}\int_{\Omega_0}\nabla P(t,\mathbf{x})\,\mathrm{d}\mathbf{x} & \text{for } \mathbf{x}\in\Omega_0,\, t>0\,,\\ -\Delta P(t,\mathbf{x}) = -\xi K_d & \text{for } \mathbf{x}\in\Omega_0,\, t>0\,,\\ P(t,\mathbf{x}) = [\alpha - \beta\mu(t,\mathbf{x})]_+ & \text{for } \mathbf{x}\in\partial\Omega_0,\, t>0\,. \end{cases}$$

5.5.3 Non-dimensionalization

Let us introduce the following typical quantities for non-dimensionalization:

$$\begin{array}{llll} \overline{L} = R, & \overline{P} = \alpha = \frac{\overline{F}\,\overline{L}^2}{\overline{L}}, & \overline{F} = \frac{\overline{P}}{\overline{L}} = \frac{\alpha}{R} = \xi\overline{V}, \\ \overline{V} = \frac{\alpha}{R\xi}, & \overline{T} = \frac{\overline{L}}{\overline{V}} = \frac{\xi R^2}{\alpha}, & \overline{C} = N_c\overline{L}^{-2} = \frac{N_c}{R^2}, \end{array}$$

with N_c the total number of molecules.

Remark 25. *The typical pressure corresponds to a maximal incoming pressure of the fluid at the boundary of the domain.*

Now, write (p,u,c,v) the non-dimensionalized analogous to (P,U,C,V). For simplicity, we keep the same notation for μ. Denote $D' = \frac{D}{\overline{L}\,\overline{V}} = \frac{D\xi}{\alpha}$, $\delta := \frac{\beta N_c}{\alpha R^2}$ and $k_d := \frac{\xi R^2}{\alpha}K_d$.

No exchange case The non-dimensionalized problem writes:

$$\begin{cases} u(t,\mathbf{x}) = -\nabla p(t,\mathbf{x}) - \frac{\xi}{\xi_1}\int_{\Omega_0}\nabla p(t,\mathbf{x})\mathbf{x} & \text{on } \Omega_0\,,\\ -\Delta p(t,\mathbf{x}) = -k_d & \text{on } \Omega_0\,,\\ p(t,\mathbf{x}) = [1-\delta c(t,\mathbf{x})]_+ & \text{on } \partial\Omega_0\,, \end{cases} \tag{5.42}$$

where the domain velocity is:

$$v(t) = \frac{\xi}{\xi_1}\int_{\Omega_0}\nabla p(t,\mathbf{x})\;\mathrm{d}\mathbf{x}\,. \tag{5.43}$$

The convection-diffusion problem writes

$$\begin{cases} \partial_t c(t,\mathbf{x}) + \operatorname{div}\;(c(t,\mathbf{x})u(t,\mathbf{x}) - D'\nabla c(t,\mathbf{x})) = 0 & \text{on } \Omega_0\,,\\ (D'\nabla c(t,\mathbf{x}) - c(t,\mathbf{x})u(t,\mathbf{x}))\cdot\mathbf{n} = 0 & \text{on } \partial\Omega_0\,. \end{cases} \tag{5.44}$$

Moreover, the global mass is prescribed:

$$\int_{\Omega_0} c(t,\mathbf{x})\;\mathrm{d}\mathbf{x} = M\,. \tag{5.45}$$

Dynamical exchange case In the problem with activation of the marker at the membrane, the non-dimensionalized problem writes:

$$\begin{cases} u(t,\mathbf{x}) = -\nabla p(t,\mathbf{x}) - \frac{\xi}{\xi_1}\int_{\Omega_0}\nabla p(t,\mathbf{x})\mathbf{x} & \text{on } \Omega_0\,, \\ -\Delta p(t,\mathbf{x}) = -k_d & \text{on } \Omega_0\,, \\ p(t,\mathbf{x}) = [1-\delta\mu(t,\mathbf{x})]_+ & \text{on } \partial\Omega_0\,, \end{cases} \tag{5.46}$$

where the domain velocity is:

$$v(t) = \frac{\xi}{\xi_1}\int_{\Omega_0}\nabla p(t,\mathbf{x})\,\mathrm{d}\mathbf{x}\,, \tag{5.47}$$

the exchange dynamics write

$$\frac{\partial}{\partial t}\mu(t,\mathbf{x}) = k_{\text{on}}c(t,\mathbf{x}) - k_{\text{off}}\mu(t,\mathbf{x})\,,$$

where $k_{\text{on/off}} = \frac{\xi R^2}{\alpha}K_{\text{on/off}}$, and the convection-diffusion problem is

$$\begin{cases} \partial_t c + \text{div}\ (cu - D'\nabla c) = 0 & \text{on } \Omega_0\,, \\ (D'\nabla c - cu)\cdot\mathbf{n} = -k_{\text{on}}c + k_{\text{off}}\mu & \text{on } \partial\Omega_0\,. \end{cases} \tag{5.48}$$

Moreover, the global mass is prescribed:

$$\int_{\Omega_0} c(t,\mathbf{x})\,\mathrm{d}\mathbf{x} + \int_{\partial\Omega_0}\mu(t,\mathbf{x})\,\mathrm{d}\mathbf{x} = M\,. \tag{5.49}$$

Remark 26 (On the cell velocity)**.** *Using the boundary condition on p in (5.46), we can compute*

$$\begin{aligned} v(t) &= \frac{\xi}{\xi_1}\int_{\Omega_0}\nabla p(t,\mathbf{x})\,\mathrm{d}\mathbf{x} = \frac{\xi}{\xi_1}\int_{\partial\Omega_0} p(t,\mathbf{x})\mathbf{n}\,\mathrm{d}\mathbf{x}\,, \\ &= -\frac{\delta\xi}{\xi_1}\int_{\partial\Omega_0} c(t,\mathbf{x})\mathbf{n}\,\mathrm{d}\mathbf{x}\,, \end{aligned}$$

where $c(t,\mathbf{x})$ is replaced by $\mu(t,\mathbf{x})$ in the dynamical exchange case. This expression generalizes the one used in Maiuri et al. [2015].

5.5.4 The one-dimensional case

The previous model in a two-dimensional domain of fixed circular shape allows for numerical simulations involving interaction with environment. However, theoretical results stays out of reach. In the following, we adapt the model in a one-dimensional setting, so that the feedback loop between the fluid and the molecular marker fits into a simpler mathematical framework: we drop the positive part function in the expression of the boundary pressure. We will see in the next chapter that powerful characterization of cell persistence can be obtained.

For real numbers $a < b$, write $\Omega_0 = (a,b)$. Equation (5.43) rewrites to

$$v(t) = \frac{\xi}{\xi_1}(p(t,b) - p(t,a))\,. \tag{5.50}$$

Moreover, using that $\partial_{xx}p(t,x) = k_d$, we can write

$$p(t,x) = \frac{k_d}{2}(x-a)^2 + d(x-a) + p(t,a)\,, \tag{5.51}$$

where

$$d = \frac{p(t,b)-p(t,a)}{b-a} - \frac{k_d}{2}(b-a)\,.$$

Now, as

$$u(t,\mathbf{x}) = -\partial_x p(t,\mathbf{x}) - \frac{\xi}{\xi_1}(p(t,b)-p(t,a))\,,$$

replacing p in the expression gives

$$\begin{aligned} u(t,x) &= -k_d\left(x - \frac{a+b}{2}\right) - \left(\frac{1}{(b-a)} + \frac{\xi}{\xi_1}\right)(p(t,b)-p(t,a))\,, \\ &= -k_d\left(x - \frac{a+b}{2}\right) + \delta\left(\frac{1}{(b-a)} + \frac{\xi}{\xi_1}\right)(c(t,a)-c(t,b))\,, \end{aligned}$$

by the boundary conditions in (5.42).

We end up with the following non-linear and non-local convection-diffusion equation

$$\begin{cases} \partial_t c = \partial_x\left(D'\partial_x c - cu\right) & \text{on } (a,b),\ \text{for } t>0\,, \\ 0 = D'\partial_x c - cu & \text{on } \{a,b\},\ \text{for } t>0\,, \end{cases} \tag{5.52}$$

with $\delta = \frac{\beta N_c}{\alpha R^2} > 0$ and we recall that $D' = \frac{D\xi}{\alpha} \geq 0$. In the one dimensional setting, $R = {}^{(b-a)}/_{2}$. The domain velocity writes

$$v(t) = \delta\frac{\xi}{\xi_1}(c(t,a)-c(t,b))\,.$$

From now on, in order to simplify the computations we will assume that $a+b=0$. In such a case the velocity simply rewrites as

$$u(t,x) = -k_d x - \delta\left(\frac{1}{2b} + \frac{\xi}{\xi_1}\right)(c(t,a)-c(t,b))\,. \tag{5.53}$$

We find a model that presents some similarities with the model studied in Calvez et al. [2012, 2010]; Hawkins et al. [2009]; Lepoutre et al. [2014]; Muller et al. [2016] to describe yeast cell polarisation. The main difference here is the presence of an additional drift towards the cell center.

Dynamical exchange case

In the case with activation of the marker at the membrane, we end up with the similar problem. The exchange of markers at the boundary is described by

$$\begin{cases} \frac{\partial}{\partial t}\mu(t,a) = k_{\text{on}}c(t,a) - k_{\text{off}}\mu(t,a)\,,\ , \\ \frac{\partial}{\partial t}\mu(t,b) = k_{\text{on}}c(t,b) - k_{\text{off}}\mu(t,b)\,, \end{cases} \tag{5.54}$$

The fluid velocity writes

$$\begin{aligned} u(t,x) &= -k_d\left(x - \frac{a+b}{2}\right) - \left(\frac{1}{(b-a)} + \frac{\xi}{\xi_1}\right)(p(t,b)-p(t,a))\,, \\ &= -k_d\left(x - \frac{a+b}{2}\right) - \delta\left(\frac{1}{(b-a)} + \frac{\xi}{\xi_1}\right)(\mu(t,a)-\mu(t,b))\,, \end{aligned}$$

and is the advection velocity in the following non-linear and non-local convection-diffusion equation:

$$\begin{cases} \partial_t c = \partial_x \left(D' \partial_x c - c u \right) & \text{on } (a,b), \text{ for } t > 0\,, \\ k_{\text{on}} c - k_{\text{off}} \mu = D' \partial_x c - c u & \text{on } \{a\}, \text{ for } t > 0\,, \\ k_{\text{off}} \mu - k_{\text{on}} c = D' \partial_x c - c u & \text{on } \{b\}, \text{ for } t > 0\,. \end{cases} \tag{5.55}$$

while the domain velocity writes

$$v(t) = \delta \frac{\xi}{\xi_1} \left(\mu(t,a) - \mu(t,b) \right) .$$

Without lost of generalities, assume that $a + b = 0$ to get

$$u(t,x) = -k_d x - \delta \left(\frac{1}{2b} + \frac{\xi}{\xi_1} \right) \left(\mu(t,a) - \mu(t,b) \right). \tag{5.56}$$

The advection dynamics is then composed of an attractive drift towards the cell center, and a repulsive drift from the boundary that depends on the global asymmetry factor $\mu(t,a) - \mu(t,b)$.

Conclusions In this chapter, we have built minimal models of cell migration based on a macroscopic description of the cytoskeleton, and a generic principle able to relate cell migration and polarisation. The more realistic model consists in a two dimensional free boundary problem, where actin polymerization and depolymerization induce actin flows. They are responsible for the apparition of friction forces, deformation of the membrane, and also for the advection of polarity cues away from the edge. These molecules are supposed to exert a feedback on polymerization, hence on the flow. Moreover, cell shape has a non trivial effect on the whole dynamics.

In an attempt to obtain theoretical results, we simplified the model by neglecting the cell deformation. The resulting model is less realistic, but easier to handle analytically and numerically. We will see in chapter 7 how numerical simulations of this model can be enriched by the effect of a signal, noise, or event obstacles in the environment. Finally, the one-dimensional simplification of this model consists in a non-linear and non-local convection-diffusion equation, for which an analytical study can be performed. This is detailed in the next chapter 6.

Bibliography

Akhshi, T. K., Wernike, D., and Piekny, A. (2014). Microtubules and actin crosstalk in cell migration and division. Cytoskeleton (Hoboken), 71(1):1–23. 175

Ben Amar, M., Cummings, L., and Pomeau, Y. (2003). Transition of a moving contact line from smooth to angular. Physics of Fluids (1994-present), 15(10):2949–2960. 166

Ben Amar, M., Manyuhina, O., and Napoli, G. (2011). Cell motility: a viscous fingering analysis of active gels. The European Physical Journal Plus, 126(2):1–15. 165, 166, 171

Blanch-Mercader, C. and Casademunt, J. (2013). Spontaneous motility of actin lamellar fragments. Physical Review Letters, 110(7). 167, 171, 174

Callan-Jones, A. C., Joanny, J.-F., and Prost, J. (2008). Viscous-fingering-like instability of cell fragments. Physical Review Letters, 100(25). 164, 165, 167, 173, 179

Callan-Jones, A. C. and Voituriez, R. (2013). Active gel model of amoeboid cell motility. New Journal of Physics, 15(2):025022. 162, 178, 179

Calvez, V., Hawkins, R. J., Meunier, N., and Voituriez, R. (2012). Analysis of a Nonlocal Model for Spontaneous Cell Polarization. SIAM Journal on Applied Mathematics, 72(2):594–622. 184

Calvez, V., Meunier, N., and Voituriez, R. (2010). A one-dimensional Keller–Segel equation with a drift issued from the boundary. Comptes Rendus Mathematique, 348(11):629–634. 184

Dang, I., Gorelik, R., Sousa-Blin, C., Derivery, E., Guérin, C., Linkner, J., Nemethova, M., Dumortier, J. G., Giger, F. A., Chipysheva, T. A., Ermilova, V. D., Vacher, S., Campanacci, V., Herrada, I., Planson, A.-G., Fetics, S., Henriot, V., David, V., Oguievetskaia, K., Lakisic, G., Pierre, F., Steffen, A., Boyreau, A., Peyriéras, N., Rottner, K., Zinn-Justin, S., Cherfils, J., Bièche, I., Alexandrova, A. Y., David, N. B., Small, J. V., Faix, J., Blanchoin, L., and Gautreau, A. (2013). Inhibitory signalling to the Arp2/3 complex steers cell migration. Nature, 503(7475):281–4. 161, 175

De Gennes, P.-G. (1979). Scaling concepts in polymer physics. Cornell university press. 161

De Gennes, P. G. and Prost, J. (1993). The physics of liquid crystals. Oxford. 160

Dembo, M. and Wang, Y.-L. (1999). Stresses at the cell-to-substrate interface during locomotion of fibroblasts. Biophysical journal, 76(4):2307–2316. 165

Hawkins, R. J., Bénichou, O., Piel, M., and Voituriez, R. (2009). Rebuilding cytoskeleton roads: active-transport-induced polarization of cells. Phys Rev E Stat Nonlin Soft Matter Phys, 80(4 Pt 1):040903. 184

Head, D. A., Levine, A. J., and MacKintosh, F. C. (2003). Distinct regimes of elastic response and deformation modes of cross-linked cytoskeletal and semiflexible polymer networks. Phys Rev E Stat Nonlin Soft Matter Phys, 68(6 Pt 1):061907. 161

Heckman, C. and Plummer, H. (2013). Filopodia as sensors. Cellular signalling, 25(11):2298–2311. 177

Joanny, J.-F. and Prost, J. (2009). Active gels as a description of the actin-myosin cytoskeleton. HFSP J, 3(2):94–104. 161, 162

Jülicher, F., Kruse, K., Prost, J., and Joanny, J.-F. (2007). Active behavior of the cytoskeleton. Physics Reports, 449(1):3–28. 162, 163

Krause, M. and Gautreau, A. (2014). Steering cell migration: lamellipodium dynamics and the regulation of directional persistence. Nat Rev Mol Cell Biol, 15(9):577–90. 161

Kruse, K., Joanny, J. F., Jülicher, F., and Prost, J. (2006). Contractility and retrograde flow in lamellipodium motion. Phys Biol, 3(2):130–7. 162, 173, 179

Kruse, K., Joanny, J. F., Jülicher, F., Prost, J., and Sekimoto, K. (2005). Generic theory of active polar gels: a paradigm for cytoskeletal dynamics. Eur Phys J E Soft Matter, 16(1):5–16. 162

Lawson, C. D. and Burridge, K. (2014). The on-off relationship of Rho and Rac during integrin-mediated adhesion and cell migration. Small GTPases, 5(1):e27958. 175

Lepoutre, T., Meunier, N., and Muller, N. (2014). Cell polarisation model : the 1D case. Journal des Mathematiques Pures et Appliquees, 101(2):152–171. 184

Lidke, D. S., Lidke, K. A., Rieger, B., Jovin, T. M., and Arndt-Jovin, D. J. (2005). Reaching out for signals: filopodia sense EGF and respond by directed retrograde transport of activated receptors. J Cell Biol, 170(4):619–26. 177

Machacek, M., Hodgson, L., Welch, C., Elliott, H., Pertz, O., Nalbant, P., Abell, A., Johnson, G. L., Hahn, K. M., and Danuser, G. (2009). Coordination of Rho GTPase activities during cell protrusion. Nature, 461(7260):99–103. 175

MacKintosh, F., Käs, J., and Janmey, P. (1995). Elasticity of semiflexible biopolymer networks. Physical review letters, 75(24):4425. 161

Maiuri, P., Rupprecht, J.-F., Wieser, S., Ruprecht, V., Bénichou, O., Carpi, N., Coppey, M., De Beco, S., Gov, N., Heisenberg, C.-P., Lage Crespo, C., Lautenschlaeger, F., Le Berre, M., Lennon-Dumenil, A.-M., Raab, M., Thiam, H.-R., Piel, M., Sixt, M., and Voituriez, R. (2015). Actin flows mediate a universal coupling between cell speed and cell persistence. Cell, 161(2):374–86. 161, 164, 168, 175, 176, 181, 183

Maiuri, P., Terriac, E., Paul-Gilloteaux, P., Vignaud, T., McNally, K., Onuffer, J., Thorn, K., Nguyen, P. A., Georgoulia, N., Soong, D., et al. (2012). The first world cell race. Current Biology, 22(17):R673–R675. 168

Muller, N. (2013). Études mathématiques et numériques de problèmes non-linéaires et non-locaux issus de la biologie. PhD thesis, Université Paris Descartes. 181

Muller, N., Piel, M., Calvez, V., Voituriez, R., Gonçalves-Sá, J., Guo, C.-L., Jiang, X., Murray, A., and Meunier, N. (2016). A predictive model for yeast cell polarization in pheromone gradients. PLoS Comput Biol, 12(4):e1004795. 184

Oliver, T., Dembo, M., and Jacobson, K. (1999). Separation of propulsive and adhesive traction stresses in locomoting keratocytes. The Journal of cell biology, 145(3):589–604. 165

Parsons, J. T., Horwitz, A. R., and Schwartz, M. A. (2010). Cell adhesion: integrating cytoskeletal dynamics and cellular tension. Nat Rev Mol Cell Biol, 11(9):633–43. 160

Prost, J., Jülicher, F., and Joanny, J. (2015). Active gel physics. Nature Physics, 11(2):111–117. 162, 164

Renkawitz, J., Schumann, K., Weber, M., Lämmermann, T., Pflicke, H., Piel, M., Polleux, J., Spatz, J. P., and Sixt, M. (2009). Adaptive force transmission in amoeboid cell migration. Nature cell biology, 11(12):1438–1443. 168

Ridley, A. J. (2011). Life at the leading edge. Cell, 145(7):1012–22. 164, 171

Ridley, A. J., Schwartz, M. A., Burridge, K., Firtel, R. A., Ginsberg, M. H., Borisy, G., Parsons, J. T., and Horwitz, A. R. (2003). Cell migration: integrating signals from front to back. Science, 302(5651):1704–9. 175

Sackmann, E. (2015). How actin/myosin crosstalks guide the adhesion, locomotion and polarization of cells. Biochim Biophys Acta, 1853(11 Pt B):3132–42. 175

Sens, P. and Plastino, J. (2015). Membrane tension and cytoskeleton organization in cell motility. Journal of Physics: Condensed Matter, 27(27):273103. 174

Svitkina, T. M. and Borisy, G. G. (1999). Arp2/3 complex and actin depolymerizing factor/cofilin in dendritic organization and treadmilling of actin filament array in lamellipodia. J Cell Biol, 145(5):1009–26. 163

Theriot, J. A. and Mitchison, T. J. (1992). Comparison of actin and cell surface dynamics in motile fibroblasts. The Journal of cell biology, 119(2):367–377. 165

Vigneaux, P. (2007). Méthodes Level Set pour des problèmes d'interface en microfluidique. PhD thesis, Université Sciences et Technologies-Bordeaux I. 174

Wilhelm, J. and Frey, E. (2003). Elasticity of stiff polymer networks. Phys Rev Lett, 91(10):108103. 161

Wittmann, T. and Waterman-Storer, C. M. (2001). Cell motility: can Rho GTPases and microtubules point the way? Journal of cell science, 114(21):3795–3803. 175

Wottawah, F., Schinkinger, S., Lincoln, B., Ananthakrishnan, R., Romeyke, M., Guck, J., and Käs, J. (2005). Optical rheology of biological cells. Physical review letters, 94(9):098103. 161, 162, 165

Chapter 6

Analysis of a 1D non-local and non-linear Fokker-Planck equation

Contents

6.1 The boundary non-linear Fokker-Planck equation 190
6.2 Global existence and asymptotic analysis for sub-critical mass $M < 1$ 193
6.3 Critical case $M = 1$ 198
6.4 The Super-critical case $M > 1$ 200
6.4.1 Stationary solutions 200
6.4.2 Blow-up for a modified equation 201
6.4.3 Blow-up in the Super-critical case 203
6.5 Dynamical exchange of markers at the boundary: prevention of blow-up and asymptotic behaviour 204
6.6 Perspectives 207

In this work, in collaboration with Nicolas Meunier and Raphaël Voituriez (LJP and LPTMC, UPMC), we study the one-dimensional form of the crawling model defined in a domain of fixed circular shape. The migration model reduces to a non-linear and non-local Fokker-Planck equation, where the advection term depends on boundary quantities. This work is related to a model of yeast cells polarisation defined on the half-line, composed of a non-local attractive drift to the boundary [Calvez et al., 2012, 2010; Hawkins et al., 2009; Lepoutre et al., 2014; Muller et al., 2016].

Using similar tools (entropy techniques, logarithmic Sobolev inequality), we prove the following dichotomy behaviour: in the subcritical and critical case, we show the existence of a unique stationary profile of exponential shape. Convergence is obtained using a Lyapunov functional for $M < 1$, and using the convergence to zero of the relative entropy for $M = 1$. Exponential decay to equilibrium is proved in both cases using the logarithmic Sobolev inequality. In the supercritical case, we show that there exists a unique symmetric stationary profile. Moreover, for a specific range of mass, there exists two non-symmetric supplementary equilibrium profiles, corresponding to polarized states. The three of them are explicit. Finally, we show that for an asymmetric enough initial profile, the solution blows-up in finite time. This result is obtained thanks to a concentration-comparison principle. From the biological point of vue, the blow-up can be interpreted as a polarised state, but still shows that the model is not smooth enough. It is possible to avoid this singularity by considering separately cytoplasmic markers and membrane-bound markers.

In this case, the advection term depends on the trapped markers, and this is enough to prevent the blow-up to appear.

The plan of this work is as follows. In Section 6.1, we introduce the model, compare its structure to the polarisation model Hawkins et al. [2009], and present the mathematical results obtained. In Section 6.2, 6.3, and 6.4, we analyse with full details the one-dimensional case. In Section 6.5, we briefly study a model with exchange of markers at the boundary in the one-dimensional case. This work has been submitted for publication.

6.1 The boundary non-linear Fokker-Planck equation

Let us first recall the principles followed to construct the model, that were detailed in the last chapter. The actin cytoskeleton is described as a fluid of local velocity u and pressure p. It is assumed to transport a marker of the cell rear, that also diffuses in the domain, such that its mass is conserved. The concentration in marker on the domain's boundary lowers the fluid pressure, hence acts negatively on the actin flows able to carry the marker away. Finally, the domain's velocity is a result of the mechanical equilibrium of the global system.

In a one-dimensional setting, for $\Omega = (-1, 1)$, and with all constants set to one, we have seen that this problem resumes to an advection-diffusion equation, where the advection is non-linear and non-local:

$$\begin{cases} \partial_t c(t,x) = \partial_x \Big(\partial_x c(t,x) + (x + c(t,-1) - c(t,1))\, c(t,x) \Big) & \text{in } \Omega\,, \\ \partial_x c(t,-1) + (c(t,-1) - c(t,1) - 1)\, c(t,-1) = 0\,, \\ \partial_x c(t,1) + (c(t,-1) - c(t,1) + 1)\, c(t,1) = 0\,, \end{cases} \tag{6.1}$$

The zero-flux boundary conditions ensure mass conservation. The cell velocity writes

$$v(t) = \frac{\delta\xi}{\xi_1}(c(t,-1) - c(t,1))\,,$$

with ξ a friction coefficient related to the friction of the actin filaments on the substrate, ξ_1 a global friction coefficient related to the drag of the passive components of the cell on the substrate, and δ a non-negative coefficient related to the feedback of the marker on the cytoskeleton dynamics.

The model (6.1) has the same structure than the one studied in Calvez et al. [2012, 2010]; Hawkins et al. [2009]; Lepoutre et al. [2014]; Muller et al. [2016] for the polarisation of yeast cells. In their works, the cell is non-motile, and its polarisation is a preliminary process for contact and mating with other cells. Polarisation is characterized by the local aggregation of a *front* marker in a part of the membrane, Cdc42 proteins. Their spatial repartition is governed by cytoplasmic diffusion and active transportation towards the membrane by the cytoskeleton. Notice that the direction of advection is reversed compared to our problem.

The feedback of the marker's concentration on the advection field is also reversed: aggregation on the membrane increases the attractive field towards this pool. Therefore, the system consists in a competition between diffusion and an attractive non-linear drift towards the membrane.

The corresponding problem is defined on the half-line, where $\{x = 0\}$ accounts for the cell membrane. Write $\Omega = (0, +\infty)$, and consider the concentration in markers $n : \mathbb{R}_+ \times \Omega \to \mathbb{R}_+$. We have

$$\begin{cases} \partial_t n(t,x) = \partial_x \Big(\partial_x n(t,x) + n(t,0) n(t,x) \Big) \,, & x > 0 \,, \\ \partial_x n(t,0) + n(t,0)^2 = 0 \,, \\ n(0,x) = n^0(x) \,, & x > 0 \,. \end{cases} \tag{6.2}$$

A particular feature of this problem relies on the fact that for a super-critical mass of markers, any weak solution of (6.2) with non-increasing initial data blows-up (i.e become unbounded) in finite time. For sub-critical and critical mass, under some regularity assumptions, global existence of a weak solution is established, the asymptotic behaviour of the solution is explicit, and rates of convergence are given.

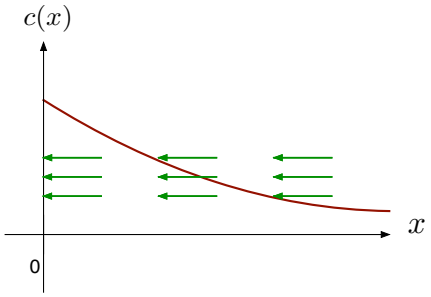

Figure 6.1 – Representation of the marker concentration (in red) and the global advection field (in green), that competes with diffusion.

Characteristics of the migration model

Let us discuss the specific features of our model. Despite a similar structure, the active description of the cytoskeleton (polymerisation, depolymerisation) yields non-trivial differences.

First, the polarisation marker in our model characterizes the rear. Instead of reinforcing an attractive drift, its concentration on the membrane lowers its local repulsion. This mechanism accounts for a local inhibition of polymerisation. Now, since the boundary is made of two points, both local non-repulsive effects combine via the Darcy fluid assumption, and give rise to a non-local drift $c(t,-1) - c(t,1)$.

The linear drift towards the cell center results from actin depolymerization. It tends to homogenize the concentration on the boundary, hence acts with the diffusion.

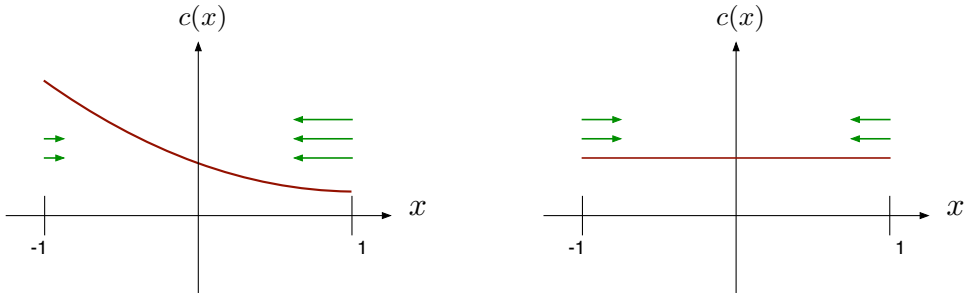

Figure 6.2 – Representation of the marker concentration (in red) and the local advection field (in green), that combine the repulsive drift from the boundary and the drift towards the cell center. In the non-homogeneous case, the boundary with the lowest concentration has the largest advection flow, and vice versa. In the homogeneous case, only the drift to the center exists.

Overall, the ingredients of the model seem less likely to generate singularities than the polarisation model. The only openly attractive drift is directed towards the cell center. However, the local repulsion turns into a global drift due to the fluid description. Therefore, it is natural to question the ability of the model to provide a polarised profile. Other questions related to its mathematical properties are the following: can we find a similar dichotomy behaviour ? Is a blow-up likely to occur for this system ? Do non-homogeneous stationary profiles appear ?

Mathematical results

We are looking for a solution to (6.1). As it is classical we start by giving a proper definition of weak solutions, adapted to our context:

Definition 8. *We say that $c(t,x)$ is a weak solution of (6.1) on $(0,T)$ if it satisfies:*

$$c \in L^\infty\left(0,T;L^1_+(-1,1)\right)\ , \quad \partial_x c \in L^1\left((0,T)\times(-1,1)\right)\ , \tag{6.3}$$

and $c(t,x)$ is a solution of (6.1) in the sense of distribution in $\mathcal{D}'(-1,1)$.

Since the flux $\partial_x c(t,x) + (c(t,-1) - c(t,1) + x)\, c(t,x)$ belongs to $L^1\left((0,T)\times(-1,1)\right)$, the solution is well-defined in the distributional sense under assumption (6.3). In fact we can write

$$\int_0^T \left(c(t,-1) - c(t,1)\right)\, \mathrm{dt} = -\int_0^T \int_{-1}^1 \partial_x c(t,x)\, \mathrm{dx}\, \mathrm{dt}\,.$$

Let us now observe that the non-negativity of a solution is preserved. Indeed if c is solution in L^1_x, since $\mathrm{sgn}(c)\partial^2_{xx} c \le \partial^2_{xx}|c|$, then

$$\frac{\mathrm{d}}{\mathrm{dt}} \int_{-1}^1 \left(|c| - c\right)\, \mathrm{dx} \le 0.$$

This proves that if $|c_0| = c_0$ almost everywhere (initial data non-negative) then $|c| = c$ almost everywhere for later times.

Moreover, weak solutions in the sense of Definition 8 are mass-preserving: $M = \int_{-1}^1 c_0(x)\, \mathrm{dx} = \int_{-1}^1 c(t,x)\, \mathrm{dx}$. A simple computation on the first momentum defined by $\mathbf{J}(t) = \int_{-1}^1 x c(t,x)\, \mathrm{dx}$, leads to

$$\frac{\mathrm{d}}{\mathrm{dt}}\mathbf{J}(t) = (1-M)\left(c(t,-1) - c(t,1)\right) - \mathbf{J}(t)\,. \tag{6.4}$$

Note that $\mathbf{J}(t) \ge -M$ since $\int_{-1}^1 (x+1)c(t,x)\, \mathrm{dx} \ge 0$.

The main aim of this paper is to provide some results on the long time asymptotics of the solution to (6.1) and to give estimates on the convergence rates in cases of convergence. To this end, we first look for stationary states. Similarly to Calvez et al. [2012, 2010], we will prove that the following dichotomy occurs. In the case $M \le 1$, there exists a unique stationary state $G_M(x) := M exp(-x^2/2)/\int_{-1}^1 exp(-y^2/2)\, \mathrm{dy}$ towards which the solution converges and the asymptotic result is obtained through the convergence to zero of a suitable Lyapunov functional $\mathbf{L}$ defined in (6.7) in the case $M < 1$, and through the convergence to zero of the relative entropy $\mathbf{H}$ defined in (6.6) in the case $M = 1$. Moreover, in both cases, using the logarithmic Sobolev inequality with a suitable function, we obtain an exponential decay to equilibrium.

Theorem 17. *Assume that the initial datum c_0 satisfies both $c_0 \in L^1(-1,1)$ and $\int_{-1}^{1} c_0(x)\log c_0(x)\,\mathrm{d}x < +\infty$. Assume in addition that $M \leq 1$, then there exists a global weak solution of (6.1) that satisfies the following estimates for all $T > 0$,*

$$\begin{aligned} \sup_{t\in(0,T)} \int_{-1}^{1} c(t,x)\log c(t,x)\,\mathrm{d}x &< +\infty\,, \\ \int_0^T \int_{-1}^{1} c(t,x)\left(\partial_x \log c(t,x)\right)^2 \mathrm{d}x\,\mathrm{d}t &< +\infty\,. \end{aligned}$$

Moreover, the solution strongly converges in L^1 towards the unique stationary state $G_M(x)$ and the rate is exponential.

Solutions of (6.1) may become unbounded in finite time (so-called blow-up). This occurs if the mass M is above the critical mass: $M > 1$, and for an asymmetric enough initial profile.

Theorem 18. *Assume $M > 1$ and the first moment shifted of 1 is small: $\tilde{\mathbf{J}}(0) < (M-1)/2$. Assume in addition that c_0 satisfies $c_0(-1) - c_0(1) > 1$. Then the solution to (6.1) with initial data $c(0,x) = c_0(x)$ blows-up in finite time.*

In Figure 6.3, we illustrate Theorems 17 and 18.

Although in the present biological context, blow-up of solutions is interpreted as cell polarisation, such a blow-up in finite time might be questionable. Indeed a strong instability drives the system towards an inhomogeneous state and blow-up corresponds to the case where the drift becomes infinite. The boundary conditions in (6.1) which is responsible for infinite drift turns out to be unrealistic from a biophysical viewpoint. On the way towards a more realistic model, we distinguish between cytoplasmic content $c(t,x)$ and the concentration of trapped molecules on the boundary at $x = \pm 1$: $\mu_\pm(t)$. Then the exchange of molecules at the boundary is described by very simple kinetics.

6.2 Global existence and asymptotic analysis for sub-critical mass $M < 1$

In this section we prove Theorem 17 in the case $M < 1$. The proof is decomposed in three steps. First we compute the stationary state of (6.1), then we build a Lyapunov functional, this allows establishing a-priori estimates. Finally we investigate long-time behaviour of solutions in the case $M < 1$ using entropy methods. We stress out that the method for proving global existence in this case strongly relies on the existence of a Lyapunov functional, Lemma 8. This is why we analyse the global existence and the long time behaviour all in all. Note that the proof is very close to the one given in Calvez et al. [2012] and in Lepoutre et al. [2014]. The differences concern the expression of the stationary state and the domain geometry. In Calvez et al. [2012]; Lepoutre et al. [2014], the stationary state is the family $\{\alpha \exp\left(-\alpha x - x^2/2\right)\}_\alpha$, and the domain is the half-line.

Let us start with the existence of a unique stationary state.

Lemma 7. *If $M < 1$ equation (6.1) admits a unique stationary state given by $G_M = M\exp(-x^2/2)/\int_{-1}^{1}\exp(-y^2/2)\,\mathrm{d}y$.*

Proof. An easy computation shows that any stationary state for (6.1) is either G_M (which is symmetric) or of the form G_α for $\alpha = G_\alpha(-1) - G_\alpha(1) \neq 0$ to be found. For $\alpha > 0$, it writes

$$G_\alpha(x) = \frac{\alpha}{1-\exp(-2\alpha)}\exp\Big(-\alpha(x+1) - \frac{x^2-1}{2}\Big)\,. \tag{6.5}$$

It remains to find α such that the mass constraint $\int_{-1}^{1} G_\alpha(x)\,\mathrm{dx} = \mathrm{M}$ is satisfied. This rewrites $P(\alpha) = M$, P being the function defined by:

$$P(\alpha) \;=\; \int_0^{2\alpha} \frac{1}{1-\exp(-2\alpha)} \exp\left(-y - \frac{1}{2}\left(\left(\frac{y}{\alpha}-1\right)^2 - 1\right)\right) \mathrm{dy}\,.$$

We observe that $P(\alpha) > \int_0^{2\alpha} \frac{1}{1-\exp(-2\alpha)} \exp(-y)\,\mathrm{dy} = 1$, hence there is no stationary state of the form G_α with $\alpha > 0$.

The case $\alpha < 0$ is done similarly. □

Lyapunov functional As it is classical we note the relative entropy

$$\mathbf{H}(u|v) = \int_{-1}^{1} u(x) \log\left(\frac{u(x)}{v(x)}\right) \mathrm{dx}, \tag{6.6}$$

and the Fisher information

$$\mathbf{I}(u|v) = \int_{-1}^{1} u(x) \left(\partial_x \left(\log \frac{u(x)}{v(x)}\right)\right)^2 \mathrm{dx}.$$

Note that $\mathbf{H}(c|G_M) \geq M \log M$ for all $t > 0$ by Jensen's inequality. We introduce a Lyapunov functional for equation (6.1):

$$\mathbf{L}(t) = \mathbf{H}(c|G_M) + \frac{\mathbf{J}(t)^2}{2(1-M)}\,. \tag{6.7}$$

Let Γ_c be defined by

$$\Gamma_c(x) = A_c \exp\left(-\left(c(t,-1) - c(t,1)\right)\, x - \frac{x^2}{2}\right)\,, \tag{6.8}$$

with

$$A_c = \frac{M}{\int_{-1}^{1} \exp\left(-\left(c(t,-1) - c(t,1)\right)\, y - \frac{y^2}{2}\right) \mathrm{dy}}\,. \tag{6.9}$$

Lemma 8. *If $M < 1$, then the Lyapunov functional $\mathbf{L}$ is non-increasing:*

$$\frac{\mathrm{d}}{\mathrm{dt}}\mathbf{L}(t) = -\mathbf{D}(t) \leq 0\,, \tag{6.10}$$

where the dissipation is

$$\mathbf{D}(t) = \mathbf{I}(c|\Gamma_c) + \frac{1}{(1-M)}\Big(\left(c(t,-1) - c(t,1)\right)(1-M) - \mathbf{J}(t)\Big)^2\,. \tag{6.11}$$

Proof. We compute the evolution of the entropy:

$$\frac{\mathrm{d}}{\mathrm{dt}}\mathbf{H}(c|G_M)(t) = \int_{-1}^{1} \partial_t c(t,x) \left(\log(c(t,x)) + \frac{x^2}{2} + 1 - \log\left(\frac{M}{\int_{-1}^{1} e^{-\frac{y^2}{2}}\,\mathrm{dy}}\right)\right) \mathrm{dx}\,,$$

where $\int_{-1}^{1} \partial_t c(t,x)(1 - \log(M/\int_{-1}^{1} e^{-\frac{y^2}{2}}\,\mathrm{dy}))\,\mathrm{dx} = 0$ by mass conservation. Hence,

$$\begin{aligned}
\frac{\mathrm{d}}{\mathrm{dt}}\mathbf{H}(c|G_M)(t) &= -\int_{-1}^{1}\Big(\partial_x c(t,x) + \big(x + c(t,-1) - c(t,1)\big)c(t,x)\Big)\left(\frac{\partial_x c(t,x)}{c(t,x)} + x\right)\mathrm{dx} \\
&= -\int_{-1}^{1} c(t,x)\Big(\partial_x \log c(t,x) + x\Big)^2\,\mathrm{dx} + \mathrm{(c(t,-1) - c(t,1))^2} - \mathrm{(c(t,-1) - c(t,1))}\,\mathbf{J}(\mathrm{t}) \\
&= -\int_{-1}^{1} c(t,x)\Big(\partial_x \log c(t,x) + x + c(t,-1) - c(t,1)\Big)^2\,\mathrm{dx} \\
&\quad + (M-1)\,(c(t,-1) - c(t,1))^2 + (c(t,-1) - c(t,1))\,\mathbf{J}(t)\,. \qquad (6.12)
\end{aligned}$$

We can eliminate $c(t,-1) - c(t,1)$ from (6.12) in the two following steps:

$$\begin{aligned}
(c(t,-1) - c(t,1))\,\mathbf{J}(t) &= \frac{\mathbf{J}(t)}{(1-M)}\frac{\mathrm{d}}{\mathrm{dt}}\mathbf{J}(t) + \frac{\mathbf{J}(t)^2}{(1-M)} \\
&= -\frac{\mathrm{d}}{\mathrm{dt}}\frac{\mathbf{J}(t)^2}{2(1-M)} + \frac{2\mathbf{J}(t)}{(1-M)}\frac{\mathrm{d}}{\mathrm{dt}}\mathbf{J}(t) + \frac{\mathbf{J}(t)^2}{(1-M)}\,, \qquad (6.13)
\end{aligned}$$

leading to

$$-\frac{1}{(1-M)}\left(\frac{\mathrm{d}}{\mathrm{dt}}\mathbf{J}(t)\right)^2 = (M-1)\,(c(t,-1) - c(t,1))^2 + \frac{2\mathbf{J}(t)}{(1-M)}\frac{\mathrm{d}}{\mathrm{dt}}\mathbf{J}(t) + \frac{\mathbf{J}(t)^2}{(1-M)}\,. \qquad (6.14)$$

Combining (6.12) – (6.13) – (6.14), we obtain

$$\mathbf{D}(t) = \int_{-1}^{1} c(t,x)\Big(\partial_x \log c(t,x) + x + c(t,-1) - c(t,1)\Big)^2\,\mathrm{dx} + \frac{1}{(1-\mathrm{M})}\left(\frac{\mathrm{d}}{\mathrm{dt}}\mathbf{J}(\mathrm{t})\right)^2,$$

and the proof of Lemma 8 is complete. □

A priori estimates We now derive a priori bounds for solutions to (6.1) in the classical sense.

Proposition 23 (Main a priori estimate)**.** *Assume that $\int_{-1}^{1} c_0 \log c_0\,\mathrm{dx} < +\infty$. Let c be a classical solution to (6.1). If $M < 1$, then the following global estimates hold true for all $T > 0$:*

$$\begin{aligned}
\sup_{t\in(0,T)}\int_{-1}^{1} c(t,x)\log c(t,x)\,\mathrm{dx} &< +\infty\,, \\
\int_0^T\int_{-1}^{1} c(s,x)(\partial_x \log c(s,x))^2\,\mathrm{dx}\,\mathrm{ds} &< +\infty\,.
\end{aligned}$$

Proof. The proof follows from Lemma 8. Indeed, integrating (6.10) in time, it yields that

$$\begin{aligned}
&\mathbf{H}(c|G_M)(t) + \frac{\mathbf{J}(t)^2}{2(1-M)} + \int_0^t\int_{-1}^{1} c(s,x)\Big(\partial_x \log c(s,x) + x + c(s,-1) - c(s,1)\Big)^2\,\mathrm{dx}\,\mathrm{ds} \\
&+\frac{1}{(1-M)}\int_0^t\left(\frac{\mathrm{d}}{\mathrm{dt}}\mathbf{J}(s)\right)^2\mathrm{ds} = \mathbf{H}(\mathrm{c}|\mathrm{G_M})(0) + \frac{\mathbf{J}(0)^2}{2(1-\mathrm{M})}\,. \qquad (6.15)
\end{aligned}$$

Since $\mathbf{H}(c|G_M) \geq M\log M$, it remains to prove that $c(t,-1) - c(t,1)$ belongs to L^2 locally in time. We first derive the following trace-type inequality:

$$\begin{aligned}
(c(t,-1) - c(t,1))^2 &= \left(\int_{-1}^{1}\partial_x c(t,x)\,\mathrm{dx}\right)^2 \\
&\leq \left(\int_{-1}^{1} c(t,x)\,\mathrm{dx}\right)\left(\int_{-1}^{1} c(t,x)\,(\partial_x \log c(t,x))^2\,\mathrm{dx}\right). \qquad (6.16)
\end{aligned}$$

Furthermore, recalling that

$$2(1-M)\left(c(t,-1)-c(t,1)\right)\mathbf{J}(t)=\frac{\mathrm{d}}{\mathrm{dt}}\mathbf{J}(t)^2+2\mathbf{J}(t)^2\,,$$

and

$$\frac{\mathrm{d}}{\mathrm{dt}}\mathbf{J}(t)^2+\mathbf{J}(t)^2+\left(\frac{\mathrm{d}}{\mathrm{dt}}\mathbf{J}(t)\right)^2=(1-M)^2\left(c(t,-1)-c(t,1)\right)^2\geq 0\,,$$

we deduce that

$$\begin{aligned}&2\left(c(t,-1)-c(t,1)\right)\mathbf{J}(t)+\frac{1}{(1-M)}\left(\frac{\mathrm{d}}{\mathrm{dt}}\mathbf{J}(t)\right)^2\\ =\;&(1-M)\left(c(t,-1)-c(t,1)\right)^2\geq 0\,.\end{aligned}\tag{6.17}$$

which together with inequality (6.16) yields that

$$\begin{aligned}&\int_{-1}^{1}c(t,x)\Big(\partial_x\log c(t,x)+x+c(t,-1)-c(t,1)\Big)^2\,\mathrm{dx}+\frac{1}{(1-\mathrm{M})}\left(\frac{\mathrm{d}}{\mathrm{dt}}\mathbf{J}(\mathrm{t})\right)^2\\ =\;&\int_{-1}^{1}c(t,x)\left(\partial_x\log c(t,x)\right)^2\,\mathrm{dx}+(\mathrm{M}-2)\left(\mathrm{c}(\mathrm{t},-1)-\mathrm{c}(\mathrm{t},1)\right)^2+2\left(\mathrm{c}(\mathrm{t},-1)-\mathrm{c}(\mathrm{t},1)\right)\mathbf{J}(\mathrm{t})\\ &+\int_{-1}^{1}x^2c(t,x)\,\mathrm{dx}-2\mathrm{M}+2\left(\mathrm{c}(\mathrm{t},-1)+\mathrm{c}(\mathrm{t},1)\right)+\frac{1}{(1-\mathrm{M})}\left(\frac{\mathrm{d}}{\mathrm{dt}}\mathbf{J}(\mathrm{t})\right)^2\\ \geq\;&\left(M+\frac{1}{M}-2\right)\left(c(t,-1)-c(t,1)\right)^2-2M\,.\end{aligned}\tag{6.18}$$

The quantity $M+M^{-1}-2$ is positive since $M<1$. Hence, using (6.15) and (6.18) we can prove that $c(t,-1)-c(t,1)$ belongs to L^2 locally in time. Next, using again (6.18) togther with (6.17), we see that

$$\begin{aligned}&\int_{-1}^{1}c(t,x)\Big(\partial_x\log c(t,x)+x+c(t,-1)-c(t,1)\Big)^2\,\mathrm{dx}+\frac{1}{(1-\mathrm{M})}\left(\frac{\mathrm{d}}{\mathrm{dt}}\mathbf{J}(\mathrm{t})\right)^2\\ \geq\;&\int_{-1}^{1}c(t,x)\left(\partial_x\log c(t,x)\right)^2\,\mathrm{dx}+(\mathrm{M}-2)\left(\mathrm{c}(\mathrm{t},-1)-\mathrm{c}(\mathrm{t},1)\right)^2-2\mathrm{M}\,.\end{aligned}\tag{6.19}$$

Hence, $\int_{-1}^{1}c(t,x)\left(\partial_x\log c(t,x)\right)^2\,\mathrm{dx}$ belongs to L^1 locally in time. □

To prove existence of weak solutions in the sense of Definition 8 one should perform a regularization procedure. In this work we focus on long-time dynamics and we will not detail this regularization procedure. Such a regularization procedure is classical and we refer to Calvez et al. [2012] for more details.

Long-time behaviour To prove convergence of $c(t,\cdot)$ towards G_M we develop the following strategy. We use the previous a priori estimates which enable to pass to the limit after extraction. The main argument (apart from passing to the limit) consists in identifying the possible configurations c_∞ for which the dissipation $\mathbf{D}$ vanishes. This occurs if and only if both positive terms in (6.11) are zero. Thanks to (6.4), this means that $\mathbf{J}_\infty=(1-M)\left(c_\infty(-1)-c_\infty(1)\right)$ on the one hand, and on the other hand,

$$\partial_x\log c_\infty(x)+x+c_\infty(-1)-c_\infty(1)=0\,,$$

which yields that $c_\infty\equiv G_M$.

Rate of convergence As it is classical when the equilibrium state is a gaussian function, the natural tool is a logarithmic Sobolev inequality established by Gross in Gross [1975] that we first recall. Although we are dealing here with a non linear problem this method will be fruitful.

Lemma 9 (Logarithmic Sobolev inequality)**.** *Let $\nu(x)dx = \exp(-V(x))dx$ be a measure with smooth density on $[-1,1]$. Assume that $V''(x) \geq 1$ then, for $u \geq 0$ satisfying $\int_{-1}^{1} u(x)\,\mathrm{dx} = \int_{-1}^{1} \nu(\mathrm{x})\,\mathrm{dx}$, we have*

$$\int_{-1}^{1} u(x) \log\left(\frac{u(x)}{\nu(x)}\right) \mathrm{dx} \leq \frac{1}{2}\int_{-1}^{1} \mathrm{u(x)}\left(\partial_{\mathrm{x}}\left(\log\frac{\mathrm{u(x)}}{\nu(\mathrm{x})}\right)\right)^2 \mathrm{dx}\,.$$

First, recalling (6.10) and (6.11), we deduce that

$$\frac{\mathrm{d}}{\mathrm{dt}}\mathbf{L}(t) = -\mathbf{D}(t) = -\mathbf{I}(c|\Gamma_c) - \frac{1}{(1-M)}\Big(\big(c(t,-1)-c(t,1)\big)(1-M) - \mathbf{J}(t)\Big)^2\,.$$

Our aim is to apply a logarithmic Sobolev inequality to $\mathbf{H}(c|\Gamma_c)$. We first observe that

$$\begin{aligned}\frac{\mathrm{d}}{\mathrm{dt}}\mathbf{L}(t) + 2\mathbf{L}(t) &= -\mathbf{I}(c|\Gamma_c) - (1-M)\left(c(t,-1)-c(t,1)\right)^2 + 2\mathbf{H}(c|G_M)\\ &\quad +2\left(c(t,-1)-c(t,1)\right)\mathbf{J}(t)\,,\end{aligned}$$

and we decompose the relative entropy as follows

$$\begin{aligned}\mathbf{H}(c|G_M) &= \int_{-1}^{1} c(t,x)\log\left(\frac{c(t,x)}{G_M(x)}\right)\mathrm{dx}\\ &= \int_{-1}^{1} c(t,x)\log\left(\frac{c(t,x)}{\Gamma_c(x)}\right)\mathrm{dx} + \int_{-1}^{1}\mathrm{c(t,x)}\log\left(\frac{\Gamma_{\mathrm{c}}(\mathrm{x})}{\mathrm{G_M(x)}}\right)\mathrm{dx}\,.\end{aligned}$$

Recalling the definition (6.8) of Γ_c we deduce that

$$\begin{aligned}&\int_{-1}^{1} c(t,x)\log\left(\frac{\Gamma_c(x)}{G_M(x)}\right)\mathrm{dx} = \int_{-1}^{1}\mathrm{c(t,x)}\log\left(\frac{\int_{-1}^{1}\exp\left(-\mathrm{y}^2/2\right)\,\mathrm{dy}}{\mathrm{M}}\right)\mathrm{dx}\\ &+\int_{-1}^{1} c(t,x)\log\Big(A_c\exp\Big(-\left(c(t,-1)-c(t,1)\right)\,x\Big)\Big)\,\mathrm{dx}\\ =\;& M\log\left(\frac{\int_{-1}^{1}\exp\left(-y^2/2\right)\,\mathrm{dy}}{\int_{-1}^{1}\exp\left(-\left(c(t,-1)-c(t,1)\right)y - \frac{y^2}{2}\right)\mathrm{dy}}\right) - \left(c(t,-1)-c(t,1)\right)\mathbf{J}(t)\,,\end{aligned}$$

thanks to the definition (6.9) of A_c. Therefore,

$$\begin{aligned}2\mathbf{H}(c|G_M) &= 2\mathbf{H}(c|\Gamma_c) + 2M\log\left(\frac{\int_{-1}^{1}\exp\left(-x^2/2\right)\,\mathrm{dx}}{\int_{-1}^{1}\exp\left(-\left(c(t,-1)-c(t,1)\right)x - \frac{x^2}{2}\right)\mathrm{dx}}\right)\\ &\quad -2\left(c(t,-1)-c(t,1)\right)\mathbf{J}(t)\,.\end{aligned} \tag{6.20}$$

Finally, applying a logarithmic Sobolev inequality (Lemma 9) to the measure $\Gamma_c(x)\,\mathrm{dx}$ and

using that $-(1-M)\left(c(t,-1)-c(t,1)\right)^2 \leq 0$, we obtain

$$\begin{aligned}\frac{\mathrm{d}}{\mathrm{dt}}\mathbf{L}(t)+2\mathbf{L}(t) &= -\mathbf{I}(c|\Gamma_c)-(1-M)\left(c(t,-1)-c(t,1)\right)^2+2\mathbf{H}(c|\Gamma_c)\\ &\quad +2M\log\left(\frac{\int_{-1}^{1}\exp\left(-x^2/2\right)\,\mathrm{dx}}{\int_{-1}^{1}\exp\left(-\left(c(t,-1)-c(t,1)\right)x-\frac{x^2}{2}\right)\,\mathrm{dx}}\right)\\ &\leq 2M\log\left(\frac{\int_{-1}^{1}\exp\left(-x^2/2\right)\,\mathrm{dx}}{\int_{-1}^{1}\exp\left(-\left(c(t,-1)-c(t,1)\right)x-\frac{x^2}{2}\right)\,\mathrm{dx}}\right)\\ &= -2M\log\left(\int_{-1}^{1}\exp\left(-\left(c(t,-1)-c(t,1)\right)x\right)\frac{G_M(x)}{M}\,\mathrm{dx}\right)\\ &\leq 0\,,\end{aligned}$$

thanks to Jensen's inequality. Hence

$$\frac{\mathrm{d}}{\mathrm{dt}}\mathbf{L}(t)+2\mathbf{L}(t)\leq 0\,,$$

leading to

$$\mathbf{H}(c|G_M)\leq \mathbf{L}(0)\exp(-2t)\,.$$

A rate of convergence for the L^1 norm is obtained by using the Csiszár-Kullback inequality, [Csiszàr, 1967; Kullback, 1968], that we recall now.

Proposition 24 (Csiszár-Kullback inequality)**.** *For any non-negative functions $f,g\in L^1(-1,1)$ such that $\int_{-1}^{1}f(x)\,\mathrm{dx}=\int_{1}^{1}\mathrm{g(x)}\,\mathrm{dx}=\mathrm{M}$, we have that*

$$\|f-g\|_1^2\leq 2M\int_{-1}^{1}f(x)\log\left(\frac{f(x)}{g(x)}\right)\,\mathrm{dx}\,. \tag{6.21}$$

Hence, the following decay estimate holds:

$$\|c(t,x)-G_M(x)\|_{L^1} \leq \sqrt{2M\mathbf{L}(0)}\exp(-t)\,.$$

6.3 Critical case $M=1$

Similarly, we can prove the existence of a stationary solution.

Lemma 10. *For $M=1$, equation (6.1) admits a unique stationary solution given by G_1.*

Proof. The proof is similar to the one of lemma 7. □

In this part we cannot follow the strategy developped in Section 6.2 since we crucially used $M<1$. In the case $M=1$, from (6.12) it follows that

$$\frac{\mathrm{d}}{\mathrm{dt}}\mathbf{H}(c|G_1)=-\mathbf{I}(c|\Gamma_c)+\left(c(t,-1)-c(t,1)\right)\mathbf{J}(t)\,, \tag{6.22}$$

and

$$\begin{aligned}\mathbf{H}(c|G_1) &= \mathbf{H}(c|\Gamma_c)+\log\left(\frac{\int_{-1}^{1}\exp\left(-x^2/2\right)\,\mathrm{dx}}{\int_{-1}^{1}\exp\left(-\left(c(t,-1)-c(t,1)\right)x-\frac{x^2}{2}\right)\,\mathrm{dx}}\right)\\ &\quad -\left(c(t,-1)-c(t,1)\right)\mathbf{J}(t)\,.\end{aligned}$$

Then, together with the logarithmic Sobolev inequality $2\mathbf{H}(c|\Gamma_c) \le \mathbf{I}(c|\Gamma_c)$, we deduce that

$$\frac{\mathrm{d}}{\mathrm{dt}}\mathbf{H}(c|G_1) \le -\mathbf{H}(c|\Gamma_c) - \mathbf{H}(c|G_1) + \log\left(\frac{\int_{-1}^1 \exp\left(-x^2/2\right)\,\mathrm{dx}}{\int_{-1}^1 \exp\left(-\left(c(t,-1)-c(t,1)\right)x - \frac{x^2}{2}\right)\,\mathrm{dx}}\right).$$

Consequently, using again Jensen's inequality, it follows that

$$\frac{\mathrm{d}}{\mathrm{dt}}\mathbf{H}(c|G_1) \le -\mathbf{H}(c|G_1) \le 0\,. \tag{6.23}$$

Consequently we deduce that $0 \le \mathbf{H}(c|G_1)(t) \le \mathbf{H}(c|G_1)(0)$, hence

$$\int_{-1}^1 c(t,x)\log c(t,x)\,\mathrm{dx} \le \mathrm{C}_0\,, \quad \text{a.e. t} \in (0,+\infty)\,.$$

A priori bound To obtain a control on the dissipation of entropy, we follow the strategy developped in Calvez et al. [2012]. Consider the even function $\Lambda : \mathbb{R} \to \mathbb{R}_+$ such that $\Lambda(0) = 0$, and $\Lambda'(u) = (\log(u))_+^{1/2}$ for $u > 0$. Then, it is non-increasing on $(-\infty, 0)$, non-decreasing on $(0, +\infty)$, convex and superlinear, and for all D, there exists $A \in \mathbb{R}_+$ such that for any $u \in (-\infty, -A) \cup (A, +\infty)$, $\Lambda(u)^2 \ge (1+D)C_0u^2$. Using again a trace-type inequality, we get

$$\begin{aligned}
\Lambda\left(c(t,-1)-c(t,1)\right)^2 &= \left(-\int_{-1}^1 \partial_x\Lambda(c(t,x)-c(t,1))\,\mathrm{dx}\right)^2,\\
&= \left(-\int_{-1}^1 \Lambda'(c(t,x)-c(t,1))c(t,x)\partial_x\log(c(t,x))\,\mathrm{dx}\right)^2,\\
&\le \left(\int_{-1}^1 c(t,x)\left|\Lambda'(c(t,x)-c(t,1))\right|^2\,\mathrm{dx}\right)\left(\int_{-1}^1 c(t,x)(\partial_x\log(c(t,x)))^2\,\mathrm{dx}\right)\\
&\le \left(\int_{-1}^1 c(t,x)\log(c(t,x))_+\,\mathrm{dx}\right)\left(\int_{-1}^1 c(t,x)(\partial_x\log(c(t,x)))^2\,\mathrm{dx}\right)\\
&\le C_0\left(\int_{-1}^1 c(t,x)(\partial_x\log(c(t,x)))^2\,\mathrm{dx}\right). \qquad (6.24)
\end{aligned}$$

Moreover, recall that we have

$$\begin{aligned}
\frac{\mathrm{d}\mathbf{H}(\mathrm{c}|\mathrm{G}_1)(\mathrm{t})}{\mathrm{dt}} &= \alpha(t)\mathbf{J}(t) - \int_{-1}^1 c(t,x)\left(\partial_x\log(c(t,x)) + \alpha(t) + x\right)^2\,\mathrm{dx}\,, \qquad (6.25)\\
&= \alpha(t)^2 - \alpha(t)\mathbf{J}(t) + 2(1-c(t,1)-c(t,-1)) - \mathbf{K}(t) - \int_{-1}^1 c(t,x)\left(\partial_x\log(c(t,x))\right)^2\,\mathrm{dx}\,,\\
&\le \alpha(t)^2 - \alpha(t)\mathbf{J}(t) + 2 - \int_{-1}^1 c(t,x)\left(\partial_x\log(c(t,x))\right)^2\,\mathrm{dx}\,,
\end{aligned}$$

with $\mathbf{K}(t) = \int_{-1}^1 x^2c(t,x)\,\mathrm{dx} \ge 0$. Combining (6.23) and (6.24), it leads to

$$\frac{\mathrm{d}\mathbf{H}(\mathrm{c}|\mathrm{G}_1)(\mathrm{t})}{\mathrm{dt}} \le \begin{cases} 0 & \text{if } |\alpha(t)| \le A\\ -\frac{\Lambda(\alpha(t))^2}{C_0} + \alpha(t)^2 + 2 - \alpha(t)\mathbf{J}(t) \le -D\alpha(t)^2 + 2 - \alpha(t)\mathbf{J}(t) & \text{if } |\alpha(t)| > A\,. \end{cases}$$

We can assume $A > \sqrt{2}$, so that $\alpha(t)^2 > 2$. In the case $|\alpha(t)| > A$, as $\mathbf{J}(t) = \mathbf{J}(0)e^{-t}$, we have $-\alpha(t)\mathbf{J}(t) \leq \alpha(t)^2|\mathbf{J}(0)|$, and

$$-D\alpha(t)^2 + 2 - \alpha(t)\mathbf{J}(t) \leq -(D - 1 - |\mathbf{J}(0)|)\alpha(t)^2 .$$

Take $D = 2 + |\mathbf{J}(0)|$. Then,

$$\frac{\mathrm{d}\mathbf{H}(\mathrm{c}|\mathrm{G}_1)(\mathrm{t})}{\mathrm{dt}} \leq \begin{cases} 0 & \text{if } |\alpha(t)| \leq A \\ -\alpha(t)^2 & \text{if } |\alpha(t)| > A . \end{cases}$$

Now, on the set $E = \{t : |\alpha(t)| > A\}$, we have

$$\int_E \alpha(t)^2 \,\mathrm{dt} \leq \mathbf{H}(\mathrm{c}|\mathrm{G}_1)(0) , \tag{6.26}$$

giving a L^2 control on $\alpha(t)$.

Finally, using (6.25) and (6.26), we prove that $\int_0^t \int_{-1}^1 c(s,x) \left(\partial_x \log(c(s,x))\right)^2 \,\mathrm{dx}\,\mathrm{dt}$ is bounded for all $t \in (0,T)$. Then, proposition 23 is still verified, and we can similarly prove the global existence of weak solutions in the critical case.

Long-time behaviour The convergence of $c(t,\cdot)$ towards G_M is proved as in the sub-critical case.

Rate of convergence By (6.23), we know that

$$\mathbf{H}(c|G_1)(t) \leq \mathbf{H}(c|G_1)(0)e^{-t} .$$

Hence, the Csiszár-Kullback inequality leads to the following estimation:

$$\|c(t,x) - G_M(x)\|_{L^1} \quad \leq \quad \sqrt{2M\mathbf{H}(c|G_1)(0)}\exp(-t/2) .$$

6.4 The Super-critical case $M > 1$

We prove now that depending on the mass, the problem (6.1) admits one or three stationary solutions. Then, we prove that if the initial condition is asymmetric enough, a blow-up occurs in finite time, and we are able to give a quantitative criterion for its apparition. The proof is based on the blow-up analysis for a modified problem, followed by the use of a concentration-comparison principle to deduce the blow-up in our case. Numerical simulations displayed in figure 6.3 show the apparition of a blow-up.

6.4.1 Stationary solutions

We establish now the following lemma.

Lemma 11. *Denote* $M_0 = \frac{1}{2}\int_{-1}^1 exp\left(-\frac{x^2-1}{2}\right) \mathrm{dx} > 1$. *Then,*

- *for* $M \in (1, M_0)$, *equation* (6.1) *admits exactly three stationary states: the symmetric solution* G_M, *and two asymmetric solutions* $G_{\pm\alpha}$, *with*

$$G_\alpha(x) = \frac{\alpha}{1 - \exp(-2\alpha)} \exp\Big(- \alpha(x+1) - \frac{x^2-1}{2}\Big) ,$$

for some $\alpha > 0$ *defined by the mass constraint* $\int_{-1}^1 G_\alpha(x)\,\mathrm{dx} = \mathrm{M}$.

- *for $M \geq M_0$, G_M is the only stationary solution.*

Proof. We have seen in the proof of lemma 7 that the only possible stationary solutions are of the form G_M and G_α. It is straightforward that for all $M > 1$, G_M is solution and satisfies the mass constraint. For G_α, let us denote $M_\alpha = \int_{-1}^{1} G_\alpha(x)\,\mathrm{dx}$. We know that $M_\alpha > 1$. It remains to characterize the set $I = \{M_\alpha,\, \alpha > 0\}$ of attainable mass values. As we were not able to characterize I explicitly, we performed a numerical simulation of M_α as a function of α (see figure 6.5, a)). Notice that M_0 is defined such that $\lim_{\alpha\to 0} G_\alpha = G_{M_0}$, leading to the result. □

6.4.2 Blow-up for a modified equation

In this section we consider the following modified equation of (6.1):

$$\partial_t c(t,x) = \partial_x\Big(\partial_x c(t,x) + \left(-1 + c(t,-1) - c(t,1)\right) c(t,x)\Big)\,, \tag{6.27}$$

where $c(t,x)$ is defined for $t > 0$ and $x \in (-1,1)$, together with zero-flux boundary conditions:

$$\begin{cases} \partial_x c(t,-1) + \left(c(t,-1) - c(t,1) - 1\right) c(t,-1) = 0\,, \\ \partial_x c(t,1) + \left(c(t,-1) - c(t,1) - 1\right) c(t,1) = 0\,, \end{cases} \tag{6.28}$$

and an initial condition: $c(t=0,x) = c_0(x)$. The total mass will also be denoted by M, i.e. $M = \int_{-1}^{1} c(t,x)\,\mathrm{dx}$.

In this part we will prove that solutions to (6.27) - (6.28) blow-up in finite time when mass is super-critical $M > 1$ and c_0 is decreasing and satisfies $c_0(-1) - c_0(1) > 1$. To do so we prove that the first momentum shifted in $x = -1$ of c, $\tilde{\mathbf{J}}(t) = \int_{-1}^{1}(x+1)c(t,x)\,\mathrm{dx}$ cannot remain positive for all time. This technique was first used by Nagai [1995], then by many authors in various contexts. In a first step, in Lemma 12, we establish that the assumption that c_0 is a decreasing function such that $c_0(-1) - c_0(1) > 1$ and that the $\tilde{\mathbf{J}}(0)$ is sufficiently small guarantee that $c(t,\cdot)$ is also decreasing and satisfies $c(t,-1) - c(t,1) > 1$ for any existence time $t > 0$. In a second step, in Proposition 25, we prove the blow-up character.

Lemma 12. *Assume that $M > 1$. Assume in addition that the initial condition c_0 of (6.27) is decreasing, satisfies $c_0(-1) - c_0(1) > 1$ and $\int_{-1}^{1}(x+1)c_0(x)\,\mathrm{dx} < (\mathrm{M}-1)/2$. Then any solution c to (6.27), if it exists, is non-increasing and satisfies $c(t,-1) - c(t,1) > 1$.*

Proof. Since we supposed that $c_0(-1) - c_0(1) > 1$, it remains true at least until a time $t_0 \in (0,T)$, where T is the existence time. We choose the maximal t_0 possible. For all $t \in [0,t_0]$, $c(t,\cdot)$ is decreasing. In fact the derivative $u(t,x) = \partial_x c(t,x)$, satisfies the following parabolic type equation without any source term:

$$\partial_t u(t,x) = \partial_{xx} u(t,x) + \partial_x\Big(\left(-1 + c(t,-1) - c(t,1)\right) u(t,x)\Big)\,. \tag{6.29}$$

The solution is initially non-positive, and also initially non-positive on the boundary due to (6.28) - (6.28) and the assumption $c_0(-1) - c_0(1) > 1$. From classical strong maximum principle, we deduce that $c(t,\cdot)$ is decreasing for all $t \in [0,t_0]$.

Therefore, for all $t \in [0,t_0]$, $-\partial_x c(t,x)/\left(c(t,-1) - c(t,1)\right)$ is a probability density. From Jensen's inequality, we deduce the following interpolation estimate:

$$\left(\int_{-1}^{1}(x+1)\frac{-\partial_x c(t,x)}{c(t,-1)-c(t,1)}\,\mathrm{dx}\right)^2 \leq \int_{-1}^{1}(x+1)^2\frac{-\partial_x c(t,x)}{c(t,-1)-c(t,1)}\,\mathrm{dx}\,,$$

hence, using that $c(t,-1) > c(t,1)$ for any time $t \in [0,t_0]$, it follows that

$$(M - 2c(t,1))^2 \leq (c(t,-1) - c(t,1)) \left(2\int_{-1}^{1} (x+1)c(t,x)\,\mathrm{dx} - 4\mathrm{c(t,1)} \right) . \tag{6.30}$$

Consequently, for all t in $[0,t_0]$, the first momentum shifted in $x=-1$, $\tilde{\mathbf{J}}(t) = \int_{-1}^{1}(x+1)c(t,x)\,\mathrm{dx}$, which is non-negative and such that $2\tilde{\mathbf{J}}(t) \geq 4c(t,1)$, for all t in $[0,t_0]$, thanks to (6.30), satisfies:

$$\begin{aligned} \frac{\mathrm{d}}{\mathrm{dt}}\tilde{\mathbf{J}}(t) &\leq M + (1-M)\left(c(t,-1) - c(t,1)\right) \leq (1-M)\frac{(M-2c(t,1))^2}{2\tilde{\mathbf{J}}(t) - 4c(t,1)} + M \\ &\leq (1-M)\frac{M^2 - 4Mc(t,1)}{2\tilde{\mathbf{J}}(t)} + M\,, \end{aligned} \tag{6.31}$$

as $M > 1$. Using again that $2\tilde{\mathbf{J}}(t) \geq 4c(t,1)$, we deduce that

$$\frac{\mathrm{d}}{\mathrm{dt}}\tilde{\mathbf{J}}(t) \leq \frac{M(1-M)}{2\tilde{\mathbf{J}}(t)}\left(M - 2\tilde{\mathbf{J}}(t)\right) + M \leq \frac{M^2(1-M)}{2\tilde{\mathbf{J}}(t)}\left(1 - \frac{2\tilde{\mathbf{J}}(t)}{M-1}\right) .$$

Since $\tilde{\mathbf{J}}(0) < (M-1)/2$ and $\tilde{\mathbf{J}}(t) \geq 0$ we deduce that for all $t \in [0,t_0]$: $\frac{\mathrm{d}}{\mathrm{dt}}\tilde{\mathbf{J}}(t) \leq 0$, hence $\tilde{\mathbf{J}}(t) \leq \tilde{\mathbf{J}}(0) < \frac{M-1}{2}$. Consequently, using (6.30), it follows that for all t in $[0,t_0]$,

$$c(t-1) - c(t,1) \geq \frac{M\left(M - 2\tilde{\mathbf{J}}(0)\right)}{2\tilde{\mathbf{J}}(0)} \geq \frac{M}{M-1} > 1\,,$$

hence $t_0 = T$ is the existence time of c. □

We can now prove a blow-up result on (6.27) - (6.28).

Proposition 25. *Assume $M > 1$ and that the first moment shifted in 1 is initially small: $\tilde{\mathbf{J}}(0) < (M-1)/2$. Assume in addition that c_0 is decreasing and satisfies $c_0(-1) - c_0(1) > 1$. Then the solution to (6.27) - (6.28) with initial data $c(0,x) = c_0(x)$ blows-up in finite time.*

Proof. From Lemma (12) it follows that

$$\frac{\mathrm{d}}{\mathrm{dt}}\tilde{\mathbf{J}}(t) \leq \frac{M^2(1-M)}{2\tilde{\mathbf{J}}(t)}\left(1 - \frac{2\tilde{\mathbf{J}}(t)}{M-1}\right) \leq \frac{M^2(1-M)}{2\tilde{\mathbf{J}}(t)}\left(1 - \frac{2\tilde{\mathbf{J}}(0)}{M-1}\right) . \tag{6.32}$$

Hence, since $\tilde{\mathbf{J}}(0) < (M-1)/2$, we deduce the inequality

$$\tilde{\mathbf{J}}(t) \leq \tilde{\mathbf{J}}(0) + \frac{(1-M)M^2}{2}\left(1 - \frac{2\tilde{\mathbf{J}}0)}{M-1}\right)\int_0^t \frac{1}{\tilde{\mathbf{J}}(s)}\,\mathrm{ds}\,. \tag{6.33}$$

We introduce the auxiliary function $\mathbf{K}(t) = \tilde{\mathbf{J}}(0) + \frac{(1-M)M^2}{2}\left(1 - \frac{2\tilde{\mathbf{J}}(0)}{M-1}\right)\int_0^t \tilde{\mathbf{J}}(s)^{-1}\,\mathrm{ds}$. It is positive, it satisfies $\mathbf{K}(t) \geq \tilde{\mathbf{J}}(t)$ together with the following differential inequality:

$$\frac{\mathrm{d}}{\mathrm{dt}}\mathbf{K}(t) = \frac{(1-M)M^2}{2\tilde{\mathbf{J}}(t)}\left(1 - \frac{2\tilde{\mathbf{J}}(0)}{M-1}\right) \leq \frac{(1-M)M^2}{2\mathbf{K}(t)}\left(1 - \frac{2\tilde{\mathbf{J}}(0)}{M-1}\right) ,$$

hence,

$$\frac{\mathrm{d}}{\mathrm{dt}}\mathbf{K}(t)^2 \leq (1-M)M^2\left(1-\frac{2\tilde{\mathbf{J}}(0)}{M-1}\right) < 0\,.$$

We obtain a contradiction: the maximal time of existence T^* is necessarily finite when $M > 1$. On the other hand, following Jäger and Luckhaus [1992], it can be proved that the modulus of integrability has to become singular at T^*:

$$\lim_{K\to+\infty}\left(\sup_{t\in(0,T^*)}\int_{-1}^{1}(c(t,x)-K)_+\,\mathrm{dx}\right) > 0\,.$$

Otherwise a truncation method enables to prove local existence by replacing c with $(c-K)_+$ for K sufficiently large. □

6.4.3 Blow-up in the Super-critical case

In this part, we prove Theorem 18. To do so, following Lepoutre et al. [2014], we state a so-called concentration-comparison principle on the equation obtained from (6.1) after space integration. This principle together with the use of a subsolution that blows-up allow proving the blow-up character of solutions to (6.1) above the critical mass.

Lemma 13. *Let $C, \bar{C}, \underline{C}$ be non-decreasing (in space) functions in $C^1(0,T;C^2([-1,1]))$ satisfying*

$$\begin{cases} \partial_t C(t,x) - \partial_{xx}C(t,x) - \Big(x + \partial_x C(t,-1) - \partial_x C(t,1)\Big)\partial_x C(t,x) = 0\,, \\ \partial_t \bar{C}(t,x) - \partial_{xx}\bar{C}(t,x) - \Big(x + \partial_x \bar{C}(t,-1) - \partial_x \bar{C}(t,1)\Big)\partial_x \bar{C}(t,x) \geq 0\,, \\ \partial_t \underline{C}(t,x) - \partial_{xx}\underline{C}(t,x) - \Big(x + \partial_x \underline{C}(t,-1) - \partial_x \underline{C}(t,1)\Big)\partial_x \underline{C}(t,x) \leq 0\,, \\ C(t,-1) = \bar{C}(t,-1) = \underline{C}(t,-1) = 0\,. \end{cases} \tag{6.34}$$

Assume that $\underline{C}(0,\,\cdot\,) \leq C(0,\,\cdot\,) \leq \bar{C}(0,\,\cdot\,)$ and that $\partial_x\bar{C}(0,-1) - \partial_x\bar{C}(0,1) > \partial_x\underline{C}(0,-1) - \partial_x\underline{C}(0,1)$, then the following inequality holds true for all $0 < t \leq T$:

$$\underline{C}(t,.) < \bar{C}(t,.).$$

Proof. From (6.34), we deduce that $\delta C = \bar{C} - \underline{C}$ satisfies the parabolic inequation

$$\begin{aligned} &\partial_t \delta C(t,x) - \partial_{xx}\delta C(t,x) - \Big(x + \partial_x \bar{C}(t,-1) - \partial_x \bar{C}(t,1)\Big)\partial_x \delta C(t,x) \\ &\geq \Big(\Big(\partial_x \bar{C}(t,-1) - \partial_x \bar{C}(t,1)\Big) - \Big(\partial_x \underline{C}(t,-1) - \partial_x \underline{C}(t,1)\Big)\Big)\partial_x \underline{C}(t,x)\,, \end{aligned}$$

with $\bar{C}(t,-1) = \underline{C}(t,-1) = 0$. Since we supposed that $\partial_x\bar{C}(0,-1) - \partial_x\bar{C}(0,1) > \partial_x\underline{C}(0,-1) - \partial_x\underline{C}(0,1)$, it remains true at least until a time $T' \in (0,T)$, and we choose the maximal T' possible. Since $\partial_x\underline{C} \geq 0$, on the time interval $[0,T']$, we have

$$\begin{cases} \partial_t \delta C(t,x) - \partial_{xx}\delta C(t,x) - \Big(\partial_x \bar{C}(t,-1) - \partial_x \bar{C}(t,1)\Big)\partial_x \delta C(t,x) - x\partial_x \delta C(t,x) \geq 0\,, \\ \bar{C}(t,-1) = \underline{C}(t,-1) = 0\,. \end{cases}$$

Hence, by strong maximum principle [Evans, 1998], $\bar{C} > \underline{C}$ on $(0,T') \times (-1,1)$. Furthermore, by Hopf Lemma (see Evans [1998]), we also have

$$\begin{cases} \partial_x \delta C(T',-1) = \partial_x \bar{C}(T',-1) - \partial_x \underline{C}(T',-1) > 0\,, \\ \partial_x \delta C(T',1) = \partial_x \bar{C}(T',1) - \partial_x \underline{C}(T',1) < 0\,. \end{cases}$$

As T' is maximal we immediately conclude that $T' = T$. □

Proof. Proof of Theorem 18. Let $\underline{c}_0$ be a decreasing function such that $\underline{c}_0(x) \leq c_0(x)$ for all $x \in [-1,1]$ and which satisfies $\int_{-1}^{1} \underline{c}_0(x)\,\mathrm{dx} > 1$. Assume in addition that $c_0(-1) - c_0(1) > \underline{c}_0(-1) - \underline{c}_0(1) > 1$. Finally assume that $\int_{-1}^{1}(x+1)\underline{c}_0(x)\,\mathrm{dx} < (\mathrm{M}-1)/2$, where we recall that $M = \int_{-1}^{1} c(t,x)\,\mathrm{dx} > 1$. First according to Proposition 25, we know that the solution $\underline{c}$ to (6.27) - (6.28) with initial data $\underline{c}(0,x) = \underline{c}_0(x)$ blows-up in finite time.

We will now prove that the distribution function $\underline{C}(t,x) = \int_{-1}^{x} \underline{c}(t,y)\,\mathrm{dy}$ satisfies

$$\partial_t \underline{C}(t,x) - \partial_{xx}\underline{C}(t,x) - \Big(x + \partial_x \underline{C}(t,-1) - \partial_x \underline{C}(t,1)\Big)\partial_x \underline{C}(t,x) \leq 0\,.$$

Indeed integrating (6.27) - (6.28) in space, one obtains

$$\partial_t \underline{C}(t,x) - \partial_{xx}\underline{C}(t,x) - \Big(-1 + \partial_x \underline{C}(t,-1) - \partial_x \underline{C}(t,1)\Big)\partial_x \underline{C}(t,x) = 0\,.$$

Hence,

$$\partial_t \underline{C}(t,x) - \partial_{xx}\underline{C}(t,x) - \Big(x + \partial_x \underline{C}(t,-1) - \partial_x \underline{C}(t,1)\Big)\partial_x \underline{C}(t,x) = -(x+1)\partial_x \underline{C}(t,x) \leq 0\,,$$

where the last inequality follows from the non-decreasing character of $\underline{C}(t,\cdot)$ together with $x \geq -1$. Hence, from Lemma 13, it follows that $\underline{C}(t,.) < \bar{C}(t,.)$ for all time below the existence time T, where $\bar{C}(t,.)$ is any function defined in (6.34). In particular, for c solution to (6.1) with initial data $c(0,x) = c_0(x)$, we can set $\bar{C}(t,x) = \int_{-1}^{x} c(t,y)\,\mathrm{dy}$, which yields the blow-up character of c. □

6.5 Dynamical exchange of markers at the boundary: prevention of blow-up and asymptotic behaviour

In Section 6.4, we proved that finite time blow-up occurs in the basic model (6.1) when mass is super-critical $M > 1$. Such a behaviour is not realistic from a biological viewpoint. Here we modifiy the model model (6.1) by considering markers that are sticked to the boundary and thus create the attracting drift. More precisely, in this part we will study the stationary states associated with the following model:

$$\begin{cases} \partial_t c(t,x) = \partial_{xx} c(t,x) + \partial_x\left((x + \mu_-(t) - \mu_+(t))\,c(t,x)\right)\,, \quad t>0\,,\, x \in (-1,1) \\ \frac{\mathrm{d}}{\mathrm{dt}}\mu_-(t) = c(t,-1) - \mu_-(t)\,, \\ \frac{\mathrm{d}}{\mathrm{dt}}\mu_+(t) = c(t,1) - \mu_+(t)\,, \end{cases} \tag{6.35}$$

together with the flux condition at the boundary:

$$\begin{cases} \partial_x c(t,-1) + (-1 + \mu_-(t) - \mu_+(t))\,c(t,-1) = \frac{\mathrm{d}}{\mathrm{dt}}\mu_-(t)\,, \\ \partial_x c(t,1) + (1 + \mu_-(t) - \mu_+(t))\,c(t,1) = -\frac{\mathrm{d}}{\mathrm{dt}}\mu_+(t)\,. \end{cases} \tag{6.36}$$

The quantities $\mu_\pm$ represent the concentrations of markers which are sticked to the boundary and thus create the attracting drift $\mu_-(t) - \mu_+(t)$. The dynamics of $\mu_\pm$ is driven by simple attachment/detachment kinetics. The mass of molecular markers is shared between the free particles $c(t,x)$ and the particles on the boundary $\mu_\pm(t)$. The boundary condition (6.36) guarantees conservation of the total mass:

$$\int_{-1}^{1} c(t,x)\,\mathrm{dx} + \mu_-(\mathrm{t}) + \mu_+(\mathrm{t}) = \mathrm{M}\,. \tag{6.37}$$

From (6.37), we easily deduce that finite time blow-up cannot occur since $|\mu_-(t) - \mu_+(t)|$ is bounded by M. We denote by $m(t)$ the mass of free particles:

$$m(t) = \int_{-1}^{1} c(t,x)\,\mathrm{dx}\,.$$

The conservation of mass reads

$$\frac{\mathrm{d}}{\mathrm{dt}} m(t) + \frac{\mathrm{d}}{\mathrm{dt}}\left(\mu_-(t) + \mu_+(t)\right) = 0\,.$$

Stationary solutions (c, μ_-, μ_+) are characterized by:

$$\begin{cases} c(x) = c(-1)e^{-\frac{x^2-1}{2} - \alpha(x+1)}\,,\ x \in (-1,1) \\ \alpha = c(-1)(1 - e^{-2\alpha})\,, \\ \int_{-1}^{1} c(x)\,\mathrm{dx} + \mathrm{c}(-1) + \mathrm{c}(1) = \mathrm{M}\,, \\ (\mu_-, \mu_+) = (c(-1), c(1))\,, \end{cases}$$

where we have denoted $\alpha = c(-1) - c(1)$.

We establish the following lemma.

Lemma 14. *Denote* $M_0 = 1 + \frac{1}{2}\int_{-1}^{1} exp\left(-\frac{x^2-1}{2}\right)\,\mathrm{dx} > 1$. *Then,*

- *for* $M \leq M_0$, *the problem* (6.35) - (6.36) *admits a unique symmetric stationary solution* G_M *defined by:*

$$G_M(x) = \frac{M}{2 + \int_{-1}^{1} e^{-\frac{x^2-1}{2}}\,\mathrm{dx}} e^{-\frac{x^2-1}{2}}\,\mathrm{dx}\,. \tag{6.38}$$

- *for* $M > M_0$, *there are two other asymmetric solutions* $G_{\pm\alpha}$, *with*

$$G_\alpha(x) = \frac{\alpha}{1 - e^{-2\alpha}} e^{-\frac{x^2-1}{2} - \alpha(x+1)}\,,$$

for some $\alpha > 0$ *defined by the mass constraint*

$$M_\alpha := \frac{\alpha}{1 - e^{-2\alpha}}\left(2 + \int_{-1}^{1} e^{-\frac{x^2-1}{2} - \alpha(x+1)}\,\mathrm{dx}\right) - \alpha = M\,.$$

Proof. A simple computation yields that any stationary solution is either of the form G_M or of the form G_α. It is straightforward that for all $M > 0$, G_M is solution and satisfies the mass constraint. For G_α, we need to characterize the set $I = \{M_\alpha,\ \alpha > 0\}$. It can be proved that for all $\alpha > 0$, $M_\alpha = M_{-\alpha}$, and $M_\alpha \sim_{+\infty} \alpha$, and that $\lim_{\alpha\to 0} M_\alpha = M_0$. As before, we performed a numerical simulation of M_α as a function of α (see figure 6.5, b)), leading to $I = (M_0, +\infty)$, hence the result. □

Numerical simulations for this model are presented in figure 6.4.

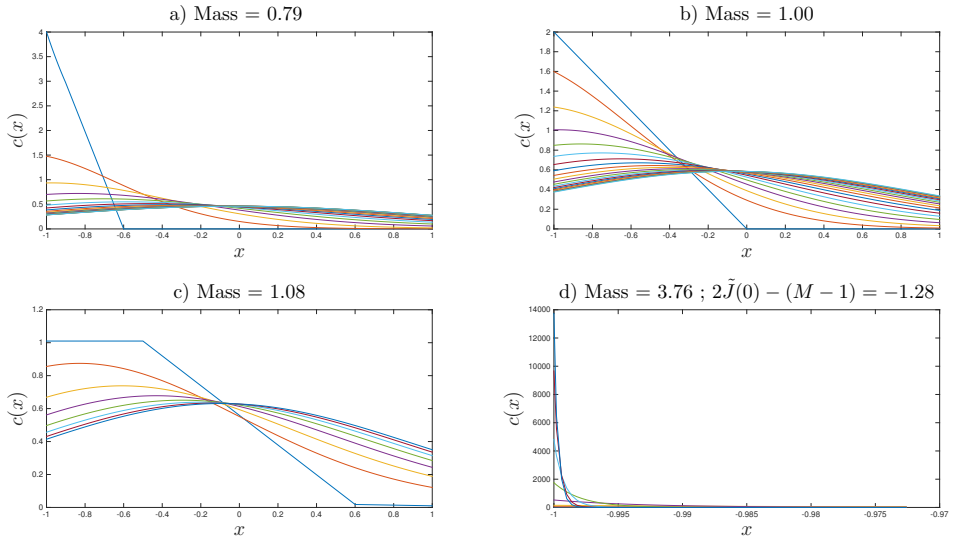

Figure 6.3 – Numerical simulations of the spatial concentration profile $c(x)$ of the marker in the simple model. Each plot corresponds to a different initial profile and mass : a) sub-critical case ; b) critical case ; c), d) super-critical case. Each curve represents the concentration profile at a specific time. Parameters: $T = 4$; $dt = 10^{-2}$; $dx = 2 * 10^{-3}$.

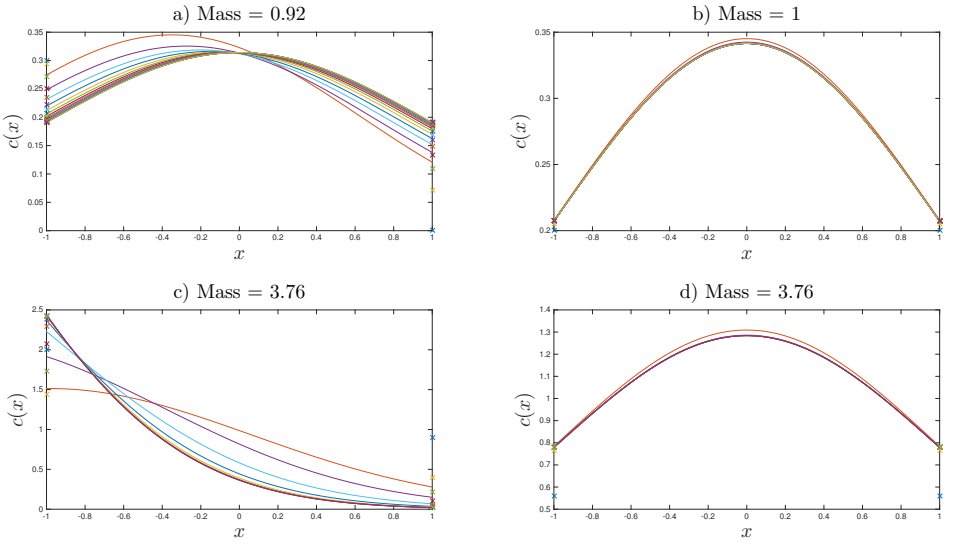

Figure 6.4 – Numerical simulations of the spatial concentration profile $c(x)$ of the marker, for the dynamical exchange model. Each plot corresponds to a different initial profile and mass : a) sub-critical case ; b) critical case ; c), d) super-critical case. Each curve represents the concentration profile at a specific time. Parameters: $T = 20$; $dt = 10^{-2}$; $dx = 2 * 10^{-3}$.

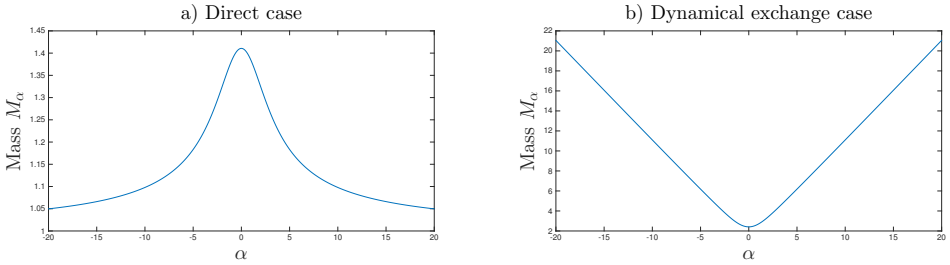

Figure 6.5 – Mass of G_α as a function of α for a) the direct case ; b) the dynamical exchange case.

6.6 Perspectives

In this work, we presented a model of 1D cell migration based on the diffusion and advection of a molecular marker inside the cell, that itself exerts a feedback on this dynamics. The marker's spatial repartition is supposed to be characteristic of the polarisation state of the cell. The resulting equation, a non linear and non local Fokker-Planck equation, was shown to admit a dichotomy behaviour at equilibrium. Below and at the critical mass, polarisation is not possible. Above the critical mass, and below a limiting mass M_0, the system admits two polarised equilibria. Moreover, we have proved that for initial concentrations "steep enough", a blow up occurs in finite time, corresponding to a polarised state, but mainly showing that the model lacks regularity and that there is room for improvement. We next presented a more realistic model, where attachment-detachment kinetics of the marker at the membrane is taken into account. In this case, we were able to prove again a dichotomy behaviour for the existence of asymmetric steady states, and that the additional dynamics at the boundary is enough to prevent the blow up apparition.

A few questions remain today unresolved, and will be the object of a future work. The stability of either symmetric or asymmetric stationary states ought to be discussed, as prospective numerical simulations suggest non trivial results. Also, in the super critical case, it is of interest to search for a quantitative criterion to discriminate between the three stationary solutions. Finally, the controllability of the cell velocity can be studied.

This model was designed to investigate the initiation of polarisation during motion. In order to describe a whole displacement, a stochastic instability could be included in the marker's dynamics. Then, the dichotomy's result could be investigated at long time scales. The question of an external signal perturbing the molecular dynamics is of similar nature.

A natural continuation consists in studying the corresponding 2D model, in order to investigate at least numerically polarisation initiation. Moreover, the inclusion of stochastic fluctuations in the dynamics would allow for numerical simulations of realistic trajectories. As a consequence, the impact of various external triggers such as chemical signals and mechanical obstacles can be investigated.

Bibliography

Calvez, V., Hawkins, R. J., Meunier, N., and Voituriez, R. (2012). Analysis of a Nonlocal Model for Spontaneous Cell Polarization. SIAM Journal on Applied Mathematics, 72(2):594–622. 189, 190, 192, 193, 196, 199

Calvez, V., Meunier, N., and Voituriez, R. (2010). A one-dimensional Keller–Segel equation with a drift issued from the boundary. Comptes Rendus Mathematique, 348(11):629–634. 189, 190, 192

Csiszàr, I. (1967). Information-type measures of difference of probability distributions and indirect observations. Studia Sci. Math. Hungar., 2:299–318. 198

Evans, L. C. (1998). Partial differential equations. Graduate studies in mathematics. American Mathematical Society, Providence (R.I.). 203

Gross, L. (1975). Logarithmic Sobolev inequalities. American Journal of Mathematics, 97(4):1061–1083. 197

Hawkins, R. J., Bénichou, O., Piel, M., and Voituriez, R. (2009). Rebuilding cytoskeleton roads: active-transport-induced polarization of cells. Phys Rev E Stat Nonlin Soft Matter Phys, 80(4 Pt 1):040903. 189, 190

Jäger, W. and Luckhaus, S. (1992). On explosions of solutions to a system of partial differential equations modelling chemotaxis. Transactions of the american mathematical society, 329(2):819–824. 203

Kullback, S. (1968). On the convergence of discrimination information (corresp.). IEEE Transactions on Information Theory, 14(5):765–766. 198

Lepoutre, T., Meunier, N., and Muller, N. (2014). Cell polarisation model : the 1D case. Journal des Mathematiques Pures et Appliquees, 101(2):152–171. 189, 190, 193, 203

Muller, N., Piel, M., Calvez, V., Voituriez, R., Gonçalves-Sá, J., Guo, C.-L., Jiang, X., Murray, A., and Meunier, N. (2016). A predictive model for yeast cell polarization in pheromone gradients. PLoS Comput Biol, 12(4):e1004795. 189, 190

Nagai, T. (1995). Blow-up of radially symmetric solutions to a chemotaxis system. Advances in Mathematical Sciences and Applications, 5:581–601. 201

Chapter 7

The discoidal 2D model

Contents

7.1 Introduction . . . 209
7.2 Models under study . . . 211
7.3 Cell intrinsic activity: first results . . . 212
7.3.1 Non motile case . . . 212
7.3.2 The motile case . . . 213
7.4 Stochastic effects . . . 217
7.4.1 Random initial profile . . . 217
7.4.2 Noised activity: depolymerization/transport . . . 217
7.5 Stimulation by a chemical signal . . . 223
7.5.1 Signal acting on the boundary . . . 224
7.5.2 Intracellular response . . . 226
7.6 Mechanical interaction . . . 230
7.6.1 Non-interpenetration . . . 230
7.6.2 Forces of contact on the fluid . . . 232
7.7 Conclusions . . . 233
7.8 Discretization . . . 234
7.8.1 Finite volume discretization . . . 234
7.8.2 Finite elements discretization . . . 241

7.1 Introduction

In this chapter our goal is to investigate the different migratory behaviours that can arise when dealing with the model we propose. This is a joint work with Nicolas Meunier and Raphaël Voituriez. The feedback loop underlying the dynamics is as follows: the boundary concentration in molecular markers acts on the fluid pressure at the boundary as a polymerization inhibitor: the larger the concentration, the lower the pressure. Next, in the case of an inhomogeneous concentration, the cell domain moves. The global friction arising from this displacement enhances the retrograde actin flow velocity that transport the markers, leading to a reinforced molecular asymmetry.

From the mathematical viewpoint, the model presents a competition between different trends. First, the diffusion of the marker classically competes with convection. But the advection field itself is the result of a competition between the local molecular asymmetry

at the boundary of the domain, eventually reinforced by the global domain's velocity, and the depolymerization leading to a drift towards the cell center. In the one dimensional case, we have seen that for a feedback of the molecular concentration at the boundary on the pressure that is not bounded below, the dynamics is well understood and is reminiscent of the Keller-Segel model in two dimensions. In the more realistic two dimensional case and for a bounded feedback, we use a numerical approach to show that the model has a two-state behaviour which represents the two states of the cell: polarised or unpolarised.

More precisely, in our model the non linearity in the advection field has two origins: the actin retrograde flow and the global passive drag. In order to illustrate the role of the global passive drag in the polarisation process, we perform numerical simulations with a null global friction, so that the displacement of the cell does not interfere with the intracellular dynamics. Then, we consider the case of a non zero global friction. Since the velocity exerts a global feedback on the molecular dynamics it reinforces the polarisation and we observe a dichotomous behaviour, with either non motile or motile states depending on the global mass of molecules. However, as it was already observed for the 1D case in chapter 6, the analysis of this model is not as simple and its dynamics does not only rely on a critical mass. We observe that the initial condition and the parameters involved in the model still play a role, so that we were unable to obtain a clear treshold between these different behaviours. This study is a first step which should be poursued both on the numerical viewpoint by a systematic analysis and from the mathematical viewpoint by the study of existence of (global) solutions. In this chapter, we use either a finite volume discretization in polar coordinates or finite elements. Since it is classical the numerical scheme corresponding to the finite volume discretization is postponed to the last section of this chapter.

Next, we want to perturb the system with stochastic fluctuations. Indeed, the multi-scale model being minimal, the description of the molecular activity reduces to a single-agent dynamics, when the real activity involves a large number of molecules in permanent interaction organized in feedback loops (see figure 7.1). It is therefore natural to use stochastic fluctuations to account for its mesoscopic read-out. The importance of fluctuations for cell trajectories was already underlined at the protrusion scale in Caballero et al. [2014].

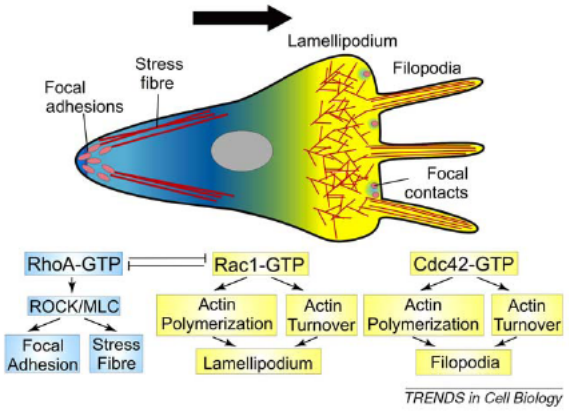

Figure 7.1 – Figure of a simplified molecular regulatory pathway involved in the cytoskeleton regulation. Source: Mayor and Carmona-Fontaine [2010].

In a first approach, we use a pointwise randomly distributed initial concentration, to see wether asymmetry could appear. However, this does not describe the fluctuations related to the activity itself, and we need for that purpose to add time-dependent fluctuations with a stochastic process. The simplest choice consists in having a noised interaction

between the molecular scale and the fluid: the action of the marker on polymerization at the boundary fluctuates. It has to be noted that the spatial correlation amounts to defining the processes on angular areas, which is not very satisfatory. In addition, the experimentally observed oscillations occur in the cell domain. The following step is thus based on a space-time stochastic process: the Q-Wiener process, acting on the marker's convection.

We choose to perform the corresponding numerical simulations using a finite elements discretization with FreeFem++. This is partly due to the easier way to handle the Q-Wiener process. But the model's flexibility is promising and will be used in future works for comparison with experimental assays on more complex settings. For that purpose, the use of FreeFem++ is preferred. We also choose a Stokes description of the fluid rather than the Darcy one to provide more stability.

7.2 Models under study

Let us recall the problems obtained in chapter 5 defined on a fixed domain Ω_0. Recall that ξ_1 is the global friction coefficient related to the passive drag, while ξ is the friction coefficient related to the actin filaments rubbing against the substrate. Denote k_d the depolymerization rate , D' the diffusion rate , δ the intensity of the coupling between the concentration and the pressure at the boundary, and $k_{\text{on/off}}$ the attachment/detachment rates for the marker at the membrane. In the case without activation at the membrane, the cell velocity writes

$$v(t) = \frac{\xi}{\xi_1} \int_{\partial\Omega_0} [1 - \delta c(t, \mathbf{x})]_+ \mathbf{n} \, \mathrm{d}\mathbf{x} \,, \tag{5.43}$$

while c is replaced by μ in the model with activation.

Remark 27. *In the following, in particular in the description of numerical simulations, the notation* $\gamma = \frac{\xi}{\xi_1}$ *may arise.*

Direct model The model (5.42)-(5.44) writes

$$\begin{cases} u(t, \mathbf{x}) = -\nabla p(t, \mathbf{x}) - \frac{\xi}{\xi_1} \int_{\Omega_0} \nabla p(t, \mathbf{x}) \, \mathrm{d}\mathbf{x} & \text{in } \Omega_0 \,, \\ -\Delta p(t, \mathbf{x}) = -k_d & \text{in } \Omega_0 \,, \\ p(t, \mathbf{x}) = [1 - \delta c(t, \mathbf{x})]_+ & \text{on } \partial\Omega_0 \,, \end{cases} \tag{7.1}$$

with the convection-diffusion problem

$$\begin{cases} \partial_t c(t, \mathbf{x}) + \nabla \cdot \left(c(t, \mathbf{x}) u(t, \mathbf{x}) - D' \nabla c(t, \mathbf{x}) \right) = 0 & \text{in } \Omega_0 \,, \\ \left(D' \nabla c(t, \mathbf{x}) - c(t, \mathbf{x}) u(t, \mathbf{x}) \right) \cdot \mathbf{n} = 0 & \text{on } \partial\Omega_0 \,. \end{cases} \tag{7.2}$$

The conserved marker mass writes

$$M = \int_{\Omega_0} c(t, \mathbf{x}) \, \mathrm{d}x \,.$$

Finally, the advection velocity rewrites

$$u(t, \mathbf{x}) = -\nabla p(t, \mathbf{x}) - \frac{\xi}{\xi_1} \int_{\partial\Omega_0} [1 - \delta c(t, \mathbf{x})]_+ \mathbf{n} \, \mathrm{d}\mathbf{x} \,. \tag{7.3}$$

The convection-diffusion problem is therefore nonlinear and non local. The non linear expression of the polymerization, $[1 - \delta c(t, \mathbf{x})]_+$ acts on both levels: at the local scale on

the pressure boundary values, and at the global scale as an boundary integral quantity. We have seen in the one dimensional case that for a linear expression $(1 - \delta c(t, \mathbf{x}))$, the coupling could induce an unbounded advection field leading to a blow-up. In this case, we deal with bounded terms, so that the model does not carry any such singularity.

Exchange model In the case where the markers are activated by binding to the membrane, the pressure boundary condition changes, and the problem (5.46)-(5.48) writes

$$\begin{cases} u(t,\mathbf{x}) = -\nabla p(t,\mathbf{x}) - \frac{\xi}{\xi_1}\int_{\Omega_0} \nabla p(t,\mathbf{x})\,\mathrm{d}\mathbf{x} & \text{in } \Omega_0\,, \\ -\Delta p(t,\mathbf{x}) = -k_d & \text{in } \Omega_0\,, \\ p(t,\mathbf{x}) = [1-\delta\mu(t,\mathbf{x})]_+ & \text{on } \partial\Omega_0\,, \end{cases} \tag{7.4}$$

with the following equation for the exchange dynamics:

$$\frac{\partial}{\partial t}\mu(t,\mathbf{x}) = k_{\mathrm{on}} c(t,\mathbf{x}) - k_{\mathrm{off}}\mu(t,\mathbf{x})\,, \tag{7.5}$$

and the convection-diffusion problem is

$$\begin{cases} \partial_t c + \nabla\cdot(cu - D'\nabla c) = 0 & \text{in } \Omega_0\,, \\ (D'\nabla c - cu)\cdot\mathbf{n} = k_{\mathrm{off}}\mu - k_{\mathrm{on}} c & \text{on } \partial\Omega_0\,. \end{cases} \tag{7.6}$$

The marker mass is conserved between the cytoplasmic and membrane-bound markers:

$$M = \int_{\Omega_0} c(t,\mathbf{x})\,\mathrm{d}\mathbf{x} + \int_{\partial\Omega_0} \mu(t,\mathbf{x})\,\mathrm{d}\mathbf{x}\,.$$

Finally, the advection velocity rewrites

$$u(t,\mathbf{x}) = -\nabla p(t,\mathbf{x}) - \frac{\xi}{\xi_1}\int_{\partial\Omega_0} [1-\delta\mu(t,\mathbf{x})]_+\mathbf{n}\,\mathrm{d}\mathbf{x}\,. \tag{7.7}$$

7.3 Cell intrinsic activity: first results

In this section, we perform numerical experiments on the system for single-cell motion on a surface, without any external stimulation. Since the non linearity of the convection has two different origins, we start by considering the case where the global friction is infinite. In such a situation the cell velocity is equal to zero and we call it the non motile case. From the modelling viewpoint, this means that the intracellular activity is not coupled to the the cell motion, so that no displacement can arise. Then in a second step we consider the complete model that we call the motile one. Furthermore we start with the case without exchange on the boundary, before considering the case with exchange that is more realistic. The numerical simulations presented below were produced using Matlab. For each configuration, we will first investigate the non motile state: the cell velocity will be put to zero, so that the observed behaviour results only from the internal process. Then, we will let the velocity impact on the polarisation via the associated passive drag.

7.3.1 Non motile case

Model without exchange at the boundary

We perform numerical simulations of the system (7.1)-(7.2) with $\xi_1 \to +\infty$. In that situation, the concentration of markers at the boundary is directly responsible for the

pressure at the boundary. We were only able to observe relaxation towards a Gaussian symmetric profile centered in $(0, 0)$. Even in the case of an asymmetric initial condition, the combined effect of diffusion and depolymerization led to a stationary centered Gaussian profile. This can be interpreted as follows: if the concentration in the marker-rich region is low enough so that the local pressure is non zero, then the marker is advected away from the boundary, and the system relaxes to a non motile profile. It the local pressure is zero, then the marker will still experience the drift to the center (for a non zero depolymerization rate), and in any case the diffusion. Therefore, the local concentration lowers, and the first case of figure applies. We can suppose that the asymmetry-enhancing processing being only local, they can not counterbalance the constant drift to the center and diffusion.

For any mass, the solution was observed to converge to a non motile profile as displayed in figure 7.2: the local repulsive forces at the membrane are not sufficient to induce a sustained global asymmetry, even starting with a polarised initial condition.

It is possible to exhibit an initial condition asymmetric enough so that the supports of c and p were disjoint and the advection field was null where the marker was located. In this case, for non trivial diffusion coefficient and depolymerization rate, the solution relaxes to a non motile profile.

In the following, we will consider the attachment kinetics at the membrane, that allows for more stability and a more realistic description of the dynamics.

With activation

We performed numerical simulations of the model including the activation of markers at the boundary, that is to say (7.4)-(7.5)-(7.6) with $\xi_1 \to +\infty$. In this situation, only the captured markers at the membrane modify the boundary pressure and the cell velocity. The activation kinetics adding a time lag to the dynamics, we can assume that an asymmetry can be maintained for a longer time, so that a sustained polarised profile emerges.

However, the simulations showed qualitatively similar results as for the model without activation. The attachment dynamics led to larger relaxation times. Having largely unbalanced attachment/detachment rates, with a strong attachment and rare detachment allows an initially asymmetric profile to be maintained, but is not realistic.

7.3.2 The motile case

In the non motile case we were not able to obtain a dichotomous behaviour by changing the mass value, the parameters in the dynamics, or the initial condition. Let us now allow the cell displacement. This cell displacement could be given. In such a case it would not change the nature of the model. But the main novelty of our model is two fold: first such a displacement results from the intracellular activity and second the displacement acts on the marker's dynamics. Mathematically speaking, the cell velocity results from the fluid equations which model the actin flow and it modifies the equation by adding a supplementary global coupling.

As explained above, considering a non zero global friction ξ/ξ_1 let the cell velocity interfere with the intracellular dynamics. It acts as a bias that amplifies the local effect of the retrograde flow. We perform numerical simulations of the system (7.4)-(7.5)-(7.6).

We are looking for parameter settings that allow having different dynamics for a changing mass. We consider a low mass $M = 0.05$ and a larger one $M = 1$, for the same parameter set. In the first case, the dynamics is diffusive. In order to illustrate this dynamics, we display in figure 7.4 a kymograph that represents the concentration in attached markers

at the boundary as a function of time. We can see the initially polarized profile getting more homogeneous with time, meaning that depolarisation occurs.

For a large mass, polarisation is rapidly enhanced (see figures 7.3 and 7.5). This shows that for this parameter setting, the coupling with the cell velocity is tight.

Performing numerical simulations for our model with exchange allowed illustrating the different behaviours that can arise. We have seen that it is possible to exhibit sets of parameters for which the system relaxes to a non-polarised Gaussian-type profile, and others for which a sustained motile profile emerges. Let us now consider stochastic fluctuations and their impact on the system.

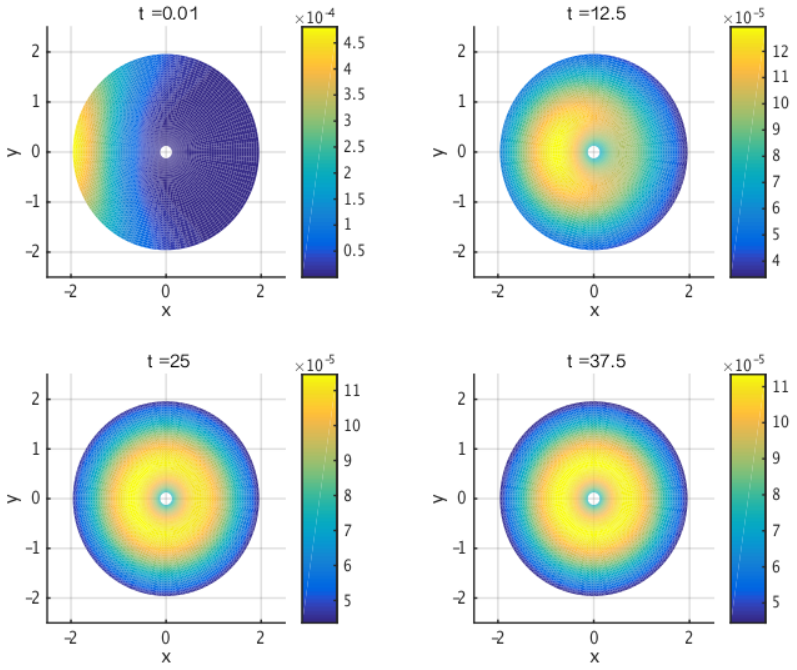

Figure 7.2 – Numerical simulations of the concentration dynamics in $\Omega = B(0,R) \setminus B(0,R_{\min})$, without exchange at the membrane, and without motion (problem (7.1)-(7.2)). The parameters are chosen as follows: the small mass is $M = 0.01$; $\xi = 1$; $\alpha = \delta = 30$; $D = 5$; $k_d = 2$. The time step is $\Delta t = 10^{-2}$.

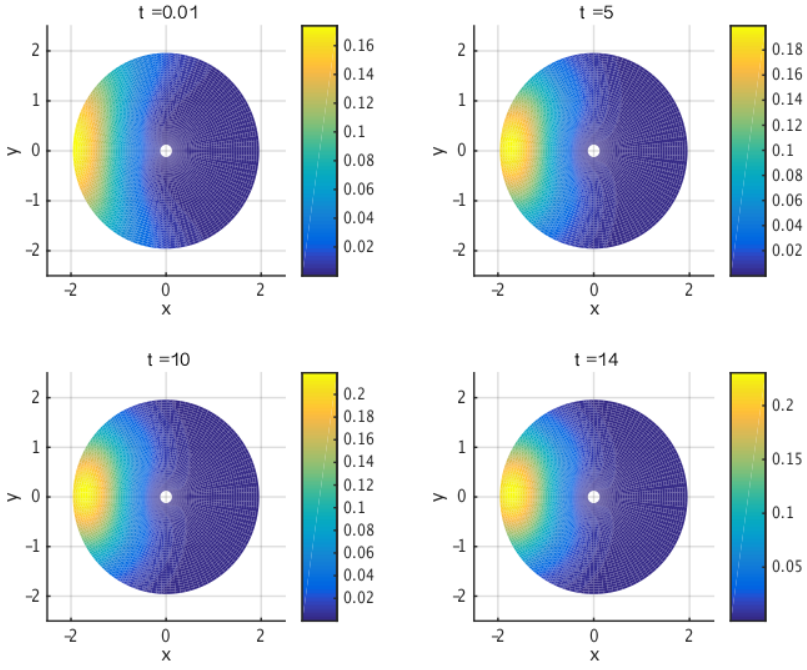

Figure 7.3 – Numerical simulations of the concentration dynamics in $\Omega = B(0,R) \setminus B(0,R_{\min})$, with attachment at the membrane and motion, in the case of polarisation, for the problem (7.4)-(7.5)-(7.6). The attachment rate is $k_{\text{on}} = 10$ while $k_{\text{off}} = 10$. The parameters are chosen as follows: the mass is $M = 1$; $\xi = 1$; $\xi_1 = 10$; $\alpha = 30$; $\delta = 30$; $D = 2$; $k_d = 2$. The time step is $\Delta t = 10^{-2}$. The initial condition is a gaussian function centered in (R, π) and with unity variance.

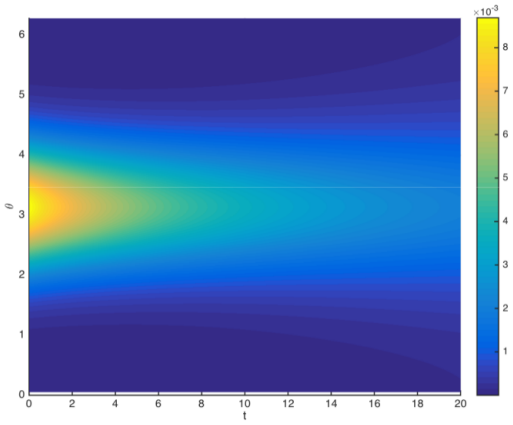

Figure 7.4 – Kymograph corresponding to the concentration in attached markers for the case of depolymerization in the problem (7.4)-(7.5)-(7.6). Time is represented in abscissa, and the angle θ in ordinate. The color shows the concentration. The parameters are chosen as follows: the mass is $M = 1$; $\xi = 1$; $\xi_1 = 10$; $\alpha = 30$; $\delta = 30$; $D = 2$; $k_d = 2$. The time step is $\Delta t = 10^{-2}$. The initial condition is a gaussian function centered in (R, π) and with unity variance.

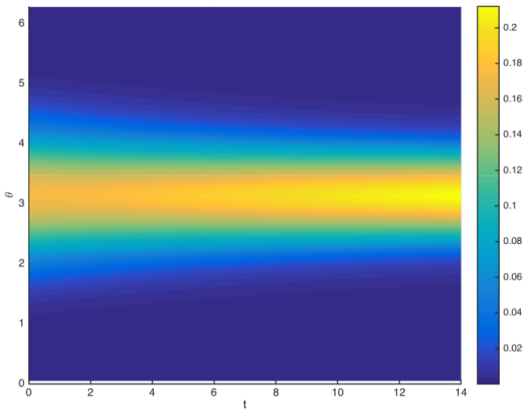

Figure 7.5 – Kymograph corresponding to the concentration in attached markers for the numerical simulation in figure 7.3. Time is represented in abscissa, and the angle θ in ordinate. The color shows the concentration.

7.4 Stochastic effects

The intracellular dynamics was proved to be able to provide motile and non motile profiles. We investigate now the effect of stochastic fluctuations arising in the system. Due to the microscopic scale, and to the large number of agents, these fluctuations can be large enough at the mesoscopic scale to perturb the dynamics. In terms of numerical simulations, it will be useful to get transitions between migratory phenotypes (motile and non motile), that could lead to realistic cell trajectories.

Since the noise brings larger distortions in the concentration than in the deterministic case, the choice of $p(t,\mathbf{x}) = [1-\delta c(t,\mathbf{x})]_+$ is now too constraining. Therefore, we choose now a smooth decreasing function:

$$p(t,\mathbf{x}) = \exp(-\delta c(t,\mathbf{x})) \quad \text{on } \partial\Omega_0\,. \tag{7.8}$$

This choice corresponds to $p(t,\mathbf{x}) = \alpha\exp(-\frac{\delta R^2}{N_c}c(t,\mathbf{x}))$ before non-dimensionalization.
A first essay consists in having an initial random concentration profile.

7.4.1 Random initial profile

In this part, we use a random initial concentration profile. The concentration at each discretization node corresponds to a uniform random variable. Take $Y \sim \mathcal{U}(0,1)$ a random variable following the uniform law on $(0,1)$. Then, we have for all $j \in \{1,\dots,N_r\}$ and $k \in \{1,\dots,N_\theta\}$,

$$c^0_{(j,k)} = Y\,.$$

The mass is then normalized to a given value. We perform numerical simulations of the problem (7.4)-(7.5)-(7.6) with a modified boundary condition on the pressure (7.8). In the simulation displayed in figure 7.6, we can see that the dynamics may lead to a sustained polarised state.

We consider now the same parameters but for a small mass $M = 0.001$. The system then converges to a non motile profile (see figure 7.7).

As explained in the study of the one dimensional case, the model's behaviour does not rely only on a critical mass, but also on the initial condition and on the parameters. Then, searching for an intermediate condition, that allows for both behaviours for different realisations of the initial condition is challenging.

As before, the system is dominated by diffusion for low masses and by convection for larger values. Even if we did not enlight a parameter state that brought both behaviours, it is reasonable to think that other types of fluctuations may be best suited for that purpose.

7.4.2 Noised activity: depolymerization/transport

It is reasonable to think that stochastic fluctuations occur on the whole cell domain. Indeed, molecules that are regulators of the cytoskeleton dynamics can also interact with the actin filaments in the cell body. These interaction could generate macroscopic effects. For example, myosin motors, that are also advected inward by actin filaments, may induce depolymerization. Under their activity, actin filaments are brought together until the constraint gets too large, after what the pointed ends shrink. Moreover, oscillations observed on the actin gel are likely to be related to the Rho regulation pathway. Adding a coupling with the description of a molecular feedback loop is thus something to investigate in a future work (see a related work in annex).

As a consequence, introducing space-time stochastic fluctuations seems relevant. The previous reasoning pushes us to define a noised and time-dependent depolymerization rate

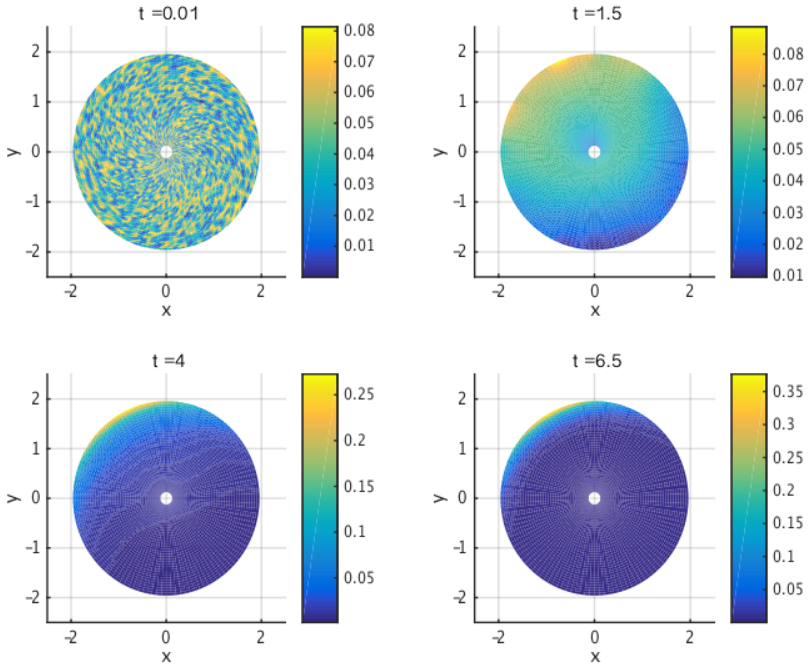

Figure 7.6 – Numerical simulations of the concentration dynamics in Ω, for the problem (7.4)-(7.5)-(7.6) with the boundary condition on the pressure (7.8). The attachment rate is $k_{\text{on}} = 10$ while $k_{\text{off}} = 10$. The mass is $M = 1$; $\xi = 1$; $\alpha = 30$; $\delta = 30$; $D = 5$; $k_d = 2$. The time step is $\Delta t = 10^{-2}$. The initial condition is uniformly distributed.

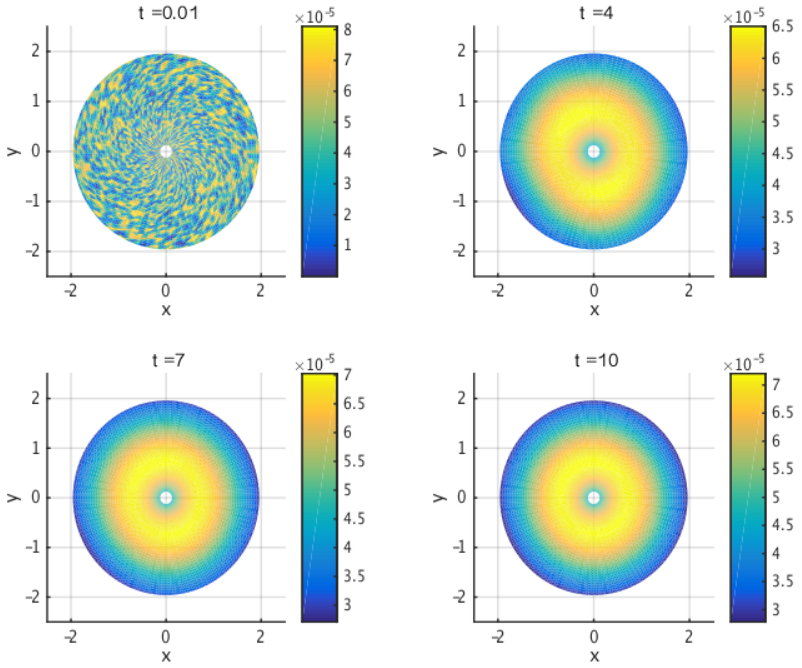

Figure 7.7 – Numerical simulations of the concentration dynamics in Ω, for the problem (7.4)-(7.5)-(7.6) with the modified boundary condition on the pressure (7.8). The attachment rates are $(k_{\text{on}}, k_{\text{off}}) = (10, 10)$. The mass is $M = 0.001$; $\xi = 1$; $\alpha = 30$; $\delta = 30$; $D = 5$; $k_d = 2$; $\Delta t = 10^{-2}$. The initial condition is random uniform on each node.

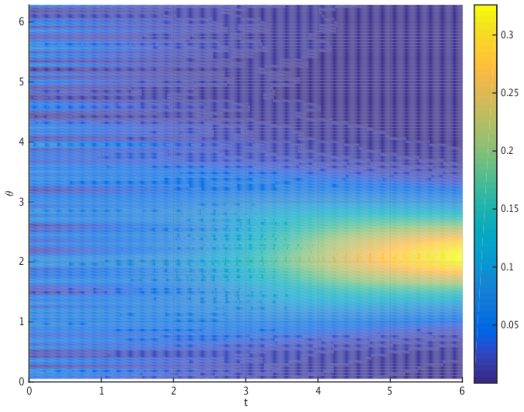

Figure 7.8 – Kymograph corresponding to the concentration in attached markers case in figure 7.6. Time is represented in abscissa, and the angle θ in ordinate. The color shows the concentration.

k_d. However, the implications on the model are too important, in particular in the perspective of studying a free boundary model. For this reason, we decide to perturb the advection field of the molecule, that is the direct consequence of the fluid displacement.

It is known that a space-time white noise, that is uncorrelated in time and space, may lead to non trivial effects [Walsh, 2005], and the corresponding numerical scheme may not converge. A natural way to circumvent this issue is to consider a space-correlated noise.

The Q-Wiener process

Let us first give the definition of the Q-Wiener process on $L^2(\Omega_0)$. The definition comes from Peszat and Zabczyk [2007] and the method and detailed proofs can be found in Boulakia et al. [2015].

Definition 9. *Let Q be a non-negative symmetric trace-class operator on $L^2(\Omega_0)$: it is compact and the trace function is well defined independently of the basis. Then, there exists a probability space $(\Omega_0, \mathcal{F}, \mathbb{P})$ on which we can define a stochastic process $(W_t^Q,\, t \in \mathbb{R}_+)$ on $L^2(\Omega_0)$ such that*

- *for each $t \in \mathbb{R}_+$, W_t^Q is a $L^2(\Omega_0)$-valued random variable,*
- *we have $W_0^Q = 0_{L^2(\Omega_0)}$ $\mathbb{P}$-almost surely,*
- *$(W_t^Q,\, t \in \mathbb{R}_+)$ has independent and stationary increments:*
  - *independent increments: for any sequence $t_1 < \cdots < t_n$, the random variables $W_{t_2}^Q - W_{t_1}^Q, \ldots, W_{t_n}^Q - W_{t_{n-1}}^Q$ are independent.*
  - *stationary increments: for any $s < t$, $W_t^Q - W_s^Q \overset{\text{law}}{=} W_{t-s}^Q$.*
- *$(W_t^Q,\, t \in \mathbb{R}_+)$ is a Gaussian process: $\forall t \in \mathbb{R}_+$, $\forall \phi \in L^2(\Omega_0)$, (W_t^Q, ϕ) is a real centered Gaussian random variable with variance $t(Q\phi, \phi)$,*
- *$(W_t^Q,\, t \in \mathbb{R}_+)$ is a $L^2(\Omega_0)$-valued pathwise continuous process $\mathbb{P}$-almost surely.*

Now, let us define a non-negative symmetric linear operator Q on $L^2(\Omega_0)$ that admits a kernel q.

Definition 10. *Let Q be a non-negative symmetric linear operator on $L^2(\Omega_0)$: for all $(\phi_1, \phi_2) \in L^2(\Omega_0)^2$,*

$$(Q\phi_1, \phi_2) = (Q\phi_2, \phi_1)\,, \quad (Q\phi_1, \phi_1) \geq 0\,.$$

Let q denote a non-negative symmetric real-valued integrable function on Ω_0^2. We say that Q has the kernel q if

$$\forall \phi \in L^2(\Omega_0),\ \forall x \in \Omega_0,\ Q\phi(x) = \int_{\Omega_0} \phi(y) q(x,y)\,\mathrm{d}y\,. \tag{7.9}$$

In this case, Q is a trace class operator, with trace given by

$$Tr(Q) = \int_{\Omega_0} q(x,x)\,\mathrm{d}x\,.$$

In the following, we will use a so-called Gaussian kernel q_ζ defined for a correlation length $\zeta > 0$ by

$$\forall (x,y) \in \Omega_0^2,\ q_\zeta(x,y) = \frac{1}{\zeta^2} e^{-\frac{\pi}{4\zeta^2}|x-y|^2}\,. \tag{7.10}$$

The covariance between two points (t,x) and (s,y) in $\mathbb{R}_+ \times \Omega_0$ then writes

$$\mathbb{E}\left[W_t^Q(x) W_s^Q(y)\right] = t \wedge s\, q_\zeta(x,y)\,.$$

One says that the correlations in time are *white* while the correlations in space are *colored* by the kernel q. If ζ tends to zero, the process tends to a space-time white noise. For $\zeta \neq 0$, the noise is regular in space. Moreover, the process $(W_t^Q(x),\ (t,x) \in \mathbb{R}_+ \times \overline{\Omega}_0)$ equipped with this kernel admits a space-time continuous version.

For our numerical simulations, we choose to follow the finite elements discretization method proposed by Boulakia et al. [2015]. As we will see, it amounts to simulate a Gaussian vector. Moreover, since our goal is to deal with specific geometric settings, and in further works with free boundary domains, it is preferable to implement the model using FreeFem++.

Finite elements discretization The finite elements discretization of our Q-Wiener process reduces to an interpolation [Boulakia et al., 2015]. Write $(\psi_i)_{1 \leq N_h}$ the P^1 basis, in the finite element space E^h. Then,

$$W_t^{Q,h} = \sum_{i=1}^{N_h} w_i \psi_i\,, \tag{7.11}$$

with $(w_i)_{1 \leq i \leq N_h}$ a centered Gaussian vector with a time-dependent covariance matrix $(tq(P_i, P_j))_{1 \leq i,j \leq N_h}$. Since the process is used in the (explicit) advection term, one only has at each time step to update the covariance matrix and generate a new Gaussian vector.

The practical generation of such a vector is classical. For a centered Gaussian vector denoted x with covariance matrix Σ, one can write

$$X = BY\,,$$

with $Y_i \sim \mathcal{N}(0,1)$, and B such that $\Sigma = BB^t$. For an invertible Σ, this is its Cholesky decomposition.

Results

For these simulations, we use as an initial condition a Gaussian function centered in $(0,0)$. For that purpose, we perform finite elements simulations of this phenomenon with FreeFem++, for a similar problem formulated in the referential of the moving cell. Moreover, to have more regularity, we use a Stokes flow instead of a Darcy flow, and choose a boundary condition on the normal component of the stress tensor, see remark 28 for more details.

We solve

$$\begin{cases} -\Delta p(t,\mathbf{x}) = -k_d & \text{in } \Omega_0\,, \\ -\eta\Delta u(t,\mathbf{x}) + \nabla p(t,\mathbf{x}) = -(u(t,\mathbf{x}) + \gamma \int_{\Omega_0} \nabla p(t,\mathbf{x})\,\mathrm{d}\mathbf{x}) & \text{in } \Omega_0\,, \\ (\eta(\nabla u(t,\mathbf{x}) + {}^t\nabla u(t,\mathbf{x})) - p(t,\mathbf{x})\mathrm{Id})\cdot\mathbf{n} = \exp(-\delta\mu(t,\mathbf{x}))\mathbf{n} & \text{on } \partial\Omega_0\,, \end{cases} \tag{7.12}$$

together with the following problem for the molecular dynamics: writing $w_t^Q \in L^2(\Omega_0)^2$ for a realisation of the random variable $(W_t^{Q,1}, W_t^{Q,2})$, and $e \in \mathbb{R}_+$,

$$\begin{cases} \partial_t c + \mathrm{div}\,\left(c(u + ew_t^Q) - D'\nabla c\right) = 0 & \text{in } \Omega_0\,, \\ \left(D'\nabla c - c(u + ew_t^Q)\right)\cdot\mathbf{n} = -k_{\mathrm{on}}c + k_{\mathrm{off}}\mu & \text{on } \partial\Omega_0\,, \\ \frac{\partial}{\partial t}\mu(t,\mathbf{x}) = k_{\mathrm{on}}c(t,\mathbf{x}) - k_{\mathrm{off}}\mu(t,\mathbf{x}) & \text{on } \partial\Omega_0\,. \end{cases} \tag{7.13}$$

The domain's displacement is obtained as an output by

$$v(t) = \gamma \int_{\Omega_0} \nabla p(t,\mathbf{x})\,\mathrm{d}\mathbf{x}\,, \tag{7.14}$$

and gives rise to the trajectories displayed in figure 7.10. For a given intensity of noise, we vary the coupling parameter δ between the molecular and fluid scale, and plot the corresponding trajectories.

Moreover, simulations with a highly correlated Q-Wiener process showed an initially Gaussian concentration profile become quickly highly polarized. The cell was then initially non motile, and the stochastic fluctuations led it to fast motion. This simulation is not displayed here. The parameters used are the following: $T = 5$, $\Delta t = 0.01$, $D = 0.27$, $\xi = 0.77$, $\eta = 0.2$, $\delta = 0.1$, $\gamma = 10$. The Q-Wiener process has range $e = 5$, and correlation coefficient $\zeta = 0.77$. The initial condition was a Gaussian function centered in $(0,0)$ and of unity standard deviation. This large polarisation may be due to the low friction for the fluid or to the large velocity coefficient γ.

Remark 28. *In these simulations, the fluid model used was a Stokes problem with a prescribed normal component of the stress tensor at the boundary. Both formulations have a physical meaning for cell migration. If one imposes the normal fluid velocity as a function of polymerization, this means that actin polymerized at its own speed regardless of the applied force, which is realistic for low forces inside the fluid. Imposing $\sigma\cdot\mathbf{n}$ at the boundary is more relevant for larger forces, above which polymerization stops. Both formulations are accepted in the physics community, and their validity depends on the underlying microscopic model. Studying the differences arising in the two settings and their microscopic origin will be the object of a future work.*

Our 2D discoid model for cell migration is based on the assumption that the actin retrograde flow is the cell motor in the case of cell crawling on the substrate. In addition we have incorporated a feedback loop with a polarity marker that is transported by the

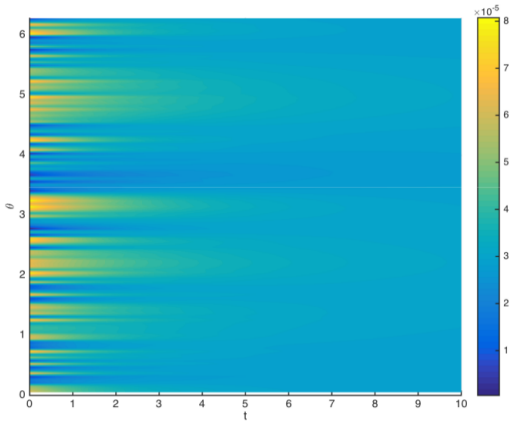

Figure 7.9 – Kymograph corresponding to the concentration in the attached markers for the simulation displayed in figure 7.7. Time is represented in abscissa, and the angle θ in ordinate. The color shows the concentration.

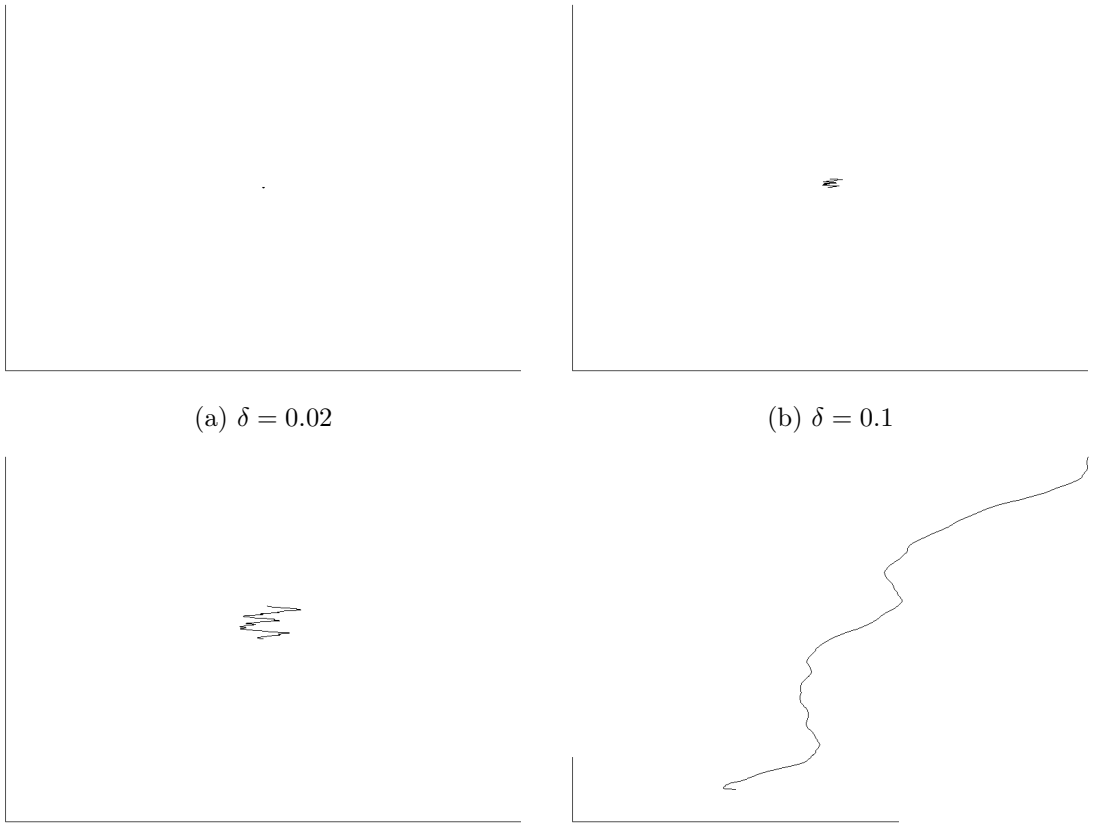

(a) $\delta = 0.02$ (b) $\delta = 0.1$

(c) $\delta = 0.15$ (d) $\delta = 0.2$

Figure 7.10 – Numerical trajectories for the Stokes model of migration (7.12)-(7.13) with a varying coupling between the molecular scale and the fluid. The horizontal and vertical segments correspond to a length 1 and are displayed for comparison purposes. Parameters: $T = 5$, $\Delta t = 0.01$, $D = 0.27$, $\xi = 0.75$, $\eta = 0.2$, $\gamma = 10$. The Q-Wiener process has range $e = 1$, and correlation coefficient $\zeta = 1$.

actin flow itself and which is implied in the polymerization process. In the case where there is no exchange on the boundary it is witnessed that the whole problem may lead to blow-up of the solution for large marker mass value. Numerical simulations provide the dichotomous behaviour of the model. In order to have a more realistic model we enriched it by considering exchange at the boundary. For this less singular model, numerical simulations provide different migratory behaviours that were biologically observed: motile and non motile. Moreover, in a third step, we enriched the model in order to describe the fluctuations related to the signalling pathway involved during the polymerization and depolymerization processes by considering a noised activity. For this less singular model, numerical simulations provide different migratory trajectories that were biologically observed, validating the derivation of the model. We emphasize that these are the first steps towards a precise description of cell migration and we propose that, like the capacity of Keller-Segel equations to describe cell aggregation behaviours associated with chemotaxis, our model constitutes a phenomenological minimal framework to describe the formation of local regions of increased marker concentrations associated with cell migration.

So far the main outputs of the model are the dynamics and directionality of polarisation without external solicitations. Let us now add some external signal.

7.5 Stimulation by a chemical signal

We have seen that a cell's intrinsic dynamics can produce several migration phenotypes with variable persistence. But crawling cells in vivo ensure their functions by interacting with the medium or other cells, and responding to external stimuli. One of the most studied guidance process in cell migration is chemotaxis: attractant molecules (chemokines) are released in the medium by cells. Membrane receptors are able to sense these signals, and induce a molecular response, that translates into a reaction at the cellular scale. This could not happen without an internal amplification mechanism. As a consequence, the protrusive activity is oriented towards the direction of higher signal [Friedl and Wolf, 2003; Kortholt et al., 2013; Servant et al., 1999]. The most frequent configurations consist in a gradient of signal, but symmetry-breaking due to a homogeneous signal in the medium was also witnessed [Wang, 2009].

In this part we will describe how we enrich our model in order to take into account the phenomenon of receptor polarisation. The main ingredient is that long-range spatial coupling is critical in the gradient detection process, but at the molecular level, many different mechanisms could produce this coupling including the transport and recycling of the signal receptor itself. The model's strength is its independence from the details of the molecular mechanisms that determine the long-range coupling parameter. In the future the model could be enriched with molecular details.

This is a first step in the description of the competition between intracellular effects and the cell's environment. In particular, here, the polarisation machinery that we describe is rear-focused, while the effect of chemoattractant signals are witnessed on front-specific processes. Therefore, this coupling allows having descriptions of antagonist cellular functions in the same model. In the end, the noised system with an external chemical signal could be used to perform numerical simulations of the chase of a bacterium by immune cells for example.

In a first approach, we model the effect of a gradient in signal perceived at the boundary.

7.5.1 Signal acting on the boundary

A cell is able to sense a concentration in signal at the membrane via its receptors. Then, an amplification loop inside the cell allows for an efficient cellular response.

We investigate now the case of an external signal that acts directly on the polymerization at the boundary, using the finite volume setting with the stochastic fluctuations at the boundary. Indeed, the interaction between the molecular and fluid scales is composed of loops of molecular reactions that imply a large number of agents. The feedback on the pressure at the boundary can therefore be assumed noisy. Denote S the concentration in signal felt at the cell membrane $\partial\Omega_0$. We assume that it is constant in time, and that its detection on the cell membrane by specific receptors acts on the maximal pressure of the fluid. Moreover, the number of receptors being bounded, we choose a bounded response to the signal, using a threshold value S_c. As a consequence, the boundary condition for the pressure p in polar coordinates now writes

$$p(t,R,\theta) = R\kappa(t,\theta)\frac{S(\theta)}{S(\theta)+S_c}e^{-\delta\frac{c(t,R,\theta)}{R}} \qquad \text{on } C(0,R)\,,$$

where $\kappa(t,\theta)$ is the stochastic fluctuations term, and S is defined by

$$S(\theta) = \left(\cos(\theta-\theta_0)\frac{0.1}{2}+1\right)S_{\text{mean}}\,, \qquad \text{for } \theta\in\mathbb{R}/2\pi\mathbb{Z}\,,$$

and θ_0 denotes the orientation of the gradient of signal, and S_{mean} its mean intensity.

The fluctuation process From the mathematical point of vue, we need now a stochastic process for the fluctuations. A relevant choice is the Ornstein-Uhlenbeck process. It can be seen as a diffusion process drifted to its mean value, or equivalently as a noisy relaxation process. More precisely, taking one as a mean value, and using the notation $(B(t))_{t\geq 0}$ for a standard Brownian motion, we write

$$\mathrm{d}Z(t) = -\lambda(Z(t)-1)\,\mathrm{d}t + \sigma\,\mathrm{d}B(t)\,, \tag{7.15}$$

where $\lambda>0$ is the damping rate, and $\sigma>0$ the standard deviation.

The solution of equation (7.15) writes

$$Z(t) = 1 + e^{-\lambda t}(Z(0)-1) + \sigma\int_0^t e^{-\lambda(t-s)}\,\mathrm{d}B_s\,. \tag{7.16}$$

Now, since

$$\begin{aligned}\mathbb{E}\left[\int_0^t e^{-\lambda(t-s)}\,\mathrm{d}B_s\right] &= 0\,,\\ \mathbb{E}\left[\left(\int_0^t e^{-\lambda(t-s)}\,\mathrm{d}B_s\right)^2\right] &= \int_0^t e^{-2\lambda(t-s)}\,\mathrm{d}s = \frac{1-e^{2\lambda t}}{2\lambda}\,,\end{aligned}$$

(see e.g Revuz and Yor [2005]) we can write

$$\mathbb{E}[Z(t)] = 1 + e^{-\lambda t}(\mathbb{E}[Z(0)]-1)\,, \tag{7.17}$$

and for the variance

$$\begin{aligned} Var(Z(t)) &= \mathbb{E}\left[(Z(t)-\mathbb{E}[Z(t)])^2\right], \\ &= \mathbb{E}\left[\left((Z(0)-\mathbb{E}[Z(0)])e^{-\lambda t}+\sigma\int_0^t e^{-\lambda(t-s)}\,\mathrm{d}B_s\right)^2\right], \\ &= \frac{\sigma^2}{2\lambda}+e^{-2\lambda t}\left(Var(Z(0))-\frac{\sigma^2}{2\lambda}\right). \end{aligned} \tag{7.18}$$

Therefore, taking a random initial value

$$Z(0)\sim\mathcal{N}\left(1,\frac{\sigma^2}{2\lambda}\right),$$

the process has a constant mean equal to 1, and constant variance equal to $\frac{\sigma^2}{2\lambda}$.

Remark 29. *Since the variance of the process is independent on the value of Z, it can lead to negative values. Since the 99%-confidence interval for a normal distribution $\mathcal{N}(1,\sigma_0^2)$ is $[1-3\sigma,1+3\sigma]$, we need to pick (λ,σ) such that $\frac{\sigma}{\sqrt{2\lambda}}\leq\frac{1}{3}$.*

We do not aim here at defining rigorously a space continuous correlated process at the boundary. For now, we simply assume that the boundary is split into angular areas and a different process is defined on each one. Finally, the space-discontinuous fluctuation process writes

$$\kappa(t,\theta)=\sum_{i=1}^{N_a}\kappa_i(t)\mathbb{1}_{\theta\in\Theta_i},$$

with $(\Theta_i)_i$ the angular decomposition of $\mathbb{R}/2\pi\mathbb{Z}$. Moreover,

$$\kappa_i(t)=\max(0,Z_i(t)),$$

Discretization

Taking a random variable $\epsilon\sim\mathcal{N}(0,1)$, we rewrite equation (7.16) as

$$Z(t)=1+e^{-\lambda t}(Z(0)-1)+\sigma\sqrt{\frac{1-e^{-2\lambda t}}{2\lambda}}\epsilon. \tag{7.19}$$

Therefore, using the time discretization $t^n=n\Delta t$, we can write

$$Z(t^{n+1})=1+e^{-\lambda\Delta t}(Z(t^n)-1)+\sigma\sqrt{\frac{1-e^{-2\lambda\Delta t}}{2\lambda}}\epsilon. \tag{7.20}$$

It amounts to doing the following: the stochastic fluctuation at the time step $n+1$ results from a random variable initialized at time step n following a distribution $\mathcal{N}\left(1,\frac{\sigma^2}{2\lambda}\right)$, that evolves during a time Δt with the Ornstein-Uhlenbeck dynamics.

Results

Finally, we perform numerical simulations of the following problem: extending our notations for κ and S for $\mathbf{x}\in\partial\Omega_0=C(0,R)$, the fluid problem writes

$$\begin{cases} u(t,\mathbf{x})=-\nabla p(t,\mathbf{x})-\frac{\xi}{\xi_1}\int_{\partial\Omega_0}\exp(-\delta\mu(t,\mathbf{x}))\mathbf{n}\,\mathrm{d}\mathbf{x}. & \text{in } \Omega_0, \\ -\Delta p(t,\mathbf{x})=-k_d & \text{in } \Omega_0, \\ p(t,\mathbf{x})=\kappa(t,\mathbf{x})\frac{S(\mathbf{x})}{S(\mathbf{x})+S_c}e^{-\delta\mu(t,\mathbf{x})} & \text{on } \partial\Omega_0, \end{cases} \tag{7.21}$$

together with the following problem for the molecular content:

$$\begin{cases} \partial_t c + \nabla \cdot (cu - D'\nabla c) = 0 & \text{in } \Omega_0\,, \\ (D'\nabla c - cu)\cdot \mathbf{n} = k_{\text{off}}\mu - k_{\text{on}}c & \text{on } \partial\Omega_0\,, \\ \frac{\partial}{\partial t}\mu = k_{\text{on}}c - k_{\text{off}}\mu & \text{on } \partial\Omega_0\,. \end{cases} \tag{7.22}$$

We observed that keeping the same parameters for the dynamics, the signal and the stochastic processes, we could exhibit a parameter space for which a changing mass produced different behaviours from an initially uniform concentration profile. For a low mass $M = 0.1$, the stochastic fluctuations did not induce the recognition of the signal, and the molecular concentration stayed globally centered Gaussian (see figure 7.11).

For a larger mass $M = 1$, the system showed a polarised profile in the direction of the signal gradient (see figure 7.12). We did not observe transient polarisation in different directions, as can be witnessed in the case of yeast cells polarisation. However, the yeast cells does not migrate in the case of polarisation. In the case of a migrating cell, it is observed that it senses its environment before "choosing" a direction of motion. Therefore, our simulations are indeed effective to produce different levels of response to an attractive chemical signal.

7.5.2 Intracellular response

We introduce the signal in the system by modelling the resulting intracellular response. This is similar to what we did in 7.4.2: the stochastic fluctuations related to what happened at the boundary was described on the resulting process: the convection. Therefore, we combine now the Q-Wiener process with the expression of a signal in the convection term. This amounts to having a noised response to the chemical signal.

For that purpose, we perform finite elements simulations of this problem with FreeFem++, for the problem formulated for a Stokes flow and a prescribed normal component of the stress tensor σ at the boundary. Moreover, to show the cell displacement in the numerical simulations, we solve the problem formulated for a moving domain: write $(\tilde{p}, \tilde{u}, \tilde{c}, \tilde{\mu}, \tilde{v})$ the corresponding functions defined on $\mathbb{R}_+ \times \Omega(\,\cdot\,)$. We solve for $t > 0$,

$$\begin{cases} -\Delta\tilde{p}(t,\mathbf{X}) = -k_d & \text{in } \Omega(t)\,, \\ -\eta\Delta\tilde{u}(t,\mathbf{X}) + \nabla\tilde{p}(t,\mathbf{X}) = -(\tilde{u}(t,\mathbf{X}) + \tilde{v}(t)) & \text{in } \Omega(t)\,, \\ \sigma\cdot\mathbf{n} = \exp(-\delta\tilde{\mu}(t,\mathbf{X}))\mathbf{n} & \text{on } \partial\Omega(t)\,, \end{cases} \tag{7.23}$$

together with the following problem for the molecular dynamics: for $S : \Omega(t) \to \mathbb{R}_+$ the signal function, and a a sensitivity parameter, we write

$$\begin{cases} \partial_t\tilde{c} + \operatorname{div}\left(\tilde{c}(\tilde{u} + \tilde{v} + ew_t^Q + a\nabla S) - D'\nabla\tilde{c}\right) = 0 & \text{in } \Omega(t)\,, \\ \left(D'\nabla\tilde{c} - \tilde{c}(\tilde{u} + ew_t^Q + a\nabla S)\right)\cdot\mathbf{n} = -k_{\text{on}}\tilde{c} + k_{\text{off}}\tilde{\mu} & \text{on } \partial\Omega(t)\,, \\ \frac{\partial}{\partial t}\tilde{\mu} + \tilde{v}\cdot\nabla\tilde{\mu} = k_{\text{on}}\tilde{c} - k_{\text{off}}\tilde{\mu} & \text{on } \partial\Omega(t)\,. \end{cases} \tag{7.24}$$

The domain's displacement is obtained as an output by

$$v(t) = \gamma\int_{\Omega_0}\nabla p(t,\mathbf{x})\,\mathrm{d}\mathbf{x}\,, \tag{7.25}$$

As a first approach, we use a simplified framework for the definition of the response S to a signal.

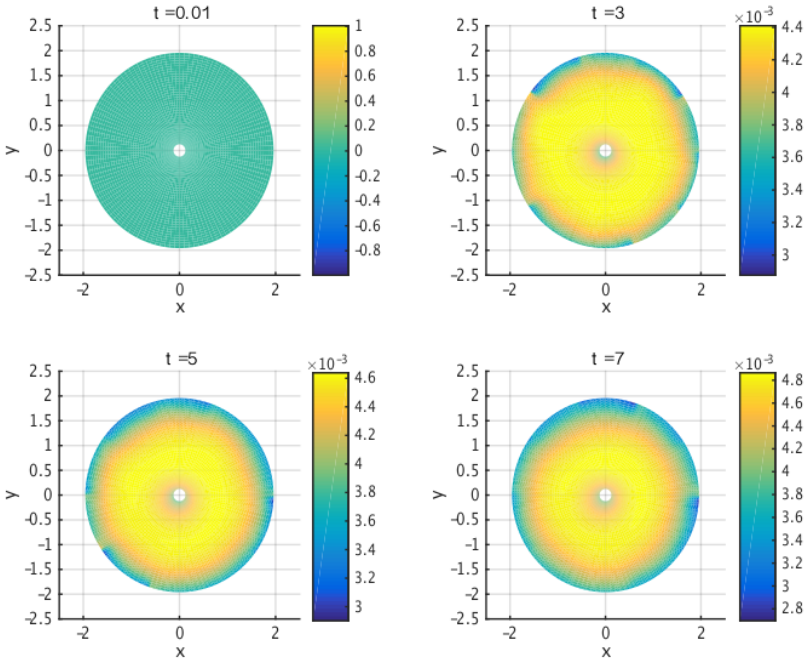

Figure 7.11 – Numerical simulations of the concentration dynamics in Ω, with a chemical attractive signal in the environment. The problem solved is (7.21)-(7.22). Parameters: $(k_{\text{on}}, k_{\text{off}}) = (10, 10)$; $(M, \xi, \alpha, \delta, D, k_d) = (0.1, 1, 300, 15, 5, 2)$. Signal: $(S_m, S_c) = (2, 5)$; fluctuations: $(\lambda, \sigma) = (4, \frac{\sqrt{2\lambda}}{3})$. The time step is $\Delta t = 10^{-2}$. The initial condition is uniform.

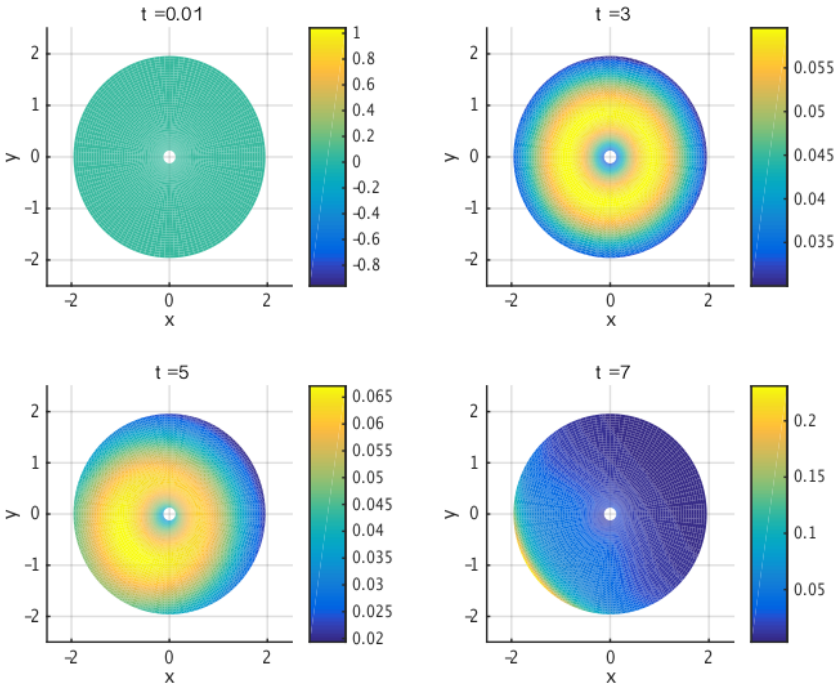

Figure 7.12 – Numerical simulations of the concentration dynamics in Ω, with a chemical attractive signal in the environment, with a stochastic perception. The problem solved is (7.21)-(7.22). Parameters: $(k_{\text{on}}, k_{\text{off}}) = (10, 10)$; $(M, \xi, \alpha, \delta, D, k_d) = (1, 1, 300, 15, 5, 2)$. Signal: $(S_m, S_c) = (2, 5)$; fluctuations: $(\lambda, \sigma) = (4, \frac{\sqrt{2\lambda}}{3})$. The time step is $\Delta t = 10^{-2}$. The initial condition is uniform.

Consider a point-source for the signal in the medium. In order to avoid resolving a problem on the whole space, we start by defining the concentration of signal felt at each point of the cell membrane as a direct function of the distance to the source point $\mathbf{x}_S$. More precisely,

$$S(\mathbf{X}) = \frac{1}{1 + 0.1 \parallel \mathbf{X} - \mathbf{x}_S \parallel^2} \,. \tag{7.26}$$

Moreover, we define an intracellular dynamics for S so that the signal and the intracellular effectors of its response are merged into the same quantity. In the following, we will call it the stimulus. It is assumed to diffuse in the domain, and is degraded at rate d. Finally, this amounts to solving the following problem:

$$\begin{aligned} -\Delta S(\mathbf{X}) + dS(\mathbf{X}) &= 0 \quad \text{in } \Omega(t)\,, \\ S(\mathbf{X}) &= \frac{1}{1 + 0.1 \parallel \mathbf{X} - \mathbf{x}_S \parallel^2} \quad \text{on } \partial\Omega(t)\,. \end{aligned}$$

In a future work, we will use a more realistic description of the signal, where it is produced in a point-source in the global domain, and diffuses in space while being degraded.

In the following numerical simulations in figures 7.14 and 7.15, we show the displacement of the cellular domain in the direction of the source of the signal. In the first case, the cell stops at the source point despite its polarisation, whereas in the second case the cell is too focused on its polarisation to find the source.

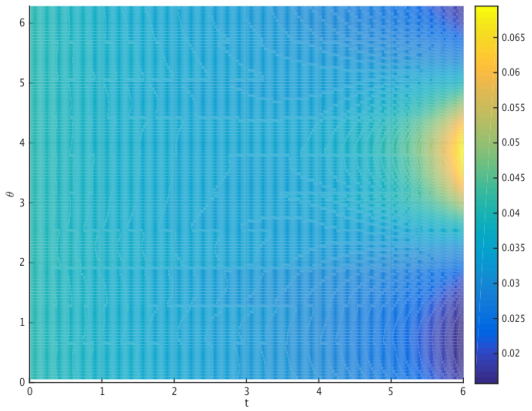

Figure 7.13 – Kymograph corresponding to the concentration of attached markers in the case of an attractive signal with a stochastic perception for $M = 1$ as displayed in figure 7.12. Time is represented in abscissa, and the angle θ in ordinate. The color shows the concentration.

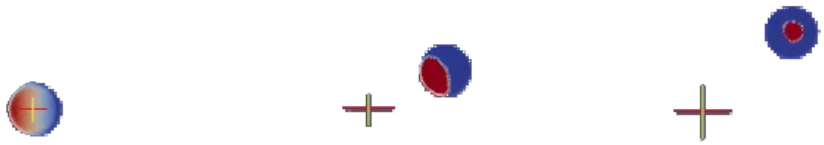

Figure 7.14 – Numerical simulations of the motion of a cell under the action of an attractive signal. The problem solved is (7.23)-(7.24)-(7.25). In this case, the cell feels the signal and responds strongly enough to counterbalance its own polarisation.

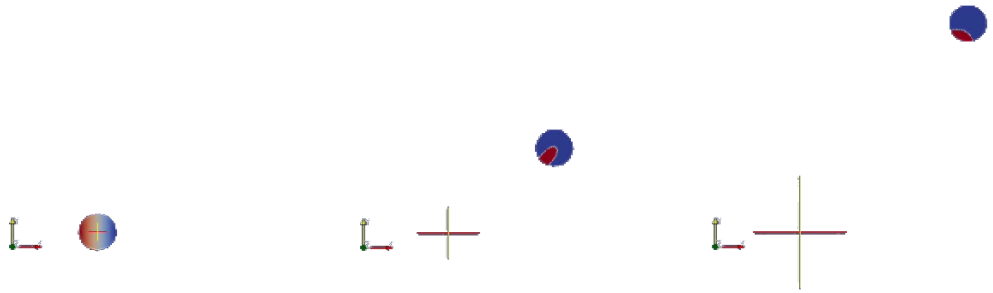

Figure 7.15 – Numerical simulations of the motion of a cell under the action of an attractive signal. The problem solved is (7.23)-(7.24)-(7.25). In this case, the cell feels the signal enough to slow down, but remains focused on its own dynamics.

7.6 Mechanical interaction

We have seen in the previous section how chemical signals could be included in the model by describing either their detection on the boundary or the consequences of this detection inside the cell. Recently, the ability of mechanical cues to induce and direct migration was investigated [Caballero et al., 2015]. The corresponding forces that exert on the cell affect the intracellular dynamics, leading to an adaptation of the cells behaviour. It is believed that the active character of the cytoskeleton is directly involved in the interaction. Therefore, the multi-scale character of our model, and the fluid description of the cytoskeleton is adapted to that type of experimental setting.

Several numerical contact models exist and some of them are widely used, in particular for modelling crowd motions [Maury and Venel, 2008, 2011]. In this part, we focus on a basic contact situation where a cell is migrating perpendicularly towards a wall. We will first impose the velocity at the time of contact without using any splitting technique. Our aim is to model the adaptive response of the polarity marker and to quantify the time it will take for the cell to go away from the wall. This approach will be enriched in further works in relation with the existing numerical contact models. We begin with the simplest description of non-interpenetration.

7.6.1 Non-interpenetration

In this section, we study the simplest mechanical interaction that arises in the contact with an obstacle. The cell can not go further in the direction of the obstacle. For that purpose, in numerical simulations, we prescribe a null velocity whenever the cell's velocity is not compatible with non-interpenetration. More precisely, the following happens (see figure 7.16): consider the situation where the cell velocity is given by V such that $V = V \cdot e_x$, and where the wall is located at $x_{\mathcal{O}}$, while the cell center is located in $x_{\mathcal{C}}(t)$ at time t, assuming that $x_{\mathcal{C}}(0) \leq x_{\mathcal{O}}$ (see figure 7.17). Finally, denote $d : \mathbb{R}_+ \to \mathbb{R}_+$ the distance function such that $d(t) = |x_{\mathcal{C}} - x_{\mathcal{O}}|$. Then, the following occurs:

1. while $d(t) > R$, the cell's dynamics corresponds to its own activity.
2. When $d(t) \leq R$, a contact appears. In order to avoid interpenetration the first option is to impose that the cell velocity then equals zero.

   $\to$ Since the cell velocity affects the intracellular dynamics see (5.46)-(5.48), the marker concentration evolves. If the cell velocity is given by (5.43), this gives a new cell velocity value which we call the cell desired velocity.
3. Finally, by adaptation to the global motion, a new displacement is "proposed", and this feedback loop operates until an acceptable velocity arises. In the model we will consider that the cell velocity is given by the cell desired velocity (which is computed from its internal state) if it is an acceptable velocity in the sense that it is compatible with non interpenetration.

In this very simple model, when there is contact the cell velocity is equal to zero until the cell desired velocity becomes acceptable. The novelty here is that the desired velocity is directly linked to the cell internal state which also depends on its velocity. Hence, according to the studies we have previously performed, if we consider some noise, if the cell velocity is zero, there will be a time for which the internal state of the cell will give rise to an acceptable velocity. Of course since diffusion and noise are at work for this to happen, we expect such a process to be long.

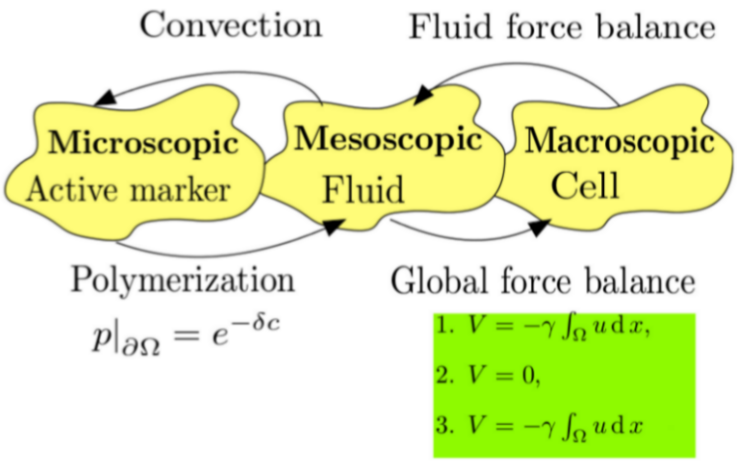

Figure 7.16 – Schemes for the different steps in dealing with a mechanical contact.

Discrete setting

Imposing a null velocity directly may lead to unrealistic behaviours. Let us now discuss more realistic options for a discrete time setting. Indeed, similarly as in the previous case, for a highly polarised cell that is not in contact with the obstacle at time t_n but has a large velocity v^n, so that its next position ought to be beyond the obstacle, the algorithm prescribes to stop. Then, the cell would be stuck at a non-zero distance from the obstacle until depolarisation induces a velocity low enough to move forward.

To avoid these types of non-physical phenomena, two options can be considered:

- a first possibility consists in adapting the velocity v^n so that the cell is brought exactly to contact. This option is still not physical, and implies an arbitrary velocity.
- one could otherwise compute the adapted time step $\Delta t'$ such that the cell reaches the obstacle at time $t^n + \Delta t'$ with a velocity v^n. This method requires to solve again the convection-diffusion problem for a time step $\Delta t'$. The following time steps then can be put back to normal.

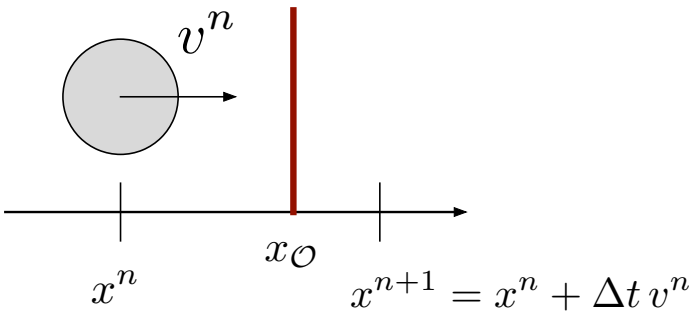

Figure 7.17 – The case of interpenetration.

Remark 30. *Another option in this case is to prescribe a velocity that leads exactly to the contact. As a consequence, for large velocities the cell would not stay at a given distance to the obstacle until it gets an acceptable velocity.*

Numerics

In terms of numerical simulations, this method requires to check at each time step the distance between the cell and each obstacle put into the setting, so that the occurrence of contact or interpenetration is detected. Then, it suffices to impose a zero velocity.

A numerical illustration was performed in the finite elements setting using FreeFem++. More precisely, we numerically solve

$$\begin{cases} -\Delta\tilde{p}(t,\mathbf{X}) = -k_d & \text{in } \Omega(t)\,, \\ -\eta\Delta\tilde{u}(t,\mathbf{X}) + \nabla\tilde{p}(t,\mathbf{X}) = -(\tilde{u}(t,\mathbf{X}) + \tilde{v}(t)) & \text{in } \Omega(t)\,, \\ \sigma\cdot\mathbf{n} = \exp(-\delta\tilde{\mu}(t,\mathbf{X})) & \text{on } \partial\Omega(t)\,, \end{cases} \tag{7.27}$$

with σ the fluid's stress tensor, together with the following problem for the molecular dynamics:

$$\begin{cases} \partial_t\tilde{c} + \operatorname{div}\ (\tilde{c}(\tilde{u}+\tilde{v}) - D'\nabla\tilde{c}) = 0 & \text{in } \Omega(t)\,, \\ (D'\nabla\tilde{c} - \tilde{c}\tilde{u})\cdot\mathbf{n} = -k_{\text{on}}\tilde{c} + k_{\text{off}}\tilde{\mu} & \text{on } \partial\Omega(t)\,, \\ \frac{\partial}{\partial t}\tilde{\mu} + \tilde{v}\cdot\nabla\tilde{\mu} = k_{\text{on}}\tilde{c} - k_{\text{off}}\tilde{\mu} & \text{on } \partial\Omega(t)\,. \end{cases} \tag{7.28}$$

Then, the domain's displacement is obtained by

$$\tilde{v}(t) = (\mathbb{1}_{d(t)>R} + \mathbb{1}_{d(t)\leq R}\mathbb{1}_{\gamma\int_{\Omega(t)}\nabla\tilde{p}(t,\mathbf{X})\,\mathrm{d}\mathbf{X}\leq 0}) \int_{\Omega(t)} \nabla\tilde{p}(t,\mathbf{X})\,\mathrm{d}\mathbf{X}\,, \tag{7.29}$$

and $d'(t) = -\tilde{v}(t)$.

The cell is initially polarised and migrates towards a wall. The loss of polarisation is observed after contact, and the stochastic fluctuations inside the cell contributes to the adaptation, and eventually the recovery of a motile phenotype. This is a characteristic example illuminating the issue of depolarisation time of a cell.

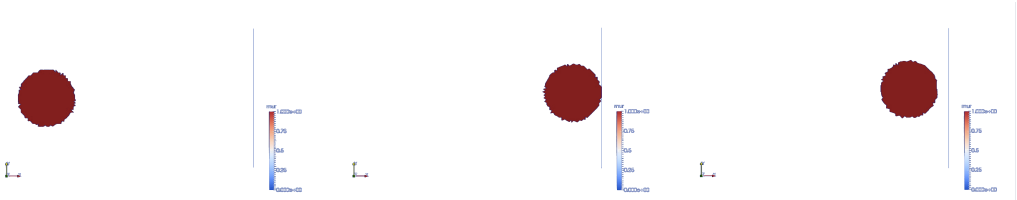

Figure 7.18 – Numerical simulations of the motion of a discoidal cell towards a wall at different times. The problem solved is (7.27)-(7.28)-(7.29). The cell stops at the contact, before moving further away due to its internal activity.

In the case where either the polarisation or the noise is low enough, contact with the wall may induce a permanent loss of motility.

If this approach is promising, and will be pursued by using more expert numerical methods, it is a first option that does not provide a mechanical description of the contact. Indeed, at the contact zone, new forces are applied on the cell and directly impact the intracellular dynamics [Mayor and Carmona-Fontaine, 2010].

7.6.2 Forces of contact on the fluid

Aiming at a realistic description on the contact in terms of forces, we consider again the global force balance equation (5.34) in the case of a local contact, before non-dimensionalization:

$$\xi_1 V(t) + \xi\int_{\Omega(t)} \tilde{U}(t,\mathbf{X}) + V(t)\,\mathrm{d}\mathbf{x} + F_{\text{contact}}(t) = 0\,, \tag{7.30}$$

where F_{contact} is the force exerted by the obstacle on the boundary at the contact point. In this setting, if the velocity V is the "desired" but non acceptable velocity, then the contact force ought to write

$$F_{\text{contact}}(t) = -\xi \left(V(t)|\Omega| + \int_{\Omega(t)} \tilde{U}(t, \mathbf{X}) \, \mathrm{d}\mathbf{X} \right) . \tag{7.31}$$

This force appears in the force balance equation for the fluid (see figure 7.19), as an external force applied at the boundary. In the case of a "frontal" contact, the force is exerted in the normal direction at the boundary, so that the Stokes problem writes

$$\begin{aligned} -\eta \Delta \tilde{U} + \nabla \tilde{P} &= -\xi(\tilde{U} + V) && \text{in } \Omega(t) , \\ \sigma \cdot \mathbf{n} := (\eta(\nabla \tilde{U} + {}^t\nabla \tilde{U}) - \tilde{P}\mathrm{Id}) \cdot \mathbf{n} &= (e^{-\delta \tilde{C}} + F_{\text{contact}})\mathbf{n} && \text{on } \partial\Omega(t) , \\ \nabla \cdot \tilde{U} &= -k_d && \text{in } \Omega(t) . \end{aligned} \tag{7.32}$$

Finally, a numerical method to describe this interaction consists in detecting any contact issue, and then in solving the new Stokes problem with contact to simulate the fluid response to the contact. This idea will be pursued in a future work.

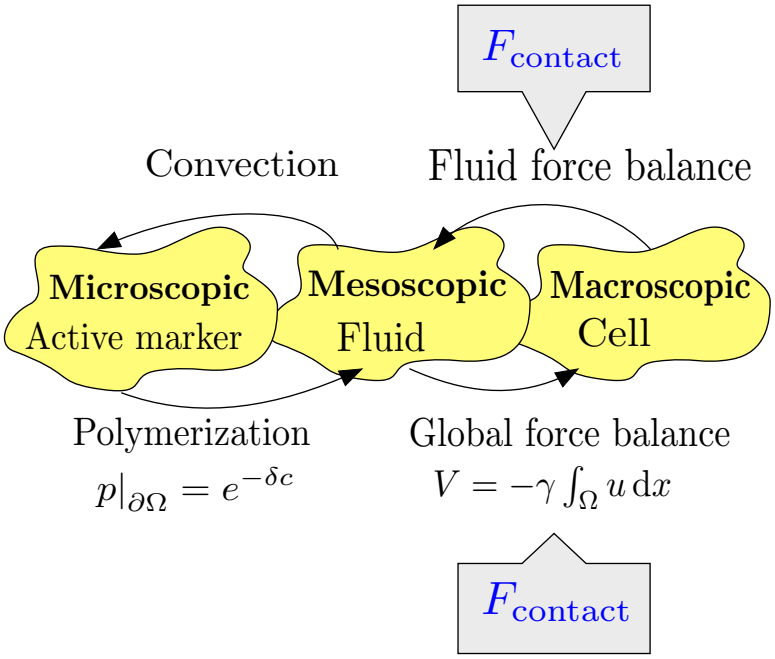

Figure 7.19 – Scheme of the system under a mechanical contact.

7.7 Conclusions

Finally, in this chapter, we have investigated first the intrinsic dynamics leading to migration in the model. Our two dimensional discoid model for cell migration is based on the interaction between the molecular and the mesoscopic fluid scale. More precisely, we follow the idea such that the actin retrograde flow is a key component in the context of cell crawling. It realizes the connection between the microscopic scale by transporting a molecular regulator of its dynamics. It is also involved in the macroscopic motion by means of global force equilibrium and friction forces. The converse feedback is of same nature, as the

global motion reinforces the actin flows by friction. Numerical simulations showed that this global friction was necessary to counteract the global drift to the center due to the actin flows, and provide different migratory behaviours, motile and non motile. Moreover, spatially correlated stochastic fluctuations were considered in the activity of the cytoskeleton. They account for the large stochasticity involved in molecular signalling pathways of the cytoskeleton functions, that are not precisely described here. Providing an intrinsic active character, they allowed getting numerical trajectories of different natures that were biologically observed, validating the derivation of the model. Next, we investigated the model confronted with external stimulations, either chemical or mechanical. In combination with stochastic perturbations, the model provides a realistic framework for these settings, and will be used further on for comparison with experimentations. As an example, microfluidics experiments using micro-pillars were made by the team of Magali Faivre (INL, Lyon 1) for the sorting of cancer cells by their motility. Recent experiments investigate the ability of cells to adapt to a difference in hydraulic pressure in micro-channels. The cells were witnessed to mainly avoid paths connected to dead-ends, which is thought to be similar to the displacement of dendritic cells in lymph vessels. A proposed explanation relies on the mechanical interaction between the active cytoskeleton and the micro-channels. With that in mind, confrontation of the model with experimental data is a work in project, in the spirit of Muller et al. [2016], in collaboration with the team of Matthieu Piel.

Moreover, the combination of both types of signal is also of interest. Finally, further works could be made in the direction of interaction between cells and collective migration. Overall, our model constitutes a phenomenological minimal multiscale and self-regulated framework to describe the formation of local regions of increased marker concentrations associated with cell migration.

7.8 Discretization

7.8.1 Finite volume discretization

We introduce now the finite volume discretization of the model in a 2D domain. We assume that the cytokeleton domain is an annulus $\Omega_0 = B(0,R) \setminus B(0,R_{min}) \subset \mathbb{R}^2$, where $B(0,R_{min})$ accounts for the nucleus. We consider a zero-flux boundary condition on $C(0,R_{min})$, the circle of center $(0,0)$ and radius R_{min}. As a consequence, it will be natural to study the problem in polar coordinates.

Polar formulation

Advection-diffusion problem Let us first recall the problem on c on $\Omega_0 = B(0,R) \setminus B(0,R_{min})$ with $\vec{n}_{\mathbf{x}}$ the unit normal vector to Ω_0 at point $\mathbf{x} \in \partial\Omega_0$:

$$\partial_t c(t,\mathbf{x}) = \nabla.\left(D'\nabla c(t,\mathbf{x}) - c(t,\mathbf{x})\,\mathbf{u}(t,\mathbf{x})\right), \text{ in } \Omega_0\,, \tag{7.33}$$

$$(D'\nabla c(t,\mathbf{x}) - c(t,\mathbf{x})\,\mathbf{u}(t,\mathbf{x})).\mathbf{n} = 0, \text{ on } C(0,R), \tag{7.34}$$

$$(D'\nabla c(t,\mathbf{x}) - c(t,\mathbf{x})\,\mathbf{u}(t,\mathbf{x})).\mathbf{n} = 0, \text{ on } C(0,R_{min}). \tag{7.35}$$

Let $\mathbf{x} = (r\cos(\theta), r\sin(\theta)) \in \Omega$, and $\tilde{c}$ the polar function such that $\frac{1}{r}\tilde{c}(t,r,\theta) = c(t,\mathbf{x})$ with $(r,\theta) \in [R_{\min}, R] \times \mathbb{R}/2\pi\mathbb{Z}$. Then,

$$\begin{aligned}
\partial_t \tilde{c}(t,r,\theta) &= \partial_r \left(D' r \partial_r \left(\frac{\tilde{c}(t,r,\theta)}{r} \right) - \tilde{c}(t,r,\theta)\mathbf{u}_r(t,r,\theta) \right) \\
&+ \partial_\theta \left(\frac{1}{r^2}(D'\partial_\theta \tilde{c}(t,r,\theta) - \tilde{c}(t,r,\theta)\mathbf{u}_\theta(t,r,\theta)) \right) \text{ in } \Omega_0\,, \qquad (7.36)\\
0 &= D' R \partial_r \left(\frac{\tilde{c}(t,R,\theta)}{R} \right) - \tilde{c}(t,R,\theta)\mathbf{u}_r(t,R,\theta), \text{ on } C(0,R)\,, \qquad (7.37)\\
0 &= D' R_{min} \partial_r \left(\frac{\tilde{c}(t,R_{min},\theta)}{R_{min}} \right) - \tilde{c}(t,R_{min},\theta)\mathbf{u}_r(t,R_{min},\theta), \text{ on } C(0,R_{min})\,. \qquad (7.38)
\end{aligned}$$

Poisson problem on p The advection velocity in the advection-diffusion problem writes $u(t,\mathbf{x}) = -\nabla p(t,\mathbf{x}) - \frac{\xi}{\xi_1}\int_{\Omega_0} \nabla p(t,\mathbf{x})\,\mathrm{d}\mathbf{x}$, where the pressure p is solution of the following problem:

$$\begin{aligned}
-\Delta p(t,\mathbf{x}) &= -k_d, \text{ in } \Omega_0\,, \qquad (7.39)\\
p(t,\mathbf{x}) &= [1 - \delta c(t,\mathbf{x})]_+, \text{ on } C(0,R)\,, \qquad (7.40)\\
p(t,\mathbf{x}) &= 0, \text{ on } C(0,R_{min})\,, \qquad (7.41)
\end{aligned}$$

where the pressure condition on $C(0,R_{min})$ is arbitrary, and fix the pressure values. Let us consider these equations in polar coordinates with $\frac{1}{r}\tilde{p}(t,r,\theta) = p(t,\mathbf{x})$ for $(r,\theta) \in [R_{min}, R] \times \mathbb{R}/2\pi\mathbb{Z}$. We have

$$\begin{aligned}
-\partial_r \left(r\partial_r \left(\frac{\tilde{p}(r,\theta)}{r} \right) \right) - \frac{1}{r^2}\partial_{\theta\theta}\tilde{p}(r,\theta) &= -k_d\, r, \qquad \text{in } \Omega_0, \qquad (7.42)\\
\tilde{p}(t,R,\theta) &= R\left[1 - \delta\frac{\tilde{c}(t,R,\theta)}{R}\right]_+ \qquad \text{on } C(0,R), \qquad (7.43)\\
\tilde{p}(t,R_{min},\theta) &= 0 \qquad \text{on } C(0,R_{min}). \qquad (7.44)
\end{aligned}$$

Discretization

Let $t^n = n\,\Delta t$ be the time discretization, and $\{r_j = R_{min} + (j - 1/2)\,\Delta r, j \in \{1,...,N_r\}\}$ the space discretization of the bounded interval $[R_{min}, R]$, such that $r_{N_r+1/2} = R$, (therefore $N_R = \frac{R-R_{min}}{\Delta r}$). Similarly, $\{\theta_k = k\,\Delta\theta, k \in \{1,...,N_\theta\}\}$ is the space discretization of the periodic interval $\mathbb{R}/2\pi\mathbb{Z}$. We introduce the control volumes $W_{(j,k)} \subset \mathbb{R}^2$ and $V_k \subset \mathbb{R}/2\pi\mathbb{Z}$ with

$$\begin{aligned}
V_k &= \left(\theta_{k-\frac{1}{2}}, \theta_{k+\frac{1}{2}}\right)\,,\\
W_{(j,k)} &= \left(r_{j-\frac{1}{2}}, r_{j+\frac{1}{2}}\right) \times V_k\,.
\end{aligned}$$

Let $\tilde{c}^n_{(j,k)}$ (resp. μ^n_k) be the approximated value of the exact solution $\tilde{c}(t^n, r_j, \theta_k)$ (resp.

$\mu(t^n, \theta_k)$), and $\tilde{p}^n_{(j,k)}$ be the approximated value of the exact solution $\tilde{p}(t^n, r_j, \theta_k)$:

$$\begin{aligned}
\tilde{c}^n_{(j,k)} &= \frac{1}{\Delta r \Delta\theta} \iint_{W(j,k)} \tilde{c}(t^n, r, \theta)\, \mathrm{d}r\, \mathrm{d}\theta\,, \\
\mu^n_k &= \frac{1}{\Delta\theta} \int_{V_k} \mu(t^n, \theta)\, \mathrm{d}\theta\,, \\
\tilde{p}^n_{(j,k)} &= \frac{1}{\Delta r \Delta\theta} \iint_{W(j,k)} \tilde{p}(t^n, r, \theta)\, \mathrm{d}r\, \mathrm{d}\theta\,.
\end{aligned}$$

Moreover, we write u^n and v^n the corresponding discretized velocity functions at time t^n.

In the case without activation at the membrane, the resolution is made as follows: for $n \geq 0$, knowing $\tilde{c}^n$ allows to compute $\tilde{p}^n$, then u^n and v^n. Finally, $\tilde{c}^{n+1}$ is computed using u^n, and so on.

Problem on $\tilde{p}$ Write $\mathcal{F}$ for the numerical flux. Then, we have the following scheme for equation (7.42): for $(j,k) \in \{1, ..., N_r\} \times \{1, ..., N_\theta\}$,

$$-\left(\frac{\mathcal{F}_{(j+\frac{1}{2},k)} - \mathcal{F}_{(j-\frac{1}{2},k)}}{\Delta r} + \frac{\mathcal{F}_{(j,k+\frac{1}{2})} - \mathcal{F}_{(j,k-\frac{1}{2})}}{\Delta\theta} \right) = -k_d r\,.$$

The finite volume numerical fluxes are defined by

$$\mathcal{F}_{(j+\frac{1}{2},k)} = r_{j+\frac{1}{2}} \frac{\frac{\tilde{p}_{(j+1,k)}}{r_{j+1}} - \frac{\tilde{p}_{(j,k)}}{r_j}}{\Delta r}, \qquad \mathcal{F}_{(j-\frac{1}{2},k)} = r_{j-\frac{1}{2}} \frac{\frac{\tilde{p}_{(j,k)}}{r_j} - \frac{\tilde{p}_{(j-1,k)}}{r_{j-1}}}{\Delta r},$$
$$\mathcal{F}_{(j,k+\frac{1}{2})} = \frac{1}{r_j^2} \frac{\tilde{p}_{(j,k+1)} - \tilde{p}_{(j,k)}}{\Delta\theta}, \qquad \mathcal{F}_{(j,k-\frac{1}{2})} = \frac{1}{r_j^2} \frac{\tilde{p}_{(j,k)} - \tilde{p}_{(j,k-1)}}{\Delta\theta}.$$

The Dirichlet boundary conditions (7.44)-(7.43) are imposed using ghost values $\tilde{p}_{(0,k)}$ and $\tilde{p}^n_{(N_r+1,k)}$. For $k \in \{1, ..., N_\theta\}$,

$$\mathcal{F}_{(\frac{1}{2},k)} = \frac{r_{\frac{1}{2}}}{r_1} \frac{\tilde{p}_{(1,k)}}{\Delta r}\,,$$

since $\tilde{p}_{(0,k)} = 0$. Now, $\tilde{p}^n_{(N_r+1,k)} = r_{N_r} \left[1 - \delta \frac{\tilde{c}^n_{(N_r,k)}}{r_{N_r}}\right]_+$, the corresponding flux writes

$$\mathcal{F}_{(N_r+\frac{1}{2},k)} = r_{N_r+\frac{1}{2}} \frac{\frac{r_{N_r}}{r_{N_r+1}} \left(1 - \delta \frac{\tilde{c}^n_{(N_r,k)}}{r_{N_r}}\right) - \frac{\tilde{p}_{(N_r,k)}}{r_{N_r}}}{\Delta r}\,.$$

Therefore, the term $\frac{r_{N_r} r_{N_r+\frac{1}{2}}}{r_{N_r+1}\Delta r} \left[1 - \delta \frac{\tilde{c}^n_{(N_r,k)}}{r_{N_r}}\right]$ will be included in the right hand side of the matricial problem.

Similarly, the periodic conditions impose for $j \in \{1, ..., N_r\}$,

$$\mathcal{F}_{(j,N_\theta+\frac{1}{2})} = \mathcal{F}_{(j,\frac{1}{2})} = \frac{1}{r_j^2} \frac{\tilde{p}_{(j,1)} - \tilde{p}_{(j,N_\theta)}}{\Delta\theta}.$$

We define the column vector $\mathcal{P}$ by $\mathcal{P}(k + (j-1)N_\theta) = \tilde{p}_{(j,k)}$ with $(j,k) \in \{1, ..., N_r\} \times \{1, ..., N_\theta\}$:

$$\mathcal{P} = \left(\tilde{p}_{(1,1)} \cdots \tilde{p}_{(1,N_\theta)}\, \tilde{p}_{(2,1)} \cdots \tilde{p}_{(2,N_\theta)} \cdots \tilde{p}_{(N_r,N_\theta)}\right)^T$$

For $\Delta r = \Delta\theta$ the stiffness matrix $\mathcal{A}_p$ is defined by

$$\mathcal{A}_p = \begin{pmatrix} \frac{r_{1/2}+r_{1+1/2}}{r_1} I_{N_\theta} & -\frac{r_{1+\frac{1}{2}}}{r_2} I_{N_\theta} & & & \\ \ddots & \ddots & \ddots & & \\ & -\frac{r_{j-\frac{1}{2}}}{r_{j-1}} I_{N_\theta} & \frac{r_{j-\frac{1}{2}}+r_{j+\frac{1}{2}}}{r_j} I_{N_\theta} & -\frac{r_{j+\frac{1}{2}}}{r_{j+1}} I_{N_\theta} & \\ & & \ddots & \ddots & \ddots \\ & & & -\frac{r_{N_r-\frac{1}{2}}}{r_{N_r-1}} I_{N_\theta} & \frac{r_{N_r-\frac{1}{2}}+r_{N_r+\frac{1}{2}}}{r_{N_r}} I_{N_\theta} \end{pmatrix} + \begin{pmatrix} \frac{1}{r_1^2}A & & & & \\ & \frac{1}{r_2^2}A & & & \\ & & \ddots & & \\ & & & \frac{1}{r_{N_r-1}^2}A & \\ & & & & \frac{1}{r_{N_r}^2}A \end{pmatrix} \tag{7.45}$$

where the second matrix accounts for the angular diffusion, with $A \in M_{N_\theta}(\mathbb{R})$ the classical diffusion matrix with periodic flux boundary conditions:

$$A = \begin{pmatrix} 2 & -1 & & & -1 \\ -1 & 2 & \ddots & & \\ & \ddots & \ddots & \ddots & \\ & & \ddots & 2 & -1 \\ -1 & & & -1 & 2 \end{pmatrix}. \tag{7.46}$$

The right-hand side in (7.42) and the flux boundary condition (7.43) on $C(0, R_{max})$ imposes this right hand side column vector of length $N_r\, N_\theta$:

$$\mathcal{R}_p^n = -k_d \begin{pmatrix} (r_1)_k \\ \vdots \\ (r_j)_k \\ \vdots \\ (r_{N_r})_k \end{pmatrix} + \frac{r_{N_r} r_{N_r+\frac{1}{2}}}{r_{N_r+1}\Delta r} \begin{pmatrix} 0 \\ \vdots \\ 0 \\ \left[1 - \delta \frac{\tilde{c}^n_{N_r,k}}{r_{N_r}}\right]_{+k} \end{pmatrix}.$$

We use a standard numerical method to invert the symmetric positive definite matrix $\frac{1}{\Delta r^2}\mathcal{A}$ and then resolve at each time step

$$\mathcal{P} = \left(\frac{1}{\Delta r^2}\mathcal{A}_p\right)^{-1} \mathcal{R}_p^n.$$

Equations for u and v The equation on v in polar coordinates writes

$$v(t) = \frac{\xi}{\xi_1} \int_0^{2\pi} \left[1 - \delta \frac{\tilde{c}(t, R, \theta)}{R}\right]_+ \mathbf{n}\, \mathrm{d}\theta\,. \tag{7.3}$$

We compute numerically the velocity in cartesian coordinates $v^n_{\text{cart}} := (v^n_x, v^n_y)^T$.

Since $\tilde{c}^n_{(j,k)} = \frac{1}{\Delta r \Delta\theta}\int_{W(j,k)} \tilde{c}(t^n, r, \theta)\,\mathrm{d}r\,\mathrm{d}\theta$, this amounts to compute

$$v^n_x = \frac{\xi}{\xi_1}\Delta\theta \sum_{k=1}^{N_\theta} \left[1 - \delta \tilde{c}^n_{(N_r,k)}\right]_+ \cos(\theta_k)\,, \tag{7.47}$$

$$v^n_y = \frac{\xi}{\xi_1}\Delta\theta \sum_{k=1}^{N_\theta} \left[1 - \delta \frac{\tilde{c}^n_{(N_r,k)}}{R}\right]_+ \sin(\theta_k)\,. \tag{7.48}$$

Then, a polar change of coordinates leads to $v^n := (v^n_r, v^n_\theta)^T$.

For the fluid velocity, we have

$$u(t,\mathbf{x}) = -\nabla p(t,\mathbf{x}) - v(t)\,, \tag{7.3}$$

that rewrites

$$u(t,r,\theta) = -\left(\partial_r\left(\frac{\tilde{p}(t,r,\theta)}{r}\right) + v_r\right)\vec{e_r} - \left(\frac{1}{r}\partial_\theta \tilde{p}(t,r,\theta) + v_\theta\right)\vec{e_\theta}\,, \tag{7.49}$$

since $u_r = u(t,\mathbf{x})\cdot\vec{e_r}$ and $u_\theta = r u(t,\mathbf{x})\cdot\vec{e_\theta}$. We define at time t^n

$$u^n_{(j+\frac{1}{2},k)} = -\frac{\frac{\tilde{p}_{(j+1,k)}}{r_{j+1}} - \frac{\tilde{p}_{(j,k)}}{r_j}}{\Delta r} - v^n_r\,, \qquad u^n_{(j-\frac{1}{2},k)} = -\frac{\frac{\tilde{p}_{(j,k)}}{r_j} - \frac{\tilde{p}_{(j-1,k)}}{r_{j-1}}}{\Delta r} - v^n_r\,,$$

$$u^n_{(j,k+\frac{1}{2})} = -\frac{1}{r_j}\frac{\tilde{p}_{(j,k+1)} - \tilde{p}_{(j,k)}}{\Delta\theta} - v^n_\theta\,, \qquad u^n_{(j,k-\frac{1}{2})} = -\frac{1}{r_j}\frac{\tilde{p}_{(j,k)} - \tilde{p}_{(j,k-1)}}{\Delta\theta} - v^n_\theta\,.$$

Equation on $\tilde{c}$ For simplicity, we call again $\mathcal{F}$ the numerical fluxes. We can write the following scheme for equation (7.36): for $(j,k) \in \{1,...,N_r\}\times\{1,...,N_\theta\}$,

$$\frac{\tilde{c}^{n+1}_{(j,k)} - \tilde{c}^n_{(j,k)}}{\Delta t} = \frac{\mathcal{F}_{(j+\frac{1}{2},k)} - \mathcal{F}_{(j-\frac{1}{2},k)}}{\Delta r} + \frac{\mathcal{F}_{(j,k+\frac{1}{2})} - \mathcal{F}_{(j,k-\frac{1}{2})}}{\Delta\theta}.$$

We define now the numerical fluxes. The diffusion part is implicit, while the advection is explicit due to the nonlinearity in the expression of v. We have:

$$\mathcal{F}_{(j+\frac{1}{2},k)} = D'\, r_{j+\frac{1}{2}}\, \frac{\frac{\tilde{c}^{n+1}_{(j+1,k)}}{r_{j+1}} - \frac{\tilde{c}^{n+1}_{(j,k)}}{r_j}}{\Delta r} - A^{up}\left(u^n_{(j+\frac{1}{2},k)}, \tilde{c}^n_{(j,k)}, \tilde{c}^n_{(j+1,k)}\right),$$

$$\mathcal{F}_{(j-\frac{1}{2},k)} = D'\, r_{j-\frac{1}{2}}\, \frac{\frac{\tilde{c}^{n+1}_{(j,k)}}{r_j} - \frac{\tilde{c}^{n+1}_{(j-1,k)}}{r_{j-1}}}{\Delta r} - A^{up}\left(u^n_{(j-\frac{1}{2},k)}, \tilde{c}^n_{(j-1,k)}, \tilde{c}^n_{(j,k)}\right),$$

$$\mathcal{F}_{(j,k+\frac{1}{2})} = \frac{1}{r_j^2}\left(D'\,\frac{\tilde{c}^{n+1}_{(j,k+1)} - \tilde{c}^{n+1}_{(j,k)}}{\Delta\theta} - A^{up}\left(u^n_{(j,k+\frac{1}{2})}, \tilde{c}^n_{(j,k)}, \tilde{c}^n_{(j,k+1)}\right)\right),$$

$$\mathcal{F}_{(j,k+\frac{1}{2})} = \frac{1}{r_j^2}\left(D'\,\frac{\tilde{c}^{n+1}_{(j,k)} - \tilde{c}^{n+1}_{(j,k-1)}}{\Delta\theta} - A^{up}\left(u^n_{(j,k-\frac{1}{2})}, \tilde{c}^n_{(j,k-1)}, \tilde{c}^n_{(j,k)}\right)\right),$$

where A^{up} is the advection term expressed by

$$A^{up}(u, x_-, x_+) = \begin{cases} u\,x_-, & \text{if } u > 0,\\ u\,x_+, & \text{if } u < 0. \end{cases} \tag{7.50}$$

The zero flux boundary conditions (7.37)-(7.38) imposes that $\mathcal{F}_{(\frac{1}{2},k)} = \mathcal{F}_{(N_r+\frac{1}{2},k)} = 0$ for $k \in \{1,...,N_\theta\}$.

Similarly, the periodic conditions impose for $j \in \{1, ..., N_r\}$

$$\mathcal{F}_{(j,N_\theta+\frac{1}{2})} = \mathcal{F}_{(j,\frac{1}{2})} = \frac{1}{r_j^2}\left(D' \frac{\tilde{c}^{n+1}_{(j,1)} - \tilde{c}^{n+1}_{(j,N_\theta)}}{\Delta\theta} - A^{up}\left(u^n_{(j,\frac{1}{2})}, \tilde{c}^n_{(j,N_\theta)}, \tilde{c}^n_{(j,1)}\right)\right).$$

We define the column vector $\mathcal{C}^n$ by $\mathcal{C}^n(k + (j-1)N_\theta) = \tilde{c}^n_{(j,k)}$ with $(j,k) \in \{1, ..., N_r\} \times \{1, ..., N_\theta\}$:

$$\mathcal{C}^n = \left(\tilde{c}^n_{(1,1)} \dots \tilde{c}^n_{(1,N_\theta)} \tilde{c}^n_{(2,1)} \dots \tilde{c}^n_{(2,N_\theta)} \dots \tilde{c}^n_{(N_r,N_\theta)}\right)^T.$$

The diffusion matrix this time writes

$$\mathcal{A} = \begin{pmatrix} \frac{r_{1/2}}{r_1} I_{N_\theta} & -\frac{r_{1+\frac{1}{2}}}{r_2} I_{N_\theta} & & & \\ \ddots & \ddots & \ddots & & \\ & -\frac{r_{j-\frac{1}{2}}}{r_{j-1}} I_{N_\theta} & \frac{r_{j-\frac{1}{2}}+r_{j+\frac{1}{2}}}{r_j} I_{N_\theta} & -\frac{r_{j+\frac{1}{2}}}{r_{j+1}} I_{N_\theta} & \\ & & \ddots & \ddots & \ddots \\ & & & -\frac{r_{N_r-\frac{1}{2}}}{r_{N_r-1}} I_{N_\theta} & \frac{r_{N_r+\frac{1}{2}}}{r_{N_r}} I_{N_\theta} \end{pmatrix} + \begin{pmatrix} \frac{1}{r_1^2}A & & & & \\ & \frac{1}{r_2^2}A & & & \\ & & \ddots & & \\ & & & \frac{1}{r_{N_r-1}^2}A & \\ & & & & \frac{1}{r_{N_r}^2}A \end{pmatrix}, \tag{7.51}$$

where the second matrix accounts for the angular diffusion, with $A \in M_{N_\theta}(\mathbb{R})$ the classical diffusion matrix with periodic flux boundary conditions:

$$A = \begin{pmatrix} 2 & -1 & & & -1 \\ -1 & 2 & \ddots & & \\ & \ddots & \ddots & \ddots & \\ & & \ddots & 2 & -1 \\ -1 & & & -1 & 2 \end{pmatrix}. \tag{7.52}$$

Now, for the advection term A^{up} defined by equation (7.50), we write $(u)^+ = \max(u, 0)$ and $(u)^- = \min(u, 0)$ so that $A^{up}(u, \tilde{c}_{j,k}, \tilde{c}_{j,k+1}) = (u)^+ c_{j,k} + (u)^- c_{j,k+1}$. Therefore, we introduce the following diagonal matrices for $j \in \{1, ..., N_r\}$, $U^+_{j+\frac{1}{2}} \in M_{N_\theta}(\mathbb{R})$ and $U^-_{j+\frac{1}{2}} \in M_{N_\theta}(\mathbb{R})$:

$$U^\pm_{j+\frac{1}{2}} = \begin{pmatrix} \ddots & & & & \\ & (u^n_{(j+\frac{1}{2},k-1)})^\pm & & & \\ & & (u^n_{(j+\frac{1}{2},k)})^\pm & & \\ & & & (u^n_{(j+\frac{1}{2},k+1)})^\pm & \\ & & & & \ddots \end{pmatrix}.$$

Thus we can define the advection matrix:

$$\mathcal{B}^n = \begin{pmatrix} U^+_{\frac{3}{2}} & U^-_{\frac{3}{2}} & & & & \\ & \ddots & \ddots & & & \\ & & U^+_{j+\frac{1}{2}} & U^-_{j+\frac{1}{2}} & & \\ & & & \ddots & U^-_{N_r-\frac{1}{2}} & \\ & & & & 0 & \end{pmatrix} - \begin{pmatrix} 0 & & & & & \\ U^+_{\frac{3}{2}} & \ddots & & & & \\ & U^+_{j-\frac{1}{2}} & U^-_{j-\frac{1}{2}} & & & \\ & & \ddots & \ddots & & \\ & & & U^+_{N_r-\frac{1}{2}} & U^-_{N_r-\frac{1}{2}} & \end{pmatrix}$$
$$+ \begin{pmatrix} \frac{1}{r_1^2}B^n & & & & & \\ & \frac{1}{r_2^2}B^n & & & & \\ & & \ddots & & & \\ & & & \frac{1}{r^2_{N_r-1}}B^n & & \\ & & & & \frac{1}{r^2_{N_r}}B^n & \end{pmatrix} \tag{7.53}$$

where the discrete advection matrix $B^n \in M_{N_\theta}(\mathbb{R})$ with periodic flux condition on the boundary is defined as in Allaire [2005]

$$B^n = \begin{pmatrix} \left(u^n_{\frac{3}{2}}\right)^+ & \left(u^n_{\frac{3}{2}}\right)^- & & & & \\ & \ddots & \ddots & & & \\ & & \left(u^n_{j+\frac{1}{2}}\right)^+ & \left(u^n_{j+\frac{1}{2}}\right)^- & & \\ & & & \ddots & \left(u^n_{N_\theta-\frac{1}{2}}\right)^- & \\ \left(u^n_{N_\theta+\frac{1}{2}}\right)^- & & & & \left(u^n_{N_\theta+\frac{1}{2}}\right)^+ & \end{pmatrix} \tag{7.54}$$
$$- \begin{pmatrix} \left(u^n_{\frac{1}{2}}\right)^- & & & & & \left(u^n_{\frac{1}{2}}\right)^+ \\ \left(u^n_{\frac{3}{2}}\right)^+ & \ddots & & & & \\ & \left(u^n_{j-\frac{1}{2}}\right)^+ & \left(u^n_{j-\frac{1}{2}}\right)^- & & & \\ & & \ddots & \ddots & & \\ & & & \left(u^n_{N_\theta-\frac{1}{2}}\right)^+ & \left(u^n_{N_\theta-\frac{1}{2}}\right)^- & \end{pmatrix}.$$

In the direct model, we have at each time step

$$\frac{\mathcal{C}^{n+1}-\mathcal{C}^n}{\Delta t} = -\frac{D'}{\Delta r^2}\mathcal{A}\mathcal{C}^{n+1} - \frac{1}{\Delta r}\mathcal{B}^n\mathcal{C}^n.$$

We use a standard numerical method to invert the matrix $I_{N_rN_\theta} + \frac{\Delta t}{\Delta r^2}\mathcal{A}$ and then resolve at each time step

$$\mathcal{C}^{n+1} = \left(I_{N_rN_\theta} + \frac{\Delta t}{\Delta r^2}\mathcal{A}\right)^{-1}\left(I_{N_rN_\theta} - \frac{\Delta t}{\Delta r}\mathcal{B}^n\right)\mathcal{C}^n.$$

The exchange case

If there is an activation dynamics at the external membrane, the corresponding equation writes in polar coordinates

$$\partial_t \mu(t,R,\theta) = k_{\text{on}} c(t,R,\theta) - k_{\text{off}} \mu(t,R,\theta)\,, \qquad \text{on } C(0,R)\,. \tag{7.55}$$

At each time step, the implicit discretization of equation (7.55) for $k \in \{1,...,N_y\}$ writes

$$-\Delta t k_{\text{on}} \tilde{c}_k^{n+1} + (1 + \Delta t\, k_{\text{off}}) \mu_k^{n+1} = \mu_k^n\,, \tag{7.56}$$

as it can be numerically treated with the problem on the concentration.

Problem on the concentration In the convection-diffusion problem, the boundary condition (7.37) writes on $C(0,R)$

$$D' R \partial_r \left(\frac{\tilde{c}(t,R,\theta)}{R} \right) - \tilde{c}(t,R,\theta) u_r(t,R,\theta) = k_{\text{off}}\, \mu(t,R,\theta) - k_{\text{on}}\, \tilde{c}(t,R,\theta)\,, \tag{7.57}$$

and it can be treated implicitly. Indeed, this leads to

$$\mathcal{F}_{(N_r+\frac{1}{2},k)} = k_{\text{off}} \mu_k^{n+1} - k_{\text{on}} \tilde{c}_{N_r,k}^{n+1}$$

for $k \in \{1,...,N_\theta\}$.

For simplicity, we describe the cytoplasmic concentration and the attached marker concentration in the same matricial problem on

$$\mathcal{E}^n = \left(\tilde{C}^n_{(1,1)} \dots \tilde{C}^n_{(1,N_\theta)} \tilde{C}^n_{(2,1)} \dots \tilde{C}^n_{(2,N_\theta)} \dots \tilde{C}^n_{(N_r,N_\theta)} \mu_1^n \dots \mu_{N_r}^n \right)^T.$$

We have at each time step

$$\left(I_{(N_r+1)N_\theta} + \frac{\Delta t}{\Delta r^2} \mathcal{A}_\mu \right) \mathcal{E}^{n+1} = \left(I_{(N_r+1)N_\theta} - \frac{\Delta t}{\Delta r} \mathcal{B}_\mu^n \right) \mathcal{E}^n\,,$$

where $\mathcal{A}_\mu$ and $\mathcal{B}_\mu^n$ are similar to $\mathcal{A}$ and $\mathcal{B}^n$, except for the additional terms accounting for (7.56) and (7.57).

Problem on the pressure The pressure boundary condition on $C(0,R)$ (7.43) rewrites

$$\tilde{p}(t,R,\theta) = R \left[1 - \delta \frac{\mu(t,R,\theta)}{R} \right]_+ \qquad \text{on } C(0,R)\,. \tag{7.58}$$

Therefore, one only has to change the source term in the matricial problem.

Equation for the cell velocity The cell velocity now verifies

$$v(t) = \frac{\xi}{\xi_1} \int_0^{2\pi} \left[1 - \delta \frac{\mu(t,R,\theta)}{R} \right]_+ \mathbf{n}\, \mathrm{d}\theta\,,$$

and is computed similarly as in the no exchange case.

7.8.2 Finite elements discretization

In the following, we will also perform numerical simulations using finite elements discretizations and the software FreeFem++. In a first approach, we chose to simulate the model without activation at the membrane. Moreover, we impose a Stokes flow instead of a Darcy flow, which brings more regularity. More precisely, for η the viscosity, the fluid problem writes

$$\begin{aligned} -\eta \Delta u + \nabla p &= -\xi(u+v) && \text{in } \Omega(t)\,, \\ \sigma \cdot \mathbf{n} := (\eta(\nabla u + {}^t\nabla u) - p\mathrm{Id}) \cdot \mathbf{n} &= e^{-\delta c}\mathbf{n} && \text{on } \partial\Omega(t)\,, \\ \nabla \cdot u &= -k_d && \text{in } \Omega(t)\,. \end{aligned} \tag{7.59}$$

Weak form

Stokes equation

Multiplying the force balance equation by a test function w and integrating over Ω leads to

$$\int_{\Omega(t)} \nabla p \cdot w - \eta \triangle u \cdot w \, \mathrm{d}\mathbf{x} = -\xi \int_{\Omega(t)} (u+v) \cdot w \, \mathrm{d}\mathbf{x} \, .$$

Remark 31. *For $\nabla \cdot u =$ constant, it is known (see Alouges and Maury [2013]) that the Green identity leads to*

$$\int_{\partial\Omega(t)} ({}^t\nabla u \cdot \mathbf{n}) \cdot w \, \mathrm{d}S = \int_{\Omega(t)} {}^t\nabla u : \nabla w \, \mathrm{d}\mathbf{x} \, .$$

Therefore,

$$\int_{\Omega(t)} \Delta u \cdot w \, \mathrm{d}\mathbf{x} + \int_{\Omega(t)} \nabla u : (\nabla w + {}^t\nabla w) \, \mathrm{d}\mathbf{x} = \int_{\partial\Omega(t)} w \cdot (\nabla u + {}^t\nabla u) \cdot \mathbf{n} \, \mathrm{d}S \, .$$

After integration by parts, the left-hand side rewrites

$$\int_{\partial\Omega(t)} pw \cdot \mathbf{n} \, \mathrm{d}S - \int_{\Omega(t)} p\nabla \cdot w \, \mathrm{d}\mathbf{x} - \eta \left(\int_{\partial\Omega(t)} w \cdot (\nabla u + {}^t\nabla u) \cdot \mathbf{n} \, \mathrm{d}S - \int_{\Omega(t)} \nabla u : (\nabla w + {}^t\nabla w) \, \mathrm{d}\mathbf{x} \right) ,$$

hence we have $\forall w \in H^1(\Omega)^2$,

$$\int_{\partial\Omega(t)} pw \cdot \mathbf{n} - \eta w \cdot (\nabla u + {}^t\nabla u) \cdot \mathbf{n} \, \mathrm{d}S - \int_{\Omega(t)} p\nabla \cdot w \, \mathrm{d}\mathbf{x} + \eta \int_{\Omega(t)} \nabla u : (\nabla w + {}^t\nabla w) \, \mathrm{d}\mathbf{x} = -\xi \int_{\Omega(t)} (u+v) \cdot w \, \mathrm{d}\mathbf{x} \, .$$

Boundary condition Now, for the boundary condition, we have

$$\int_{\partial\Omega(t)} \left((\eta(\nabla u + {}^t\nabla u) - p\mathrm{Id}) \cdot \mathbf{n} \right) \cdot w \, \mathrm{d}\mathbf{x} \quad = \quad \int_{\partial\Omega(t)} k_p w \cdot \mathbf{n} \, \mathrm{d}S \, .$$

Recalling that $k_p(t, \mathbf{x}) = e^{-\delta c(t,\mathbf{x})}$, we have

$$+ \int_{\partial\Omega(t)} e^{-\delta c} w \cdot \mathbf{n} \, \mathrm{d}S - \int_{\Omega(t)} p\nabla \cdot w \, \mathrm{d}\mathbf{x} + \eta \int_{\Omega(t)} \nabla u : (\nabla w + {}^t\nabla w) \, \mathrm{d}\mathbf{x} = -\xi \int_{\Omega(t)} (u+v) \cdot w \, \mathrm{d}\mathbf{x} \, .$$

Divergence equation

For the divergence equation on u, let us multiply by a scalar test function q that vanishes on the domain's boundary, and integrate by parts. We obtain

$$\int_{\Omega(t)} q\nabla \cdot u \, \mathrm{d}\mathbf{x} = -\int_{\Omega(t)} q k_d \, \mathrm{d}x \Leftrightarrow -\int_{\Omega(t)} u \cdot \nabla q \, \mathrm{d}\mathbf{x} = -\int_{\Omega(t)} q k_d \, \mathrm{d}x \, .$$

Bibliography

Allaire, G. (2005). Analyse numérique et optimisation: Une introduction à la modélisation mathématique et à la simulation numérique. Editions Ecole Polytechnique. 240

Alouges, F. and Maury, B. (2013). Variational methods for computational fluid dynamics. 242

Boulakia, M., Genadot, A., and Thieullen, M. (2015). Simulation of spdes for excitable media using finite elements. Journal of Scientific Computing, 65(1):171–195. 219, 220

Caballero, D., Comelles, J., Piel, M., Voituriez, R., and Riveline, D. (2015). Ratchetaxis: Long-range directed cell migration by local cues. Trends Cell Biol, 25(12):815–27. 230

Caballero, D., Voituriez, R., and Riveline, D. (2014). Protrusion fluctuations direct cell motion. Biophys J, 107(1):34–42. 210

Friedl, P. and Wolf, K. (2003). Tumour-cell invasion and migration: diversity and escape mechanisms. Nat Rev Cancer, 3(5):362–74. 223

Kortholt, A., Keizer-Gunnink, I., Kataria, R., and Van Haastert, P. J. M. (2013). Ras activation and symmetry breaking during dictyostelium chemotaxis. J Cell Sci, 126(Pt 19):4502–13. 223

Maury, B. and Venel, J. (2008). A mathematical framework for a crowd motion model. Comptes Rendus Mathematique, 346(23):1245–1250. 230

Maury, B. and Venel, J. (2011). A discrete contact model for crowd motion. ESAIM: Mathematical Modelling and Numerical Analysis, 45(1):145–168. 230

Mayor, R. and Carmona-Fontaine, C. (2010). Keeping in touch with contact inhibition of locomotion. Trends in cell biology, 20(6):319–328. 210, 232

Muller, N., Piel, M., Calvez, V., Voituriez, R., Gonçalves-Sá, J., Guo, C.-L., Jiang, X., Murray, A., and Meunier, N. (2016). A predictive model for yeast cell polarization in pheromone gradients. PLoS Comput Biol, 12(4):e1004795. 234

Peszat, S. and Zabczyk, J. (2007). Stochastic partial differential equations with Lévy noise: An evolution equation approach, volume 113. Cambridge University Press. 219

Revuz, D. and Yor, M. (2005). Continuous martingales and Brownian motion. Number 293 in Grundlehren der mathematischen Wissenschaften. Springer, Berlin, corr. 3. print. of the 3. ed edition. 224

Servant, G., Weiner, O. D., Neptune, E. R., Sedat, J. W., and Bourne, H. R. (1999). Dynamics of a chemoattractant receptor in living neutrophils during chemotaxis. Mol Biol Cell, 10(4):1163–78. 223

Walsh, J. B. (2005). Finite element methods for parabolic stochastic pde's. Potential Analysis, 23(1):1–43. 219

Wang, F. (2009). The signaling mechanisms underlying cell polarity and chemotaxis. Cold Spring Harbor perspectives in biology, 1(4):a002980. 223

Part III

Appendices

Appendix A

An integro-differential equation for 1D cell migration

In this part, we present a work that was made in collaboration with Bérénice Grec, Bertrand Maury, Nicolas Meunier and Laurent Navoret that led to the publication of a conference proceeding [Etchegaray et al., 2015].

A.0.3 Introduction

Cell migration is a fundamental biological phenomenon involved for example in development, wound healing, cancer and immune response. Understanding its key features is therefore a burning issue.

Some cells can move on an adherent substrate by a *crawling* process, where motion comes from the formation of finger-like extensions named *filopodia* that adhere to the substrate for some time. When the cell contracts, non-adherent filopodia retract, whereas adherent ones exert forces that induce motion. We refer to Ananthakrishnan and Ehrlicher [2007] for a complete description of cell crawling.

When a cell is set on a flat homogenous substrate, it performs a random-like motion. However, it can also become polarized and move in a preferential direction. How this direction is chosen is a question that is still driving many experimental and modeling efforts. In Caballero et al. [2014], a non-homogenous substrate impose geometrical constraints that are sufficient to direct 1D cell motion. This paper focuses on the 1D motion brought forth by the filopodial activity.

We introduce a simplified model of 1D cell migration relying on the filopodial activity. In what follows, the substrate is supposed to be flat and homogenous, but more complex settings could also be described. Let us consider the center of mass of the cell, whose position at time t is denoted $x(t) \in \mathbb{R}$. Force equilibrium leads to

$$C\frac{dx}{dt}(t) = -F_\ell(t) + F_r(t), \tag{A.1}$$

where $F_r \geq 0$ (resp. $F_\ell \geq 0$) is the force exerted by filopodia located on the right (resp. on the left) of the cell and C is the friction parameter, that can be set equal to $1nN.h.\mu m^{-1}$ Johnston et al. [2008].

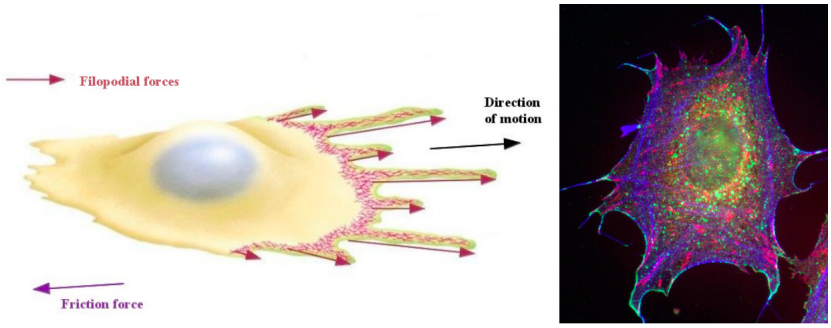

Figure A.1 – Illustration of a moving cell, and picture of a fibroblast [Johnston et al., 2008; Lodish, 2002].

We can now focus on the forces $F_{r,\ell}$. Following biological knowledge, we assume that the forces exerted by filopodia on the cell at time t depend on:

- densities of filopodia sent to the right and left, denoted by $\psi_{r,\ell} > 0$,
- their existence time, fixed by the lifetime function $\mathcal{P} : \mathbb{R}^+ \to \mathbb{R}^+$,
- the force $f_{r,\ell}$ exerted by one filopodium on the cell, related to its orientation. Moreover, we assume that $f_{r,\ell} = f_{r,\ell}(x(t'), x(t))$ depends on the positions of both the tip of the filopodium, related to the cell position at creation time t', and the actual cell position.

Consequently, equation (A.1) rewrites as an integro-differential equation

$$\begin{aligned} &\frac{dx}{dt}(t) = \int_0^t \mathcal{P}(a)\Big(\psi_r f_r(x(t-a), x(t)) - \psi_\ell f_\ell(x(t-a), x(t))\Big)da, \\ &x(0) = x_0, \end{aligned} \tag{A.2}$$

where $\psi_{r,\ell}$ are positive constants, $x : \mathbb{R}^+ \to \mathbb{R}$, and $f_{r,\ell} : \mathbb{R}^2 \to \mathbb{R}$. Let us assume for simplicity that $x_0 = 0$.

Problem (A.2) can be treated more or less easily depending on the force functions $f_{r,\ell}$. In this work, we shall first investigate one case of non-linear elastic force, where only existence and uniqueness of a solution can be proved. Then, we shall consider a simplified case of linear force functions, where a linear Volterra equation can be obtained. We shall see how this formalism allows us to get more information on the sign, boundedness and asymptotic behaviour of the solution in general, as well as explicit solutions for some special cases.

A.0.4 Non-linear force functions

Let us start with the force functions

$$f_r(y, x) = k\left[\ell - (x - y)\right]_+, \quad \text{and} \quad f_\ell(y, x) = k\left[\ell - (y - x)\right]_+,$$

where $[.]_+$ denotes the positive part function and $k, \ell \in \mathbb{R}^+$ are two constants. Taking $f_r(x(t-a), x(t))$ and $f_\ell(x(t-a), x(t))$, it corresponds to the hypothesis of filopodia having a constant size ℓ, and exerting elastic forces as long as the cell at position $x(t)$ has not reached their tips $x(t-a) \pm \ell$. Equation (A.2) now writes

$$\begin{aligned} \frac{dx}{dt}(t) = k\int_0^t \mathcal{P}(a)\Big(&\psi_r[\ell + x(t-a) - x(t)]_+ \\ &- \psi_\ell\left[\ell + x(t) - x(t-a)\right]_+\Big)da. \end{aligned} \tag{A.3}$$

Existence and uniqueness

We prove the following result :

Theorem 19. *For $\mathcal{P} \in L^1(\mathbb{R}^+)$, there exists a unique solution $x \in \mathcal{C}^1(\mathbb{R}^+, \mathbb{R})$ of (A.3).*

Proof. After integration, equation (A.3) writes

$$x(t) = k \int_0^t \int_0^s \mathcal{P}(a)\Big(\psi_r\big[x(s-a) + \ell - x(s)\big]_+ - \psi_\ell\big[x(s) - x(s-a) + \ell\big]_+\Big) da ds =: \Phi(x)(t)$$

with

$$\begin{array}{rccc} \Phi : & \big(\mathcal{C}([0,T],\mathbb{R}), \| \ \|_\infty\big) & \longrightarrow & \big(\mathcal{C}([0,T],\mathbb{R}), \| \ \|_\infty\big) \\ & x & \longmapsto & \Phi(x) = (t \mapsto \Phi(x)(t)), \end{array}$$

for some $T \geq 0$. We are looking for existence and uniqueness of a fixed point for Φ. Let us construct a sequence $(x^n)_{n\geq 0}$ in $\mathcal{C}([0,T],\mathbb{R})$ such that

$$x^0 \equiv x_0, \quad x^{n+1} = \Phi(x^n) \ \forall n \geq 0.$$

As $[0,T]$ is compact, $\big(\mathcal{C}([0,T],\mathbb{R}), \| \ \|_\infty\big)$ is a Banach space and we can use the Banach fixed-point theorem. All we need to show now is that Φ is a contraction mapping. Considering $(y,z) \in \big(\mathcal{C}([0,T],\mathbb{R}), \| \ \|_\infty\big)^2$ and denoting

$$g_{s,a}(y) = y(s-a) + \ell - y(s), \quad \text{and} \quad h_{s,a}(y) = y(s) - y(s-a) + \ell,$$

we have

$$\begin{aligned} \|\Phi(y) - \Phi(z)\|_\infty = \sup_{t\in[0,T]} \Big| k \int_0^t \int_0^s \mathcal{P}(a)\Big(\psi_r\big([g_{s,a}(y)]_+ - [g_{s,a}(z)]_+\big) \\ - \psi_\ell\big([h_{s,a}(y)]_+ - [h_{s,a}(z)]_+\big)\Big) da ds \Big| \\ \leq kT \sup_{s\in[0,T]} \int_0^s |\mathcal{P}(a)| \times \Big(\psi_r\big|[g_{s,a}(y)]_+ - [g_{s,a}(z)]_+\big| \\ + \psi_\ell\big|[h_{s,a}(y)]_+ - [h_{s,a}(z)]_+\big|\Big) da, \end{aligned}$$

since $\psi_{r,\ell} \geq 0$. Denote $\psi := \psi_r + \psi_\ell$. Now, for $(A,B) \in \mathbb{R}^2$, the inequality $\big|[A]_+ - [B]_+\big| \leq \big|A - B\big|$ holds, leading to

$$\begin{aligned} \| \Phi(y) - \Phi(z) \|_\infty &\leq kT \sup_{s\in[0,T]} \int_0^s \psi\, |\mathcal{P}(a)| \, \big|(y-z)(s-a) - (y-z)(s)\big| da, \\ &\leq 2kT\psi \, \| \mathcal{P} \|_{L^1(\mathbb{R}+)} \| \, y - z \, \|_\infty . \end{aligned}$$

For T small enough such that $2k\psi \, \| \mathcal{P} \|_{L^1(\mathbb{R}+)} \, T < 1$, we deduce that Φ is a contraction mapping. As a consequence of the Banach fixed-point theorem, there exists a unique $x \in \mathcal{C}([0,T],\mathbb{R})$ which is solution of (A.3).

Iterating the same reasoning on time intervals of size T, one can extend this result to prove that (A.3) admits a unique solution $x \in \mathcal{C}(\mathbb{R}^+,\mathbb{R})$. Finally, using (A.3), it is clear that $x \in \mathcal{C}^1(\mathbb{R}^+,\mathbb{R})$, and this concludes the proof. □

Numerical simulations

We consider the lifetime function $\mathcal{P} : a \mapsto e^{-a}$. This means that a density of filopodia will exponentially decrease with time, as more and more filopodia will have disappeared. For the filopodia's length, we use an experimental value from Caballero et al. [2014]. Moreover, we impose a bias on the densities of filopodia ($\psi_r > \psi_\ell$).

Figure A.2 represents the cell position and velocity over time computed with an explicit Euler time discretization and a rectangle integration method of equation (A.3). What can be observed is that the bias in the produced forces seems to lead to a non-zero asymptotic velocity. Further simulations with different parameter values and/or lifetime functions confirm this tendency.

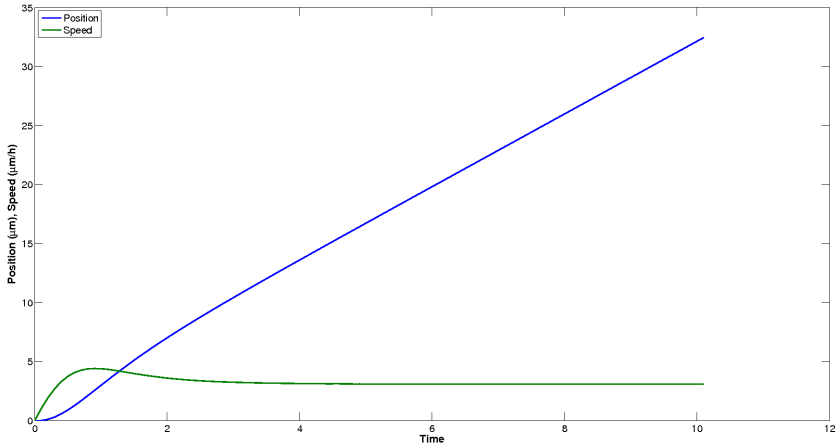

Figure A.2 – Numerical simulation of a particle speed and trajectory during $T = 10h$, for $dt = 10^{-2}h$, $C = 1nN.h.\mu m^{-1}$, $k = 1nN.\mu m^{-1}$, $\ell = 20.5\mu m$, and $(\psi_r, \psi_\ell) = (1.5, 1)$.

A.0.5 Linear forces

The presence of the positive part function in the previous case prevents getting analytical properties of the solution. In this section, we will take the following linearized forces functions:

$$f_r(x(t-a), x(t)) = k\left(x(t-a) + \ell - x(t)\right),$$
$$f_\ell(x(t-a), x(t)) = k\left(x(t) - x(t-a) + \ell\right),$$

with $k, \ell \in \mathbb{R}^+$. This assumption is less relevant from the modelling point of vue, since if the cell overtakes the tip of a filopodium, then it will experience a force in the opposite direction. However, for k small enough, and an appropriate lifetime function, we can assume that the cell is slow enough so that it does not reach any existing filopodium tip.

Equation (A.2) can be written as a linear Volterra equation, which will lead to more analytical results.

Linear Volterra equation formalism

Let us rewrite equation (A.2):

$$\begin{aligned} v(t) &= k\int_0^t \mathcal{P}(a)\Big(\psi_r(x(t-a) + l - x(t)) - \psi_\ell(x(t) - x(t-a) + \ell)\Big)da \\ &= kl(\psi_r - \psi_\ell)\int_0^t \mathcal{P}(a)da + k\psi\int_0^t \mathcal{P}(a)\left(x(t-a) - x(t)\right)da. \end{aligned} \tag{A.4}$$

Denoting $Q : t \mapsto \int_0^t \mathcal{P}(a)da$ and integrating by parts, we obtain

$$v(t) = k\ell(\psi_r - \psi_\ell)Q(t) + k\psi\left(\int_0^t Q(a)v(t-a)da - Q(t)x(t)\right),$$

since $Q(0) = 0$ and $x(0) = 0$. After the change of variable $s = t - a$, we get

$$v(t) = f(t) - k\psi\int_0^t (Q(t) - Q(t-s))v(s)ds, \tag{A.5}$$

$$\text{with} \quad f(t) = k\ell(\psi_r - \psi_\ell)Q(t). \tag{A.6}$$

which is a linear Volterra integro-differential equation on v.

Existence and uniqueness of a solution

With similar arguments to Theorem 19, we can prove the following property:

Theorem 20. *For $\mathcal{P} \in L^1(\mathbb{R}^+)$, equation (A.5) admits a unique solution $v \in \mathcal{C}(\mathbb{R}^+, \mathbb{R})$.*

Remark 32 (The resolvent formalism)**.** *Let us define the operator*

$$h \star v : t \mapsto \int_0^{+\infty} h(t,s)v(s)ds.$$

Equation (A.5) can then be written as a convolution-like equation:

$$v(t) + (h \star v)(t) = f(t), \ \textit{with}$$
$$h(t,s) = k\psi(Q(t) - Q(t-s))\mathbf{1}_{[0,t]}(s).$$

Existence and uniqueness of a solution can be proved by showing that h is a Volterra kernel of L^∞ type. For more details, we refer to Gripenberg et al. [1990].

Sign and boundedness property

We now prove a result showing how important the function f is in controlling the migration. Indeed, it captures no less than the range of forces exerted with k, aging, and the potential asymmetry $\psi_r - \psi_\ell$ in the formation of filopodia.

Theorem 21. *If $\mathcal{P}$ is positive and decreasing, then the solution to equation (A.5) satisfies*

$$\psi_r \geq \psi_\ell \quad \Rightarrow \quad \forall t \geq 0,\ v(t) \in [0, f(t)],$$
$$\psi_r \leq \psi_\ell \quad \Rightarrow \quad \forall t \geq 0,\ v(t) \in [f(t), 0].$$

Proof. First, let us assume that $\psi_r \geq \psi_\ell$. As a consequence, $\forall t \geq 0,\ f(t) \geq 0$ and $f'(t) \geq 0$. By derivation of (A.5), we obtain

$$v'(t) = f'(t) - k\psi(Q(t) - Q(0))v(t) - k\psi\int_0^t (\mathcal{P}(t) - \mathcal{P}(t-s))v(s)ds,$$

with $f'(t) = k\ell(\psi_r - \psi_\ell)\mathcal{P}(t)$. Suppose there exists t^* such that $\forall t < t^*,\ v(t) > 0$ and $v(t^*) = 0$, then

$$v'(t^*) = f'(t^*) - k\psi Q(t^*)v(t^*) - k\psi\int_0^{t^*} (\mathcal{P}(t^*) - \mathcal{P}(t^* - s))v(s)ds$$

is positive (since all the terms are positive). Consequently, $\forall t \geq 0,\ v(t) \geq 0$. This implies that $x(t-a) - x(t) \leq 0,\ \forall t \geq a \geq 0$. Going back to the equivalent equation (A.4), this shows that $\forall t \geq 0,\ v(t) \leq f(t)$. Now, let us assume that $\psi_\ell \geq \psi_r$, which means that $\forall t \geq 0,\ f(t) \leq 0$ and $f'(t) \leq 0$. In a similar way, if there exists t^* such that $\forall t < t^*,\ v(t) < 0$ and $v(t^*) = 0$, then $v'(t^*)$ is negative. And considering again (A.4), we easily show that $\forall t \geq 0,\ v(t) \geq f(t)$, which concludes the proof. □

Asymptotic velocity

We now give an expression for the asymptotic velocity of the cell. Here again, f has a crucial importance. The proof of the following result is similar to the one done in a forthcoming work Grec et al. [2012], and we do not repeat it here.

Theorem 22. *Let v be the solution of (A.5), and denote $\gamma = \lim_{t\to+\infty} f(t)$. Assume that v is uniformly continuous on $\mathbb{R}^+$. Then,*

$$v(t) \underset{t\to+\infty}{\longrightarrow} v_\infty = \begin{cases} \frac{\gamma}{1+k\psi\int_0^{+\infty} a\mathcal{P}(a)da} & \text{if } a \mapsto a\mathcal{P}(a) \in L^1(\mathbb{R}^+), \\ 0 & \text{if } a \mapsto a\mathcal{P}(a) \notin L^1(\mathbb{R}+). \end{cases}$$

Having two different cases can be interpreted as follows: if the mean lifetime of filopodia is finite, then the cell is permanently escaping from the action of older forces. As a consequence, if $\psi_r - \psi_\ell \neq 0$, it can get off its position all the time. However, if the mean lifetime of filopodia is infinite, all of them exert elastic forces on the cell, which will be stabilized in finite time.

A.0.6 Particular cases

Some choices of function $\mathcal{P}$ can give more explicit information on the solution.

Infinite existence time of forces ($\mathcal{P} \equiv 1$).

Taking $\mathcal{P} \equiv 1$, we are considering elastic forces that never disappear. Here, $\mathcal{P}$ does not fulfill the hypothesis of Theorem 20, but Theorem 22 applies. Equation (A.5) writes

$$v(t) \quad = \quad k\ell(\psi_r - \psi_\ell)t - k\psi\int_0^t sv(s)ds,$$

and can be solved after derivation with the variation of constants method, to give

$$v(t) = v(0)e^{-k\psi t^2/2} + \ell\sqrt{\frac{k\pi}{2}}(\psi_r - \psi_\ell)\sqrt{e^{-\frac{k\psi t^2}{2}}\left(1 - e^{-\frac{k\psi t^2}{2}}\right)}. \tag{A.7}$$

Figure A.3 represents the solution v as well as the corresponding forcing function f. As expected, the cell is stabilized in finite time. Moreover, we can observe numerically the sign and boundedness property (given in Theorem 21), where in this case the $f(t)$ bound is optimal.

It is easy to check analytically the convergence of v to $v_\infty = 0$ since we have the following equivalence:

$$v(t) \underset{t\to+\infty}{\sim} \ell\sqrt{\frac{k\pi}{2}}(\psi_r - \psi_\ell)e^{-k\psi t^2/4}.$$

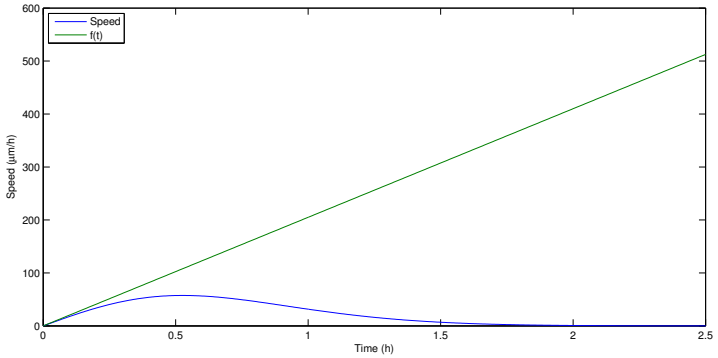

Figure A.3 – Graph of $t \mapsto v(t)$ and $t \mapsto f(t)$ for $\mathcal{P} \equiv 1$, with $C = 1nN.h.\mu m^{-1}$, $\ell = 20.5\mu m$, $k = 5nN.\mu m^{-1}$, $(\psi_r, \psi_\ell) = (6, 4)$ and $v(0) = 0$.

Exponential decay ($\mathcal{P}(a) = e^{-a}$)

We assume now that $\mathcal{P}(a) = e^{-a}$, which was the function chosen in Section A.0.4. All the results demonstrated before apply. However, we can actually directly solve the equation. Noting that $Q(t) = 1 - e^{-t}$, equation (A.5) becomes

$$v(t) = k\ell(\psi_r - \psi_\ell)(1 - e^{-t}) - k(\psi_r + \psi_\ell)e^{-t}A(t), \tag{A.8}$$
$$\text{with} \quad A(t) = \int_0^t (e^s - 1)v(s)ds.$$

Proposition 26. *The solution to (A.8) is given by:*

$$v(t) = k\ell(\psi_r - \psi_\ell)\left(1 - e^{-t}\right) - k^2 l(\psi_r - \psi_\ell)\psi e^{-(k\psi+1)t+k\psi-k\psi e^{-t}} J(t), \tag{A.9}$$
$$\textit{with} \quad J(t) = \int_0^t (e^s + e^{-s} - 2)e^{k\psi(s-1+e^{-s})}ds.$$

Proof. Deriving A with respect to time leads to:

$$A'(t) = k\ell(\psi_r - \psi_\ell)(e^t + e^{-t} - 2) - k\psi(1 - e^{-t})A(t).$$

Now, by the variation of constant method, we find

$$A(t) = k\ell(\psi_r - \psi_\ell)e^{-k\psi(t-1+e^{-t})} \int_0^t (e^s + e^{-s} - 2)e^{k\psi(s-1+e^{-s})}ds,$$

leading to expression (A.9). □

As a consequence, an asymptotic equivalent of the solution can be given.

Theorem 23. *The following equivalence holds:*

$$v(t) \underset{t\to+\infty}{\sim} k\ell(\psi_r - \psi_\ell)\left(1 - \frac{k\psi}{k\psi+1} - \frac{k\psi}{k\psi-1}e^{-2t} + 2e^{-t}\right), \tag{A.10}$$

and v converges to the asymptotic velocity

$$v_\infty := k\ell(\psi_r - \psi_\ell)\left(1 - \frac{k\psi}{k\psi+1}\right).$$

Proof. Using the following equivalence

$$\int_0^t e^{\alpha s} ds \underset{t\to+\infty}{\sim} \frac{e^{\alpha t}}{\alpha},$$

we easily obtain

$$J(t) \underset{t\to+\infty}{\sim} e^{-k\psi}\left(\frac{e^{(k\psi+1)t}}{k\psi+1} + \frac{e^{(k\psi-1)t}}{k\psi-1} - 2\frac{e^{k\psi t}}{k\psi}\right).$$

Considering expression (A.9), we have :

$$v(t) \underset{t\to+\infty}{\sim} kl(\psi_r-\psi_\ell)\left[1 - k\psi e^{-(k\psi+1)t}\left(\frac{e^{(k\psi+1)t}}{k\psi+1} + \frac{e^{(k\psi-1)t}}{k\psi-1} - 2\frac{e^{k\psi t}}{k\psi}\right)\right],$$

which leads to the result. □

We can then deduce that the asymptotic behaviour of the cell depends on the range of filopodial forces k, on the global filopodial activity ψ, and on the asymmetry $\psi_r - \psi_\ell$. Moreover, the bigger k and ψ are, the faster the cell velocity reaches equilibrium. The non-trivial equilibrium is a consequence of the lifetime function that lets newer forces lead motion, whereas the older ones are "silenced". The initial asymmetry is then maintained over time. On Figure A.4, a numerical simulation illustrates this behaviour.

Constant existence time ($\mathcal{P}(a) = 1_{[0,\tau]}(a)$)

Now, let us look at $\mathcal{P}(a) = 1_{[0,\tau]}(a)$ with $\tau > 0$, meaning that all filopodia exert forces during the same finite amount of time. For $t \geq 0$, we have

$$Q(t) = \begin{cases} t & \text{if } t < \tau, \\ \tau & \text{if } t \geq \tau. \end{cases}$$

Existence and uniqueness of a continuous solution to (A.5) comes from Theorem 20. Moreover, we can find an explicit solution for $t \leq \tau$, and bounds for the solution for $t \geq \tau$. Equation (A.5) then writes

$$v(t) = k\ell(\psi_r-\psi_\ell)t - k\psi\int_0^t sv(s)ds, \qquad \text{for } t \leq \tau, \tag{A.11}$$

$$v(t) = k\ell\tau(\psi_r-\psi_\ell) - k\psi\int_{t-\tau}^t v(s)(\tau-(t-s))ds, \qquad \text{for } t \geq \tau. \tag{A.12}$$

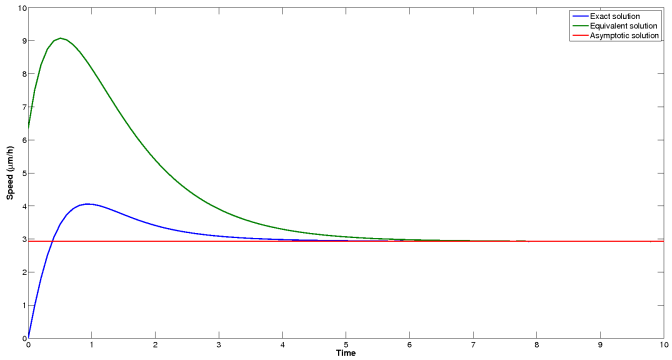

Figure A.4 – Numerical simulation of the exact solution, its equivalent at infinity and the asymptotic velocity for $C = 1nN.h.\mu m^{-1}$, $k = 1nN.\mu m^{-1}$, $\ell = 20.5\mu m$ and $(\psi_r, \psi_\ell) = (1.5, 1)$.

Theorem 24. *The unique solution to equations (A.11)-(A.12) satisfies*

$$v(t) = \ell(\psi_r - \psi_\ell)\sqrt{\frac{k\pi}{2\psi}}\sqrt{(1 - e^{\frac{-k\psi}{2}t^2})} \qquad \text{for } t \leq \tau, \tag{A.13}$$

$$v(\tau)\exp\left(-k\psi\frac{(t^2-\tau^2)}{2}\right) \leq v(t) \leq k\ell(\psi_r - \psi_\ell) \qquad \text{for } t \geq \tau. \tag{A.14}$$

Proof. Let us first study the case where $t \leq \tau$. By derivation of (A.11), we have:

$$v'(t) = k\ell(\psi_r - \psi_\ell) - k\psi t v(t),$$

and the variation of constant method leads to expression (A.11).

Let us now consider the case where $t \geq \tau$. After a change of variable, equation (A.12) becomes

$$v(t) = k\ell\tau(\psi_r - \psi_\ell) - k\psi\int_0^\tau (\tau - s)v(t-s)ds, \tag{A.15}$$

$$= k\ell\tau(\psi_r - \psi_\ell) - k\psi\int_0^t (t - s)v(t-s)ds + h(t), \tag{A.16}$$

with

$$h(t) = k\psi\int_\tau^t (t-s)v(t-s)ds + k\psi\int_0^\tau (t-\tau)v(t-s)ds.$$

Since $\mathcal{P}$ is positive and decreasing, we deduce from Theorem 21 that $\forall t \geq 0,\ v(t) \geq 0$. Hence, we know that $h \geq 0$ on $[\tau, +\infty[$. Moreover, derivating h in t, we obtain

$$\begin{aligned} h'(t) &= k\psi\left(\int_\tau^t \frac{d}{dt}((t-s)v(t-s))ds + \int_0^\tau \frac{d}{dt}((t-\tau)v(t-s))ds\right), \\ &= k\psi\left((t-\tau)v(t) + (x(t) - x(t-\tau))\right) \geq 0, \end{aligned}$$

as $v \geq 0$. Then, derivating equation (A.16) leads to

$$v'(t) \geq -k\psi t v(t),$$

from which we deduce

$$v(t) \geq v(\tau)\exp\left(-k\psi\frac{(t^2-\tau^2)}{2}\right),$$

leading to the first inequality. Moreover, as $v \geq 0$, the second one is obtained from equation (A.15), and this concludes the proof. □

A.0.7 Conclusions and perspectives

In this paper, we have introduced a simple deterministic model of 1D cell migration, based on the filopodial activity of the cell. It describes the formation of antagonist elastic forces by filopodia on each side of the cell.

This model is not able to describe realistic trajectories, as the filopodial activity is taken constant, but it relates explicitly filopodial statistics to the cell velocity and asymptotic behaviour, and hence represents a first step in the global description of cell trajectories from filopodial activity.

In this work, we have studied a realistic case where filopodia stop exerting a force as soon as the cell has overtook their tips. In this case, the highly non-linear force prevent us from getting more than an existence and uniqueness result.

The case of linear elastic forces is richer, as it gave more information about the sign, boundedness and asymptotic behaviour of the solution. It is important to keep in mind that the linear model is realistic only in a particular setting: if the cell is slow enough, and filopodia's lifetime short enough, then they won't be reached by the cell. Typical velocity and filopodium lifetime are closely related to the cell type and experimental setting. Indeed, considering the force $k\ell$ exerted by a filopodium of length ℓ on the substrate, it is known that ℓ is variable among cell types. Moreover, k highly depends on the rigidity of the substrate: the more it is rigid, the larger the forces are Lo et al. [2000]. Another key-player in the filopodial forces is the adhesiveness of the substrate, that scales how strong it is coupled to filopodia, hence how large forces will be. However, a very adherent substrate is also less likely to let go of filopodia during the contraction of the cell, leading to a longer lifetime for them. This results in a bell-shaped curve relating velocity and adhesiveness, as described in Palecek et al. [1997]. As a consequence, it is likely that for a substrate of low (or very large) adhesiveness and low rigidity, cells velocity would be low enough so that the linear model fits with experimental conditions. This first-step model describing filopodial activity and trajectories is simple enough to give analytical information about the cell velocity, but still rich enough to be compared to different kinds of experimental 1D migration assays. In future works, it will be crucial to consider non constant densities of filopodia, to take into account the effect of motion itself on the filopodial activity. This would probably lead to much more realistic trajectories, where changes of direction would be described.

Appendix B

Algorithm for numerical trajectories analysis

In the spirit of Caballero et al. [2014], an analysis of cell trajectories in terms of persistence was performed experimentally for various cell mutants, and for which measures of the protrusive dynamics were made. Using our model, we developped an algorithm able to generate numerical trajectories and to derive the same typical quantities. This is an ongoing joint work with David Caballero (IBEC), Nicolas Meunier, Daniel Riveline (IGBMC), and Raphaël Voituriez. Measures of persistence consist in:

- the persistence length L_{pe}, defined as the mean length of path between two changes of direction. Numerically, it is defined with a treshold in the angle of motion, set as $12,5° = 0.22rad$.
- the persistence time and speed $\boldsymbol{T_{pe}}, \boldsymbol{V_{pe}}$,associated with L_{pe}.
- the pausing time $\boldsymbol{T_{pa}}$, defined as the time during which the cell's velocity is 0, only if it lasts more than $0.5h$. Numerically, it means that we will have pausing time either bigger than $0.5h$, either equal to $0h$.

Parameters on the protrusive dynamics can be fitted on experimental measure. The friction coefficient γ and the polarisation coefficient α are free.

Analysis of numerical trajectories

Experimental movies last 40h, and consist in pictures taken every 5 minutes. We use an algorithm that can generates a trajectory, and split it in persistent paths and pausing states, from which we can get mean values for L_{pe}, T_{pe}, V_{pe} and T_{pa}. Moreover, we can mark on the trajectory all persistent paths discriminated, as well as pausing periods. Four types of events can be detected :

→ Pausing.

→ Stopping (shorter than a pause) and the cell doesn't change of direction after it.

→ Stopping leading to a change of direction.

→ Changing of direction without pausing or stopping.

Algorithm

- Simulate a trajectory.
- Remove data such that the sampling frequency is of about $5min$ (to get the same precision as experimentally).
- Take starting index i, and running index $j = i$.

$\star$ While $i \leq i_{max}$, let j run throught vectors Time, Module, Argument from i while

$\boldsymbol{j \leq j_{max}}$ AND $\boldsymbol{Module(v_j) \neq 0}$ AND $\boldsymbol{\mid Argument(v_j) - Argument(v_i) \mid \leq 0.22.}$

Then, consider all options.

- If $j = j_{max}$, **end** (the last portion of trajectory is neglected).
- Else, if $Module(v_j) = 0$, there is either a pause or a stop.
  - $\rightarrow$ Let k be the next index such that $Module(v_k) \neq 0$.
  - $\rightarrow$ If $Time(k) - Time(j) > 0.5h$, then **pause** :
    - store the distance between points I and J, and the corresponding time and speed.
    - store indexes i and j for the plot.
    - store the pausing time between J and K.
    - store one index of pausing state (e.g j or $k-1$).
    - take $i = k$, $j = i$, and go back from $\star$.
  - $\rightarrow$ Else : there is **no pause**.
    - If $\mid Argument(v_k) - Argument(v_i) \mid \leq 0.22$, no change of direction. Take $j = k$ and go back from $\star$ (i unchanged).
    - If there is a change of direction during the pause, then
      - $\hookrightarrow$ Store the distance between points I and J, and the corresponding time and speed.
      - $\hookrightarrow$ Store indexes i and j for the plot.
      - $\hookrightarrow$ Store pausing time $= 0$ (and no index of pausing to store).
      - $\hookrightarrow$ Take $i = k$, $j = i$, and go back from $\star$.
- Else : there is a **change of direction without stopping**.
  - $\rightarrow$ Store the distance between points I and J, and the corresponding time and speed.
  - $\rightarrow$ Store indexes i and j for the plot.
  - $\rightarrow$ Take $i = j$ and go back from $\star$.

An example of analyzed trajectory is given in figure B.1.

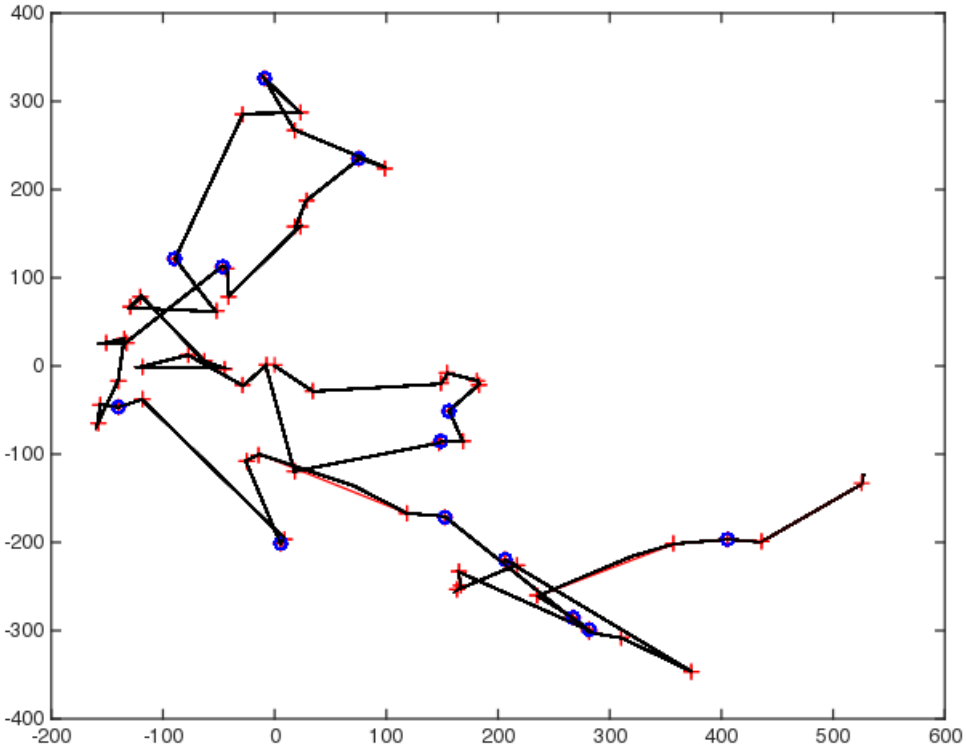

Figure B.1 – Numerical analysis of a trajectory. Parameters: $T = 40$, $\Delta t = 10^{-4}$, $c = 20$, $r = 9.6$, $\alpha = 1$, $\eta = 5 \cdot 10^{-5}$. The red crosses show persistent paths. Blue circles show pauses.

Appendix C

Un modèle de régulation moléculaire oscillatoire

La régulation de la dynamique du cytosquelette se fait en grande partie par le rôle des molécules de la famille des RhoGTPases. Dans ce travail en collaboration avec Bertrand Maury et Alexis Gautreau, nous avons défini et simulé numériquement un modèle de circuit de régulation moléculaire supposé capable de produire des oscillations en temps. La boucle de signalement est la suivante :

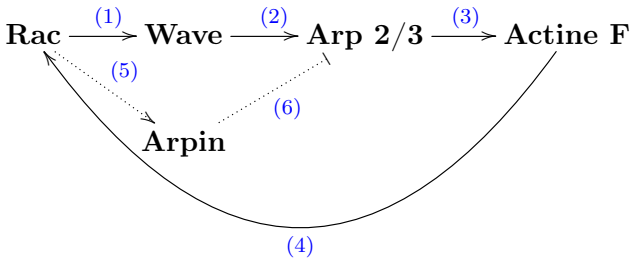

(1) **Rac** est capable d'activer localement divers Facteurs de Nucléation dans la cellule (Nucleation Promoting Factor). Au niveau du lamelllipode, il s'agit du complexe **Wave** (présent sur sa périphérie).

(2) Le complexe **Wave** possède une terminaison de type *VCA* (structure tripartite de type C : fonction carboxyle -COOH). Le motif Acide lui sert à se lier à **Arp2/3**. Le reste de la molécule sert à activer le complexe.

(3) Le complexe **Wave-Arp2/3** est "activé", c'est-à-dire qu'il peut se fixer à deux **filaments d'actine** simultanément. Ils forment alors un angle d'environ 70°. Le complexe Wave se détache alors, tandis qu'Arp2/3 maintient le branchement.

(4) Localement, la polymérisation de l'**actine** réactive **Rac** via la *Coronin1A* et le facteur d'échange de Rac *β-Pix*, aussi appelé *ArhGEF7*.

L'action de ces molécules est schématisée ci-dessous [Castro-Castro et al., 2011]:

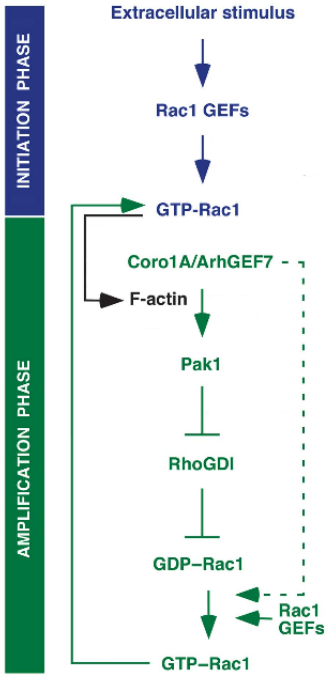

Figure C.1 – Schéma de la régulation de la translocation et activation de Rac1 par CoroninA, menant à l'amplification des signaux Rac1. Les flèches en pointillés correspondent à des étapes hypothétiques.

Le schéma peut être synthétisé comme suit: la forme active de Rac est **GTP-Rac1**, tandis que sa forme inactive est **GDP-Rac1**. La transition entre ces formes se fait grâce à des facteurs d'échange Rac1-GEF, comme par exemple *ArhGEF7* (qui est également une protéine permettant de stocker Rac1 au bord de la membrane). La molécule RhoGDI (Rho-GDP Dissociation Inhibitor) est capable de former un complexe avec Rac1, et de l'éloigner de la membrane pour l'isoler dans le cytosol. En présence d'actine, les molécules *ArhGEF7* et *Coronin1A* activent Pak1, qui est capable d'inhiber l'action de RhoGDI : pour cela, il forme un complexe Pak1-RhoGDI et par phosphorylation, entraîne la dissociation du complexe RhoGDI-Rac1. Les molécules Rac-GDP ainsi libérées sont transloquées vers les zones membranaires riches en actine, et activées grâce à *Coronin1A* et des *Rac1-GEF*.

(5) L'activation de **Rac** recrute des molécules d'**Arpin** actives, localement à la périphérie du lamellipode.

(6) Arpin est une molécule possédant un domaine terminal de type C très mobile, contenant le motif Acide responsable de l'attachement à **Arp2/3**. Il ne possède pas le motif VC que possède Wave (qui est responsable de l'activation d'Arp2/3). Il y a donc **compétition** entre Arpin et Wave pour la formation d'un complexe avec Arp2/3.

Nous présentons maintenant quelques observations concernant la molécule Arpin [Dang et al., 2013]. En l'absence de cette molécule, la formation du lamellipode est rapide, et les protrusions sont plus fréquentes et plus persistantes. Lorsqu'elle est présente, des protrusions se créent toujours, mais les cycles de croissance sont plus nombreux et durent moins longtemps.

C.1 Modélisation locale

Nous nous attachons d'abord à modéliser la boucle de réaction sans tenir compte des effets spatiaux.

C.1.1 Modèle 1.1 à 6 espèces

Nous modélisons ici la chaine de réactions, sans considération spatiale. Les concentrations totales en chaque espèce (forme active + inactive) est donc constante, et nous les supposons toutes égales à 1. Les variables considérées sont les suivantes :

R	la concentration en Rac actif. La concentration en Rac non actif est donc $1 - R$.
W	la concentration en Wave actif.
$Arpin$	la concentration en Arpin actif.
$A^+_{2/3}$	la concentration en complexe Wave-Arp2/3.
$A^-_{2/3}$	la concentration en complexe Arpin-Arp2/3.
	Nous supposons que les protéines Arp2/3 se présentent sous forme active (Wave-Arp2/3), inactive
$ActF$	la concentration en filaments d'actine branchés.
	L'actine F se présente sous l'état libre, et l'état branché.

Modèle 1.1-a : cinétique enzymatique

Nous supposons que les réactions d'activation se font selon une cinétique de type Michaelis-Menten. N'ayant aucune information particulière sur le passage de la forme active à non active des espèces, les taux de transition correspondants sont pris constants pour chacune. Nous obtenons ainsi le système suivant :

$$\begin{cases} \dfrac{dR(t)}{dt} = \alpha_1\big(1-R(t)\big)\dfrac{ActF(t)^{n_1}}{K_1^{n_1}+ActF(t)^{n_1}} - \beta_1 R(t) \\ \dfrac{dW(t)}{dt} = \alpha_2\big(1-W(t)\big)\dfrac{R(t)^{n_2}}{K_2^{n_2}+R(t)^{n_2}} - \beta_2 W(t) \\ \dfrac{dArpin(t)}{dt} = \alpha_3\big(1-Arpin(t)\big)\dfrac{R(t)^{n_3}}{K_3^{n_3}+R(t)^{n_3}} - \beta_3 Arpin(t) \\ \dfrac{dA^+_{2/3}(t)}{dt} = \alpha_4\big(1-A^+_{2/3}(t)-A^-_{2/3}(t)\big)\dfrac{W(t)^{n_4}}{K_4^{n_4}+W(t)^{n_4}} - \beta_4 A^+_{2/3}(t) \\ \dfrac{dA^-_{2/3}(t)}{dt} = \alpha_5\big(1-A^+_{2/3}(t)-A^-_{2/3}(t)\big)\dfrac{Arpin(t)^{n_5}}{K_5^{n_5}+Arpin(t)^{n_5}} - \beta_5 A^-_{2/3}(t) \\ \dfrac{dActF(t)}{dt} = \alpha_6\big(1-ActF(t)\big)\dfrac{A^+_{2/3}(t)^{n_6}}{K_6^{n_6}+A^+_{2/3}(t)^{n_6}} - \beta_6 ActF(t) \\ \big(R(0),W(0),Arpin(0),A^+_{2/3}(0),A^-_{2/3}(0),ActF(0)\big) = \big(R_0,W_0,Arp_0,A^+_0,A^-_0,ActF_0\big). \end{cases} \tag{C.1}$$

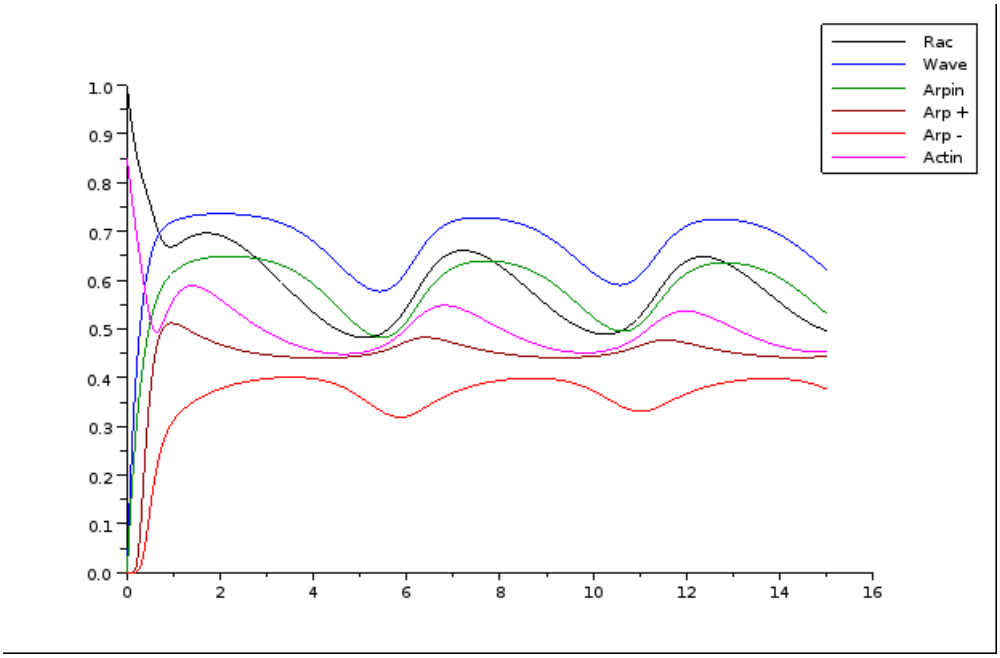

Figure C.2 – Simulations numériques du modèle 1.

i	α_i	β_i	n_i	K_i
1	3	1	8	0.5
2	3	1	8	0.5
3	2	1	8	0.5
4	2.95	1	8	0.5
5	3	1	8	0.5
6	3	1	8	0.5

Table C.1 – Paramètres correspondants.

Influence des valeurs initiales	
Si $[R_0] = 1$:	Si $[R_0] = 0$:
$ActF_0$: pas de contrainte.	$ActF_0 \geq 0.85$.
$A_0^- \leq 0.03$.	$W_0 \geq 0.85$.
$Arp_0 < 0.03$.	$Arp_0^+ \geq 0.85$.

Modèle 1.1-b : utilisation de fonction de Heaviside

Dans le modèle précédent, les termes de la forme $\dfrac{ActF(t)^n}{K^n + ActF(t)^n}$ servent à représenter la réponse à l'évolution de la concentration $ActF$. L'entier n permet d'obtenir différentes intensités de réponses. Lorsque $n \to +\infty$, cette fonction tend vers la fonction $x \mapsto H(x - K)$, où H est une Heaviside, et K est le seuil d'activation.

Nous pouvons donc réécrire le modèle ainsi :

$$
\begin{cases}
\dfrac{dR(t)}{dt} &= \alpha_1\big(1-R(t)\big)H\left(ActF(t)-K_1\right) &-\beta_1 R(t)\\
\dfrac{dW(t)}{dt} &= \alpha_2\big(1-W(t)\big)H\left(R(t)-K_2\right) &-\beta_2 W(t)\\
\dfrac{dArpin(t)}{dt} &= \alpha_3\big(1-Arpin(t)\big)H\left(R(t)-K_3\right) &-\beta_3 Arpin(t)\\
\dfrac{dA^+_{2/3}(t)}{dt} &= \alpha_4\big(1-A^+_{2/3}(t)-A^-_{2/3}(t)\big)H\left(W(t)-K_4\right) &-\beta_4 A^+_{2/3}(t)\\
\dfrac{dA^-_{2/3}(t)}{dt} &= \alpha_5\big(1-A^+_{2/3}(t)-A^-_{2/3}(t)\big)H\left(Arpin(t)-K_5\right) &-\beta_5 A^-_{2/3}(t)\\
\dfrac{dActF(t)}{dt} &= \alpha_6\big(1-ActF(t)\big)H\left(A^+_{2/3}(t)(t)-K_6\right) &-\beta_6 ActF(t)\\
\big(R(0),W(0),Arpin(0),A^+_{2/3}(0),A^-_{2/3}(0),ActF(0)\big) = \big(R_0,W_0,Arp_0,A^+_0,A^-_0,ActF_0\big).
\end{cases}
\tag{C.2}
$$

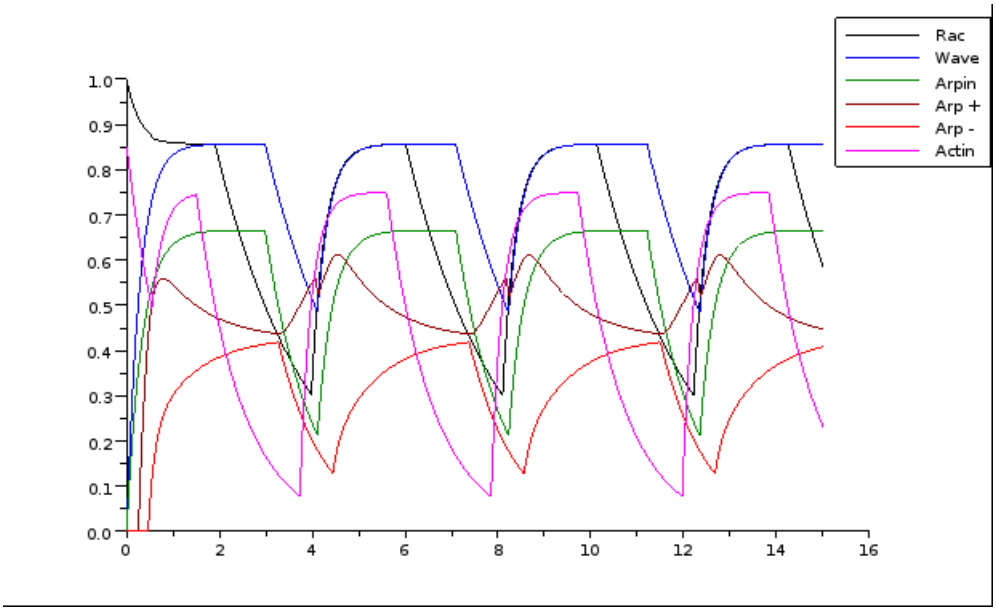

Figure C.3 – Simulation numérique du modèle simplifié 1.

i	α_i	β_i	K_i
1	3	0.5	0.5
2	3	0.5	0.5
3	2	1	0.5
4	2.95	1	0.5
5	3	1	0.5
6	3	1	0.5

Table C.2 – Paramètres correspondants.

C.1.2 Modèle 1.2 à 3 espèces

Nous pouvons décrire le même phénomène en prenant en compte seulement 3 espèces :

→ L'actine F, de concentration $ActF$.

→ Le complexe actif Arp2/3 + Wave, de concentration $A^+_{2/3}$.

→ Le complexe non actif Arp2/3 + Arpin, de concentration $A^-_{2/3}$.

Nous formulons les hypothèses suivantes :

(1) L'actine F branché induit la formation des complexes $Arp^+_{2/3}$ et $Arp^-_{2/3}$.

(2) Le complexe $Arp^+_{2/3}$ provoque à son tour l'augmentation de la concentration en actine F branché.

(3) La concentration totale en molécule Arp (libre, occupée ou activée) est constante, normalisée à 1.

La compétition pour la formation de complexes $Arp^+_{2/3}$ et $Arp^-_{2/3}$ est donc encore décrite. Cela correspond au diagramme suivant :

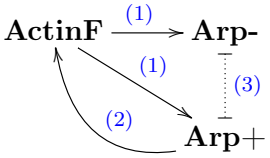

Modèle 1.2-a : cinétique enzymatique

$$\begin{cases} \dfrac{dActF(t)}{dt} &= \alpha_1(1-ActF(t))\dfrac{A^+_{2/3}(t)^{n_1}}{K_1^{n_1}+A^+_{2/3}(t)^{n_1}} - \beta_1 ActF(t) \\ \dfrac{dA^+_{2/3}(t)}{dt} &= \alpha_2(1-A^+_{2/3}(t)-A^-_{2/3}(t))\dfrac{ActF(t)^{n_2}}{K_2^{n_2}+ActF(t)^{n_2}} - \beta_2 A^+_{2/3}(t) \\ \dfrac{dA^-_{2/3}(t)}{dt} &= \alpha_3(1-A^+_{2/3}(t)-A^-_{2/3}(t))\dfrac{ActF(t)^{n_3}}{K_3^{n_3}+ActF(t)^{n_3}} - \beta_3 A^-_{2/3}(t) \end{cases}$$

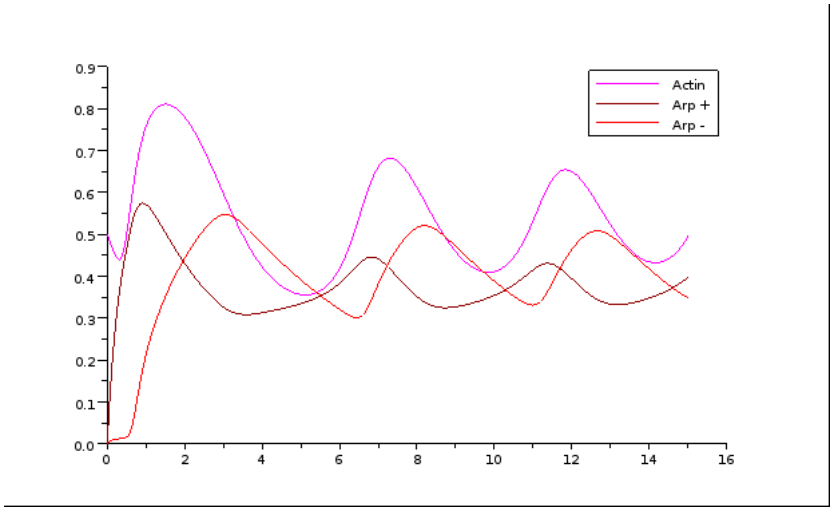

Figure C.4 – Modèle 1.2-a

i	α_i	β_i	n_i	K_i	Intervalle pour la condition initiale.
1	3	0.5	8	0.45	[0.25 , 1]
2	3	1	2	0.4	[0,1]
3	2	0.2	15	0.6	[0,0.51]

Table C.3 – Paramètres correspondants à la courbe "Modèle 1.2-a".

Remark 33. *En dehors des plages de conditions initiales données dans le tableau (pour ces paramètres), on obtient un état stable (0,0,0).*

Les portraits de phase correspondants sont les suivants :

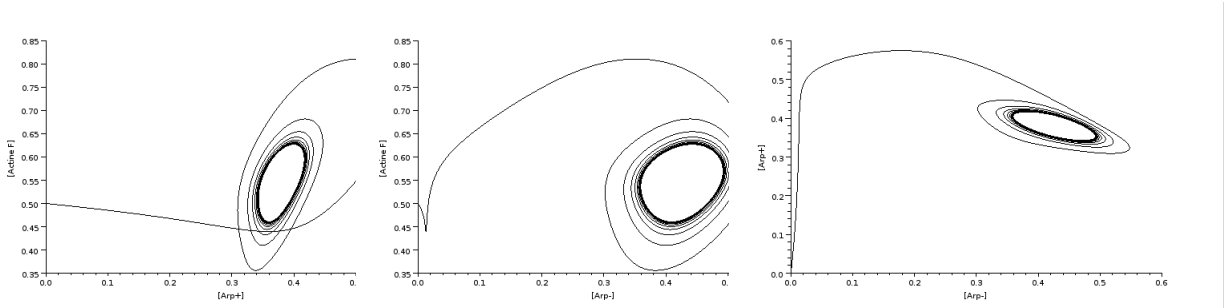

Actine F / $Arp^+_{2/3}$ Actine F / $Arp^-_{2/3}$ $Arp^+_{2/3}/Arp^-_{2/3}$

Modèle 1.2-b : utilisation de fonctions de Heaviside

Là aussi, nous pouvons représenter les réactions d'activation par des fonctions de Heaviside.

$$\begin{cases} \dfrac{dActF(t)}{dt} &= \alpha_1(1-ActF(t))H\left(A^+_{2/3}(t)-K_1\right)-\beta_1 ActF(t) \\ \dfrac{dA^+_{2/3}(t)}{dt} &= \alpha_2(1-A^+_{2/3}(t)-A^-_{2/3}(t))H\left(ActF(t)-K_2\right)-\beta_2 A^+_{2/3}(t) \\ \dfrac{dA^-_{2/3}(t)}{dt} &= \alpha_3(1-A^+_{2/3}(t)-A^-_{2/3}(t))H\left(ActF(t)-K_3\right)-\beta_3 A^-_{2/3}(t) \end{cases}$$

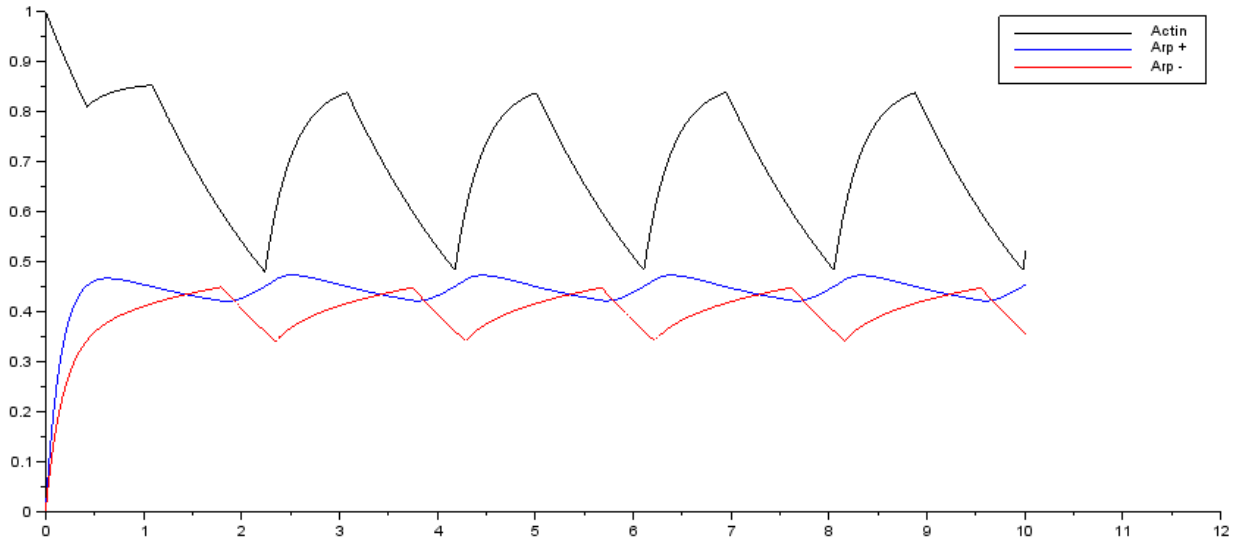

i	α_i	β_i	K_i
1	3	0.5	0.5
2	3	0.5	0.5
3	2	1	0.5

Table C.4 – Paramètres pour la simulation du modèle 1.2-b.

C.2 Modèle 2 : diffusion sur la membrane

Nous ajoutons maintenant une dimension spatiale, en représentant la membrane cellulaire par un domaine $\Omega = [0, l]$, avec $l \geq 0$, sur lequel les protéines diffusent.

C.2.1 Modèle 2.1 : hypothèse non réaliste

Dans un premier temps, les espèces autres que l'actineF diffusent, mais seulement sous leur forme active (ou sous forme de complexe). Cela revient à dire que les mêmes espèces sous formes inactive ou libre diffusent si peu en comparaison que leur concentration à tout moment peut être considérée homogène et constante. Cela permet de limiter le modèle à 6 équations, mais cette hypothèse reste très peu satisfaisante.

Modèle 2.1-a : modèle à 6 espèces

Le modèle s'écrit maintenant

$$\begin{cases} \dfrac{\partial R}{\partial t} = D_1 \triangle R + \alpha_1\big(1-R\big)\dfrac{ActF^{n_1}}{K_1^{n_1}+ActF^{n_1}} - \beta_1 R \\ \dfrac{\partial W}{\partial t} = D_2 \triangle W + \alpha_2\big(1-W\big)\dfrac{R^{n_2}}{K_2^{n_2}+R^{n_2}} - \beta_2 W \\ \dfrac{\partial Arpin}{\partial t} = D_3 \triangle Arpin + \alpha_3\big(1-Arpin\big)\dfrac{R^{n_3}}{K_3^{n_3}+R^{n_3}} - \beta_3 Arpin \\ \dfrac{\partial A^+_{2/3}}{\partial t} = D_4 \triangle A^+_{2/3} + \alpha_4\big(1-A^+_{2/3}-A^-_{2/3}\big)\dfrac{W^{n_4}}{K_4^{n_4}+W^{n_4}} - \beta_4 A^+_{2/3} \\ \dfrac{\partial A^-_{2/3}}{\partial t} = D_5 \triangle A^-_{2/3} + \alpha_5\big(1-A^+_{2/3}-A^-_{2/3}\big)\dfrac{Arpi5^{n_5}}{K_5^{n_5}+Arpin^{n_5}} - \beta_5 A^-_{2/3} \\ \dfrac{\partial ActF}{\partial t} = \alpha_6\big(1-ActF\big)\dfrac{{A^+_{2/3}}^{n_6}}{K_6^{n_6}+{A^+_{2/3}}^{n_6}} - \beta_6 ActF \\ \big(R(0),W(0),Arpin(0),A^+_{2/3}(0),A^-_{2/3}(0),ActF(0)\big) = \big(R_0,W_0,Arp_0,A^+_0,A^-_0,ActF_0\big), \end{cases} \tag{C.3}$$

avec des conditions de bord périodiques pour les 5 premières espèces.

Modèle 2.1-b : modèle à 3 espèces

Comme précédemment, en réduisant le modèle à 3 espèces, nous obtenons :

$$\begin{cases} \dfrac{\partial A^+_{2/3}}{\partial t} = D_1 \triangle A^+_{2/3} + \alpha_1(1-A^+_{2/3}-A^-_{2/3})\dfrac{ActF^{n_1}}{K_1^{n_1}+ActF^{n_1}} - \beta_1 A^+_{2/3} \\ \dfrac{\partial A^-_{2/3}}{\partial t} = D_2 \triangle A^-_{2/3} + \alpha_2(1-A^+_{2/3}-A^-_{2/3})\dfrac{ActF^{n_2}}{K_2^{n_2}+ActF^{n_2}} - \beta_2 A^-_{2/3} \\ \dfrac{\partial ActF}{\partial t} = D_3 \triangle ActF + \alpha_3(1-ActF)\dfrac{{A^+_{2/3}}^{n_3}}{K_3^{n_3}+{A^+_{2/3}}^{n_3}} - \beta_3 ActF \\ \big(ActF(0),A^+_{2/3}(0),A^-_{2/3}(0)\big) = \big(ActF_0,A^+_0,A^-_0\big), \end{cases}$$

avec des conditions de bord périodiques.

Nous obtenons les simulations numériques suivantes :

$\boldsymbol{i}$	$\boldsymbol{\alpha_i}$	$\boldsymbol{\beta_i}$	$\boldsymbol{n_i}$	$\boldsymbol{K_i}$
1	3	1	2	0.4
2	2	0.2	15	0.6
3	3	0.5	8	0.45
$T=100$			$l=100$	

Table C.5 – Paramètres pour la simulation du modèle 2.1-b.

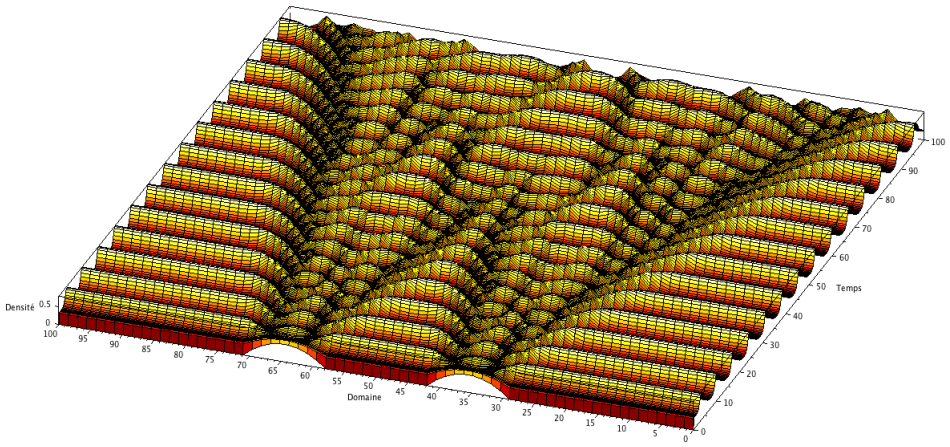

Figure C.5 – Simulation numérique de l'évolution de la concentration en ActineF branché sur la membrane au cours du temps, avec une condition initiale à deux maxima.

Bibliography

Ananthakrishnan, R. and Ehrlicher, A. (2007). The forces behind cell movement. Int J Biol Sci, 3(5):303–17. III

Caballero, D., Voituriez, R., and Riveline, D. (2014). Protrusion fluctuations direct cell motion. Biophys J, 107(1):34–42. III, VI, XIII

Castro-Castro, A., Ojeda, V., Barreira, M., Sauzeau, V., Navarro-Lérida, I., Muriel, O., Couceiro, J. R., Pimentel-Muíños, F. X., del Pozo, M. A., and Bustelo, X. R. (2011). Coronin 1a promotes a cytoskeletal-based feedback loop that facilitates rac1 translocation and activation. The EMBO Journal, 30:3913–3927. XVII

Dang, I., Gorelik, R., Sousa-Blin, C., Derivery, E., Guérin, C., Linkner, J., Nemethova, M., Dumortier, J. G., Giger, F. A., Chipysheva, T. A., Ermilova, V. D., Vacher, S., Campanacci, V., Herrada, I., Planson, A.-G., Fetics, S., Henriot, V., David, V., Oguievetskaia, K., Lakisic, G., Pierre, F., Steffen, A., Boyreau, A., Peyriéras, N., Rottner, K., Zinn-Justin, S., Cherfils, J., Bièche, I., Alexandrova, A. Y., David, N. B., Small, J. V., Faix, J., Blanchoin, L., and Gautreau, A. (2013). Inhibitory signalling to the arp2/3 complex steers cell migration. Nature, 503(7475):281–4. XVIII

Etchegaray, C., Grec, B., Maury, B., Meunier, N., and Navoret, L. (2015). Integral Methods in Science and Engineering: Theoretical and Computational Advances, chapter An Integro-Differential Equation for 1D Cell Migration, pages 195–207. Springer International Publishing, Cham. III

Grec, B., Maury, B., Meunier, N., and Navoret, L. (2012). The role of ligands binding in shear induced leukocyte rolling. VIII

Gripenberg, G., Londen, S.-O., and Staffans, O. (1990). Volterra integral and functional equations, volume 34. Cambridge University Press. VII

Johnston, S. A., Bramble, J. P., Yeung, C. L., Mendes, P. M., and Machesky, L. M. (2008). Arp2/3 complex activity in filopodia of spreading cells. BMC cell biology, 9(1):1. III, IV

Lo, C.-M., Wang, H.-B., Dembo, M., and Wang, Y.-l. (2000). Cell movement is guided by the rigidity of the substrate. Biophysical journal, 79(1):144–152. XII

Lodish, et al Harvey, D. B. (2002). Molecular Cell Biology, 4th Edition. W H Freeman & Co, fourth edition edition edition. IV

Palecek, S. P., Loftus, J. C., Ginsberg, M. H., Lauffenburger, D. A., Horwitz, A. F., et al. (1997). Integrin ligand binding properties govern cell migration speed through cell-substratum adhesiveness. Nature, 385(6616):537–540. XII

université PARIS-SACLAY | École doctorale de mathématiques Hadamard (EDMH)

Mathematical and numerical modelling of cell migration

Keywords. *Cell migration ; population process ; Fokker-Planck equation ; non linear and non local convection-diffusion equation ; asymptotic analysis ; numerical simulations.*

Abstract: Cell migration is fundamental for physiological and pathological phenomena (immune response, embryogenesis, tumor metastasis). The intracellular processes responsible for cell motion have a complex self-organized activity spanning different scales in time and space. In this doctoral thesis, we develop minimal models of individual cell migration relying on a multiscale interaction.
In a first part, we build stochastic particle models of migration. We study the case of a leukocyte carried by the blood flow that develops adhesive bonds with the artery wall. Then, we investigate the case of a cell crawling on an adhesive surface. In both situations, key intracellular processes are described using population models. Renormalizations lead to continuous stochastic equations giving stationary characteristics of the dynamics (stopping times, non motile or directional stationary states).
In a second part, we build a deterministic model of migration in a discoïdal cell domain. The actin cytoskeleton is described by a fluid whose activity is carried by boundary terms. It reinforces cell polarisation by advecting a molecule that regulates the cytoskeleton dynamics. The one dimensional analysis reveals a dichotomic behaviour (global existence or possible blow-up, polarised or unpolarised stationary states). Numerical simulations in two dimensions using finite volumes and finite elements methods illustrate this system's dynamics.

Modélisation mathématique et numérique de la migration cellulaire

Mots-clés. *Migration cellulaire ; processus de population ; équation de Fokker-Planck ; convection-diffusion non linéaire non locale ; analyse asymptotique ; simulations numériques.*

Résumé : Les déplacements cellulaires sont essentiels pour des phénomènes physiologiques et pathologiques (réponse immunitaire, embryogenèse, invasion tumorale). Les processus cellulaires à l'origine du déplacement forment une activité complexe, auto-organisée et multi-échelle en temps et en espace. Dans cette thèse, nous développons des modèles minimaux de migration basés sur des interactions multi-échelles.
Dans une première partie, nous construisons deux modèles stochastiques particulaires de migration. Nous étudions d'abord le cas d'un leucocyte porté par le sang qui créé des liens avec la paroi artérielle. Puis, nous nous intéressons au cas d'une cellule rampant sur une surface. Dans ces situations, des processus intracellulaires clés sont décrits au moyen de processus de population. Par renormalisation, nous obtenons des modèles limites continus, ainsi que des caractéristiques stationnaires (temps d'arrêt, état asymptotique).
Dans une seconde partie, nous développons un modèle déterministe de migration dans un domaine cellulaire disque. Le cytosquelette d'actine est décrit par un fluide dont le caractère actif est porté par les termes de bord. Il renforce la polarisation cellulaire en transportant une molécule régulatrice de sa dynamique. L'analyse du modèle unidimensionnel met en évidence un comportement dichotomique (existence globale ou éventuel blow-up, état stationnaire exclusivement non motile ou apparition d'états stationnaires motiles). Des simulations numériques en deux dimensions par volumes et éléments finis illustrent la dynamique du système.

Université Paris-Saclay
Espace Technologique/Immeuble Discovery
Route de l'Orme aux merisiers RD 128,
91190 Saint-Aubin France